

DISCOVERY AND DEVELOPMENT OF NOVEL, SELECTIVE METABOTROPIC
GLUTAMATE RECEPTOR 7 NEGATIVE AND POSITIVE ALLOSTERIC
MODULATORS; A GENERAL, ENANTIOSELECTIVE SYNTHESIS OF 2-
SUBSTITUTED THIOMORPHOLINES AND THIOMORPHOLINE 1,1-DIOXIDES; AND
TOTAL SYNTHESIS OF NATURAL (-)- AND UNNATURAL (+)-MELEARORIDE A

By

Carson W. Reed

Dissertation

Submitted to the Faculty of the
Graduate School of Vanderbilt University
in partial fulfillment of the requirements

for the degree of
DOCTOR of PHILOSOPHY
in

Chemistry

January 31, 2020

Nashville, Tennessee

Approved:

Craig W. Lindsley, Ph. D.

Gary A. Sulikowski, Ph. D.

Steven D. Townsend, Ph. D.

Colleen M. Niswender, Ph. D.

To my parents and my brother for always believing in me

To Chelsea, the love of my life, for her never-ending love and support

ACKNOWLEDGMENTS

The following work was generously supported by financial assistance from the Vanderbilt University Department of Chemistry, the Vanderbilt Institute of Chemical Biology Fellowship, NIMH grant R21 MH102548, CDMRP/DoD award W81XWH-17-1-0266, a Basic research grant from rettsyndrome.org, and the William K. Warren, Jr. and the William K. Warren Foundation who funded the William K. Warren, Jr. Chair in Medicine.

I would not have made it this far in my professional career without the generous help of the following people. Most importantly, I owe all my success at Vanderbilt University to my advisor and mentor Dr. Craig Lindsley. Craig, thank you for first giving me the opportunity to rotate through your lab as a first-year graduate student. After joining your lab, you have always been there to answer any of my questions, and as a result, you have molded me into the independent researcher that I am today. You make me strive to become a better scientist each and every day. Additionally, I would like to thank the members of my committee, Dr. Steve Townsend, Dr. Gary Sulikowski, and Dr. Colleen Niswender, for their additional guidance and mentorship that I have received through all of the milestones of my graduate career.

To current Lindsley lab members (Jeanette Bertron, Jacob Kalbfleisch, Caitlin Kent, and Jade Williams) and also Dr. Samantha Yohn, thank you for the years of not only collegiate discussion, but also friendship. Thank you for always being there to bounce ideas off of and for helping me persevere through the lows of graduate school.

Your friendship is much appreciated. I wish you all the best in your future endeavors. To past Lindsley lab members (especially Dr. Kevin McGowan, Dr. Mark Fulton, and Dr. Daniel Jeffries), I thank you for all of your guidance and support you have given me throughout my graduate journey. To all the members of the Rett Syndrome Team (especially Dr. Colleen Niswender, Dr. Rocco Gogliotti, Nicole Fisher, and Sheryl Vermudez), I thank you for allowing me to join your weekly meetings to learn more about the biology associated with my project. To the various members of the VCNDD leadership, DMPK (especially Dr. Annie Blobaum), and molecular pharmacology teams, I thank you all for contributing to this work.

To all the members of my graduate cohort, I thank you for your friendship. A special shout-out to Caleb Jones, John Terrell, and Jeanette Bertron for your senses of humor which always seemed to bring a smile to my face even on the worst of days.

I also am indebted to numerous people who have helped me along the way prior to entering my graduate studies at Vanderbilt University. First, I would like to thank Dr. Justin K. Wyatt for inspiring my love for organic chemistry. Ever since my first day in your undergraduate sophomore organic chemistry class, I was captivated by the subject matter. Your enthusiasm for the subject was indeed contagious. Thank you for giving a kid, who had no experience performing research at the time, the opportunity to learn chemistry and basic research techniques during multiple summers under your mentorship.

Next, I would like to thank both Dr. Craig Beeson and especially Dr. Christopher Lindsey for their mentorship during my time at MitoChem Therapeutics, LLC as a

research associate. Many thanks are due to Chris for his leadership/mentorship and for teaching me what to expect before I began my graduate studies. Thank you for helping me to learn a few new named reactions and advanced organic chemistry concepts every day.

To my parents and my brother, thank you for all of the love and support you have so graciously given to me these past years. Thank you for understanding the requirements of a Ph.D. program and helping me to face all of my stress and anxiety. You have always believed in me and have encouraged me to achieve great things throughout my professional development.

Last but certainly not least, I would like to thank my wonderful wife, Chelsea. Thank you for pushing me to not only become a better scientist, but also a better person. Thank you for understanding the stress and levels of commitment that are required for obtaining a Ph.D. and for being my rock to lean on during this time. Thank you for believing in me even at times when I stopped believing in myself. I love you with all my heart, always and forever.

TABLE OF CONTENTS

	Page
DEDICATION.....	ii
ACKNOWLEDGMENTS.....	iii
LIST OF TABLES.....	xi
LIST OF FIGURES.....	xiii
LIST OF SCHEMES.....	xv
LIST OF ABBREVIATIONS.....	xvii
CHAPTER	
I. Discovery and Development of Novel, Selective Metabotropic Glutamate Receptor 7 Negative Allosteric Modulators.....	1
Background and Introduction.....	1
G Protein-Coupled Receptors: Metabotropic Glutamate Receptors.....	1
Metabotropic Glutamate Receptor 7 (mGlu ₇) and Known Physiological Roles.....	4
Orthosteric vs. Allosteric Probe Development Strategies.....	7
mGlu ₇ Tool Compounds: Negative Allosteric Modulators and Allosteric Antagonists.....	10
Potential Therapeutic Avenue for mGlu ₇ NAMs: Anxiety-Related Disorders.....	12
Conclusion.....	13
Materials and Methods.....	14
General Synthetic Methods and Instrumentation.....	14
Primary Screening (Calcium Mobilization) Assay.....	16
<i>In Vitro</i> DMPK Methods: Intrinsic Clearance in Murine and Rat Liver Microsomes.....	17
Mouse and Rat Plasma Protein Binding.....	18
Mouse and Rat Brain Homogenate Binding.....	19
Metabolite Identification in Rat Hepatic S9.....	20
LC/MS/MS Analysis of Samples from <i>In Vitro</i> Assays.....	20

<i>In Vivo</i> PK Methods.....	21
Time Course PK and Single Time Point Tissue Distribution Studies.....	21
Mouse Tissue Distribution Studies.....	22
Plasma and Brain Sample Preparation.....	22
LC/MS/MS Bioanalysis of Samples from <i>In Vivo</i> Assays.....	23
Extracellular Field Potential Recordings.....	23
Eurofins Lead Profiling Data.....	24
Behavioral Pharmacology: Animals.....	25
Behavioral Pharmacology: Elevated Zero Maze (EZM).....	25
Behavioral Pharmacology: Light-Dark Box.....	25
Behavioral Pharmacology: Marble Burying Assay.....	26
Behavioral Pharmacology: Data Analysis.....	26
Discovery and Development of Novel, Selective Metabotropic Glutamate Receptor 7 Negative Allosteric Modulators.....	27
High-Throughput Screening Campaign: Identification of VU6009748.....	27
Initial SAR of Western Aromatic Ring: Analogs 1.13-1.34	28
SAR of the Southern Heterocyclic Ring: Analogs 1.35-1.59	32
SAR Around the Eastern Aromatic Ring: Analogs 1.63-1.96	36
Assessment of VU6010608 (1.23) as a Viable Tool Compound.....	41
Addressing the Potential Metabolic Liabilities of 1.23 : Discovery of VU6012962.....	44
Addressing the True Metabolic Liability of VU6010608 (1.23): Amide Hydrolysis.....	52
Elongation of the Amide Linker: Discovery of Phenoxy Benzamide Linker.....	54
Extended Amide Linker Replacements: Carbamate Congeners...60	
Extended Amide Linker Replacements: Des-Carbonyl Analogs...65	
Heterocycles as Viable Amide Replacements.....	68
1,3,4-Oxadiazole and 1,2,4-Oxadiazole Heterocyclic Analog.....	70
Conclusion.....	81
Experimental Methods.....	82
General Synthetic Methods and Instrumentation.....	82
References for Chapter I.....	123
Appendix A: Relevant Spectra for Chapter I.....	130
II. Progress Towards the Development of Metabotropic Glutamate Receptor 7 Positive Allosteric Modulators.....	255

Background and Introduction.....	255
Known mGlu ₇ Orthosteric and Allosteric Agonists, and Positive Allosteric Modulators.....	255
Neurodevelopmental Disorders: Rett Syndrome (RTT).....	258
Known Mutations of <i>Mecp2</i> Gene Responsible for RTT.....	260
The Correlation Between mGlu ₇ and RTT.....	262
Therapeutic Strategies for Treating RTT.....	265
Conclusion.....	267
Materials and Methods.....	268
General Synthetic Methods and Instrumentation.....	268
Primary Screening (Calcium Mobilization) Assay.....	270
<i>In Vitro</i> DMPK Methods: Intrinsic Clearance in Murine and Rat Liver Microsomes.....	271
Mouse and Rat Plasma Protein Binding.....	272
Mouse and Rat Brain Homogenate Binding.....	273
LC/MS/MS Analysis of Samples from <i>In Vitro</i> Assays.....	274
<i>In Vivo</i> PK Methods.....	274
Time Course PK and Single Time Point Tissue Distribution Studies.....	275
Mouse Tissue Distribution Studies.....	275
Plasma and Brain Sample Preparation.....	276
LC/MS/MS Bioanalysis of Samples from <i>In Vivo</i> Assays.....	276
Eurofins Lead Profiling Data.....	277
Progress Towards the Development of Metabotropic Glutamate Receptor 7 Positive Allosteric Modulators.....	277
Identification of Molecular Switch: Discovery of VU6014181.....	277
SAR of Western Heterocyclic Ring.....	281
SAR of Piperazine Linkers.....	286
SAR of Alternative Alkoxy Groups.....	292
SAR of Buchwald-Hartwig Library.....	297
Identification of Potential <i>In Vivo</i> Tool Compounds.....	300
Addressing Potential Metabolic Sites of Quinoline Scaffold.....	301
Conclusions/Future Directions.....	305
Experimental Methods.....	306
General Synthetic Methods and Instrumentation.....	306
References for Chapter II.....	320
Appendix B: Relevant Spectra for Chapter II.....	328
III. A General, Enantioselective Synthesis of 2-Substituted Thiomorpholines and Thiomorpholine 1,1-Dioxides.....	355

Background and Introduction.....	355
Importance of Saturated Azaheterocycles.....	355
Traditional Methods for Synthesizing Substituted Thiomorpholine Heterocycles.....	356
Recent Thiomorpholine Synthetic Strategies Using Transition Metals.....	358
Proposed Synthetic Strategy for Accessing Chiral 2-Substituted Thiomorpholines Using Organocatalysis.....	361
Materials and Methods.....	364
General Synthetic Methods and Instrumentation.....	364
General Enantioselective Synthesis of 2-Substituted Thiomorpholines and Thiomorpholine 1,1-Dioxides.....	366
Synthesis of C2-Symmetric Organocatalysts 3.31 and 3.32	366
Synthesis of β -chloroalcohols (<i>R</i>)- 3.41a-h and (<i>S</i>)- 3.42a-h	366
Synthesis of Cyclization Precursors: Thioesters 3.45a-h and 3.46a- h	368
Optimization of the Deprotection/Cyclization Cascade: Synthesis of Chiral C2-Substituted Thiomorpholines 3.47a-h and 3.48a-h	369
Synthesis of Chiral C2-Substituted Thiomorpholine 1,1-Dioxides 3.49	371
Conclusion.....	372
Experimental Methods.....	372
General Synthetic Methods and Instrumentation.....	372
References for Chapter III.....	409
Appendix C: Spectra and Chiral SFC Traces for Chapter III.....	413
 IV. Total Synthesis of Natural (-)-and Unnatural (+)-Melearoride A.....	 508
Background and Introduction.....	508
Importance of Natural Products.....	508
Isolation and Biological Activity of Melearoride A (4.8a).....	511
Synthesis of PF1163B (4.11): A Related Natural Product.....	513
Necessity of a Novel, Modular Synthetic Approach for Accessing Additional Analogs of This Family of Natural Products.....	515
Materials and Methods.....	516
General Synthetic Methods and Instrumentation.....	516
Total Synthesis of Natural (-)- and Unnatural (+)-Melearoride A.....	518
Retrosynthetic Analysis for 4.8a and 4.8b	518
Synthesis of Chiral Epoxides 4.29a and 4.29b	519
Synthesis of Chiral Tosylates 4.30a and 4.30b	520

Optimizing the Formation of Alcohol 4.38a	521
Synthesis of Esters 4.39a and 4.39b	523
Synthesis of Natural (-)-Melearoride A 4.8a and Unnatural (+)- Melearoride A 4.8b	524
Conclusion.....	525
Experimental Methods.....	526
General Synthetic Methods and Instrumentation.....	526
References for Chapter IV.....	541
Appendix D: Relevant NMR Spectra for Chapter IV.....	545

LIST OF TABLES

Chapter I

Table	Page
1.1 SAR around the western aromatic ring – analogs 1.13-1.34	29
1.2 SAR of the southern heterocyclic ring – analogs 1.35-1.59	33
1.3 SAR of the eastern aromatic ring – analogs 1.63-1.96	37
1.4 Eurofins lead profile panel for 1.23 . Significant activity is defined as >50% inhibition at a 10 μ M concentration of 1.23 . Data courtesy of Eurofins.....	41
1.5 Alternative alkoxy groups surveyed – analogs 1.105-1.132	46
1.6 Eurofins lead profile panel for 1.127 . Significant activity is defined as >50% inhibition at a 10 μ M concentration of 1.127 . Data courtesy of Eurofins.....	49
1.7 SAR of traditional amide bioisosteres – analogs 1.133-1.140	53
1.8 SAR of elongated amide analogs 1.141 ; 1.147-1.172	56
1.9 SAR of carbamate analogs 1.173 ; 1.177-1.204	61
1.10 SAR of des-carbonyl analogs 1.210-1.230	66
1.11 SAR of diversity-oriented heterocyclic linker library.....	68
1.12 SAR of 1,3,4-oxadiazole analogs 1.250-1.271	71
1.13 SAR of 1,2,4-oxadiazole analogs 1.275-1.288	75
1.14 SAR of 1,3,4-oxadiazole: southern heterocyclic ring – analogs 1.289-1.315	78

Chapter II

Table	Page
2.1 Eurofins lead profiling panel of VU6014181 (2.18). Significant activity is defined as >50% inhibition at a 10 μ M concentration of 2.18 . Data courtesy of Eurofins.....	279
2.2 SAR of western heterocyclic ring: analogs 2.25-2.50	282
2.3 SAR of piperazine linkers: analogs 2.56-2.82	288
2.4 SAR of alternative alkoxy groups: analogs 2.85-2.111	293
2.5 SAR of enantiomers of both 2.91 and 2.98	297
2.6 SAR of 8-aminoquinoline analogs 2.114-2.124	298
2.7 Rat <i>in vivo</i> PK parameters for potential tool compounds 2.91 , 2.101 , 2.103 , and 2.121	301
2.8 SAR of quinolones 2.130-2.131 and <i>N</i> -methyl quinolones 2.132-2.133	303
2.9 SAR of fused imidazo- and triazolo-heterocycles 2.135-2.137	305

Chapter III

Table	Page
3.1 Reaction optimization of the deprotection/cyclization cascade.....	369

Chapter IV

Table	Page
4.1 Optimization of our synthetic route en route to alcohol 4.38a	521
4.2 Comparison of ^1H and ^{13}C NMR data of isolated 4.8a and synthetic 4.8a	540

LIST OF FIGURES

Chapter I

Figure	Page
1.1	Generic representation of mGlu receptor homodimer.....2
1.2	NMDA-receptor dependent mechanism of LTP.....6
1.3	Orthosteric and putative allosteric binding sites for mGlu receptors.....8
1.4	Representative allosteric ternary complex model.....9
1.5	Known mGlu ₇ NAMs and allosteric antagonists 1.1-1.310
1.6	Commonly prescribed SSRIs 1.4-1.712
1.7	Structure of HTS hit VU6009748 (1.8) and our proposed SAR strategy.....27
1.8	VU6010608 (1.23) is capable of blocking the induction of LTP at SC-CA1 synapses. Data courtesy of Branden Stansley, Ph.D.....44
1.9	Potential Metabolic Liabilities of VU6010608 (1.23).....45
1.10	Structure of VU6012962 (1.127) with respective DMPK parameters.....49
1.11	Anxiolytic behavioral assays of 1.127 : (A) elevated zero maze assay, (B) light/dark box assay, and (C) marble burying assay. VEH = vehicle and FLX = fluoxetine (positive control). Data courtesy of Samantha Yohn, Ph.D.....52
1.12	Structures of novel mGlu ₇ NAM tool compounds 1.23 , 1.127 , and 1.30782

Chapter II

Figure	Page
2.1	Known mGlu ₇ orthosteric and allosteric agonists, and positive allosteric modulators.....256
2.2	8 common mutations of the <i>Mecp2</i> gene that lead to RTT.....260
2.3	Current small molecules in ongoing clinical trials for the treatment of RTT.....266
2.4	Structures of the mGlu ₇ NAM VU6009339 (2.17) and the molecular switch mGlu ₇ PAM VU6014181 (2.18).....278

Chapter III

Figure	Page
3.1	Examples of pharmaceutically relevant thiomorpholines 3.1-3.3 and their oxidized congeners (thiomorpholine 1,1-dioxides) 3.4-3.5355
3.2	Key bond disconnections used to access β -chloro alcohols 3.28361
3.3	Jørgensen's asymmetric α -chlorination of aldehydes methodology.....362

3.4	Putative rationale for diastereofacial selectivity observed in α -chlorination reaction.....	363
------------	---	-----

Chapter IV

Figure	Page	
4.1	Representative natural product therapeutic agents 4.1-4.6	509
4.2	Structural simplification of the natural product lovastatin (4.3) leads to atorvastatin (4.7).....	511
4.3	Structures of (-)-Melearoride A (4.8a), (+)-Melearoride A (4.8b), (-)-Melearoride B (4.9) and the PF1163 Family of Related Natural Products (4.10-4.14).....	512
4.4	Retrosynthetic analysis for natural (-)-Melearoride A 4.8a	518
4.5	Retrosynthetic analysis for unnatural (+)-Melearoride A 4.8b	519
4.6	Structure of 5-membered chelate 4.42	525

LIST OF SCHEMES

Chapter I

Scheme	Page
1.1 SAR of western aromatic ring – synthesis of analogs 1.13-1.34	28
1.2 SAR of southern heterocyclic ring – analogs 1.35-1.59	33
1.3 Synthesis of analogs 1.63-1.96	36
1.4 Synthesis of 3-alkoxy analogs 1.105-1.113 and 4-alkoxy analogs 1.114-1.132	46
1.5 (A) Structure of VU6014098 (1.141) and (B) Synthesis of analogs 1.147-1.172	55
1.6 (A) Structure of VU6015158 (1.173) and (B) Synthesis of carbamate analogs 1.177-1.204	60
1.7 Synthesis of des-carbonyl analogs 1.210-1.230	65
1.8 Synthesis of (A) 1,3,4-oxadiazole analogs 1.250-1.271 and (B) 1,2,4-oxadiazole analogs 1.275-1.288	71

Chapter II

Scheme	Page
2.1 SAR of western heterocyclic ring: synthesis of analogs 2.25-2.50	281
2.2 SAR of piperazine linkers: analogs 2.56-2.82	287
2.3 SAR of alternative alkoxy groups: synthesis of analogs 2.85-2.111	292
2.4 Synthesis of alternative 8-aminoquinoline analogs 2.114-2.124	297
2.5 Synthesis of quinolone analogs 2.130-2.131 and <i>N</i> -methyl quinolones 2.132-2.133	302
2.6 Synthesis of fused imidazo- and triazolo-heterocycles 2.135-2.137	304

Chapter III

Scheme	Page
3.1 Synthetic strategies for accessing both 3- and 2-substituted thiomorpholines.....	357
3.2 Synthetic strategy developed by Bode and coworkers to obtain 3-aryl substituted thiomorpholines.....	358
3.3 Synthetic strategy developed by Stoltz and coworkers to obtain 2,2-disubstituted thiomorpholine-3-ones 3.24	360

3.4	Synthesis of diphenylpyrrolidine organocatalysts 3.31 and 3.32	366
3.5	Synthesis of β -chloro alcohols (<i>R</i>)- 3.41a-h and (<i>S</i>)- 3.42a-h	367
3.6	Synthesis of cyclization precursors: thioesters 3.45a-h and 3.46a-h	368
3.7	Synthesis of chiral C2-substituted thiomorpholines 3.47a-h and 3.48a-h	370
3.8	Synthesis of chiral C2-substituted thiomorpholine 1,1-dioxides 3.49	371

Chapter IV

Scheme	Page	
4.1	Gesson and coworker's synthetic approach to versatile intermediates 4.18 and 4.22	513
4.2	Endgame strategy utilized by Gesson and coworkers to synthesize PF1163B (4.11).....	514
4.3	Synthesis of chiral epoxides 4.29a and 4.29b	519
4.4	Synthesis of chiral tosylates 4.30a and 4.30b	520
4.5	Synthesis of esters 4.39a and 4.39b	523
4.6	Synthesis of natural (-)-Melearoride A 4.8a and unnatural (+)-Melearoride A 4.8b	525

LIST OF ABBREVIATIONS

° C	Degrees Celsius
7-TM	Seven-transmembrane domain
AcOH	Acetic acid
ADMET	Adsorption, distribution, metabolism, excretion, and toxicity
AMPA	α -amino-3-hydroxy-5-methyl-4-isoxazolepropionic acid
B ₂ pin ₂	Bis(pinacolato)diboron
BBB	Blood-brain barrier
BDNF	Brain-derived neurotrophic factor
BH ₃ •SMe ₂	Borane dimethylsulfide complex
BHB	Brain homogenate binding
Bn	Benzyl
Boc	<i>tert</i> -butyloxycarbonyl
B(OMe) ₃	Trimethylborate
Ca ²⁺	Calcium
cAMP	Cyclic adenosine monophosphate
CHO	Chinese hamster ovary
CL _{HEP}	Predicted hepatic clearance
CL _{INT}	Intrinsic clearance
cLogP	Partition coefficient between <i>n</i> -octanol and water
CNS	Central Nervous System
CRD	Cysteine rich domain
CREB1	cAMP responsive element binding protein 1
CTD	C-terminal domain
CuI	Copper (I) iodide
Cu(OTf) ₂	Copper (II) triflate
DALYs	Disability adjusted life years
DAT	Dopamine transporter
DCC	<i>N,N'</i> -dicyclohexylcarbodiimide
DCM	Dichloromethane

DFT	Density functional theory
DIAD	Diisopropyl azodicarboxylate
DIEA	<i>N,N</i> -Diisopropylethylamine
DMF	Dimethylformamide
DMA	Dimethylacetamide
DMAP	4-(Dimethylamino)pyridine
DMF•DMA	Dimethylformamide dimethylacetal
DMPK	Drug metabolism and pharmacokinetics
EC ₅₀	Half maximal effective concentration
ELFN1	Extracellular leucine rich repeat and fibronectin type III domain containing I
ESI	Electrospray ionization
Et ₃ N	Triethylamine
Et ₂ O	Diethyl ether
EtOAc	Ethyl acetate
EtOH	Ethanol
F	Bioavailability
FDA	Food and drug administration
fEPSPs	Field excitatory postsynaptic potential
<i>f_u</i>	Fraction unbound
GABA	γ-aminobutyric acid
GDP	Guanosine diphosphate
GEF	Guanine nucleotide exchange factor
GPCR	G protein-coupled receptor
GTP	Guanosine triphosphate
H ₂	Hydrogen gas
H ₅ IO ₆	Periodic acid
H ₂ NOSO ₃ H	Hydroxylamine- <i>O</i> -sulfonic acid
H ₂ O	Water
HEK	Human embryonic kidney
HEPES	4-(2-hydroxyethyl)-1-piperazineethanesulfonic acid
HFIP	Hexafluoroisopropanol

HMG-CoA	β -hydroxy β -methylglutaryl-CoA
HPLC	High-performance liquid chromatography
HRMS	High-resolution mass spectrometry
HTS	High-throughput screening
IC ₅₀	Half maximal inhibitory concentration
IGF-1	Insulin-like growth factor-1
IP	Intraperitoneal
IP3	Inositol 1,4,5-triphosphate
IV	Intravenous
K ₂ CO ₃	Potassium carbonate
K ₃ PO ₄	Potassium phosphate tribasic
K _p	Brain:plasma partition coefficient
K _{p_{uu}}	Unbound brain:plasma partition coefficient
L-AP4	L-2-amino-4-phosphonobutyric acid
LC/MS	Liquid chromatography / Mass spectrometry
LiAlH ₄	Lithium aluminum hydride
LiBH ₄	Lithium borohydride
LiI	Lithium Iodide
LiOH	Lithium hydroxide
LTP	Long term potentiation
M	Muscarinic receptor
MBD	Methyl-CpG-binding domain
<i>m</i> CPBA	<i>meta</i> -chloroperoxybenzoic acid
Me ₃ P	Trimethylphosphine
MeCN	Acetonitrile
Mecp2	Methyl-CpG-binding protein 2
Mel	Iodomethane
MeOH	Methanol
Mg	Magnesium
MgCl ₂	Magnesium chloride
mGlu	Metabotropic glutamate

MgSO ₄	Magnesium sulfate
MS	Molecular sieves
MsCl	Mesyl chloride
MW	Molecular weight
Na ⁺	Sodium
NaBH ₄	Sodium borohydride
NaH	Sodium hydride
NaHCO ₃	Sodium bicarbonate
NaHMDS	Sodium bis(trimethylsilyl)amide
NAM	Negative allosteric modulator
NaN ₃	Sodium azide
NaOH	Sodium hydroxide
<i>n</i> -BuLi	<i>n</i> -butyl lithium
NCS	<i>N</i> -chlorosuccinimide
NMDA	<i>N</i> -methyl-D-aspartate
NMR	Nuclear magnetic resonance
PAM	Positive allosteric modulator
Pd/C	Palladium on carbon
Pd ₂ (dba) ₃	Tris(dibenzylideneacetone)dipalladium (0)
(Ph ₃ P) ₃ RhCl	Wilkinson's catalyst
PICK1	Protein interacting with C kinase-1
PK	Pharmacokinetic
POCl ₃	Phosphorus (V) oxychloride
PPh ₃	Triphenylphosphine
PSA	Polar Surface Area
PyClU	Chlorodipyrrolidinocarbenium hexafluorophosphate
PyBroP	Bromotripyrrolidinophosphonium hexafluorophosphate
Pyr	Pyridine
RTT	Rett syndrome
SAR	Structure-activity relationship
SC-CA1	Schaffer collateral CA1

SERT	Serotonin transporter
SFC	Supercritical fluid chromatography
SnAP	Stannyl amine protocol
$t_{1/2}$	Half life
T3P	Propylphosphonic anhydride
<i>t</i> -BuLi	<i>tert</i> -butyl lithium
Tf ₂ O	Triflic anhydride
TFA	Trifluoroacetic acid
THF	Tetrahydrofuran
Ti(O <i>i</i> Pr) ₄	Titanium tetraisopropoxide
TLC	Thin-layer chromatography
TMSN ₃	Trimethylsilyl azide
TOF	Time of flight
Tol	Toluene
TRD	Transcription repression domain
TrkB	Tropomyosin receptor kinase B
TsCl	<i>p</i> -toluenesulfonyl chloride
VFD	Venus flytrap domain
V _{ss}	Volume of distribution at steady state
VOID	Vanderbilt University identification number
Zn	Zinc

CHAPTER I

DISCOVERY AND DEVELOPMENT OF NOVEL, SELECTIVE METABOTROPIC GLUTAMATE RECEPTOR 7 NEGATIVE ALLOSTERIC MODULATORS

Background and Introduction

G Protein-Coupled Receptors: Metabotropic Glutamate Receptors

G protein-coupled receptors (GPCRs) encompass a wide variety of extracellular proteins that are responsible for detecting extracellular ligands and activating internal signal transduction pathways, resulting in specific cellular responses.¹⁻³ Activation of GPCRs and the subsequent induction of these cellular responses have been shown to have direct effects on endocrinal signaling pathways, anti-inflammatory/immune responses, physiological homeostasis, human behavior, and the chemical senses of smell and taste.⁴⁻⁸ As of 2016, 826 GPCRs have been identified from the human genome.³ Approximately 30% of the FDA-approved drugs target one of these GPCRs, reinforcing the notion of their attractive therapeutic potential.⁹ Given that GPCRs have the highest level of receptor expression in the central nervous system (CNS) coupled with the prevalence and burden of CNS disorders, recent effort has focused on targeting CNS GPCRs as potential therapeutic targets.¹⁰⁻¹²

Glutamate, the major excitatory and most abundant neurotransmitter in the CNS, is responsible for maintaining various physiological processes including neurotransmission, interneuron signaling, learning, memory, and cognitive function. Therefore, glutamate is regarded as one of the most important neurotransmitters

associated with neurological homeostasis.¹³⁻¹⁴ Regulation of glutamate is of paramount importance for normal physiological function. The glutamatergic hypotheses of neurological disorders postulate that disturbances in glutamatergic neurotransmission are implemented in disorders such as schizophrenia, substance abuse, mood disorders, Alzheimer's disease, and autism-spectrum disorders.¹⁵ This has led to increasing interest in a specific family of GPCRs, the metabotropic glutamate (mGlu) receptor family, as novel therapeutic targets.¹⁶⁻¹⁸

The mGlu receptors are widely distributed within the central nervous system (CNS) and are involved in modulating neuronal excitability and synaptic transmission.¹⁹⁻²⁰ mGlu receptors belong to the Class C family of GPCRs. These receptors possess a large extracellular N-terminal domain that contains the endogenous ligand binding site (Venus flytrap domain), a cysteine-rich domain, a heptahelical transmembrane domain, and an intracellular C-terminal domain responsible for interacting with specific heterotrimeric G proteins consisting of α , β , and γ subunits (**Figure 1.1**).¹⁹ The mGlu

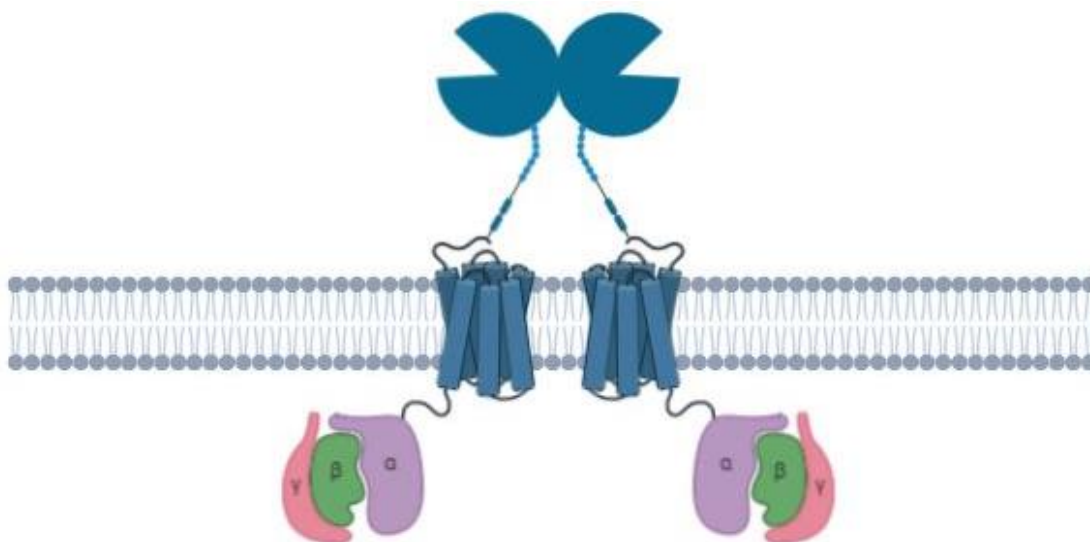


Figure 1.1: Generic representation of mGlu receptor homodimer

receptors exist and function as either constitutive homodimers or heterodimers.²¹⁻²²

The Venus flytrap domain (VFD) is responsible for binding the endogenous ligand glutamate and consists of two lobes.^{21,23-24} The name for this N-terminal domain is derived from the way these two lobes “bite” down onto glutamate after ligand binding. The cysteine rich domain (CRD) consists of nine important cysteine residues. Eight of these cysteine residues are linked together via disulfide bonds.²⁵ Upon binding of glutamate, a new disulfide bond between the ninth cysteine residue of the CRD and a cysteine residue found in one of the lobes of the VFD is formed. The new disulfide bond results in conformational changes within the receptor.²⁶ This conformational change is propagated through the CRD and the heptahelical domain, also referred to as the seven-transmembrane domain (7-TM), to the C-terminal domain of the receptor.¹⁹ As a result, the G protein associated with the C-terminal domain is enabled to act as a guanine nucleotide exchange factor (GEF).²⁷ In the inactive state, the G_{α} subunit of the heterotrimeric G protein is bound to guanosine diphosphate (GDP). Binding of glutamate and the subsequent conformational changes enable GEF activity and result in the exchange of GDP for guanosine triphosphate (GTP).²⁷ The G-protein is now considered to be “activated”, and the G_{α} subunit dissociates from the $G_{\beta\gamma}$ dimeric subunit. Both the liberated G_{α} and $G_{\beta\gamma}$ are capable of activating different second messenger cascades depending on the nature of the parent mGlu receptor/G protein pair.²⁸

The eight mGlu receptors are divided into three groups based upon their sequence homology, pharmacology, and signal-transduction mechanisms. Group I contains mGlu₁ and mGlu₅, Group II contains mGlu₂ and mGlu₃, while Group III contains

mGlu₄, mGlu₆, mGlu₇, and mGlu₈.¹⁹ Group I mGlu receptors are primarily located on postsynaptic terminals and couple to G_{q/11}, which leads to the activation of phospholipase C_β.¹⁹ This results in the hydrolysis of phosphoinositides within the plasma membrane leading to the formation of inositol 1,4,5-triphosphate (IP3) and diacyl glycerol. IP3 results in the activation of calcium channels and increases intracellular [Ca²⁺], while diacyl glycerol participates as a cofactor for the activation of protein kinase C.²⁹⁻³¹ This increase in intracellular [Ca²⁺] can promote neuronal excitability.³² In contrast to Group I mGlu receptors, both Group II and Group III mGlu receptors are primarily located on presynaptic terminals and couple to G_{i/o}.³³ Upon activation of G_{i/o}, the liberated G_α subunit inhibits adenylyl cyclase, causing a reduction of intracellular cyclic adenosine monophosphate (cAMP).³⁴ The G_{βγ} dimer is capable of modulating the activity of ion channels, leading to a decrease in intracellular [Ca²⁺] and an increase in [K⁺].³⁴ This decrease in intracellular [Ca²⁺] can inhibit neurotransmitter release.³⁵

Metabotropic Glutamate Receptor 7 (mGlu₇) and Known Physiological Roles

Considerable effort and progress has been made in assigning potential therapeutic roles for all of the mGlu receptors. While much effort has been devoted to the exploration of the physiological roles and therapeutic potentials of both group I and group II mGlu receptors, much is still unknown regarding the physiology of group III mGlu receptors.³⁶ Of these group III mGlu receptors, perhaps the least is known about mGlu₇. Preliminary genetic knockout experiments have associated mGlu₇ with neuropsychiatric disorders (anxiety, depression, and schizophrenia),

neurodevelopmental disorders (epilepsy, ADHD, and autism), and normal cognitive development (learning and memory).³⁷⁻⁴⁵

mGlu₇ is localized to the active zone of excitatory presynaptic terminals and is primarily located in the neocortex, prefrontal cortex, hippocampus, and amygdala.³⁸ Unlike other Group III mGlu receptors, mGlu₇ has a low affinity for glutamate (500 μM - 1 mM), which led to the hypothesis that mGlu₇ serves as an “emergency brake” for cells to avoid overstimulation and glutamatergic excitotoxicity.⁴⁶⁻⁴⁷ In addition to glutamatergic regulation, mGlu₇ possesses heteroreceptor characteristics, with the ability to also influence GABAergic and monoamine (dopamine, serotonin, and epinephrine) regulation.³⁹

Due to its high level of conservation in mammalian species and hippocampal localization, mGlu₇ has been implicated in important biological processes such as learning and memory; for example, Niswender and coworkers have discovered that activation of mGlu₇ is critical for the induction of long-term potentiation (LTP) at hippocampal Schaffer collateral CA1 (SC-CA1) synapses.⁴⁸ LTP is a persistent strengthening of synapses that occurs after certain types of stimulation parameters.⁴⁹ This persistent activity results in an increase in synaptic inter-transmission between these synapses, forming stronger synaptic connections.⁴⁹ Since memories are believed to be formed via strengthening of synaptic connections, activation of mGlu₇ has been hypothesized to play an important role in memory processes at SC-CA1 synapses.⁵⁰

One potential mechanism for LTP involves NMDA-receptor dependent processes (**Figure 1.2**).⁵¹ In this mechanism, postsynaptic AMPA receptors are activated by the

release of glutamate and result in the influx of Na^+ into the cell. As more glutamate is released via more frequent action potentials, more Na^+ can enter into the cell and results in the removal of the voltage-dependent Mg^{2+} block of NMDA receptors. The influx of Ca^{2+} through these “opened” NMDA receptors results in the expression of more AMPA receptors on the postsynaptic terminal. Due to the presence of these additional AMPA receptors, response to glutamate is increased which strengthens the synaptic connection.⁵¹ In the present case of SC-CA1 synapses, Niswender and coworkers found that activation of mGlu_7 results in the inhibition of GABA release from inhibitory synapses. It is this disinhibition mechanism that enables the induction of LTP at these

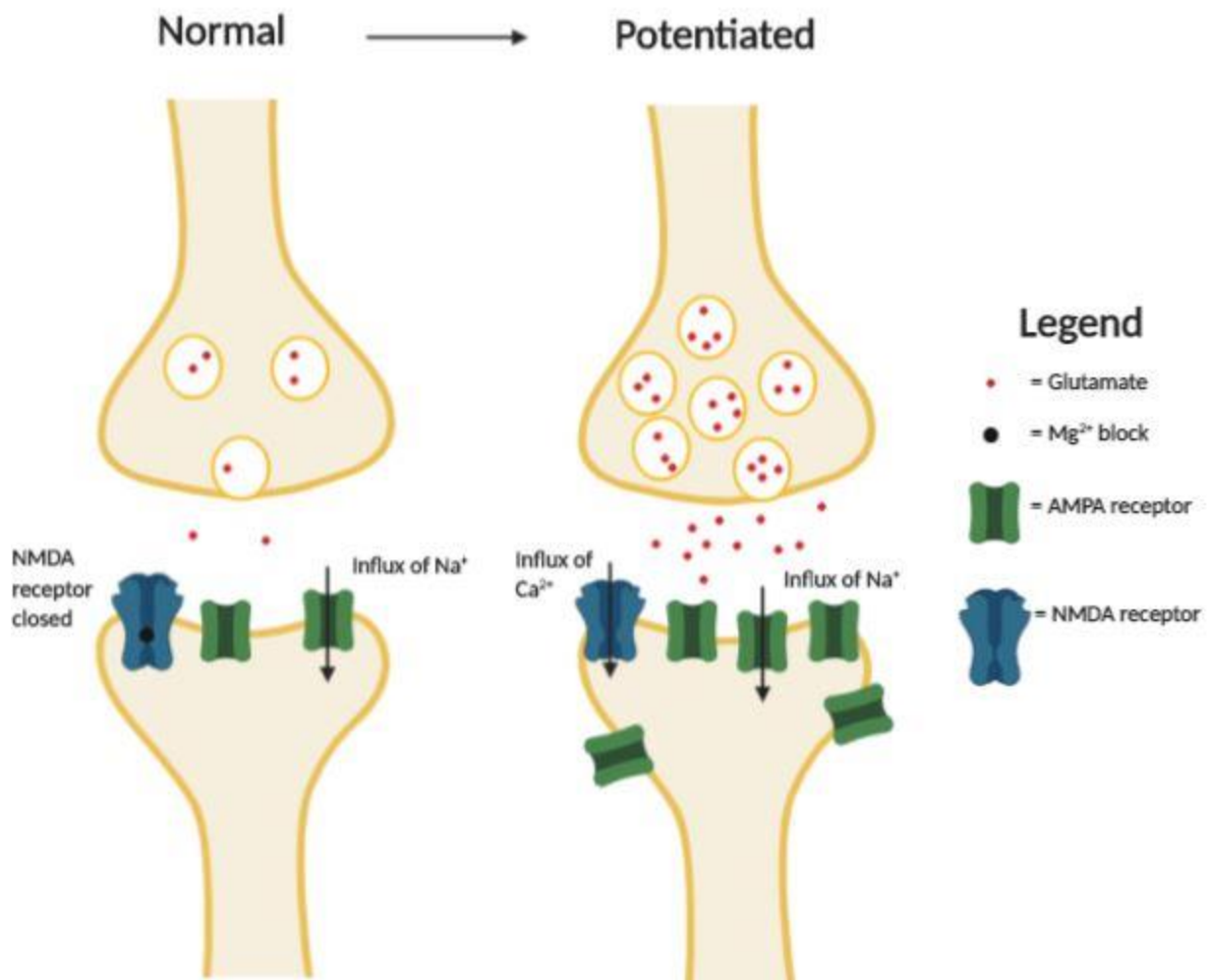


Figure 1.2: NMDA-receptor dependent mechanism of LTP

SC-CA1 synapses.⁴⁸

Orthosteric vs. Allosteric Probe Development Strategies

In order to further probe the physiological relevance of mGlu₇, fully selective *in vivo* tool compounds for mGlu₇ must be developed. Traditional probe development approaches involve targeting the orthosteric site where the endogenous ligand binds. In this case, a small molecule that binds to the orthosteric site and activates the receptor is referred to as an agonist.⁵² On the other hand, a small molecule that competes with the endogenous ligand for binding to the orthosteric site and antagonizes the receptor is referred to as an antagonist.⁵² Both agonists and antagonists can be exemplified in the “light switch” analogy. An agonist can be thought of as turning a light switch “on” (activation of the receptor), while an antagonist can be thought of as turning a light switch “off” (prevention of activation of the receptor). While this orthosteric ligand development method can be useful for certain scenarios, it can complicate matters when the therapeutic window for receptor activation is small and subtype selectivity is crucial.⁵³ For example, xanomeline, a muscarinic acetylcholine receptor 1 and 4 (M₁/M₄)-preferring orthosteric agonist, was developed in hopes of improving cognition in schizophrenia patients.⁵⁴ However, the following side effects were observed in patients (diarrhea, urination, muscle weakness, bronchorrhea, bradycardia, emesis, lacrimation, and salivation) which were indicative of cholinergic toxicity.⁵⁴⁻⁵⁵ This was attributed to overactivation of the muscarinic receptors and off-target activity at M₂ and M₃ receptors.⁵⁴⁻⁵⁵

Traditional orthosteric ligand development strategies cannot be used for developing effective *in vivo* tool compounds for mGlu₇ for additional reasons. Pursuing

orthosteric analogs of the endogenous ligand glutamate would result in the formation of amino acid-like small molecules which would suffer from poor *in vivo* pharmacokinetic (PK) properties. These small, charged molecules would suffer from high hepatic clearance and would not be able to cross the blood brain barrier following traditional administration pathways. To further exacerbate this problem, the orthosteric binding site of all mGlu receptors is highly conserved, which would not enable the required level of subtype selectivity needed for interrogating the physiological importance of a single mGlu receptor.¹⁹

In order to achieve this level of subtype selectivity amongst the mGlu receptors, an allosteric modulation strategy is the preferred method.⁵⁶ As a whole, allosteric modulators bind to a site which is distinct from the orthosteric site (**Figure 1.3**). For mGlu receptors, these allosteric binding sites are usually found within the 7-TM domain.⁵⁷⁻⁵⁹ Binding of an allosteric modulator within the 7-TM domain results in new interactions between the ligand and specific amino acid residues (referred to as the

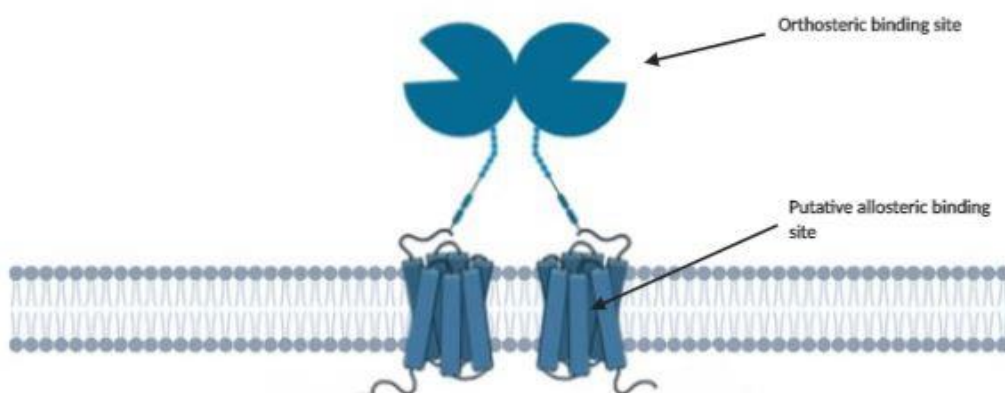


Figure 1.3: Orthosteric and putative allosteric binding sites for mGlu receptors

“trigger switch” and the “transmission switch” domains) which results in conformational changes of the receptor.⁶⁰

Allosteric modulators can be classified as either positive allosteric modulators (PAMs), negative allosteric modulators (NAMs), or neutral allosteric ligands (NALs). Upon binding of an allosteric modulator, the effect that the endogenous ligand has on the native receptor can be either potentiated (PAM) or antagonized (NAM).⁶¹ This is possible because these allosteric modulators can stabilize either active conformations of the receptor that promote orthosteric ligand binding (PAMs) or inactive conformations of the receptor that hinder orthosteric ligand binding (NAMs).⁶¹ This can be described by the mathematical relationship presented in the allosteric ternary complex model shown in **Figure 1.4**.⁶² As a result, PAMs are capable of increasing the potency and/or efficacy of an orthosteric agonist when that orthosteric agonist is present (positive cooperativity), while NAMs reduce the affinity and/or efficacy of an orthosteric agonist when that orthosteric agonist is present (negative cooperativity).⁶³ In the case of a NAL, the allosteric ligand will bind and occupy an allosteric site but will neither potentiate nor

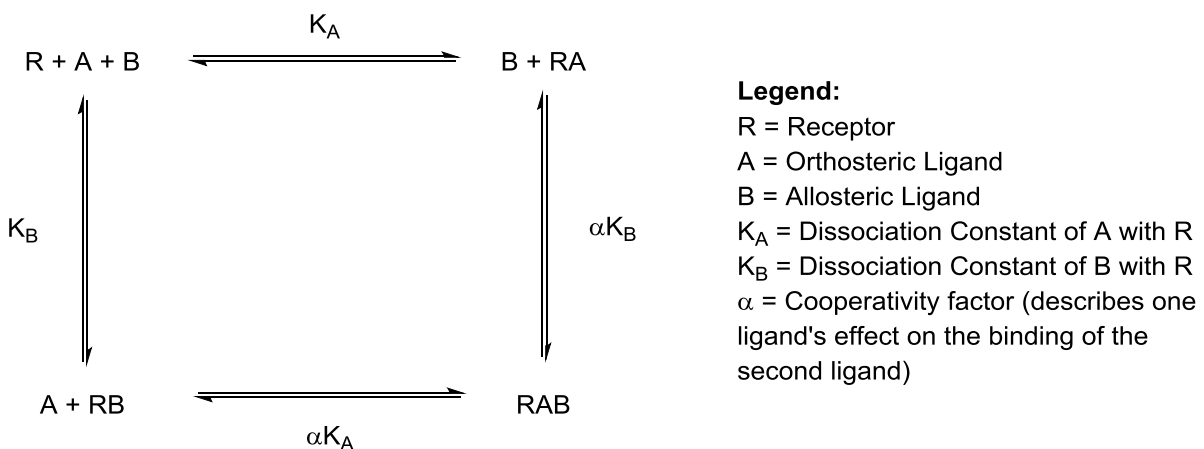


Figure 1.4: Representative allosteric ternary complex model

antagonize the effect that the endogenous ligand has on the native receptor. As opposed to the “light switch” analogy for orthosteric agonists and antagonists, allosteric modulators can be described using the “dimmer switch” analogy. The specific level of activity of a receptor can be modulated to a certain degree in either direction as opposed to defined “on” and “off” states. Therefore, the modulatory capability of allosteric ligands, combined with their potential subtype selectivity, make them the preferred probe development strategy for studying the physiological roles of mGlu₇.

mGlu₇ Tool Compounds: Negative Allosteric Modulators and Allosteric Antagonists

The majority of data associated with mGlu₇ prior to 2005 came from genetic knockout experiments. mGlu₇ knockout mice have been shown to have epileptic, anxiolytic, and antidepressant phenotypes, deficits in learning, amygdala-dependent learning, amygdala-fear extinction response, impaired working memory, and conditioned taste aversion.³⁷⁻⁴⁵ Recently, significant effort has been devoted to the development of selective negative allosteric modulators (NAMs) and allosteric antagonists in order to elucidate and validate the pharmacology of mGlu₇ (**Figure 1.5**). In 2007, isoxazolopyridone **1.1** (MMPIP) was discovered to be a potent mGlu₇ NAM.⁶⁴

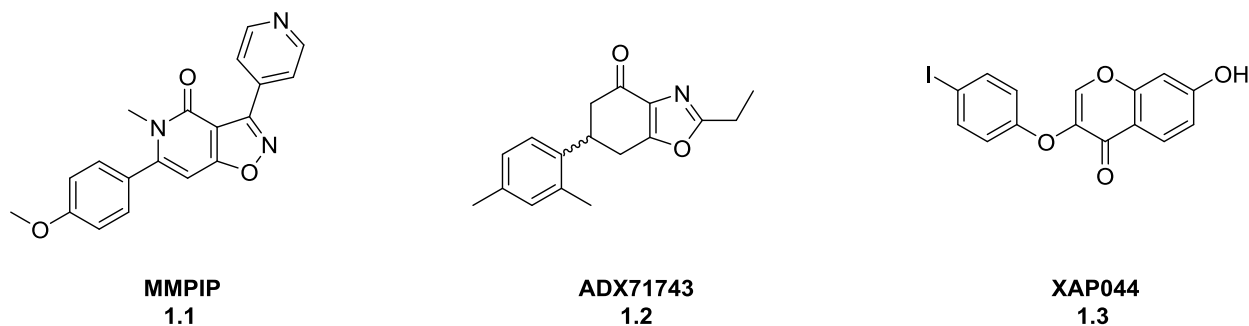


Figure 1.5: Known mGlu₇ NAMs and allosteric antagonists **1.1-1.3**

However, further investigation led to the discovery that **1.1** displays complex pharmacology in different cellular contexts (mGlu₇ IC₅₀ = 70 nM utilizing G_{α15} calcium mobilization assay versus mGlu₇ IC₅₀ = 718 nM utilizing G_{αi/o} thallium flux assay) and does not show *in vitro* efficacy in electrophysiology experiments performed at SC-CA1 synapses.⁶⁴⁻⁶⁶ This complex pharmacology has precluded the further use of MMPIP as a viable mGlu₇ tool compound. In 2013, ADX71743 (**1.2**) was discovered to be a potent mGlu₇ NAM (rat mGlu₇ IC₅₀ = 88 nM and human mGlu₇ IC₅₀ = 63 nM) by Addex Therapeutics.⁶⁷ ADX71743 (**1.2**) was subsequently utilized as an *in vivo* mGlu₇ tool compound. Lütjens and coworkers were able to show that **1.2** displayed an anxiolytic-like profile in mice using both the marble burying assay and the elevated plus maze assay.⁶⁷ However, the low CNS penetrance of **1.2** required Lütjens and coworkers to dose the mice with relatively high dosing paradigms of **1.2** (50-150 mg/kg) via subcutaneous administration.⁶⁷ In addition, **1.2** displayed weak mGlu₂ activity in our cell assays and contains an undesirable ketone moiety.⁶⁸ Most recently, **1.3** (XAP044), an allosteric antagonist, was reported in 2014.⁶⁹ Interestingly, **1.3** was shown to engage a binding pocket localized to the Venus flytrap domain (VFD).⁷⁰ However, **1.3** displayed weak mGlu₇ activity (mGlu₇IC₅₀ = 5.5 μM) in comparison to **1.2**. In addition, the isoflavone scaffold of **1.3** complicates the pharmacological interpretation around this molecule and analogs thereof. This scaffold has the potential to be a pan-assay interference compound (PAIN) via redox activity and should be avoided for optimization efforts.⁷¹ With all of these data, the further development of tool compounds for mGlu₇ devoid of aforementioned pitfalls is necessary to better understand the pharmacological complexities associated with this receptor.

Potential Therapeutic Avenue for *mGlu*₇ NAMs: Anxiety-Related Disorders

According to the World Health Organization (WHO) in 2010, the leading cause of disability-adjusted life-years (DALYs) in the United States was attributed to neuropsychiatric disorders, a broad term encompassing mental, behavioral, and neurological deficits.⁷² Over the past decade, physicians have reported an exponential increase in patients presenting with such disorders or their corresponding symptoms. Therefore, immense effort has been devoted to unveiling the etiology of these diseases to elucidate potential therapeutic avenues. For example, one of the pioneering forms of treatment for broad anxiety disorders and depression is the use of selective serotonin reuptake inhibitors (SSRIs) such as Zoloft (**1.4**), Celexa (**1.5**), Prozac (**1.6**), and Cymbalta (**1.7**) (**Figure 1.6**). This therapy was developed in response to the serotonin hypothesis of depression, which attributed the presentation of anxiety and depression to deficits in brain serotonin levels.⁷³⁻⁷⁵ However, the clinical efficacy of SSRIs is variable, suggesting that the pharmacological mechanisms associated with this particular disease may be more complex than originally hypothesized.^{10,76-77} As such, additional hypotheses involving the major excitatory neurotransmitter, glutamate, the major inhibitory neurotransmitter, γ -aminobutyric acid (GABA), and their association with

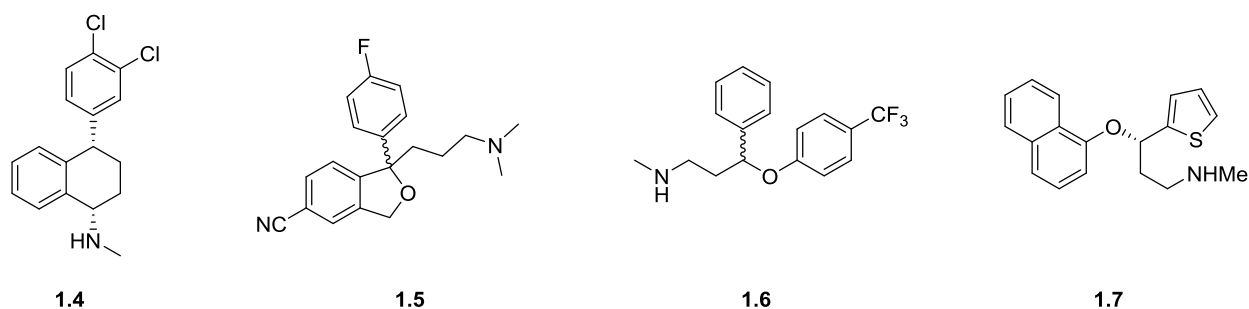


Figure 1.6: Commonly prescribed SSRIs 1.4-1.7

disease-state aberrant neuroplasticity, have been proposed to supplement the serotonin imbalance hypothesis.^{10,76-77} Recent attention has focused on the glutamatergic system, and in particular, metabotropic glutamate (mGlu) receptors, as potential therapeutic targets for the treatment of such neuropsychiatric disorders.¹¹⁻¹²

Given the localization of mGlu₇ in the neocortex, prefrontal cortex, hippocampus, amygdala, and locus coeruleus, and the knowledge that mGlu₇ knockout animals display anxiolytic profiles, it has been hypothesized that selective negative allosteric modulation of mGlu₇ may be effective in eliciting anxiolytic behaviors and may provide an alternative therapeutic strategy for treating anxiety.⁷⁸ However, mGlu₇ knockout mice also display epileptic phenotypes.³⁷ It has been shown that protein-protein interactions between mGlu₇ and PICK1 and mGlu₇ and ELFN1 are important for mGlu₇ cell surface expression and cellular trafficking.⁷⁹⁻⁸³ Disruptions of these protein-protein interactions result in seizure phenotypes in mice.⁷⁹⁻⁸³ At this point, it is not clear whether or not mGlu₇ NAMs would disrupt such protein-protein interactions and warrants further exploration before any therapeutic applications can be rationalized.

Conclusion

After conducting a high-throughput screening (HTS) campaign, we will identify novel mGlu₇ NAM chemotypes that can be optimized through traditional medicinal chemistry approaches en route to a suitable tool compound. Structure-activity relationships (SAR) will be used to guide our chemical approaches, as there is no known crystal structure of the seven transmembrane domain of mGlu₇. Although considerably more challenging, by targeting putative allosteric sites as opposed to the highly conserved orthosteric site, we hope to achieve the necessary subtype selectivity

required for *in vitro* and/or *in vivo* validation and behavioral studies. The following sections of this chapter will summarize our efforts that led to the discovery of both novel *in vitro* and *in vivo* mGlu₇ NAM tool compounds.

Materials and Methods

General Synthetic Methods and Instrumentation

All NMR spectra were recorded on a 400 MHz AMX Bruker NMR spectrometer. ¹H and ¹³C chemical shifts are reported in δ values in ppm downfield with the deuterated solvent as the internal standard. Data are reported as follows: chemical shift, multiplicity (s = singlet, d = doublet, t = triplet, q = quartet, b = broad, m = multiplet), integration, coupling constant (Hz). Low resolution mass spectra were obtained on an Agilent 6120 or 6150 with ESI source. MS parameters were as follows: fragmentor: 70, capillary voltage: 3000 V, nebulizer pressure: 30 psig, drying gas flow: 13 L/min, drying gas temperature: 350 °C. Samples were introduced via an Agilent 1290 UHPLC comprised of a G4220A binary pump, G4226A ALS, G1316C TCC, and G4212A DAD with ULD flow cell. UV absorption was generally observed at 215 nm and 254 nm with a 4 nm bandwidth. Column: Waters Acquity BEH C18, 1.0 x 50 mm, 1.7 μm. Gradient conditions: 5% to 95% CH₃CN in H₂O (0.1% TFA) over 1.4 min, hold at 95% CH₃CN for 0.1 min, 0.5 mL/min, 55 °C. High resolution mass spectra were obtained on an Agilent 6540 UHD Q-TOF with ESI source. MS parameters were as follows: fragmentor: 150, capillary voltage: 3500 V, nebulizer pressure: 60 psig, drying gas flow: 13 L/min, drying gas temperature: 275 °C. Samples were introduced via an Agilent 1200 UHPLC

comprised of a G4220A binary pump, G4226A ALS, G1316C TCC, and G4212A DAD with ULD flow cell. UV absorption was observed at 215 nm and 254 nm with a 4 nm bandwidth. Column: Agilent Zorbax Extend C18, 1.8 μm , 2.1 x 50 mm. Gradient conditions: 5% to 95% CH_3CN in H_2O (0.1% formic acid) over 1 min, hold at 95% CH_3CN for 0.1 min, 0.5 mL/min, 40 $^\circ\text{C}$. For compounds that were purified on a Gilson preparative reversed-phase HPLC, the system comprised of a 333 aqueous pump with solvent-selection valve, 334 organic pump, GX-271 or GX-281 liquid handler, two column switching valves, and a 155 UV detector. UV wavelength for fraction collection was user-defined, with absorbance at 254 nm always monitored. Method 1: Phenomenex Axia-packed Luna C18, 30 x 50 mm, 5 μm column. Mobile phase: CH_3CN in H_2O (0.1% TFA). Gradient conditions: 0.75 min equilibration, followed by user defined gradient (starting organic percentage, ending organic percentage, duration), hold at 95% CH_3CN in H_2O (0.1% TFA) for 1 min, 50 mL/min, 23 $^\circ\text{C}$. Method 2: Phenomenex Axia-packed Gemini C18, 50 x 250 mm, 10 μm column. Mobile phase: CH_3CN in H_2O (0.1% TFA). Gradient conditions: 7 min equilibration, followed by user defined gradient (starting organic percentage, ending organic percentage, duration), hold at 95% CH_3CN in H_2O (0.1% TFA) for 7 min, 120 mL/min, 23 $^\circ\text{C}$. All reagents were purchased from Aldrich Chemical Co. and were used without purification. All final compounds were >98% pure by LCMS (254 nm, 214 nM and ELSD). Following these purification protocols, final compounds were transferred to a barcode vial and diluted to a concentration of 10 μM using molecular biology grade dimethylsulfoxide (DMSO). These compounds were registered into Dotmatics and assigned a VU identification number before being tested in the primary screening assay.

Primary Screening (Calcium Mobilization) Assay

Human mGlu₄/G_{q15}/CHO cells (30,000 cells/20 µL/well), rat mGlu₇/G_{a15}/HEK cells (15,000 cells/20 µL/well), and rat mGlu₈/G_{a15}/HEK cells (15,000 cells/20 µL/well) were plated in black-walled, clear-bottomed, TC treated, 384 well plates (Greiner Bio-One, Monroe, NC) in DMEM containing 10% dialyzed FBS, 20 mM HEPES, 100 units/mL penicillin/streptomycin, and 1 mM sodium pyruvate (Plating Medium). The cells were grown overnight at 37 °C in the presence of 5% CO₂. The next day, the medium was removed and replaced with 20 µL of 1 µM Fluo-4, AM (Life Technologies, Thermo Fisher Scientific, Grand Island, NY) prepared as a 2.3 mM stock in DMSO and mixed in a 1:1 ratio with 10% (w/v) pluronic acid F-127 and diluted in Assay Buffer (Hank's balanced salt solution, 20 mM HEPES and 2.5 mM Probenecid (Sigma-Aldrich, St. Louis, MO)) for 45 minutes at 37 °C. Dye was removed and replaced with 20 µL of Assay Buffer. For concentration-response curve experiments, compounds were serially diluted 1:3 into 10 point concentration response curves in DMSO, transferred to daughter plates using an Echo acoustic plate reformatter (Labcyte, Sunnyvale, CA) Echo, and diluted in Assay Buffer to a 2X final concentration. Calcium flux was measured using the Functional Drug Screening System 6000 or 7000 (FDSS6000/7000, Hamamatsu, Japan). After establishment of a fluorescence baseline for 4 seconds (4 images at 1 Hz; excitation, 470 ± 20 nm; emission, 540 ± 30 nm), 20 µL of test compounds were added to the cells, and the response was measured. 142 seconds later, 10 µL (5X) of an EC₂₀ concentration of glutamate was added to the cells, and the response of the cells was measured; after an additional 120 seconds, 12 µL (5X) of an EC₈₀ concentration of agonist was added and readings taken for an additional 40 seconds. Calcium fluorescence was recorded as fold over basal fluorescence and raw

data were normalized to the maximal response to glutamate. Potency (EC₅₀) and maximum response (% Glu or L-AP4 Max) for compounds were determined using a four parameter logistical equation in GraphPad Prism (La Jolla, CA) or Dotmatics (XX.XX) software. For efficacy and selectivity experiments, a constant amount of compound was applied prior to the addition of a full glutamate concentration-response curve and the shift of the EC₅₀ of the curves was calculated as “fold shift”. mGlu receptor selectivity profiling, and GIRK assay were performed as previously reported^{84-85, 45}.

In Vitro DMPK Methods: Intrinsic Clearance in Murine and Rat Liver Microsomes

Murine or rat liver microsomes (0.5 mg/mL) and 1 μM test compound were incubated in 100 mM potassium phosphate pH 7.4 buffer with 3 mM MgCl₂ at 37 °C with constant shaking. After a 5 min preincubation, the reaction was initiated by addition of NADPH (1 mM). At selected time intervals (0, 3, 7, 15, 25, and 45 min), 50 μL aliquots were taken and subsequently placed into a 96-well plate containing 150 μL of cold acetonitrile with internal standard (50 ng/mL carbamazepine). Plates were then centrifuged at 3000 rcf (4 °C) for 10 min, and the supernatant was transferred to a separate 96-well plate and diluted 1:1 with water for LC/MS/MS analysis. The *in vitro* half-life (T_{1/2}, min, Eq. 1), intrinsic clearance (CL_{INT}, mL/min/kg, Eq. 2) and subsequent predicted hepatic clearance (CL_{HEP}, mL/min/kg, Eq. 3) were determined employing the following equations:

$$(1) \quad T_{1/2} = \frac{\text{Ln}(2)}{k}$$

where k represents the slope from linear regression analysis of the natural log percent remaining of test compound as a function of incubation time

$$(2) \quad CL_{int} = \frac{0.693}{in\ vitro T_{1/2}} \times \frac{mL\ incubation}{mg\ microsomes} \times \frac{45\ mg\ microsomes}{gram\ liver} \times \frac{45^a\ gram\ liver}{kg\ body\ wt}$$

^a scale-up factor that is species specific

$$(3) \quad CL_{hep} = \frac{Q_h \cdot CL_{int}}{Q_h + CL_{int}}$$

where Q_h (hepatic blood flow) is species specific.

Mouse and Rat Plasma Protein Binding

The protein binding of each compound was determined in rat or mouse plasma via equilibrium dialysis employing HTDialysis Teflon dialysis chamber and cellulose membranes (MWCO 12-14 K) (HTDialysis LLC, Gales Ferry, CT). Plasma was added to the 96-well plate containing test compound and mixed thoroughly for a final concentration of 5 μ M. Subsequently, 150 μ L of the plasma-compound mixture was transferred to the dialysis chamber, with an accompanying 150 μ L of phosphate buffer (25 mM, pH 7.4) on the other side of the membrane. The device plate was sealed and incubated for 4 hours at 37 °C with shaking. At completion, aliquots from each chamber were diluted 1:1 with either plasma (for the buffer sample) or buffer (for the plasma sample) and transferred to a new 96-well plate, at which time ice-cold acetonitrile containing internal standard (50 ng/mL carbamazepine) (2 volumes) was added to extract the matrices. The plate was centrifuged (3000 rcf, 10 min) and supernatants transferred and diluted 1:1 (supernatant: water) into a new 96 well plate, which was then sealed in preparation for LC/MS/MS analysis. Each compound was assayed in triplicate within the same 96-well plate. Fraction unbound was determined using the following equation:

$$F_u = \frac{Conc_{buffer}}{Conc_{plasma}}$$

Mouse and Rat Brain Homogenate Binding

The brain homogenate binding of each compound was determined in brain homogenate via equilibrium dialysis employing HTDialysis Teflon dialysis chamber and cellulose membranes (MWCO 12-14 K) (HTDialysis LLC, Gales Ferry, CT). Brain tissue homogenate was prepared by diluting one volume whole mouse or rat brain tissue with one to three volumes (species specific) of phosphate buffer (25 mM, pH 7.4). The mixture was then subjected to mechanical homogenization employing a Mini-Beadbeater™ and 1.0 mm Zirconia/Silica Beads (BioSpec Products). Brain homogenate spiked with test compound and mixed thoroughly for a final concentration of 5 µM. Subsequently, 150 µL of the brain homogenate-compound mixture was transferred to the dialysis chamber with an accompanying 150 µL of phosphate buffer (25 mM, pH 7.4) on the other side of the membrane. The block was sealed and incubated for 6 hours at 37 °C with shaking. At completion, aliquots from each side of the chamber were diluted 1:1 with either brain homogenate (to the buffer side) or buffer (to the brain homogenate side) in a new 96 well plate, at which time ice-cold acetonitrile containing internal standard (50 ng/mL carbamazepine) was added to extract the matrices. The plate was centrifuged (3000 rcf, 10 min) and supernatants transferred and diluted 1:1 (supernatant: water) into a new 96 well plate, which was then sealed in preparation for LC/MS/MS analysis. Each compound was assayed in triplicate within the same 96-well plate. Fraction unbound was determined using the following equation:

$$F_{u,tissue} = \frac{1/D_f}{(1/F_{u,hom} - 1) + 1/D_f}$$

Where $F_{u,hom}$ represent the measured fraction unbound in the diluted homogenate and D_f represents dilution factor.

Metabolite Identification in Rat Hepatic S9

Compound 11a was incubated with rat hepatic S9 fractions (5 mg/mL) +/- NADPH and +/- UDPGA and PAPs. Substrates (5 or 20 μ M) were incubated at 37 °C in borosilicate glass test tubes under ambient oxygenation for 60 minutes in a potassium phosphate-buffered reaction (100 mM, pH 7.4) containing hepatic S9 from rat and $MgCl_2$ (3 mM). The total incubation volume was 0.5 mL. Reactions were initiated by the addition of substrate, terminated with the addition of 2 volumes of ice-cold acetonitrile, and subsequently centrifuged at 4000 rcf for 10 min. The resulting supernatants were dried under a stream of nitrogen and reconstituted in initial mobile phase in preparation for LC/MS analysis.

LC/MS/MS Analysis of Samples from In Vitro Assays

Samples were analyzed via electrospray ionization (ESI) on an AB Sciex API-4000 (Foster City, CA) triple-quadrupole instrument that was coupled with Shimadzu LC-10AD pumps (Columbia, MD) and a Leap Technologies CTC PAL auto-sampler (Carrboro, NC). Analytes were separated by gradient elution using a Fortis C18 3.0 x 50 mm, 3 μ m column (Fortis Technologies Ltd, Cheshire, UK) thermostated at 40 °C. HPLC mobile phase A was 0.1% formic acid in water (pH unadjusted), mobile phase B was 0.1% formic acid in acetonitrile (pH unadjusted). The gradient started at 10% B after a 0.2 min hold and was linearly increased to 90% B over 1.2 min; held at 90% B for

0.1 min and returned to 10% B in 0.1 min followed by a re-equilibration (0.9 min). The total run time was 2.5 min and the HPLC flow rate was 0.5 mL/min. The source temperature was set at 500 °C and mass spectral analyses were performed using multiple reaction monitoring (MRM), with transitions specific for each compound utilizing a Turbo-Ionspray® source in positive ionization mode (5.0 kV spray voltage).

In Vivo PK Methods

All rodent PK experiments were conducted in accordance with the National Institute of Health regulations of animal care covered in Principles of Laboratory Animal Care (National Institutes of Health publication 85-23, revised 1985) and were approved by the Institutional Animal Care and Use Committee.

Time Course PK and Single Time Point Tissue Distribution Studies

IV cassette PK experiments in rats were carried out according to methods described previously.⁸⁶ Briefly, a cassette of compounds (n = 4–5/cassette) were formulated from 10 mM solutions of compounds in DMSO. In order to reduce the absolute volume of DMSO that was administered, the compounds were combined and diluted with ethanol and PEG 400 to achieve a final concentration of 0.4–0.5 mg/mL for each compound (2 mg/mL total) administered in each cassette. The final dosing solutions consisted of approximately 10% ethanol, 40% PEG400, and 50% DMSO (v/v). For time course PK studies, each cassette dose was administered IV via the jugular vein to two dual-cannulated (carotid artery and jugular vein) adult male Sprague–Dawley rats, each weighing between 250 and 350 g (Harlan, Indianapolis, IN) for a final dose of 0.2–0.25 mg/kg per compound. Whole blood collections via the carotid artery were performed at 0.033, 0.117, 0.25, 0.5, 1, 2, 4, 7, and 24 hours post dose and

plasma samples prepared for bioanalysis. For single time point tissue distribution studies, compounds were formulated as described above (in cassette format) and dosed to male Sprague-Dawley rats for a final dose of 0.2-0.25 mg/kg per compound. Brain dissection and blood collections via the carotid artery were performed 0.25 hr post dose. The brain samples were rinsed in PBS, snap frozen and stored at -80 °C. Prior to LC/MS/MS analysis, brain samples were thawed to room temperature and subjected to mechanical homogenation employing a Mini-Beadbeater™ and 1.0 mm Zirconia/Silica Beads (BioSpec Products).

Mouse Tissue Distribution Studies

Tissue distribution studies with compound-in mice were performed by formulating the compound in 20% BCD and dosing via intraperitoneal injection to 20 week old male C57/Bl6 mice (3-4 per time point). At 0.5 hours post dose, animals were euthanized and decapitated, blood was collected via cardiac puncture and the brains were removed, thoroughly washed in cold phosphate-buffered saline, and immediately frozen on dry ice.

Plasma and Brain Sample Preparation

Plasma was separated by centrifugation (4000 rcf, 4 °C) and stored at -80 °C until analysis. On the day of analysis, frozen whole brains were weighed and diluted with 1:3 (w/w) parts of 70:30 isopropanol:water. The mixture was then subjected to mechanical homogenation employing a Mini-Beadbeater™ and 1.0 mm Zirconia/Silica Beads (BioSpec Products) followed by centrifugation. The sample extraction of plasma (20 µL) or brain homogenate (20 µL) was performed by a method based on protein precipitation using three volumes of ice-cold acetonitrile containing an internal standard

(50 ng/mL carbamazepine). The samples were centrifuged (3000 rcf, 5 min) and supernatants transferred and diluted 1:1 (supernatant: water) into a new 96-well plate, which was then sealed in preparation for LC/MS/MS analysis.

LC/MS/MS Bioanalysis of Samples from In Vivo Assays

In vivo samples were analyzed via electrospray ionization (ESI) on an AB Sciex API-4000 (Foster City, CA) triple-quadrupole instrument that was coupled with Shimadzu LC-10AD pumps (Columbia, MD) and a Leap Technologies CTC PAL auto-sampler (Carrboro, NC). Analytes were separated by gradient elution using a Fortis C18 3.0 x 50 mm, 3 μ m column (Fortis Technologies Ltd, Cheshire, UK) thermostated at 40 °C. HPLC mobile phase A was 0.1% formic acid in water (pH unadjusted), mobile phase B was 0.1% formic acid in acetonitrile (pH unadjusted). The source temperature was set at 500 °C and mass spectral analyses were performed using multiple reaction monitoring (MRM), with transitions specific for each compound utilizing a Turbospray® source in positive ionization mode (5.0 kV spray voltage). The calibration curves were constructed, and linear response was obtained by spiking known amounts of test compound in blank brain homogenate or plasma. All data were analyzed using AB Sciex Analyst software v1.5.1. The final PK parameters were calculated by noncompartmental analysis using Phoenix (version 6.2) (Pharsight Inc., Mountain View, CA).

Extracellular Field Potential Recordings

The 6-week-old male C57BL/6J mice (The Jackson Laboratory) were anesthetized with isoflurane, and the brains were removed and submerged in ice-cold cutting solution containing the following (in mM): 230 sucrose, 2.5 KCl, 8 MgSO₄, 0.5

CaCl₂, 1.25 NaH₂PO₄, 10 D-glucose, 26 NaHCO₃. Coronal slices containing the hippocampus were cut at 400 μm using a Compressstome (Precisionary Instruments). Slices were transferred to a holding chamber containing NMDG-HEPES recovery solution (in mM) as follows: 93 NMDG, 2.5 KCl, 1.2 NaH₂PO₄, 30 NaHCO₃, 20 HEPES, 25 D-glucose, 5 sodium ascorbate, 2 thiourea, 3 sodium pyruvate, 10 MgSO₄, 0.5 CaCl₂, pH 7.3, 305 mOsm, for 15 min at 32 °C. Slices were then transferred to a room temperature holding chamber for at least 1 h containing aCSF (in mM) as follows: 126 NaCl, 1.25 NaH₂PO₄, 2.5 KCl, 10 D-glucose, 26 NaHCO₃, 2 CaCl₂, 1 MgSO₄, supplemented with 600 μM sodium ascorbate for slice viability. All buffers were continuously bubbled with 95% O₂/5% CO₂. Subsequently, slices were transferred to a 30 °C submersion recording chamber where they were perfused with a CSF at a rate of 2 mL/min. Borosilicate glass electrodes were pulled using a Flaming/Brown micropipette puller (Sutter Instruments) and had a resistance of 3–5 MΩ when filled with aCSF. Paired-pulse field EPSPs (fEPSPs) were recorded by from the stratum radiatum of CA1 and evoked by electrical stimulation (200 ms duration, every 20 s) delivered through a concentric bipolar stimulating electrode placed near the CA3-CA1 border. Input– output curves were generated for each slice, and the stimulation intensity was adjusted to 50% of the maximum response. VU6010608 was prepared in DMSO vehicle (0.05%). After a 10 min baseline recording, 10 μM VU6010608 was bath-applied for 10 min followed by 2 trains of high-frequency stimulation (HFS, 2 trains of 100 Hz, 20 sec inter-stimulus interval). All slopes calculated were normalized to the average slope calculated during the predrug period (percentage of baseline).

Eurofins Lead Profiling Data

A radioligand binding panel of 68 targets (GPCRs, ion channels, transporters, and nuclear hormones) with data reported as % inhibition of radioligand binding at a 10 μ M concentration of VU6010608 and VU6012962 from two independent determinations.

Behavioral Pharmacology: Animals

All studies were carried out in accordance with the National Institute of Health Guide for the Care and Use of Laboratory Animals and approved by the Vanderbilt University Institutional Animal Care and Use Committee. Separate cohorts of C57Bl/6J male mice (8 weeks old) were used for behavioral testing. All mice were grouped housed on a 12:12 light–dark cycle with lights on at 0600. All experiments were conducted during the light phase. Food and water were available ad libitum.

Behavioral Pharmacology: Elevated Zero Maze (EZM)

Mice received i.p. injections of either vehicle (10% Tween 80) or various doses of VU6012962 (VU'962; 1-10 mg/kg) 60 minutes prior to testing. To start the EZM test, mice were lowered by their tail and placed at a randomly chosen boundary between an open and a closed zone, facing the inside of the closed zone on the elevated circular platform (40 cm off the ground, 50 cm in diameter). Activity of the mouse was monitored for five minutes via an overheard camera connected to a computer in a separate room using video acquisition and ANY-maze analysis software (Stoelting, Wood Dale, IL, USA). Data analyzed included the time spent in the open versus closed arm, the total distance traveled in the maze, and the number of arm entries. Time spent in the open versus closed arm is shown as percentage of time in open to total time. Two mice were excluded from analysis due to sedative-like effects observed at the highest dose.

Behavioral Pharmacology: Light-Dark Box

Sixty minutes prior to behavioral testing, mice received one of the following treatment conditions: vehicle (10% Tween 80; i.p.), 15 mg/kg fluoxetine (FLX; i.p.) or 3 mg/kg VU6012962 (VU'962; i.p.). Mice were individually placed into sound-attenuating chambers (27.9 × 27.9 cm; MED-OFA-510; MED Associates, St. Albans, VT, USA) containing dark box inserts that split the chamber into light (~25 lux) and dark (<5 lux) halves (Med Associates ENV-511). Beam breaks from 16 infrared beams were recorded by Activity Monitor v5.10 (MED Associates) to monitor position and behavior during a 10-min testing period. Data analyzed only included the first five minutes of the session and included total distance traveled and time spent in light to total time. Data are presented as Mean ± S.E.M and is shown as a ratio of time in light to total time

Behavioral Pharmacology: Marble Burying Assay

Mice were pretreated with either vehicle (10% Tween 80; i.p.), 15 mg/kg fluoxetine (FLX; i.p.) or 3 mg/kg VU6012962 (VU'962; i.p.). Forty-five minutes after injection, mice habituated for 15 minutes to 2.5 cm Diamond Soft Bedding (Harlan Teklad, Madison, WI, USA). Mice were then placed back in Plexiglass cages in which 15 blue marbles (14 mm diameter) were distributed in a 3 x 5 layout with 1.5 cm between each marble on top of the Diamond Soft Bedding. The amount of marbles buried was quantified following a 30 minute interval. The mice were then removed from the cages and the number of buried marbles was counted by two blinded experimenters using a criterion of greater than 2/3rd covered by bedding. Data are presented as Mean ± S.E.M. Three mice were excluded from analysis for being outliers as assessed by the Grubb's Outlier Test.

Behavioral Pharmacology: Data Analysis

Behavioral data were analyzed by a one-way analysis of variance (ANOVA) followed by post hoc Dunnett's multiple comparison test unless otherwise specified. All statistical analyses were conducted with Prism GraphPad 6 (San Diego, CA, USA). Data sets in Prism were run through the Grubb's test. Results are shown as Mean \pm S.E.M. Statistical significance was set at $P < 0.05$.

Discovery and Development of Novel, Selective Metabotropic Glutamate Receptor 7 Negative Allosteric Modulators

High-Throughput Screening Campaign: Identification of VU6009748

In order to explore novel chemotypes, a high-throughput screening (HTS) campaign was initiated on a 63,000-membered library to identify novel mGlu₇ NAM scaffolds.^{68,84} A calcium mobilization assay was used to determine the *in vitro* potency and efficacy of compounds tested for mGlu₇ activity. One of the HTS hits, VU6009748 (**1.8**) (Figure 1.7), was of particular interest. Although **1.8** was a weak mGlu₇ NAM

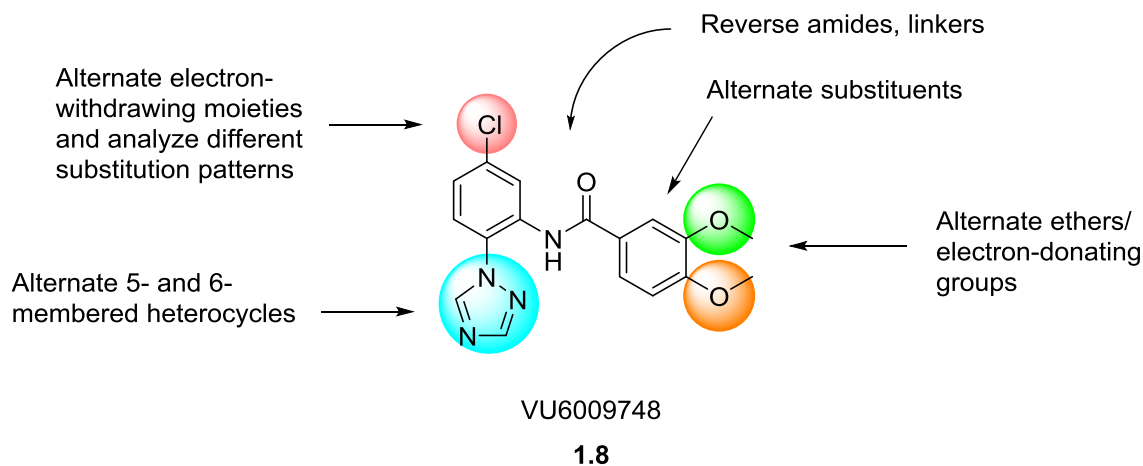


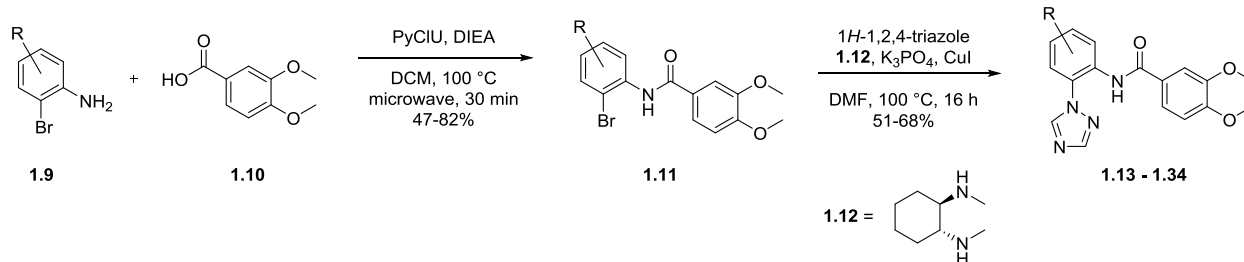
Figure 1.7: Structure of HTS hit VU6009748 (**1.8**) and our proposed SAR strategy

(mGlu₇ IC₅₀ = 5.8 μM, 19% L-AP₄_{min}), it provided us with a novel *N*-(2-(1*H*-1,2,4-triazol-1-yl)phenyl)benzamide chemotype. **Figure 1.7** also depicts the initial strategy taken for lead optimization and exploration into the structure-activity relationship (SAR) for analogs in this series.⁶⁸

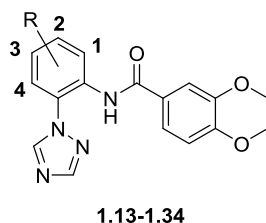
Initial SAR of Western Aromatic Ring: Analogs 1.13-1.34

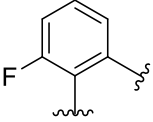
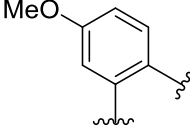
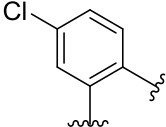
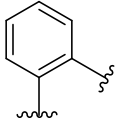
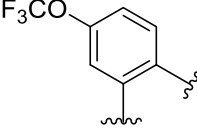
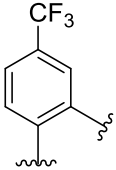
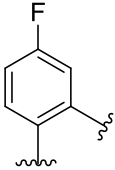
To begin our SAR campaign, we elected to first focus on the western aromatic ring of **1.8**. Specifically, we wanted to examine additional analogs containing different electron-withdrawing and electron-donating groups with different aromatic substitution patterns. The synthesis of analogs of this nature was facile (2 steps), allowing for the rapid generation of analogs (**Scheme 1.1**). Commercially available anilines **1.9** were reacted with 3,4-dimethoxybenzoic acid **1.10** under microwave-assisted PyCIU-mediated amide coupling conditions to form amides **1.11**. Modified Ullmann coupling conditions using diamine ligand **1.12** were then utilized to access analogs **1.13-1.34**.⁸⁷

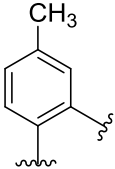
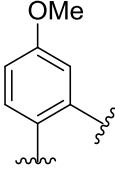
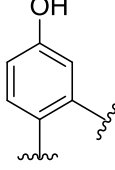
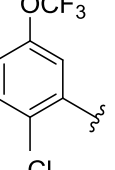
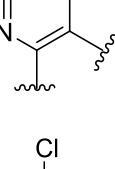
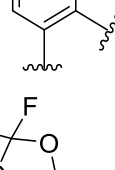
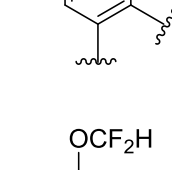
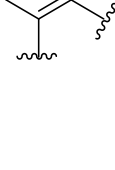
SAR data is shown below in **Table 1.1**.

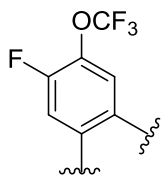


Scheme 1.1: SAR of western aromatic ring - synthesis of analogs **1.13-1.34**



Ar =	Compound Number	VOID	mGlu ₇ IC ₅₀ (μM)	mGlu ₇ % L-AP4 _{min}
	1.13	VU6010276	Inactive	N/A
	1.14	VU6010277	Inactive	N/A
	1.15	VU6010278	> 10	51%
	1.16	VU6010279	Inactive	N/A
	1.17	VU6010280	> 10	51%
	1.18	VU6010603	> 10	38%
	1.19	VU6010606	> 10	63%

	1.20	VU6010607	> 10	49%
	1.21	VU6012570	Inactive	N/A
	1.22	VU6014051	Inactive	N/A
	1.23	VU6010608	0.759	15%
	1.24	VU6012960	Inactive	N/A
	1.25	VU6012699	Inactive	N/A
	1.26	VU6012568	> 10	55%
	1.27	VU6012961	> 10	48%

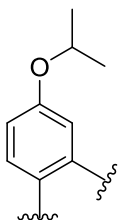


1.28

VU6013213

2.4

38%

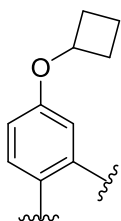


1.29

VU6014054

5.67

18%

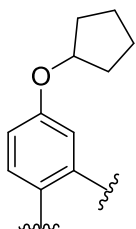


1.30

VU6014096

2.47

41%

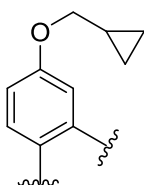


1.31

VU6014097

1.51

32%

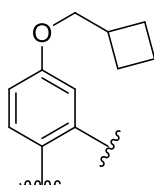


1.32

VU6014317

5.78

19%

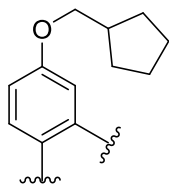


1.33

VU6014318

9.8

12%



1.34

VU6014319

1.17

11%

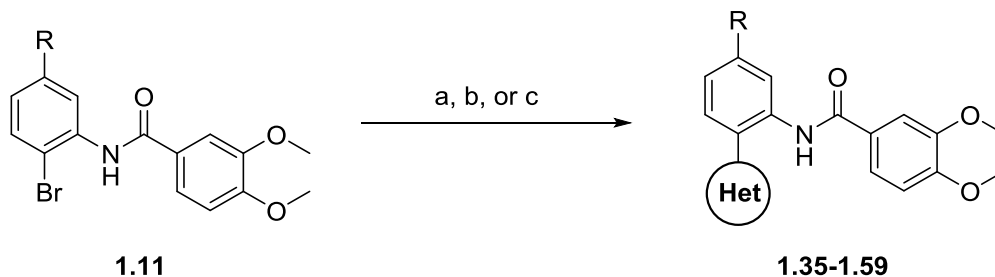
Table 1.1: SAR around the western aromatic ring – analogs **1.13-1.34**

As can be seen in **Table 1.1**, the vast majority of analogs synthesized (**1.13-1.22**) were either inactive at the mGlu₇ receptor or had potency values (IC₅₀) greater than 10 μM. Incorporation of azaheterocycles (**1.24-1.25**) was also not tolerated. However, it was found that the incorporation of a trifluoromethoxy group at the 2-position (numbering scheme established in **Table 1.1**) (**1.23**) resulted in the most potent mGlu₇ NAM thus far with an mGlu₇ IC₅₀ = 759 nM and 15% L-AP₄_{min}. Cyclization onto the western aromatic ring as the geminal difluoro-acetal **1.26** resulted in considerable loss in potency. Swapping the trifluoromethoxy group for the isosteric difluoromethoxy group (analog **1.27**) also resulted in loss of potency. Surprisingly, even the incorporation of a fluorine atom at the 3-position (analog **1.28**) resulted in a ~3-fold loss in potency (mGlu₇ IC₅₀ = 2.4 μM and 38% L-AP₄_{min}). Both sterically-hindered and cyclic alkyl groups have also been reported in the literature to serve as suitable bioisosteres for trifluoromethoxy groups.⁸⁸ However, none of these analogs (**1.29-1.34**) showed improved potency over **1.23**.

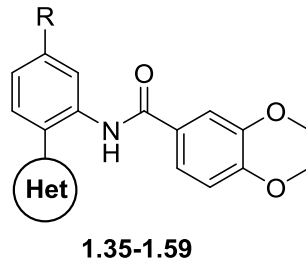
SAR of the Southern Heterocyclic Ring: Analogs 1.35-1.59

Next, we wanted to examine the effects that different 5- and 6-membered heterocycles would have on the activity of our analogs. The synthesis of analogs of this nature is shown in **Scheme 1.2**. Amides **1.11** proved to be competent coupling partners

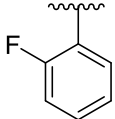
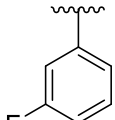
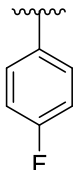
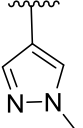
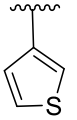
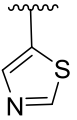
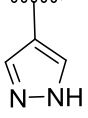
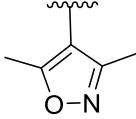
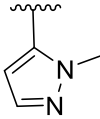
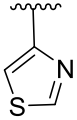
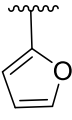
in modified Ullmann reactions (to install *N*-linked heterocycles) and Suzuki or Stille reactions (to install *C*-linked heterocycles) en route to analogs **1.35-1.59** (Table 1.2).



Scheme 1.2: SAR of southern heterocyclic ring – analogs **1.35-1.59**. Reagents and conditions: a) azaheterocycle, K_3PO_4 , CuI, DMF, 100 °C, 16 h, 51-68%; b) aryl- or heteroaryl-boronic acid, Cs_2CO_3 , Pd(dppf)Cl₂, 1,4-dioxane:H₂O (4:1), 100 °C, 16 h, 63-87%; c) heteroaryl-stannane reagent, Pd(PPh₃)₄, 1,4-dioxane, 100 °C, 16 h, 47-56%.



R =	Het	Compound Number	VOID	mGlu ₇ IC ₅₀ (μM)	mGlu ₇ % L-AP ₄ _{min}
Cl		1.35	VU6010269	> 10	55%
Cl		1.36	VU6010270	Inactive	N/A
Cl		1.37	VU6010271	> 10	48%
Cl		1.38	VU6010272	Inactive	N/A
Cl		1.39	VU6010273	Inactive	N/A

Cl		1.40	VU6010403	Inactive	N/A
Cl		1.41	VU6010404	Inactive	N/A
Cl		1.42	VU6010405	Inactive	N/A
OCF ₃		1.43	VU6011333	Inactive	N/A
OCF ₃		1.44	VU6011334	Inactive	N/A
OCF ₃		1.45	VU6011335	Inactive	N/A
OCF ₃		1.46	VU6011462	Inactive	N/A
OCF ₃		1.47	VU6011464	Inactive	N/A
OCF ₃		1.48	VU6011465	Inactive	N/A
OCF ₃		1.49	VU6011467	Inactive	N/A
OCF ₃		1.50	VU6014007	Inactive	N/A

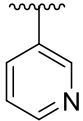
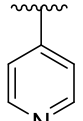
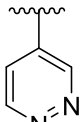
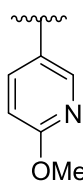
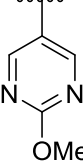
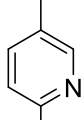
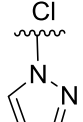
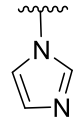
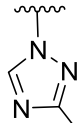
OCF ₃		1.51	VU6011457	Inactive	N/A
OCF ₃		1.52	VU6011458	Inactive	N/A
OCF ₃		1.53	VU6011342	Inactive	N/A
OCF ₃		1.54	VU6011345	Inactive	N/A
OCF ₃		1.55	VU6011459	Inactive	N/A
OCF ₃		1.56	VU6011461	Inactive	N/A
OCF ₃		1.57	VU6013214	Inactive	N/A
OCF ₃		1.58	VU6013339	Inactive	N/A
OCF ₃		1.59	VU6013906	Inactive	N/A

Table 1.2: SAR of the southern heterocyclic ring – analogs **1.35-1.59**

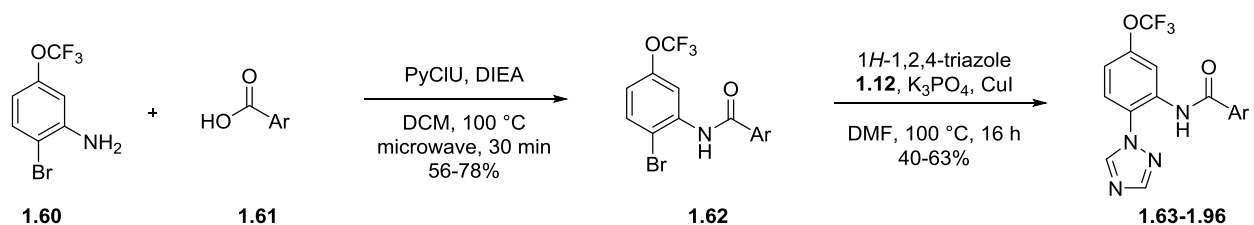
The data in **Table 1.2** show that the identity of the southern heterocycle is critical for maintaining activity at mGlu₇. Various 5- and 6-membered heterocycles were

surveyed (analogs **1.35-1.59**), but all of these compounds were either inactive or showed very weak activity ($> 10 \mu\text{M}$). Therefore, the 1,2,4-triazole motif was kept constant for further analog exploration. We hypothesize that this 1,2,4-triazole heterocycle is involved in an intramolecular hydrogen bond (IMHB) with the N-H bond of the amide. This IMHB could place an important conformational restraint within our scaffold which is necessary for activity.

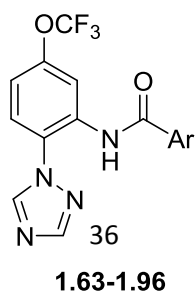
SAR Around the Eastern Aromatic Ring: Analogs **1.63-1.96**

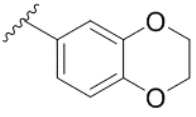
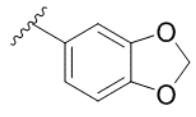
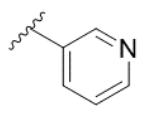
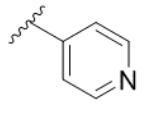
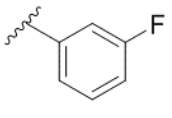
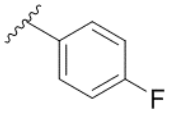
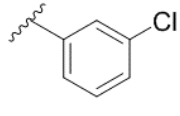
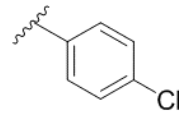
Since we had yet to explore the effect of different substituents on the eastern aromatic ring of this scaffold, we implemented a synthetic route to accommodate the synthesis of analogs of this nature (**Scheme 1.3**). Commercially available aniline **1.60** was coupled with various aryl- and heteroaryl- benzoic acids **1.61** via microwave-assisted PyClU-mediated amide coupling conditions. The resulting amides **1.62** were reacted with 1*H*-1,2,4-triazole under modified Ullmann coupling conditions to afford the desired analogs **1.63-1.96**. The results of this SAR campaign are summarized below in

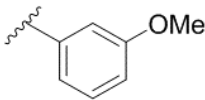
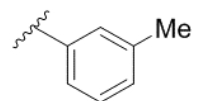
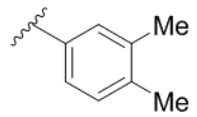
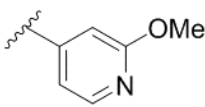
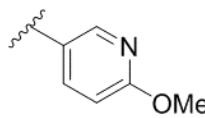
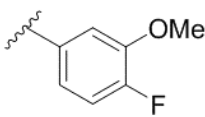
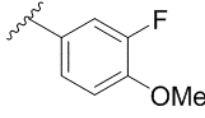
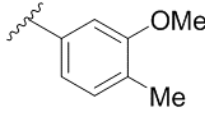
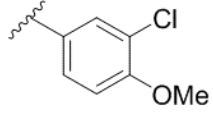
Table 1.3.

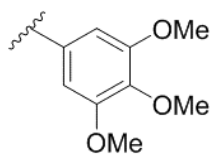


Scheme 1.3: Synthesis of analogs **1.63-1.96**



Ar =	Compound Number	VOID	mGlu ₇ IC ₅₀ (μM)	mGlu ₇ % L-AP ₄ _{min}
	1.63	VU6011109	Inactive	N/A
	1.64	VU6011110	Inactive	N/A
	1.65	VU6011112	Inactive	N/A
	1.66	VU6011122	Inactive	N/A
	1.67	VU6011113	Inactive	N/A
	1.68	VU6011114	Inactive	N/A
	1.69	VU6011135	Inactive	N/A
	1.70	VU6011118	Inactive	N/A

	1.71	VU6011115	Inactive	N/A
	1.72	VU6011118	Inactive	N/A
	1.73	VU6011131	Inactive	N/A
	1.74	VU6011214	Inactive	N/A
	1.75	VU6011116	Inactive	N/A
	1.76	VU6011209	Inactive	N/A
	1.77	VU6011210	Inactive	N/A
	1.78	VU6011208	> 10	60%
	1.79	VU6011329	Inactive	N/A

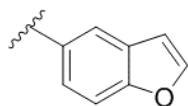


1.80

VU6011219

> 10

61%

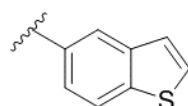


1.81

VU6011211

Inactive

N/A

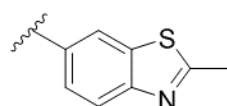


1.82

VU6011214

Inactive

N/A

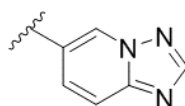


1.83

VU6011218

Inactive

N/A

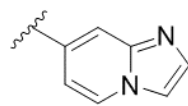


1.84

VU6011212

Inactive

N/A

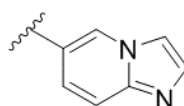


1.85

VU6011213

Inactive

N/A

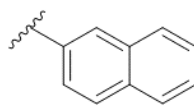


1.86

VU6011215

Inactive

N/A

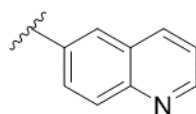


1.87

VU6011216

Inactive

N/A



1.88

VU6011216

Inactive

N/A

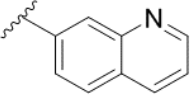
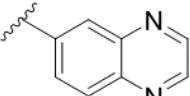
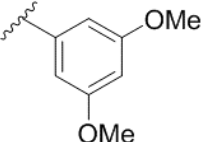
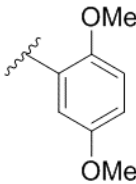
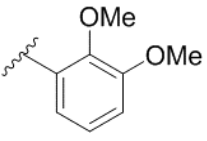
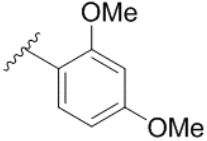
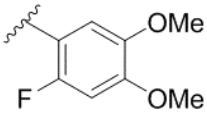
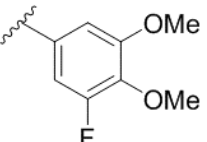
	1.89	VU6011339	Inactive	N/A
	1.90	VU6011343	Inactive	N/A
	1.91	VU6012567	Inactive	N/A
	1.92	VU6012694	Inactive	N/A
	1.93	VU6012697	Inactive	N/A
	1.94	VU6012698	Inactive	N/A
	1.95	VU6014818	> 10	51%
	1.96	VU6015155	2.22	28%

Table 1.3: SAR of the eastern aromatic ring – analogs **1.63-1.96**

As is common with trying to develop allosteric modulators of GPCRs, the SAR encountered was steep. In our case, attempts at cyclizing the two methoxy groups into either a 6-membered or 5-membered fused ring (analogs **1.63** and **1.64** respectively) led to inactive compounds. Additionally, different substituents on both aryl- and heteroaryl-groups were not tolerated (analogs **1.65-1.90**). With this information, we accepted the necessity for the dimethoxy groups on this eastern aromatic ring; however, we also wanted to probe if different dimethoxy substituent patterns were viable alternatives. Unfortunately, analogs of this nature (**1.91-1.94**) were not active. Finally, a fluorine walk around this eastern aromatic ring (analogs **1.95-1.96**) was also futile in producing an analog with improved potency when compared to **1.23**. Analog **1.95** was significantly less active than analog **1.96**. This observation lends credence to our intramolecular hydrogen bond (IMHB) hypothesis. Fluorine atom incorporation at this position in **1.95** can form a IMHB with the N-H bond of the amide, which can compete with the proposed IMHB between the N-H bond of the amide and one of the nitrogen atoms of the 1,2,4-triazole heterocycle.

*Assessment of VU6010608 (**1.23**) as a Viable Tool Compound*

1.23 was found to be highly selective for mGlu₇ (mGlu_{1,2,3,4,5,6,8} IC₅₀ > 10 μM) and displayed no ancillary pharmacology in a Eurofins lead profiling panel, meaning there was no off-target activity noted at 10 μM for 68 common GPCRs, ion channels, and transporters (**Table 1.4**). In addition, **1.23** had an attractive *in vitro* DMPK profile; **1.23** possessed an acceptable clogP (clogP = 2.86), good CNS penetration (K_p = 3.4), and moderate predicted hepatic clearance in mice (CL_{hep} = 48.5 mL/min/kg). With these data, we were excited to further explore the utility of **1.23** as a mGlu₇ tool compound.

Target/Protein	Species	% Inhibition
Adenosine A ₁	Human	19
Adenosine A _{2A}	Human	-1
Adenosine A ₃	Human	49
Adrenergic α _{1A}	Rat	35
Adrenergic α _{1B}	Rat	6
Adrenergic α _{1D}	Human	10
Adrenergic α _{2A}	Human	1
Adrenergic β ₁	Human	1
Adrenergic β ₂	Human	1
Androgen (Testosterone)	Human	9
Bradykinin B ₁	Human	5
Bradykinin B ₂	Human	-18
Calcium Channel L-Type, Benzothiazepine	Rat	15
Calcium Channel L-Type, Dihydropyridine	Rat	29
Calcium Channel N-Type	Rat	-3
Cannabinoid CB ₁	Human	28
Dopamine D ₁	Human	7
Dopamine D _{2S}	Human	1
Dopamine D ₃	Human	4
Dopamine D _{4.2}	Human	4
Endothelin ET _A	Human	6
Endothelin ET _B	Human	-11
Epidermal Growth Factor (EGF)	Human	-5
Estrogen E _α	Human	4
GABA _A , Flunitrazepam, Central	Rat	-10
GABA _A , Muscimol, Central	Rat	-3
GABA _{B1A}	Human	17
Glucocorticoid	Human	-4
Glutamate, Kainate	Rat	8
Glutamate, NMDA, Agonism	Rat	16
Glutamate, NMDA, Glycine	Rat	4
Glutamate, NMDA, Phencyclidine	Rat	14
Histamine H ₁	Human	11
Histamine H ₂	Human	3
Histamine H ₃	Human	-11
Imidazoline I ₂ , Central	Rat	12
Interleukin IL-1	Mouse	8
Leukotriene, Cysteinyl CysLT ₁	Human	1
Melatonin MT ₁	Human	10
Muscarinic M ₁	Human	3

Muscarinic M ₂	Human	2
Muscarinic M ₃	Human	6
Neuropeptide Y Y ₁	Human	4
Neuropeptide Y Y ₂	Human	1
Nicotinic Acetylcholine	Human	-7
Nicotinic Acetylcholine α 1, Bungarotoxin	Human	-5
Opiate δ ₁ (OP1, DOP)	Human	3
Opiate κ (OP2, KOP)	Human	12
Opiate μ (OP3, MOP)	Human	6
Phorbol Ester	Mouse	-1
Platelet Activating Factor (PAF)	Human	-7
Potassium Channel [K _{ATP}]	Hamster	8
Potassium Channel hERG	Human	33
Prostanoid EP ₄	Human	11
Purinergic P2X	Rabbit	-1
Purinergic P2Y	Rat	4
Rolipram	Rat	45
Serotonin (5-HT _{1A})	Human	4
Serotonin (5-HT _{2B})	Human	14
Serotonin (5-HT ₃)	Human	49
Sigma σ ₁	Human	-4
Sodium Channel, Site 2	Rat	-1
Tachykinin NK ₁	Human	-22
Thyroid Hormone	Rat	-11
Transporter, Dopamine (DAT)	Human	12
Transporter, GABA	Rat	-3
Transporter, Norepinephrine (NET)	Human	15
Transporter, Serotonin (SERT)	Human	7

Table 1.4: Eurofins lead profile panel for **1.23**. Significant activity is defined as >50% inhibition at a 10 μ M concentration of **1.23**. Data courtesy of Eurofins.

Although **1.23** possessed only a moderate predicted *in vitro* hepatic clearance, *in vivo* clearance data in rats showed that there was poor *in vitro: in vivo* correlation (*in vivo* CL_p = 64.2 mL/min/kg). Given the high *in vivo* clearance and low potency of **1.23** (mGlu₇ IC₅₀ = 759 nM), we decided that **1.23** would not be an exceptional candidate for an *in vivo* mGlu₇ tool compound. Even though these data preclude **1.23** from being a

viable *in vivo* tool compound, we still wanted to explore its utility as an *in vitro* probe. In electrophysiology experiments, administration of a mGlu₇ NAM onto brain slices of Schaffer Collateral SC-CA1 synapses has been shown to block long-term potentiation (LTP), a process contingent upon the successful activation of mGlu₇.⁴⁸ Indeed, as shown in **Figure 1.8**, Branden Stansley found that administration of **1.23** was also capable of blocking LTP at SC-CA1 synapses in wild type brain slices.⁶⁸ Given that mGlu₇ is the only mGlu receptor expressed presynaptically at SC-CA1 synapses in adult animals, we were confident to say that **1.23** negatively modulates mGlu₇ in this environment.^{48,68}

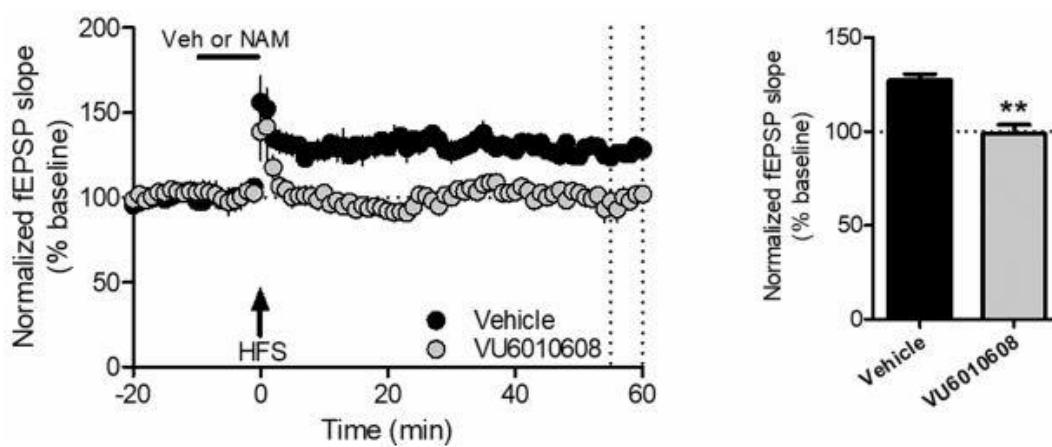


Figure 1.8: VU6010608 (**1.23**) is capable of blocking the induction of LTP at SC-CA1 synapses. Data courtesy of Branden Stansley, Ph.D.⁶⁸

Addressing the Potential Metabolic Liabilities of 1.23: Discovery of VU6012962

By analysis of the structure of **1.23**, we hypothesized that the high *in vivo* clearance could be due to two potential metabolic pathways: 1) cytochrome p450-mediated dealkylation/oxidation of the eastern 3,4-dimethoxy aryl ring or 2) amide hydrolysis (**Figure 1.9**). Therefore, two separate synthetic strategies were initiated in order to access analogs that could further address these issues.³⁴ To further guide our

efforts, metabolic ID studies were also initiated on **1.23** to determine the major mode(s) of metabolism and the resulting metabolite(s).

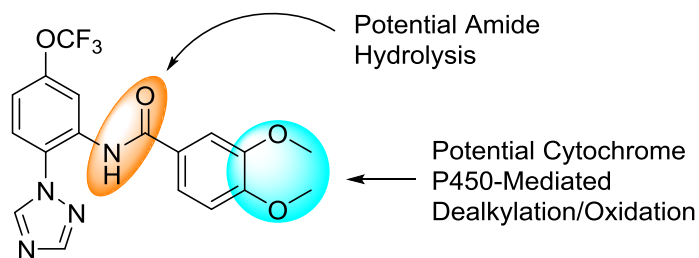


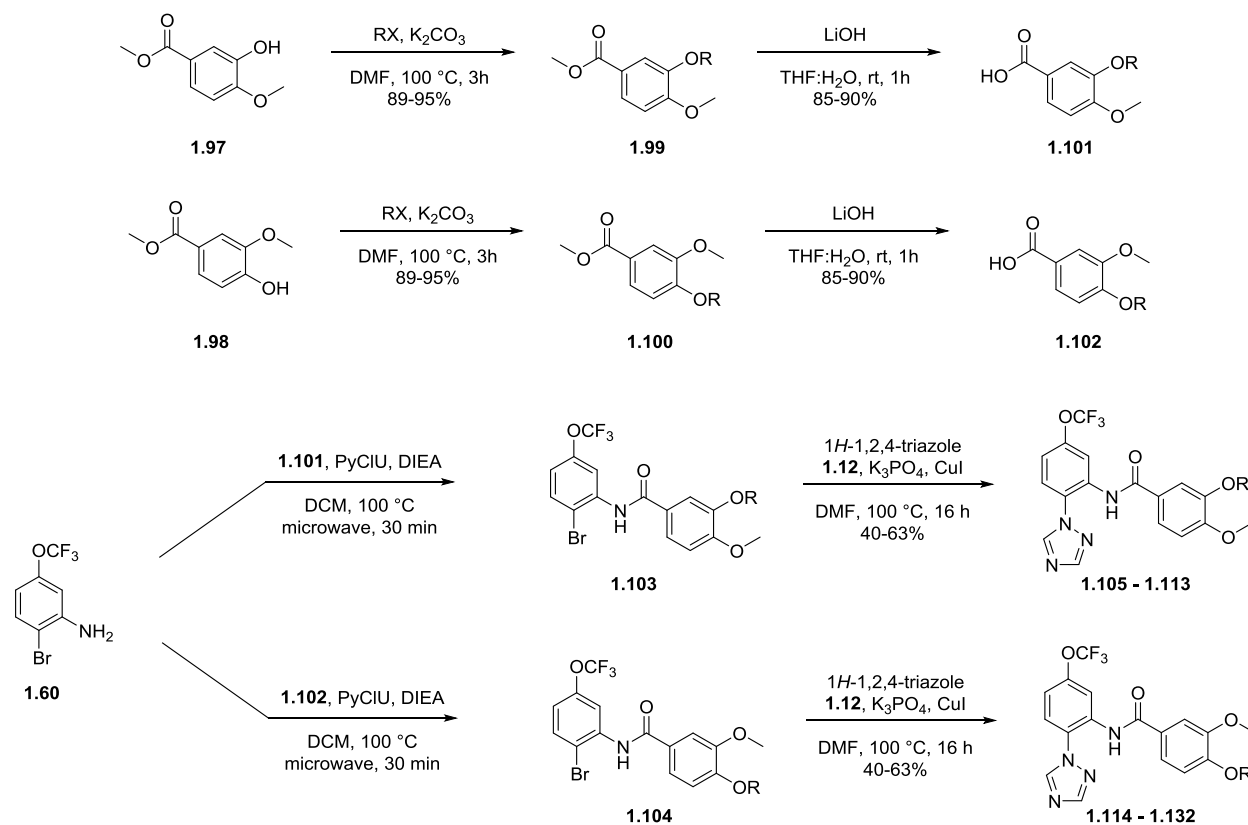
Figure 1.9: Potential metabolic liabilities of VU6010608 (**1.23**)

In order to address the potential cytochrome p450-mediated dealkylation/oxidation sequence on the eastern 3,4-dimethoxy aryl ring, we hypothesized that invocation of either the kinetic isotope effect or increasing the steric environment around the dimethoxy-motif (AKA alternative alkoxy groups) might be sufficient strategies for mitigating such a mode of metabolism. In addition to increasing steric congestion, larger alkoxy substituents at these positions might also aid in achieving a tighter fit into an allosteric pocket. The synthesis of analogs with alternative alkyl groups at both the 3- and 4-position are described below in **Scheme 1.4**.

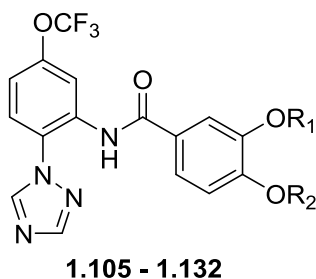
Methyl isovanillate **1.97** and methyl vanillate **1.98** were alkylated with various alkyl halides under standard conditions. The corresponding esters **1.99** and **1.100** were hydrolyzed with lithium hydroxide, followed by a microwave-assisted PyClU-mediated amide coupling with aniline **1.60** to afford amides **1.103** and **1.104**, respectively. Modified Ullmann coupling conditions were used to install the desired 1,2,4-triazole heterocycle, forming the desired both 3-alkoxy derivatives (**1.105 – 1.113**) and 4-alkoxy

derivatives (**1.114** – **1.132**). The results of these efforts are summarized below in **Table**

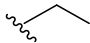
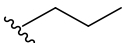
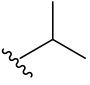
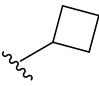
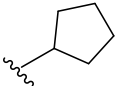
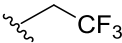
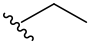
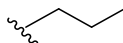
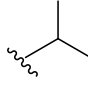
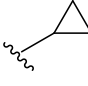



1.5.



Scheme 1.4: Synthesis of 3-alkoxy analogs **1.105-1.113** and 4-alkoxy analogs **1.114-1.132**



R ₁ =	R ₂ =	Compound Number	VID	mGlu ₇ IC ₅₀ (μM)	mGlu ₇ % L-AP ₄ _{min}
CD ₃	CH ₃	1.105	VU6014321	1.0	13%

CH ₃	CD ₃	1.106	VU6014320	1.0	13%
CD ₃	CD ₃	1.107	VU6014322	1.4	13%
	CH ₃	1.108	VU6011347	> 10	46%
	CH ₃	1.109	VU6011349	Inactive	N/A
	CH ₃	1.110	VU6011350	Inactive	N/A
	CH ₃	1.111	VU6011356	> 10	N/A
	CH ₃	1.112	VU6011351	Inactive	N/A
	CH ₃	1.113	VU6011328	Inactive	N/A
CH ₃		1.114	VU6011121	0.51	11%
CH ₃		1.115	VU6010953	0.78	19%
CH ₃		1.116	VU6010955	0.78	14%
CH ₃		1.117	VU6012964	0.71	11%
CH ₃		1.118	VU6011353	1.06	12%
CH ₃		1.119	VU6012963	> 10	28%
CH ₃		1.120	VU6013341	> 10	41%

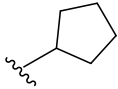
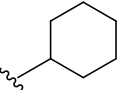
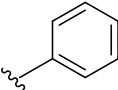
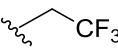
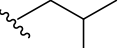
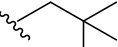
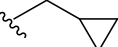
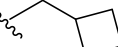
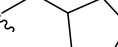
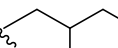
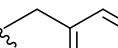
CH ₃		1.121	VU6011111	1.4	10%
CH ₃		1.122	VU6013751	2.9	10%
CH ₃		1.123	VU6014315	> 10	46%
CH ₃		1.124	VU6011327	Inactive	N/A
CH ₃		1.125	VU6013571	1.2	35%
CH ₃		1.126	VU6013572	> 10	25%
CH ₃		1.127	VU6012962	0.35	12%
CH ₃		1.128	VU6013215	1.4	15%
CH ₃		1.129	VU6014099	2.8	27%
CH ₃		1.130	VU6014100	> 10	57%
CH ₃		1.131	VU6013340	3.1	19%
CH ₃	CF ₂ H	1.132	VU6014316	> 10	48%

Table 1.5: Alternative alkoxy groups surveyed – analogs **1.105-1.132**

First, a -OCD₃ group was incorporated into the 3- (analog **1.105**) and 4-positions (analog **1.106**), and a bis -OCD₃ analog (**1.107**) was also synthesized to test the hypothesis that we can utilize the kinetic isotope effect to mitigate this potential mode of metabolism. However, no significant improvement in the predicted *in vitro* hepatic

clearance was observed when compared to **1.23**, leading us to conclude this would not be a viable solution for addressing clearance. Another strategy that was thought to potentially alter the rate of metabolism was increasing the steric environment around the two methoxy groups, which could slow the rate of cytochrome p450 enzyme activity. As a whole, alternative alkoxy groups at the 3-position (analogs **1.108-1.113**) were not tolerated, as most of these compounds lost mGlu₇ activity. However, we found that alternative alkoxy groups in the 4-position were tolerated well. In our efforts, we discovered that the incorporation of a lipophilic methylene cyclopropyl group, VU6012962 (**1.127**), led to a ~2-fold increase in potency (**Figure 1.10**). Additionally, **1.127** was found to possess favorable DMPK properties with improved predicted hepatic clearance values (**Figure 1.10**). Like our previous *in vitro* tool compound (**1.23**), **1.127** also possessed a high selectivity for mGlu₇, with no activity observed at the other mGlu receptors (mGlu_{1,2,3,4,5,6,8} IC₅₀ > 10 μM), while significant activity was only observed at one off-target receptor (Serotonin 5-HT_{2B}) in a Eurofins lead profiling panel (**Table 1.6**).

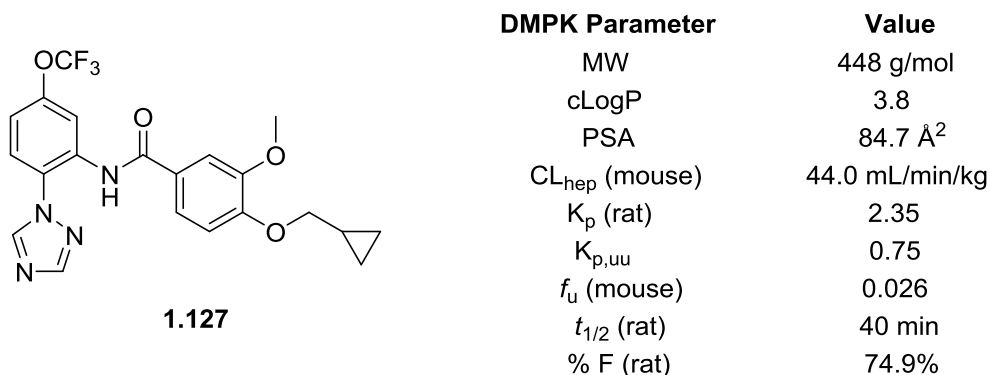


Figure 1.10: Structure of VU6012962 (**1.127**) with respective DMPK parameters

Target/Protein	Species	% Inhibition
Adenosine A ₁	Human	9
Adenosine A _{2A}	Human	-1
Adenosine A ₃	Human	45
Adrenergic α_{1A}	Rat	-3
Adrenergic α_{1B}	Rat	-5
Adrenergic α_{1D}	Human	8
Adrenergic α_{2A}	Human	-6
Adrenergic β_1	Human	6
Adrenergic β_2	Human	6
Androgen (Testosterone)	Human	-9
Bradykinin B ₁	Human	-5
Bradykinin B ₂	Human	-5
Calcium Channel L-Type, Benzothiazepine	Rat	-3
Calcium Channel L-Type, Dihydropyridine	Rat	14
Calcium Channel N-Type	Rat	-5
Cannabinoid CB ₁	Human	49
Dopamine D ₁	Human	5
Dopamine D _{2S}	Human	3
Dopamine D ₃	Human	-4
Dopamine D _{4.2}	Human	0
Endothelin ET _A	Human	0
Endothelin ET _B	Human	-5
Epidermal Growth Factor (EGF)	Human	9
Estrogen E α	Human	-3
GABA _A , Flunitrazepam, Central	Rat	3
GABA _A , Muscimol, Central	Rat	23
GABA _{B1A}	Human	5
Glucocorticoid	Human	-4
Glutamate, Kainate	Rat	-1
Glutamate, NMDA, Agonism	Rat	10
Glutamate, NMDA, Glycine	Rat	-5
Glutamate, NMDA, Phencyclidine	Rat	8
Histamine H ₁	Human	-3
Histamine H ₂	Human	2
Histamine H ₃	Human	-14
Imidazoline I ₂ , Central	Rat	5
Interleukin IL-1	Mouse	2
Leukotriene, Cysteinyl CysLT ₁	Human	-5
Melatonin MT ₁	Human	6
Muscarinic M ₁	Human	-2

Muscarinic M ₂	Human	-18
Muscarinic M ₃	Human	-2
Neuropeptide Y Y ₁	Human	3
Neuropeptide Y Y ₂	Human	-6
Nicotinic Acetylcholine	Human	-6
Nicotinic Acetylcholine α 1, Bungarotoxin	Human	11
Opiate δ ₁ (OP1, DOP)	Human	0
Opiate κ (OP2, KOP)	Human	14
Opiate μ (OP3, MOP)	Human	-6
Phorbol Ester	Mouse	-3
Platelet Activating Factor (PAF)	Human	22
Potassium Channel [K _{ATP}]	Hamster	-5
Potassium Channel hERG	Human	17
Prostanoid EP ₄	Human	10
Purinergic P2X	Rabbit	10
Purinergic P2Y	Rat	-3
Rolipram	Rat	25
Serotonin (5-HT _{1A})	Human	-1
Serotonin (5-HT_{2B})	Human	73
Serotonin (5-HT ₃)	Human	-3
Sigma σ ₁	Human	-9
Sodium Channel, Site 2	Rat	30
Tachykinin NK ₁	Human	7
Thyroid Hormone	Rat	6
Transporter, Dopamine (DAT)	Human	0
Transporter, GABA	Rat	5
Transporter, Norepinephrine (NET)	Human	4
Transporter, Serotonin (SERT)	Human	-9

Table 1.6: Eurofins lead profile panel for **1.127**. Data courtesy of Eurofins.

Due to the relative improvement of the *in vivo* clearance of **1.127** in comparison to **1.23**, we were excited to explore the utility of **1.127** as an *in vivo* tool compound. Previous mGlu₇ NAMs, such as ADX71743, have shown to be effective in mouse models of anxiety, albeit using high dosing paradigms (50-150 mg/kg).⁶⁷ Therefore, we wanted to explore the *in vivo* utility of **1.127** in mouse models of anxiety in collaboration

with the Conn lab. As shown in **Figure 1.11**, Samantha Yohn was able to show that **1.127** was efficacious in eliciting anxiolytic behavior in three mouse models of anxiety (the elevated zero maze assay, the light/dark box assay, and the marble burying assay) at doses as low as 3 mg/kg.⁸⁹

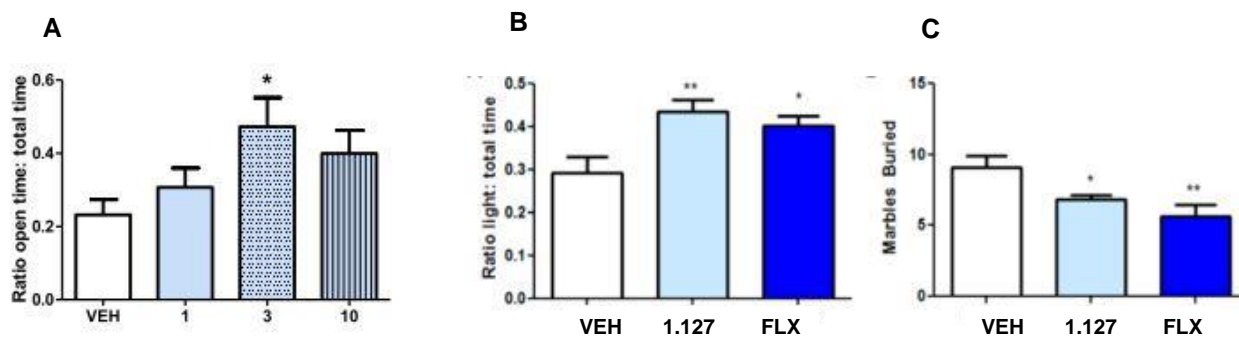
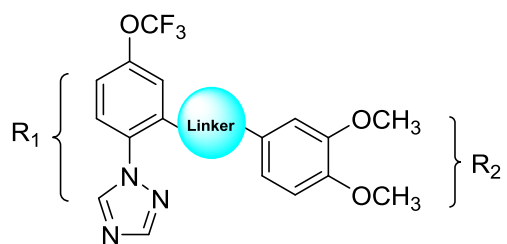


Figure 1.11: Anxiolytic behavioral assays of **1.127**: (A) elevated zero maze assay, (B) light/dark box assay, and (C) marble burying assay. VEH = vehicle and FLX = fluoxetine (positive control). Data courtesy of Samantha Yohn, Ph. D.⁸⁹

Addressing the True Metabolic Liability of VU6010608 (1.23): Amide Hydrolysis

Results from the metabolic ID studies of **1.23** revealed that while dealkylation of the dimethoxy motif occurs to an extent, the major mode of metabolism is hydrolysis of the amide. With the minimum pharmacophore and the major metabolic liability identified, we sought to address this issue by exploring a variety of different strategies that have been reported in the literature for mitigating this mode of metabolism.⁹⁰

Therefore, the first strategy we initiated was the incorporation of traditional amide bioisosteres. In theory, bioisosteres can mimic the physical and chemical properties of the amide bond, with the advantage of decreased hydrolytic liabilities. **Table 1.7** summarizes the different amide bioisosteres that we synthesized for this purpose.



1.133 - 1.140

Linker	Compound Number	VOID	mGlu ₇ IC ₅₀ (μM)	mGlu ₇ % L-AP ₄ _{min}
	1.133	VU6010268	Inactive	N/A
	1.134	VU6014004	Inactive	N/A
	1.135	VU6012560	Inactive	N/A
	1.136	VU6012695	Inactive	N/A
	1.137	VU6014705	Inactive	N/A
	1.138	VU6016247	Inactive	N/A

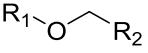
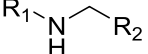
	1.139	VU6014095	> 10	56%
	1.140	VU6014706	5.9	18%

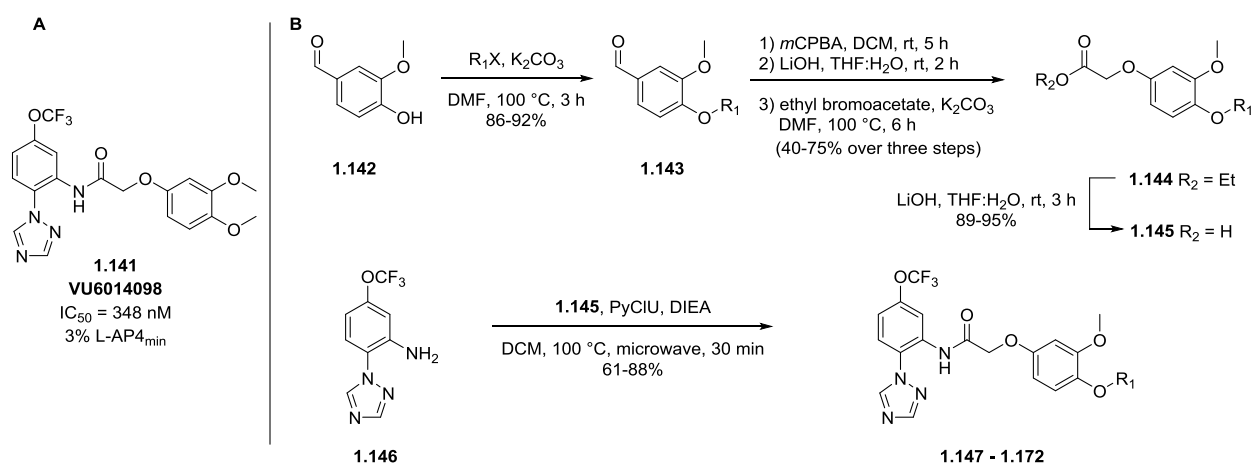
Table 1.7: SAR of traditional amide bioisosteres – analogs **1.133-1.140**

Unfortunately, the *N*-Me amide, reverse amide, urea, and sulfonamide analogs (**1.133-1.136** respectively) were not active. Additionally, α -trifluoromethyl amine **1.137** and spirocyclic oxetane **1.138** were inactive. While both phenol **1.139** and aniline **1.140** did show weak activity, their low potencies did not justify their further use in this context.

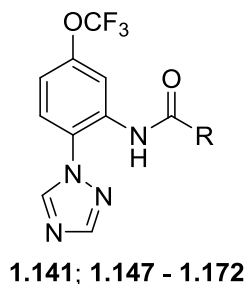
Elongation of the Amide Linker: Discovery of Phenoxy Benzamide Linker

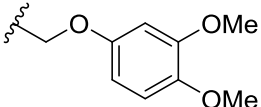
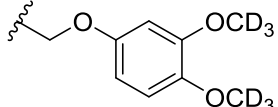
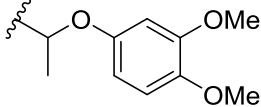
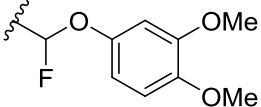
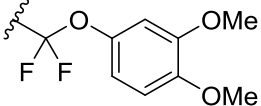
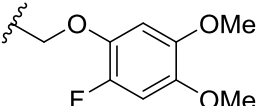
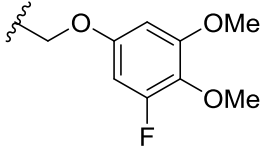
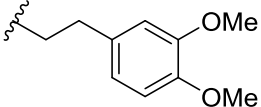
With the failure of the traditional amide bioisosteres, a rather simplistic strategy was next employed. It has been previously reported that increasing the distance between two aryl rings joined together by an amide linker can sometimes decrease the hydrolytic rates of the respective amides.⁹⁰ Therefore, analysis of previously disregarded HTS hits led to the observation that a phenoxy benzamide linker was a common motif in multiple compounds. The inclusion of such a motif was prioritized (VU6014098) (**1.141**), and to our delight, **1.141** displayed activity at mGlu₇ with a potency comparable of that to **1.127** (**Scheme 1.5 A**).

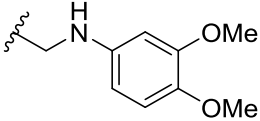
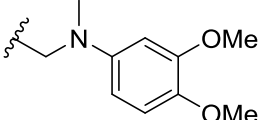
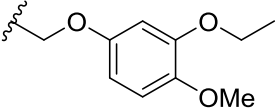
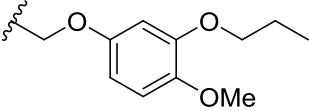
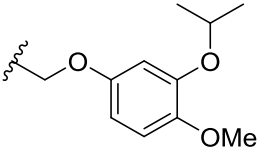
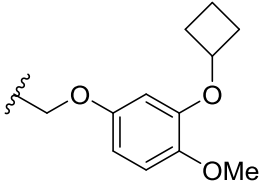
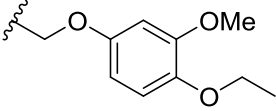
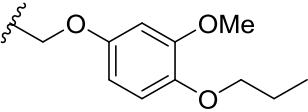
The synthesis of analogs of this nature was pursued in order to better understand the SAR associated with this new scaffold (**Scheme 1.5 B**). As representative examples, vanillin or substituted vanillin derivatives (**1.142**) were alkylated under standard conditions with a variety of alkyl halides to afford aldehydes **1.143**. Dakin oxidation and subsequent S_N2 displacement with ethyl bromoacetate led to the formation of esters **1.144**. Saponification of **1.144** afforded benzoic acids **1.145**, which were reacted with aniline **1.146** utilizing PyCIU-mediated amide bond coupling conditions to form analogs **1.147-1.172**. The results of this SAR campaign are summarized in **Table 1.8**.

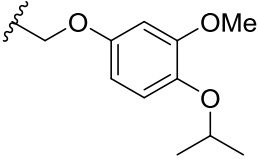
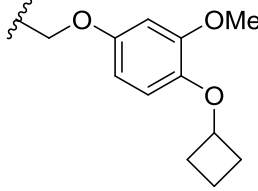
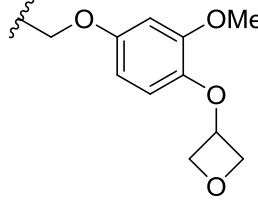
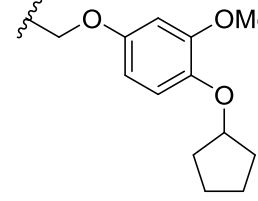
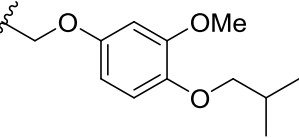
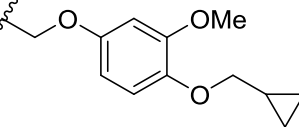
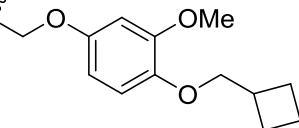


Scheme 1.5: (A) Structure of VU6014098 (**1.141**) and (B) Synthesis of analogs **1.147-1.172**.



R =	Compound Number	VUID	mGlu ₇ IC ₅₀ (μM)	mGlu ₇ % L-AP ₄ _{min}
	1.141	VU6014098	0.35	3%
	1.147	VU6015156	0.16	3%
	1.148	VU6014707	> 10	18%
	1.149	VU6014713	0.66	3%
	1.150	VU6014712	1.09	3%
	1.151	VU6014819	0.14	6%
	1.152	VU6015157	1.16	19%
	1.153	VU6015153	> 10	61%

	1.154	VU6015154	Inactive	N/A
	1.155	VU6015332	Inactive	N/A
	1.156	VU6014951	0.87	27%
	1.157	VU6014952	Inactive	N/A
	1.158	VU6014953	> 10	54%
	1.159	VU6014954	2.90	54%
	1.160	VU6014711	0.26	3%
	1.161	VU6014713	0.20	6%

	1.162	VU6014714	0.32	6%
	1.163	VU6014715	0.13	5%
	1.164	VU6014820	0.26	6%
	1.165	VU6014716	0.47	3%
	1.166	VU6014822	0.97	9%
	1.167	VU6014717	0.20	6%
	1.168	VU6014821	0.62	24%

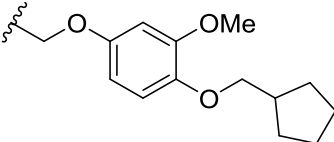
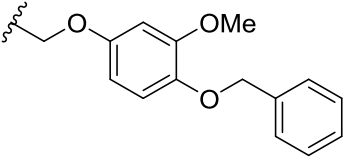
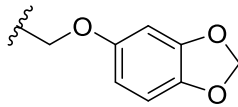
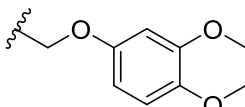
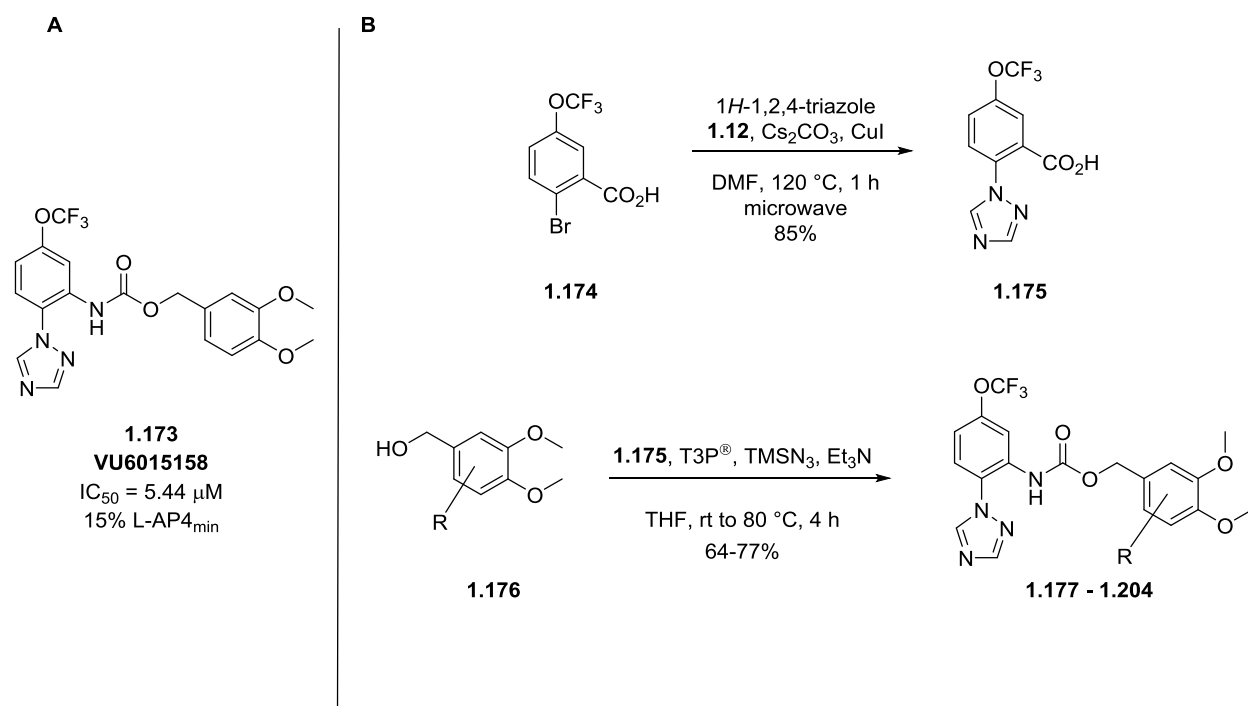
	1.169	VU6014719	2.00	64%
	1.170	VU6014720	1.35	53%
	1.171	VU6014949	Inactive	N/A
	1.172	VU6014950	0.75	22%

Table 1.8: SAR of elongated amide analogs **1.141**; **1.147-1.172**

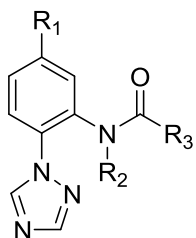
Through our efforts, we observed that the incorporation of a methyl group (analog **1.148**) in the methylene linker led to a drastic drop in potency. The incorporation of mono-fluoro and geminal difluoro groups (analog **1.149** and **1.150**, respectively) at this position also resulted in reduced potency. Both *C*-linked and *N*-linked benzamide linker alternatives (analog **1.153-1.155**) were also inactive. As we noticed before, it appeared that the only tolerated changes to the scaffold included the incorporation of alternative alkoxy groups at the 4-position of the eastern aromatic ring (analog **1.160-1.170**). Unfortunately, while some of the analogs in this series (ex: **1.147**, **1.151**, and **1.163**) were the most potent compounds to date, these compounds suffered from either high predicted hepatic clearance or plasma instability in both mice and rats. Based on these data, we elected to pursue other strategies to mitigate this amide hydrolysis.

Extended Amide Linker Replacements: Carbamate Congeners

Given the structure of **1.141**, it did not escape our attention that carbamate and/or urea functionalities in the linker might be suitable amide alternatives. Therefore, VU6015158 (**1.173**) (**Scheme 1.6 A**) was synthesized, and encouragingly, **1.173** retained activity at mGlu₇. Even though **1.173** is a weak mGlu₇ NAM (mGlu₇ IC₅₀ = 5.44 μM), we further explored the SAR around the more stable carbamate motif. Carbamate analogs were synthesized as shown in **Scheme 1.6 B**. As a representative example, Ullmann coupling of 1*H*-1,2,4-triazole with commercially available **1.174** led to the formation of benzoic acid **1.175**. A Curtius rearrangement was utilized to form the corresponding isocyanate *in situ*, followed by reaction with benzylic alcohols **1.176** to afford the corresponding carbamates **1.177-1.204**. The results for this SAR campaign are shown below in **Table 1.9**.



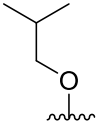
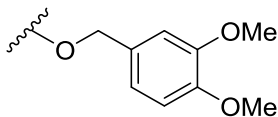
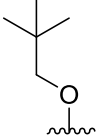
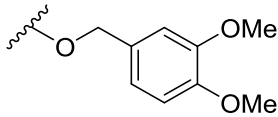
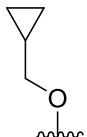
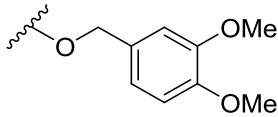
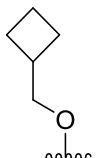
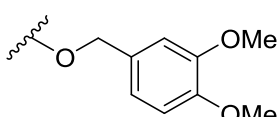
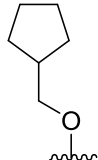
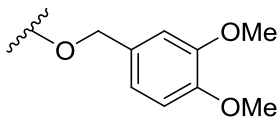
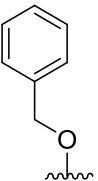
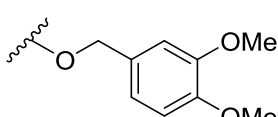
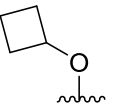
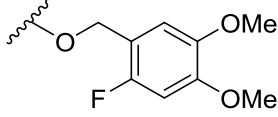
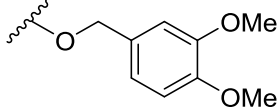
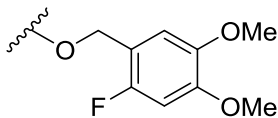
Scheme 1.6: (A) Structure of VU6015158 (**1.173**) and (B) Synthesis of carbamate analogs **1.177-1.204**



1.173, 1.177 - 1.204

R ₁ =	R ₂ =	R ₃ =	Compound Number	VUID	mGlu ₇ IC ₅₀ (μM)	mGlu ₇ % L-AP ₄ _{min}
OCF ₃	H		1.173	VU6015158	5.44	15%
OCF ₃	H		1.177	VU6015849	5.56	15%
OCF ₃	H		1.178	VU6015330	2.85	13%
OCF ₃	H		1.179	VU6015331	> 10	45%
OCF ₃	H		1.180	VU6016764	Inactive	N/A
OCF ₃	H		1.181	VU6016538	> 10	43%
OCF ₃	H		1.182	VU6016773	Inactive	N/A
OCF ₃	H		1.183	VU6016758	Inactive	N/A

OCF ₃	H		1.184	VU6015852	4.72	20%
OCF ₃	H		1.185	VU6015853	8.26	16%
OCF ₃	H		1.186	VU6015854	Inactive	N/A
OCF ₂ H	H		1.187	VU6016243	> 10	54%
	H		1.188	VU6016248	Inactive	N/A
	H		1.189	VU6016249	> 10	50%
	H		1.190	VU6015860	2.64	22%
	H		1.191	VU6015861	Inactive	N/A
	H		1.192	VU6016239	1.84	17%

	H		1.193	VU6016241	3.77	23%
	H		1.194	VU6016242	3.56	14%
	H		1.195	VU6015858	> 10	20%
	H		1.196	VU6015859	1.64	50%
	H		1.197	VU6015857	Inactive	N/A
	H		1.198	VU6016240	Inactive	N/A
	H		1.199	VU6016250	1.77	21%
OCF ₃	CH ₃		1.200	VU6015329	Inactive	N/A
OCF ₃	CH ₃		1.201	VU6015855	Inactive	N/A

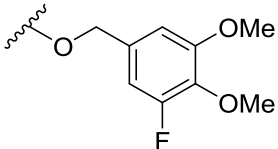
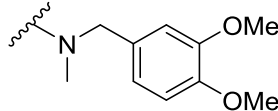
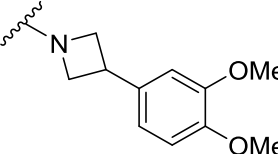
OCF ₃	CH ₃		1.202	VU6015856	Inactive	N/A
OCF ₃	H		1.203	VU6015159	Inactive	N/A
OCF ₃	H		1.204	VU6015328	Inactive	N/A

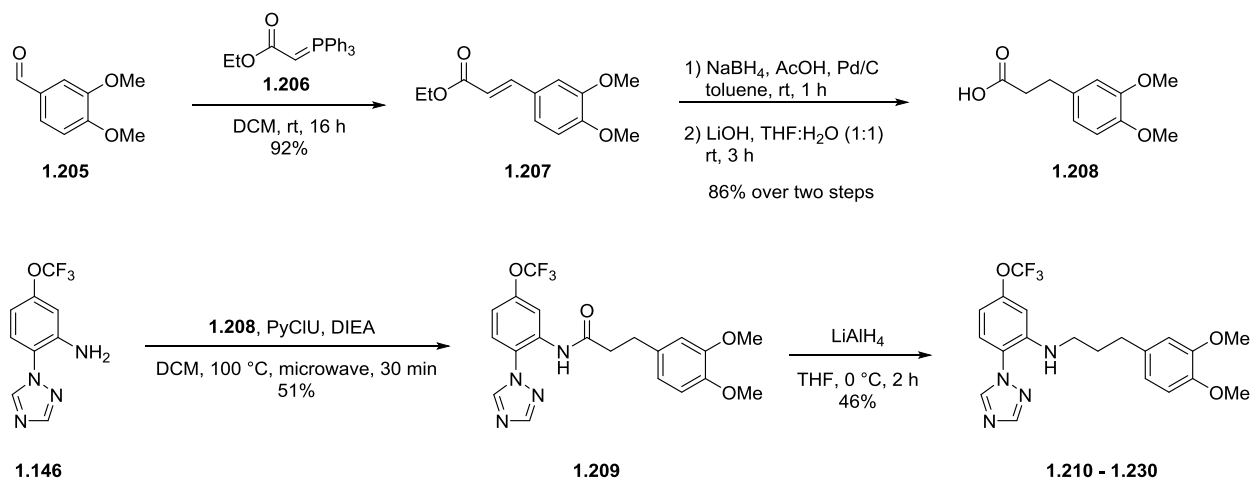
Table 1.9: SAR of carbamate analogs **1.173**, **1.177-1.204**

As shown in **Table 1.9**, the incorporation of a fluorine atom at the 6-position of the eastern aromatic ring (analog **1.178**) was conducive for potency. We hypothesize that with this elongated linker, we are no longer observing a competing intramolecular hydrogen bond interaction between this fluorine atom and the N-H bond of our amide as we had observed previously with the shorter amide linker (analog **1.95**). Unfortunately, the incorporation of azaheterocycles (analog **1.181**) and additional functionality on the methylene group of the linker (analog **1.182** and **1.183**) resulted in a loss in potency and/or activity. As previously observed, alternative alkoxy groups in the 4-position of the eastern aromatic ring (analog **1.184-1.185**) and sterically-hindered alkoxy bioisosteres on the western aromatic ring (analog **1.190**, **1.192-1.194**, **1.196**, and **1.199**) were well tolerated. Both the incorporation of the *N*-Me carbamate (analog **1.200-1.202**) and urea congeners (analog **1.203** and **1.204**) led to inactive compounds. Even with these data, the best compound in this series, **1.199**, still lacked considerably in potency when

compared to **1.127**; therefore, we elected to continue pursuing effort in finding other suitable amide replacements.

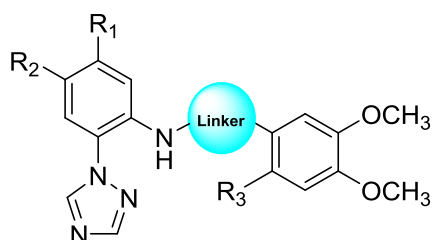
Extended Amide Linker Replacements: Des-Carbonyl Analogs

In addition to examining amide replacements, we also investigated the possibility of deleting the carbonyl of the amide, resulting in substituted aniline derivatives. In this case, there would be no amide functional group present for hydrolysis, and we may be able to exploit this in order to decrease clearance. Therefore, the synthesis of des-carbonyl analogs was initiated. As a representative example, homologated aniline VU6015848 (**1.210**) was synthesized according to **Scheme 1.7**. In this case, Wittig reaction of 3,4-dimethoxybenzaldehyde **1.205** and resonance-stabilized ylide **1.206** afforded ester **1.207**. Reduction of the α,β -unsaturated olefin followed by saponification of the ester using lithium hydroxide resulted in the formation of homologated acids **1.208**. PyCIU-mediated amide coupling of aniline **1.146** with acids **1.208** yielded amides **1.209**, which were subsequently reduced with lithium aluminum hydride to form anilines **1.210-1.230**.



Scheme 1.7: Synthesis of des-carbonyl analogs **1.210-1.230**

Homologation of the linker was found to be beneficial for potency (comparing to aniline analog **1.140**). Different linker groups were synthesized and incorporated into the aniline scaffold as described above to further explore the SAR around compounds of this nature (**Table 1.10**).



1.210 - 1.230

R ₁ =	R ₂ =	R ₃ =	Linker =	Compound Number	VOID	mGlu ₇ IC ₅₀ (μM)	mGlu ₇ % L-AP ₄ _{min}
OCF ₃	H	H		1.210	VU6015848	1.6	10%
OCF ₃	H	H		1.211	VU6016244	2.98	10%
OCF ₃	H	H		1.212	VU6016497	1.97	6%
OCF ₃	H	H		1.213	VU6017724	2.47	12%
OCF ₃	H	H		1.214	VU6017981	2.92	5%
OCF ₃	H	F		1.215	VU6016771	1.3	10%
OCF ₃	H	F		1.216	VU6017722	2.81	10%
OCF ₃	H	F		1.217	VU6016769	1.2	6%

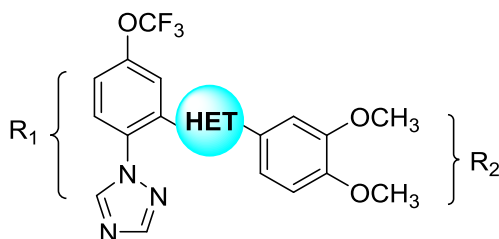
OCF ₃	H	F		1.218	VU6017983	5.36	10%
OCF ₃	F	H		1.219	VU6016532	5.95	12%
OCF ₃	F	H		1.220	VU6016533	> 10	18%
Cl	H	H		1.221	VU6016759	1.64	11%
Cl	H	H		1.222	VU6016760	0.92	8%
Cl	H	H		1.223	VU6016765	2.81	8%
Cl	H	H		1.224	VU6017740	7.52	18%
Cl	H	H		1.225	VU6017980	2.94	7%
Cl	H	F		1.226	VU6017738	4.53	11%
Cl	H	F		1.227	VU6017741	2.86	7%
Cl	H	F		1.228	VU6017982	6.14	14%
Cl	F	H		1.229	VU6016766	4.66	19%
Cl	F	H		1.230	VU6016767	5.73	18%

Table 1.10: SAR of des-carbonyl analogs **1.210** – **1.230**

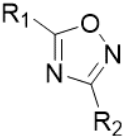
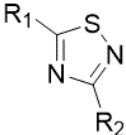
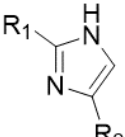
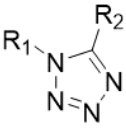
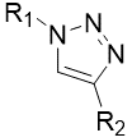
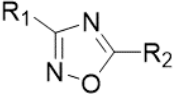
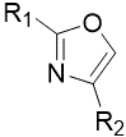
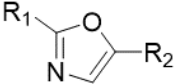
We observed that both OCF₃- and Cl- substituted analogs were tolerated, in addition to a variety of different alkyl linkers differing in either their steric or electronic properties. However, the analogs from this series suffered from high predicted hepatic clearance in mice (e.g. mouse predicted CL_{hep} for analog **1.222** = 87.2 mL/min/kg). Additionally, high plasma protein binding and rat brain homogenate binding were observed in *in vitro* and *in vivo* PK experiments, likely due to the presence of the N-H bond of the aniline functional group. These data precluded us from further exploring this scaffold.⁸⁹

Heterocycles as Viable Amide Replacements

Recently, the use of heterocycles as amide bond mimics has been reported in the literature.⁹⁰ Therefore, a vast array of heterocyclic linker congeners of **1.23** were synthesized (**Table 1.11**). We discovered that the incorporation of 1,3,4-oxadiazole (VU6017094) (**1.231**) and 1,2,4-oxadiazole (VU6017095) (**1.232**) heterocycles led to moderately potent mGlu₇ NAMs, warranting additional SAR.⁹¹



Het =	Compound Number	VOID	mGlu ₇ IC ₅₀ (μM)	mGlu ₇ % L-AP ₄ _{min}
	1.231	VU6017094	1.58	7%

	1.232	VU6017095	1.32	15%
	1.233	VU6017096	> 10	42%
	1.234	VU6018504	> 10	34%
	1.235	VU6017976	Inactive	N/A
	1.236	VU6018798	> 10	32%
	1.237	VU6018797	2.39	8%
	1.238	VU6018218	7.63	21%
	1.239	VU6018226	2.08	37%

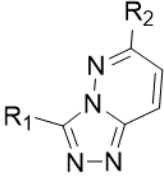
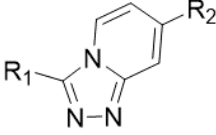
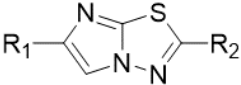
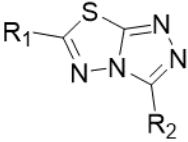
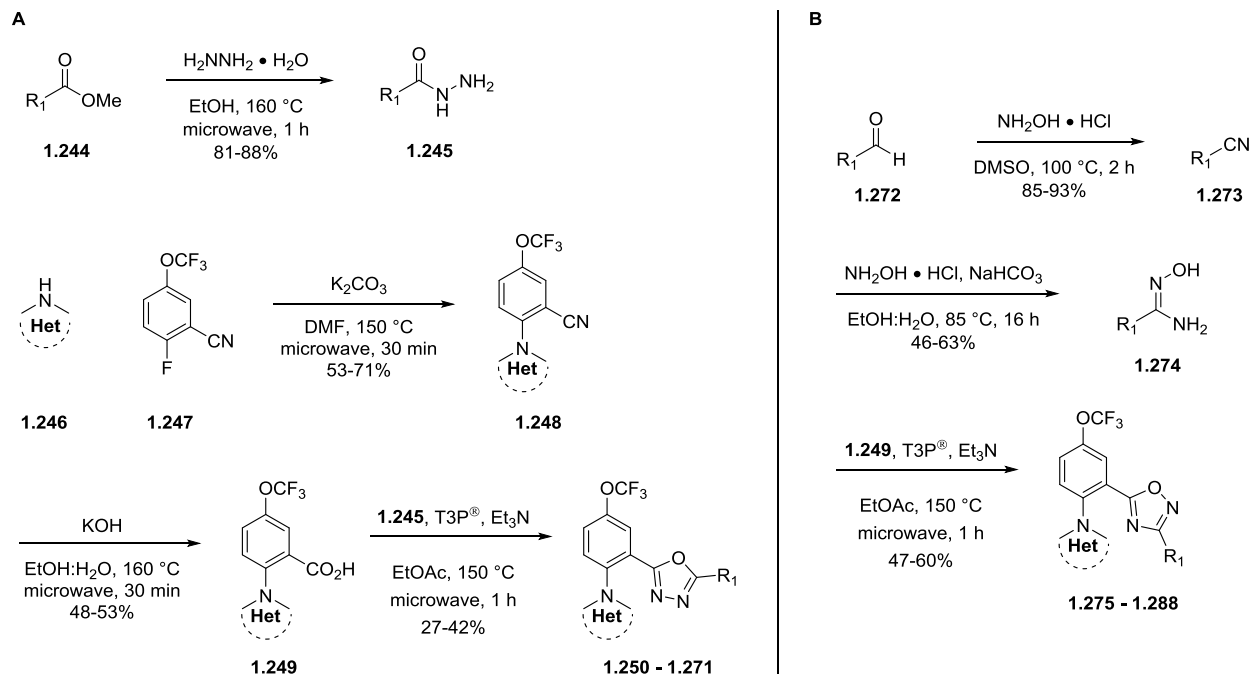
	1.240	VU6018301	Inactive	N/A
	1.241	VU6018503	Inactive	N/A
	1.242	VU6018506	Inactive	N/A
	1.243	VU6017977	Inactive	N/A

Table 1.11: SAR of diversity-oriented heterocyclic linker library

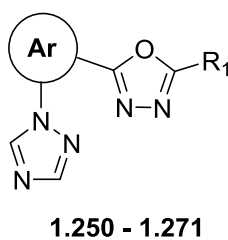
1,3,4-Oxadiazole and 1,2,4-Oxadiazole Heterocyclic Analogs

Both 1,3,4-oxadiazole and 1,2,4-oxadiazole analogs were synthesized as depicted in **Scheme 1.8**. For 1,3,4-oxadiazole variants, commercially available esters **1.244** were reacted with hydrazine to form acyl hydrazides **1.245**. A S_NAr reaction between nitrogen-containing heterocycles **1.246** and commercial **1.247** yielded nitriles **1.248**, which were subsequently hydrolyzed to benzoic acids **1.249**. A T_3P° -mediated, one-pot, microwave-assisted tandem amide coupling/condensation was utilized to afford analogs **1.250-1.271** (**Table 1.12**).⁹² For 1,2,4-oxadiazole variants, commercially available aldehydes **1.272** were transformed into nitriles **1.273**, which were reacted with hydroxylamine hydrochloride to afford the corresponding amidoximes **1.274**. Reaction of

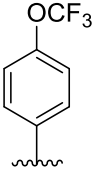
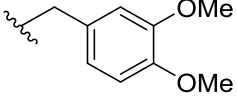
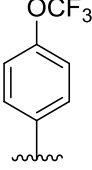
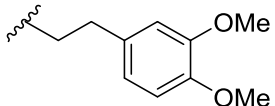
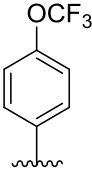
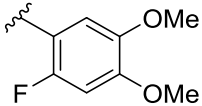
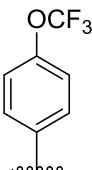
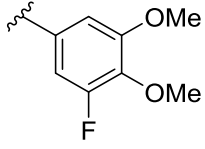
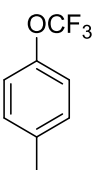
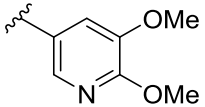
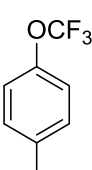
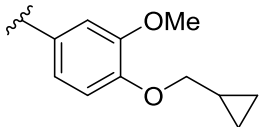
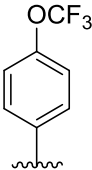
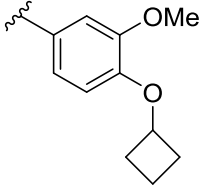
1.274 with 1.249 using the T₃P[®] conditions aforementioned resulted in analogs 1.275-1.288 (Table 1.13).⁹²

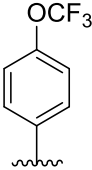
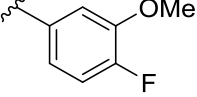
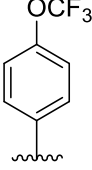
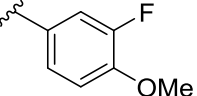
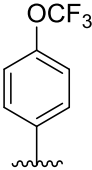
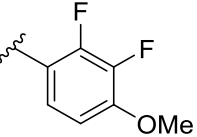
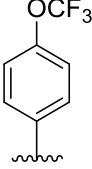
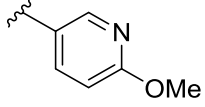
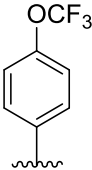
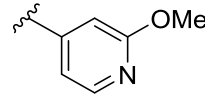
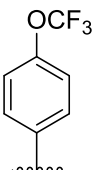
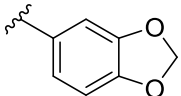
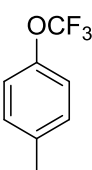
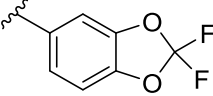


Scheme 1.8: Synthesis of (A) 1,3,4-oxadiazole analogs 1.250-1.271 and (B) 1,2,4-oxadiazole analogs 1.275-1.288



Ar	R ₁ =	Compound Number	UID	mGlu ₇ IC ₅₀ (μM)	mGlu ₇ % L-AP ₄ _{min}
		1.250	VU6017730	2.11	10%

		1.251	VU6017718	Inactive	N/A
		1.252	VU6018221	Inactive	N/A
		1.253	VU6017726	> 10	73%
		1.254	VU6017721	Inactive	N/A
		1.255	VU6017731	4.38	14%
		1.256	VU6017714	1.31	13%
		1.257	VU6017727	1.55	10%

		1.258	VU6017732	Inactive	N/A
		1.259	VU6017733	Inactive	N/A
		1.260	VU6017729	Inactive	N/A
		1.261	VU6017985	Inactive	N/A
		1.262	VU6017986	> 10	68%
		1.263	VU6017715	Inactive	N/A
		1.264	VU6017734	Inactive	N/A

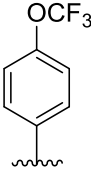
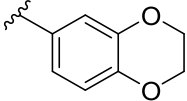
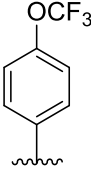
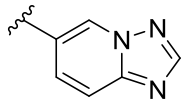
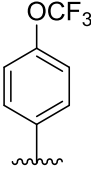
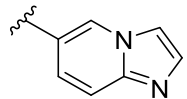
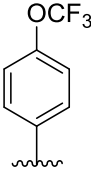
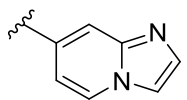
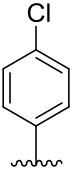
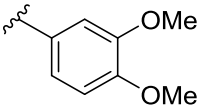
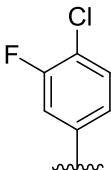
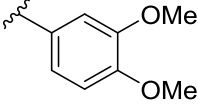
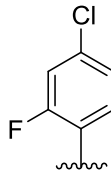
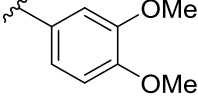
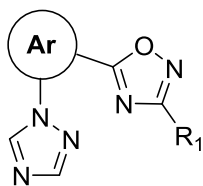
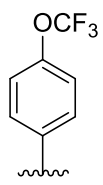
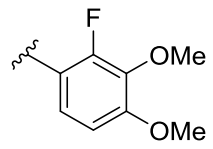
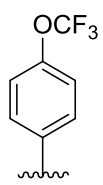
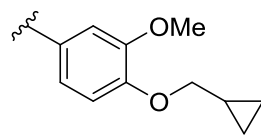
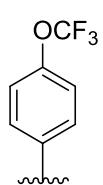
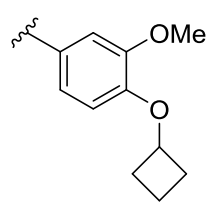
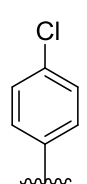
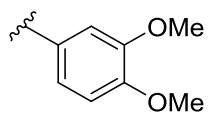
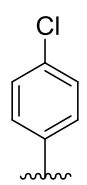
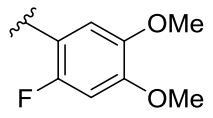
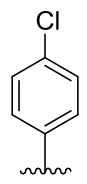
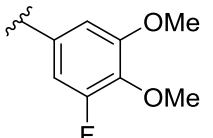
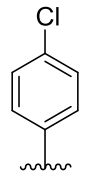
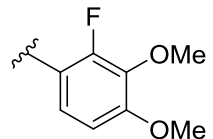
		1.265	VU6017728	Inactive	N/A
		1.266	VU6017974	Inactive	N/A
		1.267	VU6017973	Inactive	N/A
		1.268	VU6017975	Inactive	N/A
		1.269	VU6017725	> 10	34%
		1.270	VU6017742	> 10	43%
		1.271	VU6017984	Inactive	N/A

Table 1.12: SAR of 1.3.4-oxadiazole analogs **1.250-1.271**



1.275 - 1.288

Ar	R ₁ =	Compound Number	VOID	mGlu ₇ IC ₅₀ (μM)	mGlu ₇ % L-AP ₄ _{min}
		1.275	VU6018310	1.16	23%
		1.276	VU6018223	> 10	23%
		1.277	VU6018225	Inactive	N/A
		1.278	VU6017716	> 10	58%
		1.279	VU6017737	> 10	55%

		1.280	VU6017717	> 10	52%
		1.281	VU6017735	2.6	22%
		1.282	VU6017736	> 10	29%
		1.283	VU6017743	1.18	30%
		1.284	VU6018227	3.65	47%
		1.285	VU6018229	2.75	52%
		1.286	VU6018231	Inactive	N/A

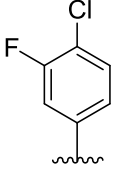
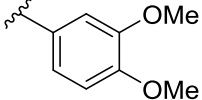
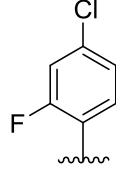
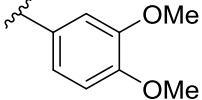
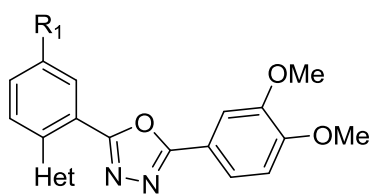
		1.287	VU6017978	> 10	52%
		1.288	VU6017979	1.03	46%

Table 1.13: SAR of 1,2,4-oxadiazole analogs **1.275-1.288**

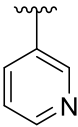
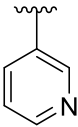
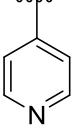
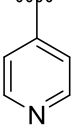
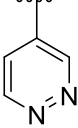
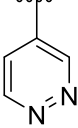
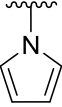
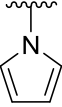
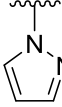
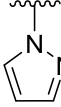
As a whole, 1,3,4-oxadiazole analogs were more potent and possessed more favorable DMPK parameters than 1,2,4-oxadiazole analogs. However, as was observed before with the other scaffolds, SAR was steep. Modifications to the eastern aromatic ring were not tolerated, and incorporation of bulky alkoxy groups at the 4-position (like those of **1.127**) did not contribute to an increase in potency or efficacy. The OCF₃ group on the western aromatic ring was found to be the optimal substituent in these cases.

However, the absence of the N-H bond of the amide led us to hypothesize that an intramolecular hydrogen bond was no longer critical for activity, meaning that the southern 1,2,4-triazole heterocycle may not be optimal for analogs of this nature. Therefore, different saturated and unsaturated *N*-linked heterocycles and *C*-linked heterocycles were surveyed for the 1,3,4-oxadiazole variants (**Table 1.14**).



1.289 - 1.315

R ₁ =	Het	Compound Number	VOID	mGlu ₇ IC ₅₀ (μM)	mGlu ₇ % L-AP ₄ _{min}
OCF ₃		1.289	VU6019274	3.53	49%
Cl		1.290	VU6019275	Inactive	N/A
OCF ₃		1.291	VU6019280	1.32	21%
Cl		1.292	VU6019281	1.48	36%
OCF ₃		1.293	VU6019282	2.24	10%
Cl		1.294	VU6019283	1.59	27%
OCF ₃		1.295	VU6019496	Inactive	N/A
Cl		1.296	VU6019493	Inactive	N/A

OCF ₃		1.297	VU6019494	Inactive	N/A
Cl		1.298	VU6019488	Inactive	N/A
OCF ₃		1.299	VU6019486	> 10	28%
Cl		1.300	VU6019489	Inactive	N/A
OCF ₃		1.301	VU6019487	> 10	28%
Cl		1.302	VU6019490	> 10	53%
OCF ₃		1.303	VU6019485	> 10	43%
Cl		1.304	VU6019484	Inactive	N/A
OCF ₃		1.305	VU6019279	2.04	51%
Cl		1.306	VU6019276	Inactive	N/A

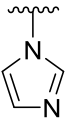
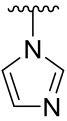
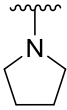
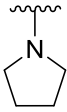
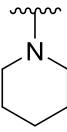
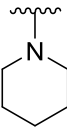
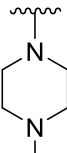
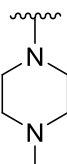
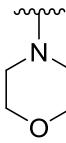
OCF ₃		1.307	VU6019278	0.57	6%
Cl		1.308	VU6019277	0.82	17%
OCF ₃		1.309	VU6020234	Inactive	N/A
Cl		1.310	VU6020232	Inactive	N/A
OCF ₃		1.311	VU6020230	5.86	65%
Cl		1.312	VU6020228	Inactive	N/A
OCF ₃		1.313	VU6020233	Inactive	N/A
Cl		1.314	VU6020229	Inactive	N/A
OCF ₃		1.315	VU6020231	1.18	23%

Table 1.14: SAR of 1,3,4-oxadiazole: southern heterocyclic ring – analogs **1.289-1.315**

As a whole, C-linked heterocycles were unproductive, either resulting in inactive compounds or compounds that lacked considerably in potency when compared to the parent 1,3,4-oxadiazole analog **1.231**. While the incorporation of saturated azacine (pyrrolidine, piperidine, morpholine, and *N*-Me piperazine) heterocycles yielded a similar result, we discovered that the incorporation of an imidazole ring (analog **1.307**) was optimal, with potency comparable to **1.23** (VU6010608). We were pleased that we were no longer limited to the intramolecular hydrogen bond restraints of the 1,2,4-triazole heterocycle, and we were excited to examine compound **1.307** further. **1.307** possessed low predicted hepatic clearance in rat ($CL_{\text{hep}} = 27.7 \text{ mL/min/kg}$) and high CNS penetration ($K_p = 4.9$, $K_{p,uu} = 0.65$).⁹¹

Conclusion

In conclusion, we have discovered three mGlu₇ NAM tool compounds containing a previously unexplored chemotype. These tool compounds include VU6010608 (**1.23**), VU6012962 (**1.127**), and VU6019278 (**1.307**) (**Figure 1.12**). Both **1.127** and **1.307** were developed to address two different metabolic liabilities of our first generation *in vitro* tool compound **1.23**. With collaboration with the Conn lab, we were able to show that **1.127** shows utility as an *in vivo* tool compound, while efforts are still ongoing with **1.307** to fully explore its potential as an alternative tool compound. We hope that with the development of these mGlu₇ selective NAMs, we can begin to learn more about the physiological role of mGlu₇ and any potential therapeutic avenues for mGlu₇ that may come as a result of these studies.

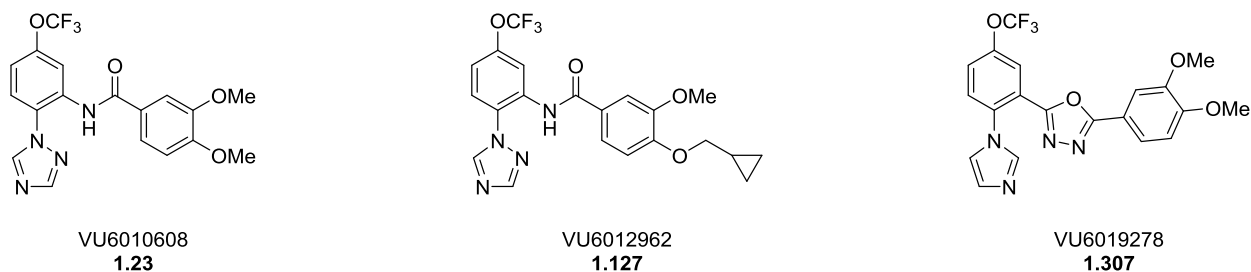


Figure 1.12: Structures of novel mGlu₇ NAM tool compounds **1.23**, **1.127**, and **1.307**

Experimental Methods

General Synthetic Methods and Instrumentation

Unless otherwise stated, all reactions were conducted in flame-dried or oven-dried glassware under inert atmospheres of argon. All commercially available reagents and reaction solvents were used as received, unless otherwise noted. All NMR spectra were recorded on a 400 MHz AMX Bruker NMR spectrometer. ¹H and ¹³C chemical shifts are reported in δ values in ppm downfield with the deuterated solvent as the internal standard. Data are reported as follows: chemical shift, multiplicity (s = singlet, d = doublet, t = triplet, q = quartet, b = broad, m = multiplet), integration, coupling constant (Hz). Low resolution mass spectra were obtained on an Agilent 6120 or 6150 with ESI source. MS parameters were as follows: fragmentor: 70, capillary voltage: 3000 V, nebulizer pressure: 30 psig, drying gas flow: 13 L/min, drying gas temperature: 350 °C. Samples were introduced via an Agilent 1290 UHPLC comprised of a G4220A binary pump, G4226A ALS, G1316C TCC, and G4212A DAD with ULD flow cell. UV absorption was generally observed at 215 nm and 254 nm with a 4 nm bandwidth.

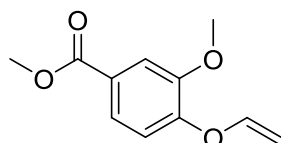
Column: Waters Acquity BEH C18, 1.0 x 50 mm, 1.7 μm . Gradient conditions: 5% to 95% CH_3CN in H_2O (0.1% TFA) over 1.4 min, hold at 95% CH_3CN for 0.1 min, 0.5 mL/min, 55 $^\circ\text{C}$. High resolution mass spectra were obtained on an Agilent 6540 UHD Q-TOF with ESI source. MS parameters were as follows: fragmentor: 150, capillary voltage: 3500 V, nebulizer pressure: 60 psig, drying gas flow: 13 L/min, drying gas temperature: 275 $^\circ\text{C}$. Samples were introduced via an Agilent 1200 UHPLC comprised of a G4220A binary pump, G4226A ALS, G1316C TCC, and G4212A DAD with ULD flow cell. UV absorption was observed at 215 nm and 254 nm with a 4 nm bandwidth.

Column: Agilent Zorbax Extend C18, 1.8 μm , 2.1 x 50 mm. Gradient conditions: 5% to 95% CH_3CN in H_2O (0.1% formic acid) over 1 min, hold at 95% CH_3CN for 0.1 min, 0.5 mL/min, 40 $^\circ\text{C}$. For compounds that were purified on a Gilson preparative reversed-phase HPLC, the system comprised of a 333 aqueous pump with solvent-selection valve, 334 organic pump, GX-271 or GX-281 liquid handler, two column switching valves, and a 155 UV detector. UV wavelength for fraction collection was user-defined, with absorbance at 254 nm always monitored.

Method 1: Phenomenex Axiapacked Luna C18, 30 x 50 mm, 5 μm column. Mobile phase: CH_3CN in H_2O (0.1% TFA). Gradient conditions: 0.75 min equilibration, followed by user defined gradient (starting organic percentage, ending S3 organic percentage, duration), hold at 95% CH_3CN in H_2O (0.1% TFA) for 1 min, 50 mL/min, 23 $^\circ\text{C}$.

Method 2: Phenomenex Axia-packed Gemini C18, 50 x 250 mm, 10 μm column. Mobile phase: CH_3CN in H_2O (0.1% TFA). Gradient conditions: 7 min equilibration, followed by user defined gradient (starting organic percentage, ending organic percentage, duration), hold at 95% CH_3CN in H_2O (0.1% TFA) for 7 min, 120 mL/min, 23 $^\circ\text{C}$. All reagents were purchased from Aldrich

Chemical Co. and were used without purification. Sure-Seal solvents were purchased from Sigma Aldrich. Analytical thin layer chromatography was performed on 250 μM silica gel 60 F₂₅₄ plates. Visualization was accomplished with UV light, and/or the use of potassium permanganate or Seebach stain followed by development with a heat gun.



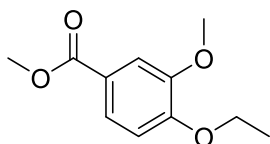
Synthesis of methyl 3-methoxy-4-(vinylloxy)benzoate (1.316)

An oven dried vial was sequentially charged with methyl vanillate (250 mg, 1.37 mmol), sodium carbonate (51.9 mg, 0.480 mmol), chloro(1,5-cyclooctadiene)iridium(I) dimer (9.21 mg, 0.0137 mmol), toluene (1.0 mL), and vinyl acetate (0.253 mL, 2.74 mmol).

The resulting solution was degassed by vigorously bubbling argon through the reaction mixture for two minutes. The vial was then heated to 110 °C, monitoring the reaction by LCMS. After 3 hours, the reaction was allowed to cool to room temperature and was filtered through a pad of celite. The resulting organic material was concentrated and purified using flash chromatography (Teledyne ISCO system; silica gel column; hexanes:EtOAc) to afford the desired material as a yellow oil (165 mg, 58% yield). ¹H NMR (400 MHz, CDCl₃) δ 7.64 (dd, J = 8.0 Hz, 1.9 Hz, 1H), 7.61 (d, J = 1.9 Hz, 1H), 7.00 (d, J = 8.3 Hz, 1H), 6.62 (dd, J = 12.0 Hz, 6.0 Hz, 1H), 4.87 (dd, J = 12.0 Hz, 2.0 Hz, 1H), 4.54 (dd, J = 4.0 Hz, 2.0 Hz, 1H), 3.93 (s, 3H), 3.90 (s, 3H); ¹³C NMR (100 MHz, CDCl₃) δ = 166.7, 149.8, 149.6, 147.7, 125.7, 123.2, 116.5, 113.3, 96.8, 56.3, 52.3 ppm. HRMS (TOF, ES⁺) calc'd for C₁₁H₁₂O₄, 208.0736; found, 208.0737.

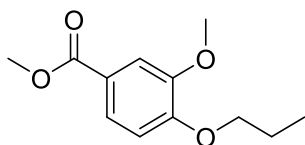
General Procedure 1: Synthesis of Esters

To a suspension of methyl vanillate (100 mg, 0.549 mmol) and potassium carbonate (154 mg, 1.10 mmol) in DMF (1 mL) was added the appropriate alkyl halide (1.10 mmol) at room temperature. The resulting suspension was then heated to 100 °C and was monitored by LCMS. Once LCMS indicated complete consumption of starting material, the reaction was diluted with DCM and quenched with the addition of water. The layers were separated, and the aqueous layer was washed with DCM x 3. The combined organic material was passed through a phase separator, concentrated, and purified via flash chromatography (Teledyne ISCO system, silica gel column, hexanes:EtOAc) to afford the desired products.



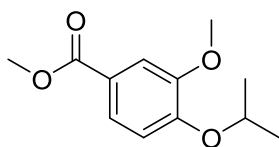
Synthesis of methyl 4-ethoxy-3-methoxybenzoate (1.100a)

This compound was synthesized according to general procedure 1. White solid (113.1 mg, 98% yield). ¹H NMR (400 MHz, CDCl₃) δ 7.65 (dd, *J* = 8.4 Hz, 2.0 Hz, 1H), 7.54 (d, *J* = 2.0 Hz, 1H), 6.86 (d, *J* = 8.4 Hz, 1H), 4.15 (q, 2H), 3.91 (s, 3H), 3.88 (s, 3H), 1.48 (t, 3H); ¹³C NMR (100 MHz, CDCl₃) δ = 167.1, 152.5, 148.9, 123.7, 122.6, 112.4, 111.4, 64.6, 56.2, 52.1, 14.8 ppm. HRMS (TOF, ES⁺) calc'd for C₁₁H₁₄O₄, 210.0892; found, 210.0890.



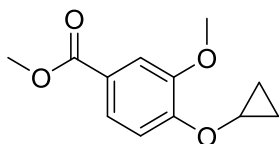
Synthesis of methyl 3-methoxy-4-propoxybenzoate (1.100b)

This compound was synthesized according to general procedure 1. Colorless oil (120.5 mg, 98% yield). ^1H NMR (400 MHz, CDCl_3) δ 7.63 (dd, $J = 8.4$ Hz, 2.0 Hz, 1H), 7.53 (d, $J = 2.0$ Hz, 1H), 6.86 (d, $J = 8.5$ Hz, 1H), 4.01 (t, 2H), 3.90 (s, 3H), 3.87 (s, 3H), 1.87 (m, 2H), 1.03 (t, 3H); ^{13}C NMR (100 MHz, CDCl_3) $\delta = 167.1, 152.8, 149.0, 123.7, 122.5, 112.5, 111.6, 70.6, 56.2, 52.1, 22.5, 10.5$ ppm. HRMS (TOF, ES+) calc'd for $\text{C}_{12}\text{H}_{16}\text{O}_4$, 224.1049; found, 224.1047.



Synthesis of methyl 4-isopropoxy-3-methoxybenzoate (1.100c)

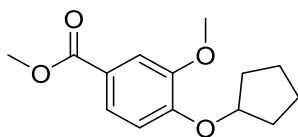
This compound was synthesized according to general procedure 1. Colorless oil (117.3 mg, 94% yield). ^1H NMR (400 MHz, CDCl_3) δ 7.62 (dd, $J = 8.5$ Hz, 2.0 Hz, 1H), 7.53 (d, $J = 2.0$ Hz, 1H), 6.87 (d, $J = 8.5$ Hz, 1H), 4.62 (m, 1H), 3.88 (s, 3H), 3.87 (s, 3H), 1.38 (d, 6H); ^{13}C NMR (100 MHz, CDCl_3) $\delta = 167.0, 151.6, 149.6, 123.5, 113.4, 112.7, 71.3, 56.1, 52.0, 22.0$ ppm. HRMS (TOF, ES+) calc'd for $\text{C}_{12}\text{H}_{16}\text{O}_4$, 224.1049; found, 224.1046.



Synthesis of methyl 4-cyclopropoxy-3-methoxybenzoate (1.100d)

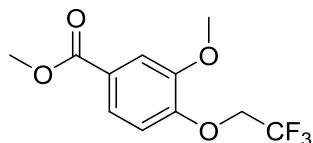
To a solution of methyl 3-methoxy-4-(vinylloxy)benzoate **C** (115 mg, 0.552 mmol) and diiodomethane (0.356 mL, 4.42 mmol) in DCE (2.0 mL) at 0 °C was added diethylzinc (4.42 mL, 4.42 mmol, 1.0 M solution in hexanes) dropwise. After the addition was

complete, the flask was allowed to slowly warm to room temperature, stirring for an additional 16 hours. The reaction was diluted with DCM, quenched with the addition of saturated NH_4Cl , and filtered through a pad of celite. The layers were separated, and the aqueous layer was washed with DCM x 3. The combined organic material was passed through a phase separator, concentrated, and purified using flash chromatography (Teledyne ISCO system; silica gel column; hexanes:EtOAc) to afford the desired material **7e** as a slight yellow oil (74.1 mg, 60% yield). ^1H NMR (400 MHz, CDCl_3) δ 7.67 (dd, $J = 8.0$ Hz, 2.0 Hz, 1H), 7.53 (d, $J = 1.9$ Hz, 1H), 7.27 (d, $J = 8.4$ Hz, 1H), 3.90 (s, 3H), 3.89 (s, 3H), 3.80 (m, 1H), 0.90-0.83 (m, 4H); ^{13}C NMR (100 MHz, CDCl_3) $\delta = 167.0, 152.6, 148.6, 123.5, 123.1, 112.7, 112.2, 56.1, 52.1, 51.9, 6.5$ ppm. HRMS (TOF, ES+) calc'd for $\text{C}_{12}\text{H}_{14}\text{O}_4$, 222.0892; found, 222.0892.



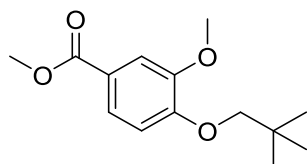
Synthesis of methyl 4-(cyclopentyloxy)-3-methoxybenzoate (1.100e)

This compound was synthesized according to general procedure 1. Colorless oil (131.4 mg, 96% yield). ^1H NMR (400 MHz, CDCl_3) δ 7.62 (dd, $J = 8.4$ Hz, 2.0 Hz, 1H), 7.51 (d, $J = 1.9$ Hz, 1H), 6.85 (d, $J = 8.4$ Hz, 1H), 4.81 (m, 1H), 3.87 (s, 3H), 3.86 (s, 3H), 1.98-1.77 (m, 6H), 1.64-1.56 (m, 2H); ^{13}C NMR (100 MHz, CDCl_3) $\delta = 167.0, 152.0, 149.4, 123.5, 122.2, 113.1, 112.6, 80.5, 56.1, 52.0, 32.9, 24.2$ ppm. HRMS (TOF, ES+) calc'd for $\text{C}_{14}\text{H}_{18}\text{O}_4$, 250.1205; found, 250.1204.



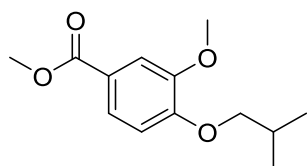
Synthesis of methyl 3-methoxy-4-(2,2,2-trifluoroethoxy)benzoate (1.100f)

This compound was synthesized according to general procedure 1. White solid (273 mg, 94% yield). $^1\text{H NMR}$ (400 MHz, CDCl_3) δ 7.64 (dd, $J = 8.4, 2.0$ Hz, 1H), 7.60 (d, $J = 1.9$ Hz, 1H), 6.96 (d, $J = 8.4$ Hz, 1H), 4.45 (q, 2H), 3.93 (s, 3H), 3.90 (s, 3H); $^{13}\text{C NMR}$ (100 MHz, CDCl_3) $\delta = 166.6, 150.7, 149.9, 125.7, 123.4$ (q, $J_{\text{CF}} = 277.0$ Hz), 123.3, 115.6, 113.5, 67.4 (q, $J_{\text{CF}} = 35.5$ Hz), 56.2, 52.3 ppm. HRMS (TOF, ES+) calc'd for $\text{C}_{11}\text{H}_{11}\text{F}_3\text{O}_4$, 264.0609; found, 264.0613.



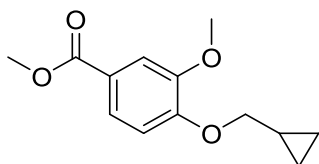
Synthesis of methyl 3-methoxy-4-(neopentyloxy)benzoate (1.100g)

This compound was synthesized according to general procedure 1. Colorless oil (219 mg, 79% yield). $^1\text{H NMR}$ (400 MHz, CDCl_3) δ 7.64 (dd, $J = 8.4, 2.0$ Hz, 1H), 7.54 (d, $J = 2.0$ Hz, 1H), 6.86 (d, $J = 8.4$ Hz, 1H), 3.89 (s, 3H), 3.88 (s, 3H), 3.67 (s, 2H), 1.06 (s, 9H); $^{13}\text{C NMR}$ (100 MHz, CDCl_3) $\delta = 167.1, 153.7, 149.3, 123.7, 122.4, 113.2, 112.0, 78.9, 56.4, 52.0, 32.2, 26.7$ ppm. HRMS (TOF, ES+) calc'd for $\text{C}_{14}\text{H}_{20}\text{O}_4$, 252.1362; found, 252.1366.



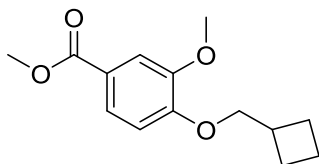
Synthesis of methyl 4-isobutoxy-3-methoxybenzoate (1.100h)

This compound was synthesized according to general procedure 1. White solid (249 mg, 95% yield). ^1H NMR (400 MHz, CDCl_3) δ 7.64 (dd, $J = 8.4, 2.0$ Hz, 1H), 7.54 (d, $J = 2.0$ Hz, 1H), 6.86 (d, $J = 8.4$ Hz, 1H), 3.90 (s, 3H), 3.88 (s, 3H), 3.82 (d, 2H), 2.18 (m, 1H), 1.04 (d, 6H); ^{13}C NMR (100 MHz, CDCl_3) $\delta = 167.1, 153.0, 149.1, 123.7, 122.5, 112.7, 111.7, 75.4, 56.3, 52.1, 28.2, 19.4$ ppm. HRMS (TOF, ES+) calc'd for $\text{C}_{13}\text{H}_{18}\text{O}_4$, 238.1205; found, 238.1206.



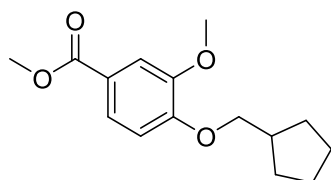
Synthesis of methyl 4-(cyclopropylmethoxy)-3-methoxybenzoate (1.100i)

This compound was synthesized according to general procedure 1. White solid (249 mg, 96% yield). ^1H NMR (400 MHz, CDCl_3) δ 7.63 (dd, $J = 8.4, 2.0$ Hz, 1H), 7.54 (d, $J = 1.9$ Hz, 1H), 6.86 (d, $J = 8.4$ Hz, 1H), 3.92 (s, 3H), 3.91 (d, 2H), 3.88 (s, 3H), 1.37-1.31 (m, 1H), 0.69-0.64 (m, 2H), 0.39-0.35 (m, 2H); ^{13}C NMR (100 MHz, CDCl_3) $\delta = 167.1, 152.7, 149.0, 123.6, 122.7, 112.4, 111.8, 74.0, 56.2, 52.1, 10.2, 3.6$ ppm. HRMS (TOF, ES+) calc'd for $\text{C}_{13}\text{H}_{16}\text{O}_4$, 236.1049; found, 236.1052.



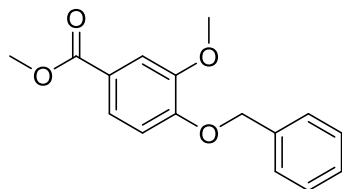
Synthesis of methyl 4-(cyclobutylmethoxy)-3-methoxybenzoate (1.100j)

This compound was synthesized according to general procedure 1. White solid (258 mg, 94% yield). ^1H NMR (400 MHz, CDCl_3) δ 7.64 (dd, $J = 8.4, 2.0$ Hz, 1H), 7.53 (d, $J = 2.0$ Hz, 1H), 6.87 (d, $J = 8.4$ Hz, 1H), 4.04 (d, 2H), 3.90 (s, 3H), 3.89 (s, 3H), 2.91-2.81 (m, 1H), 2.21-2.13 (m, 2H), 2.00-1.82 (m, 4H); ^{13}C NMR (100 MHz, CDCl_3) $\delta = 167.1, 153.0, 149.1, 123.6, 122.6, 112.7, 111.9, 73.3, 56.2, 52.1, 34.5, 25.2, 18.8$ ppm. HRMS (TOF, ES+) calc'd for $\text{C}_{14}\text{H}_{18}\text{O}_4$, 250.1205; found, 250.1207.



Synthesis of methyl 4-(cyclopentylmethoxy)-3-methoxybenzoate (1.100k)

This compound was synthesized according to general procedure 1. Colorless oil (244 mg, 84% yield). ^1H NMR (400 MHz, CDCl_3) δ 7.64 (dd, $J = 8.4, 2.0$ Hz, 1H), 7.54 (d, $J = 2.0$ Hz, 1H), 6.88 (d, $J = 8.4$ Hz, 1H), 3.93 (d, 2H), 3.90 (s, 3H), 3.88 (s, 3H), 2.45 (m, 1H), 1.90-1.83 (m, 2H), 1.68-1.57 (m, 4H), 1.41-1.34 (m, 2H); ^{13}C NMR (100 MHz, CDCl_3) $\delta = 167.1, 153.1, 149.1, 123.7, 122.5, 112.7, 111.8, 73.4, 56.3, 52.1, 39.0, 29.7, 25.4$ ppm. HRMS (TOF, ES+) calc'd for $\text{C}_{15}\text{H}_{20}\text{O}_4$, 264.1362; found, 264.1367.



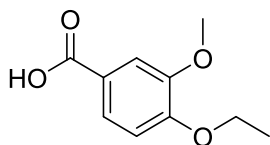
Synthesis of methyl 4-(benzyloxy)-3-methoxybenzoate (1.100L)

This compound was synthesized according to general procedure 1. White solid (278 mg, 93% yield). ^1H NMR (400 MHz, CDCl_3) δ 7.61 (dd, $J = 8.4, 2.0$ Hz, 1H), 7.57 (d, $J =$

2.0 Hz, 1H), 7.44-7.30 (m, 5H), 6.90 (d, $J = 8.4$ Hz, 1H), 5.21 (s, 2H), 3.94 (s, 3H), 3.88 (s, 3H); ^{13}C NMR (100 MHz, CDCl_3) $\delta = 167.0, 152.2, 149.3, 136.5, 128.8, 128.2, 127.3, 123.5, 123.1, 112.58, 112.56, 70.9, 56.2, 52.1$ ppm. HRMS (TOF, ES+) calc'd for $\text{C}_{16}\text{H}_{16}\text{O}_4$, 272.1049; found, 272.1049.

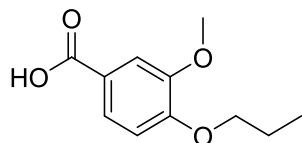
General Procedure 2: Synthesis of Benzoic Acids

To a solution of the appropriate methyl ester (1.0 eq) in THF: H₂O (1:1; 0.2 M) was added lithium hydroxide (1.5 eq). The resulting reaction was heated to 60 °C and monitored by LCMS. After 2 hours, the reaction was allowed to cool to room temperature before the organic solvent was removed *in vacuo*. The resulting aqueous solution was acidified to pH = 2 using 2 M HCl, which resulted in a white precipitate crashing out of solution. This white solid was collected via vacuum filtration, dried *in vacuo*, and carried forward to the next step without any further purification.



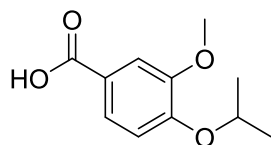
Synthesis of 4-ethoxy-3-methoxybenzoic acid (1.102a)

This compound was synthesized according to general procedure 2. White solid (88.8 mg, quantitative yield). ^1H NMR (400 MHz, DMSO-d_6) δ 7.54 (dd, $J = 8.4$ Hz, 2.0 Hz, 1H), 7.44 (d, $J = 2.0$ Hz, 1H), 7.02 (d, $J = 8.4$ Hz, 1H), 4.08 (q, 2H), 3.80 (s, 3H), 1.34 (t, 3H); ^{13}C NMR (100 MHz, DMSO-d_6) $\delta = 167.1, 151.9, 148.3, 123.1, 122.8, 112.0, 111.7, 63.8, 55.4, 14.6$ ppm. HRMS (TOF, ES+) calc'd for $\text{C}_{10}\text{H}_{12}\text{O}_4$, 196.0736; found, 196.0734.



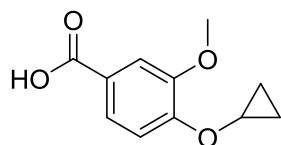
Synthesis of 3-methoxy-4-propoxybenzoic acid (1.102b)

This compound was synthesized according to general procedure 2. White solid (95.3 mg, quantitative yield). ^1H NMR (400 MHz, DMSO- d_6) δ 7.54 (dd, J = 8.4 Hz, 2.0 Hz, 1H), 7.44 (d, J = 1.9 Hz, 1H), 7.02 (d, J = 8.5 Hz, 1H), 3.98 (t, 2H), 3.80 (s, 3H), 1.75 (m, 2H), 0.97 (t, 3H); ^{13}C NMR (100 MHz, DMSO- d_6) δ = 167.1, 152.0, 148.4, 123.2, 122.8, 112.1, 111.8, 69.7, 55.5, 22.0, 10.4 ppm. HRMS (TOF, ES+) calc'd for $\text{C}_{11}\text{H}_{14}\text{O}_4$, 210.0892 ; found, 210.0889.



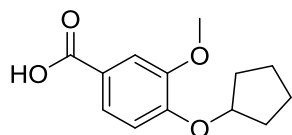
Synthesis of 4-isopropoxy-3-methoxybenzoic acid (1.102c)

This compound was synthesized according to general procedure 2. White solid (112.1 mg, quantitative yield). ^1H NMR (400 MHz, DMSO- d_6) δ 7.53 (dd, J = 8.0 Hz, 2.0 Hz, 1H), 7.44 (d, J = 2.0 Hz, 1H), 7.04 (d, J = 8.6 Hz, 1H), 4.67 (m, 1H), 3.78 (s, 3H), 1.28 (d, 6H); ^{13}C NMR (100 MHz, DMSO- d_6) δ = 167.1, 150.8, 149.0, 123.1, 122.7, 113.3, 112.4, 70.2, 55.4, 21.8 ppm. HRMS (TOF, ES+) calc'd for $\text{C}_{11}\text{H}_{14}\text{O}_4$, 210.0892 ; found, 210.0892.



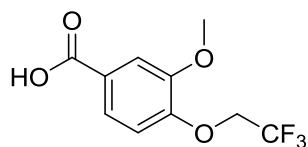
Synthesis of 4-cyclopropoxy-3-methoxybenzoic acid (1.102d)

This compound was synthesized according to general procedure 2. White solid (112.4 mg, quantitative yield). ^1H NMR (400 MHz, DMSO- d_6) δ 7.58 (dd, J = 8.4 Hz, 1.9 Hz, 1H), 7.44 (d, J = 1.8 Hz, 1H), 7.32 (d, J = 8.4 Hz, 1H), 3.89 (m, 1H), 3.77 (s, 3H), 0.83-0.78 (m, 2H), 0.70-0.66 (m, 2H); ^{13}C NMR (100 MHz, DMSO- d_6) δ = 167.1, 151.9, 148.2, 123.4, 123.0, 112.9, 112.0, 55.4, 51.4, 5.9 ppm. HRMS (TOF, ES+) calc'd for $\text{C}_{11}\text{H}_{12}\text{O}_4$, 208.0736; found, 208.0735.



Synthesis of 4-(cyclopentyloxy)-3-methoxybenzoic acid (1.102e)

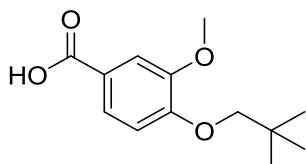
This compound was synthesized according to general procedure 2. White solid (122.0 mg, quantitative yield). ^1H NMR (400 MHz, DMSO- d_6) δ 7.53 (dd, J = 8.0 Hz, 2.0 Hz, 1H), 7.43 (d, J = 2.0 Hz, 1H), 7.01 (d, J = 8.5 Hz, 1H), 4.86 (m, 1H), 3.78 (s, 3H), 1.96-1.90 (m, 2H), 1.73-1.68 (m, 4H), 1.61-1.54 (m, 2H); ^{13}C NMR (100 MHz, DMSO- d_6) δ = 167.1, 151.0, 148.9, 123.1, 122.6, 113.1, 112.3, 79.6, 55.4, 32.3, 23.7 ppm. HRMS (TOF, ES+) calc'd for $\text{C}_{13}\text{H}_{16}\text{O}_4$, 236.1049; found, 236.1050.



Synthesis of 3-methoxy-4-(2,2,2-trifluoroethoxy)benzoic acid (1.102f)

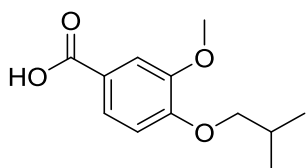
This compound was synthesized according to general procedure 2. White solid (225 mg, 95% yield). ^1H NMR (400 MHz, DMSO- d_6) δ 7.55 (dd, J = 8.4, 1.9 Hz, 1H), 7.51 (d,

$J = 1.9$ Hz, 1H), 7.17 (d, $J = 8.4$ Hz, 1H), 4.81 (q, 2H), 3.84 (s, 3H); ^{13}C NMR (100 MHz, DMSO- d_6) $\delta = 166.9, 149.9, 148.6, 125.1, 123.9$ (q, $J_{\text{CF}} = 277.0$ Hz), 122.7, 113.6, 112.7, 65.3 (q, $J_{\text{CF}} = 34.1$ Hz), 55.7 ppm. HRMS (TOF, ES+) calc'd for $\text{C}_{10}\text{H}_9\text{F}_3\text{O}_4$, 250.0453; found, 250.0454.



Synthesis of 3-methoxy-4-(neopentyloxy)benzoic acid (1.102g)

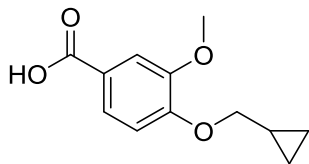
This compound was synthesized according to general procedure 2. White solid (166 mg, 88% yield). ^1H NMR (400 MHz, DMSO- d_6) δ 7.54 (dd, $J = 8.4, 1.9$ Hz, 1H), 7.44 (d, $J = 1.9$ Hz, 1H), 7.02 (d, $J = 8.4$ Hz, 1H), 3.81 (s, 3H), 3.68 (s, 2H), 1.00 (s, 9H); ^{13}C NMR (100 MHz, DMSO- d_6) $\delta = 167.1, 152.6, 148.5, 123.3, 122.8, 112.5, 112.1, 77.9, 55.8, 31.7, 26.3$ ppm. HRMS (TOF, ES+) calc'd for $\text{C}_{13}\text{H}_{18}\text{O}_4$, 238.1205; found, 238.1207.



Synthesis of 4-isobutoxy-3-methoxybenzoic acid (1.102h)

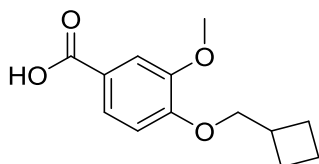
This compound was synthesized according to general procedure 2. White solid (188 mg, 91% yield). ^1H NMR (400 MHz, DMSO- d_6) δ 7.54 (dd, $J = 8.4, 1.9$ Hz, 1H), 7.44 (d, $J = 1.8$ Hz, 1H), 7.02 (d, $J = 8.4$ Hz, 1H), 3.80 (s, 3H), 3.79 (d, 2H), 2.04 (m, 1H), 0.97 (d, 6H); ^{13}C NMR (100 MHz, DMSO- d_6) $\delta = 167.1, 152.2, 148.5, 123.2, 122.8, 112.2,$

111.9, 74.4, 55.6, 27.7, 19.0 ppm. HRMS (TOF, ES+) calc'd for C₁₂H₁₆O₄, 224.1049; found, 224.1051.



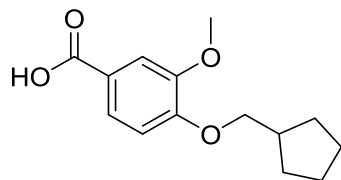
Synthesis of 4-(cyclopropylmethoxy)-3-methoxybenzoic acid (1.102i)

This compound was synthesized according to general procedure 2. White solid (199 mg, 96% yield). ¹H NMR (400 MHz, DMSO-d₆) δ 7.52 (dd, *J* = 8.4, 1.9 Hz, 1H), 7.44 (d, *J* = 1.9 Hz, 1H), 6.99 (d, *J* = 8.5 Hz, 1H), 3.86 (d, 2H), 3.81 (s, 3H), 1.28-1.19 (m, 1H), 0.60-0.55 (m, 2H), 0.34-0.30 (m, 2H); ¹³C NMR (100 MHz, DMSO-d₆) δ = 167.1, 152.0, 148.3, 123.1, 122.8, 112.0, 111.8, 72.8, 55.4, 10.1, 3.2 ppm. HRMS (TOF, ES+) calc'd for C₁₂H₁₄O₄, 222.0892; found, 222.0894.



Synthesis of 4-(cyclobutylmethoxy)-3-methoxybenzoic acid (1.102j)

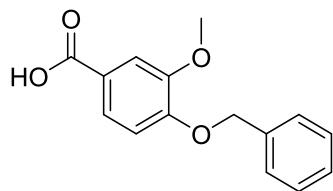
This compound was synthesized according to general procedure 2. White solid (202 mg, 93% yield). ¹H NMR (400 MHz, DMSO-d₆) δ 7.54 (dd, *J* = 8.4, 1.9 Hz, 1H), 7.43 (d, *J* = 1.9 Hz, 1H), 7.03 (d, *J* = 8.5 Hz, 1H), 4.00 (d, 2H), 3.79 (s, 3H), 2.72 (m, 1H), 2.11-2.03 (m, 2H), 1.94-1.78 (m, 4H); ¹³C NMR (100 MHz, DMSO-d₆) δ = 167.1, 152.2, 148.4, 123.2, 122.9, 112.2, 112.0, 72.3, 55.5, 33.9, 24.4, 18.1 ppm. HRMS (TOF, ES+) calc'd for C₁₃H₁₆O₄, 236.1049; found, 236.1051.



Synthesis of 4-(cyclopentylmethoxy)-3-methoxybenzoic acid (1.102k)

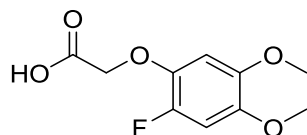
This compound was synthesized according to general procedure 2. White solid (190 mg, 91% yield). ^1H NMR (400 MHz, DMSO- d_6) δ 7.53 (dd, J = 8.4, 1.7 Hz, 1H), 7.44 (d, J = 1.6 Hz, 1H), 7.03 (d, J = 8.4 Hz, 1H), 3.89 (d, 2H), 3.80 (s, 3H), 2.32 (m, 1H), 1.80-1.72 (m, 2H), 1.62-1.51 (m, 4H), 1.36-1.28 (m, 2H); ^{13}C NMR (100 MHz, DMSO- d_6) δ = 167.1, 152.2, 148.4, 123.2, 122.8, 112.2, 112.0, 72.3, 55.6, 38.4, 29.0, 24.9 ppm.

HRMS (TOF, ES+) calc'd for $\text{C}_{14}\text{H}_{18}\text{O}_4$, 250.1205; found, 250.1211.



Synthesis of 4-(benzyloxy)-3-methoxybenzoic acid (1.102L)

This compound was synthesized according to general procedure 2. White solid (242 mg, 97% yield). ^1H NMR (400 MHz, DMSO- d_6) δ 7.54 (dd, J = 8.4, 1.9 Hz, 1H), 7.47 (d, J = 1.9 Hz, 1H), 7.45-7.32 (m, 5H), 7.13 (d, J = 8.5 Hz, 1H), 5.16 (s, 2H), 3.81 (s, 3H); ^{13}C NMR (100 MHz, DMSO- d_6) δ = 167.1, 151.6, 148.6, 136.6, 128.5, 128.0, 127.9, 123.2, 123.0, 112.4, 112.2, 69.9, 55.5 ppm. HRMS (TOF, ES+) calc'd for $\text{C}_{15}\text{H}_{14}\text{O}_4$, 258.0892; found, 258.0896.

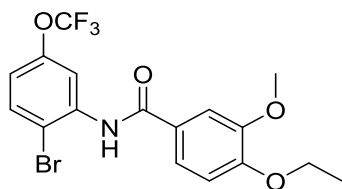


Synthesis of 2-(2-fluoro-4,5-dimethoxyphenoxy)acetic acid (1.208d)

This compound was synthesized according to general procedure 2. White solid (173 mg, 97% yield). ^1H NMR (400 MHz, DMSO- d_6) δ 6.95 (d, $J_{\text{HF}} = 12.8$ Hz, 1H), 6.80 (d, $J_{\text{HF}} = 8.4$ Hz, 1H), 4.70 (s, 2H), 3.72 (s, 3H), 3.70 (s, 3H); ^{13}C NMR (100 MHz, DMSO- d_6) $\delta = 170.1, 145.6$ (d, $J_{\text{CF}} = 235.0$ Hz), 144.9 (d, $J_{\text{CF}} = 2.0$ Hz), 143.2 (d, $J_{\text{CF}} = 8.0$ Hz), 138.4 (d, $J_{\text{CF}} = 12.0$ Hz), 102.3 (d, $J_{\text{CF}} = 2.0$ Hz), 102.1 (d, $J_{\text{CF}} = 23.0$ Hz), 66.4, 56.4, 56.3 ppm. HRMS (TOF, ES $^+$) calc'd for $\text{C}_{10}\text{H}_{11}\text{FO}_5$, 230.0591; found, 230.0592.

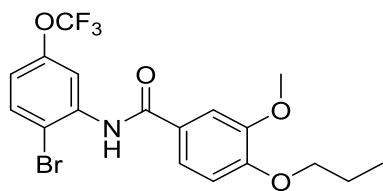
General Procedure 3: Synthesis of Benzamides

To a solution of the appropriate aniline (1.0 eq) in DCM (0.1 M) in a Biotage microwave vial was sequentially added *N,N*-diisopropylethylamine (2.0 eq), the appropriate benzoic acid (1.0 eq), and 1-(chloro-1-pyrrolidinylmethylene)pyrrolidiniumhexafluorophosphate (PyCIU) (1.0 eq). The reaction vial was sealed and heated to 100 °C for 20 minutes using a Biotage microwave reactor. After cooling to room temperature, the reaction was diluted with DCM and quenched with the addition of saturated NH_4Cl . The layers were separated, and the aqueous layer was washed with DCM x 3. The combined organic layer was passed through a phase separator, concentrated, and purified using flash chromatography (Teledyne ISCO system, silica gel column, hexanes:EtOAc).



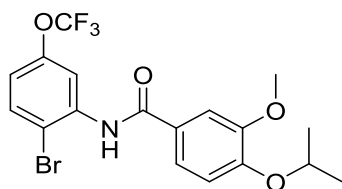
Synthesis of *N*-(2-bromo-5-(trifluoromethoxy)phenyl)-4-ethoxy-3-methoxybenzamide (1.104a)

This compound was synthesized according to general procedure 3. White solid (37.5 mg, 74% yield). ^1H NMR (400 MHz, CDCl_3) δ 8.61 (d, $J = 2.5$ Hz, 1H), 8.48 (bs, 1H), 7.58 (d, $J = 8.8$ Hz, 1H), 7.54 (d, $J = 2.1$ Hz, 1H), 7.44 (dd, $J = 8.4$ Hz, 2.1 Hz, 1H), 6.94 (d, $J = 8.4$ Hz, 1H), 6.89 (dd, $J = 8.8$ Hz, 2.0 Hz, 1H), 4.18 (q, 2H), 3.96 (s, 3H), 1.51 (t, 3H); ^{13}C NMR (100 MHz, CDCl_3) $\delta = 165.1, 152.3, 149.8, 149.2, 137.4, 132.9, 126.5, 120.6$ (q, $^1J_{\text{CF}} = 256$ Hz), 119.7, 117.2, 114.3, 111.7, 111.2, 110.7, 64.8, 56.3, 14.8 ppm. HRMS (TOF, ES+) calc'd for $\text{C}_{17}\text{H}_{15}\text{BrF}_3\text{NO}_4$, 433.0137 ; found, 433.0136.



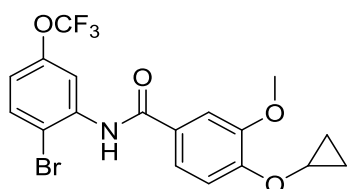
Synthesis of *N*-(2-bromo-5-(trifluoromethoxy)phenyl)-3-methoxy-4-propoxybenzamide (1.104b)

This compound was synthesized according to general procedure 3. White solid (24.6 mg, 47% yield). ^1H NMR (400 MHz, CDCl_3) δ 8.61 (d, $J = 2.4$ Hz, 1H), 8.48 (bs, 1H), 7.58 (d, $J = 8.8$ Hz, 1H), 7.54 (d, $J = 2.1$ Hz, 1H), 7.44 (dd, $J = 8.0$ Hz, 2.1 Hz, 1H), 6.94 (d, $J = 8.4$ Hz, 1H), 6.89 (dd, $J = 8.0$ Hz, 1.9 Hz, 1H), 4.06 (t, 2H), 3.95 (s, 3H), 1.91 (m, 2H), 1.07 (t, 3H); ^{13}C NMR (100 MHz, CDCl_3) $\delta = 165.1, 152.6, 149.9, 149.3, 149.2, 137.4, 132.9, 126.5, 120.6$ (q, $^1J_{\text{CF}} = 257$ Hz), 119.8, 117.2, 114.3, 111.9, 111.3, 110.7, 70.8, 56.4, 22.5, 10.6 ppm. HRMS (TOF, ES+) calc'd for $\text{C}_{18}\text{H}_{17}\text{BrF}_3\text{NO}_4$, 447.0293 ; found, 447.0288.



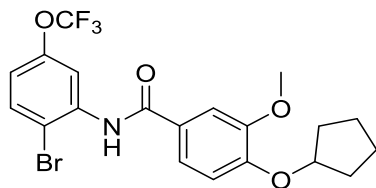
Synthesis of *N*-(2-bromo-5-(trifluoromethoxy)phenyl)-4-isopropoxy-3-methoxybenzamide (1.104c)

This compound was synthesized according to general procedure 3. White solid (56.8 mg, 65% yield). ^1H NMR (400 MHz, CDCl_3) δ 8.61 (d, $J = 2.4$ Hz, 1H), 8.48 (bs, 1H), 7.58 (d, $J = 8.8$ Hz, 1H), 7.54 (d, $J = 2.1$ Hz, 1H), 7.43 (dd, $J = 8.0$ Hz, 2.2 Hz, 1H), 6.96 (d, $J = 8.4$ Hz, 1H), 6.89 (dd, $J = 8.0$ Hz, 1.9 Hz, 1H), 4.66 (m, 1H), 3.94 (s, 3H), 1.43 (d, 6H); ^{13}C NMR (100 MHz, CDCl_3) $\delta = 165.0, 151.4, 150.5, 149.1, 137.4, 132.9, 126.5, 120.5$ (q, $^1J_{\text{CF}} = 257$ Hz), 119.6, 117.1, 114.2, 113.8, 111.5, 110.7, 71.6, 56.3, 22.1 ppm. HRMS (TOF, ES+) calc'd for $\text{C}_{18}\text{H}_{17}\text{BrF}_3\text{NO}_4$, 447.0293; found, 447.0285.



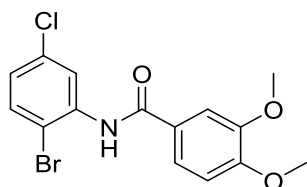
Synthesis of *N*-(2-bromo-5-(trifluoromethoxy)phenyl)-4-cyclopropoxy-3-methoxybenzamide (1.104d)

This compound was synthesized according to general procedure 3. White solid (28.6 mg, 82% yield). ^1H NMR (400 MHz, CDCl_3) δ 8.61 (d, $J = 2.2$ Hz, 1H), 8.49 (bs, 1H), 7.59 (d, $J = 8.8$ Hz, 1H), 7.54 (d, $J = 2.0$ Hz, 1H), 7.47 (dd, $J = 8.0$ Hz, 2.1 Hz, 1H), 7.35 (d, $J = 8.4$ Hz, 1H), 6.89 (m, 1H), 3.94 (s, 3H), 3.83 (m, 1H), 0.92-0.86 (m, 4H); ^{13}C NMR (100 MHz, CDCl_3) $\delta = 165.0, 152.3, 149.5, 149.2, 137.3, 132.9, 127.0, 120.5$ (q, $^1J_{\text{CF}} = 257$ Hz), 119.5, 117.2, 114.2, 113.0, 111.0, 110.7, 56.2, 52.1, 6.5 ppm. HRMS (TOF, ES+) calc'd for $\text{C}_{18}\text{H}_{15}\text{BrF}_3\text{NO}_4$, 445.0137; found, 445.0140.



Synthesis of *N*-(2-bromo-5-(trifluoromethoxy)phenyl)-4-(cyclopentyloxy)-3-methoxybenzamide (1.104e)

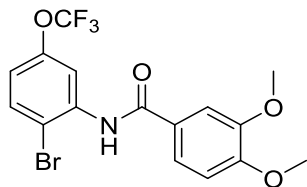
This compound was synthesized according to general procedure 3. White solid (65.7 mg, 71% yield). ^1H NMR (400 MHz, CDCl_3) δ 8.61 (d, $J = 2.4$ Hz, 1H), 8.48 (bs, 1H), 7.59 (d, $J = 8.8$ Hz, 1H), 7.53 (d, $J = 2.1$ Hz, 1H), 7.43 (dd, $J = 8.0$ Hz, 2.2 Hz, 1H), 6.94 (d, $J = 8.4$ Hz, 1H), 6.89 (dd, $J = 8.0$ Hz, 2.0 Hz, 1H), 4.86 (m, 1H), 3.93 (s, 3H), 2.03-1.84 (m, 6H), 1.68-1.63 (m, 2H); ^{13}C NMR (100 MHz, CDCl_3) $\delta = 165.1, 151.8, 150.3, 149.2, 137.4, 132.9, 126.2, 120.5$ (q, $^1J_{\text{CF}} = 255$ Hz), 119.6, 117.1, 114.2, 113.5, 111.4, 110.7, 80.8, 56.3, 33.0, 24.3 ppm. HRMS (TOF, ES+) calc'd for $\text{C}_{20}\text{H}_{19}\text{BrF}_3\text{NO}_4$, 473.0450 ; found, 473.0450.



Synthesis of *N*-(2-bromo-5-chlorophenyl)-3,4-dimethoxybenzamide (1.11b)

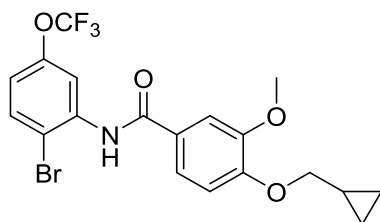
This compound was synthesized according to general procedure 3. White solid (102.1 mg, 57% yield). ^1H NMR (400 MHz, CDCl_3) δ 8.66 (d, $J = 2.5$ Hz, 1H), 8.41 (bs, 1H), 7.53 (d, $J = 2.1$ Hz, 1H), 7.48 (d, $J = 8.6$ Hz, 1H), 7.46 (dd, $J = 8.4$ Hz, 2.2 Hz, 1H), 6.99 (dd, $J = 8.6$ Hz, 2.5 Hz, 1H), 6.95 (d, $J = 8.4$ Hz, 1H), 3.97 (s, 3H), 3.96 (s, 3H); ^{13}C NMR (100 MHz, CDCl_3) $\delta = 164.9, 152.8, 149.6, 137.0, 134.7, 132.9, 126.9, 125.1,$

121.5, 119.8, 111.2, 110.9, 110.7, 56.3, 56.2 ppm. HRMS (TOF, ES+) calc'd for $C_{15}H_{13}BrClNO_3$, 368.9767 ; found, 368.9768.



Synthesis of *N*-(2-bromo-5-(trifluoromethoxy)phenyl)-3,4-dimethoxybenzamide (1.11a)

This compound was synthesized according to general procedure 3. White solid (32.6 mg, 81% yield). 1H NMR (400 MHz, $CDCl_3$) δ 8.60 (d, $J = 2.6$ Hz, 1H), 8.48 (bs, 1H), 7.58 (d, $J = 8.8$ Hz, 1H), 7.54 (d, $J = 2.8$ Hz, 1H), 7.46 (dd, $J = 8.4$ Hz, 2.1 Hz, 1H), 6.95 (d, $J = 8.4$ Hz, 1H), 6.89 (dd, $J = 8.8$ Hz, 2.0 Hz, 1H), 3.97 (s, 3H), 3.96 (s, 3H); ^{13}C NMR (100 MHz, $CDCl_3$) $\delta = 164.9, 152.8, 149.6, 149.1, 137.3, 132.9, 126.7, 120.7$ (q, $^1J_{CF} = 257$ Hz), 119.2, 117.2, 114.2, 110.9, 110.7, 110.6, 56.3, 56.2 ppm. HRMS (TOF, ES+) calc'd for $C_{16}H_{13}BrF_3NO_4$, 418.9980 ; found, 418.9981.



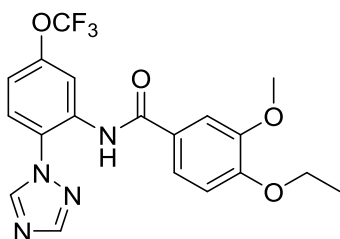
Synthesis of *N*-(2-bromo-5-(trifluoromethoxy)phenyl)-4-(cyclopropylmethoxy)-3-methoxybenzamide (1.104i)

This compound was synthesized according to general procedure 3. White solid (1.86 g, 53% yield). 1H NMR (400 MHz, $CDCl_3$) δ 8.61 (d, $J = 2.3$ Hz, 1H), 8.47 (bs, 1H), 7.58 (d, $J = 8.8$ Hz, 1H), 7.54 (d, $J = 2.1$ Hz, 1H), 7.43 (dd, $J = 8.4, 2.1$ Hz, 1H), 6.93 (d, $J = 8.4$

Hz, 1H), 6.91-6.87 (m, 1H), 3.97 (s, 3H), 3.94 (d, 2H), 1.40-1.33 (m, 1H), 0.71-0.66 (m, 2H), 0.42-0.38 (m, 2H); ^{13}C NMR (100 MHz, CDCl_3) δ = 165.0, 152.4, 149.9, 149.1, 137.3, 132.9, 126.6, 120.5 (q, J_{CF} = 256.6 Hz), 119.6, 117.1, 114.2, 112.2, 111.2, 110.7, 74.1, 56.3, 10.2, 3.6 ppm. HRMS (TOF, ES+) calc'd for $\text{C}_{19}\text{H}_{17}\text{BrF}_3\text{NO}_4$, 459.0293; found 459.0296.

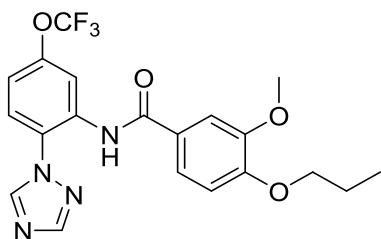
General Procedure 4: Synthesis of Triazoles

To a suspension of the appropriate benzamide (1.0 eq), 1,2,4-triazole (1.0 eq), potassium phosphate tribasic (2.5 eq), and copper (I) iodide (0.05 eq) in DMF (0.1 M) was added *trans*-*N,N'*-dimethylcyclohexane-1,2-diamine (0.10 eq). The resulting suspension was degassed by vigorously bubbling argon through the mixture for one minute. The reaction was then heated to 100 °C for 16 hours, whereupon LCMS indicated complete consumption of starting material and formation of the desired product. The reaction was diluted with EtOAc and filtered over a pad of celite. The resulting organic material was concentrated and purified using a Gilson HPLC system (30 x 50 mm column; H_2O with 0.1% TFA:acetonitrile). Fractions containing the desired product were quenched with saturated NaHCO_3 , extracted with DCM, and concentrated to liberate the product as the free base.



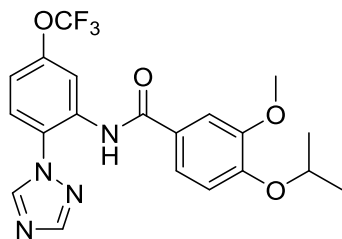
Synthesis of *N*-(2-(1*H*-1,2,4-triazol-1-yl)-5-(trifluoromethoxy)phenyl)-4-ethoxy-3-methoxybenzamide (1.114)

This compound was synthesized according to general procedure 4. White solid (15.6 mg, 60% yield). ^1H NMR (400 MHz, CDCl_3) δ 10.50 (bs, 1H), 8.76 (d, $J = 2.0$ Hz, 1H), 8.53 (s, 1H), 8.30 (s, 1H), 7.51 (d, $J = 2.1$ Hz, 1H), 7.44 (d, $J = 8.8$ Hz, 1H), 7.41 (dd, $J = 8.5$ Hz, 2.2 Hz, 1H), 7.09 (m, 1H), 6.93 (d, $J = 8.4$ Hz, 1H), 4.18 (q, 2H), 3.95 (s, 3H), 1.51 (t, 3H); ^{13}C NMR (100 MHz, CDCl_3) $\delta = 165.1, 153.1, 152.2, 149.8, 149.5, 143.9, 133.7, 126.3, 123.8, 123.6, 120.5$ (q, $^1J_{\text{CF}} = 257$ Hz), 120.1, 116.0, 115.6, 111.7, 110.9, 64.7, 56.2, 14.8 ppm. HRMS (TOF, ES+) calc'd for $\text{C}_{19}\text{H}_{17}\text{F}_3\text{N}_4\text{O}_4$, 422.1202; found, 422.1204.



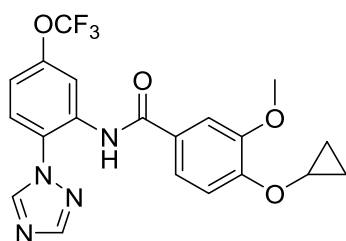
Synthesis of *N*-(2-(1*H*-1,2,4-triazol-1-yl)-5-(trifluoromethoxy)phenyl)-3-methoxy-4-propoxybenzamide (1.115)

This compound was synthesized according to general procedure 4. Colorless oil (13.7 mg, 51% yield). ^1H NMR (400 MHz, CDCl_3) δ 10.52 (bs, 1H), 8.76 (d, $J = 2.1$ Hz, 1H), 8.51 (s, 1H), 8.30 (s, 1H), 7.51 (d, $J = 2.2$ Hz, 1H), 7.43 (d, $J = 8.8$ Hz, 1H), 7.41 (dd, $J = 8.5$ Hz, 2.2 Hz, 1H), 7.09 (m, 1H), 6.93 (d, $J = 8.4$ Hz, 1H), 4.06 (t, 2H), 3.95 (s, 3H), 1.91 (m, 2H), 1.06 (t, 3H); ^{13}C NMR (100 MHz, CDCl_3) $\delta = 165.1, 153.1, 152.4, 149.7, 149.6, 143.9, 133.7, 126.2, 123.8, 123.6, 120.5$ (q, $^1J_{\text{CF}} = 257$ Hz), 120.1, 116.0, 115.6, 111.9, 111.0, 70.7, 56.2, 22.5, 10.5 ppm. HRMS (TOF, ES+) calc'd for $\text{C}_{20}\text{H}_{19}\text{F}_3\text{N}_4\text{O}_4$, 436.1358; found, 436.1358.



Synthesis of *N*-(2-(1*H*-1,2,4-triazol-1-yl)-5-(trifluoromethoxy)phenyl)-4-isopropoxy-3-methoxybenzamide (1.116)

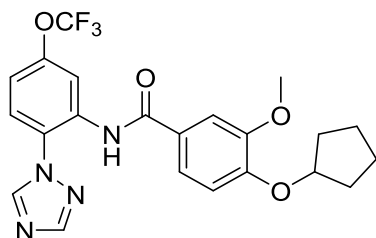
This compound was synthesized according to general procedure 4. Colorless oil (11.0 mg, 56% yield). ^1H NMR (400 MHz, CDCl_3) δ 10.51 (bs, 1H), 8.76 (d, $J = 2.0$ Hz, 1H), 8.51 (s, 1H), 8.30 (s, 1H), 7.51 (d, $J = 2.1$ Hz, 1H), 7.43 (d, $J = 8.8$ Hz, 1H), 7.40 (dd, $J = 8.4$ Hz, 2.2 Hz, 1H), 7.09 (m, 1H), 6.95 (d, $J = 8.5$ Hz, 1H), 4.66 (m, 1H), 3.94 (s, 3H), 1.42 (d, 6H); ^{13}C NMR (100 MHz, CDCl_3) $\delta = 165.1, 153.1, 151.3, 150.3, 149.8, 143.9, 133.8, 126.2, 123.8, 123.7, 120.5$ (q, $^1J_{\text{CF}} = 255$ Hz), 120.0, 116.0, 115.6, 113.7, 111.3, 71.5, 56.2, 22.1 ppm. HRMS (TOF, ES+) calc'd for $\text{C}_{20}\text{H}_{19}\text{F}_3\text{N}_4\text{O}_4$, 436.1358; found, 436.1361.



Synthesis of *N*-(2-(1*H*-1,2,4-triazol-1-yl)-5-(trifluoromethoxy)phenyl)-4-cyclopropoxy-3-methoxybenzamide (1.117)

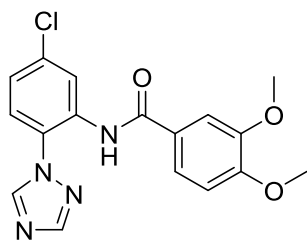
This compound was synthesized according to general procedure 4. White solid (8.7 mg, 68% yield). ^1H NMR (400 MHz, CDCl_3) δ 10.54 (bs, 1H), 8.77 (d, $J = 2.1$ Hz, 1H), 8.51 (s, 1H), 8.31 (s, 1H), 7.51 (d, $J = 2.0$ Hz, 1H), 7.44 (d, $J = 8.8$ Hz, 1H), 7.43 (dd, $J = 8.4$ Hz, 2.1 Hz, 1H), 7.33 (d, $J = 8.4$ Hz, 1H), 7.09 (dd, $J = 8.8$ Hz, 1.6 Hz, 1H), 3.93 (s,

3H), 3.82 (m, 1H), 0.90-0.84 (m, 4H); ^{13}C NMR (100 MHz, CDCl_3) δ = 165.1, 153.2, 152.3, 149.8, 149.3, 143.9, 133.7, 126.8, 123.8, 123.6, 120.5 (q, $^1J_{\text{CF}}$ = 257 Hz), 119.9, 116.0, 115.6, 113.0, 110.9, 56.1, 52.0, 6.5 ppm. HRMS (TOF, ES+) calc'd for $\text{C}_{20}\text{H}_{17}\text{F}_3\text{N}_4\text{O}_4$, 434.1202; found, 434.1204.



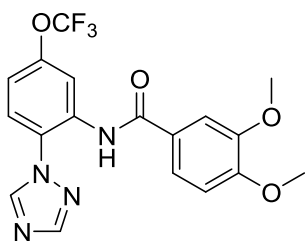
Synthesis of *N*-(2-(1*H*-1,2,4-triazol-1-yl)-5-(trifluoromethoxy)phenyl)-4-(cyclopentyloxy)-3-methoxybenzamide (1.121)

This compound was synthesized according to general procedure 4. White solid (25.3 mg, 58% yield). ^1H NMR (400 MHz, CDCl_3) δ 10.50 (bs, 1H), 8.76 (d, J = 2.1 Hz, 1H), 8.51 (s, 1H), 8.30 (s, 1H), 7.49 (d, J = 2.0 Hz, 1H), 7.43 (d, J = 8.8 Hz, 1H), 7.39 (dd, J = 8.4 Hz, 2.1 Hz, 1H), 7.08 (dd, J = 8.7 Hz, 1.6 Hz, 1H), 6.92 (d, J = 8.4 Hz, 1H), 4.85 (m, 1H), 3.92 (s, 3H), 2.02-1.83 (m, 6H), 1.67-1.62 (m, 2H); ^{13}C NMR (100 MHz, CDCl_3) δ = 165.2, 153.1, 151.7, 150.1, 149.7, 143.9, 133.8, 125.9, 123.8, 123.6, 120.5 (q, $^1J_{\text{CF}}$ = 257 Hz), 120.0, 115.9, 115.6, 113.4, 111.2, 80.7, 56.2, 33.0, 24.3 ppm. HRMS (TOF, ES+) calc'd for $\text{C}_{22}\text{H}_{21}\text{F}_3\text{N}_4\text{O}_4$, 462.1515; found, 462.1518.



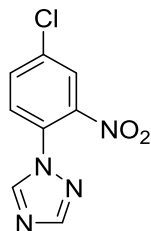
Synthesis of *N*-(5-chloro-2-(1*H*-1,2,4-triazol-1-yl)phenyl)-3,4-dimethoxybenzamide (1.8)

This compound was synthesized according to general procedure 4. White solid (49.7 mg, 51% yield). ¹H NMR (400 MHz, CDCl₃) δ 10.50 (bs, 1H), 8.81 (d, *J* = 2.3 Hz, 1H), 8.50 (s, 1H), 8.28 (s, 1H), 7.50 (d, *J* = 2.0 Hz, 1H), 7.43 (dd, *J* = 8.4 Hz, 2.0 Hz, 1H), 7.34 (d, *J* = 8.6 Hz, 1H), 7.20 (dd, *J* = 8.5 Hz, 2.3 Hz, 1H), 6.94 (d, *J* = 8.4 Hz, 1H), 3.96 (s, 3H), 3.95 (s, 3H); ¹³C NMR (100 MHz, CDCl₃) δ = 165.0, 153.0, 152.7, 149.3, 143.8, 135.8, 133.1, 126.6, 124.1, 123.4, 123.1, 120.1, 110.7, 110.6, 56.2, 56.1 ppm. HRMS (TOF, ES⁺) calc'd for C₁₇H₁₅ClN₄O₃, 358.0833 ; found, 358.0835.



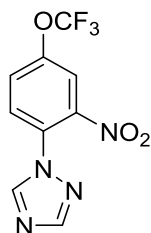
Synthesis of *N*-(2-(1*H*-1,2,4-triazol-1-yl)-5-(trifluoromethoxy)phenyl)-3,4-dimethoxybenzamide (1.23)

This compound was synthesized according to general procedure 4. White solid (11.7 mg, 60% yield). ¹H NMR (400 MHz, CDCl₃) δ 10.50 (bs, 1H), 8.77 (d, *J* = 1.9 Hz, 1H), 8.51 (s, 1H), 8.30 (s, 1H), 7.52 (d, *J* = 2.1 Hz, 1H), 7.44 (m, 2H), 7.10 (m, 1H), 6.95 (d, *J* = 8.4 Hz, 1H), 3.97 (s, 3H), 3.96 (s, 3H); ¹³C NMR (100 MHz, CDCl₃) δ = 165.1, 153.1, 152.8, 149.7, 149.4, 143.9, 133.7, 126.5, 123.8, 123.6, 120.5 (q, ¹*J*_{CF} = 257 Hz), 120.1, 116.0, 115.6, 110.7, 110.6, 56.2, 56.1 ppm. HRMS (TOF, ES⁺) calc'd for C₁₈H₁₅F₃N₄O₄, 408.1045 ; found, 408.1047.



Synthesis of 1-(4-chloro-2-nitrophenyl)-1*H*-1,2,4-triazole (1.317)

This compound was synthesized according to general procedure 4. Beige solid (2.13 g, 56% yield). ¹H NMR (400 MHz, CDCl₃) δ 8.39 (s, 1H), 8.11 (s, 1H), 8.02 (d, *J* = 2.3 Hz, 1H), 7.74 (dd, *J* = 8.5, 2.3 Hz, 1H), 7.55 (d, *J* = 8.5 Hz, 1H); ¹³C NMR (100 MHz, CDCl₃) δ = 153.4, 144.8, 144.0, 136.4, 133.9, 128.8, 128.6, 125.9 ppm. HRMS (TOF, ES+) calc'd for C₈H₅ClN₄O₂, 224.0101; found, 224.0103.



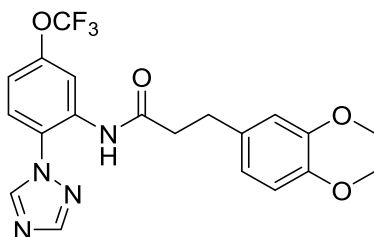
Synthesis of 1-(2-nitro-4-(trifluoromethoxy)phenyl)-1*H*-1,2,4-triazole (1.318)

This compound was synthesized according to general procedure 4. White solid (2.35 g, 49% yield). ¹H NMR (400 MHz, CDCl₃) δ 8.41 (s, 1H), 8.12 (s, 1H), 7.90 (d, *J* = 2.5 Hz, 1H), 7.67 (d, *J* = 8.5 Hz, 1H), 7.63-7.61 (m, 1H); ¹³C NMR (100 MHz, CDCl₃) δ = 153.5, 149.4 (d, *J*_{CF} = 2.0 Hz), 145.0, 144.1, 129.2, 128.7, 125.7, 120.3 (q, *J*_{CF} = 259.0 Hz), 118.4 ppm. HRMS (TOF, ES+) calc'd for C₉H₅F₃N₄O₃, 274.0314; found, 274.0315.

General Procedure 5: Synthesis of Triazoles

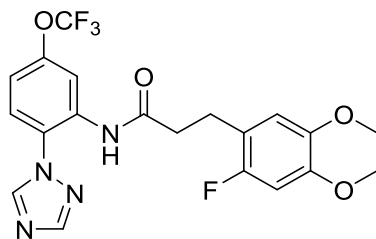
To a solution of aniline (**1.146**) (1.0 eq) in CH₂Cl₂ (0.1 M) in a Biotage microwave vial was added the appropriate benzoic acid (12, 17a-g, or 27) (1.0 eq), *N,N*-

diisopropylethylamine (3.0 eq), and chlorodipyrrolidinocarbenium hexafluorophosphate (PyClU) (1.0 eq) at room temperature. The vial was sealed and heated to 100 °C using a Biotage microwave reactor for 30 min, whereupon LCMS showed formation of the desired product. The reaction mixture was diluted with DCM and quenched with the addition of saturated NH₄Cl. The layers were separated, and the aqueous layer was washed with DCM x 3. The combined organic layer was passed through a phase separator, concentrated, and purified using a Gilson HPLC system (30 x 50 mm column; H₂O with 0.1% TFA:acetonitrile). Fractions containing the desired product were quenched with saturated NaHCO₃, extracted with DCM, and concentrated to liberate the product as the free base.



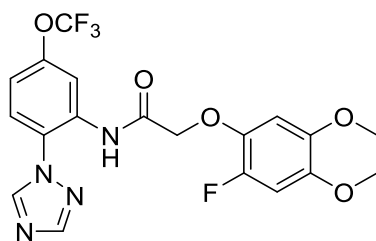
Synthesis of *N*-(2-(1*H*-1,2,4-triazol-1-yl)-5-(trifluoromethoxy)phenyl)-3-(3,4-dimethoxyphenyl)propanamide (1.209b)

This compound was synthesized according to general procedure 5. White solid (91.1 mg, 51% yield). ¹H NMR (400 MHz, CDCl₃) δ 9.52 (bs, 1H), 8.55 (d, *J* = 2.2 Hz, 1H), 8.40 (s, 1H), 8.18 (s, 1H), 7.34 (d, *J* = 8.8 Hz, 1H), 7.05 (dd, *J* = 8.7, 1.4 Hz, 1H), 6.75-6.69 (m, 3H), 3.85 (s, 3H), 3.80 (s, 3H), 2.96 (t, 2H), 2.64 (t, 2H); ¹³C NMR (100 MHz, CDCl₃) δ = 170.9, 153.1, 149.6, 149.0, 147.7, 143.7, 133.1, 132.8, 123.8, 123.6, 120.5 (q, *J*_{CF} = 257.2 Hz), 120.2, 116.1, 115.7, 111.8, 111.4, 56.0, 55.9, 40.4, 31.0 ppm. HRMS (TOF, ES⁺) calc'd for C₂₀H₁₉F₃N₄O₄, 436.1358; found, 436.1363.



Synthesis of *N*-(2-(1*H*-1,2,4-triazol-1-yl)-5-(trifluoromethoxy)phenyl)-3-(2-fluoro-4,5-dimethoxyphenyl)propanamide (1.209a)

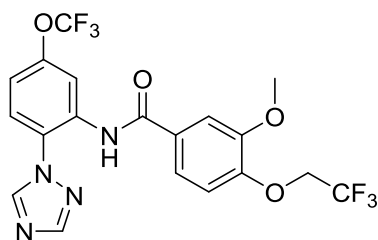
This compound was synthesized according to general procedure 5. White solid (107 mg, 57% yield). ¹H NMR (400 MHz, CDCl₃) δ 9.59 (bs, 1H), 8.55 (d, *J* = 2.1 Hz, 1H), 8.40 (s, 1H), 8.19 (s, 1H), 7.34 (d, *J* = 8.8 Hz, 1H), 7.07-7.04 (m, 1H), 6.64 (d, *J* = 7.2 Hz, 1H), 6.54 (d, *J* = 11.2 Hz, 1H), 3.83 (s, 3H), 3.75 (s, 3H), 2.96 (t, 2H), 2.63 (t, 2H); ¹³C NMR (100 MHz, CDCl₃) δ = 170.8, 155.0 (d, *J*_{CF} = 236.4 Hz), 153.1, 149.6, 148.5 (d, *J*_{CF} = 9.8 Hz), 145.1 (d, *J*_{CF} = 2.0 Hz), 143.7, 133.1, 123.7, 123.6, 120.5 (q, *J*_{CF} = 257.1 Hz), 117.3 (d, *J*_{CF} = 17.2 Hz), 116.1, 115.7, 113.0 (d, *J*_{CF} = 6.1 Hz), 100.2 (d, *J*_{CF} = 27.9 Hz), 56.4, 56.2, 38.8, 24.9 ppm. HRMS (TOF, ES⁺) calc'd for C₂₀H₁₈F₄N₄O₄, 454.1264; found, 454.1264.



Synthesis of *N*-(2-(1*H*-1,2,4-triazol-1-yl)-5-(trifluoromethoxy)phenyl)-2-(2-fluoro-4,5-dimethoxyphenoxy)acetamide (1.209d)

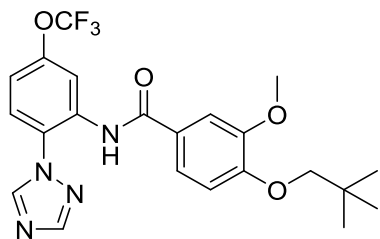
This compound was synthesized according to general procedure 5. White solid (91.6 mg, 49% yield). ¹H NMR (400 MHz, CDCl₃) δ 10.72 (bs, 1H), 8.65 (d, *J* = 2.4 Hz, 1H), 8.44 (s, 1H), 8.19 (s, 1H), 7.42 (d, *J* = 8.8 Hz, 1H), 7.14-7.11 (m, 1H), 6.73 (d, *J* = 12.1

Hz, 1H), 6.58 (d, $J = 7.9$ Hz, 1H), 4.60 (s, 2H), 3.84 (s, 6H); ^{13}C NMR (100 MHz, CDCl_3) $\delta = 167.1, 153.4$ (d, $J_{\text{CF}} = 2.5$ Hz), 149.7, 146.8 (d, $J_{\text{CF}} = 238.0$ Hz), 145.3 (d, $J_{\text{CF}} = 2.6$ Hz), 144.9 (d, $J_{\text{CF}} = 7.9$ Hz), 143.6, 137.9 (d, $J_{\text{CF}} = 12.0$ Hz), 132.7, 124.3, 124.2, 120.5 (q, $J_{\text{CF}} = 257.4$ Hz), 116.7, 115.7, 102.3 (d, $J_{\text{CF}} = 2.0$ Hz), 101.8 (d, $J_{\text{CF}} = 23.4$ Hz), 70.3, 56.8, 56.7 ppm. HRMS (TOF, ES^+) calc'd for $\text{C}_{19}\text{H}_{16}\text{F}_4\text{N}_4\text{O}_5$, 456.1057; found, 456.1063.



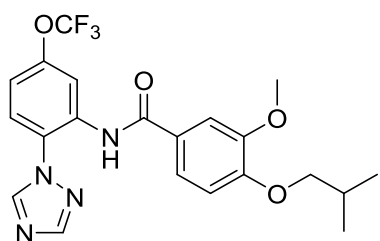
Synthesis of *N*-(2-(1*H*-1,2,4-triazol-1-yl)-5-(trifluoromethoxy)phenyl)-3-methoxy-4-(2,2,2-trifluoroethoxy)benzamide (1.124)

This compound was synthesized according to general procedure 5. White solid (16.0 mg, 41% yield). ^1H NMR (400 MHz, CDCl_3) δ 10.60 (bs, 1H), 8.74 (d, $J = 2.1$ Hz, 1H), 8.52 (s, 1H), 8.29 (s, 1H), 7.56 (d, $J = 2.0$ Hz, 1H), 7.45 (d, $J = 8.8$ Hz, 1H), 7.39 (dd, $J = 8.3, 2.0$ Hz, 1H), 7.10 (dd, $J = 8.7, 1.6$ Hz, 1H), 7.03 (d, $J = 8.3$ Hz, 1H), 4.46 (q, 2H), 3.95 (s, 3H); ^{13}C NMR (100 MHz, CDCl_3) $\delta = 164.7, 153.1, 150.6, 150.3, 149.7$ (d, $J_{\text{CF}} = 1.7$ Hz), 143.9, 133.4, 129.5, 123.9, 123.5, 123.4 (q, $J_{\text{CF}} = 277.0$ Hz), 120.5 (q, $J_{\text{CF}} = 257.0$ Hz), 119.6, 116.24, 116.16, 115.6, 112.1, 67.5 (q, $J_{\text{CF}} = 35.5$ Hz), 56.2 ppm. HRMS (TOF, ES^+) calc'd for $\text{C}_{19}\text{H}_{14}\text{F}_6\text{N}_4\text{O}_4$, 476.0919; found, 476.0923.



Synthesis of *N*-(2-(1*H*-1,2,4-triazol-1-yl)-5-(trifluoromethoxy)phenyl)-3-methoxy-4-(neopentyloxy)benzamide (1.126)

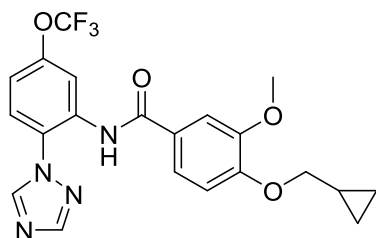
This compound was synthesized according to general procedure 5. Colorless oil (14.4 mg, 38% yield). ^1H NMR (400 MHz, CDCl_3) δ 10.51 (bs, 1H), 8.77 (d, $J = 2.1$ Hz, 1H), 8.51 (s, 1H), 8.29 (s, 1H), 7.50 (d, $J = 2.1$ Hz, 1H), 7.43 (d, $J = 8.8$ Hz, 1H), 7.41 (dd, $J = 8.4, 2.2$ Hz, 1H), 7.09 (dd, $J = 8.8, 1.7$ Hz, 1H) 6.92 (d, $J = 8.4$ Hz, 1H), 3.93 (s, 3H), 3.70 (s, 2H), 1.08 (s, 9H); ^{13}C NMR (100 MHz, CDCl_3) $\delta = 165.2, 153.3, 153.1, 150.0, 149.7$ (d, $J_{\text{CF}} = 2.0$ Hz),, 143.9, 133.8, 126.1, 123.8, 123.6, 120.5 (q, $J_{\text{CF}} = 257.3$ Hz), 120.3, 116.0, 115.6, 112.4, 111.6, 79.1, 56.5, 32.3, 26.8 ppm. HRMS (TOF, ES+) calc'd for $\text{C}_{22}\text{H}_{23}\text{F}_3\text{N}_4\text{O}_4$, 464.1671; found, 464.1675.



Synthesis of *N*-(2-(1*H*-1,2,4-triazol-1-yl)-5-(trifluoromethoxy)phenyl)-4-isobutoxy-3-methoxybenzamide (1.125)

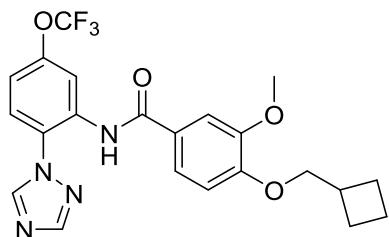
This compound was synthesized according to general procedure 5. White solid (14.8 mg, 40% yield). ^1H NMR (400 MHz, CDCl_3) δ 10.52 (bs, 1H), 8.75 (d, $J = 2.2$ Hz, 1H), 8.51 (s, 1H), 8.29 (s, 1H), 7.49 (d, $J = 2.1$ Hz, 1H), 7.43 (d, $J = 8.8$ Hz, 1H), 7.40 (dd, $J = 8.4, 2.1$ Hz, 1H), 7.07 (dd, $J = 8.8, 1.6$ Hz, 1H) 6.92 (d, $J = 8.4$ Hz, 1H), 3.93 (s, 3H),

3.83 (d, 2H), 2.19 (m, 1H), 1.05 (d, 6H); ^{13}C NMR (100 MHz, CDCl_3) δ = 165.1, 153.1, 152.7, 149.7, 143.9, 133.7, 126.2, 123.8, 123.6, 120.5 (q, J_{CF} = 257.0 Hz), 120.1, 115.9, 115.6, 112.1, 111.2, 75.6, 56.3, 28.2, 19.4 ppm. HRMS (TOF, ES+) calc'd for $\text{C}_{21}\text{H}_{21}\text{F}_3\text{N}_4\text{O}_4$, 450.1515; found, 450.1520.



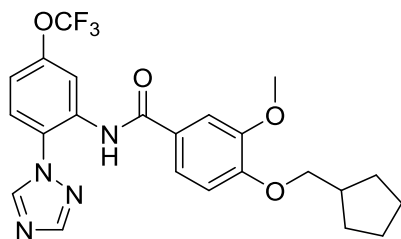
Synthesis of *N*-(2-(1*H*-1,2,4-triazol-1-yl)-5-(trifluoromethoxy)phenyl)-4-(cyclopropylmethoxy)-3-methoxybenzamide (1.127)

This compound was synthesized according to general procedure 5. Beige solid (16.2 mg, 44% yield). ^1H NMR (400 MHz, CDCl_3) δ 10.52 (bs, 1H), 8.75 (d, J = 2.2 Hz, 1H), 8.51 (s, 1H), 8.28 (s, 1H), 7.50 (d, J = 2.0 Hz, 1H), 7.43 (d, J = 8.8 Hz, 1H), 7.39 (dd, J = 8.4, 2.1 Hz, 1H), 7.07 (dd, J = 8.7, 1.7 Hz, 1H), 6.91 (d, J = 8.4 Hz, 1H), 3.95 (s, 3H), 3.92 (d, 2H), 1.39-1.32 (m, 1H), 0.69-0.65 (m, 2H), 0.40-0.36 (m, 2H); ^{13}C NMR (100 MHz, CDCl_3) δ = 165.1, 153.1, 152.3, 149.7 (d, J_{CF} = 2.0 Hz), 149.6, 143.9, 133.7, 126.3, 123.8, 123.6, 120.5 (q, J_{CF} = 257.1 Hz), 120.0, 115.9, 115.5, 112.1, 111.0, 74.1, 56.2, 10.2, 3.6 ppm. HRMS (TOF, ES+) calc'd for $\text{C}_{21}\text{H}_{19}\text{F}_3\text{N}_4\text{O}_4$, 448.1358; found, 448.1365.



Synthesis of *N*-(2-(1*H*-1,2,4-triazol-1-yl)-5-(trifluoromethoxy)phenyl)-4-(cyclobutylmethoxy)-3-methoxybenzamide (1.128)

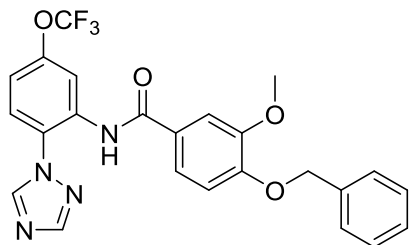
This compound was synthesized according to general procedure 5. White solid (14.8 mg, 39% yield). ¹H NMR (400 MHz, CDCl₃) δ 10.52 (bs, 1H), 8.76 (d, *J* = 2.1 Hz, 1H), 8.51 (s, 1H), 8.29 (s, 1H), 7.50 (d, *J* = 2.0 Hz, 1H), 7.43 (d, *J* = 8.8 Hz, 1H), 7.40 (dd, *J* = 8.5, 2.0 Hz, 1H), 7.08 (dd, *J* = 8.7, 1.6 Hz, 1H), 6.93 (d, *J* = 8.4 Hz, 1H), 4.06 (d, 2H), 3.93 (s, 3H), 2.87 (m, 1H), 2.21-2.14 (m, 2H), 2.04-1.83 (m, 4H); ¹³C NMR (100 MHz, CDCl₃) δ = 165.1, 153.1, 152.7, 149.8, 143.9, 133.8, 126.3, 123.8, 123.6, 120.5 (q, *J*_{CF} = 257.2 Hz), 120.1, 116.0, 115.6, 112.2, 111.2, 73.5, 56.3, 34.5, 25.2, 18.8 ppm. HRMS (TOF, ES⁺) calc'd for C₂₂H₂₁F₃N₄O₄, 462.1515; found, 462.1515.



Synthesis of *N*-(2-(1*H*-1,2,4-triazol-1-yl)-5-(trifluoromethoxy)phenyl)-4-(cyclopentylmethoxy)-3-methoxybenzamide (1.129)

This compound was synthesized according to general procedure 5. Colorless oil (18.7 mg, 48% yield). ¹H NMR (400 MHz, CDCl₃) δ 10.52 (bs, 1H), 8.76 (d, *J* = 2.0 Hz, 1H), 8.51 (s, 1H), 8.29 (s, 1H), 7.49 (d, *J* = 2.0 Hz, 1H), 7.43 (d, *J* = 8.8 Hz, 1H), 7.40 (dd, *J* = 8.4, 2.0 Hz, 1H), 7.08 (dd, *J* = 8.8, 1.6 Hz, 1H) 6.93 (d, *J* = 8.4 Hz, 1H), 3.95 (d, 2H), 3.93 (s, 3H), 2.46 (m, 1H), 1.90-1.83 (m, 2H), 1.68-1.56 (m, 4H), 1.40-1.33 (m, 2H); ¹³C NMR (100 MHz, CDCl₃) δ = 165.1, 153.1, 152.7, 149.7, 143.9, 133.7, 126.1, 123.8, 123.6, 120.5 (q, *J*_{CF} = 257.0 Hz), 120.1, 115.9, 115.6, 112.1, 111.2, 73.5, 56.3, 39.0,

29.7, 25.4 ppm. HRMS (TOF, ES+) calc'd for C₂₃H₂₃F₃N₄O₄, 476.1671; found, 476.1680.



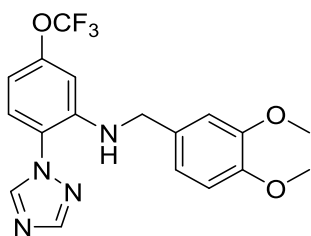
Synthesis of *N*-(2-(1*H*-1,2,4-triazol-1-yl)-5-(trifluoromethoxy)phenyl)-4-(benzyloxy)-3-methoxybenzamide (1.131)

This compound was synthesized according to general procedure 5. White solid (19.8 mg, 50% yield). ¹H NMR (400 MHz, CDCl₃) δ 10.52 (bs, 1H), 8.75 (d, *J* = 2.2 Hz, 1H), 8.50 (s, 1H), 8.28 (s, 1H), 7.53 (d, *J* = 2.1 Hz, 1H), 7.45-7.31 (m, 7H), 7.08 (dd, *J* = 8.8, 1.6 Hz, 1H), 6.94 (d, *J* = 8.4, 1H), 5.25 (s, 2H), 3.97 (s, 3H); ¹³C NMR (100 MHz, CDCl₃) δ = 165.0, 153.1, 151.9, 149.9, 149.7 (d, *J*_{CF} = 2.0 Hz), 143.9, 136.4, 133.6, 128.8, 128.3, 127.3, 126.8, 123.8, 123.6, 120.5 (q, *J*_{CF} = 257.2 Hz), 119.9, 116.0, 115.6, 112.9, 111.2, 71.0, 56.2 ppm. HRMS (TOF, ES+) calc'd for C₂₄H₁₉F₃N₄O₄, 484.1358; found, 484.1364.

General Procedure 6: Synthesis of Anilines

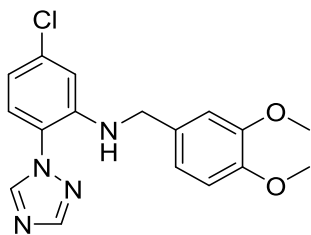
To a solution of LiAlH₄ (3.5 eq, 1.0 M stock solution in THF) cooled to 0 °C was added a solution of the appropriate triazole in THF (1.0 mL) dropwise under an inert atmosphere of argon. Upon completion of addition, the reaction was stirred at room temperature for 3 hr, whereupon LCMS indicated complete consumption of starting material and formation of the desired product. The reaction was cooled to 0 °C and quenched with the sequential addition of EtOAc and saturated aqueous Rochelle salt solution. The

resulting mixture was stirred at room temperature for 2 hr before the layers were separated. The aqueous layer was washed with EtOAc x 3. The combined organic material was passed through a phase separator, concentrated, and purified using a Gilson HPLC system (30 x 50 mm column; H₂O with 0.1% TFA:acetonitrile). Fractions containing the desired product were quenched with saturated NaHCO₃, extracted with DCM, and concentrated to liberate the product as the free base.



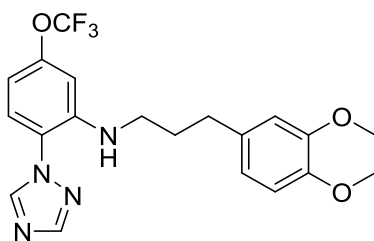
Synthesis of *N*-(3,4-dimethoxybenzyl)-2-(1*H*-1,2,4-triazol-1-yl)-5-(trifluoromethoxy)aniline (1.140a)

This compound was synthesized according to general procedure 6. White solid (26.7 mg, 51% yield). ¹H NMR (400 MHz, CDCl₃) δ 8.34 (s, 1H), 8.13 (s, 1H), 7.18 (d, *J* = 8.4 Hz, 1H), 6.87-6.81 (m, 3H), 6.62-6.58 (m, 2H), 5.87 (t, 1H), 4.28 (d, 2H), 3.86 (s, 3H), 3.84 (s, 3H); ¹³C NMR (100 MHz, CDCl₃) δ = 152.8, 150.8 (d, *J*_{CF} = 1.3 Hz), 149.4, 148.6, 143.8, 143.7, 130.1, 125.4, 120.8, 120.5 (q, *J*_{CF} = 256.3 Hz), 119.6, 111.4, 110.6, 108.2, 105.3, 56.00, 55.96, 47.5 ppm. HRMS (TOF, ES⁺) calc'd for C₁₈H₁₇F₃N₄O₃, 394.1253; found, 394.1257.



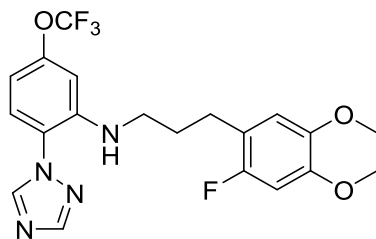
Synthesis of 5-chloro-*N*-(3,4-dimethoxybenzyl)-2-(1*H*-1,2,4-triazol-1-yl)aniline (1.140b)

This compound was synthesized according to general procedure 6. Beige solid (32.1 mg, 58% yield). ¹H NMR (400 MHz, CDCl₃) δ 8.33 (s, 1H), 8.12 (s, 1H), 7.10 (d, *J* = 8.3 Hz, 1H), 6.87-6.81 (m, 3H), 6.77 (d, *J* = 2.1 Hz, 1H), 6.71 (dd, *J* = 8.3, 2.2 Hz, 1H), 5.81 (bs, 1H), 4.28 (d, 2H), 3.86 (s, 3H), 3.85 (s, 3H); ¹³C NMR (100 MHz, CDCl₃) δ = 152.8, 149.4, 148.6, 143.8, 143.1, 136.3, 130.3, 125.2, 121.1, 119.5, 116.5, 112.8, 111.5, 110.5, 56.02, 56.0, 47.4 ppm. HRMS (TOF, ES⁺) calc'd for C₁₇H₁₇ClN₄O₂, 344.1040; found, 344.1043.



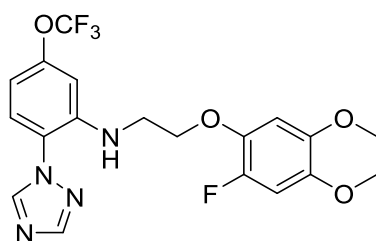
Synthesis of *N*-(3-(3,4-dimethoxyphenyl)propyl)-2-(1*H*-1,2,4-triazol-1-yl)-5-(trifluoromethoxy)aniline (1.210)

This compound was synthesized according to general procedure 6. Colorless oil (22.7 mg, 47% yield). ¹H NMR (400 MHz, CDCl₃) δ 8.31 (s, 1H), 8.16 (s, 1H), 7.15 (d, *J* = 8.4 Hz, 1H), 6.78 (d, *J* = 7.8 Hz, 1H), 6.71-6.69 (m, 2H), 6.58-6.55 (m, 2H), 5.47 (t, 1H), 3.86 (s, 3H), 3.84 (s, 3H), 3.13 (q, 2H), 2.65 (t, 2H), 1.93 (m, 2H); ¹³C NMR (100 MHz, CDCl₃) δ = 152.8, 151.0, 149.1, 147.5, 143.9, 143.8, 133.7, 125.4, 120.6, 120.5 (q, *J*_{CF} = 256.0 Hz), 120.3, 111.7, 111.4, 107.7, 104.7, 56.0, 55.9, 42.6, 32.8, 30.5 ppm. HRMS (TOF, ES⁺) calc'd for C₂₀H₂₁F₃N₄O₃, 422.1566; found, 422.1568.



Synthesis of *N*-(3-(2-fluoro-4,5-dimethoxyphenyl)propyl)-2-(1*H*-1,2,4-triazol-1-yl)-5-(trifluoromethoxy)aniline (1.215)

This compound was synthesized according to general procedure 6. Colorless oil (21.8 mg, 45% yield). ^1H NMR (400 MHz, CDCl_3) δ 8.31 (s, 1H), 8.16 (s, 1H), 7.16 (d, $J = 8.4$ Hz, 1H), 6.63-6.55 (m, 4H), 5.49 (t, 1H), 3.84 (s, 3H), 3.80 (s, 3H), 3.14 (q, 2H), 2.66 (t, 2H), 1.91 (m, 2H); ^{13}C NMR (100 MHz, CDCl_3) $\delta = 155.1$ (d, $J_{\text{CF}} = 236.0$ Hz), 152.9, 151.0, 148.3 (d, $J_{\text{CF}} = 9.8$ Hz), 145.3 (d, $J_{\text{CF}} = 2.4$ Hz), 143.9, 143.8, 125.5, 120.7, 120.5 (q, $J_{\text{CF}} = 256.0$ Hz), 118.3 (d, $J_{\text{CF}} = 17.2$ Hz), 112.9 (d, $J_{\text{CF}} = 6.4$ Hz), 107.7, 104.7, 100.3 (d, $J_{\text{CF}} = 28.4$ Hz), 56.6, 56.3, 42.6, 29.4, 26.1 ppm. HRMS (TOF, ES+) calc'd for $\text{C}_{20}\text{H}_{20}\text{F}_4\text{N}_4\text{O}_3$, 440.1472; found, 440.1472.



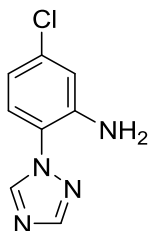
Synthesis of *N*-(2-(2-fluoro-4,5-dimethoxyphenoxy)ethyl)-2-(1*H*-1,2,4-triazol-1-yl)-5-(trifluoromethoxy)aniline (1.217)

This compound was synthesized according to general procedure 6. White solid (20.8 mg, 43% yield). ^1H NMR (400 MHz, CDCl_3) δ 8.33 (s, 1H), 8.17 (s, 1H), 7.20 (d, $J = 8.6$ Hz, 1H), 6.69-6.59 (m, 4H), 5.92 (t, 1H), 4.20 (t, 2H), 3.82 (s, 3H), 3.80 (s, 3H), 3.50 (q, 2H); ^{13}C NMR (100 MHz, CDCl_3) $\delta = 153.0$, 151.0, 147.6 (d, $J_{\text{CF}} = 237.4$ Hz), 145.2 (d,

$J_{CF} = 2.4$ Hz), 144.6 (d, $J_{CF} = 8.2$ Hz), 143.9, 143.8, 138.8 (d, $J_{CF} = 11.9$ Hz), 125.7, 121.2, 120.6 (q, $J_{CF} = 256.3$ Hz), 108.4, 105.0, 104.0 (d, $J_{CF} = 2.5$ Hz), 101.6 (d, $J_{CF} = 23.9$ Hz), 70.1, 56.7, 56.6, 43.0 ppm. HRMS (TOF, ES+) calc'd for $C_{19}H_{18}F_4N_4O_4$, 442.1264; found, 442.1265.

General Procedure 7: Synthesis of Anilines

To a solution of the appropriate *ortho*-nitro triazole compound (1.0 eq) in EtOH : H₂O (5:1) (0.3M) was sequentially added Fe powder (10.0 eq) and NH₄Cl (10.0 eq). The resulting suspension was heated to 75 °C for 4 hr, whereupon LCMS indicated complete consumption of starting material and formation of the desired product. Upon cooling to room temperature, the crude reaction mixture was filtered over a pad of celite and concentrated. The residue was dissolved in EtOAc and water. The layers were separated, and the aqueous layer was washed with EtOAc x 3. The combined organic material was washed with brine, dried over MgSO₄, filtered, concentrated, and purified via flash chromatography (Teledyne ISCO system, silica gel column, hexanes:EtOAc) to afford the desired products.

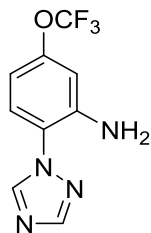


Synthesis of 5-chloro-2-(1H-1,2,4-triazol-1-yl)aniline (1.146b)

This compound was synthesized according to general procedure 7. White solid (1.01 g, 58% yield). ¹H NMR (400 MHz, CDCl₃) δ 8.33 (s, 1H), 8.14 (s, 1H), 7.10 (d, $J = 8.4$ Hz, 1H), 6.84 (d, $J = 2.2$ Hz, 1H), 6.76 (dd, $J = 8.8, 2.2$ Hz, 1H), 4.64 (bs, 2H); ¹³C NMR

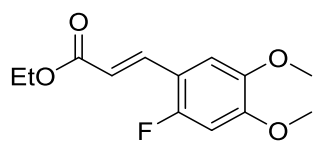
(100 MHz, CDCl₃) δ = 152.7, 143.5, 142.2, 135.7, 125.3, 121.3, 118.2, 117.1 ppm.

HRMS (TOF, ES⁺) calc'd for C₈H₇ClN₄, 194.0359; found, 194.0360.



Synthesis of 2-(1*H*-1,2,4-triazol-1-yl)-5-(trifluoromethoxy)aniline (1.146a)

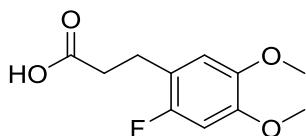
This compound was synthesized according to general procedure 7. White solid (1.1g, 53% yield). ¹H NMR (400 MHz, CDCl₃) δ 8.34 (s, 1H), 8.16 (s, 1H), 7.19 (d, *J* = 8.6 Hz, 1H), 6.70-6.69 (m, 1H), 6.67-6.64 (m, 1H), 4.64 (bs, 2H); ¹³C NMR (100 MHz, CDCl₃) δ = 152.8, 150.3 (d, *J*_{CF} = 2.0 Hz), 143.6, 142.7, 125.6, 121.1, 120.5 (q, *J*_{CF} = 256.0 Hz), 110.1, 109.4 ppm. HRMS (TOF, ES⁺) calc'd for C₉H₇F₃N₄O, 244.0572; found, 244.0574.



Synthesis of ethyl (*E*)-3-(2-fluoro-4,5-dimethoxyphenyl)acrylate (1.207a)

To a solution of 6-fluoroveratraldehyde (300 mg, 1.63 mmol) in DCM (6.52 mL) was added (carbethoxymethylene)triphenylphosphorane (681 mg, 1.95 mmol) at room temperature. The resulting solution was stirred for 16 hr at room temperature whereupon LCMS indicated complete consumption of starting material and formation of the desired product. The crude reaction mixture was concentrated and purified via flash chromatography (Teledyne ISCO system; silica gel column; hexanes:EtOAc; 0-30%

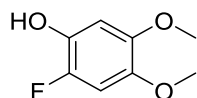
EtOAc gradient) to afford the desired material as a white solid (372 mg, 90% yield). ^1H NMR (400 MHz, CDCl_3) δ 7.77 (d, $J = 16.1$ Hz, 1H), 6.95 (d, $J_{\text{HF}} = 6.8$ Hz, 1H), 6.63 (d, $J_{\text{HF}} = 11.6$ Hz, 1H), 6.37 (d, $J = 16.1$ Hz, 1H), 4.26 (q, 2H), 3.89 (s, 3H), 3.88 (s, 3H), 1.33 (t, 3H); ^{13}C NMR (100 MHz, CDCl_3) $\delta = 167.1, 156.5$ (d, $J_{\text{CF}} = 247.0$ Hz), 152.0 (d, $J_{\text{CF}} = 10.1$ Hz), 145.7, 137.0 (d, $J_{\text{CF}} = 2.1$ Hz), 118.0 (d, $J_{\text{CF}} = 5.8$ Hz), 113.5 (d, $J_{\text{CF}} = 12.7$ Hz), 109.4 (d, $J_{\text{CF}} = 4.4$ Hz), 100.2 (d, $J_{\text{CF}} = 28.1$ Hz), 60.5, 56.4, 56.3, 14.4 ppm. HRMS (TOF, ES+) calc'd for $\text{C}_{13}\text{H}_{15}\text{FO}_4$, 254.0954; found, 254.0954.



Synthesis of 3-(2-fluoro-4,5-dimethoxyphenyl)propanoic acid (1.208a)

To a suspension of ethyl (*E*)-3-(2-fluoro-4,5-dimethoxyphenyl)acrylate (**1.207a**) (340 mg, 1.34 mmol) and Pd/C (285 mg, 0.134 mmol, 10% w/w Pd) in toluene (10.6 mL) was sequentially added acetic acid (153 μL , 2.67 mmol) and sodium borohydride (203 mg, 5.35 mmol) portionwise. The reaction was sealed and stirred at room temperature for 1 hr whereupon LCMS showed complete reduction of the α,β -unsaturated olefin. The reaction was diluted with EtOAc and filtered over a pad of celite. The crude organic material was concentrated to yield a colorless oil. This oil was redissolved in THF : H_2O (1:1) (16 mL), and lithium hydroxide (100 mg, 4.01 mmol) was added. After stirring at room temperature for 3 hr, the reaction was diluted with EtOAc and acidified to pH ~ 1 using 2 M HCl. The layers were separated, and the aqueous layer was washed with EtOAc x 3. The combined organic material was passed through a phase separator and concentrated to afford the desired material as a colorless oil (262 mg, 86% yield) which

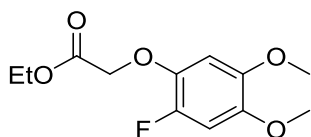
was carried forward to the next step without any further purification. ^1H NMR (400 MHz, DMSO- d_6) δ 6.86 (d, $J_{\text{HF}} = 7.5$ Hz, 1H), 6.82 (d, $J_{\text{HF}} = 11.6$ Hz, 1H), 3.72 (s, 3H), 3.71 (s, 3H), 2.75 (t, 2H), 2.48 (m, 2H); ^{13}C NMR (100 MHz, DMSO- d_6) $\delta = 173.6, 154.3$ (d, $J_{\text{CF}} = 234.0$ Hz), 148.0 (d, $J_{\text{CF}} = 10.0$ Hz), 144.9 (d, $J_{\text{CF}} = 2.0$ Hz), 117.6 (d, $J_{\text{CF}} = 17.0$ Hz), 113.4 (d, $J_{\text{CF}} = 7.0$ Hz), 100.5 (d, $J_{\text{CF}} = 28.0$ Hz), 56.0, 55.8, 34.3, 23.4 ppm. HRMS (TOF, ES+) calc'd for $\text{C}_{11}\text{H}_{13}\text{FO}_4$, 228.0798; found, 228.0798.



Synthesis of 2-fluoro-4,5-dimethoxyphenol (1.319)

To a solution of 6-fluoroveratraldehyde (300 mg, 1.63 mmol) in DCM (7.50 mL) was added 3-chloroperoxybenzoic acid (562 mg, 2.44 mmol) at room temperature portionwise. Upon completion of addition, the reaction was stirred at room temperature for 5 hr whereupon LCMS indicated complete consumption of starting materials and formation of the desired formate ester. The reaction was diluted with DCM and quenched with the addition of saturated sodium thiosulfate. The layers were separated, and the aqueous layer was washed with DCM x 3. The combined organic material was passed through a phase separator and concentrated. The crude formate ester was redissolved in THF : H₂O (1:1), and lithium hydroxide (4.89 mmol) was added. The reaction was stirred at room temperature for 1 hr before dilution with EtOAc and acidification to pH ~1 using 2 M HCl. The layers were separated, and the aqueous layer was washed with EtOAc x 3. The combined organic material was passed through a phase separator, concentrated, and purified via flash chromatography (Teledyne ISCO system; silica gel column; hexanes:EtOAc; 0-30% EtOAc gradient) to afford the desired

product as a beige solid (205 mg, 73% yield). ^1H NMR (400 MHz, CDCl_3) δ 6.68 (d, $J_{\text{HF}} = 11.6$ Hz, 1H), 6.59 (d, $J_{\text{HF}} = 8.4$ Hz, 1H), 4.79 (bd, 1H), 3.82 (s, 3H), 3.81 (s, 3H); ^{13}C NMR (100 MHz, CDCl_3) $\delta = 145.7$ (d, $J_{\text{CF}} = 2.5$ Hz), 144.5 (d, $J_{\text{CF}} = 228.3$ Hz), 142.5 (d, $J_{\text{CF}} = 7.8$ Hz), 136.6 (d, $J_{\text{CF}} = 15.0$ Hz), 102.0 (d, $J_{\text{CF}} = 2.1$ Hz), 101.0 (d, $J_{\text{CF}} = 23.2$ Hz), 56.8, 56.5 ppm. HRMS (TOF, ES^+) calc'd for $\text{C}_8\text{H}_9\text{FO}_3$, 172.0536; found, 172.0536.



Synthesis of ethyl 2-(2-fluoro-4,5-dimethoxyphenoxy)acetate (1.207d)

To a solution of 2-fluoro-4,5-dimethoxyphenol (190 mg, 1.10 mmol) in MeCN (3.17 mL) in a Biotage microwave vial was added potassium carbonate (310 mg, 2.21 mmol) and ethyl bromoacetate (244 μL , 2.21 mmol). The vial was sealed and heated to 170 $^\circ\text{C}$ for 1 hr using a Biotage microwave reactor whereupon LCMS indicated complete consumption of starting material and formation of the desired product. The reaction was diluted with EtOAc, filtered, concentrated, and purified via flash chromatography (Teledyne ISCO system; silica gel column; hexanes:EtOAc; 0-30% EtOAc gradient) to afford the desired product as a white solid (231 mg, 81% yield). ^1H NMR (400 MHz, CDCl_3) δ 6.70 (d, $J_{\text{HF}} = 5.6$ Hz, 1H), 6.67 (d, $J_{\text{HF}} = 10.2$ Hz, 1H), 4.64 (s, 2H), 4.26 (q, 2H), 3.83 (s, 3H), 3.82 (s, 3H), 1.30 (t, 3H); ^{13}C NMR (100 MHz, CDCl_3) $\delta = 169.2$, 147.4 (d, $J_{\text{CF}} = 237$ Hz), 145.1 (d, $J_{\text{CF}} = 3.0$ Hz), 144.9 (d, $J_{\text{CF}} = 8.0$ Hz), 138.5 (d, $J_{\text{CF}} = 12.0$ Hz), 104.5 (d, $J_{\text{CF}} = 2.0$ Hz), 101.5 (d, $J_{\text{CF}} = 24.0$ Hz), 69.0 (d, $J_{\text{CF}} = 3.0$ Hz), 61.4, 56.6, 56.5, 14.3 ppm. HRMS (TOF, ES^+) calc'd for $\text{C}_{12}\text{H}_{15}\text{FO}_5$, 258.0904; found, 258.0906.

References for Chapter I

1. Vassilatis, D. K.; Hohmann, J. G.; Zeng, H.; Li, F.; Ranchalis, J. E.; Mortrud, M. T.; Brown, A.; Rodriguez, S. S.; Weller, J. R.; Wright, A. C.; Bergmann, J. E.; Gaitanaris, G. A. The G protein-coupled receptor repertoires of human and mouse. *Proc. Natl. Acad. Sci.* **2003**, *100*, 4903-4908.
2. Kroeze, W. K.; Sheffler, D. G.; Rother, B. L. G-protein-coupled receptors at a glance. *J. Cell. Sci.* **2003**, *116*, 4867-4869.
3. Lv, X.; Liu, J.; Shi, Q.; Tan, Q.; Wu, D.; Skinner, J. J.; Walker, A. L.; Zhao, L.; Gu, X.; Chen, N.; Xue, L.; Si, P.; Zhang, L.; Wang, Z.; Katritch, V.; Liu, Z.; Stevens, R. C. *In vitro* expression and analysis of the 826 human G protein-coupled receptors. *Protein. Cell.* **2016**, *7*(5), 325-337.
4. Walther, C.; Ferguson, S. S. G. Minireview: Role of Intracellular Scaffolding Proteins in the Regulation of Endocrine G Protein-Coupled Receptor Signaling. *Mol. Endocrinol.* **2015**, *29*, 814-830.
5. Lombardi, M. S.; Kavelaars, A.; Heijnen, C. J. Role and modulation of G protein-coupled receptor signaling in inflammatory processes. *Crit. Rev. Immunol.* **2002**, *22*, 141-163.
6. Tao, Y. X.; Yuan, Z. H.; Xie, J. G protein-coupled receptors as regulators of energy homeostasis. *Prog. Mol. Biol. Transl. Sci.* **2013**, *114*, 1-43.
7. Rosenbaum, D. M.; Rasmussen, S. G. F.; Kobilka, B. K. The structure and function of G-protein-coupled receptors. *Nature* **2009**, *459*, 356-363.
8. Julius, D.; Nathans, J. Signaling by Sensory Receptors. *Cold Spring Harb. Perspect. Biol.* **2012**, *4*, a005991, doi:10.1101/cshperspect.a005991.
9. Overington, J. P.; Al-Lazikani, B.; Hopkins, A. L. How many drugs are there? *Nature Reviews Drug Discovery* **2006**, *5*, 993-996.
10. Lim, W. K. GPCR drug discovery: novel ligands for CNS receptors. *Recent Pat. CNS Drug Discov.* **2007**, *2*, 107-112.
11. Alavi, M. S.; Shamsizadeh, A.; Azhdari-Zarmehri, H.; Roohbakhsh, A. Orphan G protein-coupled receptors: the role in CNS disorders. *Biomed. Pharmacother.* **2018**, *98*, 222-232.
12. Santos, R.; Ursu, O.; Gaulton, A.; Bento, A. P.; Donadi, R. S.; Bologa, C. G.; Karlsson, A.; Al-Lazikani, B.; Hersey, A.; Oprea, T. I. Overington, J. P. A comprehensive map of molecular drug targets. *Nat. Rev. Drug Discov.* **2017**, *16*, 19-34.
13. Bleich, S.; Romer, K.; Wiltfang, J.; Kornhuber, J. Glutamate and the glutamate receptor system: a target for drug action. *Int. J. Geriatr. Psychiatry* **2003**, *18*, S33-S40.
14. Zhou, Y.; Danbolt, N. C. Glutamate as a neurotransmitter in the healthy brain. *J. Neural Transm.* **2014**, *121*, 799-817.
15. Moghaddam, B.; Javitt, D. From revolution to evolution: the glutamate hypothesis of schizophrenia and its implication for treatment. *Neuropsychopharmacology* **2012**, *37*, 4-15.

16. Sanacora, G.; Treccani, G.; Popoli, M. Towards a glutamate hypothesis of depression: an emerging frontier of neuropsychopharmacology for mood disorders. *Neuropharmacology* **2012**, *62*, 63-77.
17. Nicoletti, F.; Bockaert, J.; Collingridge, G. L.; Conn, P. J.; Ferraguti, F.; Schoepp, D. D.; Wroblewski, J. T.; Pin, J. P. Metabotropic glutamate receptors: from the workbench to the bedside. *Neuropharmacology* **2011**, *60*, 1017-1041.
18. Nicoletti, F.; Bruno, V.; Ngomba, R. T.; Gradini, R.; Battaglia, G. Metabotropic glutamate receptors as drug targets: what's new? *Current Opinion in Pharmacology* **2015**, *20*, 89-94.
19. Niswender, C. M.; Conn, P. J. Metabotropic glutamate receptors: physiology, pharmacology, and disease. *Annu. Rev. Pharmacol. Toxicol.* **2010**, *50*, 295-322.
20. Lindsley, C. W.; Emmitte, K. A.; Hopkins, C. R.; Bridges, T. M.; Gregory, K. J.; Niswender, C. M.; Conn, P. J. Practical strategies and concepts in GPCR allosteric modulator discovery: recent advances with metabotropic glutamate receptors. *Chem. Rev.* **2016**, *116*, 6707-6741.
21. Pin, J. P.; Galvez, T.; Prezeau, L. Evolution, structure, and activation mechanism of family 3/C G-protein-coupled receptors. *Pharmacol. Ther.* **2003**, *98*, 325-354.
22. Doumazane, E.; Scholler, P.; Zwier, J. M.; Trinquet, E.; Rondard, P.; Pin, J. P. A new approach to analyze cell surface protein complexes reveals specific heterodimeric metabotropic glutamate receptors. *FASEB.* **2011**, *25*, 66-77.
23. Tsuchiya, D.; Kunishima, N.; Kamiya, N.; Jingami, H.; Morikawa, K. Structural views of the ligand-binding cores of a metabotropic glutamate receptor complexed with an antagonist and both glutamate and Gd³⁺. *Proc. Natl. Acad. Sci.* **2002**, *99*, 2660-2665.
24. Kunishima, N.; Shimada, Y.; Tsuji, Y.; Sato, T.; Yamamoto, M.; Kumasaka, T.; Nakanishi, S.; Jingami, H.; Morikawa, K. Structural basis of glutamate recognition by a dimeric metabotropic glutamate receptor. *Nature* **2000**, *407*, 971-977.
25. Muto, T.; Tsuchiya, D.; Morikawa, A.; Jingami, H. Structures of the extracellular regions of the group II/III metabotropic glutamate receptors. *Proc. Natl. Acad. Sci.* **2007**, *104*, 3759-3764.
26. Rondard, P.; Liu, J.; Huang, S.; Malhaire, F.; Vol, C.; Pinault, A.; Labesse, G.; Pin, J-P. Coupling of agonist binding to effector domain activation in metabotropic glutamate-like receptors. *J. Biol. Chem.* **2006**, *281*, 24653-24661.
27. Stewart, A.; Fisher, R. A. Chapter one – introduction: G protein-coupled receptors and RGS proteins. *Progress in Molecular Biology and Translational Science* **2015**, *133*, 1-11.
28. Yuen, J. W. F.; Poon, L. S. W.; Chan, A. S. L.; Yu, F. W. Y.; Lo, R. K. H.; Wong, Y. H. Activation of STAT3 by specific G_α subunits and multiple G_{βγ} dimers. *The International Journal of Biochemistry and Cell Biology* **2010**, *42*, 1052-1059.
29. Bonsi, P.; Cuomo, D.; De Persis, C.; Centonze, D.; Bernardi, G.; Calabresi, P.; Pisani, A. Modulatory action of metabotropic glutamate receptor (mGluR) 5 on mGluR1 function in striatal cholinergic interneurons. *Neuropharmacology* **2005**, *49*, 104-113.
30. Chu, Z.; Hablitz, J. J. Quisqualate induces an inward current via mGluR activation in neocortical pyramidal neurons. *Brain Research* **2000**, *879*, 88-92.

31. Endoh, T. Characterization of modulatory effects of postsynaptic metabotropic glutamate receptors on calcium currents in rat nucleus tractus solitarius. *Brain Research* **2004**, *1024*, 212-224.
32. Skeberdis, V. A.; Lan, J-Y.; Opitz, T.; Zheng, X.; Bennet, M. V. L.; Zukin, R. S. mGluR1-mediated potentiation of NMDA receptors involves a rise in intracellular calcium and activation of protein kinase C. *Neuropharmacology* **2001**, *40*, 856-865.
33. Shigemoto, R.; Kinoshita, A.; Wada, E.; Nomura, S.; Ohishi, H.; Takada, M.; Flor, P. J.; Neki, A.; Abe, T.; Nakanishi, S.; Mizuno, N. Differential presynaptic localization of metabotropic glutamate receptor subtypes in the rat hippocampus. *J. Neurosci.* **1997**, *17*, 7503-7522.
34. Hinoi, E.; Ogita, K.; Takeuchi, Y.; Ohashi, H.; Maruyama, T.; Yoneda, Y. Characterization with [³H]quisqualate of group I metabotropic glutamate receptor subtype in rat central and peripheral excitable tissues. *Neurochemistry International* **2001**, *38*, 277-285.
35. Ambrosini, A.; Bresciani, L.; Fracchia, S.; Brunello, N.; Racagni, G. Metabotropic glutamate receptors negatively coupled to adenylate cyclase inhibit *N*-methyl-D-aspartate receptor activity and prevent neurotoxicity in mesencephalic neurons *in vitro*. *Mol. Pharmacol.* **1995**, *47*, 1057-1064.
36. Niswender, C. M.; Lebois, E. P.; Luo, Q.; Kim, K.; Muchalski, H.; Yin, H.; Conn, P. J.; Lindsley, C. W. Positive allosteric modulators of the metabotropic glutamate receptor subtype 4 (mGluR4): Part 1. Discovery of pyrazolo[3,4-d]pyrimidines as novel mGluR4 positive allosteric modulators. *Bioorg. Med. Chem. Lett.* **2008**, *18*, 5626-5630.
37. Sansig, G.; Bushell, T. J.; Clarke, V. R. J.; Rozov, A.; Burnashev, N.; Portet, C.; Gasparini, F.; Schmutz, M.; Klebs, K.; Shigemoto, R.; Flor, P. J.; Kuhn, R.; Knoepfel, T.; Schroeder, M.; Hampson, D. R.; Collett, V. J.; Zhang, C.; Duvoisin, R. M.; Collingridge, G. L.; van der Putten, H. Increased seizure susceptibility in mice lacking metabotropic glutamate receptor 7. *J. Neurosci.* **2001**, *21*, 8734-8745.
38. Goddyn, H.; Callaerts-Vegh, Z.; Stroobants, S.; Dirikx, T.; Vansteenwegen, D.; Hermans, D.; van der Putten, H.; D'Hooge, R. Deficits in acquisition and extinction of conditioned responses in mGluR7 knockout mice. *Neurobiology of Learning and Memory* **2008**, *90*, 103-111.
39. Palucha, A.; Klak, K.; Branski, P.; van der Putten, H.; Flor, P.; Pilc, A. Activation of the mGlu₇ receptor elicits antidepressant-like effects in mice. *Psychopharmacology* **2007**, *194*, 555-562.
40. Callaerts-Vegh, Z.; Beckers, T.; Ball, S. M.; Baeyens, F.; Callaerts, P. F.; Cryan, J. F.; Molnar, E.; D'Hooge, R. Concomitant deficits in working memory and fear extinction are functionally dissociated from reduced anxiety in metabotropic glutamate receptor 7-deficient mice. *J. Neurosci.* **2006**, *26*, 6573-6582.
41. Mitsukawa, K.; Mombereau, C.; Lötscher, E.; Uzunov, D. P.; van der Putten, H.; Flor, P. J.; Cryan, J. F. Metabotropic glutamate receptor subtype 7 ablation causes dysregulation of the HPA axis and increases hippocampal BDNF protein levels: implications for stress-related psychiatric disorders. *Neuropsychopharmacology* **2006**, *31*, 1112-1122.

42. Hölscher, C.; Schmid, S.; Pilz, P. K. D.; Sansig, G.; van der Putten, H.; Plappert, C. F. Lack of the metabotropic glutamate receptor subtype 7 selectively impairs short-term working memory but not long-term memory. *Behavioral Brain Research* **2004**, *154*, 473-481.
43. Bushell, T. J.; Sansig, G.; Collett, V. J.; van der Putten, H.; Collingridge, G. L. Altered short-term synaptic plasticity in mice lacking the metabotropic glutamate receptor mGlu₇. *The Scientific World Journal* **2002**, *2*, 730-737.
44. Masugi, M.; Yokoi, M.; Shigemoto, R.; Muguruma, K.; Watanabe, Y.; Sansig, G.; van der Putten, H.; Nakanishi, S. Metabotropic glutamate receptor subtype 7 ablation causes deficit in fear response and conditioned taste aversion. *J. Neurosci.* **1999**, *19*, 955-963.
45. Jalan-Sakrikar, N.; Field, J. R.; Klar, R.; Mattmann, M. E.; Gregory, K. J.; Zamorano, R.; Engers, D. W.; Bollinger, S. R.; Weaver, C. D.; Days, E. L.; Lewis, L. M.; Utley, T. J.; Hurtado, M.; Rigault, D.; Acher, F.; Walker, A. G.; Melancon, B. J.; Wood, M. R.; Lindsley, C. W.; Conn, P. J.; Xiang, Z.; Hopkins, C. R.; Niswender, C. M. Identification of positive allosteric modulators VU0155094 (ML397) and VU0422288 (ML396) reveals new insights into the biology of metabotropic glutamate receptor 7. *ACS Chem. Neurosci.* **2014**, *5*, 1221-1237.
46. Schoepp, D. D.; Jane, D. E.; Monn, J. A. Pharmacological agents acting at subtypes of metabotropic glutamate receptors. *Neuropharmacology* **1999**, *38*, 1431-1476.
47. Fisher, N. M.; Seto, M.; Lindsley, C. W.; Niswender, C. M. Metabotropic glutamate receptor 7: a new therapeutic target in neurodevelopmental disorders. *Front. Mol. Neurosci.* **2018**, *11*, 387. doi: 10.3389/fnmol.2018.00387.
48. Klar, R.; Walker, A. G.; Ghose, D.; Grueter, B. A.; Engers, D. W.; Hopkins, C. R.; Lindsley, C. W.; Xiang, Z.; Conn, P. J.; Niswender, C. M. Activation of metabotropic glutamate receptor 7 is required for induction of long-term potentiation at SC-CA1 synapses in the hippocampus. *J. Neurosci.* **2015**, *35*, 7600-7615.
49. Cooke, S. F.; Bliss, T. V. P. Plasticity in the human central nervous system. *Brain* **2006**, *129*, 1659-1673.
50. Bliss, T. V. P.; Collingridge, G. L. A synaptic model of memory: long-term potentiation in the hippocampus. *Nature* **1993**, *361*, 31-39.
51. Kandel, E. R.; Schwartz, J. H.; Jessell, T. M.; Siegelbaum, S. A.; Hudspeth, A. J. Principles of Neural Science. **2012**. 5th ed. New York. McGraw-Hill.
52. Flor, P. J.; Acher, F. C. Orthosteric versus allosteric GPCR activation: the great challenge of group-III mGluRs. *Biochemical Pharmacology* **2012**, *84*, 414-424.
53. Odagaki, Y. Agonists and allosteric modulators of G protein-coupled receptors as promising psychotropic drugs. *Frontiers in Clinical Drug Research – Central Nervous System* **2013**, *1*, 3-43.
54. Shannon, H.; Bymaster, E.; Calligaro, D.; Delapp, N.; Mitch, C.; Warc, J.; Olesen, P.; Sheardown, M.; Swedberg, M.; Sauerberg, P. The discovery and pharmacology of xanomeline, a muscarinic M₁ receptor agonist for Alzheimer's disease. *European Neuropsychopharmacology* **1995**, *5*, 254.
55. Bender, A. M.; Jones, C. K.; Lindsley, C. W. Classics in chemical neuroscience: xanomeline. *ACS Chem. Neurosci.* **2017**, *15*, 435-443.

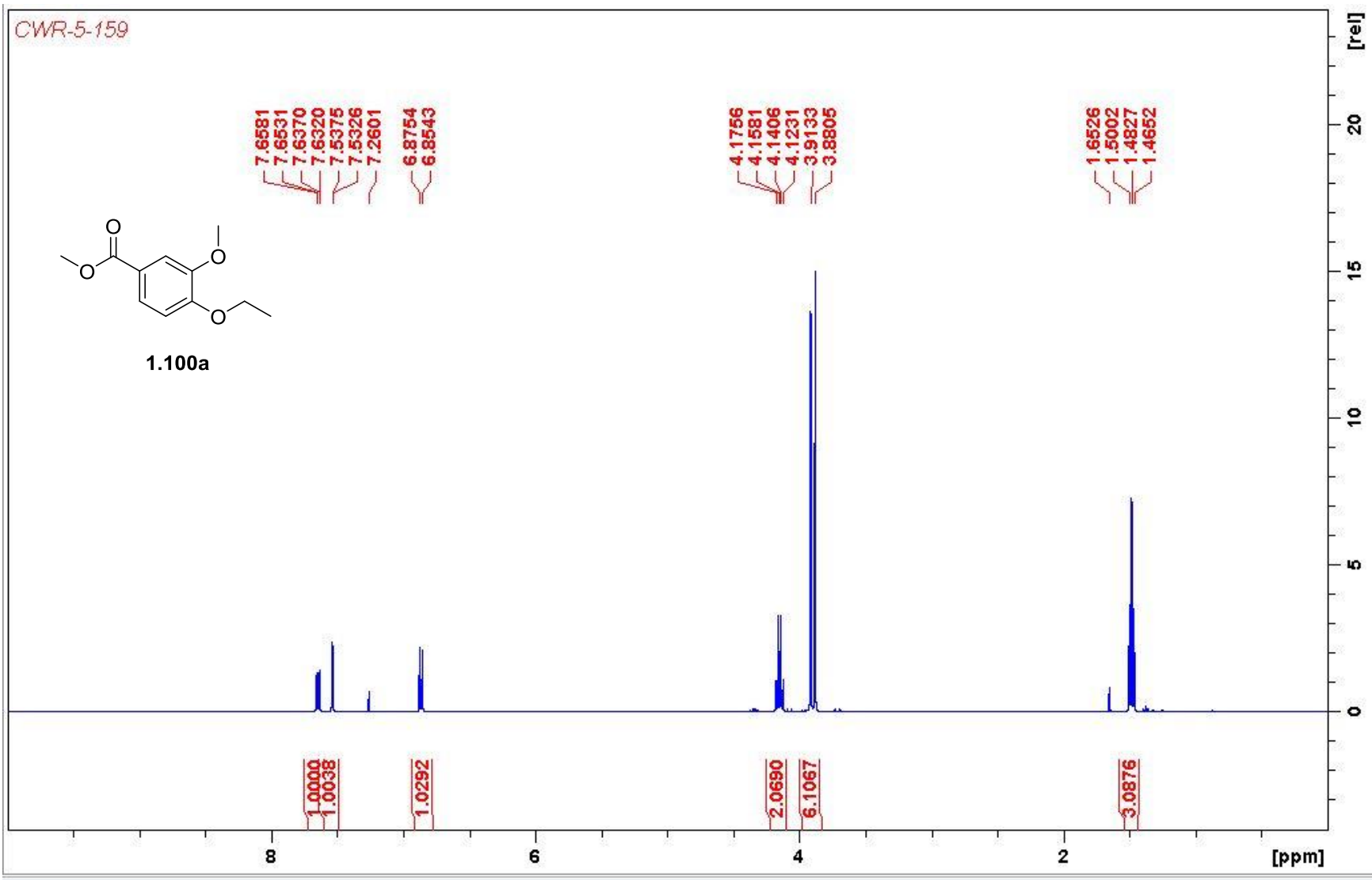
56. Conn, P. J.; Christopoulos, A.; Lindsley, C. W. Allosteric modulators of GPCRs: a novel approach for the treatment of CNS disorders. *Nat. Rev. Drug Discovery* **2009**, *8*, 41-54.
57. Farinha, A.; Lavreysen, H.; Peeters, L.; Russo, B.; Masure, S.; Trabanco, A.; Cid, J.; Tresadern, G. Molecular determinants of positive allosteric modulation of the human metabotropic glutamate receptor 2. *Br. J. Pharmacol.* **2015**, *172*, 2383-2396.
58. Dore, A. S.; Okrasa, K.; Patel, J. C.; Serrano-Vega, M.; Bennet, K.; Cooke, R. M.; Errey, J. C.; Jazayeri, A.; Khan, S.; Tehan, B.; Weir, M.; Wiggin, G. R.; Marshall, F. H. Structure of class C GPCR metabotropic glutamate receptor 5 transmembrane domain. *Nature* **2014**, *511*, 557-562.
59. Wu, H.; Wang, C.; Gregory, K. J.; Han, G. W.; Cho, H. P.; Xia, Y.; Niswender, C. M.; Katritch, V.; Meiler, J.; Cherezov, V.; Conn, P. J.; Stevens, R. C. Structure of a class C GPCR metabotropic glutamate receptor 1 bound to an allosteric modulator. *Science* **2014**, *344*, 58-64.
60. Perez-Benito, L.; Doornbos, M. L. J.; Cordomi, A.; Peeters, L.; Lavreysen, H.; Pardo, L.; Tresadern, G. Molecular switches of allosteric modulation of the metabotropic glutamate 2 receptor. *Structure* **2017**, *25*, 1153-1162.
61. May, L. T.; Leach, K.; Sexton, P. M.; Christopoulos, A. Allosteric modulation of G protein-coupled receptors. *Annu. Rev. Pharmacol. Toxicol.* **2007**, *47*, 1-51.
62. Christopoulos, A.; Mitchelson, F. Application of an allosteric ternary complex model to the technique of pharmacological resultant analysis. *J. Pharm. Pharmacol.* **1997**, *49*, 781-786.
63. Foster, D. J.; Conn, P. J. Allosteric modulation of GPCRs: new insights and potential utility for treatment of schizophrenia and other CNS disorders. *Neuron* **2017**, *94*, 431-446.
64. Suzuki, G.; Tsukamoto, N.; Fushiki, H.; Kawagishi, A.; Nakamura, M.; Kurihara, H.; Mitsuya, M.; Ohkubo, M.; Ohta, H. *In vitro* pharmacological characterization of novel isoxazolopyridone derivatives as allosteric metabotropic glutamate receptor 7 antagonists. *J. Pharmacol. Exp. Ther.* **2007**, *323*, 147-156.
65. Nakamura, M.; Kurihara, H.; Suzuki, G.; Mitsuya, M.; Ohkubo, M.; Ohta, H. Isoxazolopyridone derivatives as allosteric metabotropic glutamate receptor 7 antagonists. *Bioorg. Med. Chem. Lett.* **2010**, *20*, 726-729.
66. Niswender, C. M.; Johnson, K. A.; Miller, N. R.; Ayala, J. E.; Luo, Q.; Williams, R.; Saleh, S.; Orton, D.; Weaver, C. D.; Conn, P. J. Context-dependent pharmacology exhibited by negative allosteric modulators of metabotropic glutamate receptor 7. *Mol. Pharmacol.* **2010**, *77*, 459-468.
67. Kalinichev, M.; Rouillier, M.; Girard, F.; Royer-Urios, I.; Bournique, B.; Finn, T.; Charvin, D.; Campo, B.; Le Poul, E.; Mutel, V.; Poli, S.; Neale, S. A.; Salt, T. E.; Lütjens, R. ADX71743, a potent and selective negative allosteric modulator of metabotropic glutamate receptor 7: in vitro and in vivo characterization. *J. Pharmacol. Exp. Ther.* **2013**, *344*, 626-636.
68. Reed, C. W.; McGowan, K. M.; Spearing, P. K.; Stansley, B. J.; Roenfan, H. F.; Engers, D. W.; Rodriguez, A. L.; Engelberg, E. M.; Luscombe, V. B.; Loch, M. T.; Remke, D. H.; Rook, J. M.; Blobaum, A. L.; Conn, P. J.; Niswender, C. M.; Lindsley, C. W. VU6010608, a novel mGlu₇ NAM from a series of *N*-(2-(1*H*-1,2,4-

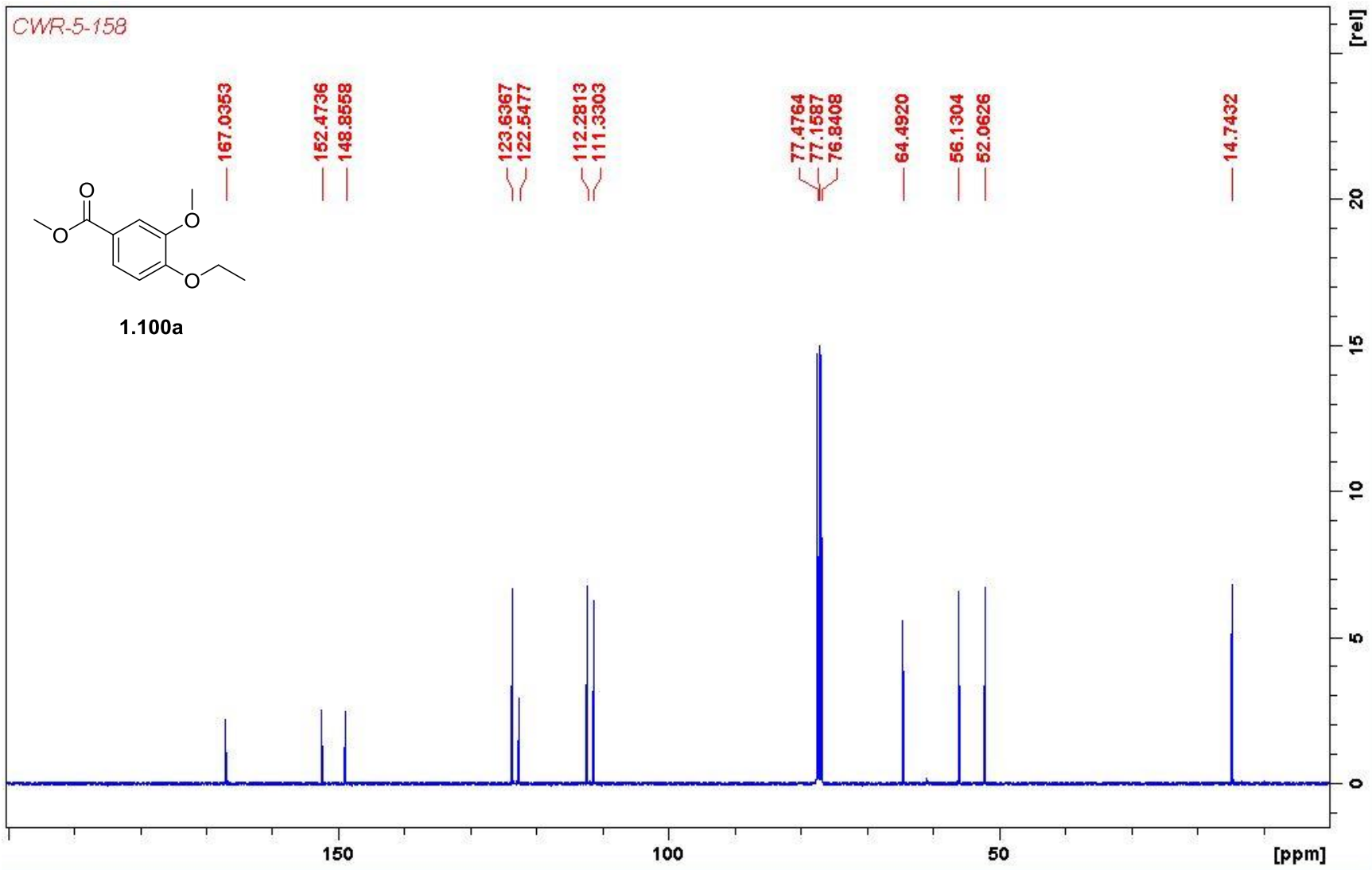
- triazol-1-yl)-5-(trifluoromethoxy)phenyl)benzamides. *ACS Med. Chem. Lett.* **2017**, *8*, 1326-1330.
69. Gee, C. E.; Peterlik, D.; Neuhäuser, C.; Bouhelal, R.; Kaupmann, K.; Laue, G.; Uschold-Schmidt, N.; Feuerbach, D.; Zimmermann, K.; Ofner, S.; Cryan, J. F.; van der Putten, H.; Fendt, M.; Vranesic, I.; Glatthar, R.; Flor, P. J. Blocking metabotropic glutamate receptor subtype 7 (mGlu₇) via the venus flytrap domain (VFTD) inhibits amygdala plasticity, stress, and anxiety-related behavior. *J. Biol. Chem.* **2014**, *289*, 10975-10987.
70. Palazzo, E.; Marabese, I.; de Novellis, V.; Rossi, F.; Maione, S. Metabotropic glutamate receptor 7: from synaptic function to therapeutic implications. *Current Neuropharmacology* **2016**, *14*, 504-513.
71. Baell, J.; Walters, M. A. Chemistry: chemical con artists foil drug discovery. *Nature* **2014**, *513*, 481-483.
72. Murray, C. J.; Atkinson, C.; Bhalla, K.; Birbeck, G.; Burstein R.; Chou, D.; Dellavalle, R.; Danaei, G.; Ezzati, M.; et. al. The state of US health, 1990-2010: burden of diseases, injuries, and risk factors. *J. Am. Med. Association* **2013**, *310*, 591-608.
73. Bunney, W. E.; Davis, J. M. Norepinephrine in depressive reactions. *Arch. Gen. Psychiatry* **1965**, *13*, 483-494.
74. Schildkraut, J. J. The catecholamine hypothesis of affective disorders: a review of supporting evidence. *Am. J. Psychiatry* **1965**, *122*, 509-522.
75. Albert, P. R.; Benkelfat, C., Descarries, L. The neurobiology of depression – revisiting the serotonin hypothesis: cellular and molecular mechanisms. *Phil. Trans. R. Soc. B* **2012**, *367*, 2378-2381.
76. Luscher, B.; Shen, Q.; Sahir, N. The GABAergic deficit hypothesis of major depressive disorder. *Mol. Psychiatry* **2011**, *16*, 383-406.
77. Miller, S.; Kesslak, J. P.; Romano, C.; Cotman, C. W. Roles of metabotropic glutamate receptors in brain plasticity and pathology. *Annals of the New York Academy of Sciences* **1995**, *757*, 460-474.
78. Cieslik, P.; Wozniak, M.; Kaczorowska, K.; Branski, P.; Burnat, G.; Chocyk, A.; Bobula, B.; Gruca, P.; Litwa, E.; Palucha-Poniewiera, A.; Wasik, A.; Pilc, A.; Wieronska, J. Negative allosteric modulators of mGlu₇ receptor as putative antipsychotic drugs. *Front. Mol. Neurosci.* **2018**, *11*, 316.
79. Perroy, J.; El Far, O.; Bertaso, F.; Pin, J. P.; Betz, H.; Bockaert, J.; Fagni, L. PICK1 is required for the control of synaptic transmission by the metabotropic glutamate receptor 7. *EMBO J.* **2002**, *21*, 2990-2999.
80. Bertaso, F.; Zhang, C.; Scheschonka, A.; de Bock, F.; Fontanaud, P.; Marin, P.; Haganir, R. L.; Betz, H.; Bockaert, J.; Fagni, L.; Lerner-Natoli, M. PICK1 uncoupling from mGluR7a causes absence-like seizures. *Nat. Neurosci.* **2008**, *11*, 940-948.
81. Zhang, C. S.; Bertaso, F.; Eulenberg, V.; Lerner-Natoli, M.; Herin, G. A.; Bauer, L.; Bockaert, J.; Fagni, L.; Betz, H.; Scheschonka, A. Knock-in mice lacking the PDZ-ligand motif of mGluR7a show impaired PKC-dependent autoinhibition of glutamate release, spatial working memory deficits, and increased susceptibility to pentylenetetrazol. *J. Neurosci.* **2008**, *28*, 8604-8614.

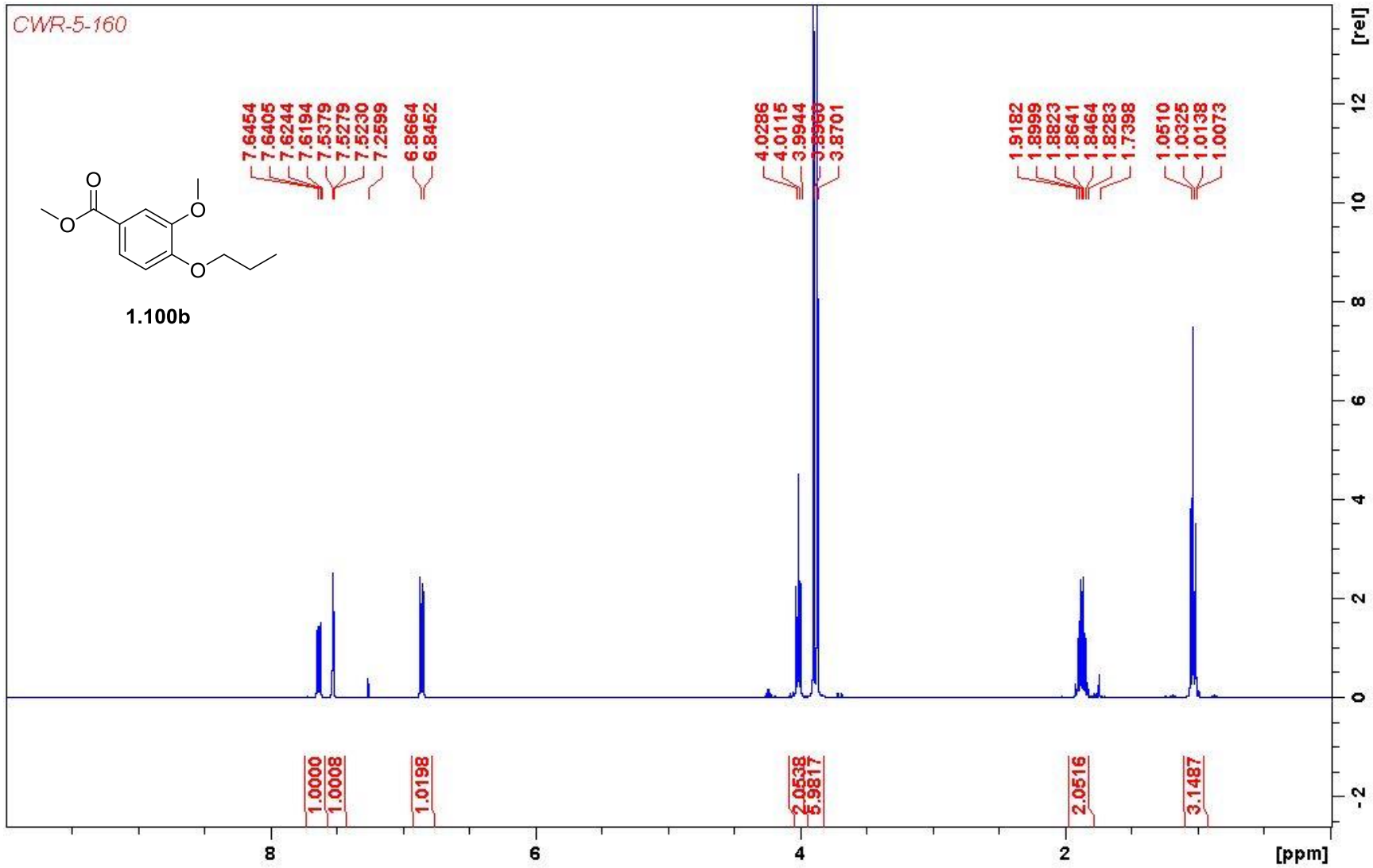
82. Tomioka, N. H.; Yasuda, H.; Miyamoto, H.; Hatayama, M.; Morimura, N.; Matsumoto, Y.; Suzuki, T.; Odagawa, M.; Odaka, Y. S.; Iwayama, Y.; Um, J. W.; Ko, J.; Inoue, Y.; Kaneko, S.; Hirose, S.; Yamada, K.; Yoshikawa, T.; Yamakawa, K.; Aruga, J. ELFN1 recruits presynaptic mGluR7 in trans and its loss results in seizures.
83. Dunn, H. A.; Patil, D. N.; Cao, Y.; Orlandi, C.; Martemyanov, K. A. Synaptic adhesion protein ELFN1 is a selective allosteric modulator of group III metabotropic glutamate receptors *in trans*. *Proc. Natl. Acad. Sci.* **2018**, *115*, 5022-5027.
84. Niswender, C. M.; Johnson, K. A.; Luo, Q.; Ayala, J. E.; Kim, C.; Conn, P. J.; Weaver, C. D. A novel assay of Gi/o-linked G protein-coupled receptor coupling to potassium channels provides new insight into the pharmacology of the group III metabotropic glutamate receptors. *Mol. Pharmacol.* **2008**, *73*, 1213-1224.
85. Jones, C. K.; Bubser, M.; Thompson, A. D.; Dickerson, J. W.; Turle-Lorenzo, N.; Amalric, M.; Blobaum, A. L.; Bridges, T. M.; Morrison, R. D.; Jadhav, S.; Engers, D. W.; Italiano, K.; Bode, J.; Daniels, J. S.; Lindsley, C. W.; Hopkins, C. R.; Niswender, C. M. The metabotropic glutamate receptor 4-positive allosteric modulator VU0364770 produces efficacy alone and in combination with L-DOPA or an adenosine A2A antagonist in preclinical rodent models of Parkinson's disease. *J. Pharmacol. Exp. Ther.* **2012**, *340*, 404-421.
86. Bridges, T. M.; Morrison, R. D.; Byers, F. W.; Luo, S.; Daniels, J. S. Use of a novel rapids and resource-efficient cassette dosing approach to determine the pharmacokinetics and CNS distribution of small molecule 7-transmembrane receptor allosteric modulators in rat. *Pharmacol. Res. Perspect.* **2014**, *2*, doi: 10.1002/prp2.77.
87. Sperotto, E.; van Klink, G. P. M.; van Koten, G.; de Vries, J. G. The mechanism of the modified Ullmann reaction. *Dalton Trans.* **2010**, *39*, 10338-10351.
88. Patani, G. A.; LaVoie, E. J. Bioisosterism: a rational approach in drug design. *Chem. Rev.* **1996**, *96*, 3147-3176.
89. Reed, C. W.; Yohn, S. E.; Washecheck, J. P.; Roenfanz, H. F.; Quitlig, M. C.; Luscombe, V. B.; Jenkins, M. T.; Rodriguez, A. L.; Engers, D. W.; Blobaum, A. L.; Conn, P. J.; Niswender, C. M.; Lindsley, C. W. Discovery of an orally bioavailable and central nervous system (CNS) penetrant mGlu₇ negative allosteric modulator (NAM) *in vivo* tool compound: *N*-(2-(1*H*-1,2,4-triazol-1-yl)-5-(trifluoromethoxy)phenyl)-4-(cyclopropylmethoxy)-3-methoxybenzamide (VU6012962). *J. Med. Chem.* **2019**, *62*, 1690-1695.
90. Meanwell, N. A. Synopsis of some recent tactical application of bioisosteres in drug design. *J. Med. Chem.* **2011**, *54*, 2529-2591.
91. Reed, C. W.; Washecheck, J. P.; Quitlig, M. C.; Jenkins, M. T.; Rodriguez, A. L.; Engers, D. W.; Blobaum, A. L.; Conn, P. J.; Niswender, C. M.; Lindsley, C. W. Surveying heterocycles as amide bioisosteres within a series of mGlu₇ NAMs: discovery of VU6019278. *Bioorg. Med. Chem. Lett.* **2019**, *29*, 1211-1214.
92. Augustine, J. K.; Vairaperumal, V.; Narasimhan, S.; Alagarsamy, P.; Radhakrishnan, A. Propylphosphonic anhydride (T3P®): an efficient reagent for the one-pot synthesis of 1,2,4-oxadiazoles, 1,3,4-oxadiazoles, and 1,3,4-thiadiazoles. *Tetrahedron* **2009**, *65*, 9989-9996.

Appendix A

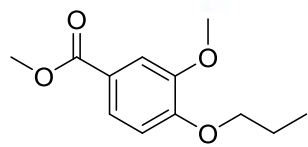
Relevant Spectra for Chapter 1







CWR-5-160



1.100b

167.0045

152.6993

148.9398

123.6040

122.4691

112.4172

111.4907

77.4766

77.1588

76.8408

70.4858

56.1357

52.0062

22.4129

10.4551

150

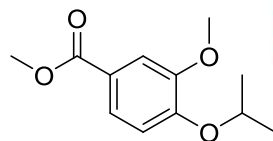
100

50

[ppm]

[rel]

CWR-5-161



1.100c

7.6351
7.6301
7.6140
7.6090
7.5330
7.5281
7.2602
6.8806
6.8594

4.6520
4.6368
4.6216
4.6064
4.5912

3.8846
3.8693

1.3816
1.3764

1.0000
0.9953

1.0762

1.0868

6.4108

6.5537

8

6

4

2

[ppm]

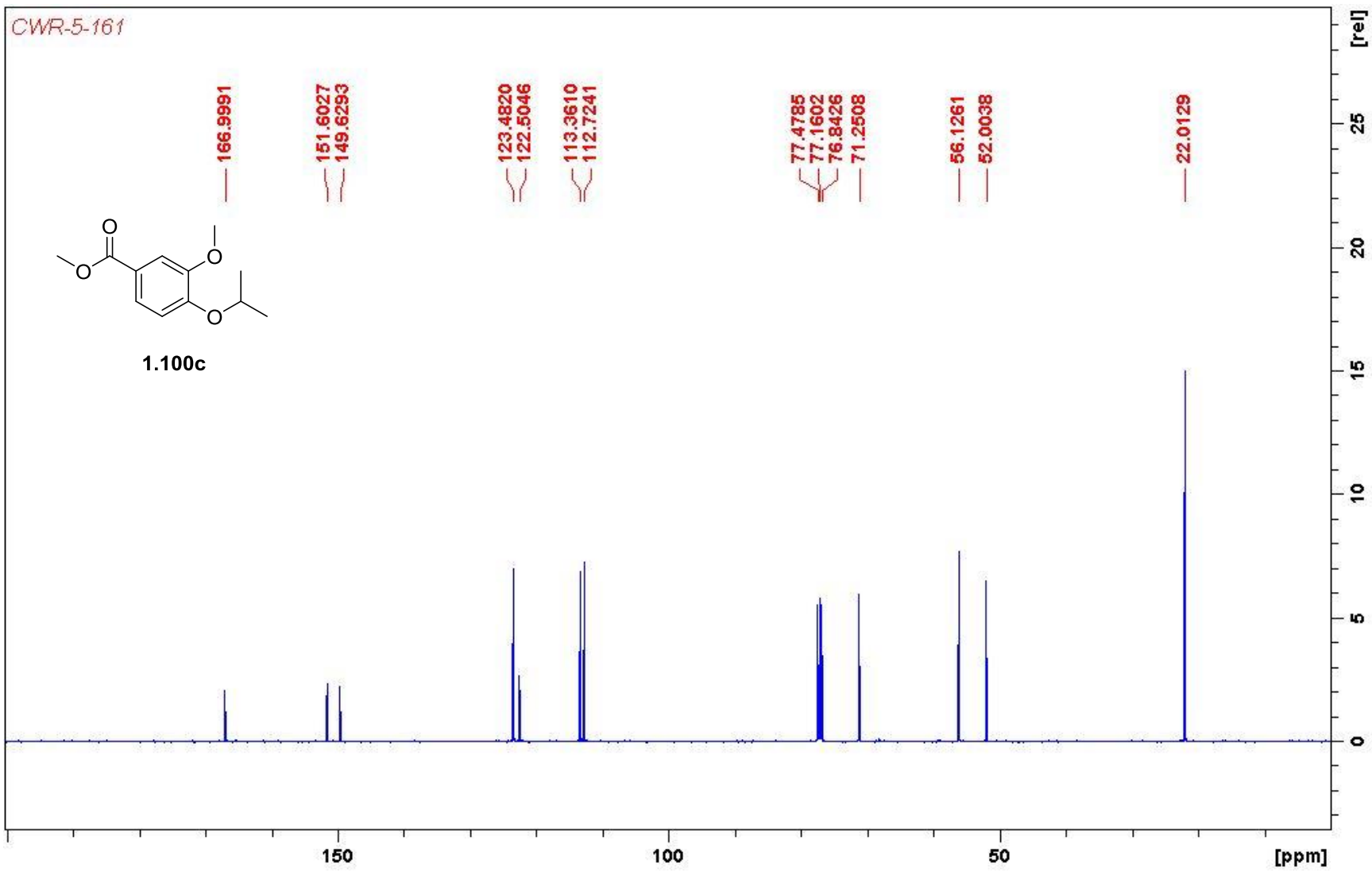
[rel]

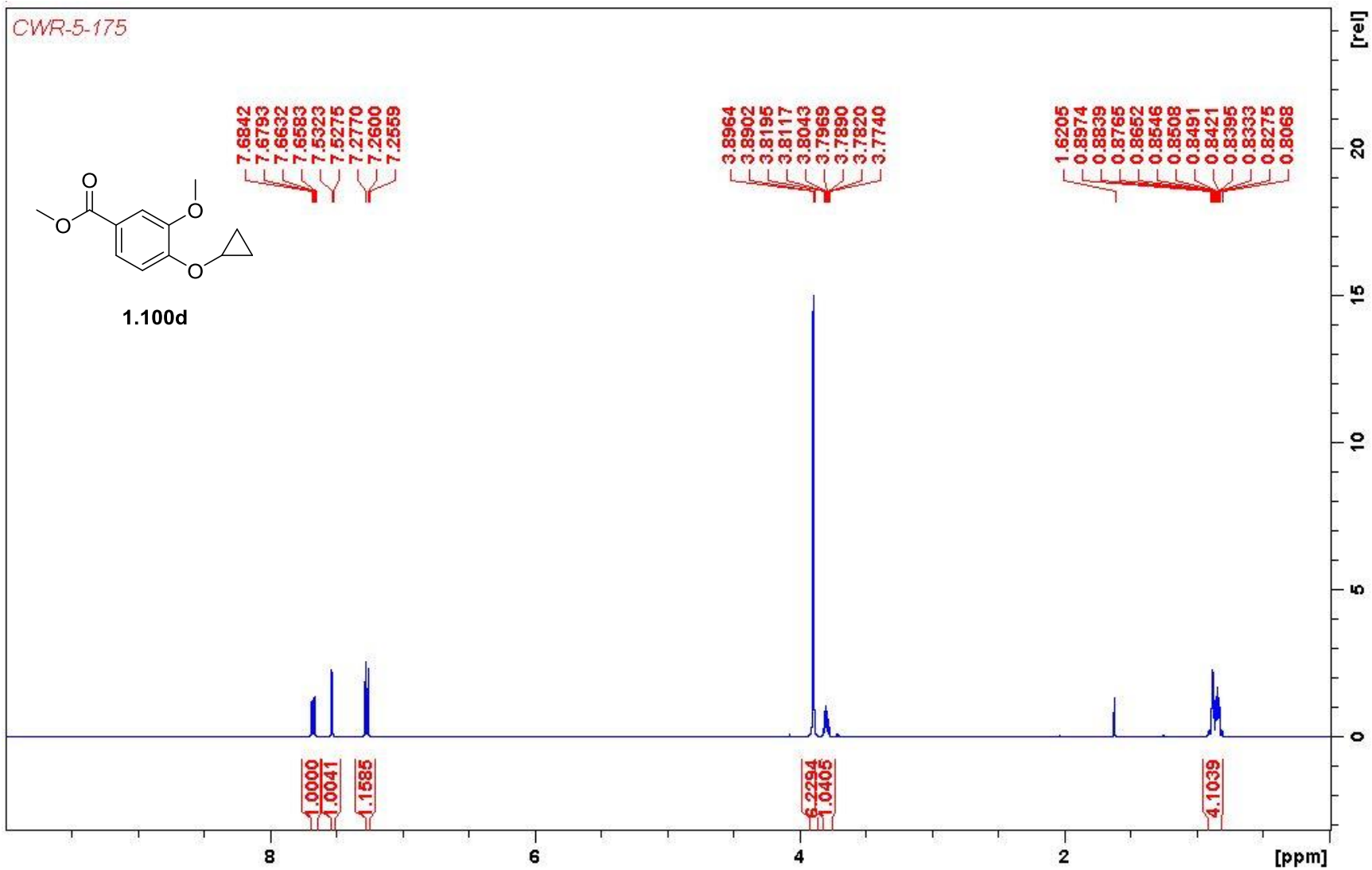
15

10

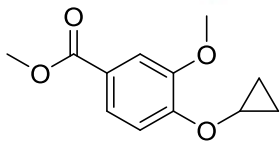
5

0





CWR-5-175



1.100d

167.0361

152.5721

148.6153

123.4962

123.0935

112.6901

112.1979

77.4783

77.1606

76.8429

56.0913

52.1135

51.9144

6.4643

20 [ref]

15

10

5

0

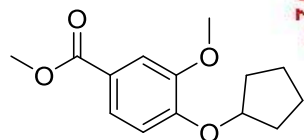
150

100

50

[ppm]

CWR-5-162



1.100e

7.6303
7.6254
7.6092
7.6043
7.5161
7.5113
7.2599
6.8596
6.8496
6.8385
4.8344
4.8270
4.8197
4.8120
4.8045
4.7968
4.7885
3.8687
3.8636
1.9829
1.9759
1.9645
1.9495
1.9346
1.9198
1.9141
1.9022
1.8938
1.8894
1.8661
1.8581
1.8543
1.8419
1.8370
1.8328
1.8296
1.8222
1.8115
1.8054
1.7952
1.7833
1.7736
1.6443
1.6316
1.6186
1.6130
1.6068
1.6027
1.5945
1.5811
1.5635

1.0000
1.0024
1.0246
1.0513
6.2209
6.4376
2.0908

[rel]

15

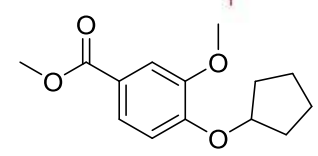
10

5

0

[ppm]

CWR-5-162



1.100e

167.0224

151.9683
149.4078

123.4841
122.2138

113.0783
112.6248

80.5006
77.4760
77.1585
76.8399

56.1345
51.9538

32.9209

24.2147

[rel]

20

15

10

5

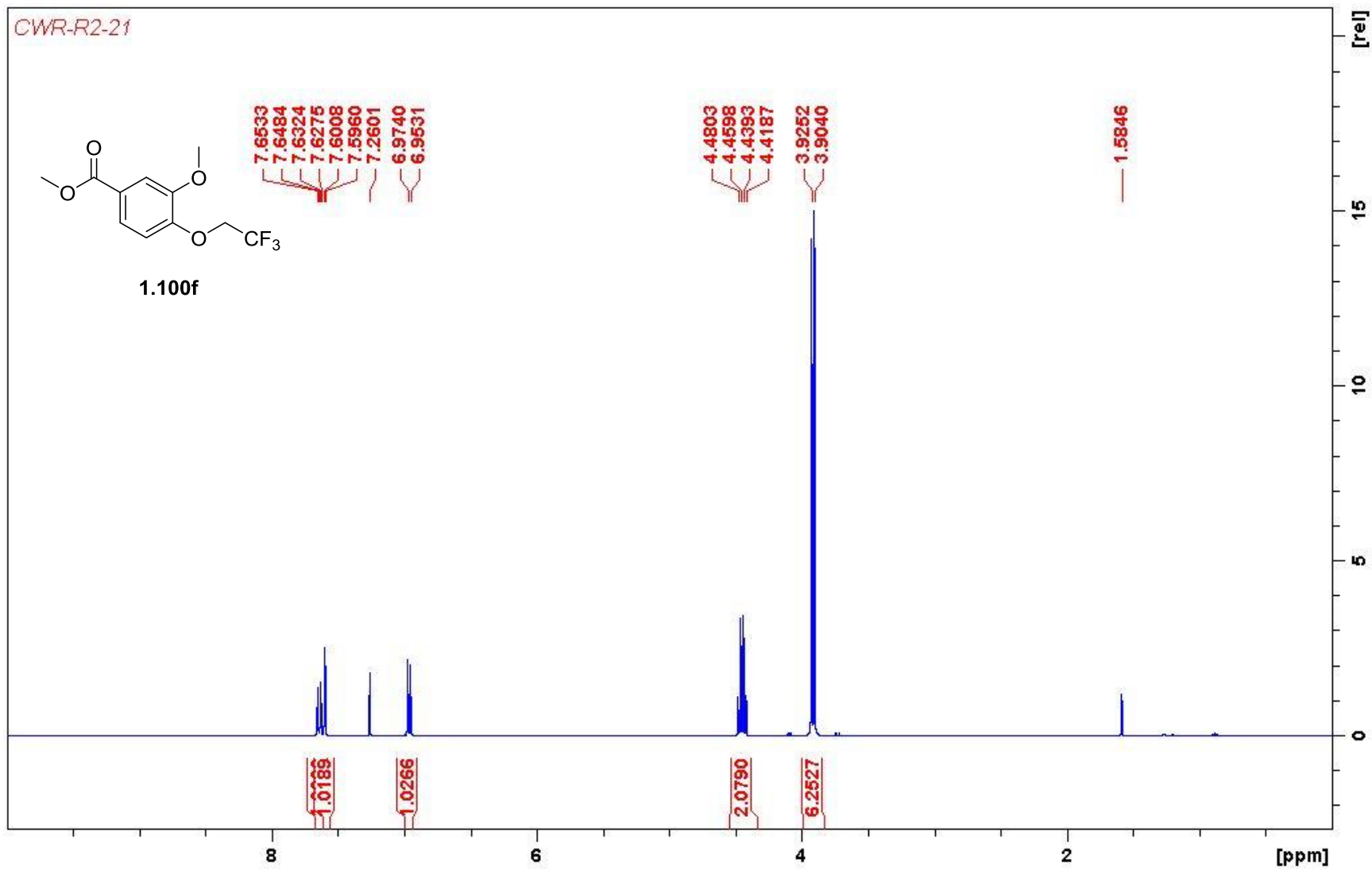
0

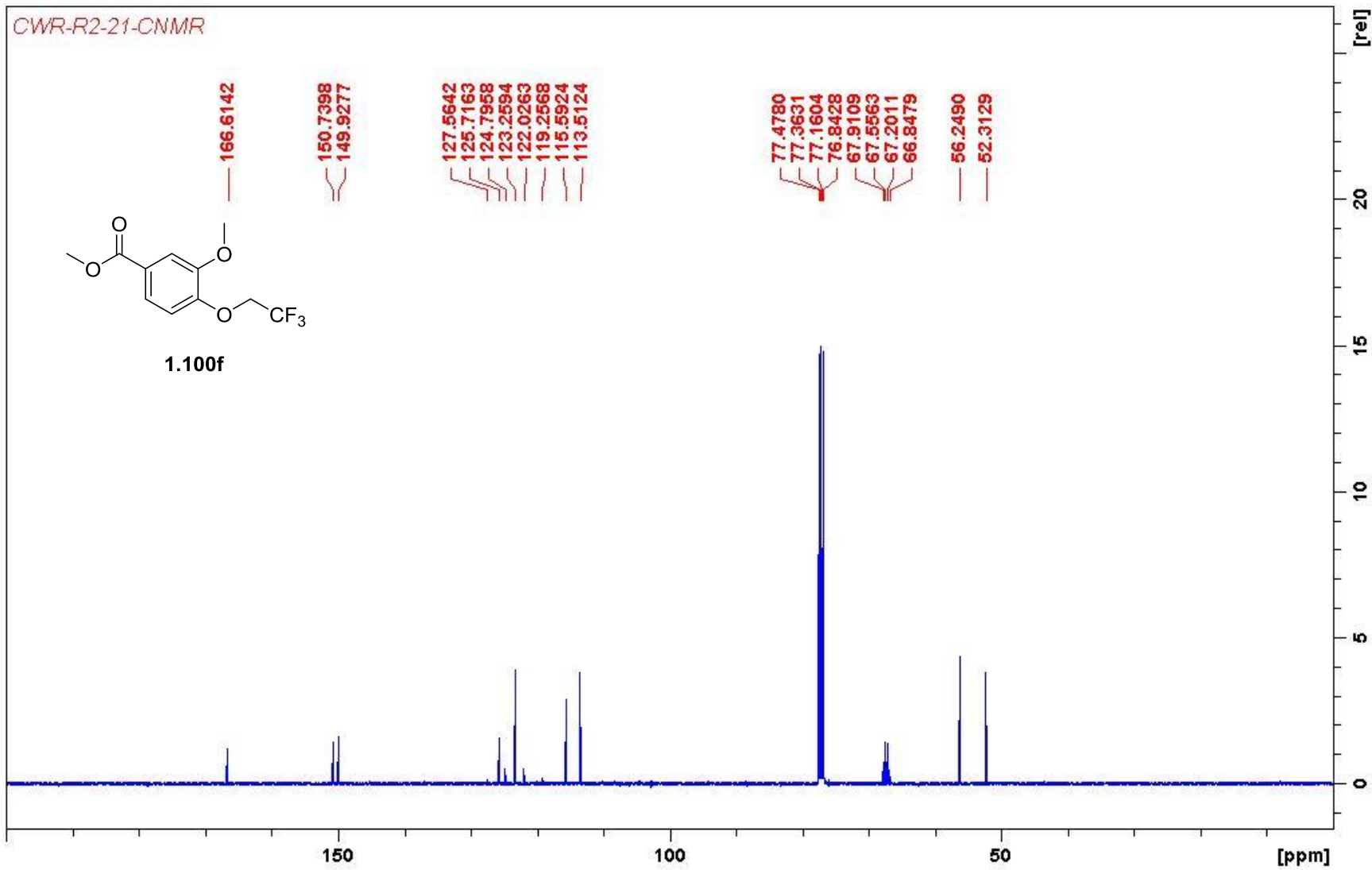
150

100

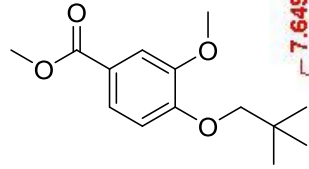
50

[ppm]





CWR-R2-26



1.100g

7.6490
7.6440
7.6280
7.6230
7.5387
7.5338
7.2600
6.8667
6.8456

3.8869
3.8800
3.6734

1.0624

1.0000
0.9094

0.9772

6.1212
2.1985

9.2625

8

6

4

2

[ppm]

[rel]

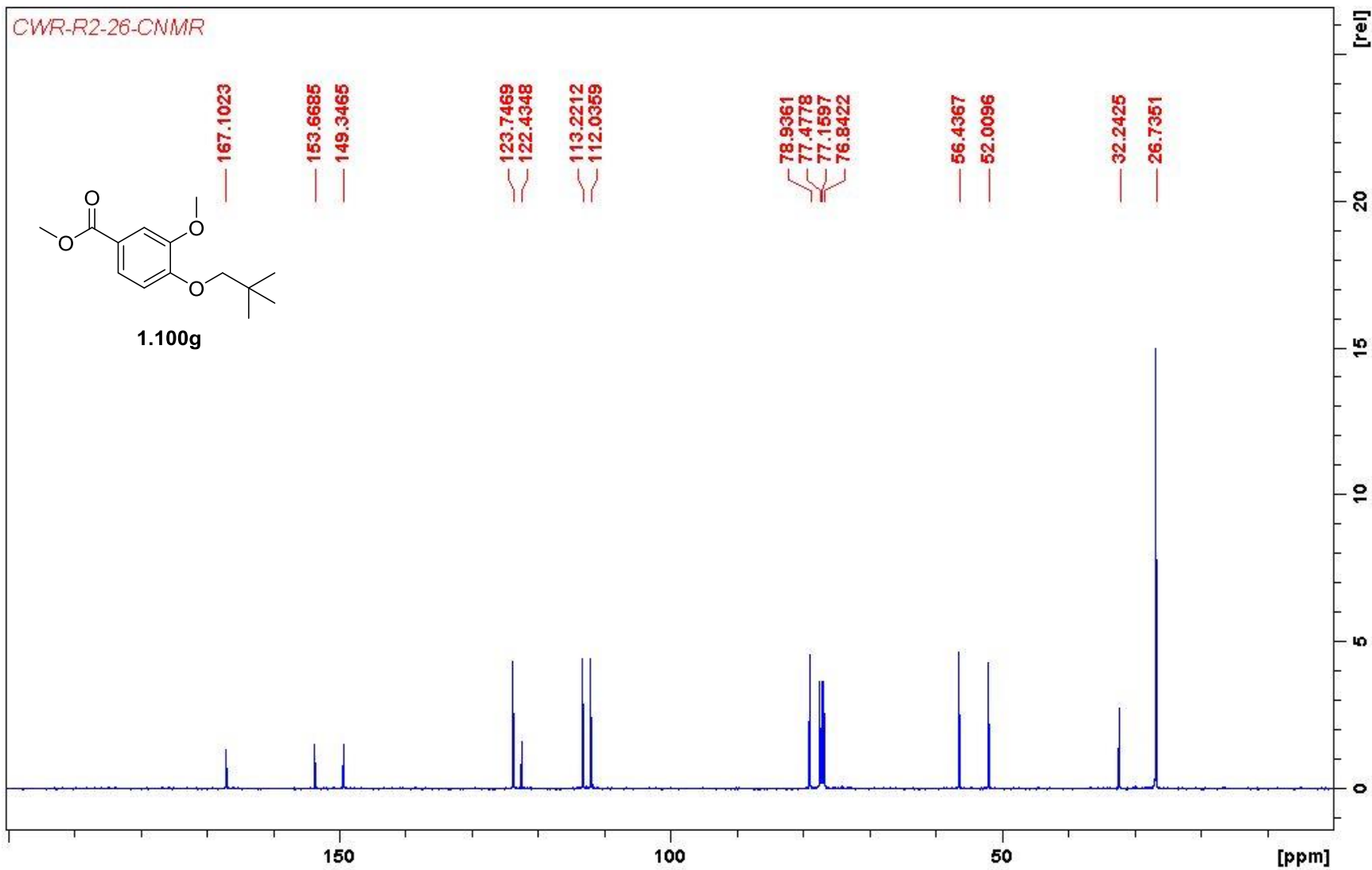
8

6

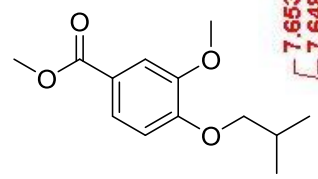
4

2

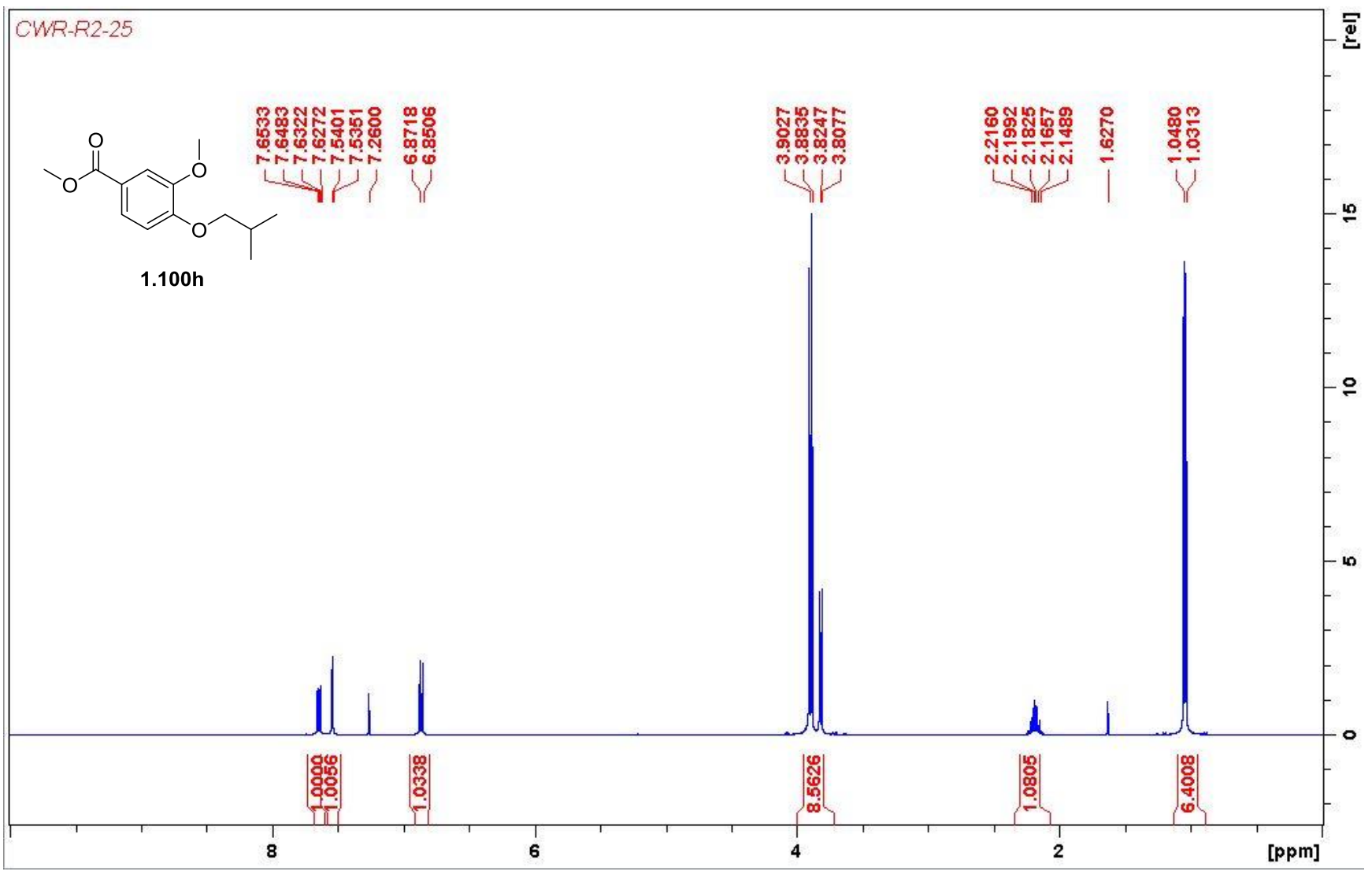
0



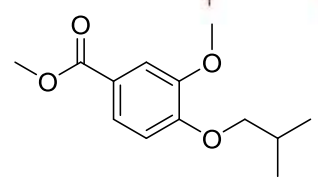
CWR-R2-25



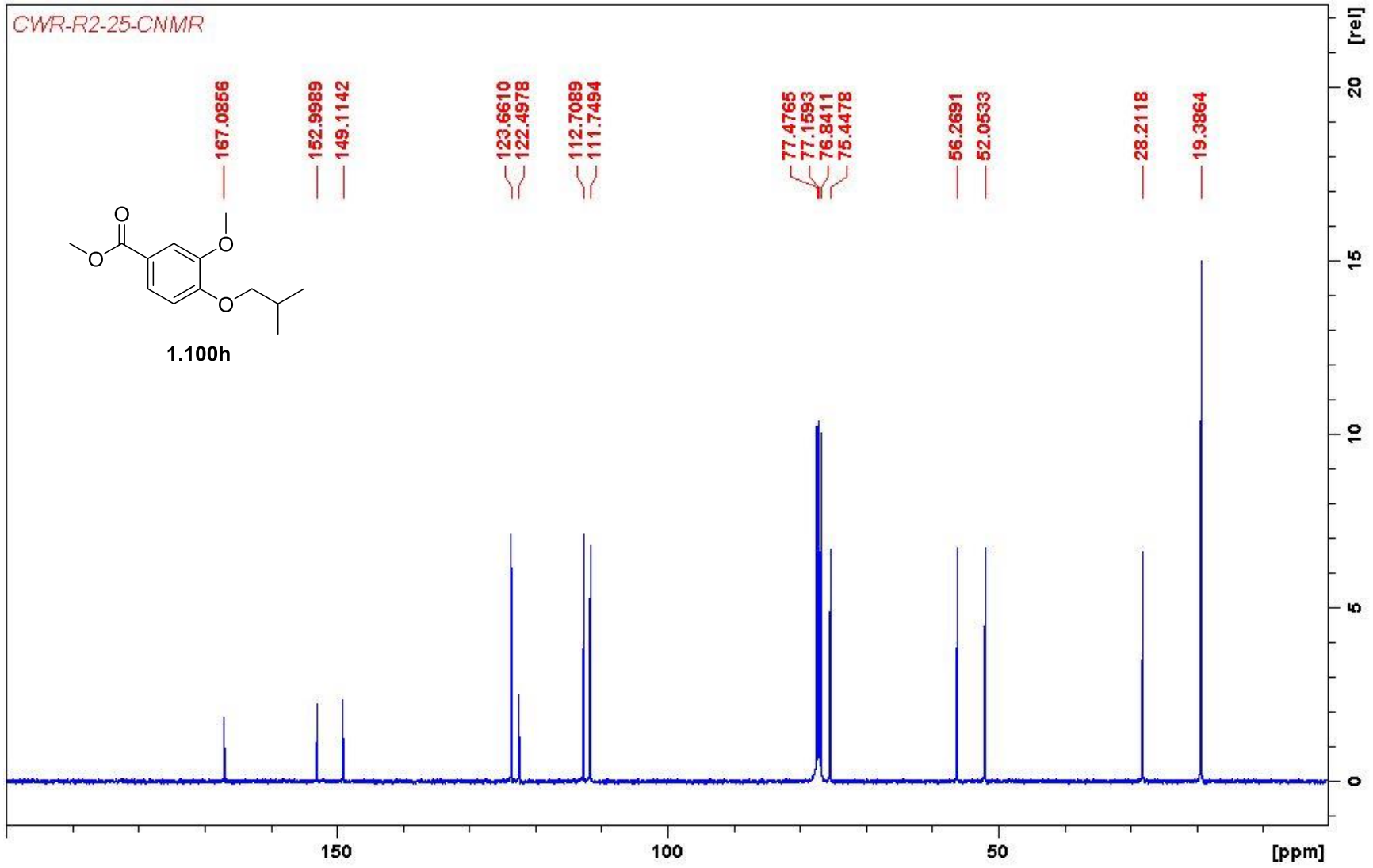
1.100h



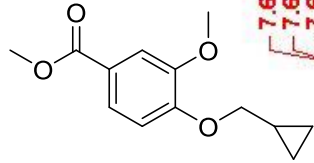
CWR-R2-25-CNMR



1.100h



CWR-R2-22



1.100i

7.6477
7.6427
7.6266
7.6217
7.5443
7.5395
7.2601
6.8681
6.8470

3.9223
3.9143
3.8967
3.8846
1.6129
1.3888
1.3811
1.3769
1.3708
1.3691
1.3632
1.3597
1.3513
1.3457
1.3428
1.3393
1.3334
1.3317
1.3255
1.3197
1.3138
0.6860
0.6737
0.6709
0.6587
0.6537
0.6509
0.6390
0.3920
0.3800

0.9743
0.9772
1.0000

7.9732

0.9698

1.9757

1.9777

8

6

4

2

[ppm]

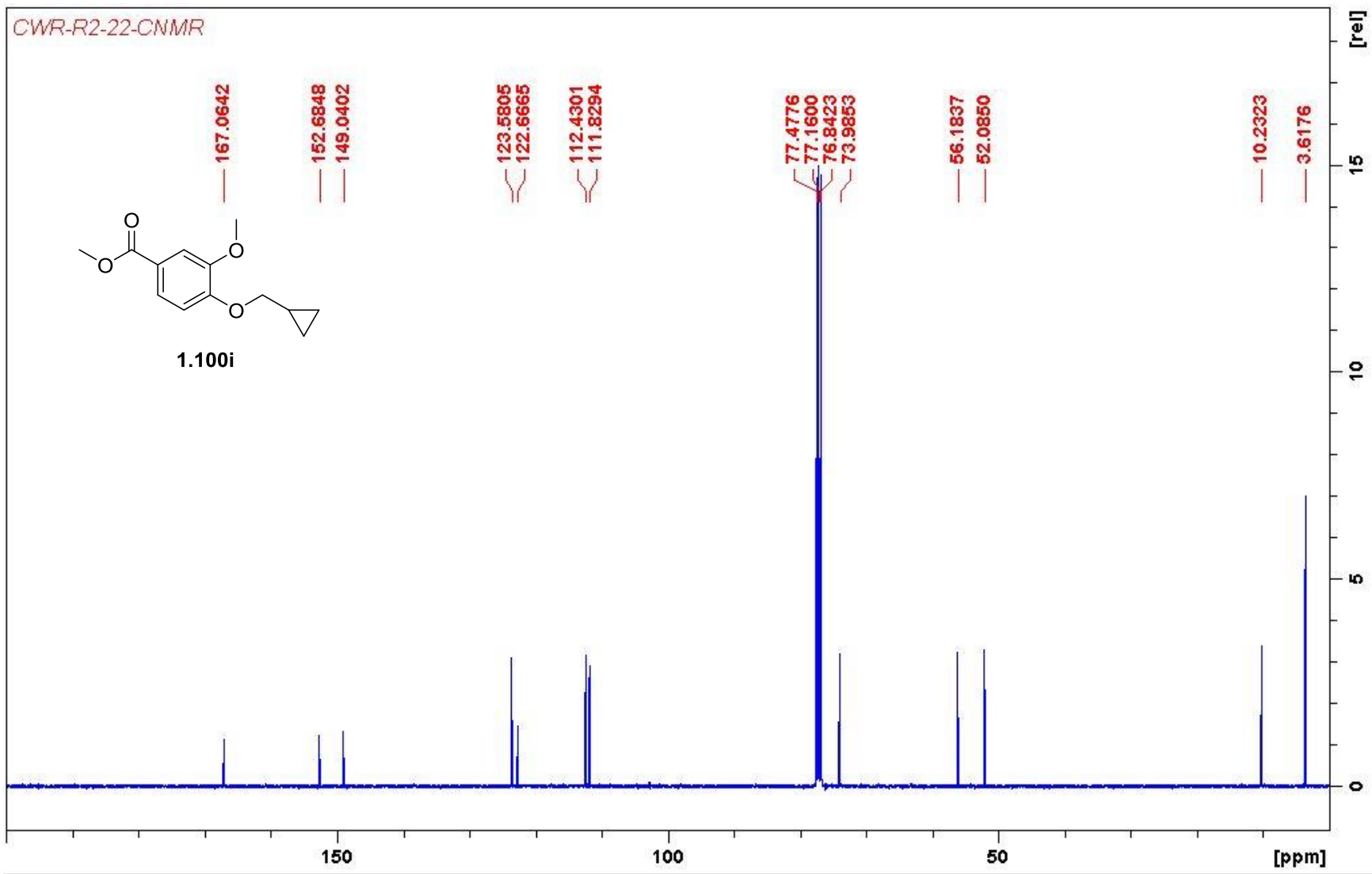
[rel]

15

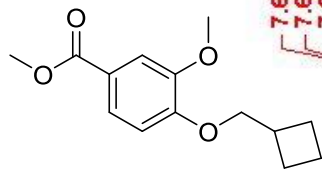
10

5

0



CWR-R2-23



1.100j

7.6554
7.6504
7.6343
7.6294
7.5354
7.5305
7.2601
6.8832
6.8621

4.0506
4.0334
3.8974
3.8850
2.8888
2.8702
2.8518
2.8339
2.1994
2.1887
2.1793
2.1689
2.1637
2.1587
2.1555
2.1519
2.1492
2.1469
2.1347
2.1305
1.9796
1.9759
1.9576
1.9420
1.9349
1.9225
1.9126
1.9008
1.8886
1.8620
1.8408
1.6144

1.0000
1.0075
1.0319

2.0748
6.1897

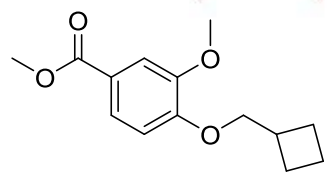
1.0002

2.0604
4.2146

[rel]

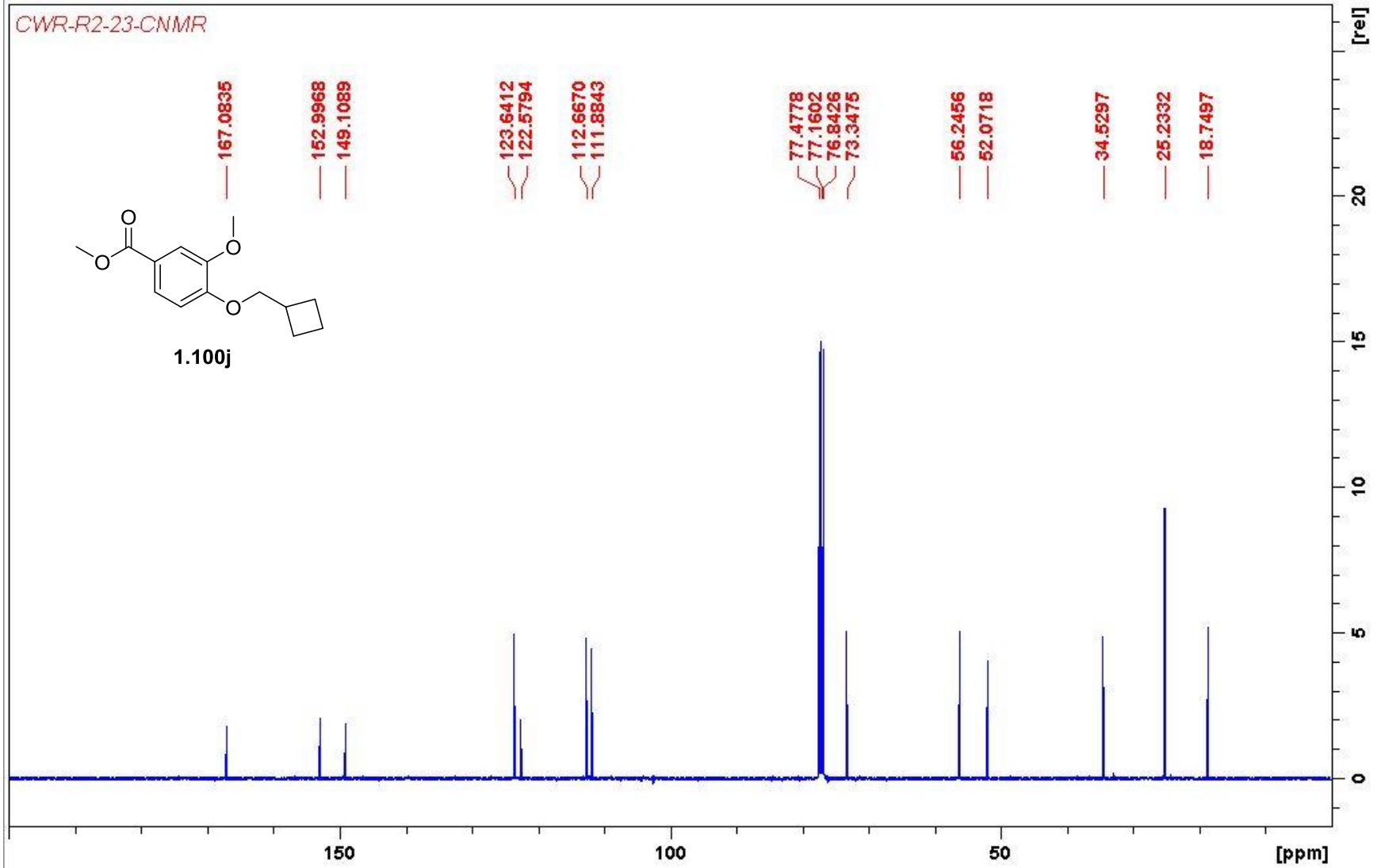
[ppm]

CWR-R2-23-CNMR

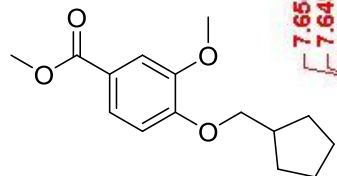


1.100j

- 167.0835
- 152.9968
- 149.1089
- 123.6412
- 122.5794
- 112.6670
- 111.8843
- 77.4778
- 77.1602
- 76.8426
- 73.3475
- 56.2456
- 52.0718
- 34.5297
- 25.2332
- 18.7497



CWR-R2-27



1.100k

7.6541
7.6491
7.6331
7.6281
7.5394
7.5344
7.2600
6.8861
6.8649

3.9392
3.9213
3.9027
3.8849
2.4730
2.4543
2.4355
1.8895
1.8862
1.8766
1.8734
1.8702
1.8573
1.8471
1.8448
1.8420
1.8378
1.8337
1.6775
1.6725
1.6650
1.6528
1.6356
1.6322
1.6264
1.6210
1.6172
1.6071
1.6001
1.5895
1.5813
1.5783
1.5708
1.5681
1.4090
1.4026
1.3906
1.3768
1.3731
1.3589
1.3419

1.0000
0.9826

1.0228

8.5851

1.0640

2.1728

4.7338

2.1506

8

6

4

2

[ppm]

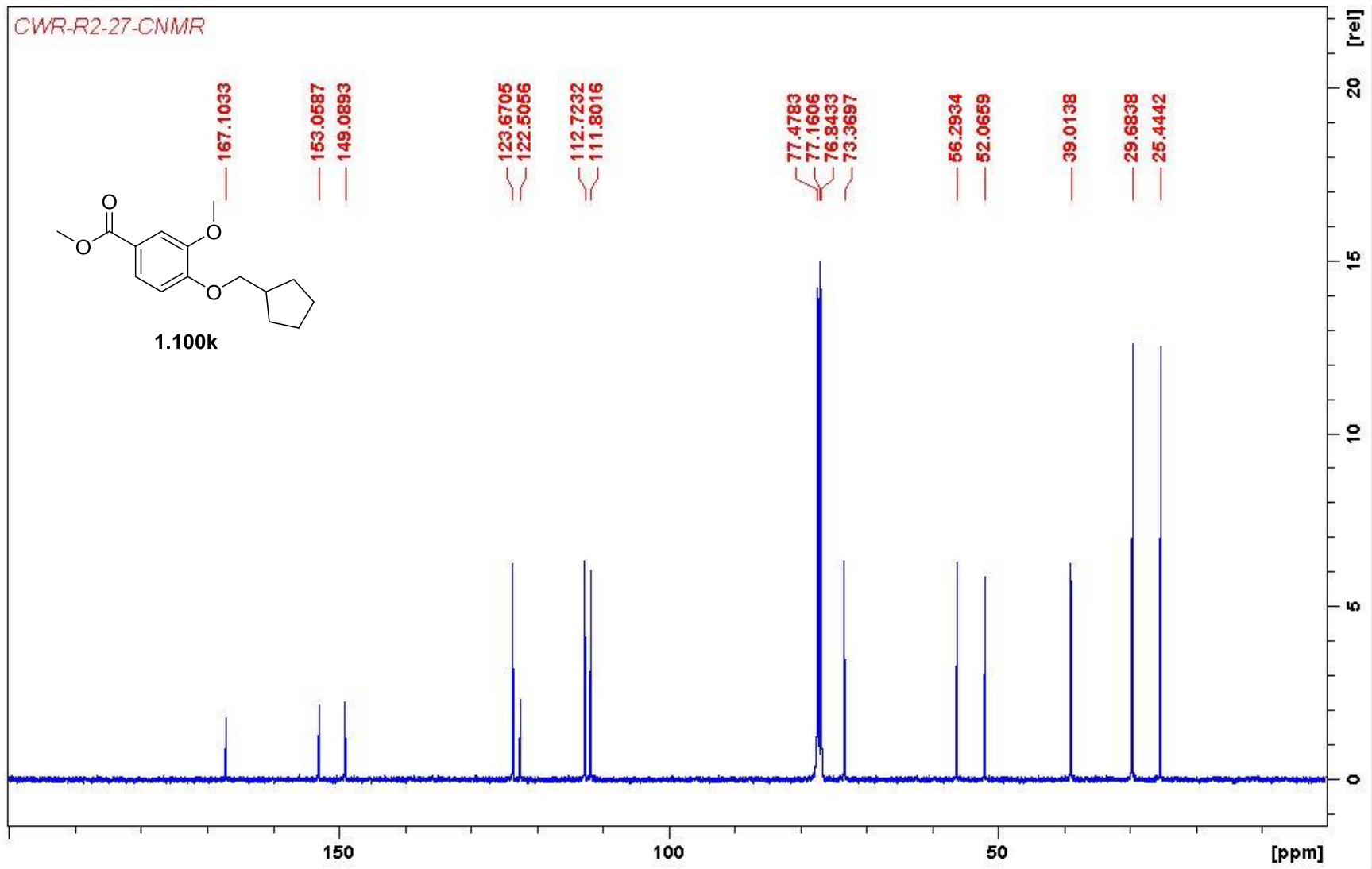
[rel]

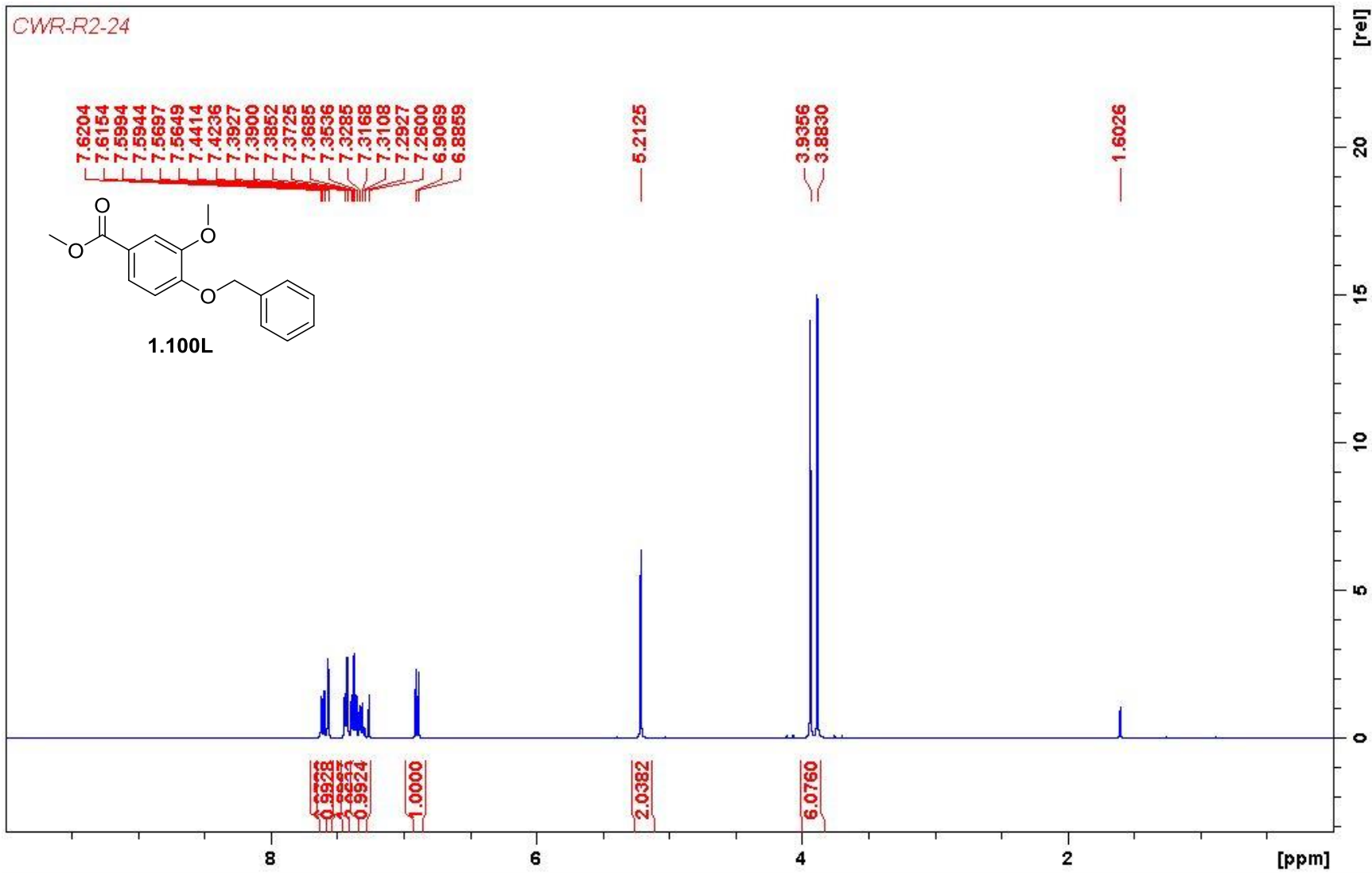
15

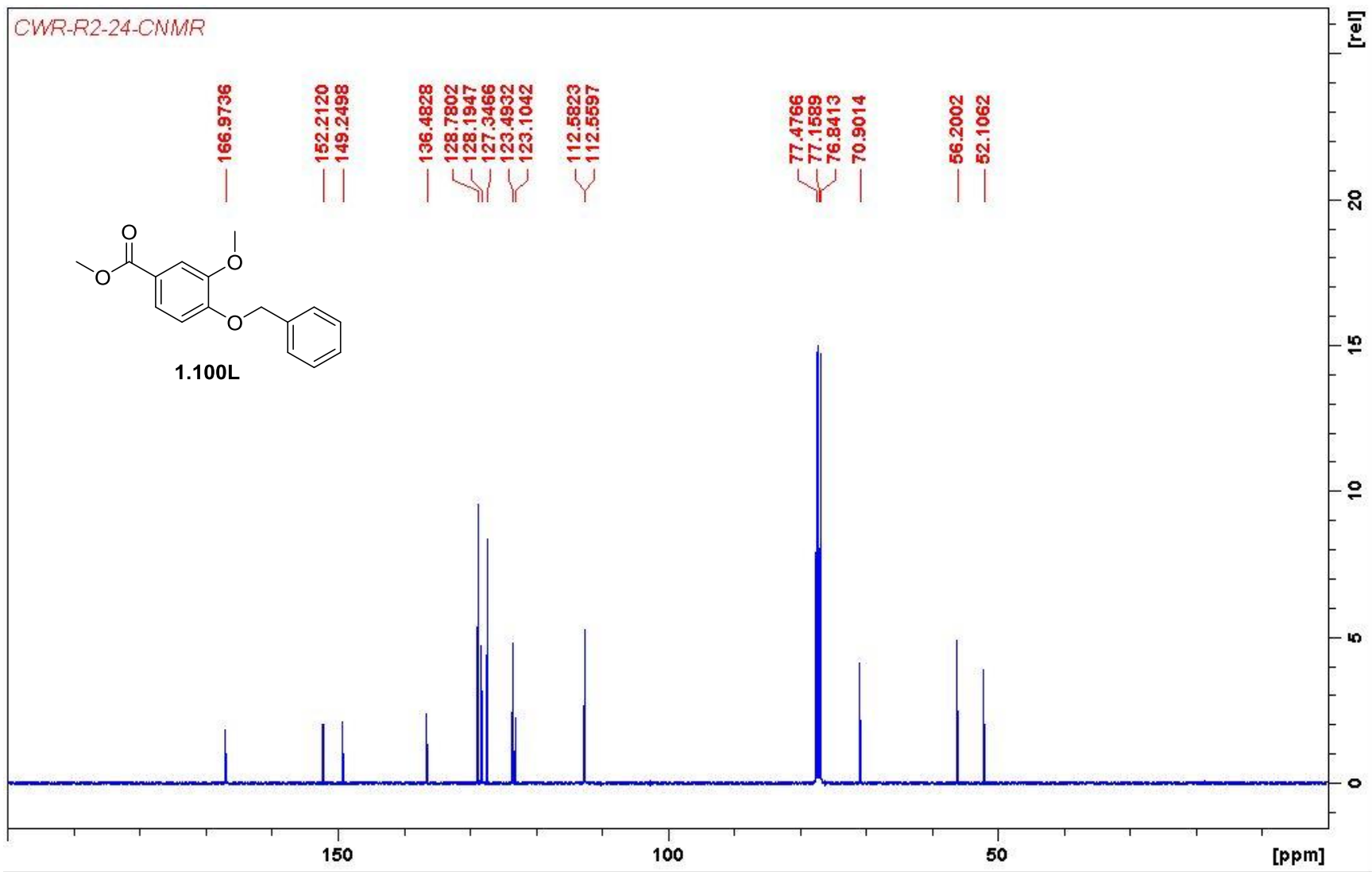
10

5

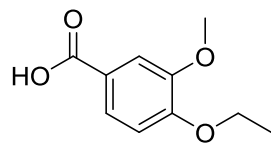
0







CWR-3-118



1.102a

7.5513
7.5464
7.5304
7.5255
7.4374
7.4325
7.0299
7.0088

4.1055
4.0881
4.0707
4.0533
3.7956

3.3266

2.5090
2.5046
2.5000
2.4955
2.4911

1.3612
1.3438
1.3264

1.0000
1.0016
1.0095

2.0211
3.0534

3.0253

8

6

4

2

[ppm]

[rel]

20

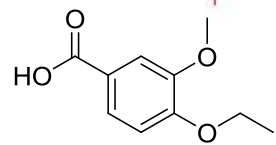
15

10

5

0

CWR-3-118



1.102a

151.8630
148.3225

123.1490
122.7653

111.9610
111.6954

63.8278

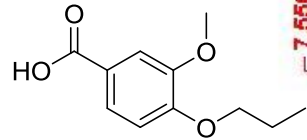
55.3831

40.1467
39.9382
39.7296
39.5206
39.3121
39.1036
38.8947

14.5795

10 [rel]
8
6
4
2
0
[ppm]

CWR-3-119



1.102b

7.5508
7.5459
7.5298
7.5249
7.4396
7.4348
7.0346
7.0134

3.9932
3.9767
3.9602
3.7985

3.3273

2.5089
2.5045
2.5000
2.4955
2.4911
1.7892
1.7711
1.7540
1.7360
1.7188
1.7009

0.9904
0.9719
0.9534

1.0000
0.9934

0.9906

2.0340
3.0313

2.0251

3.0053

8

6

4

2

[ppm]

[rel]

20

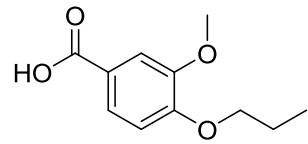
15

10

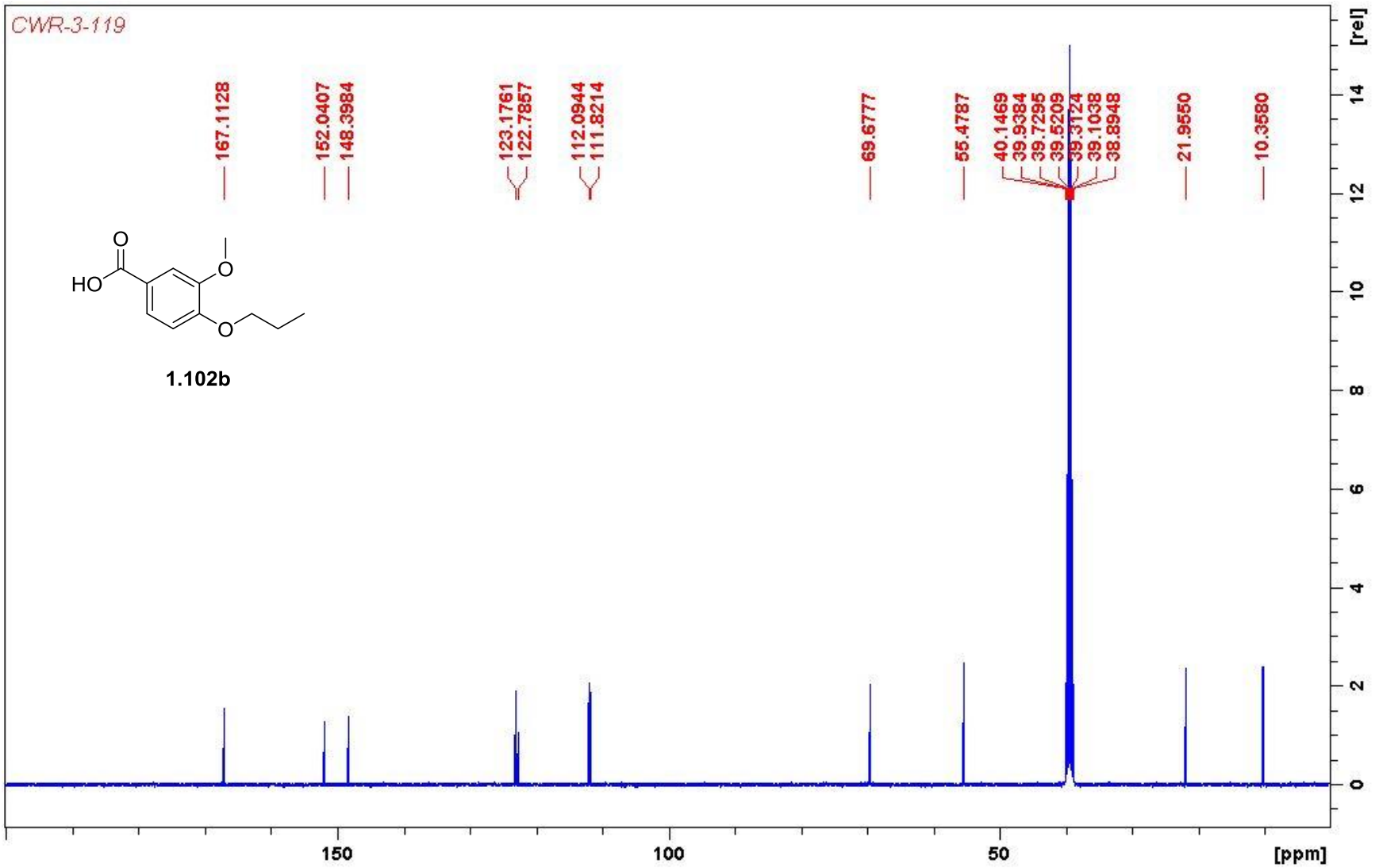
5

0

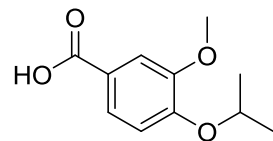
CWR-3-119



1.102b



CWR-5-167



1.102c

7.5400
7.5350
7.5190
7.5140
7.4396
7.4346
7.0466
7.0252

4.6988
4.6837
4.6686
4.6535
4.6384

3.7835

3.3297

2.5092
2.5047
2.5002
2.4957
2.4913

1.2828
1.2677

1.0000
0.9973

1.0034

1.0235

3.0748

6.1802

8

6

4

2

[ppm]

[rel]

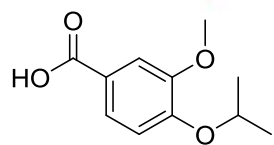
15

10

5

0

CWR-5-167



1.102c

167.0941

150.7653

149.0137

123.0669

122.7265

113.3167

112.3634

70.1784

55.3941

40.1464

39.9379

39.7290

39.5205

39.3120

39.1032

38.8945

21.7520

20 [rel]

15

10

5

0

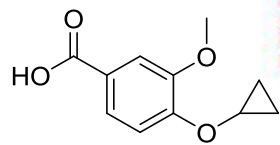
150

100

50

[ppm]

CWR-5-176



1.102d

7.5905
7.5858
7.5696
7.5649
7.4396
7.4351
7.3304
7.3094

3.9114
3.9042
3.8966
3.8891
3.8818
3.8741
3.8668
3.7747
3.3340

2.5042
2.5000
2.4959

0.8285
0.8128
0.8099
0.7954
0.7811
0.7012
0.6827
0.6626

1.0000
1.0245
0.9996

1.0878
2.9029

2.0950
1.8616

8

6

4

2

[ppm]

[rel]

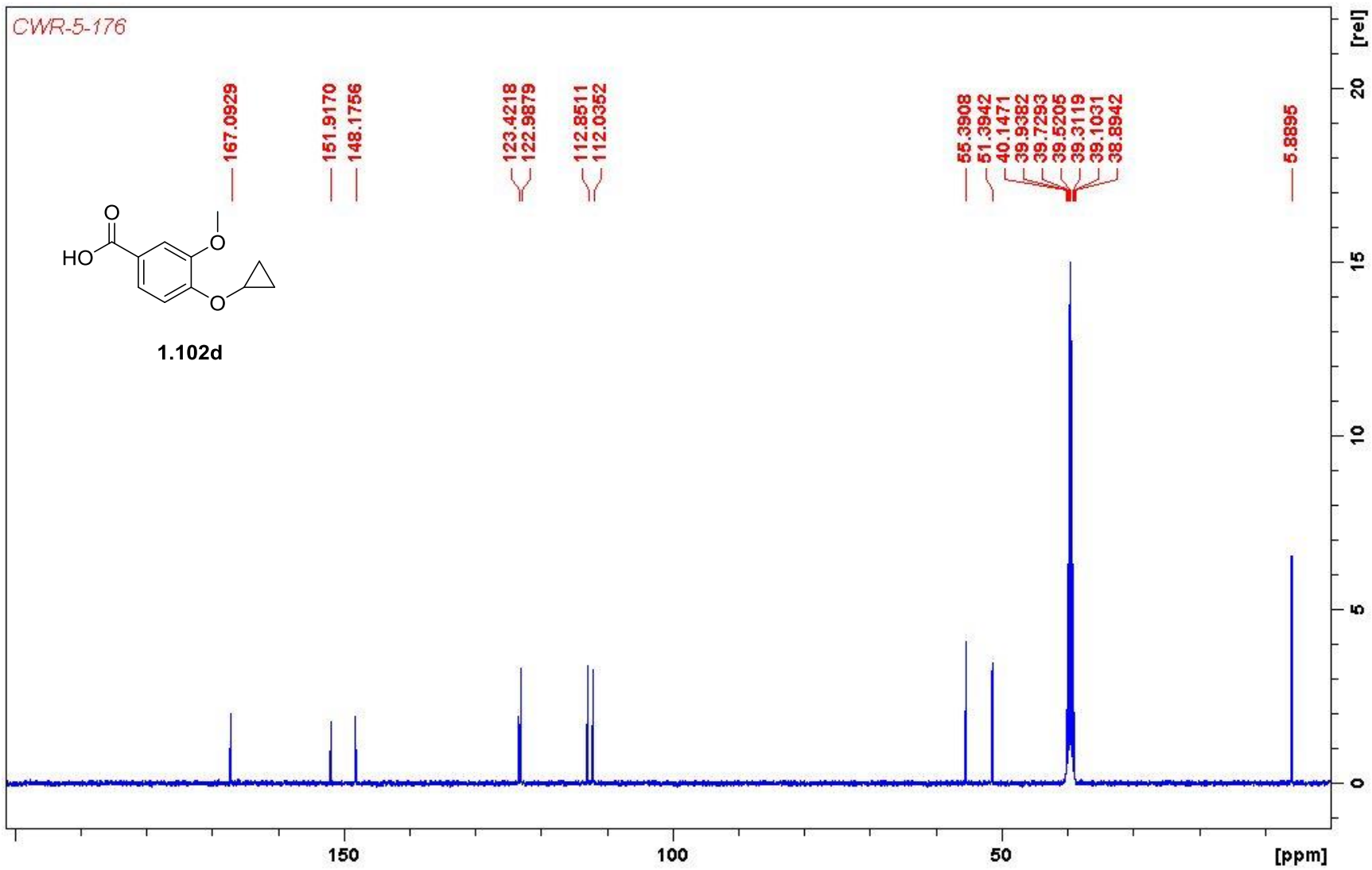
20

15

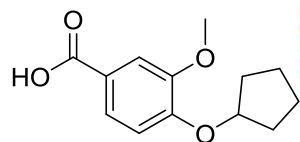
10

5

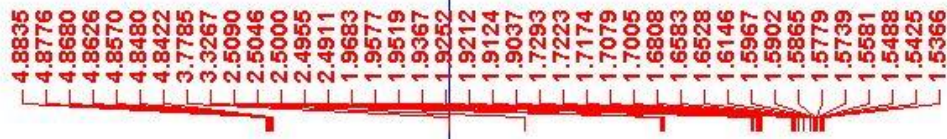
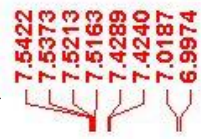
0



CWR-5-168



1.102e



8

6

4

2

[ppm]

1.0000
0.9973

1.0072

1.0064

3.0168

2.0734

4.1194

2.0192

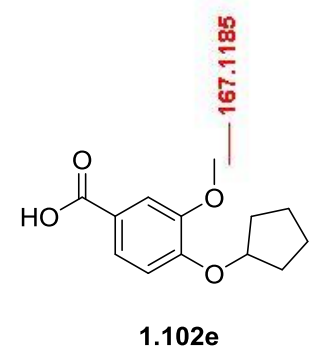
15 [rel]

10

5

0

CWR-5-168



151.0405
148.8575

123.0674
122.5989

113.1160
112.2732

79.5843

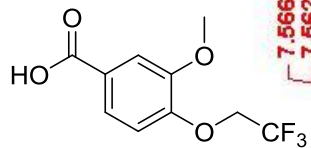
55.4480

40.1463
39.9378
39.7292
39.5203
39.3116
39.1032
38.8945
32.2767

23.6738

[rel]
14
12
10
8
6
4
2
0
[ppm]

CWR-R2-28



1.102f

7.5668
7.5620
7.5458
7.5410
7.5130
7.5083
7.1785
7.1574

4.8431
4.8211
4.7990
4.7768

3.8422

3.3337

2.5087
2.5045
2.5000
2.4956
2.4914

2.1367

2.1819

4.4639

6.6877

8

6

4

2

[ppm]

[rel]

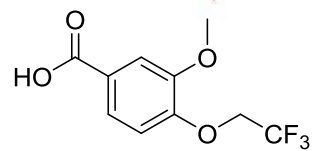
15

10

5

0

CWR-R2-28



1.102f

166.8522

149.8729

148.6203

125.2837

125.0654

122.6839

122.5215

113.6223

112.6544

65.7668

65.4257

65.0846

64.7431

55.6691

40.1459

39.9371

39.7287

39.5201

39.3111

39.1026

38.8942

[rel]

15

10

5

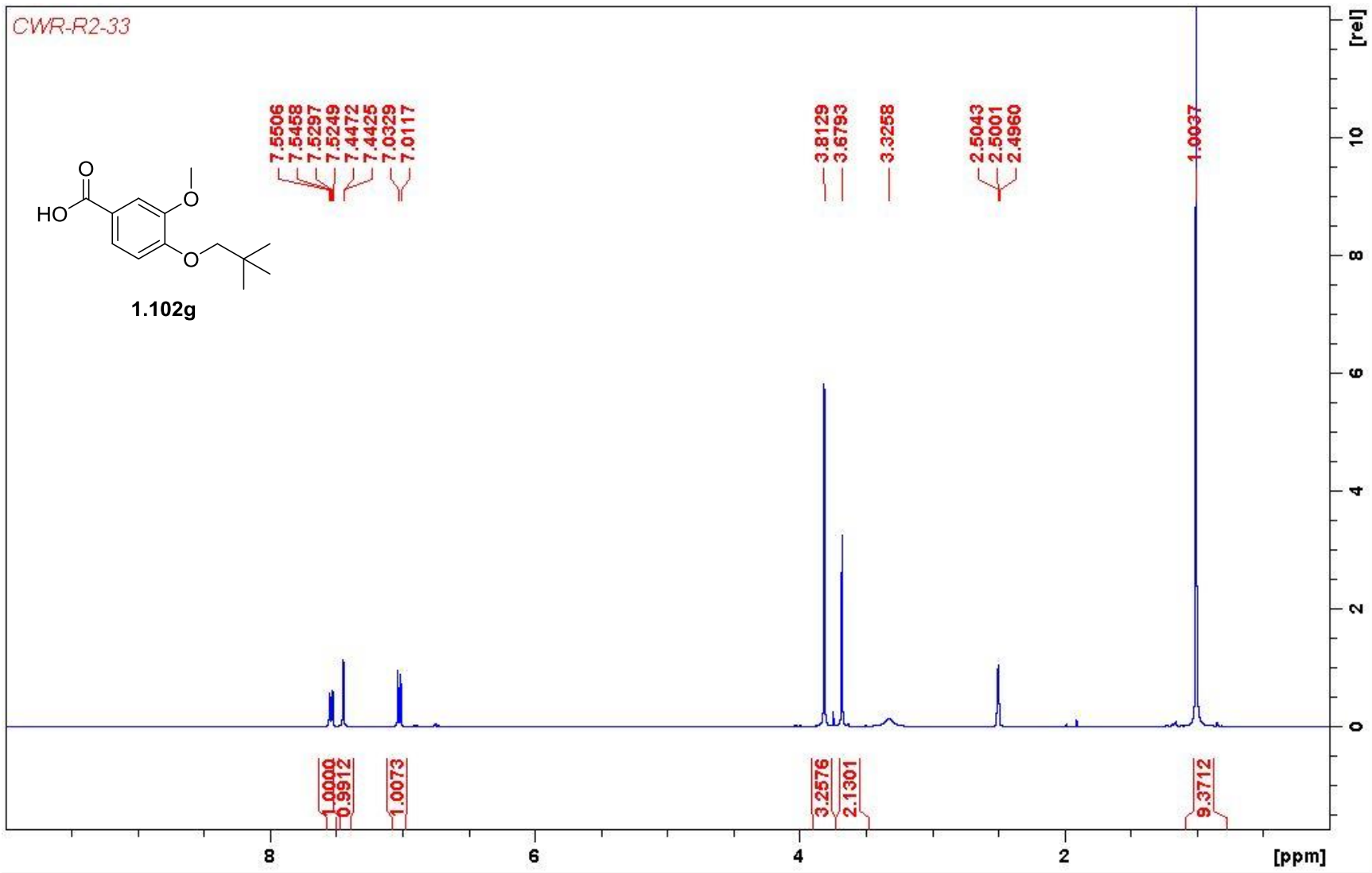
0

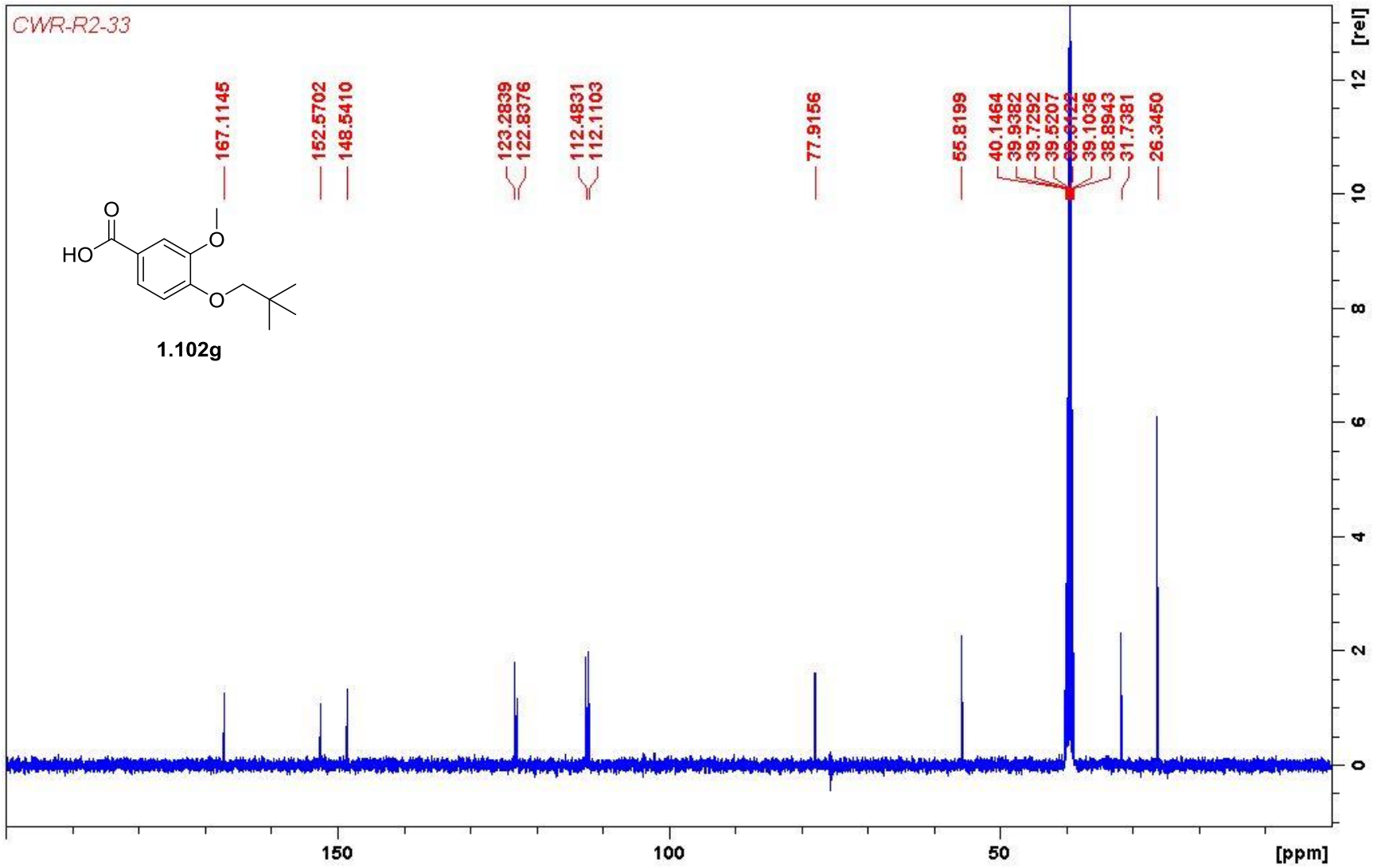
150

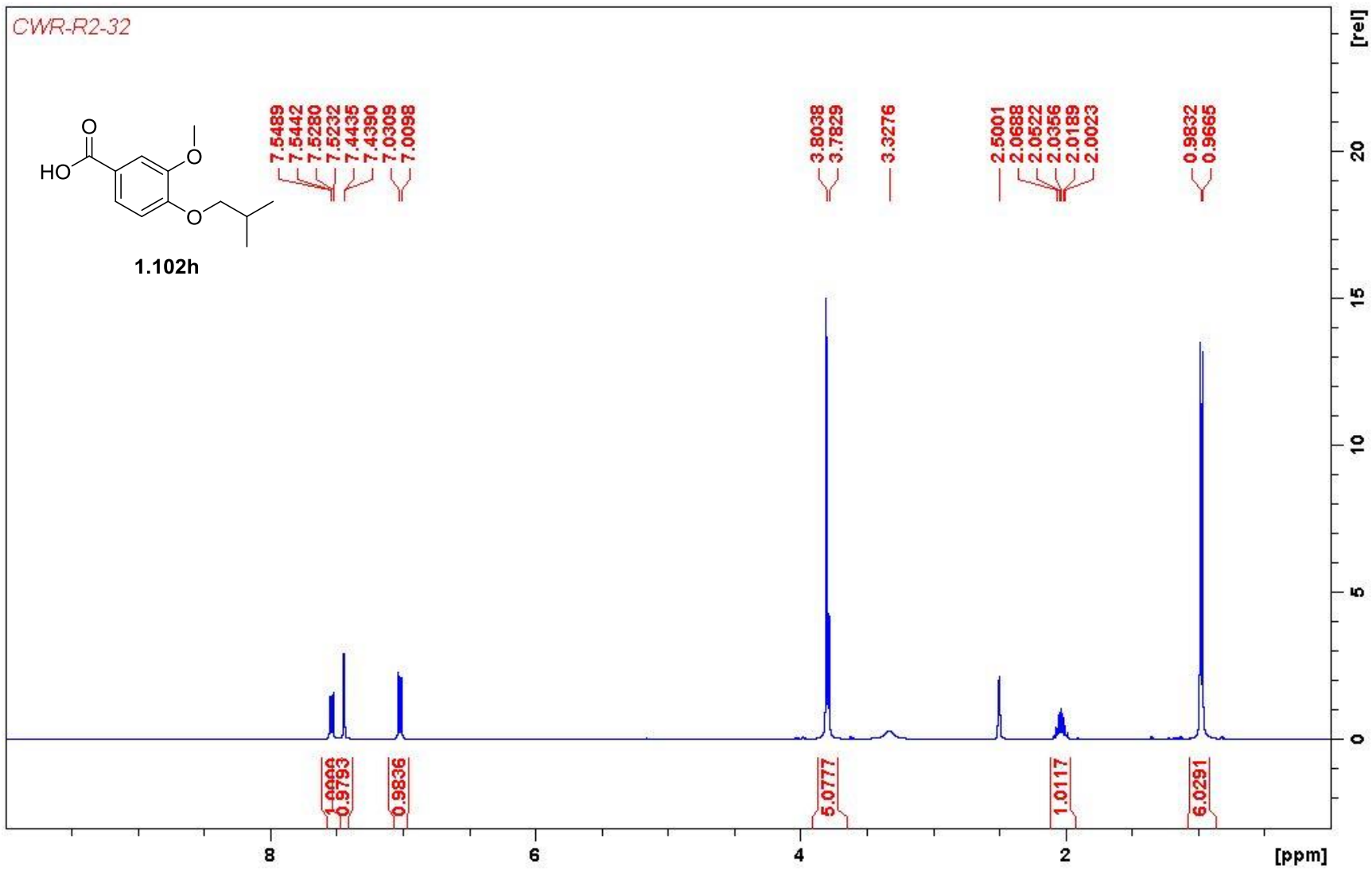
100

50

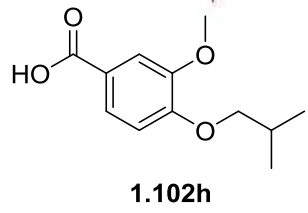
[ppm]



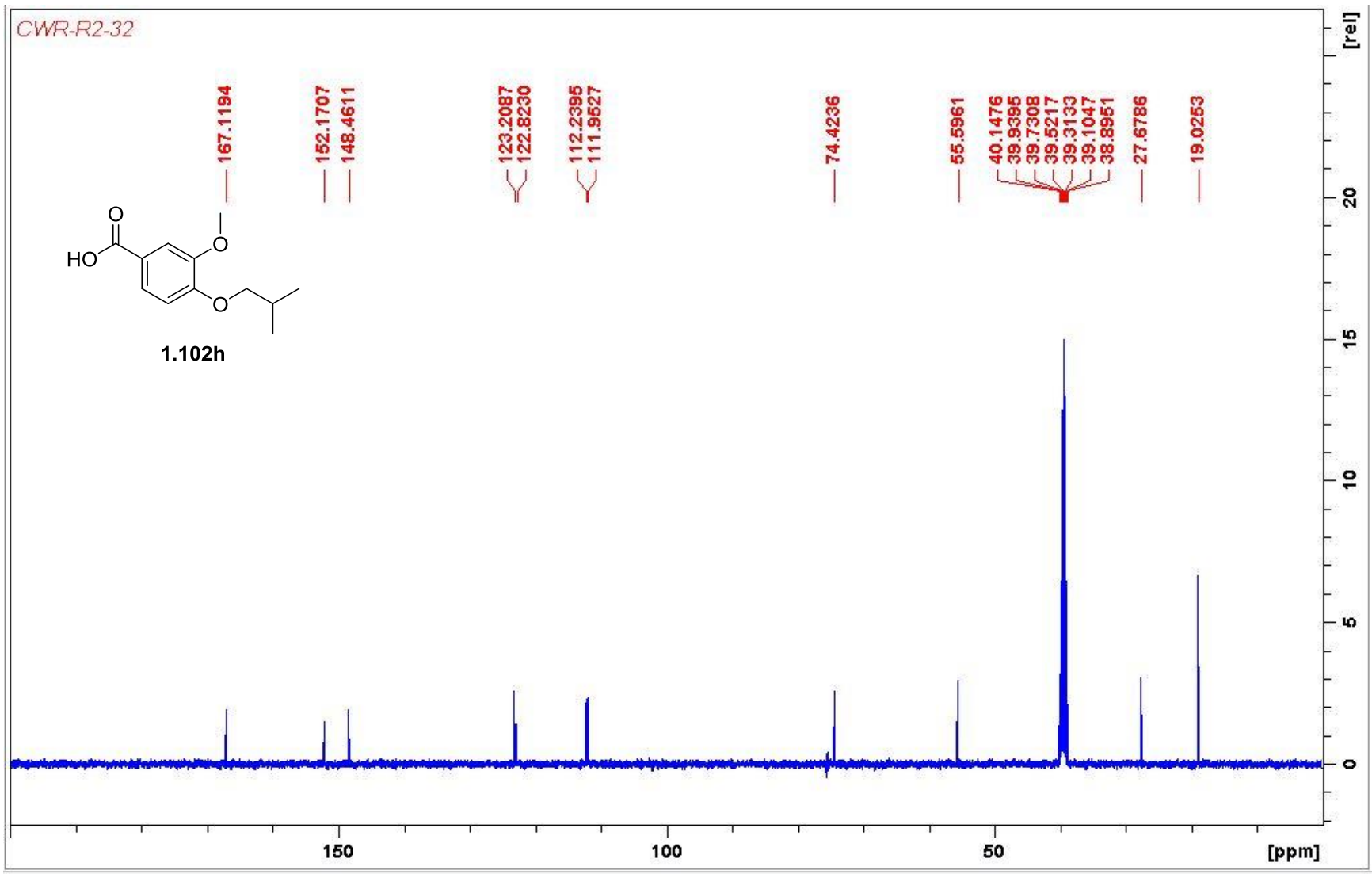


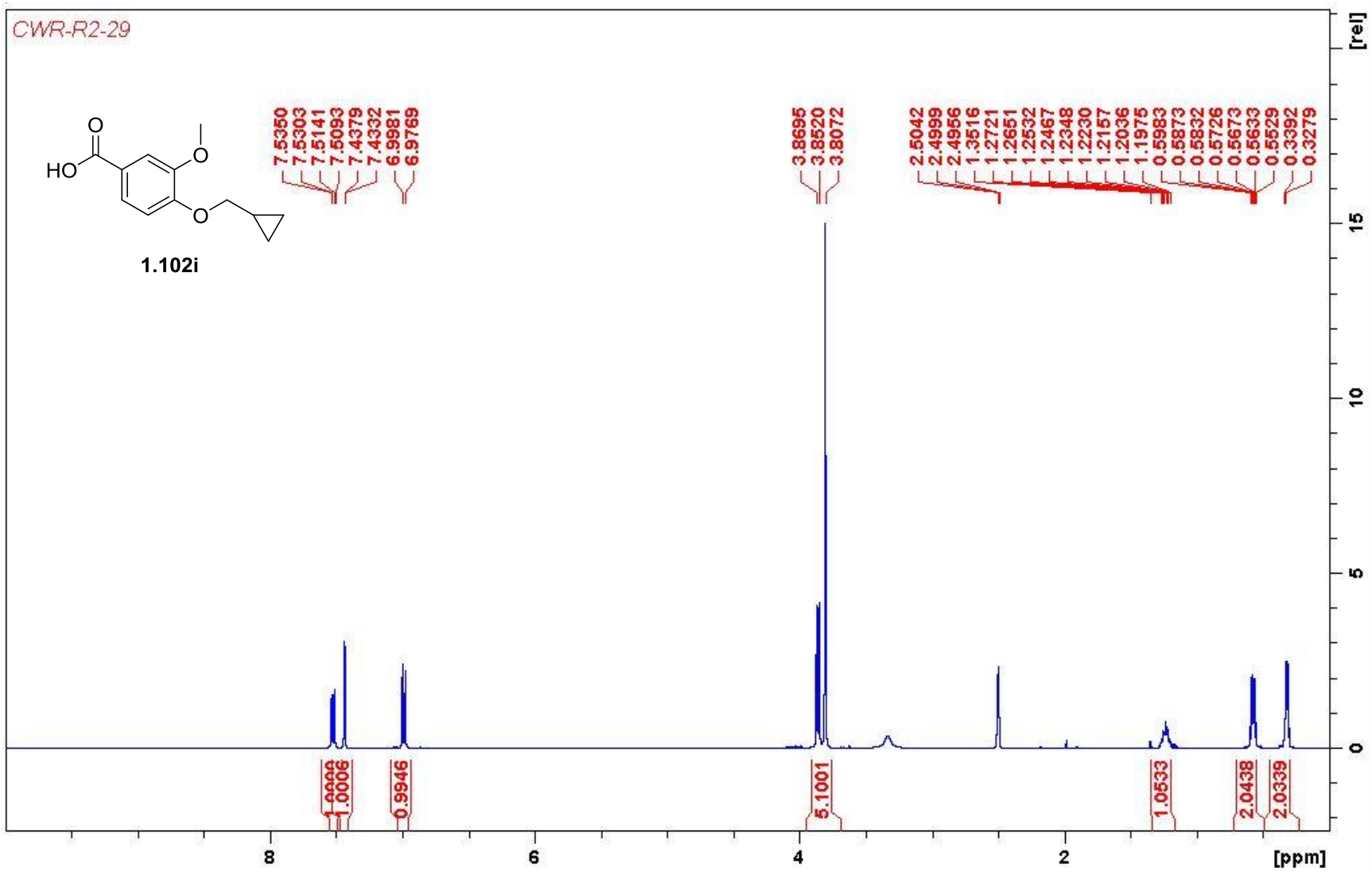


CWR-R2-32

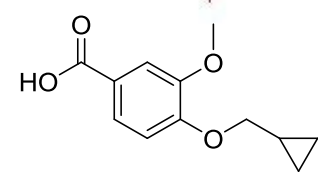


- 167.1194
- 152.1707
- 148.4611
- 123.2087
- 122.8230
- 112.2395
- 111.9527
- 74.4236
- 55.5961
- 40.1476
- 39.9395
- 39.7308
- 39.5217
- 39.3133
- 39.1047
- 38.8951
- 27.6786
- 19.0253





CWR-R2-29-CNMR



1.102i

151.9773
148.3445

123.1201
122.7601

111.9657
111.8338

72.8484

55.3807

40.1453
39.9364
39.7279
39.5193
39.3105
39.1018
38.8926

10.0501

3.2099

[rel]

20

15

10

5

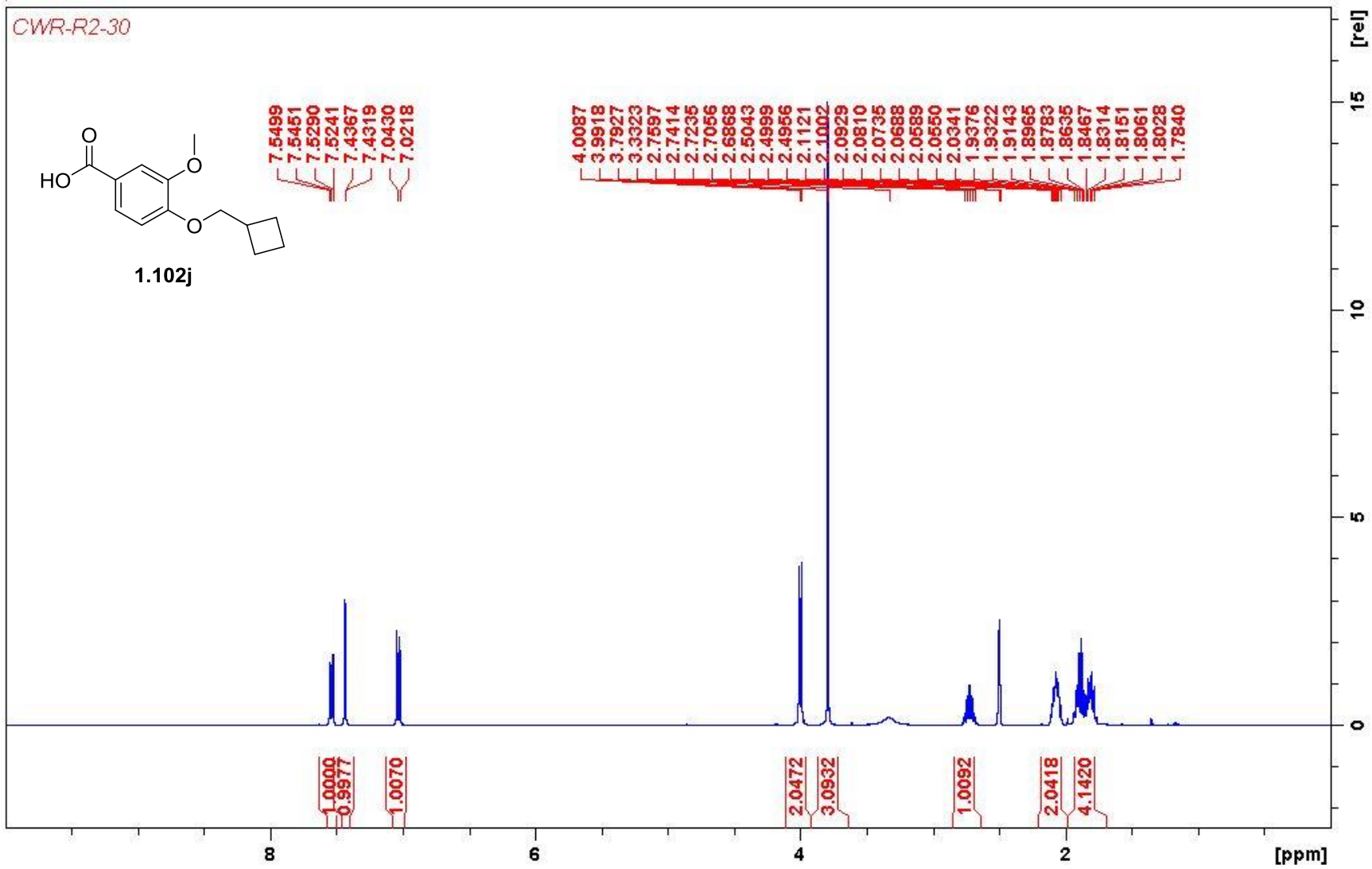
0

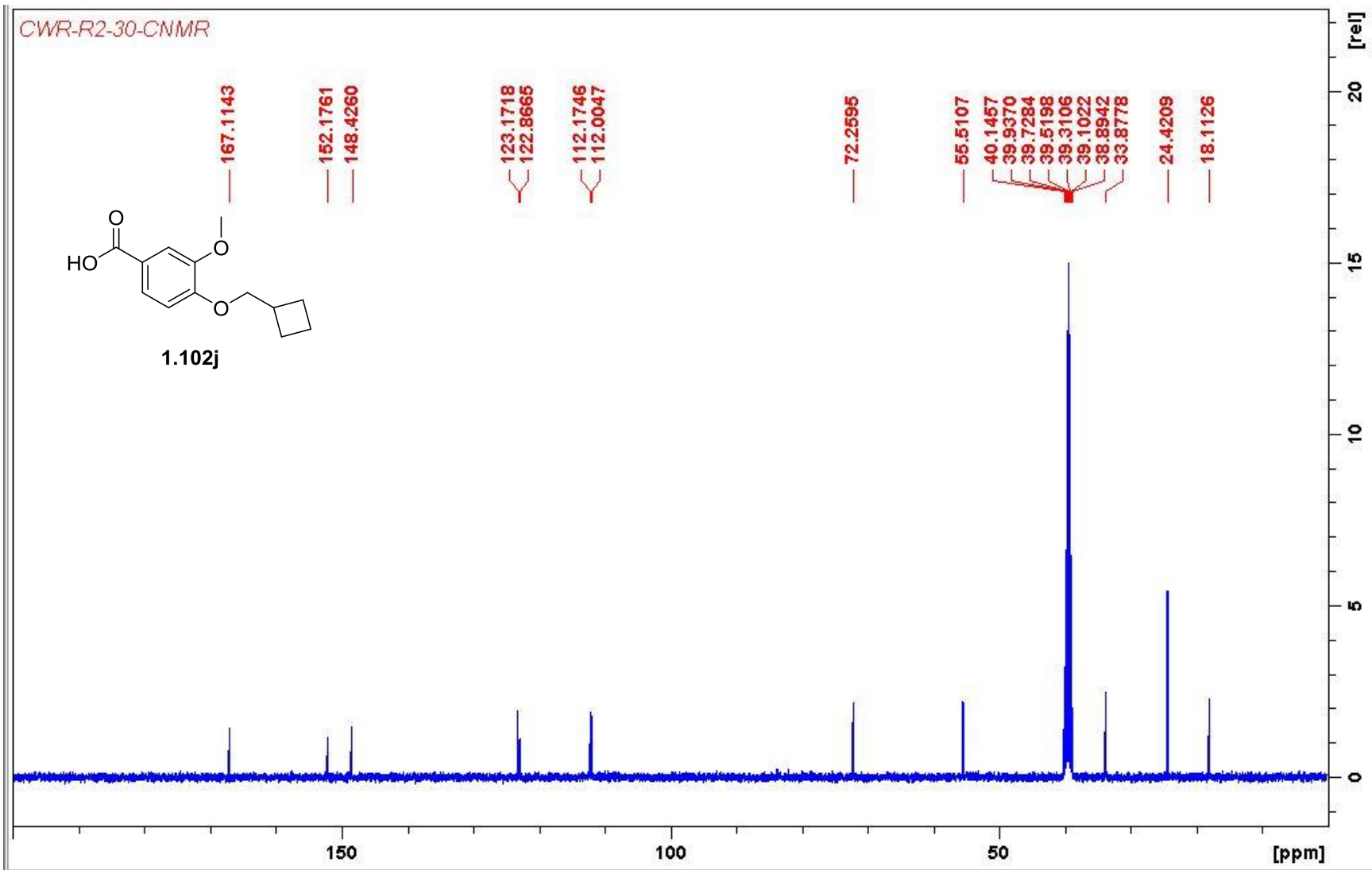
150

100

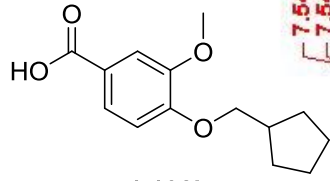
50

[ppm]





CWR-R2-34



1.102k

7.5445
7.5403
7.5236
7.5193
7.4378
7.4337
7.0405
7.0194

3.8965
3.8791
3.7976
3.3235
2.5001
2.3554
2.3371
2.3187
2.3004
2.2820
1.9073
1.7979
1.7812
1.7696
1.7517
1.7399
1.7222
1.6235
1.6034
1.5868
1.5671
1.5464
1.5375
1.5279
1.5082
1.3635
1.3480
1.3313
1.3164
1.3007
1.2837

1.0000
0.9790

0.9829

2.0935
3.0331

1.0506

2.0590
4.0466

2.1877

8

6

4

2

[ppm]

[rel]

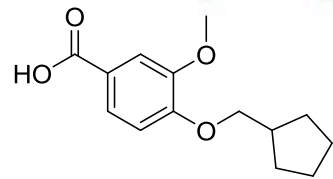
15

10

5

0

CWR-R2-34



1.102k

167.1162

152.2254

148.4133

123.1943

122.8269

112.2435

111.9892

72.3371

55.5749

40.1465

39.9388

39.7296

39.5210

39.3126

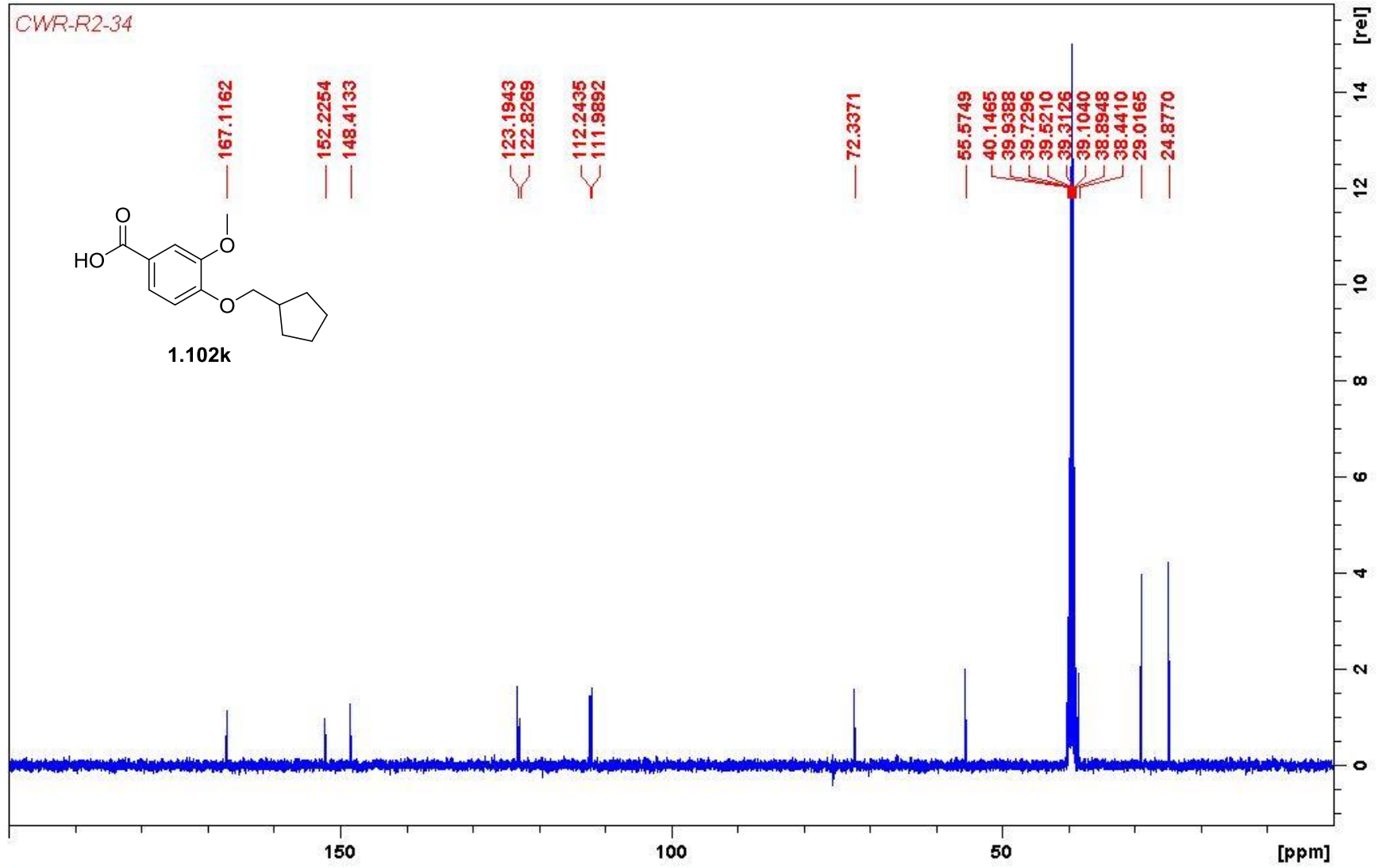
39.1040

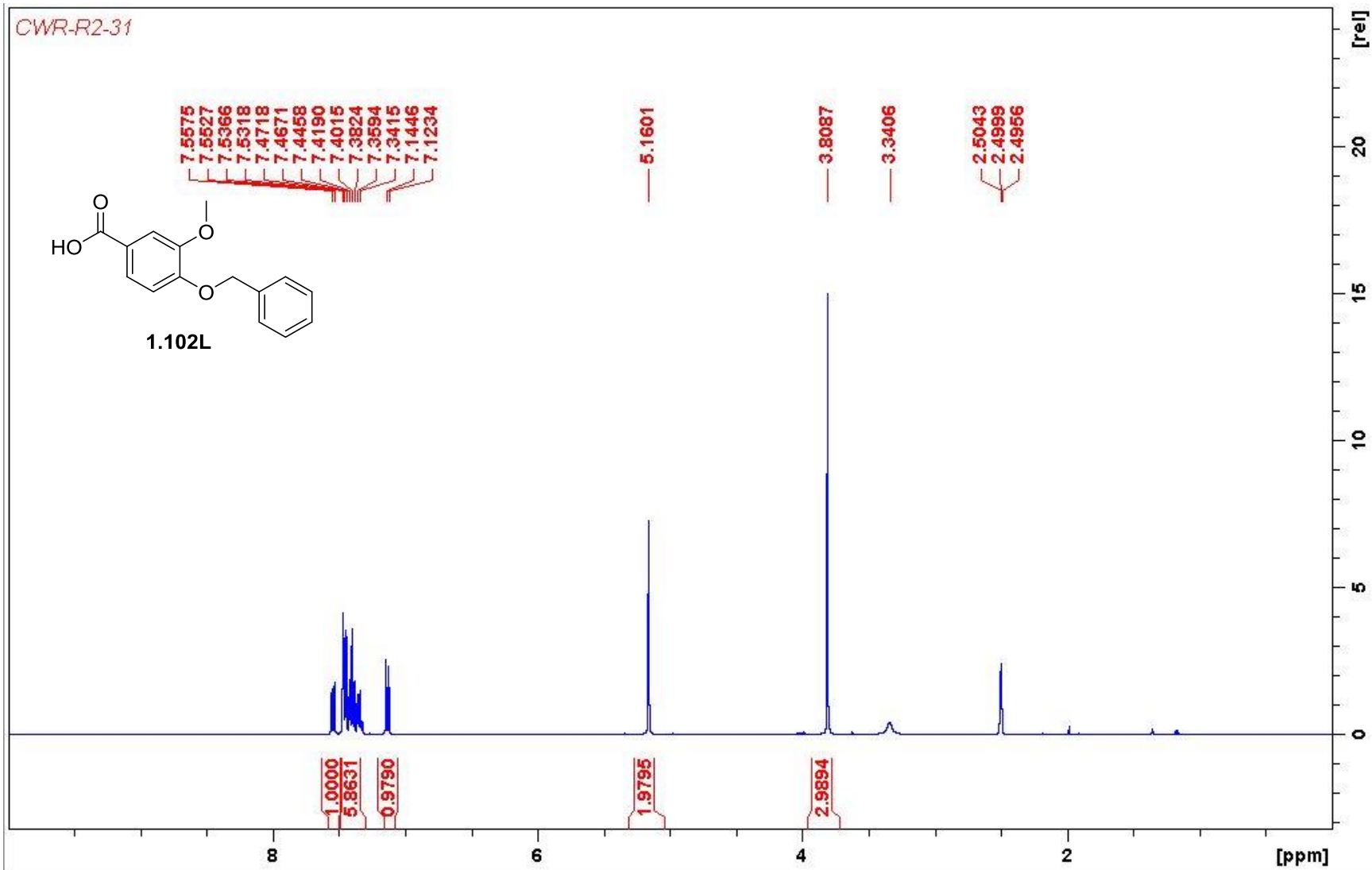
38.8948

38.4410

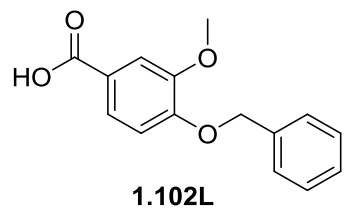
29.0165

24.8770

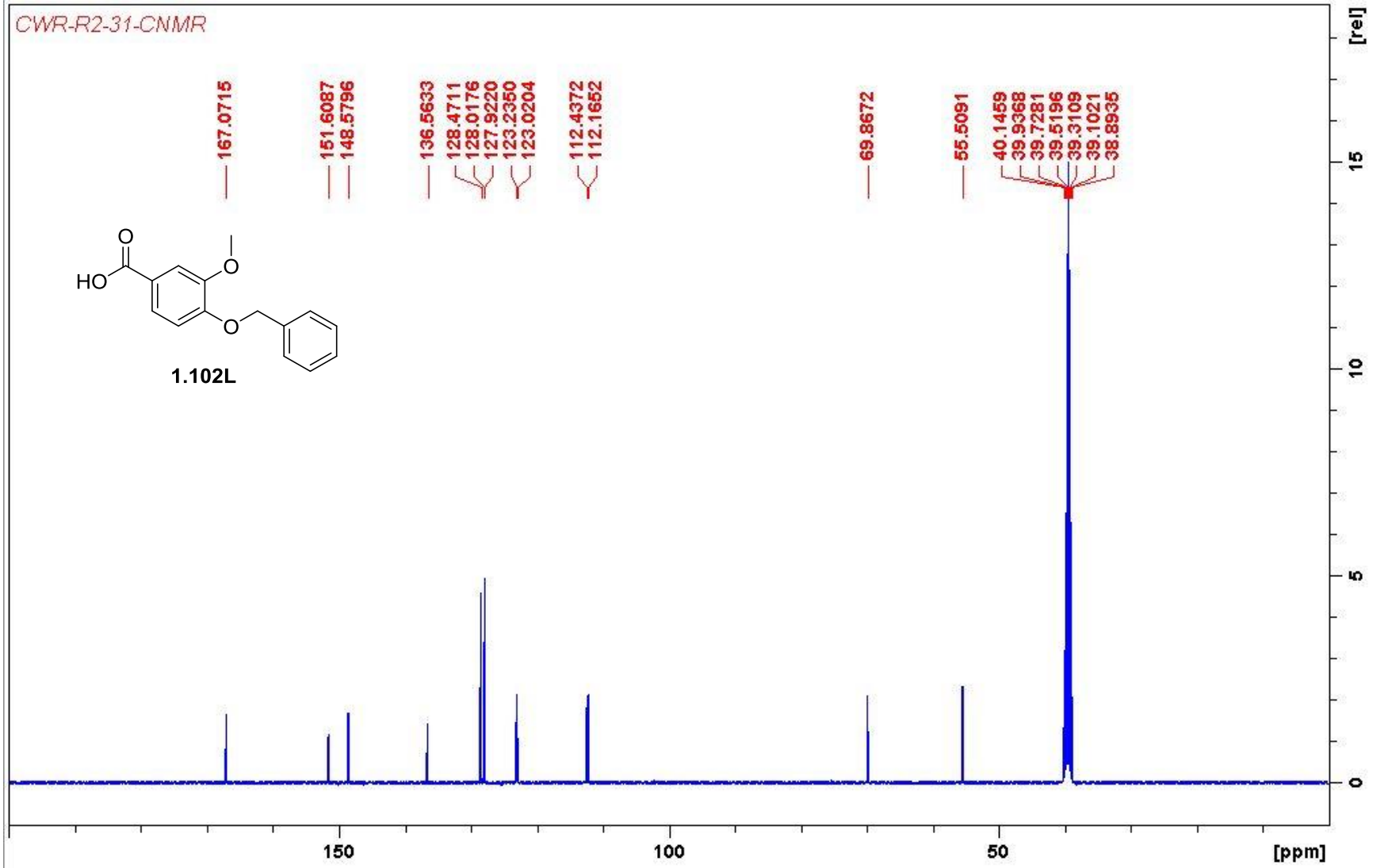




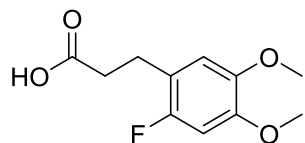
CWR-R2-31-CNMR



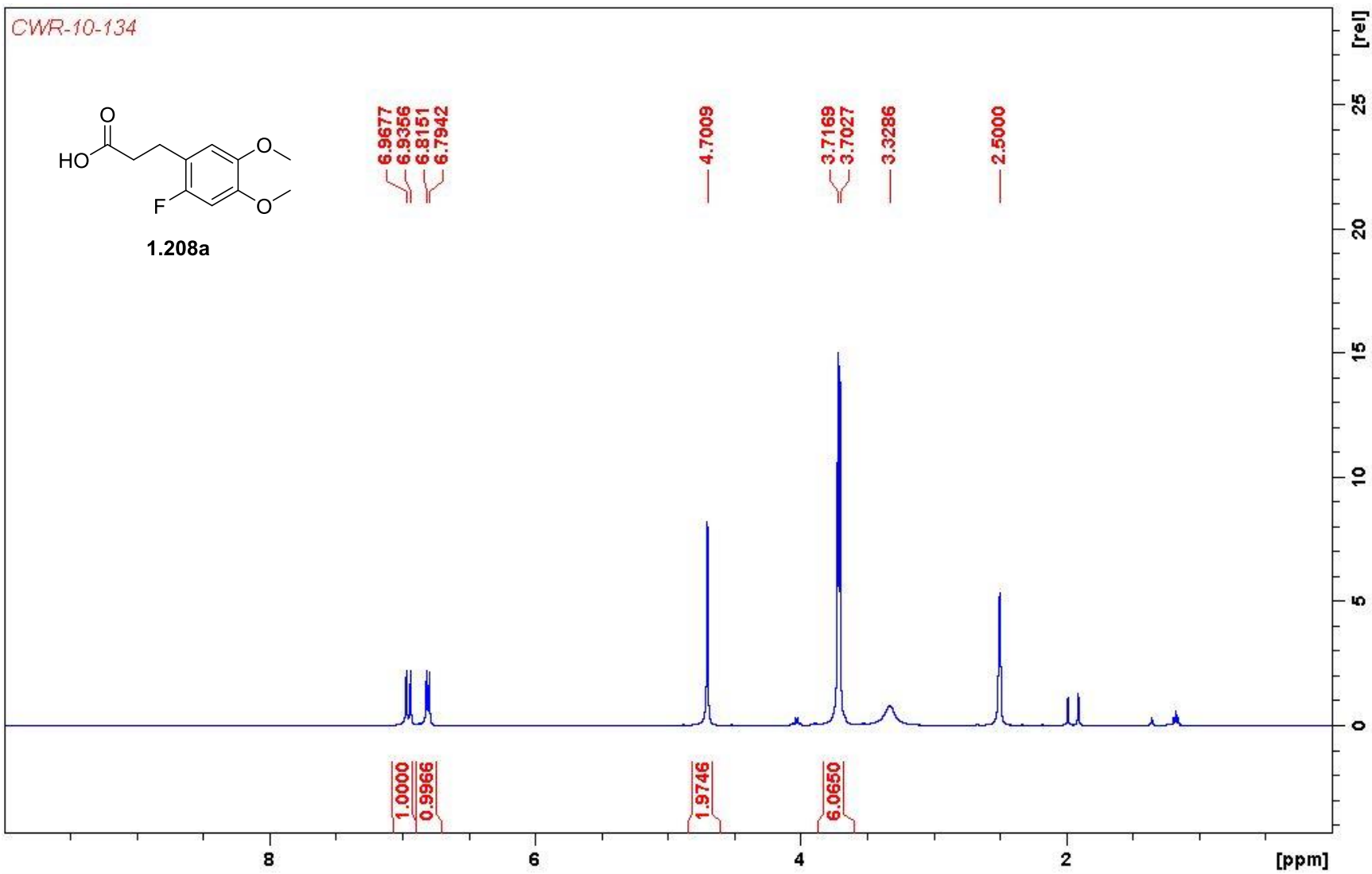
- 167.0715
- 151.6087
- 148.5796
- 136.5633
- 128.4711
- 128.0176
- 127.9220
- 123.2350
- 123.0204
- 112.4372
- 112.1652
- 69.8672
- 55.5091
- 40.1459
- 39.9368
- 39.7281
- 39.5196
- 39.3109
- 39.1021
- 38.8935

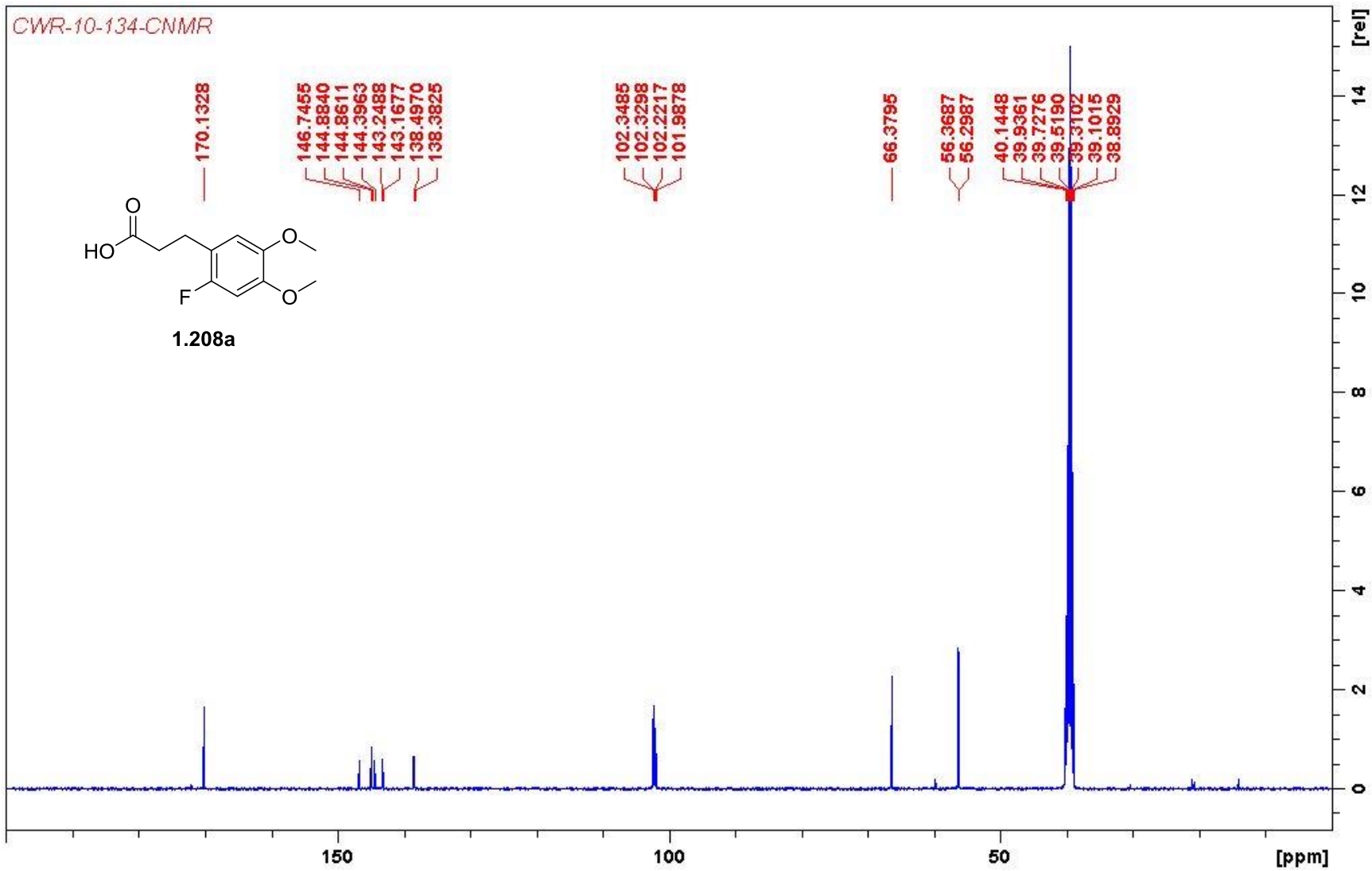


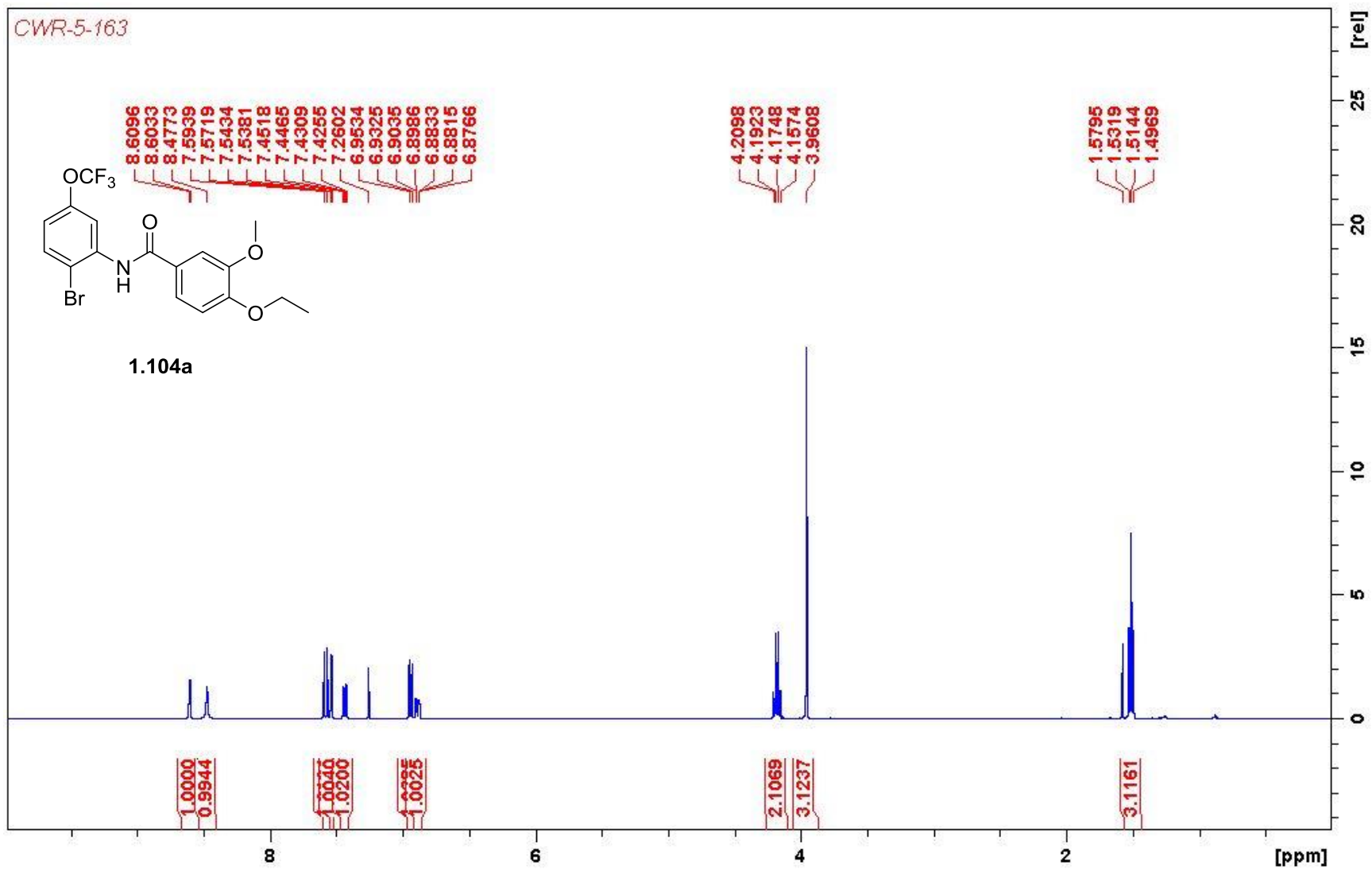
CWR-10-134

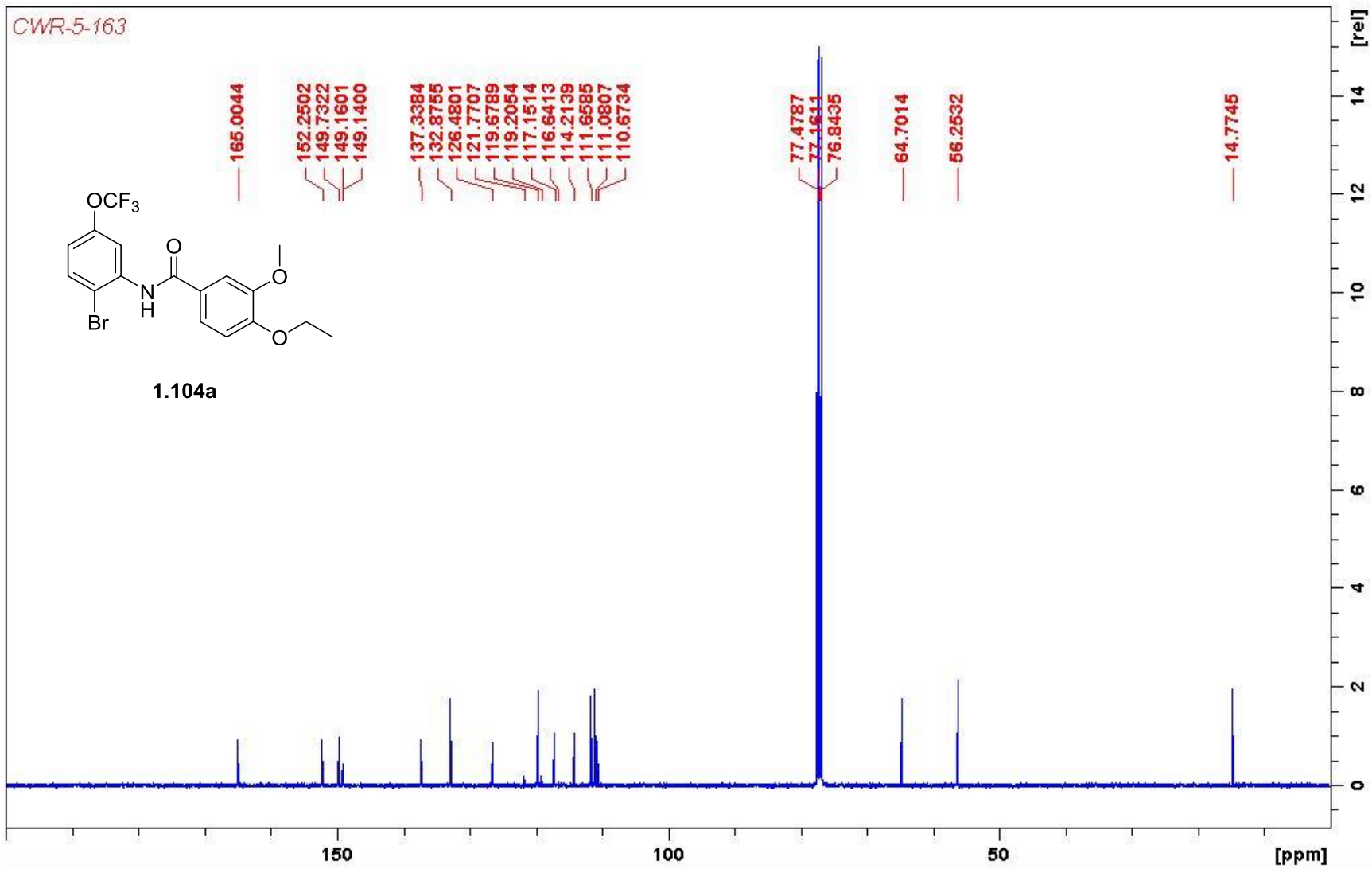


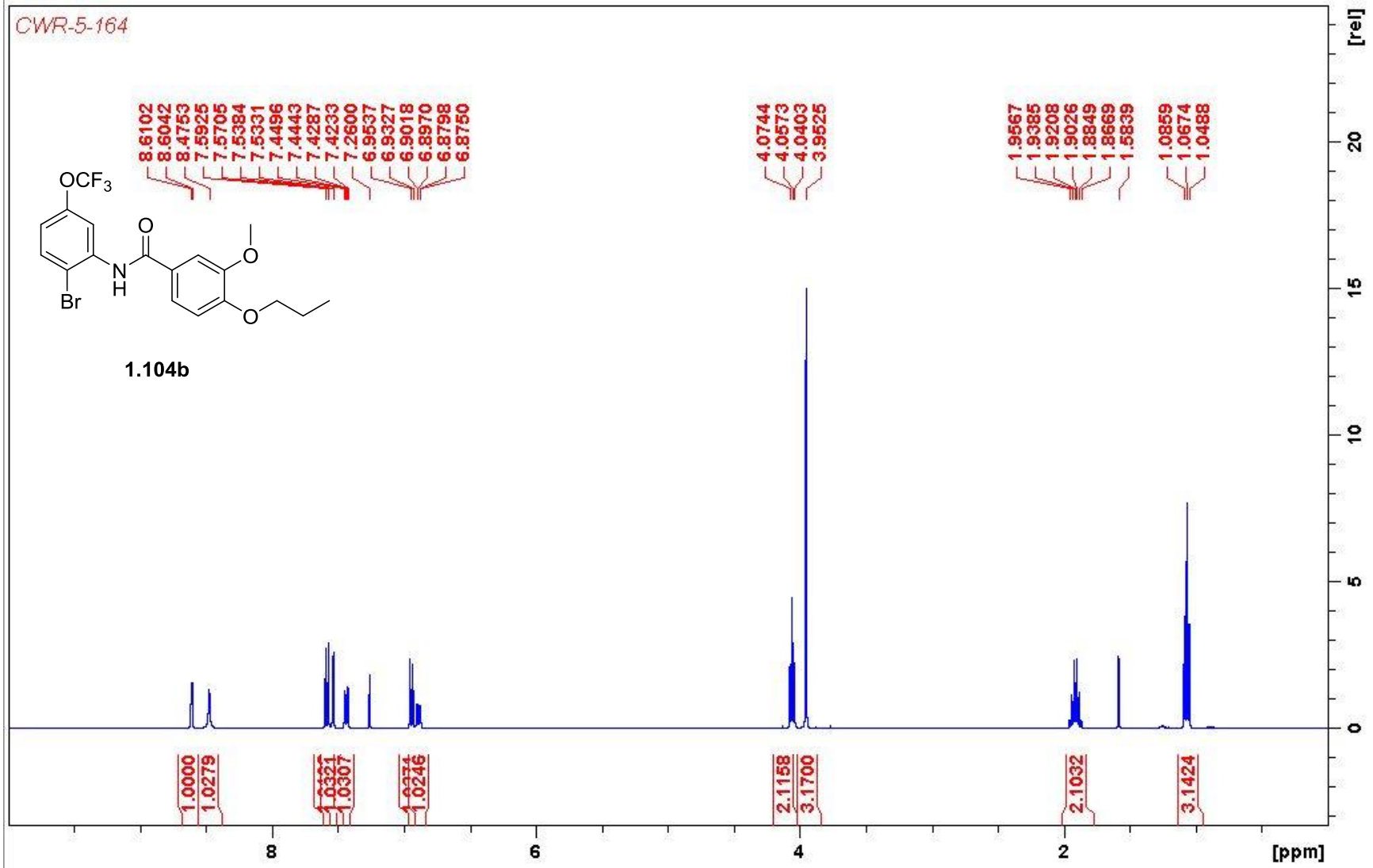
1.208a



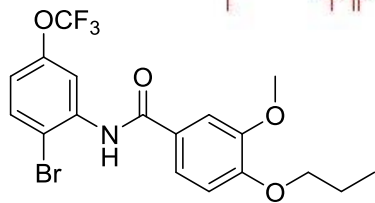




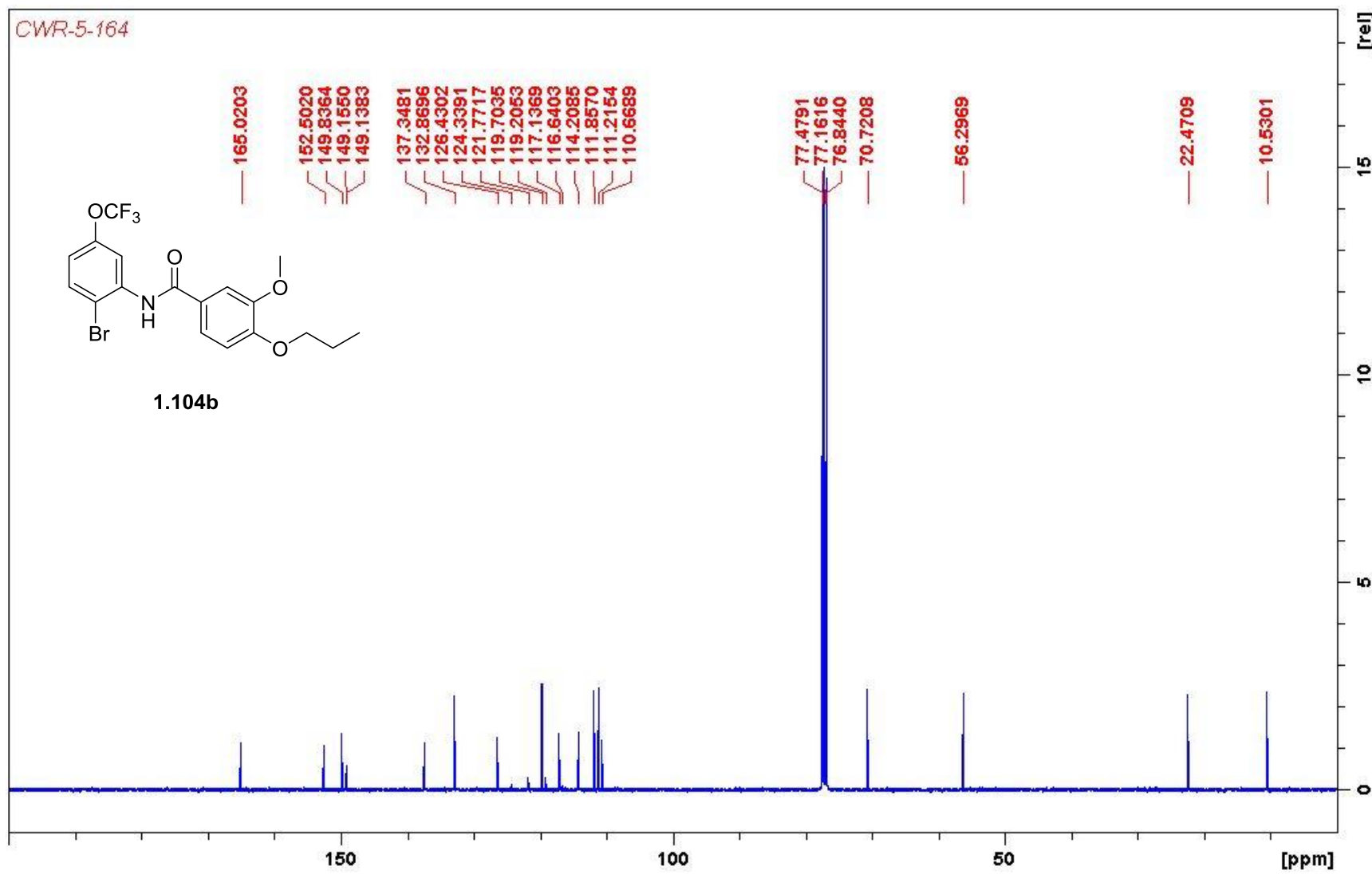


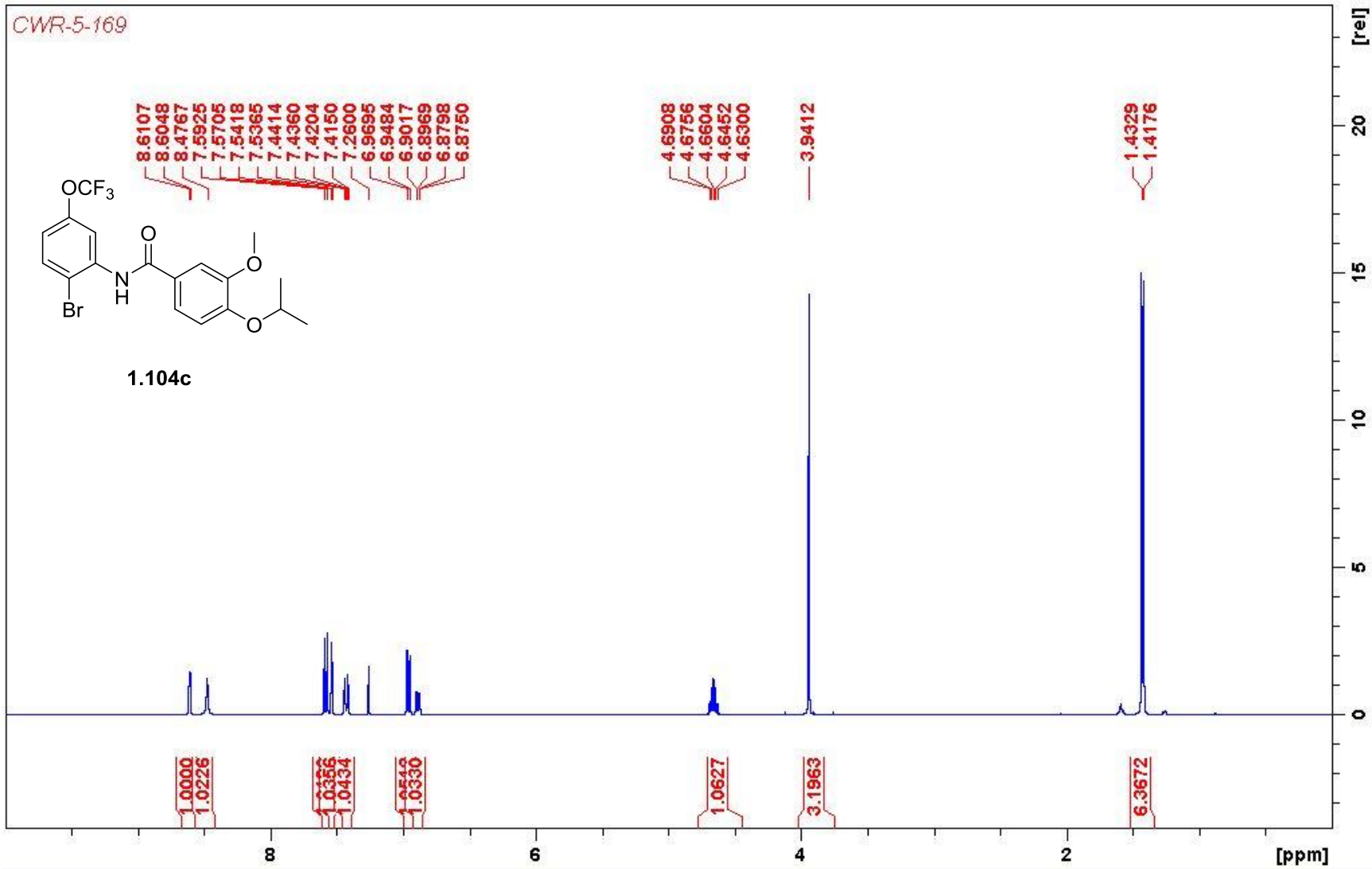


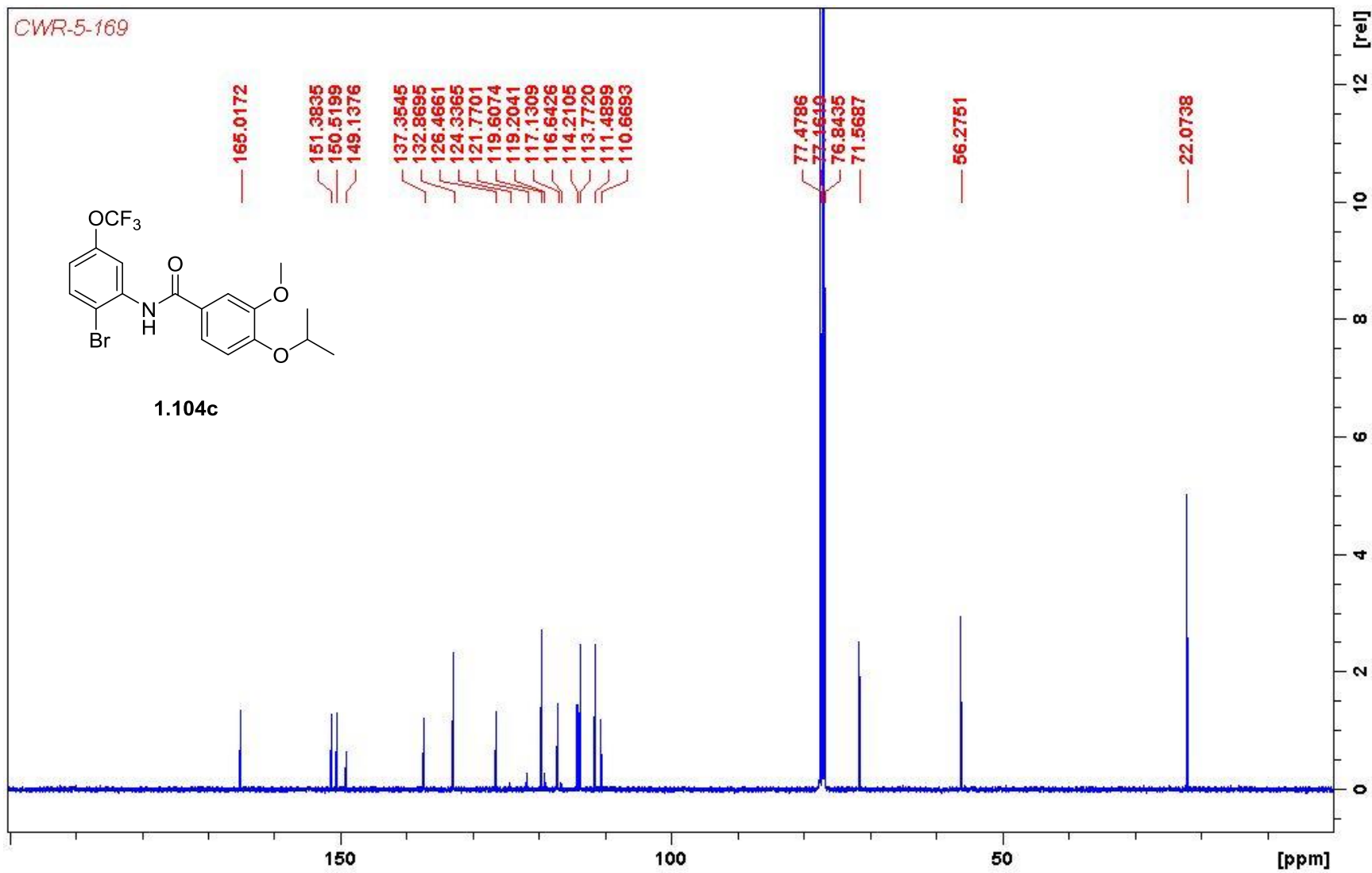
CWR-5-164

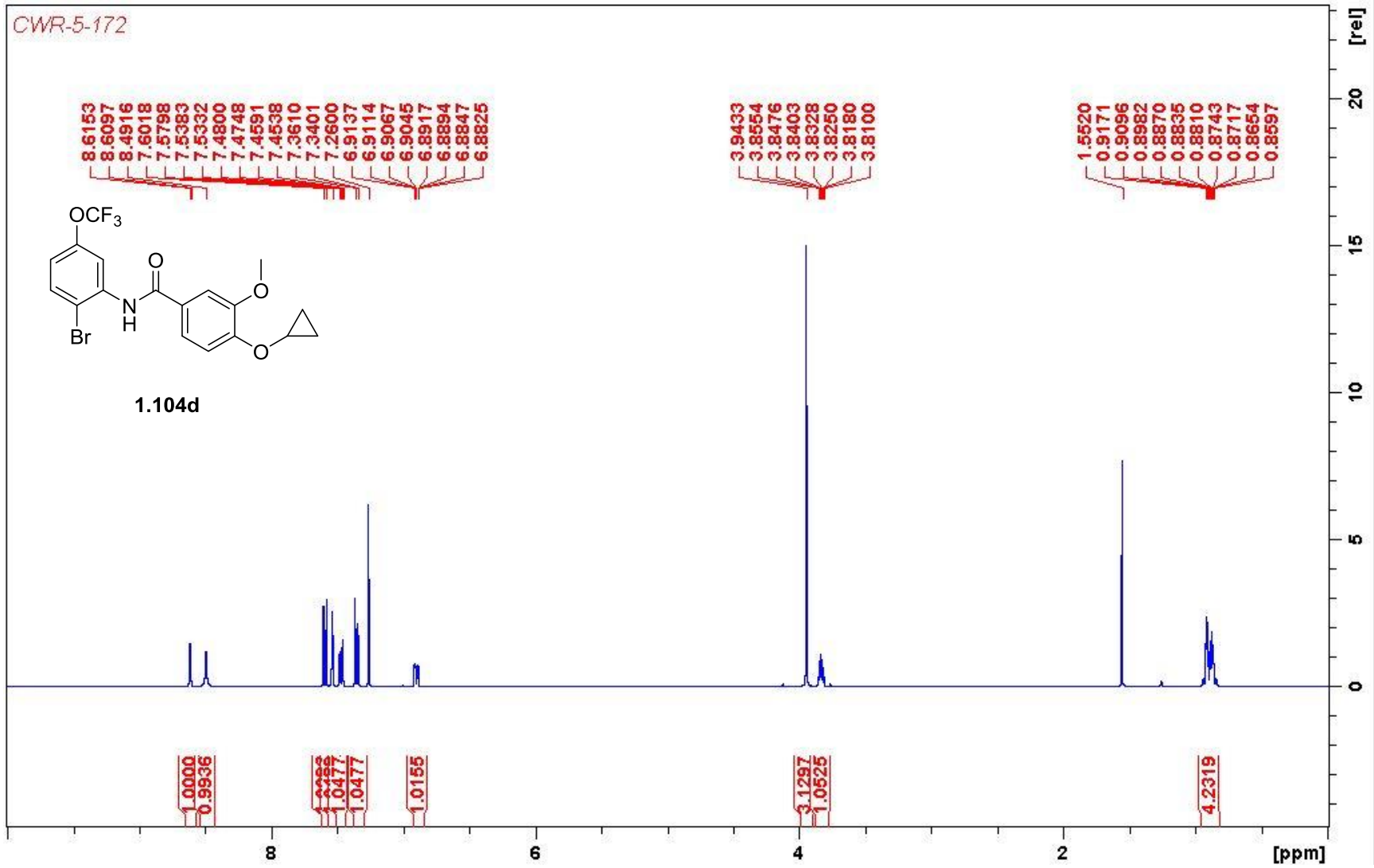


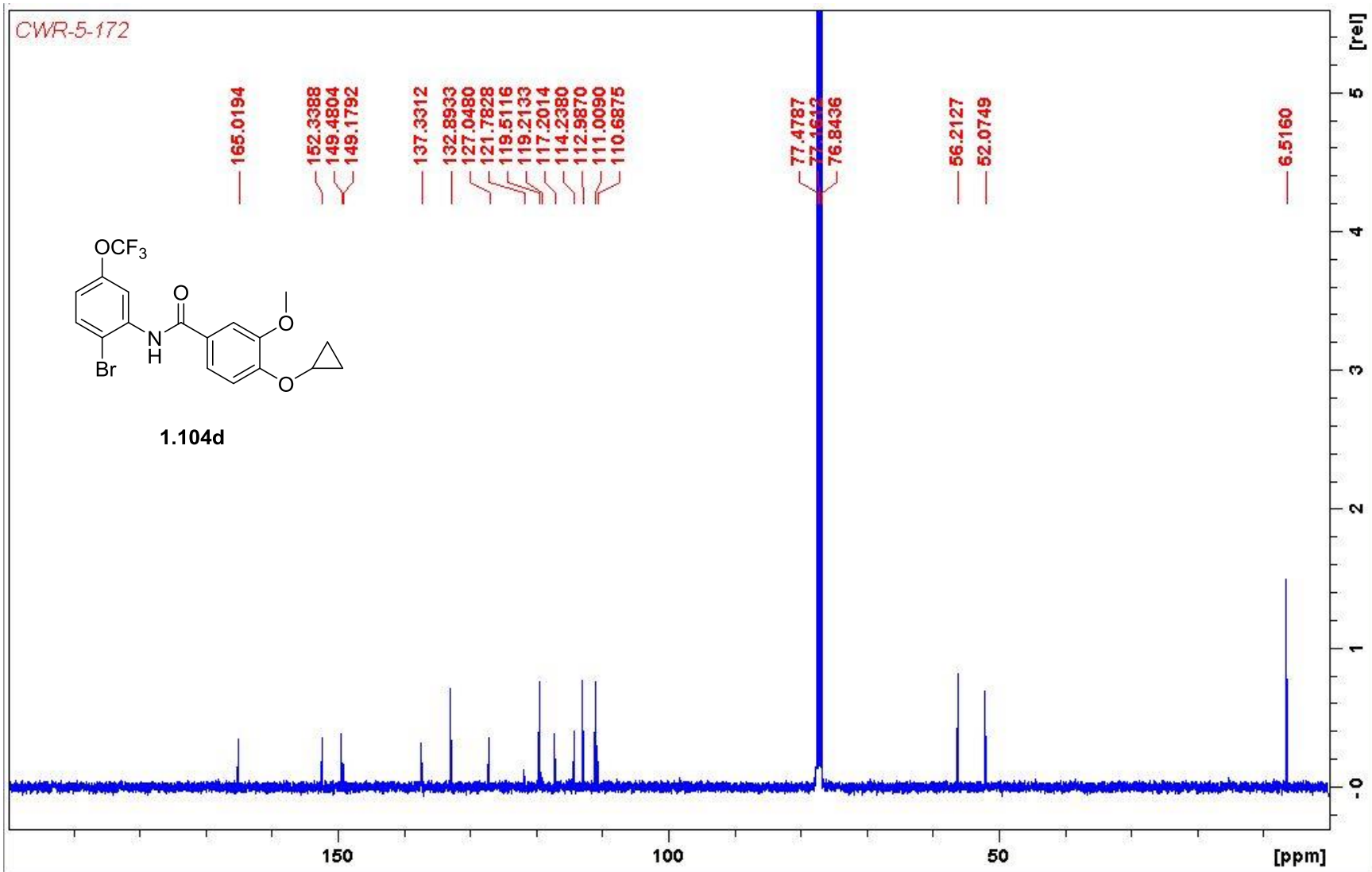
1.104b

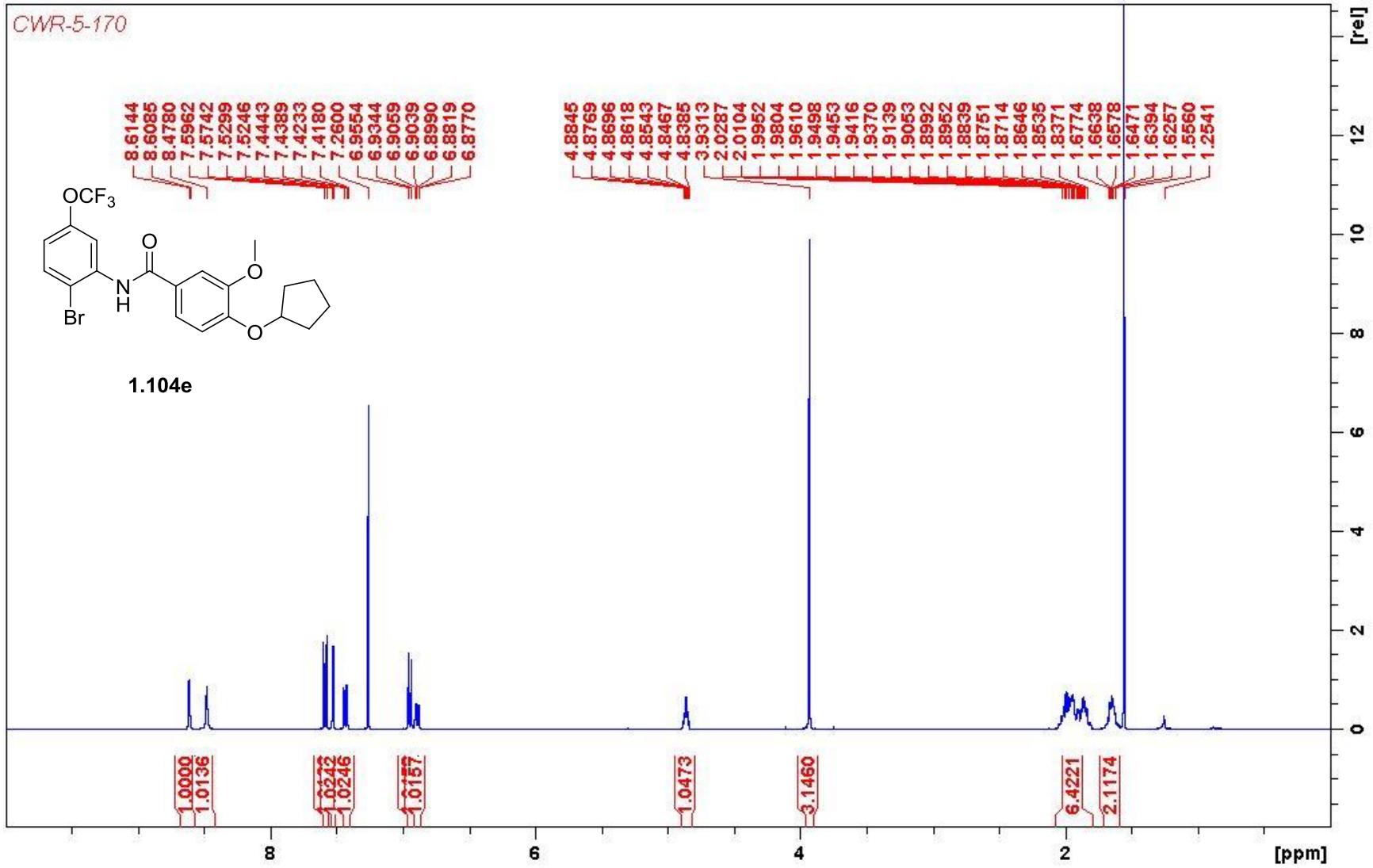


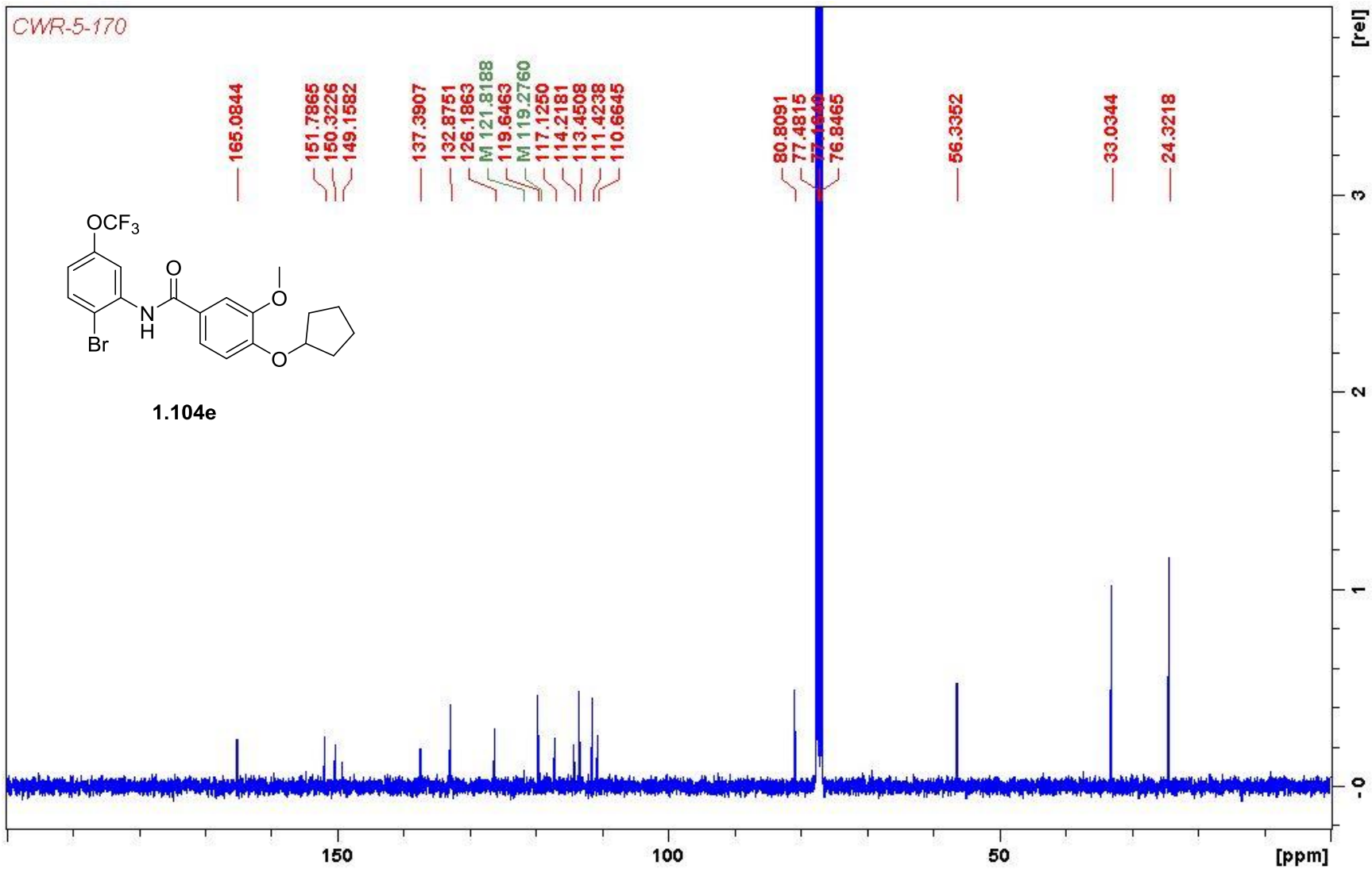


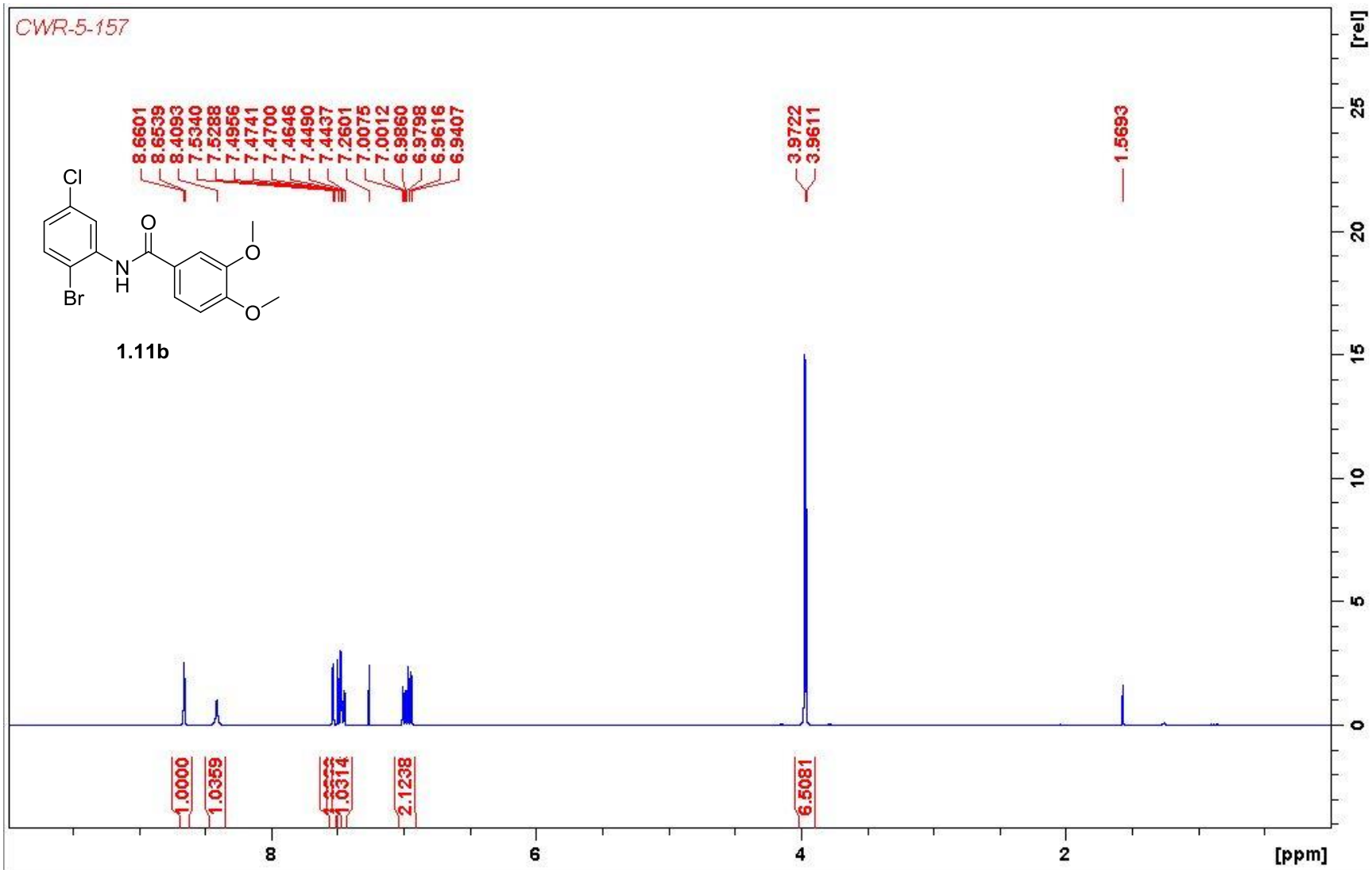


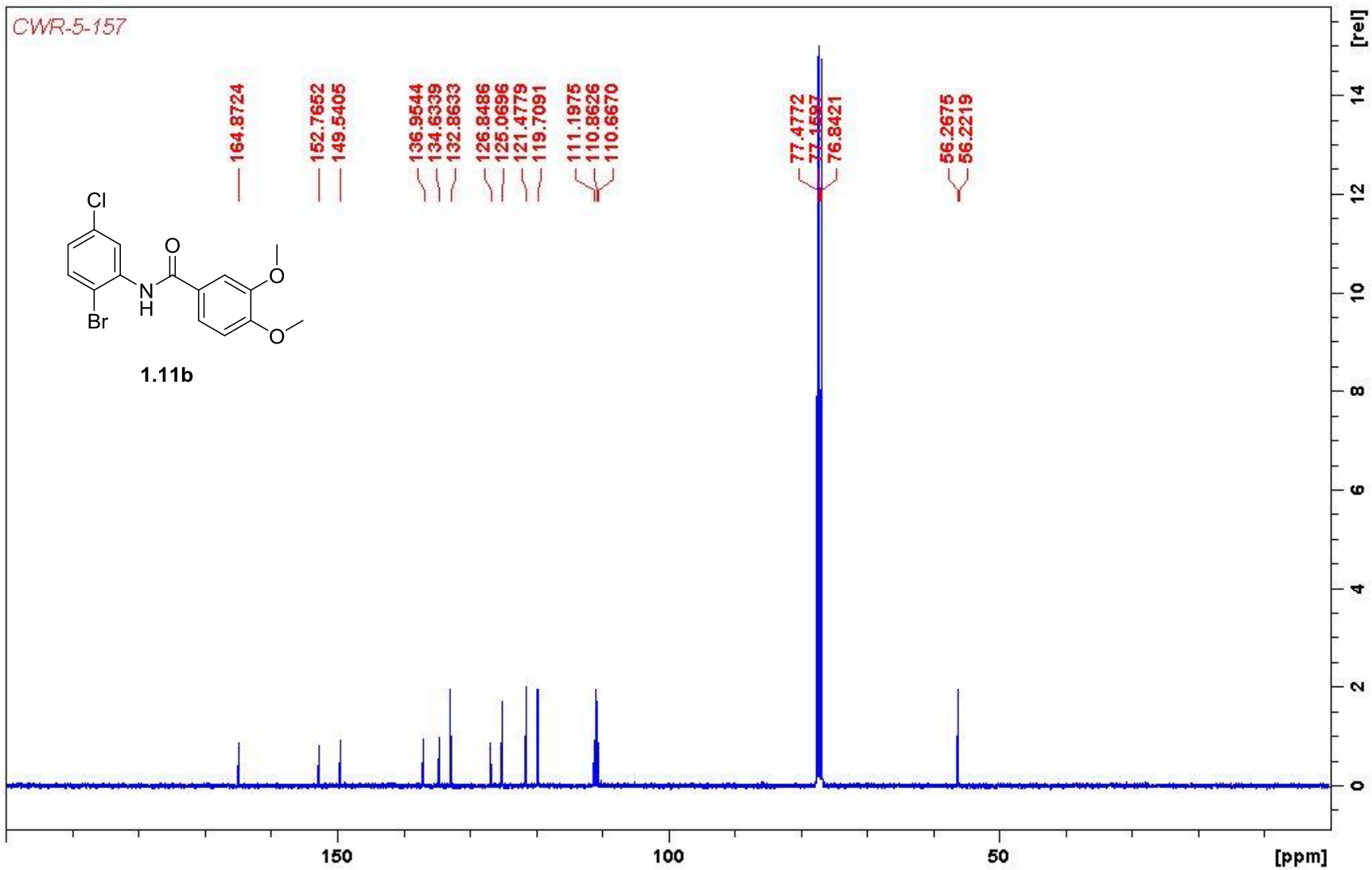


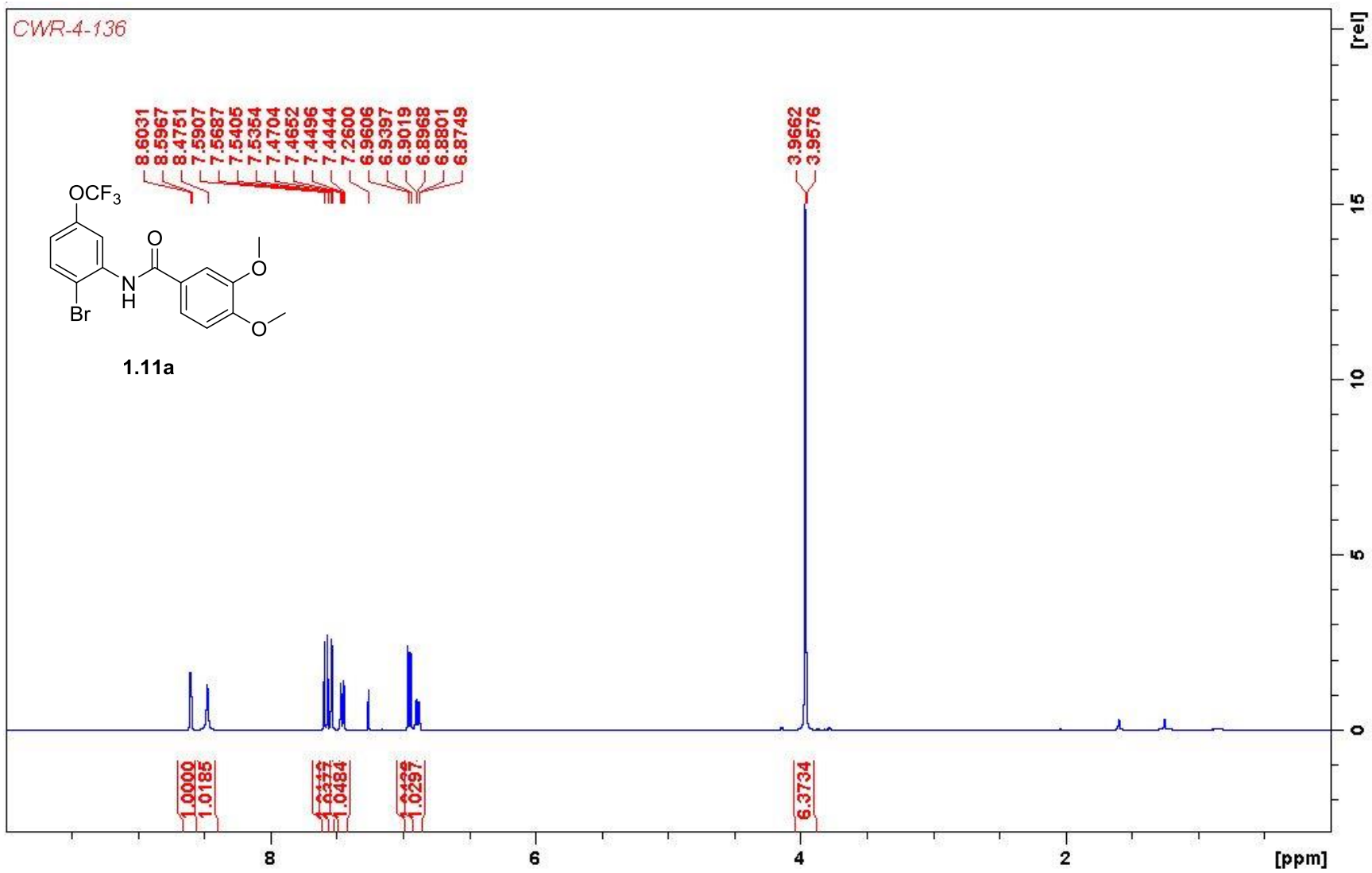


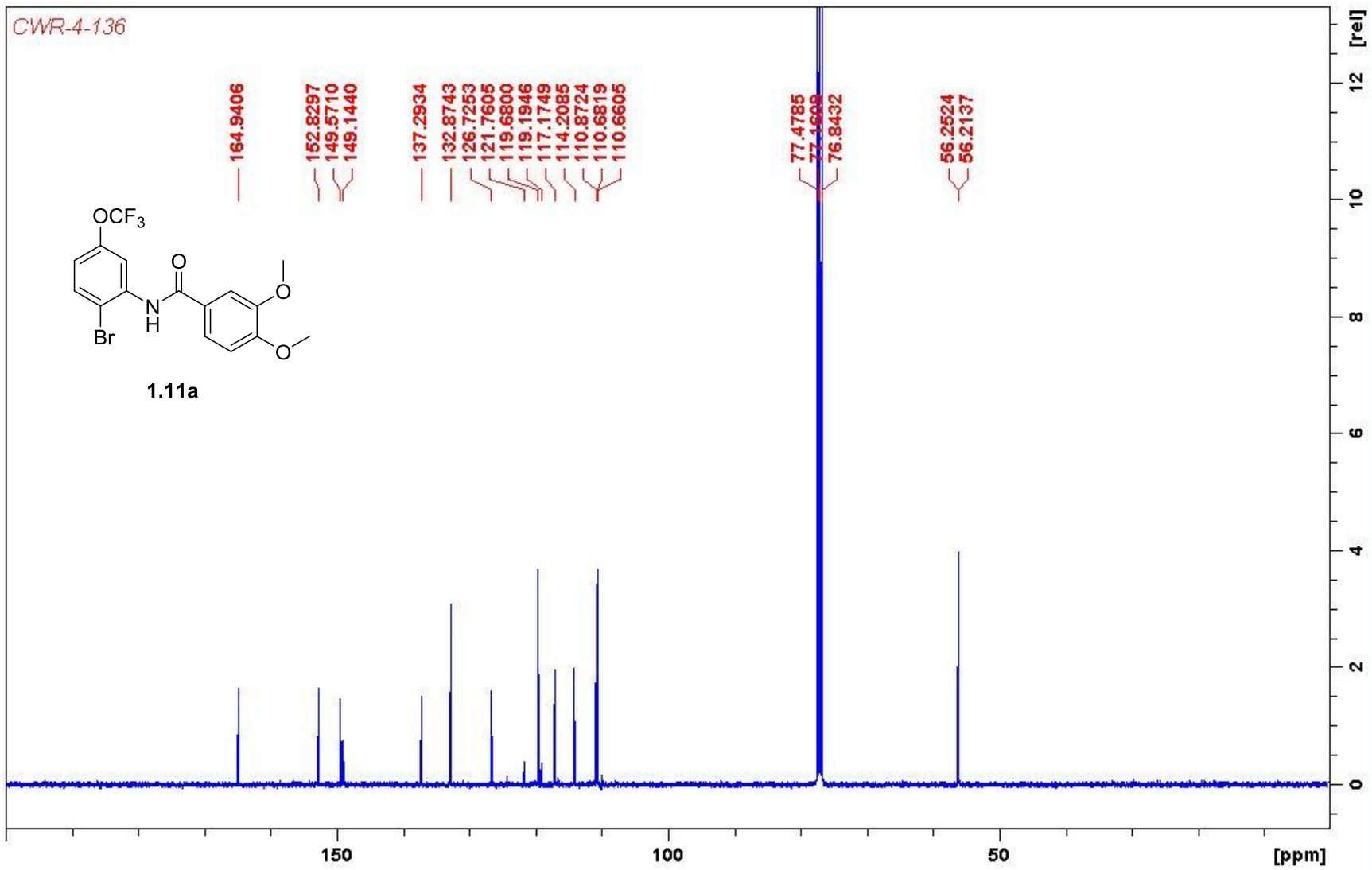


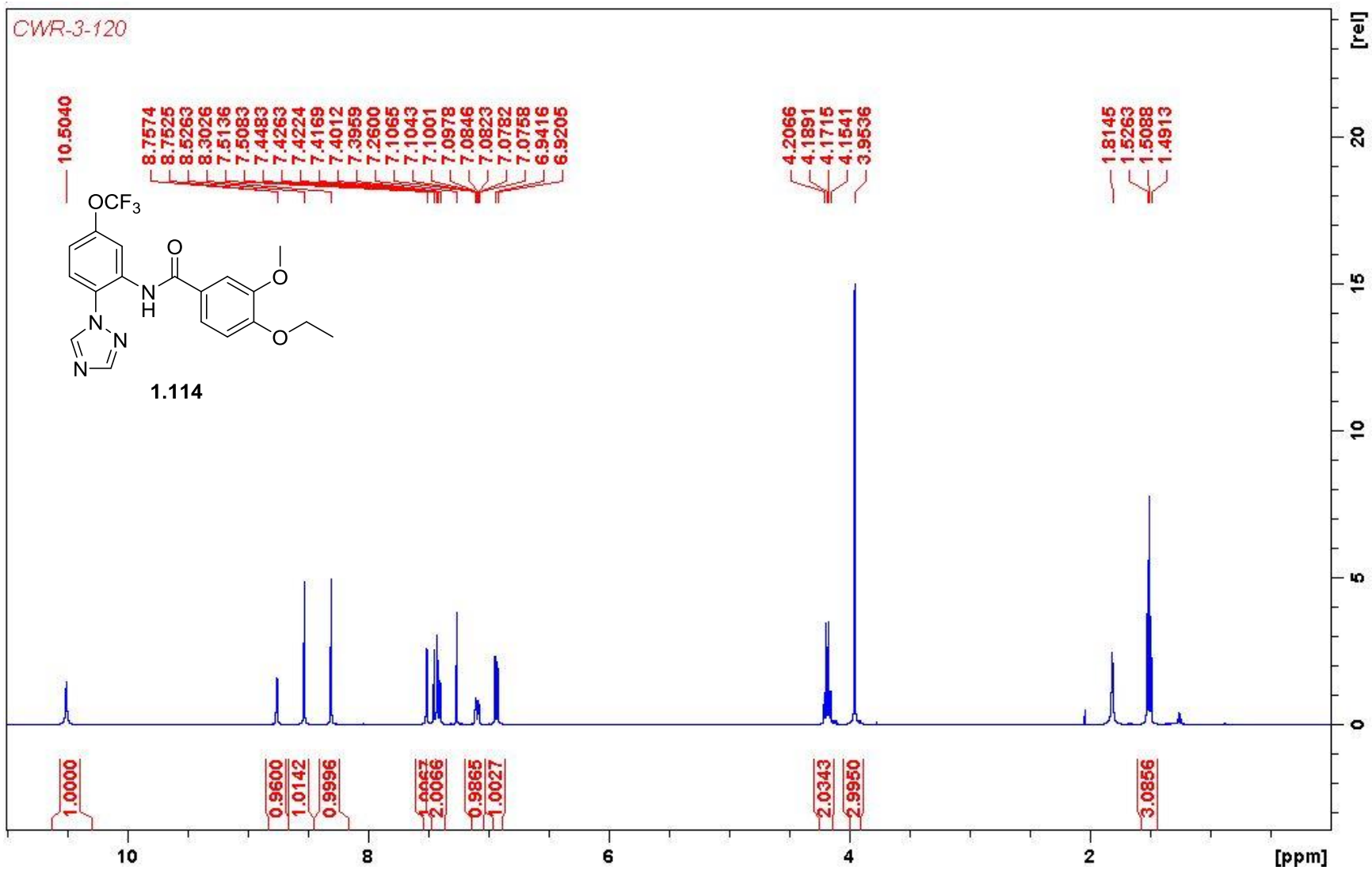


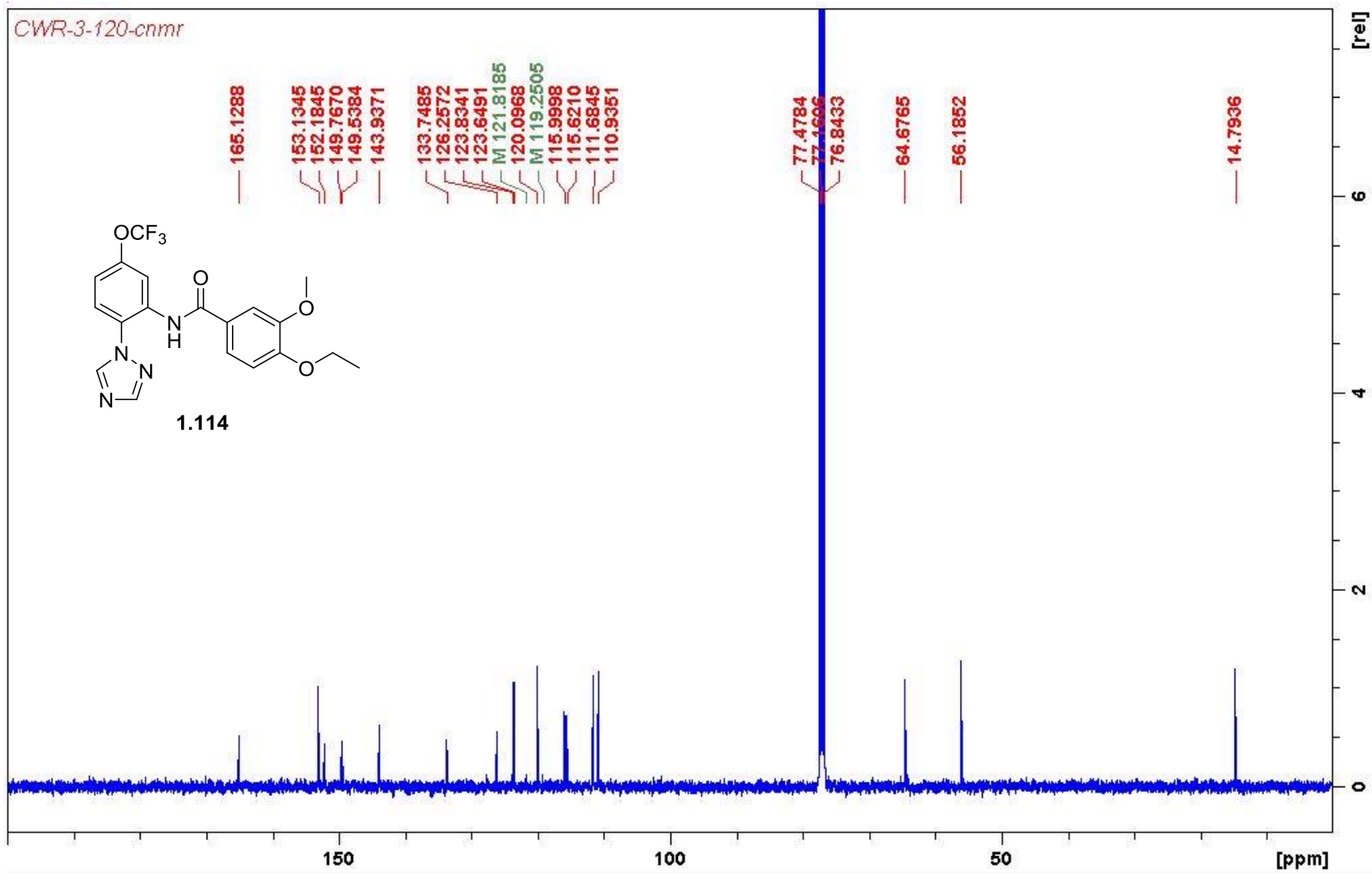


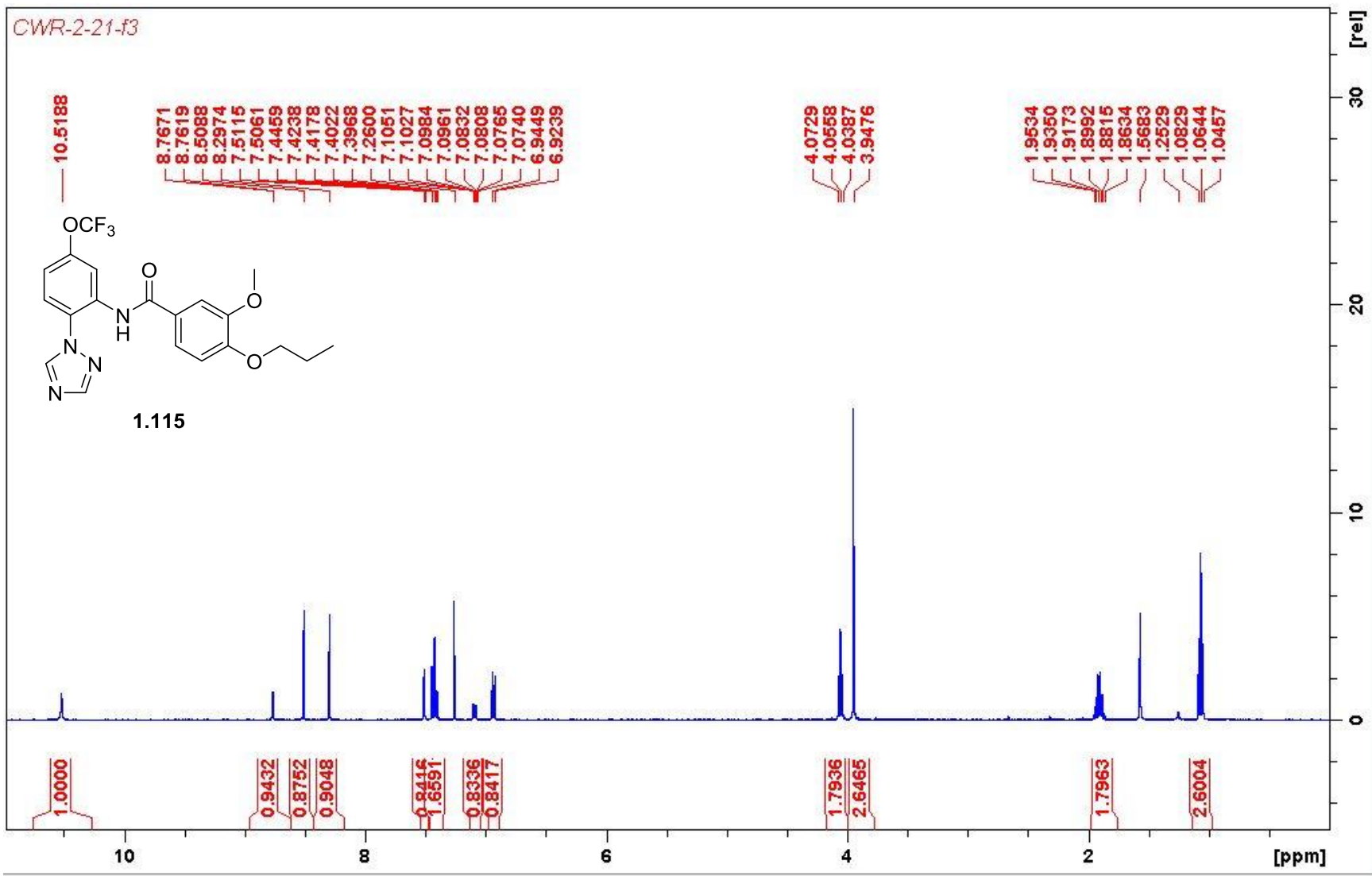


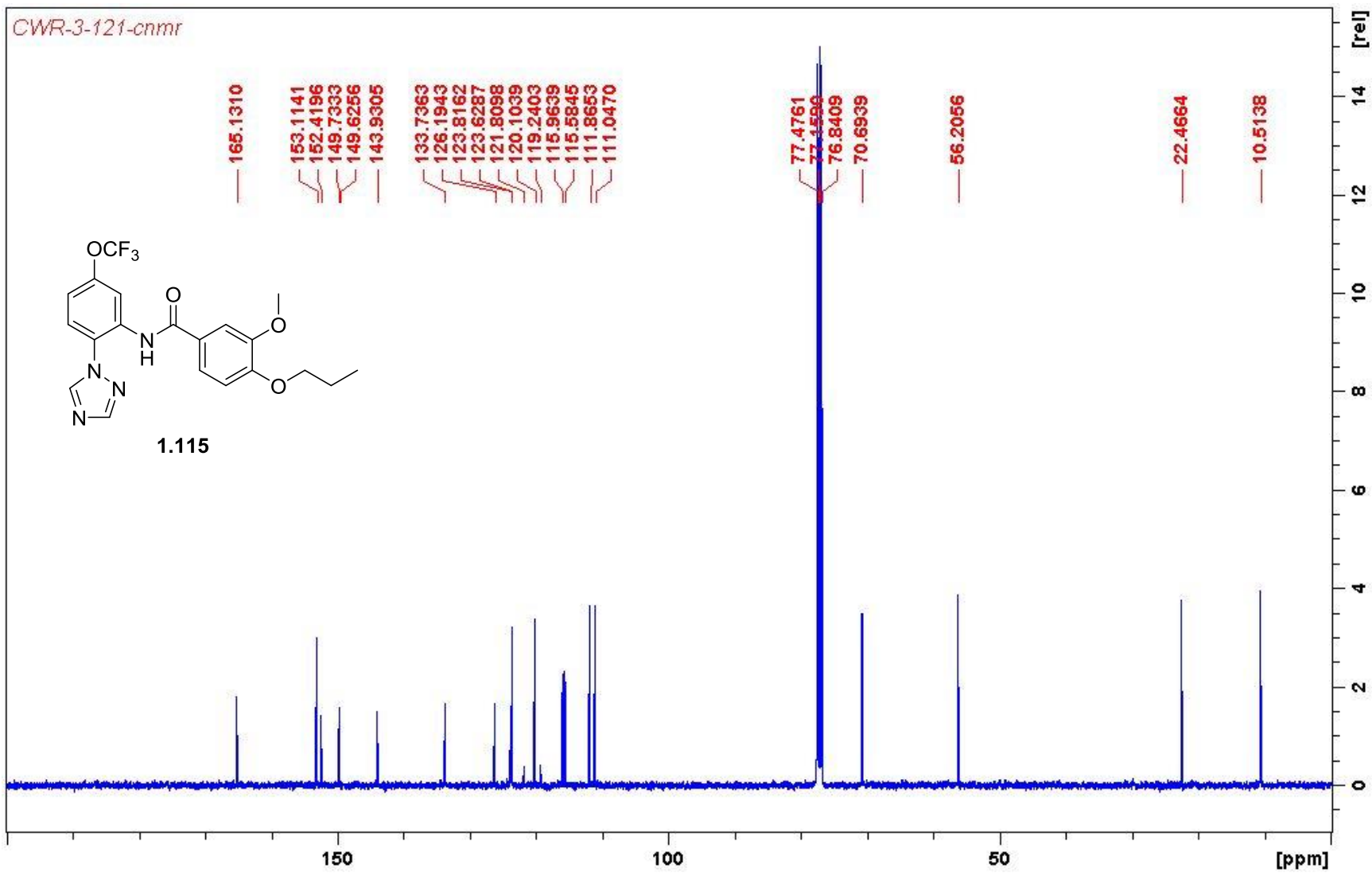


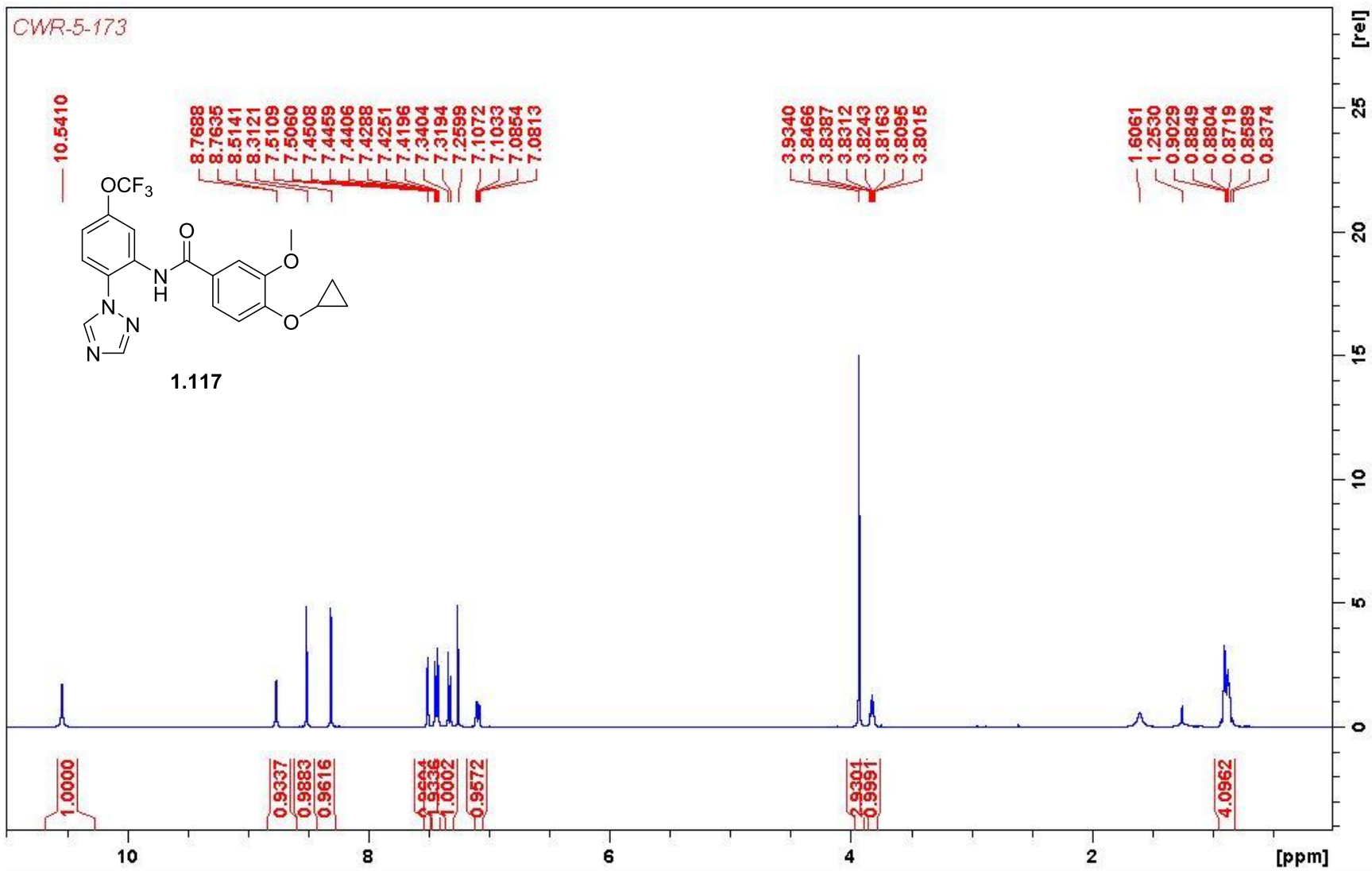


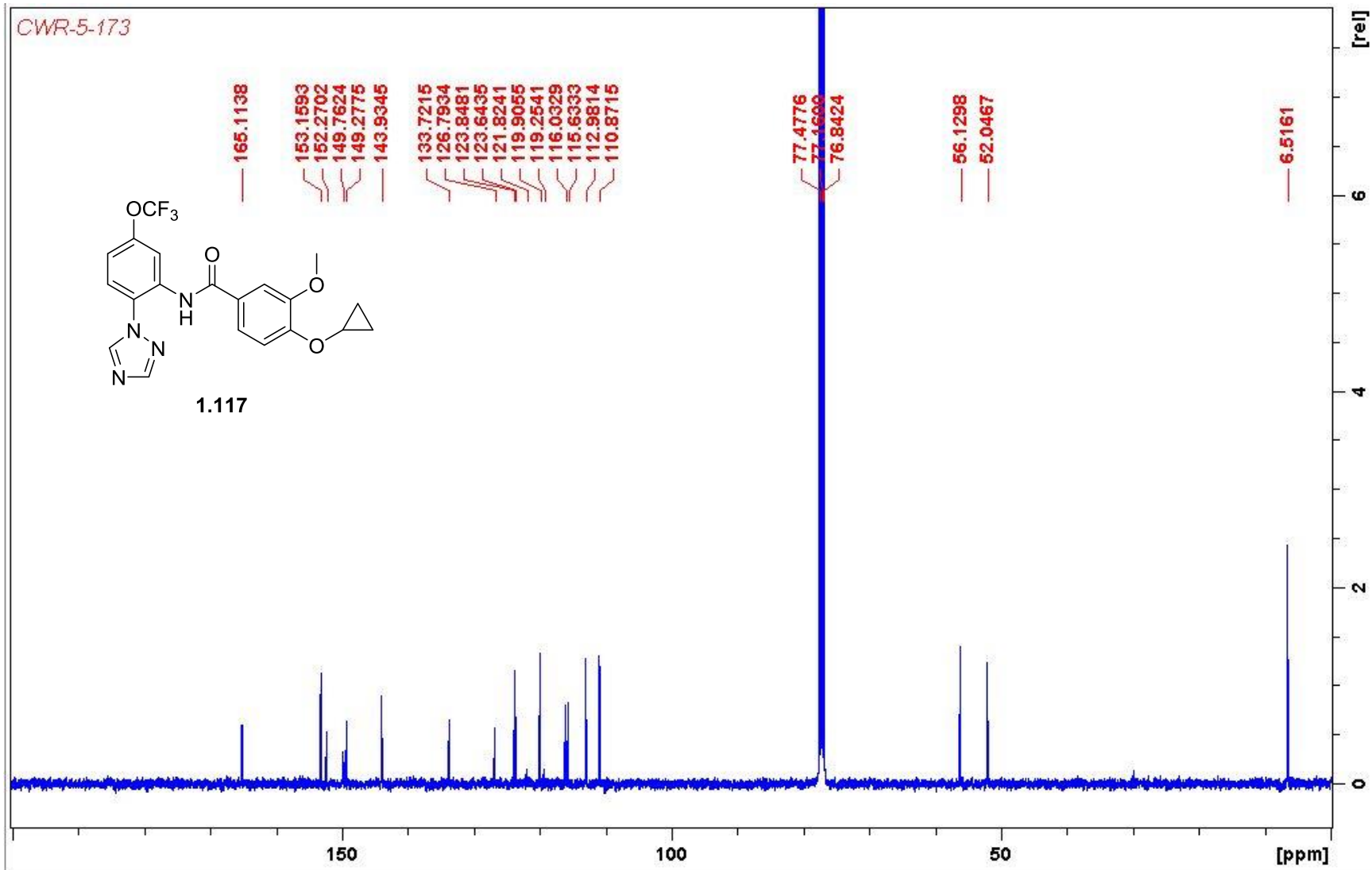


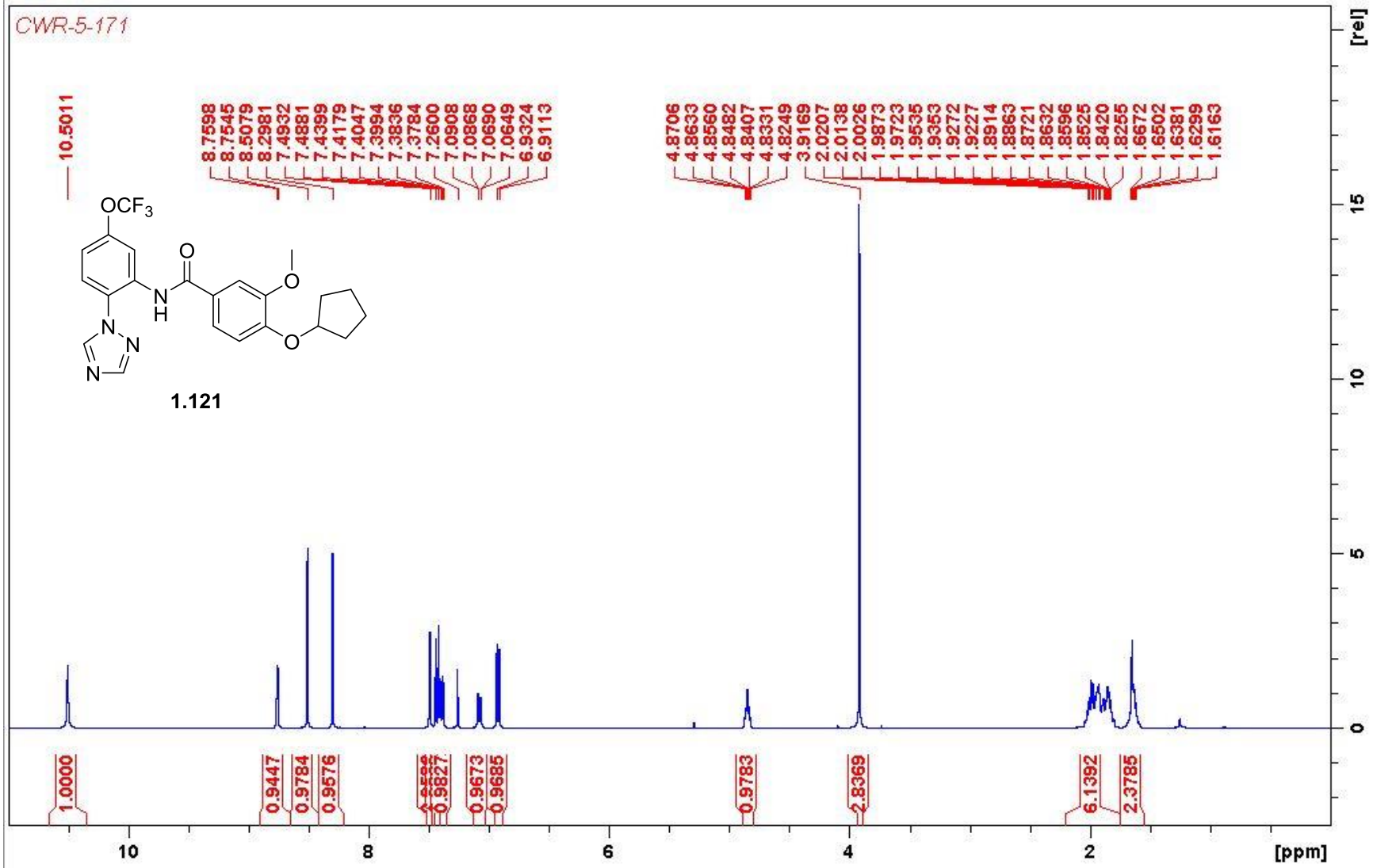


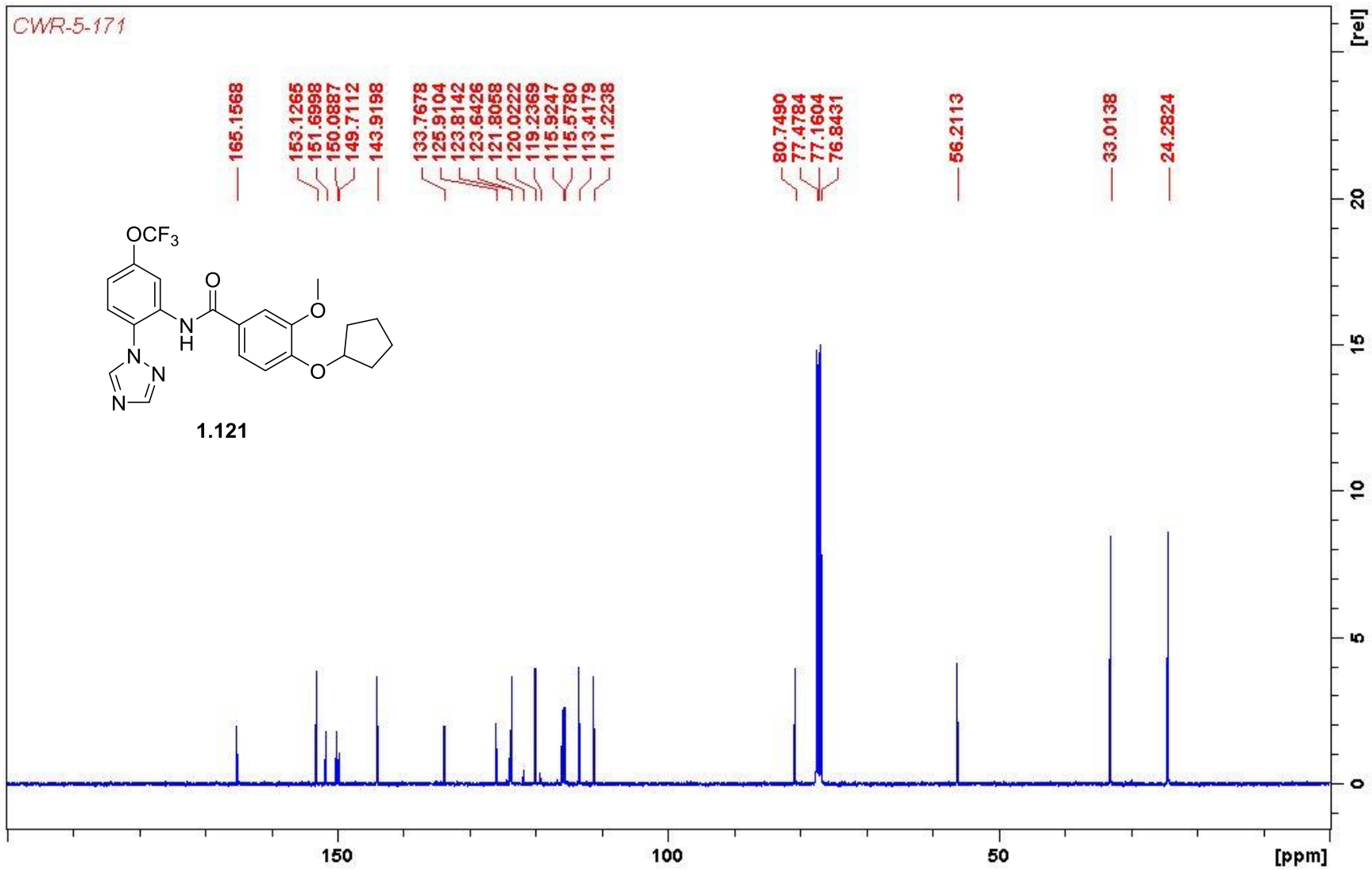


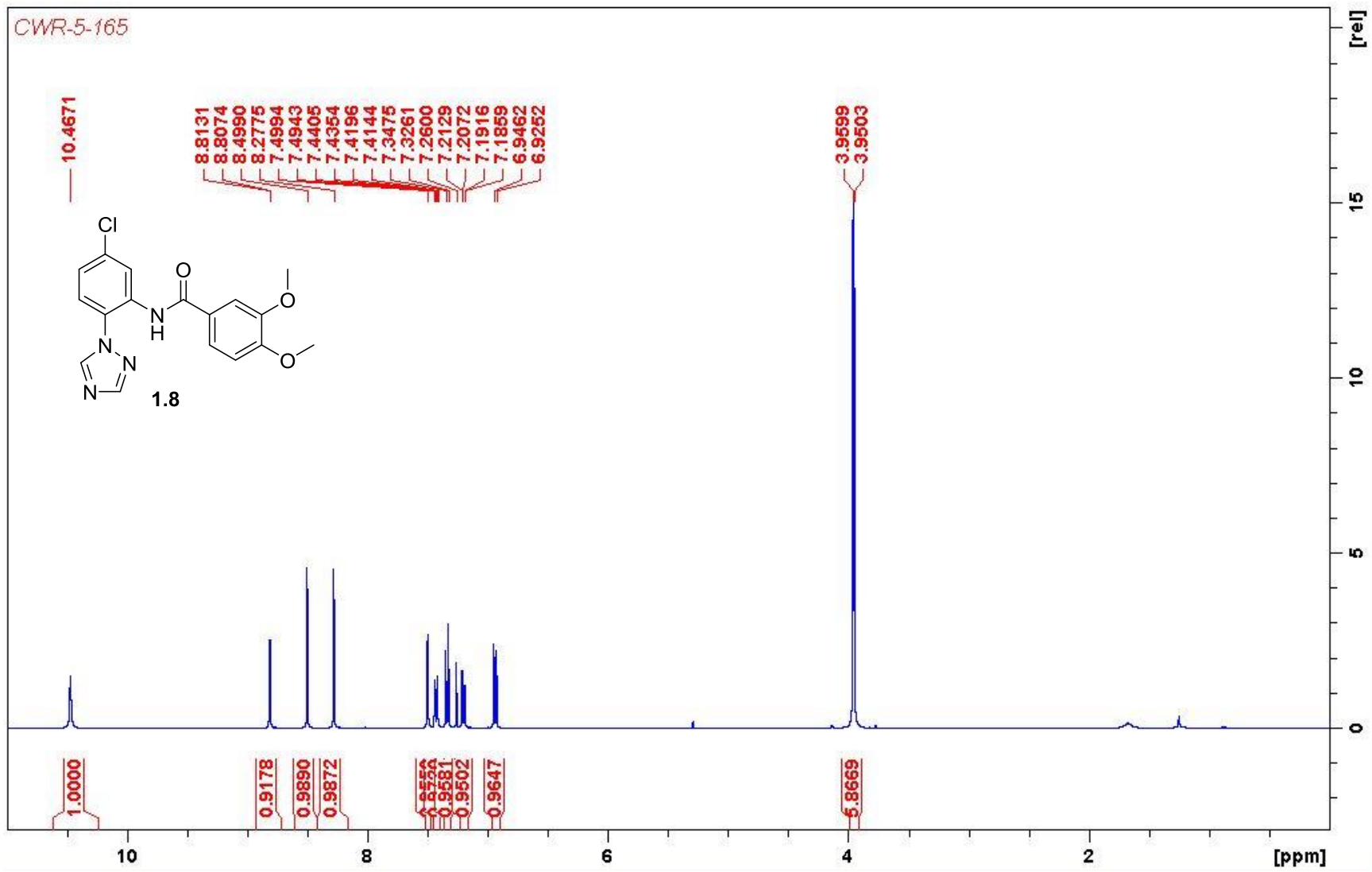


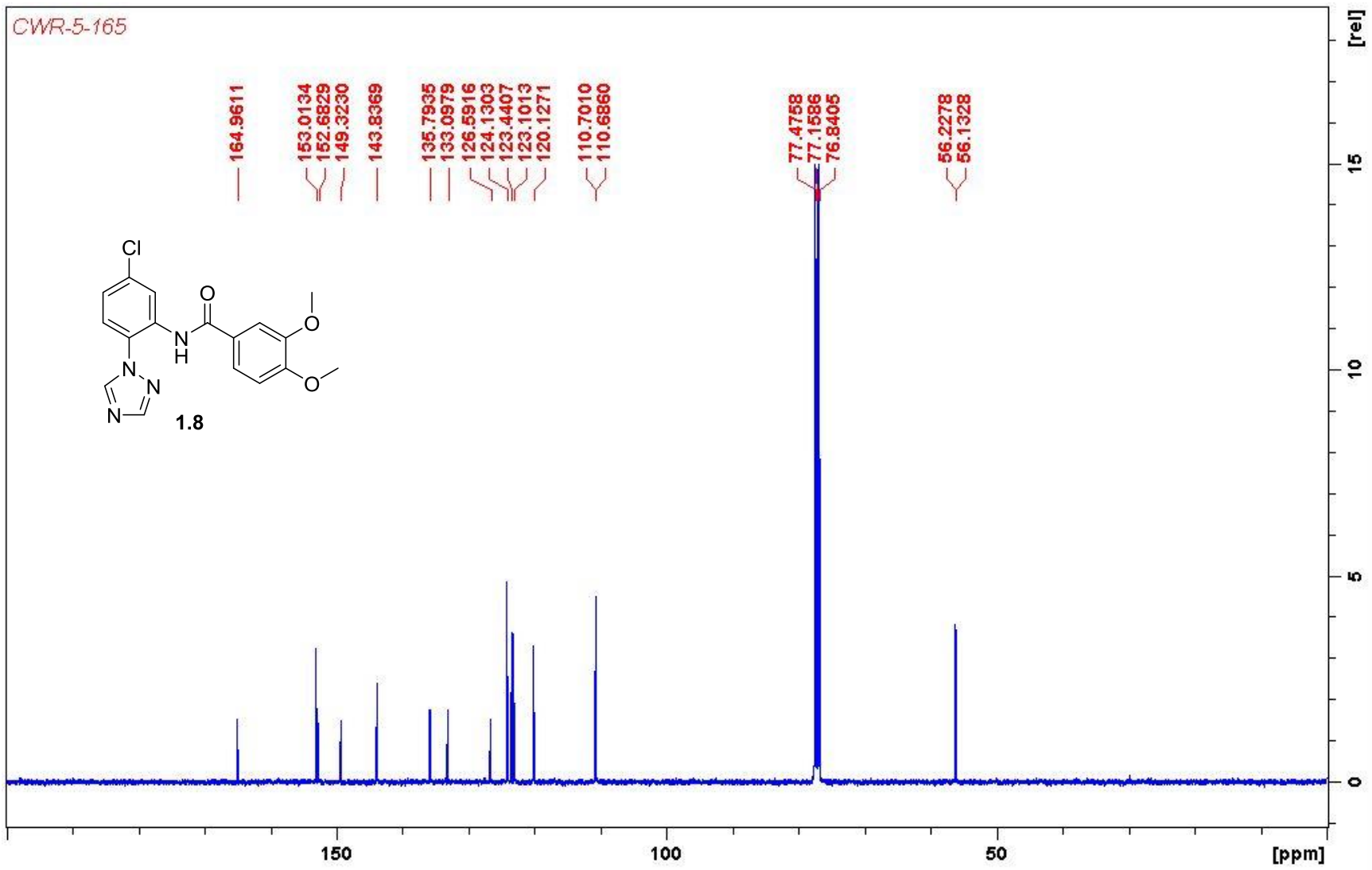


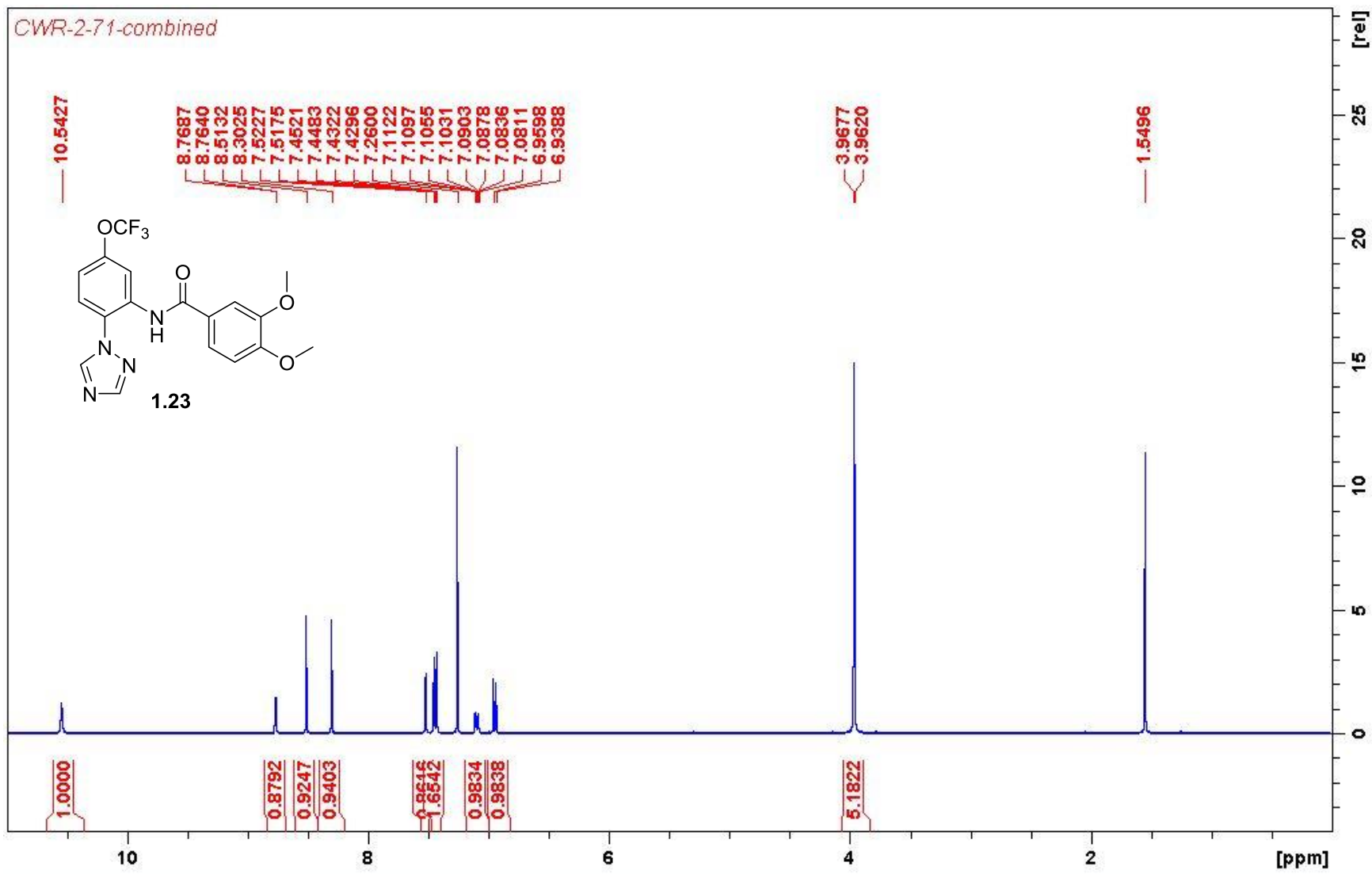


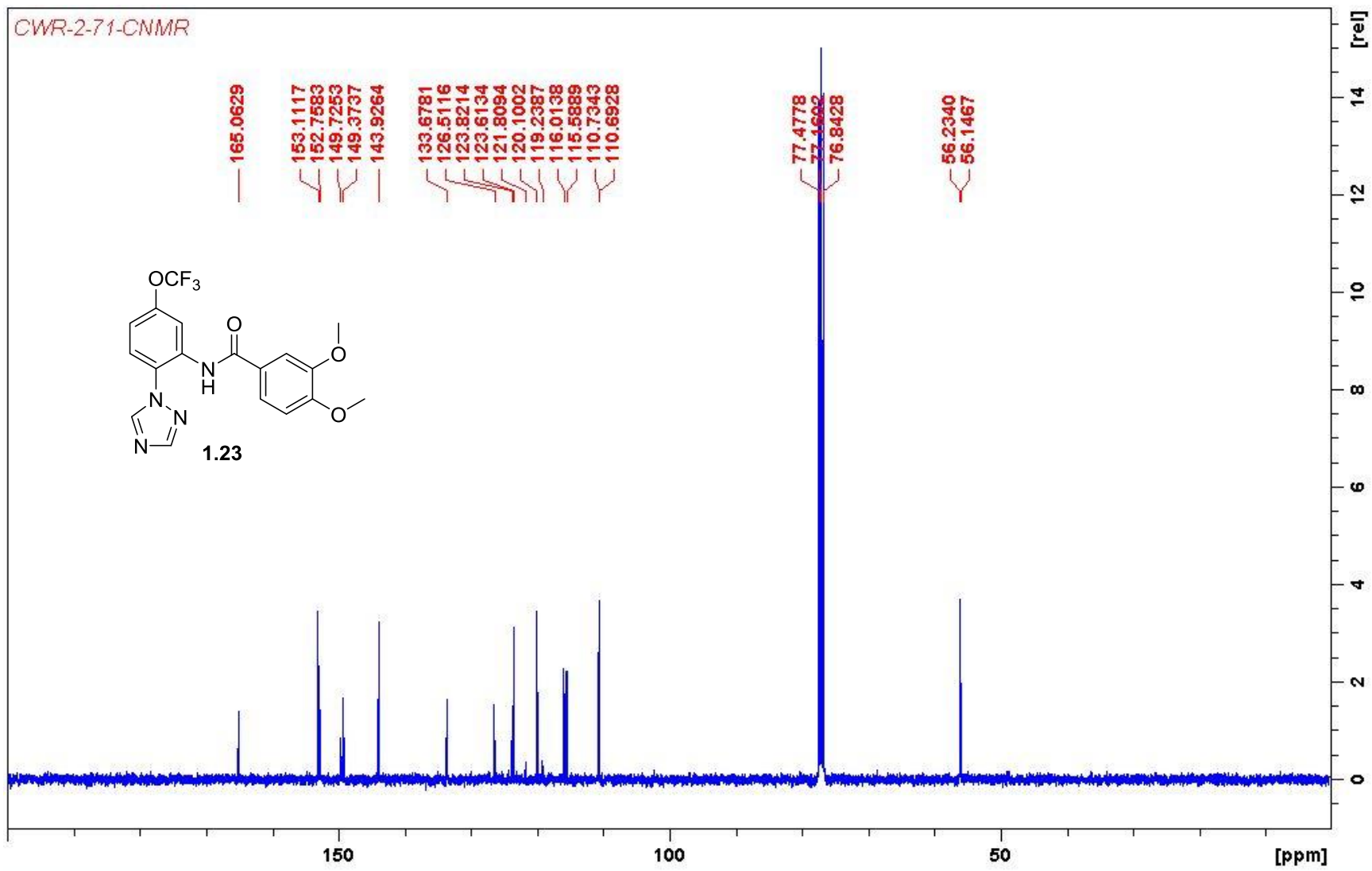


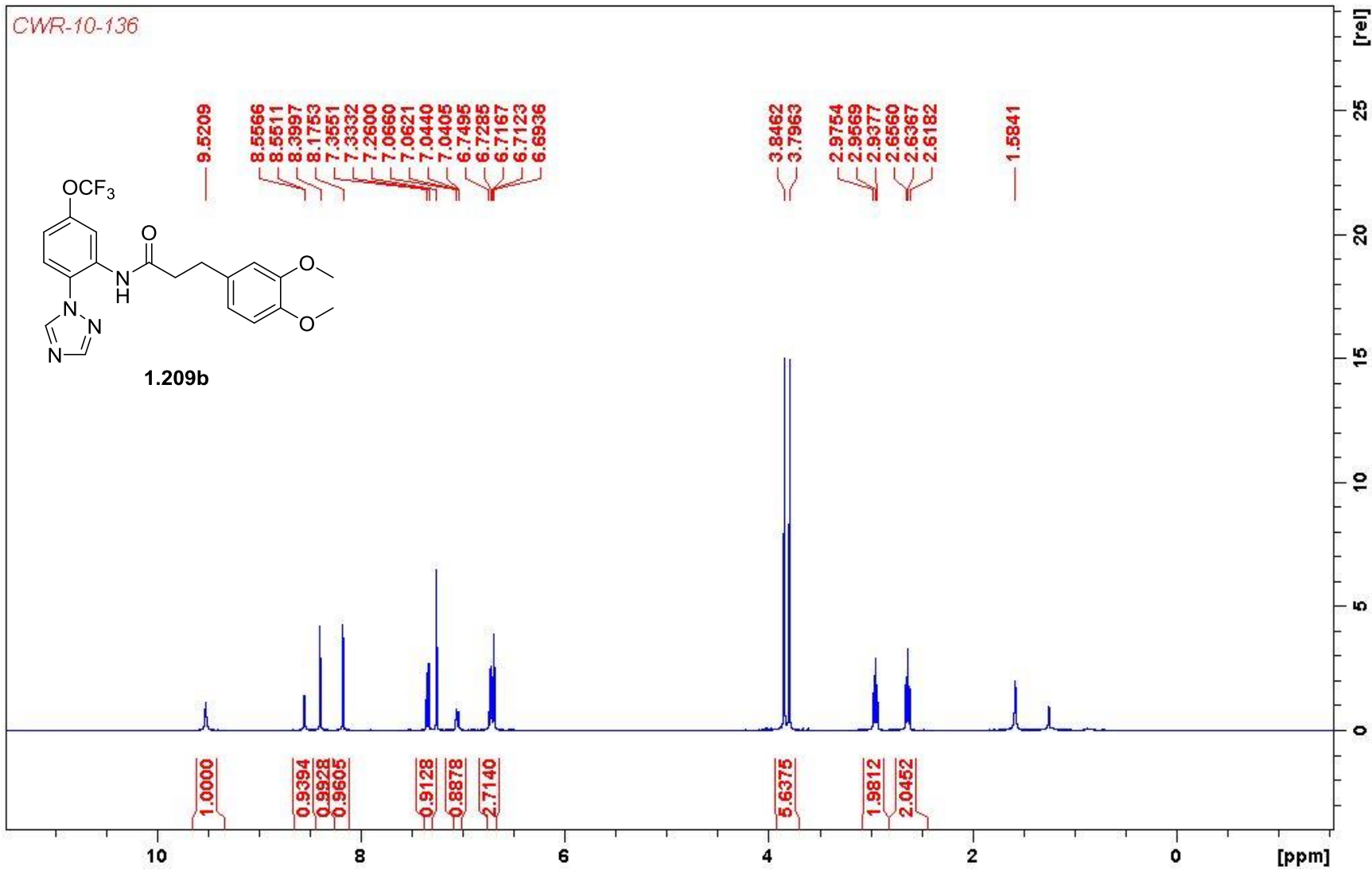


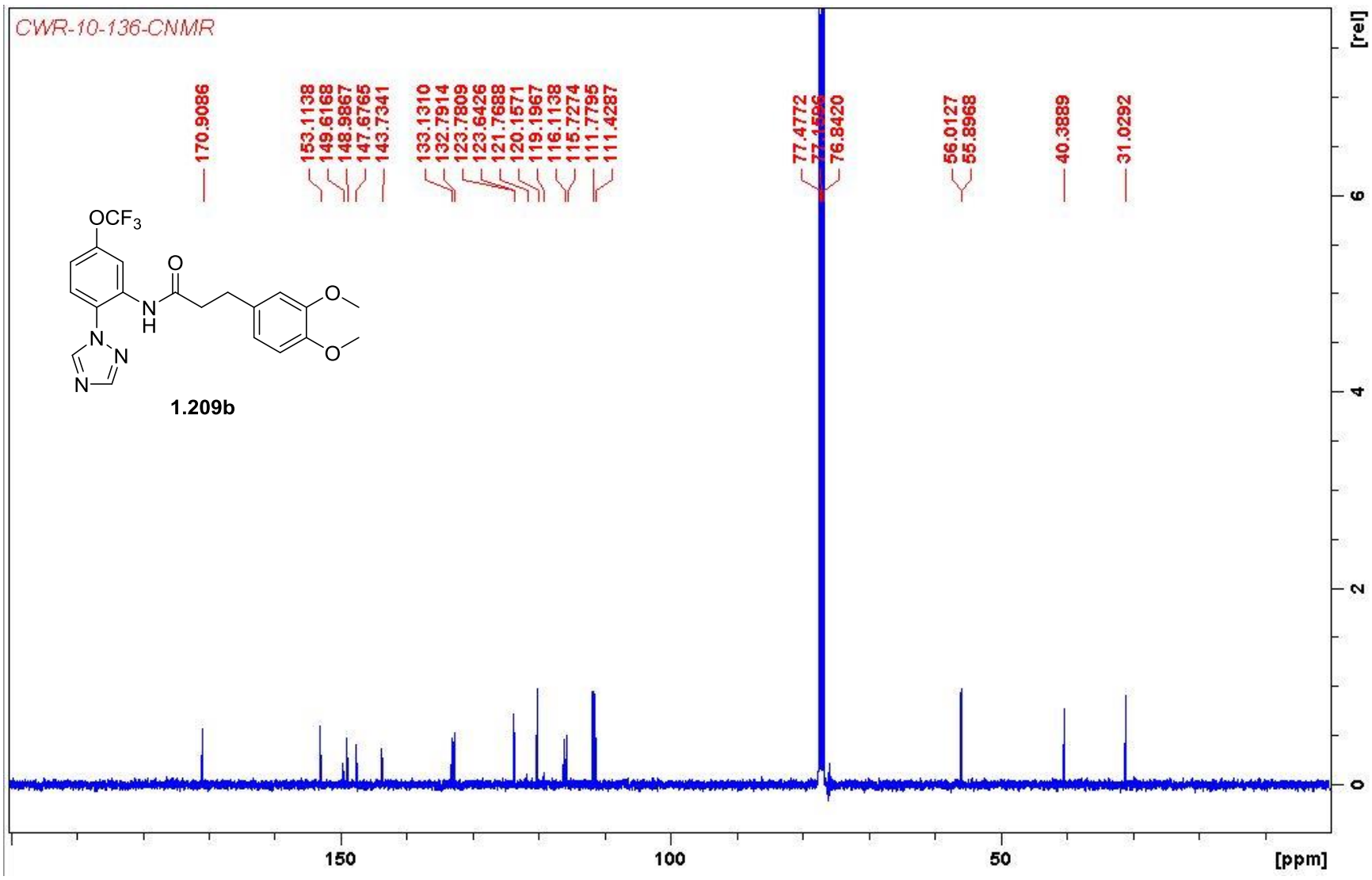




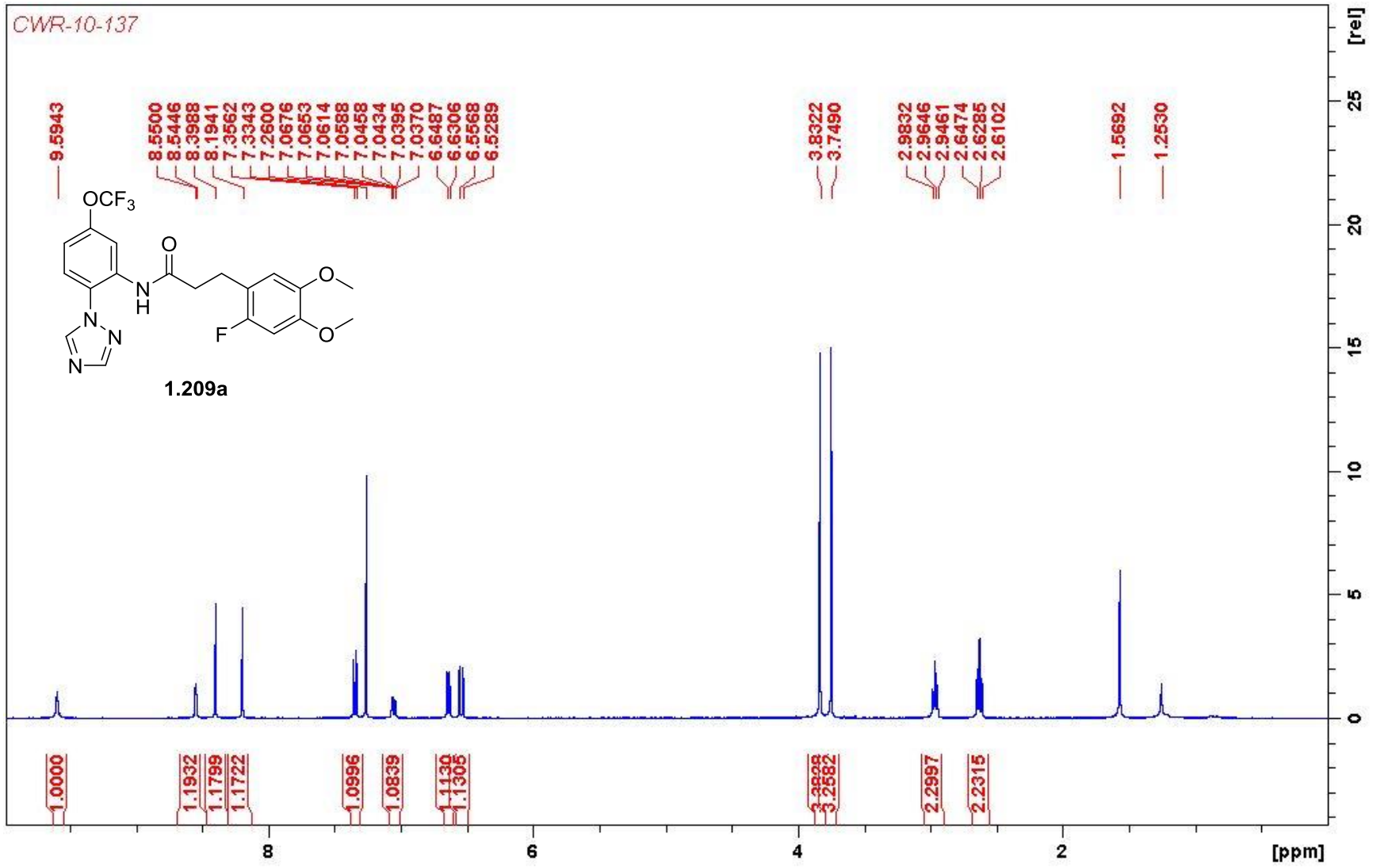




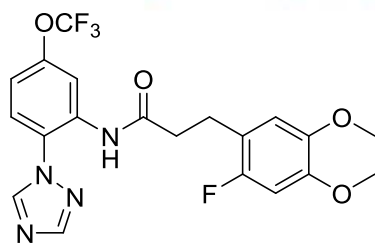




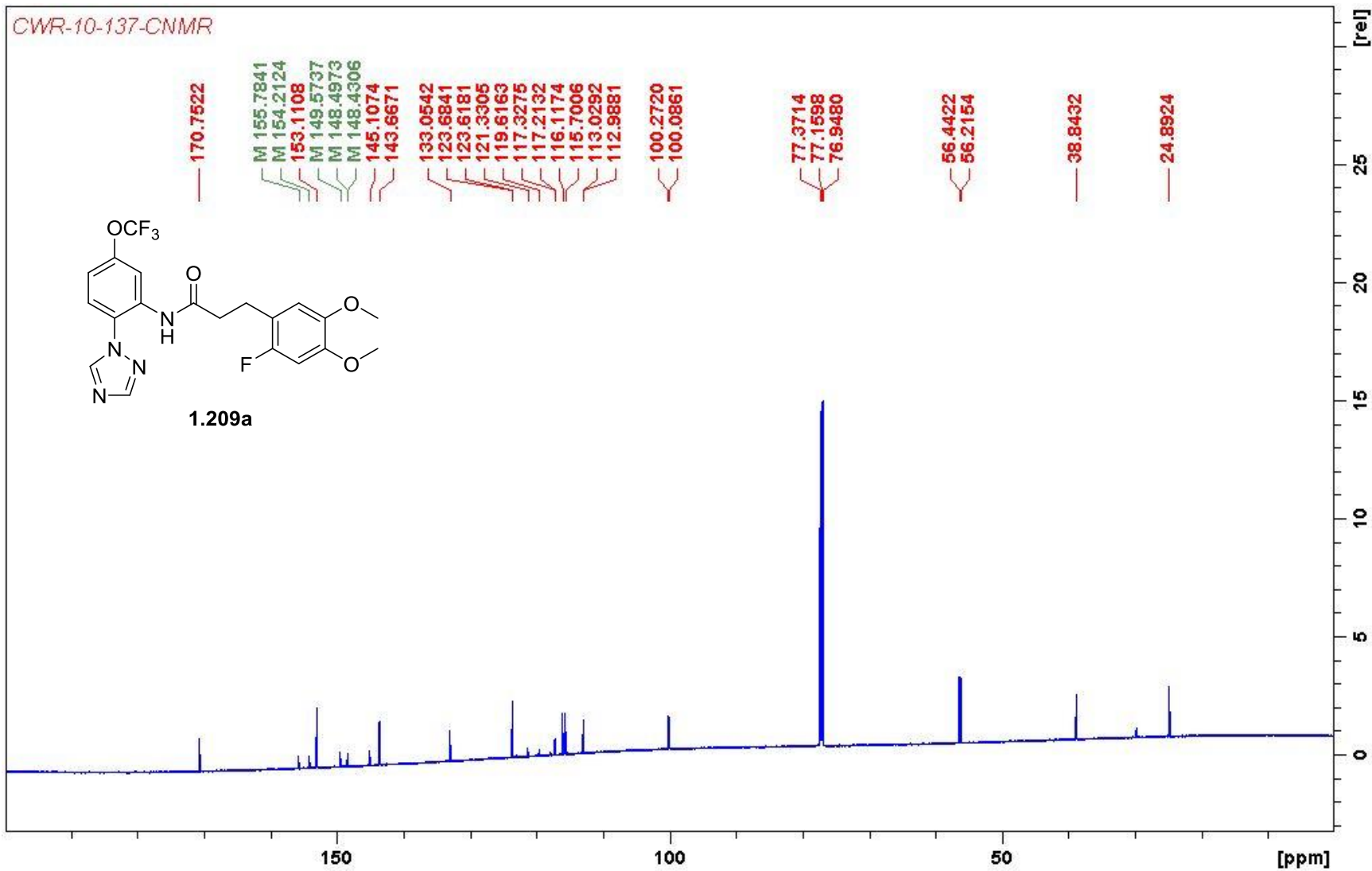
CWR-10-137

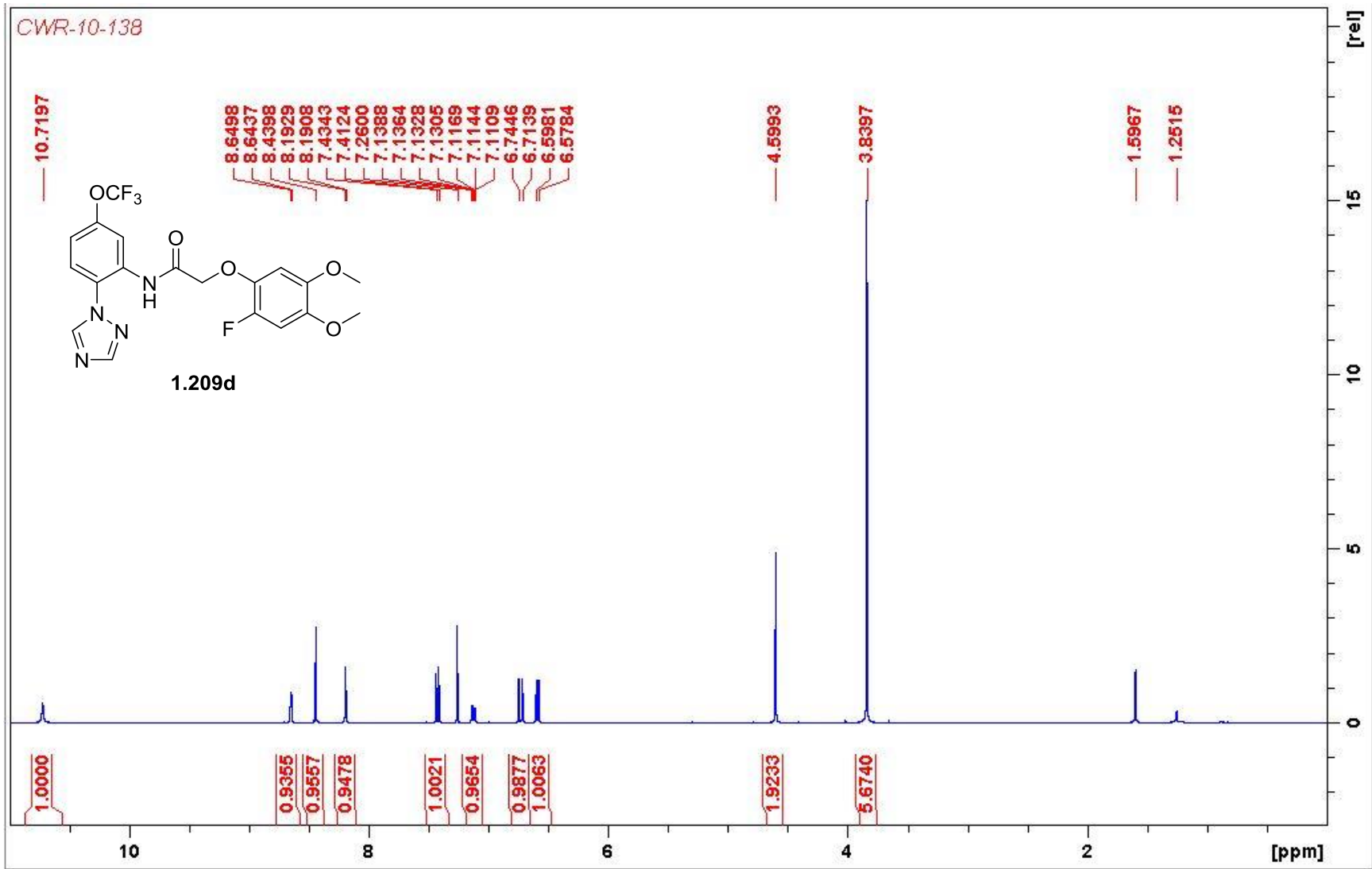


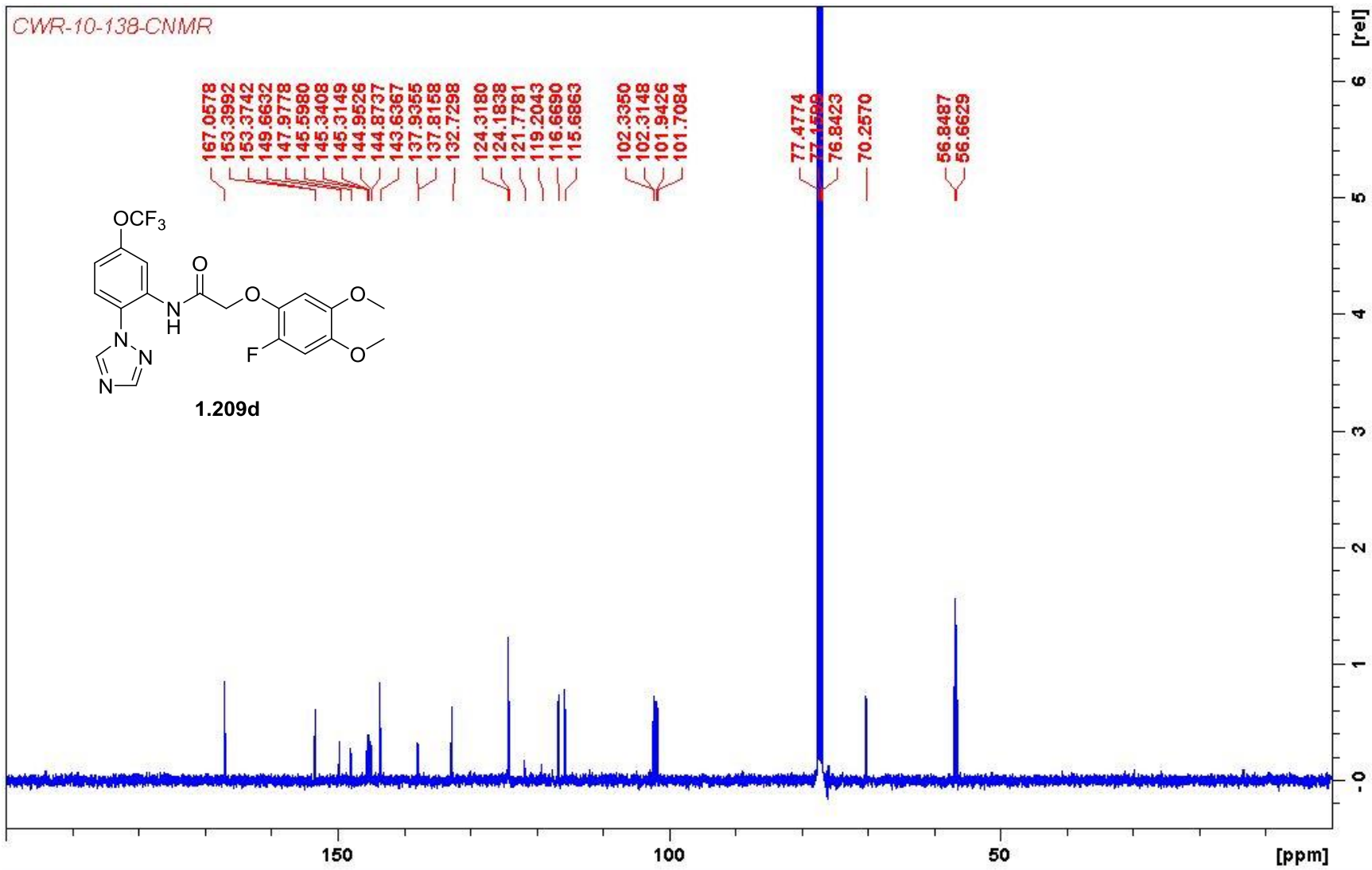
CWR-10-137-CNMR

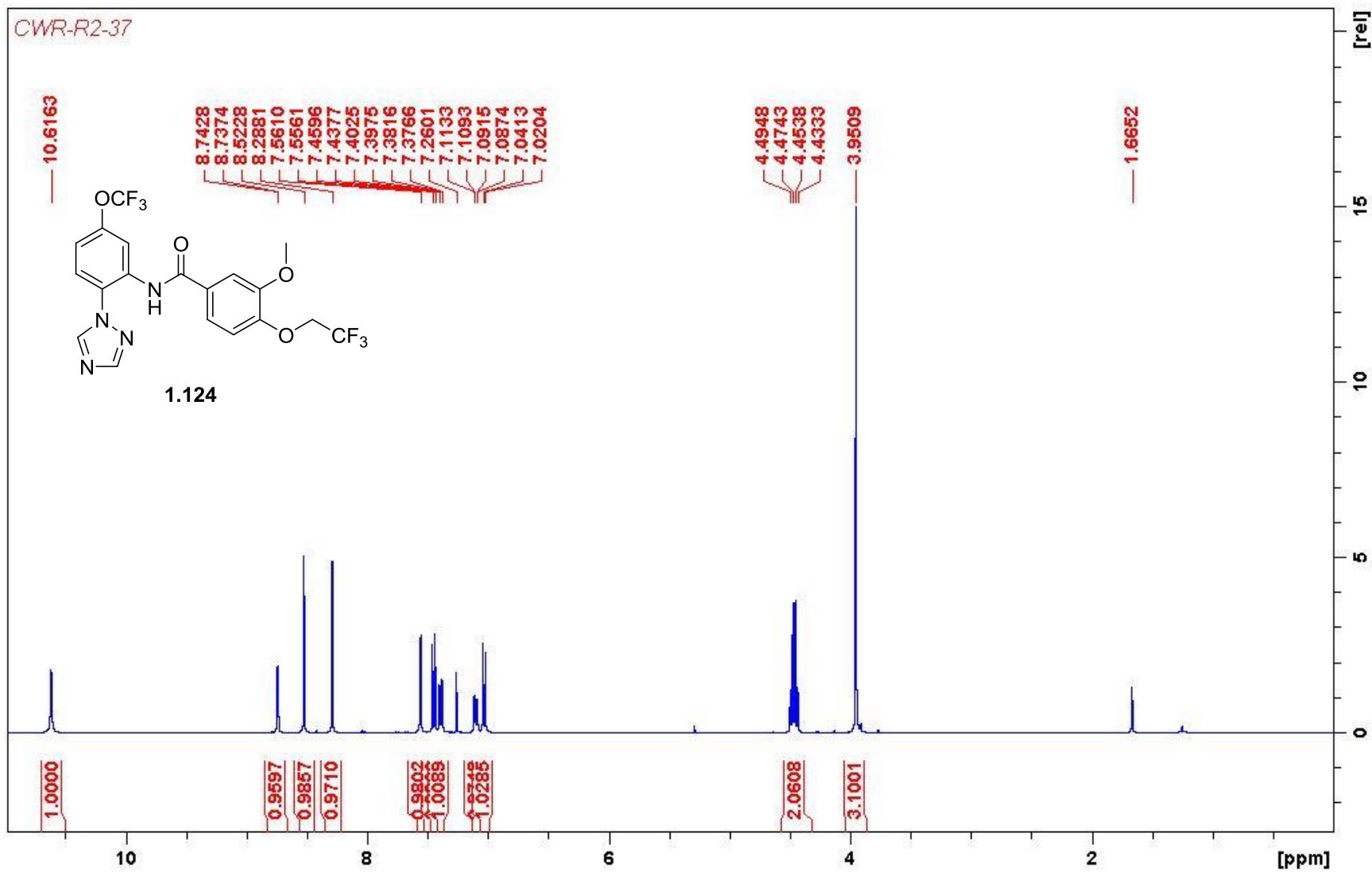


1.209a

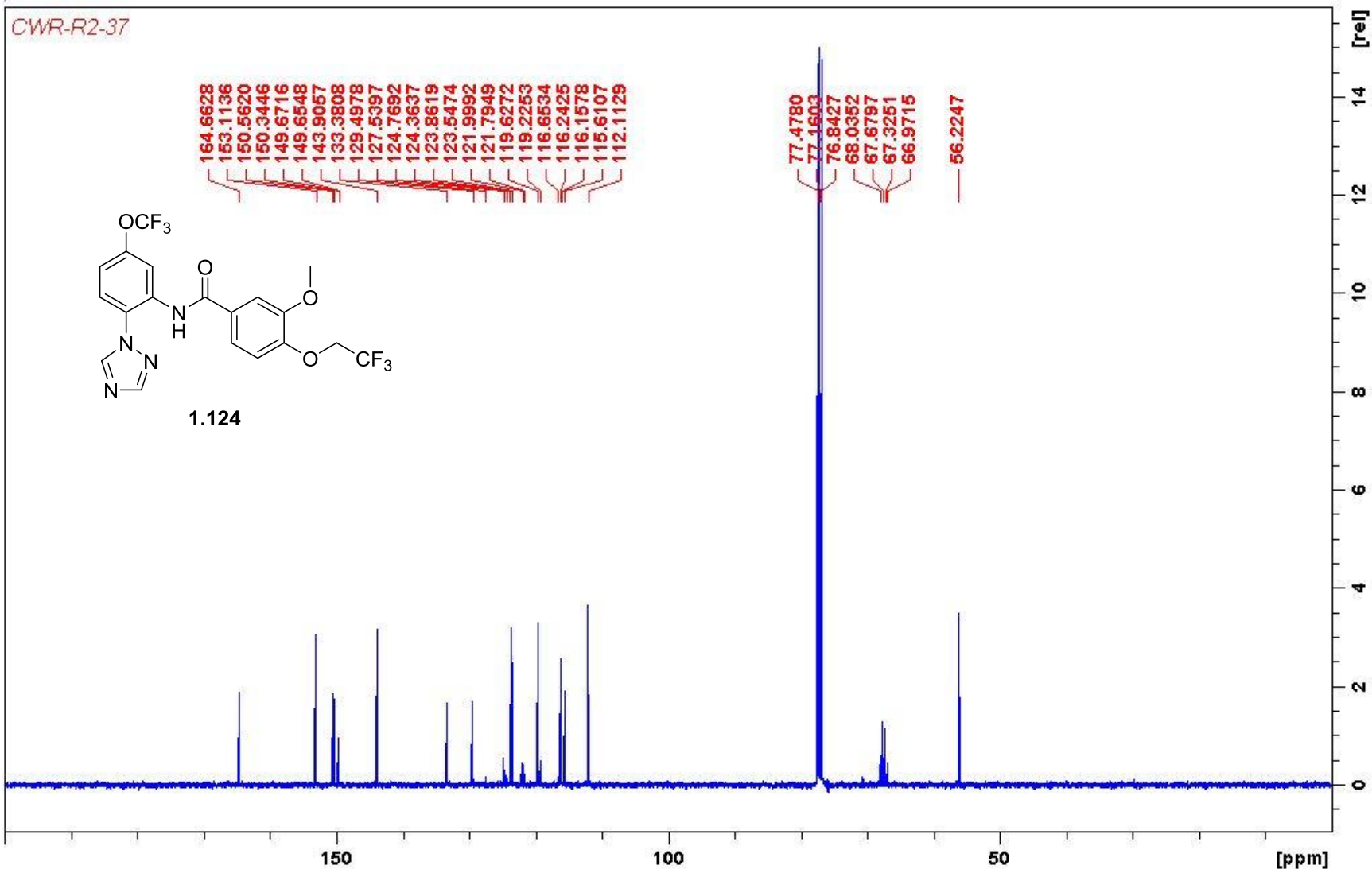


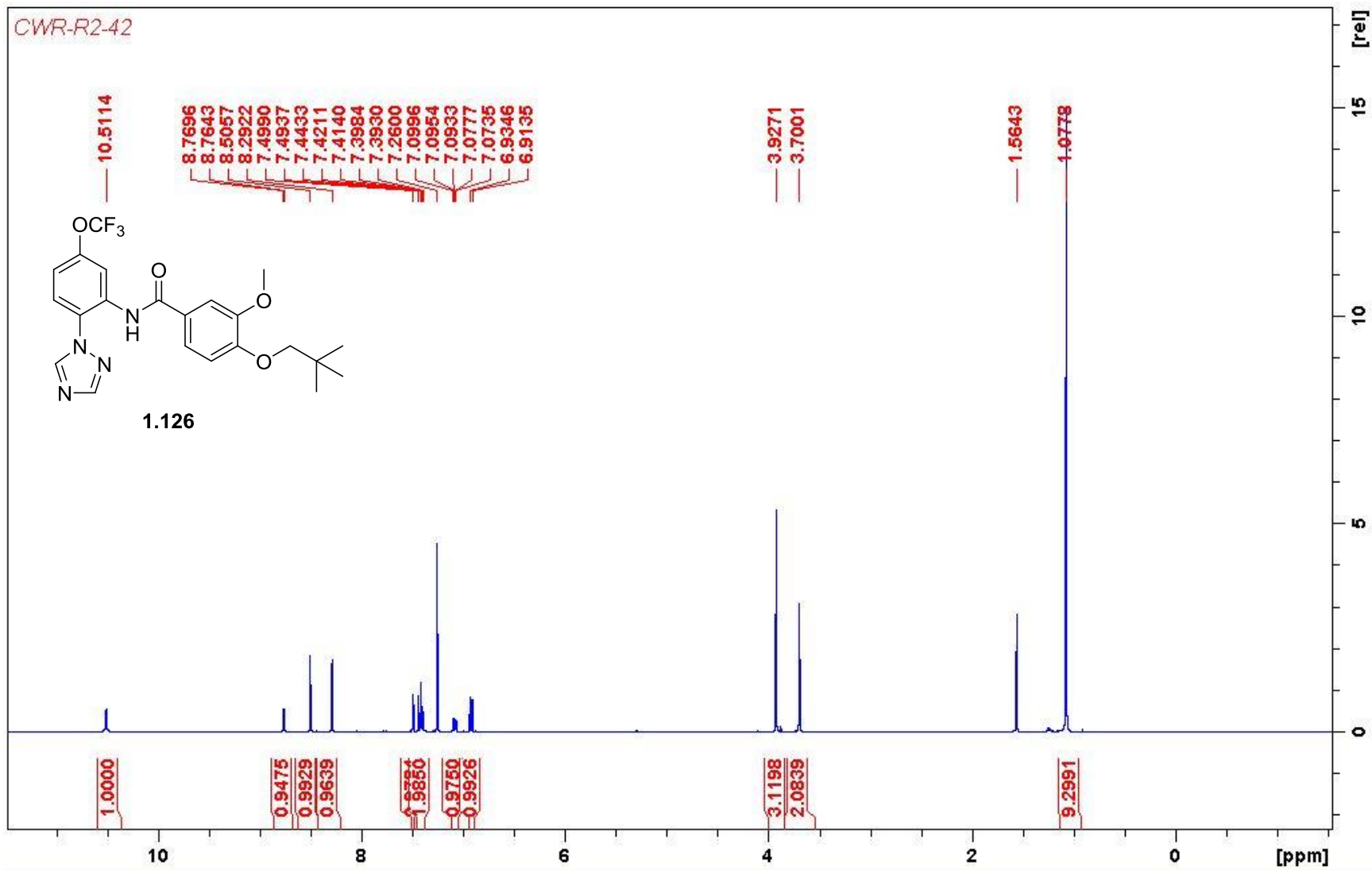


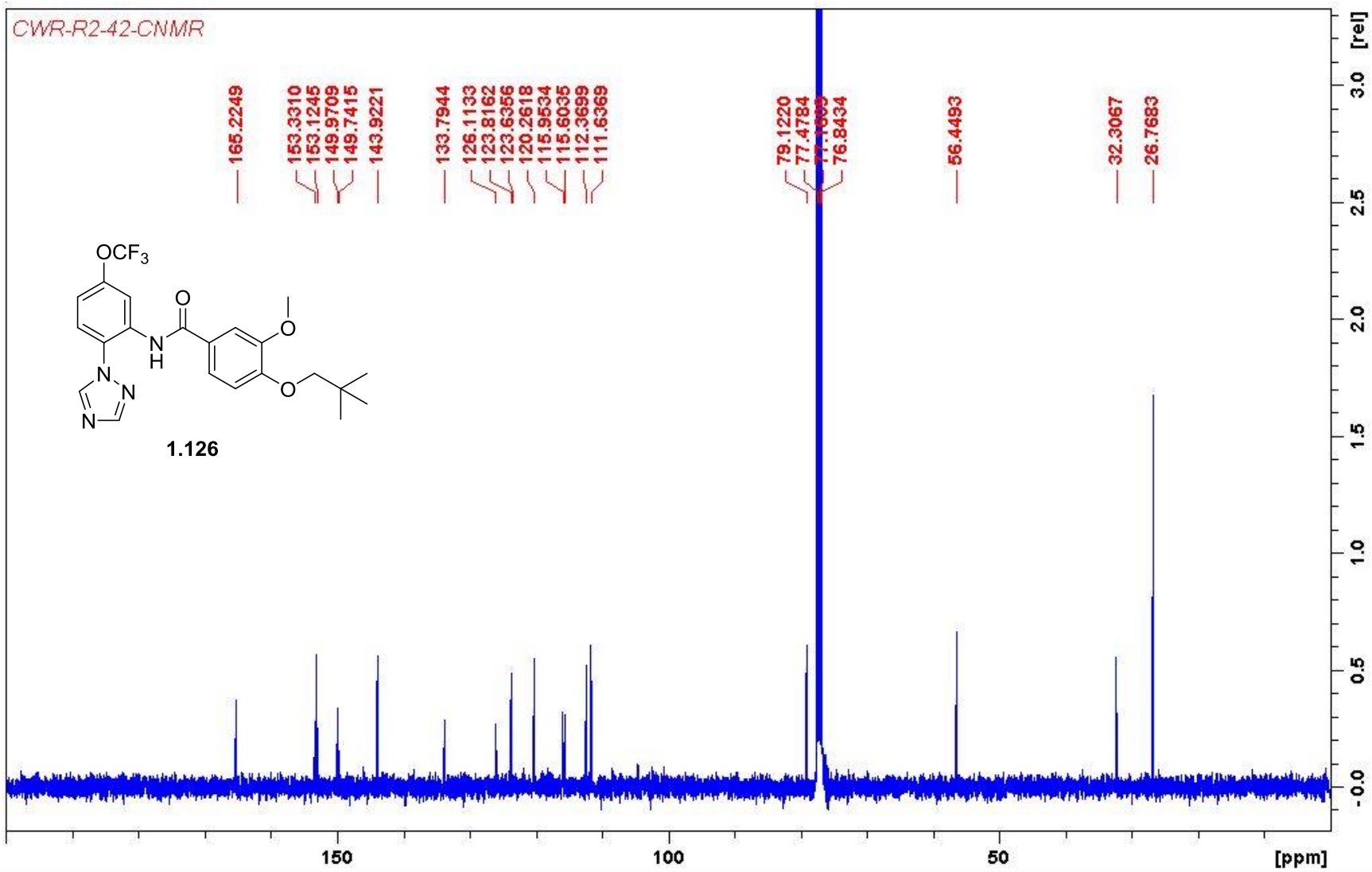


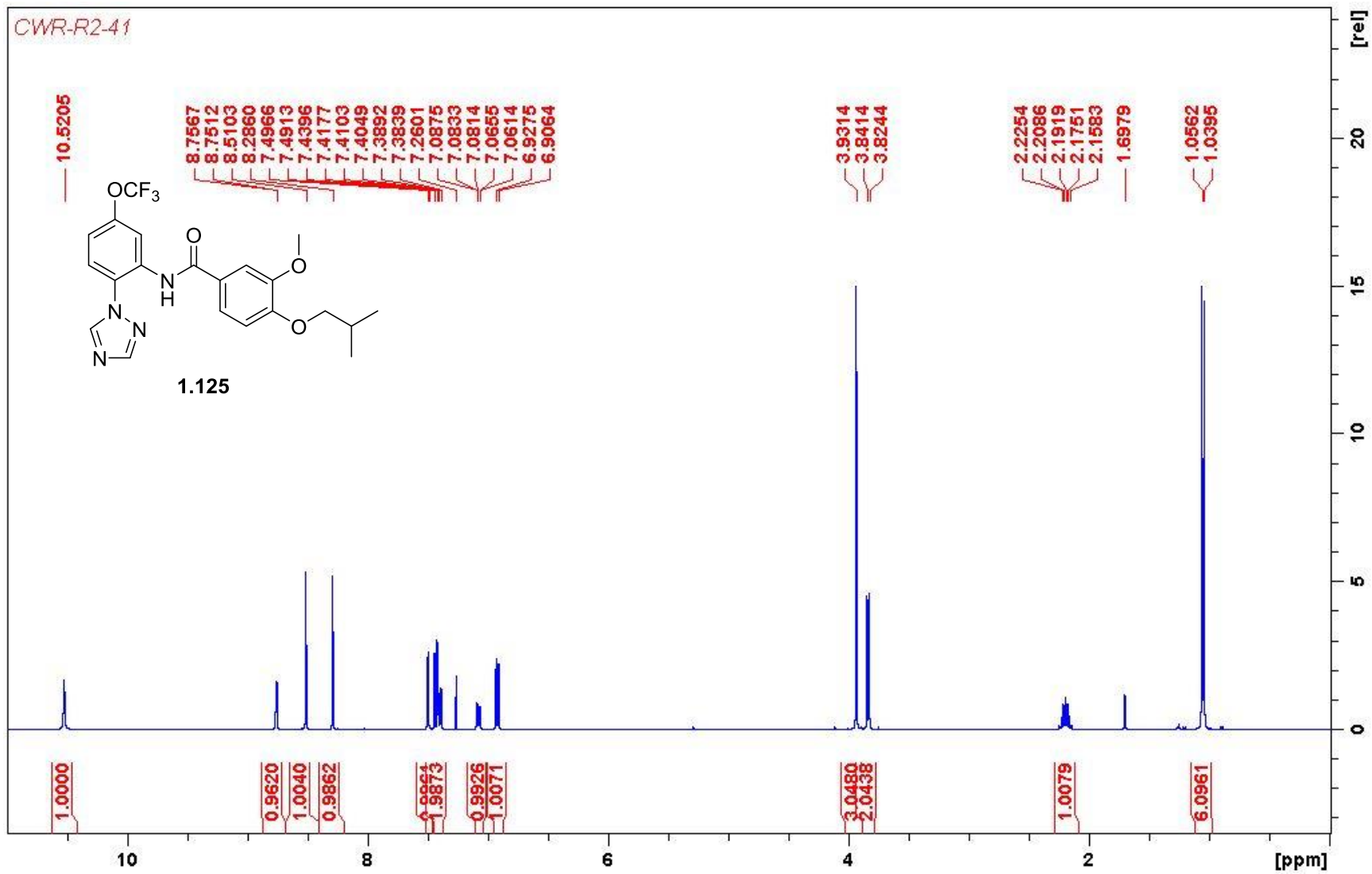


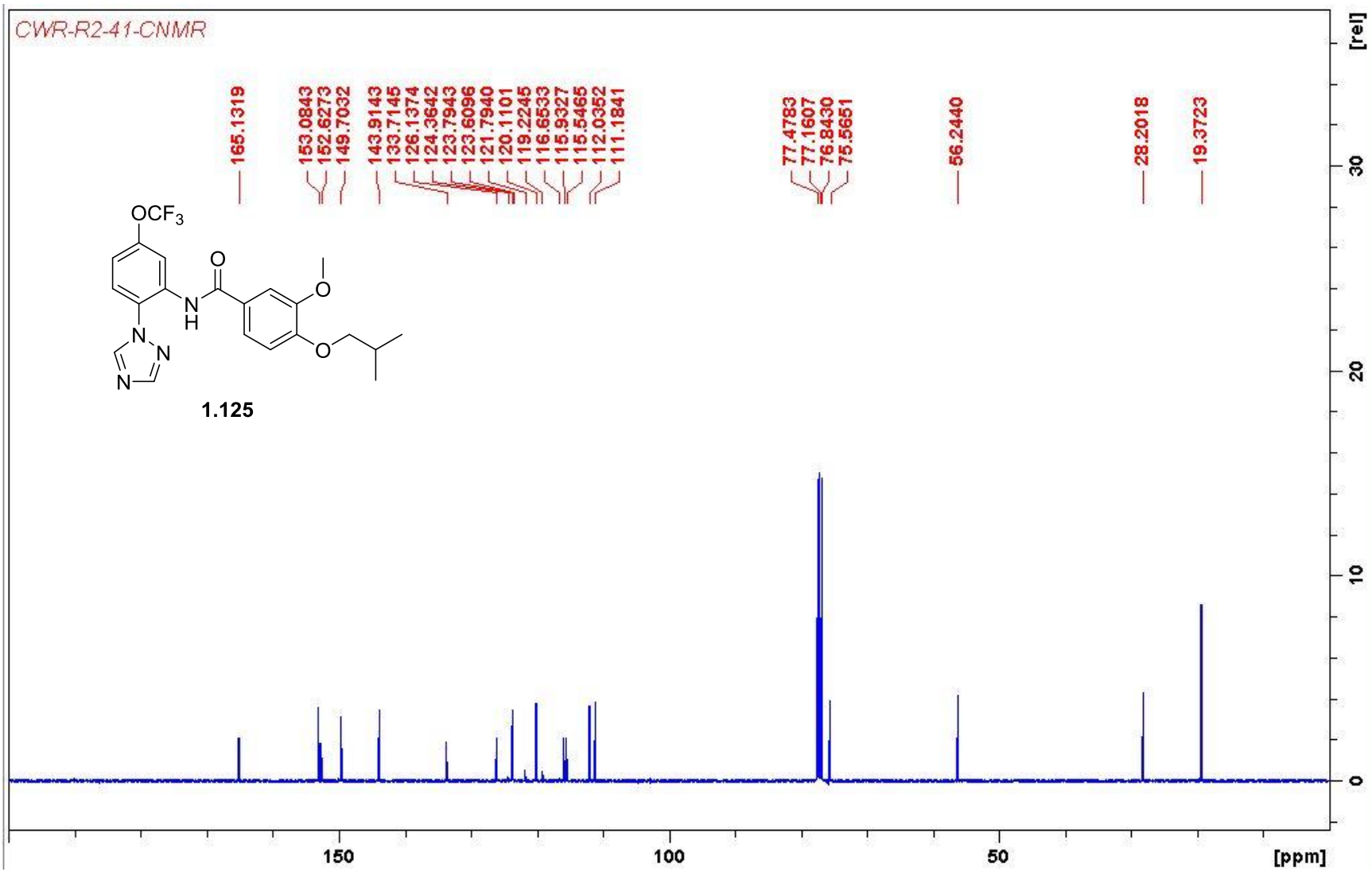
CWR-R2-37

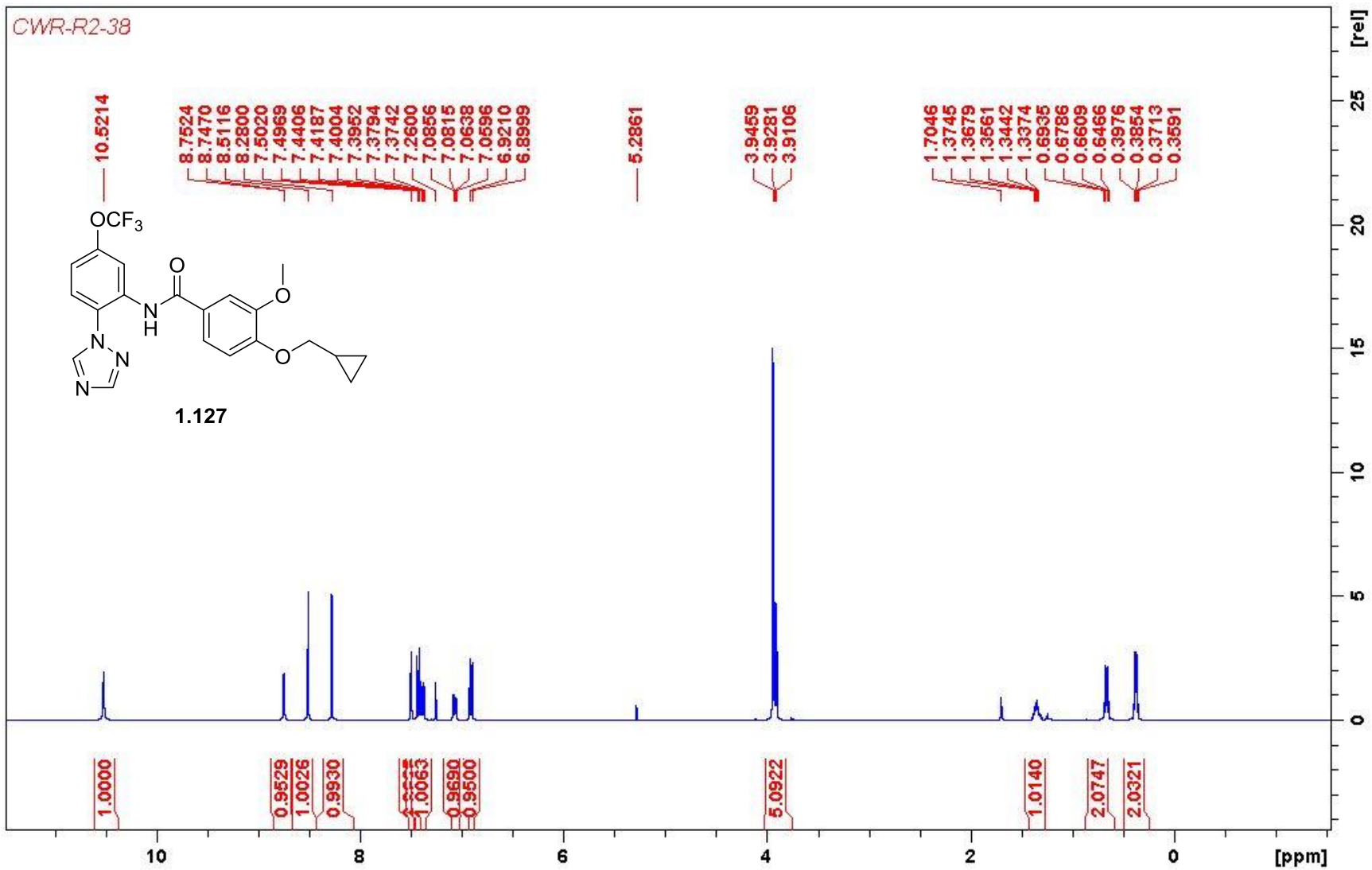




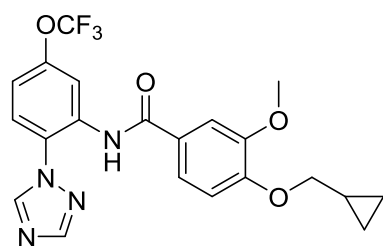








CWR-R2-38



1.127

165.0831
153.0699
152.3158
149.6828
149.6628
149.6329
143.9156
133.6740
126.3018
124.3514
123.7882
123.6045
121.7827
120.0127
119.2113
116.6404
115.9443
115.5327
112.1231
110.9673

77.4773
77.1596
76.8419
74.0961

56.1543

10.2076

3.6199

[rel]

25

20

15

10

5

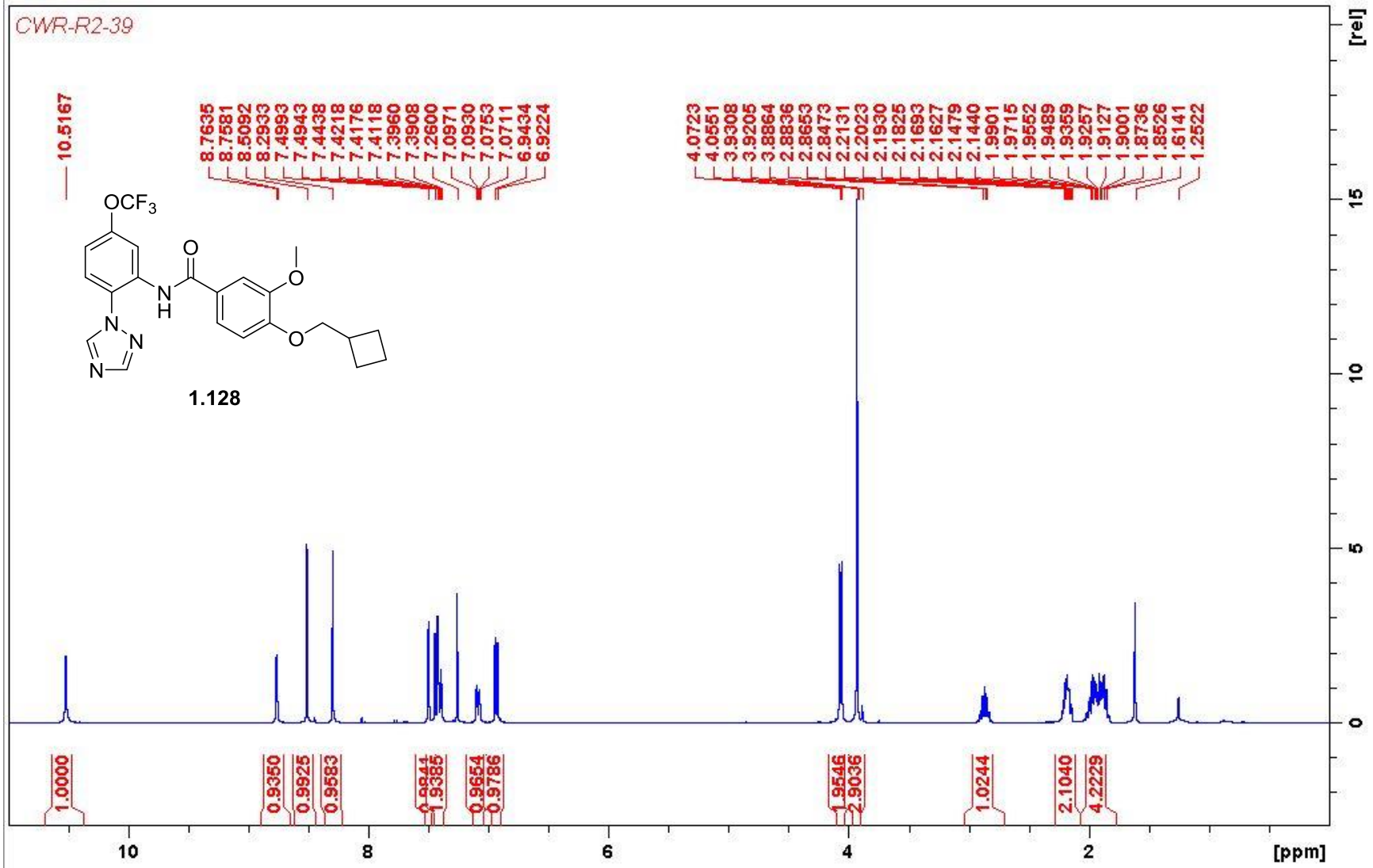
0

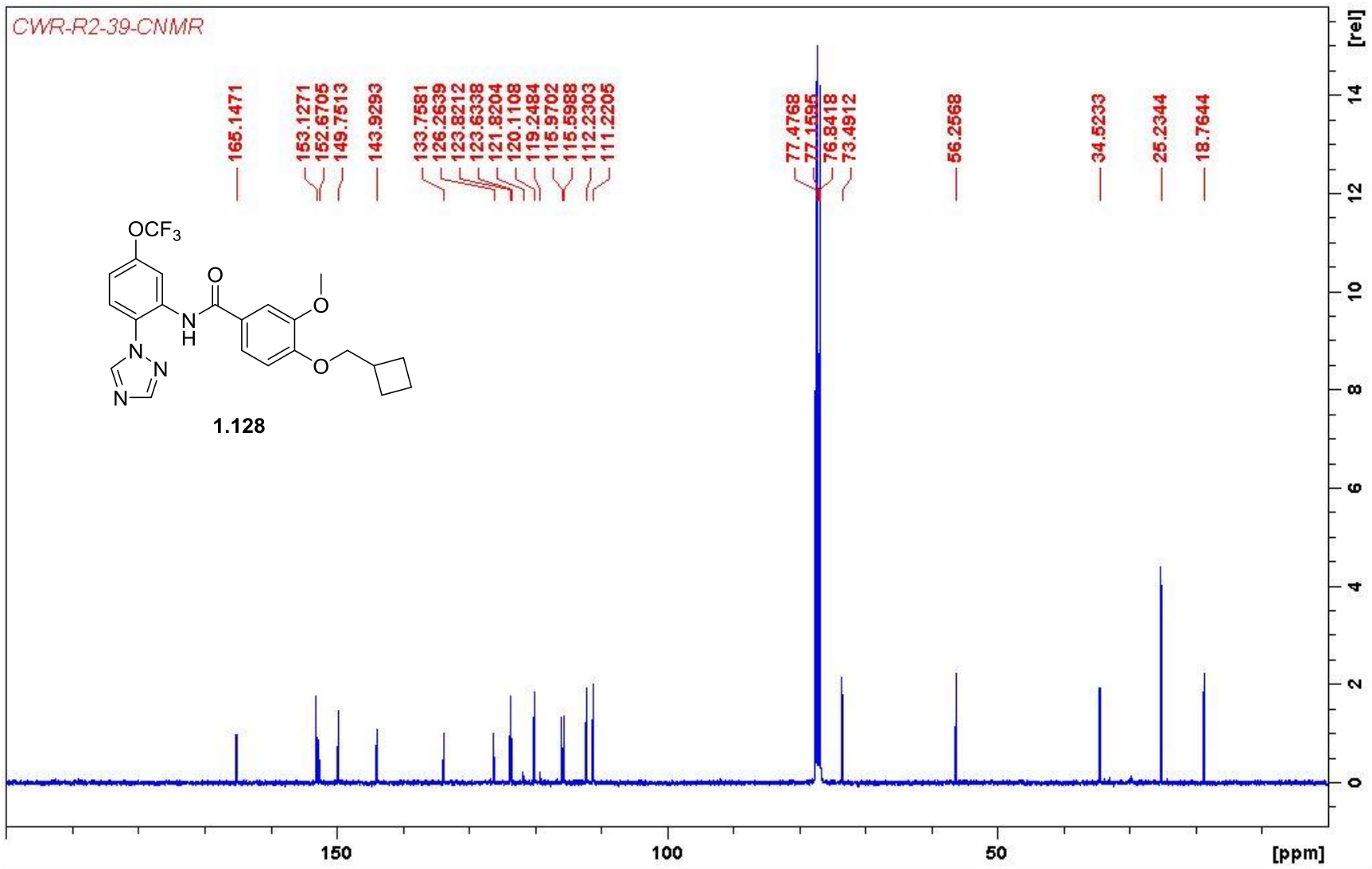
150

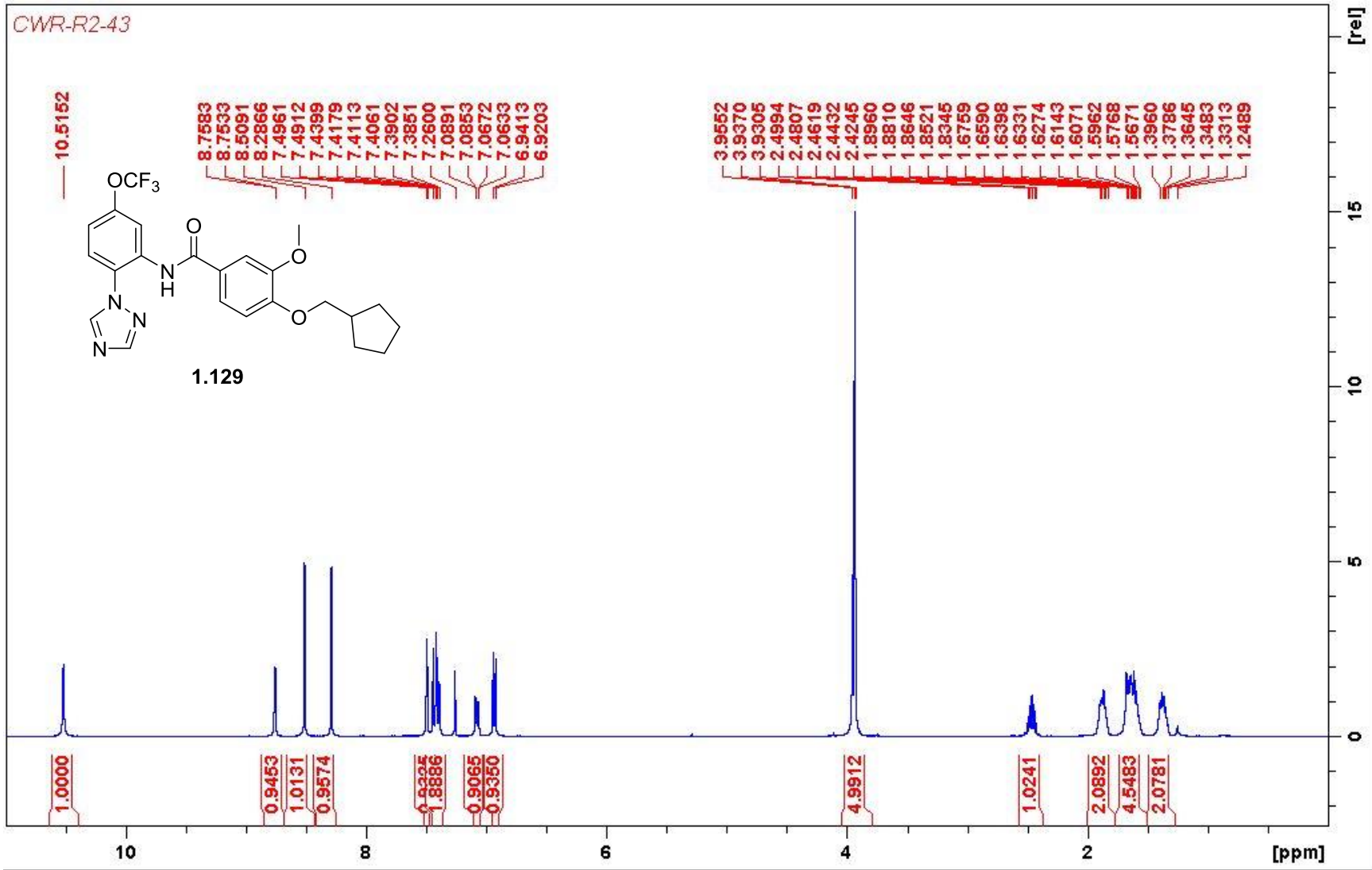
100

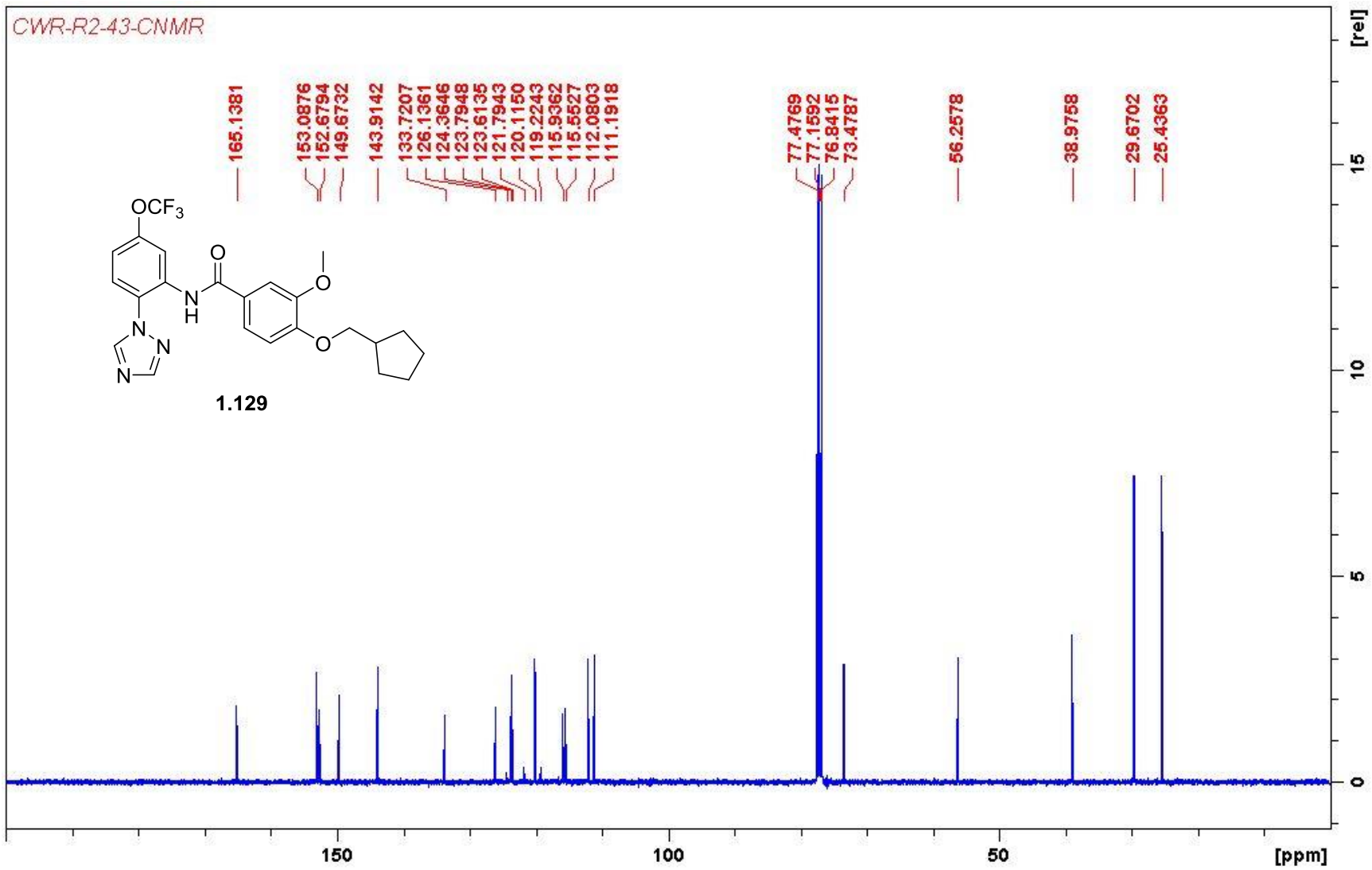
50

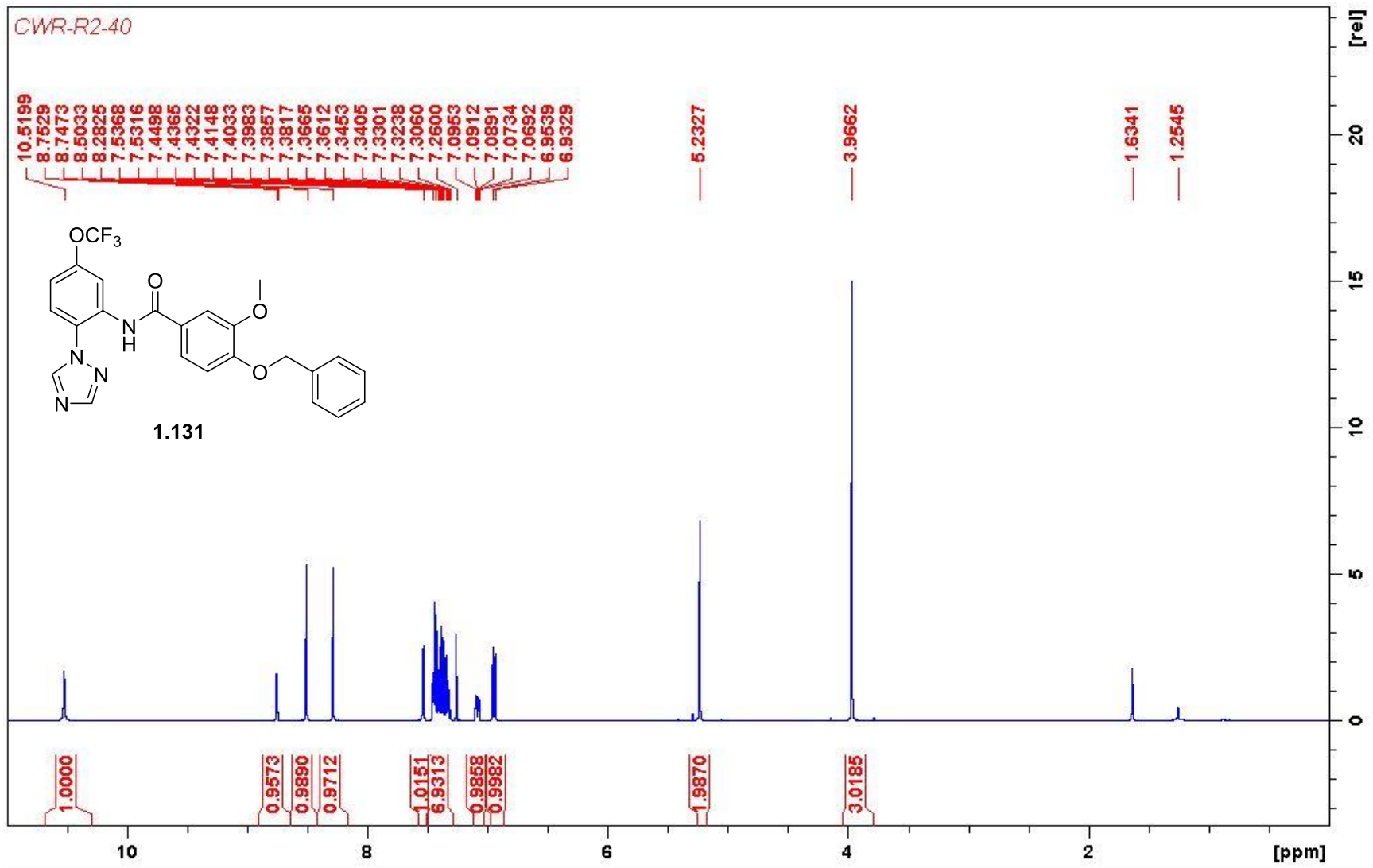
[ppm]

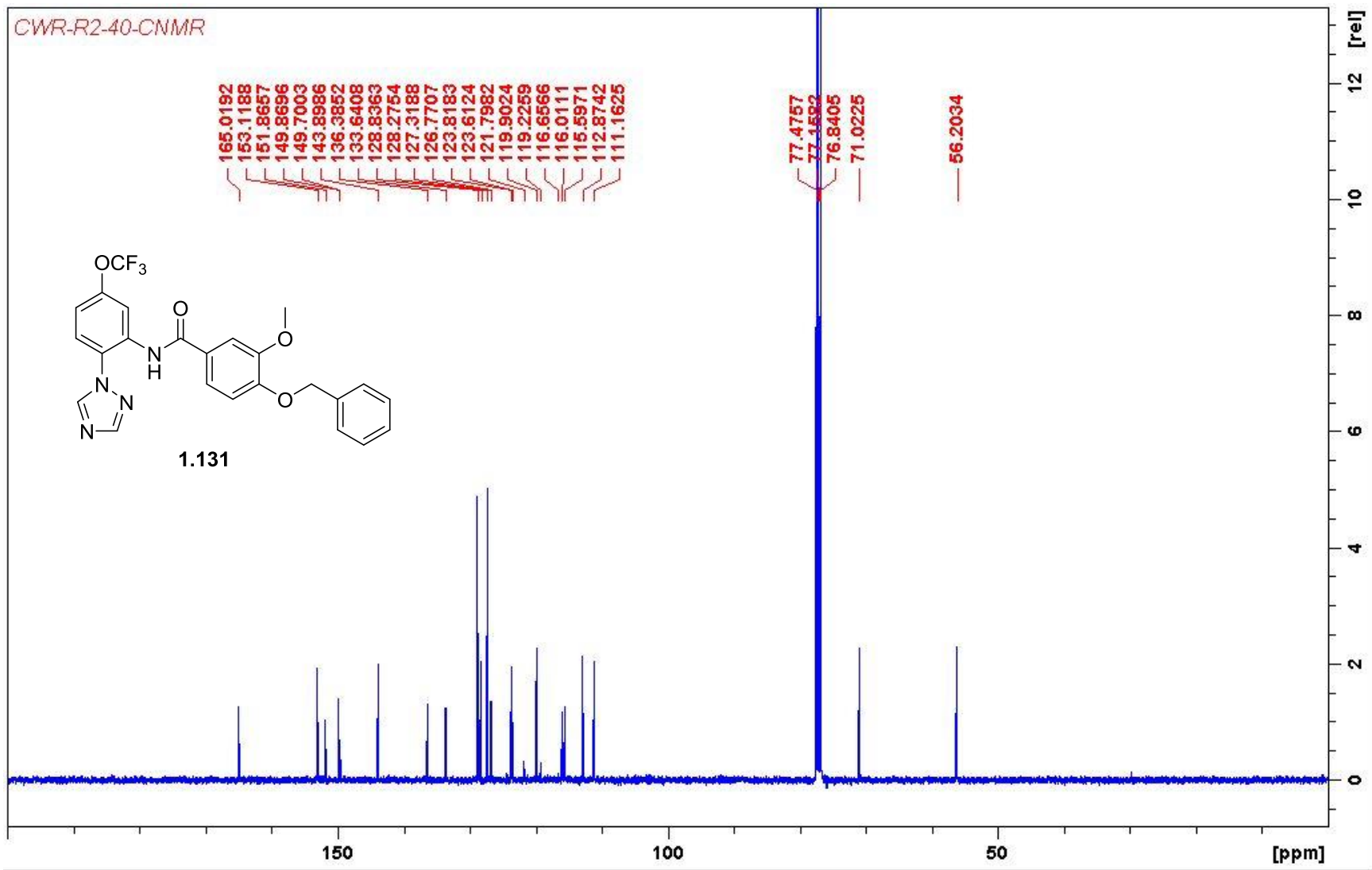




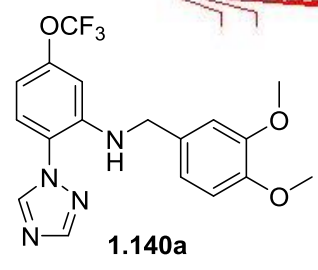






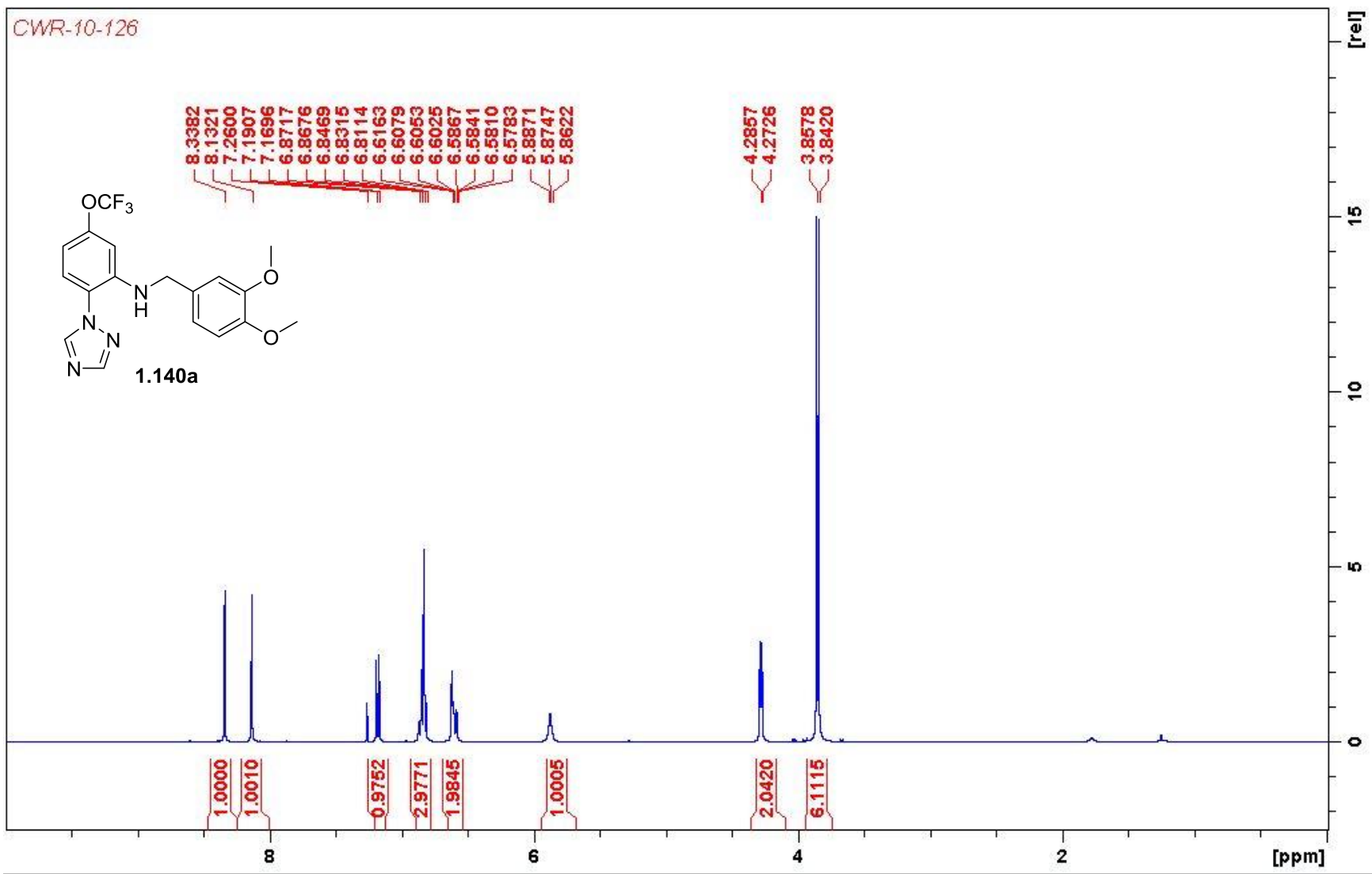


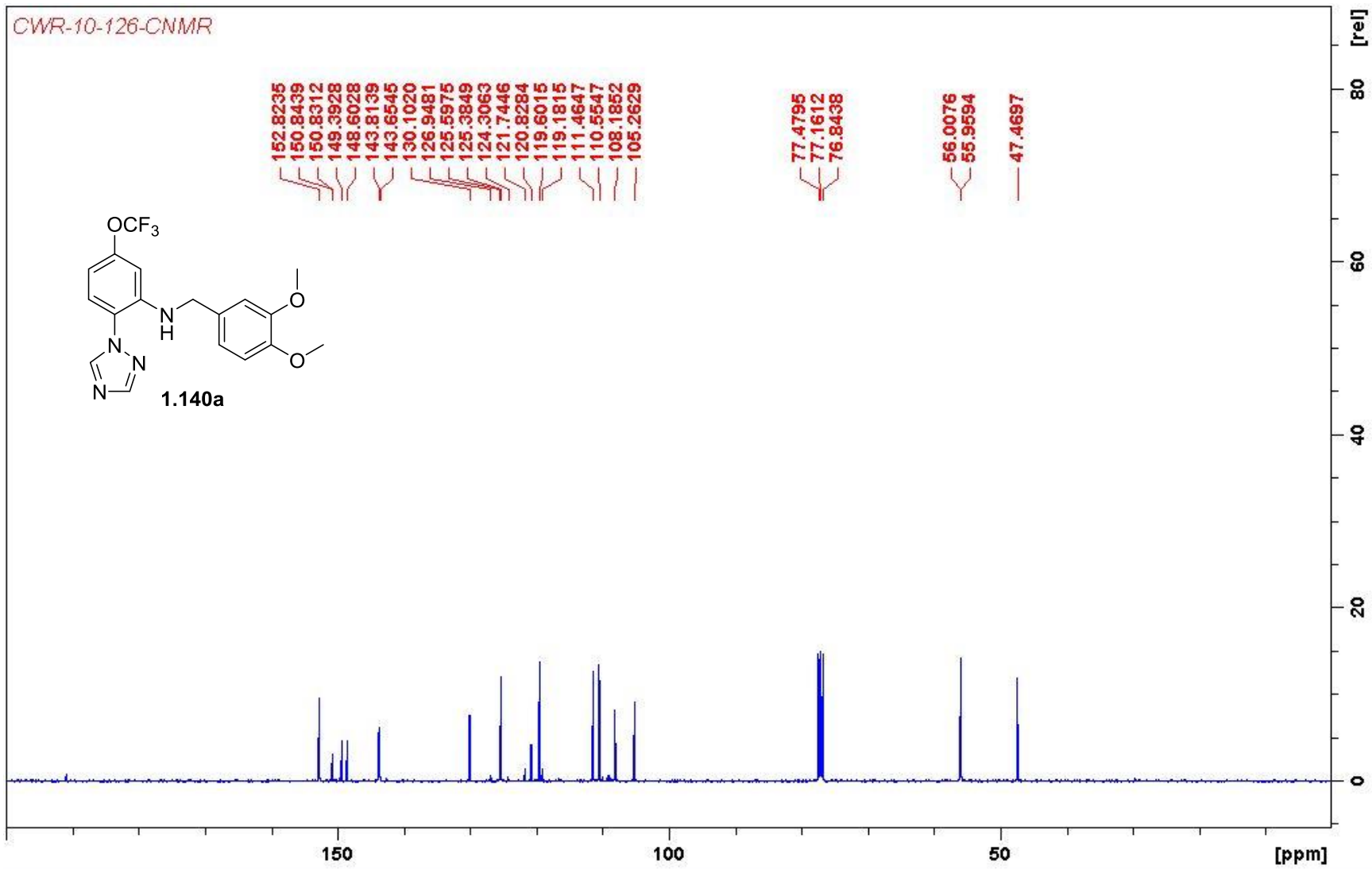
CWR-10-126

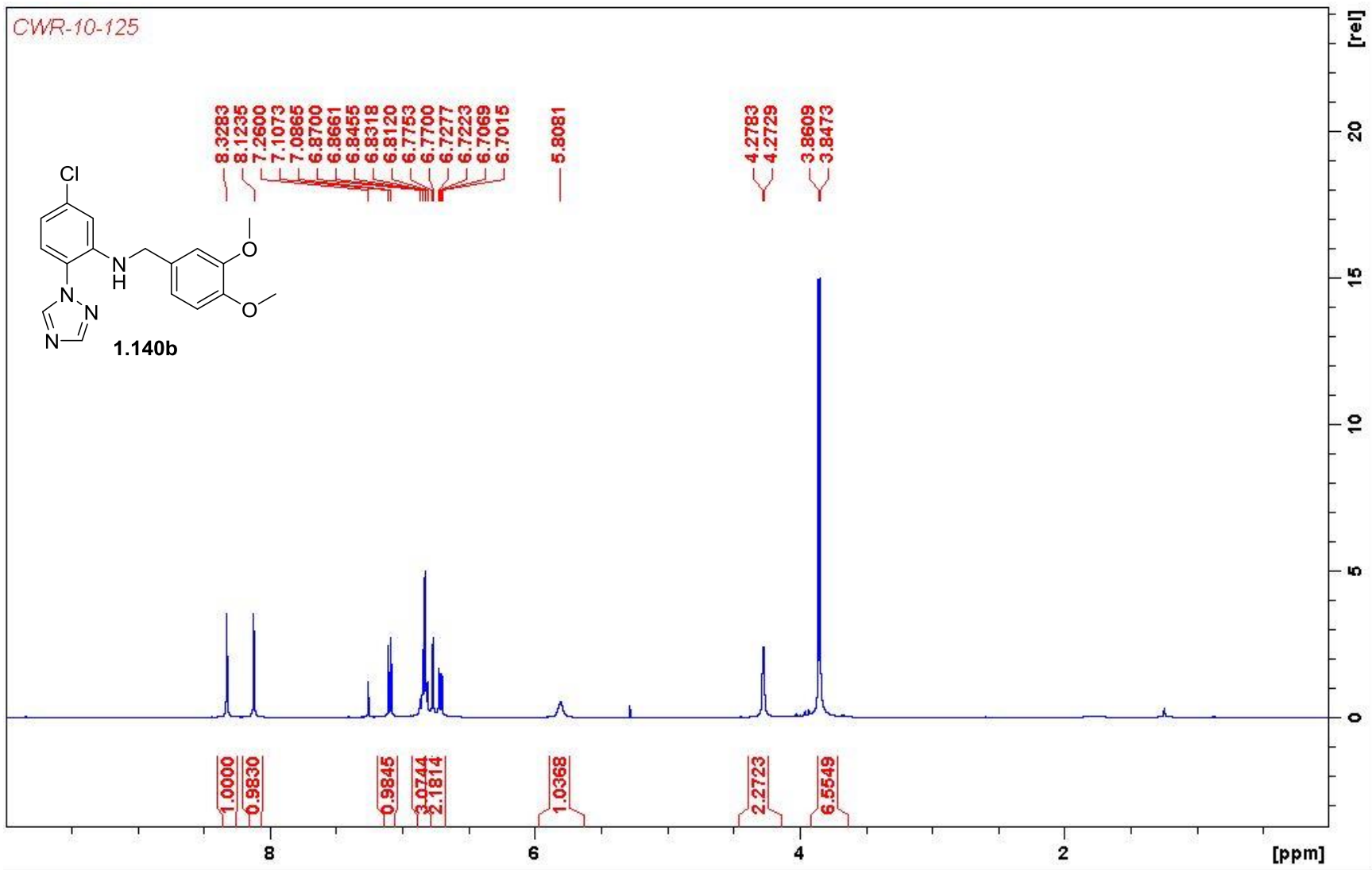


8.3382
8.1321
7.2600
7.1907
7.1696
6.8717
6.8676
6.8469
6.8315
6.8114
6.6163
6.6079
6.6053
6.6025
6.5867
6.5841
6.5810
6.5783
5.8871
5.8747
5.8622

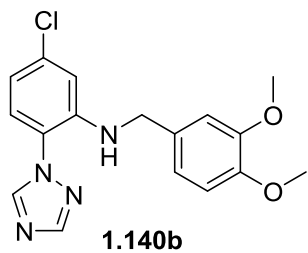
4.2857
4.2726
3.8578
3.8420







CWR-10-125-CNMR



152.7815
149.3717
148.5543
143.7581
143.1425
136.2858
130.2795
125.2067
121.0792
119.5319
116.5383
112.7589
111.4673
110.5301

77.4803
77.1623
76.8447

56.0240
55.9941

47.4242

[rel]

60

40

20

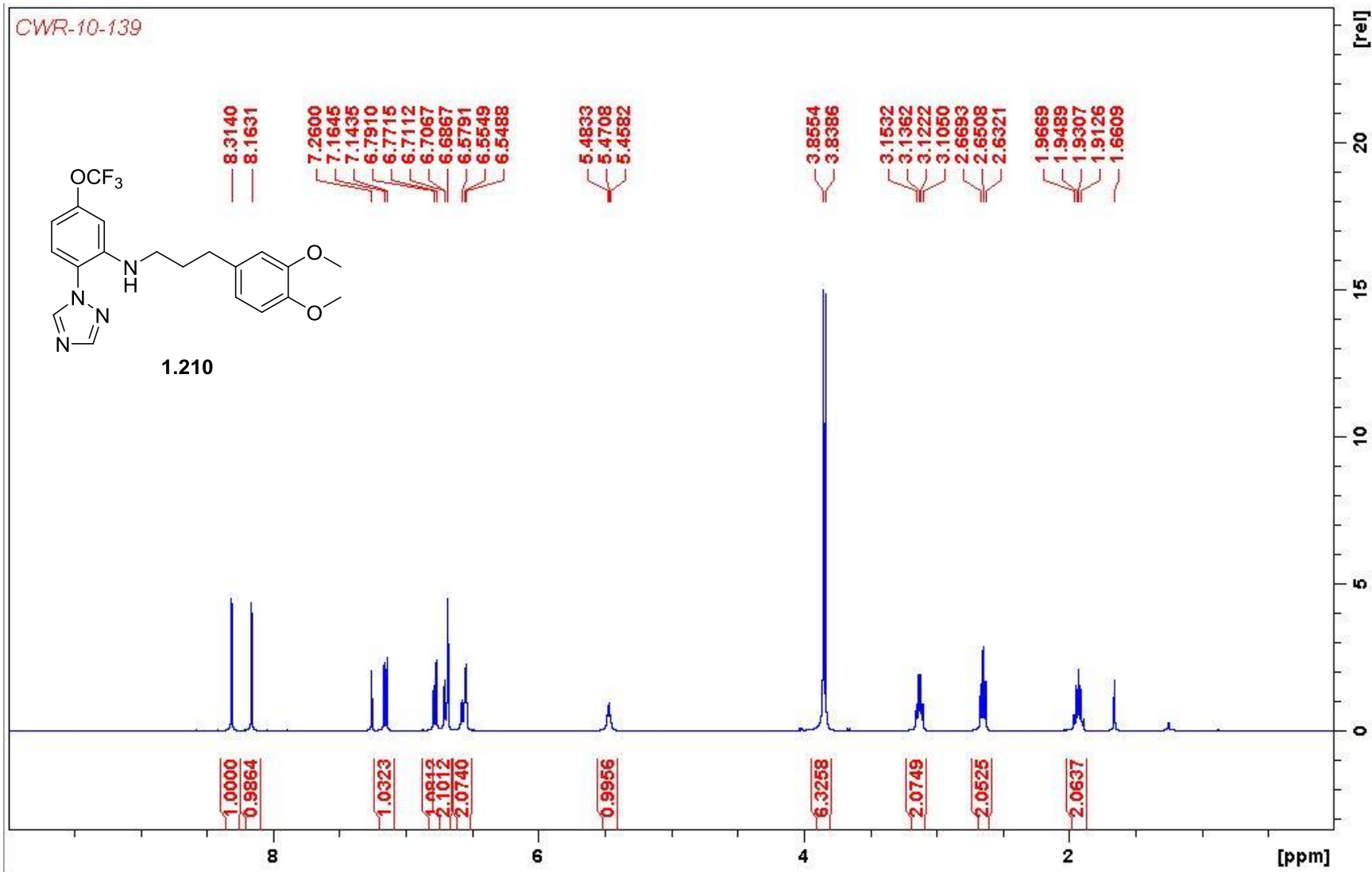
0

150

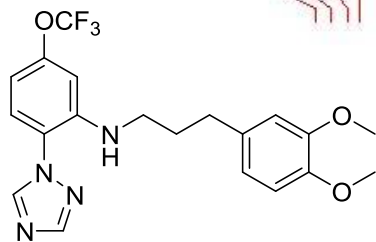
100

50

[ppm]



CWR-10-139-CNMR



1.210

152.8326
150.9720
149.0728
147.5427
143.8941
143.8467
133.6936
125.4445
124.3797
121.8178
120.6374
120.2972
119.2577
116.6974
111.7491
111.4353
107.6734
104.7205

77.4785
77.1606
76.8433

56.0473
55.9212

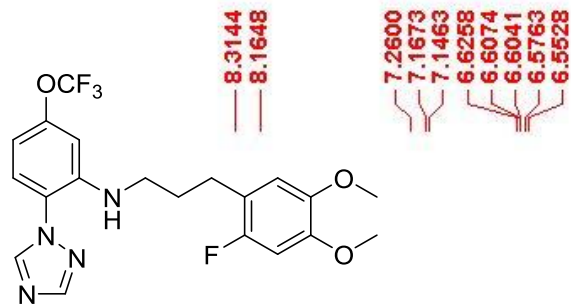
42.6072

32.7958
30.4961

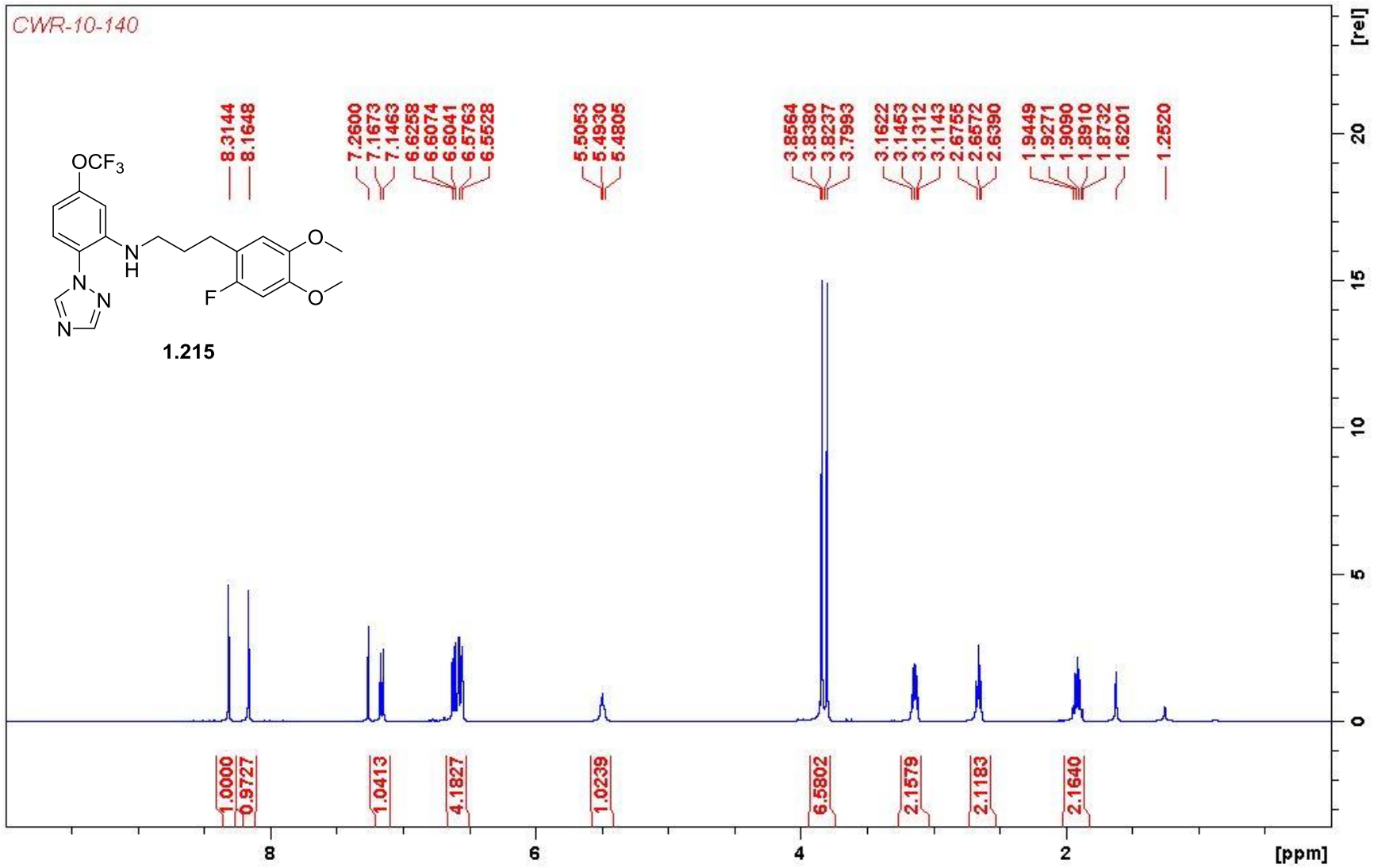
[rel]

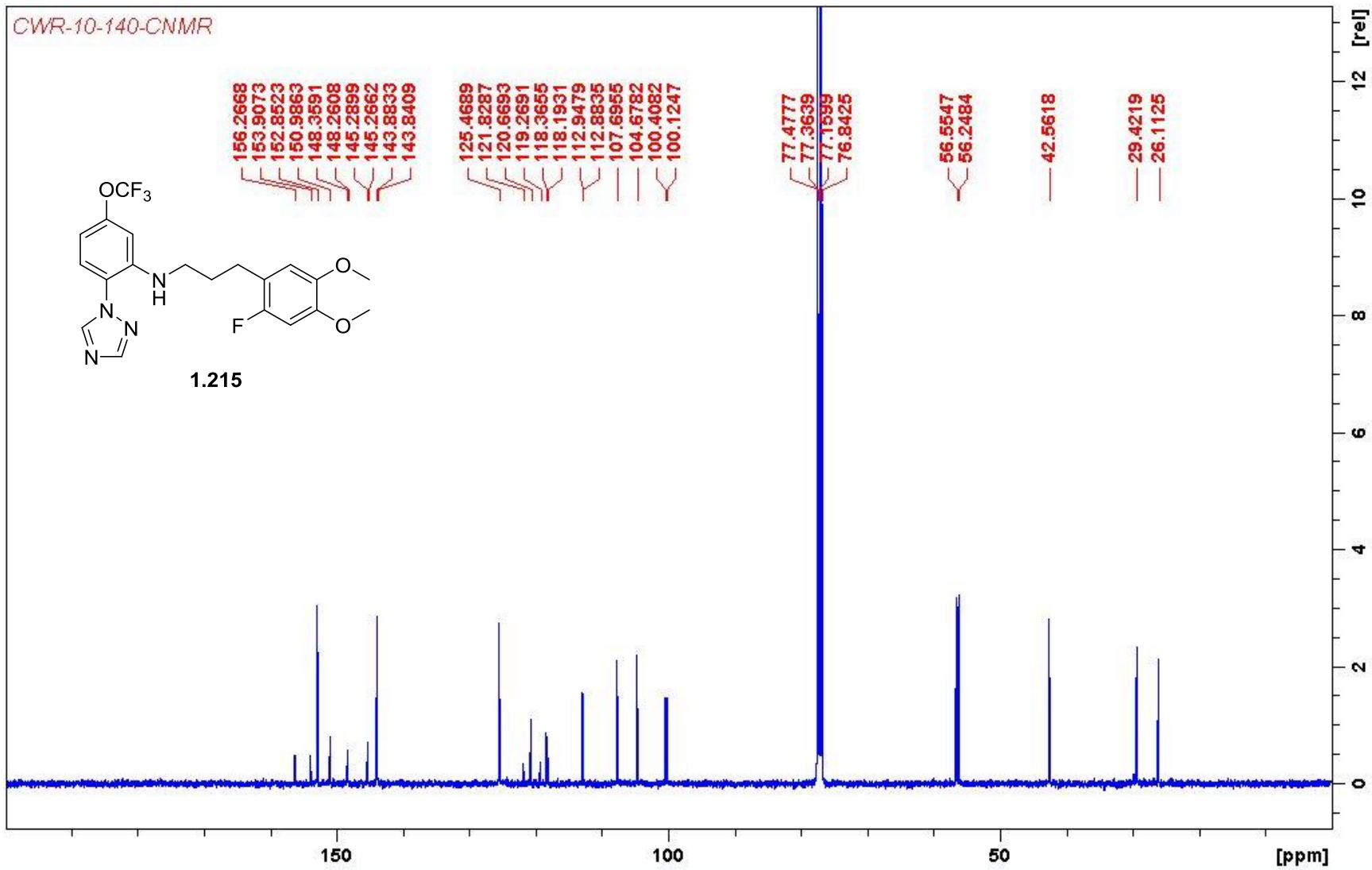
[ppm]

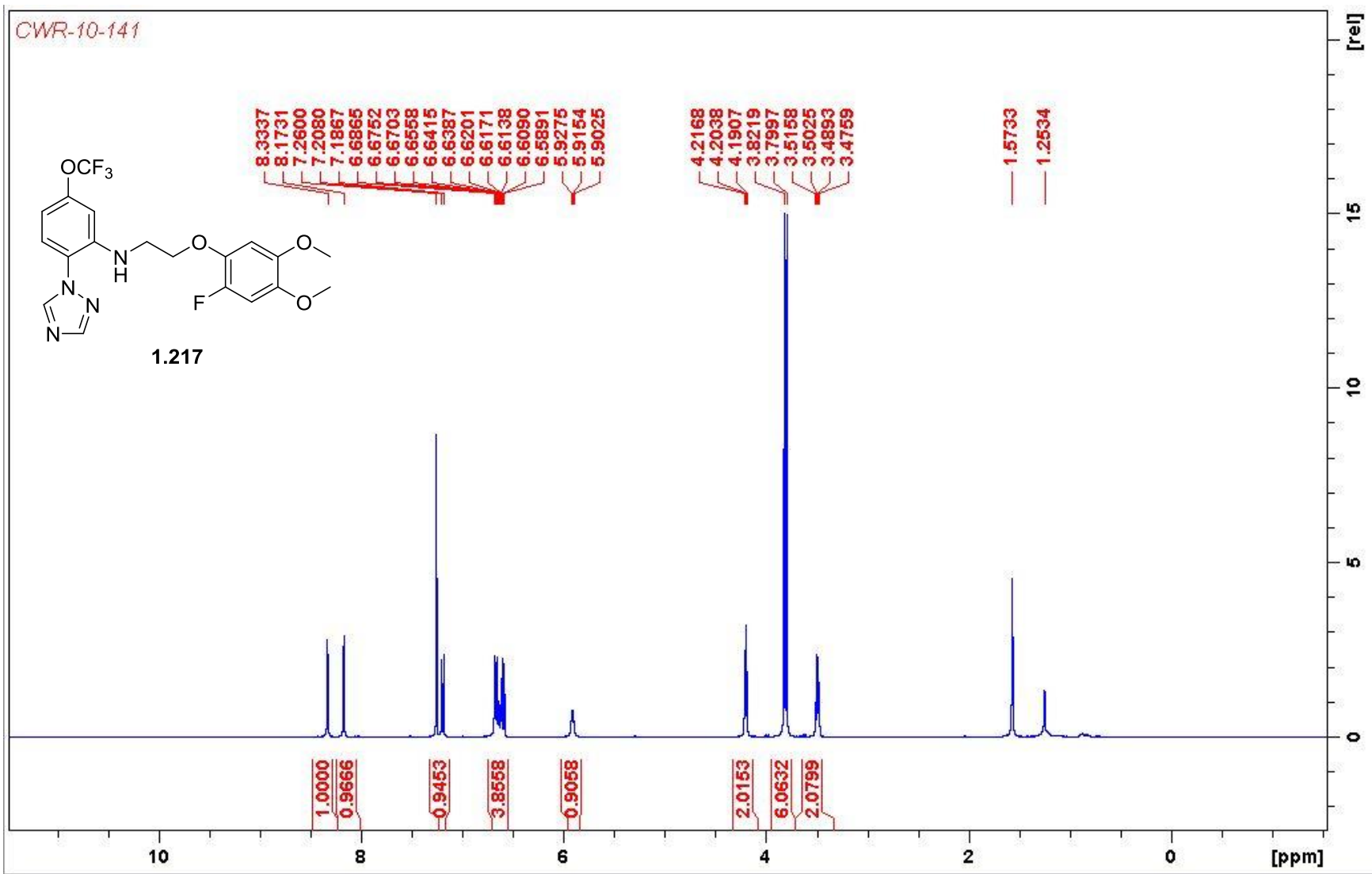
CWR-10-140

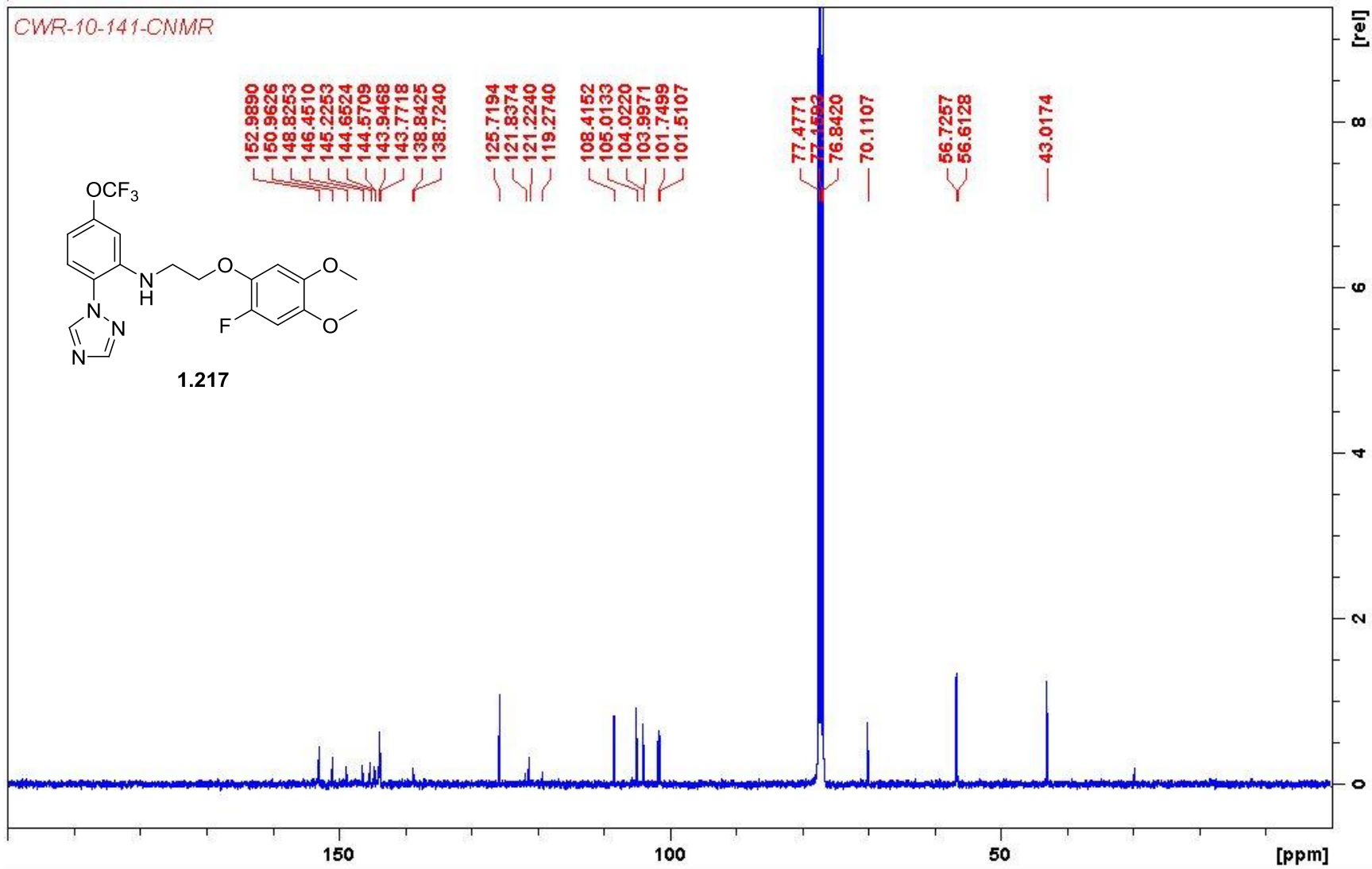


1.215

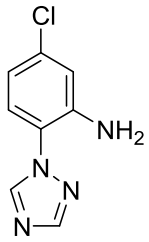




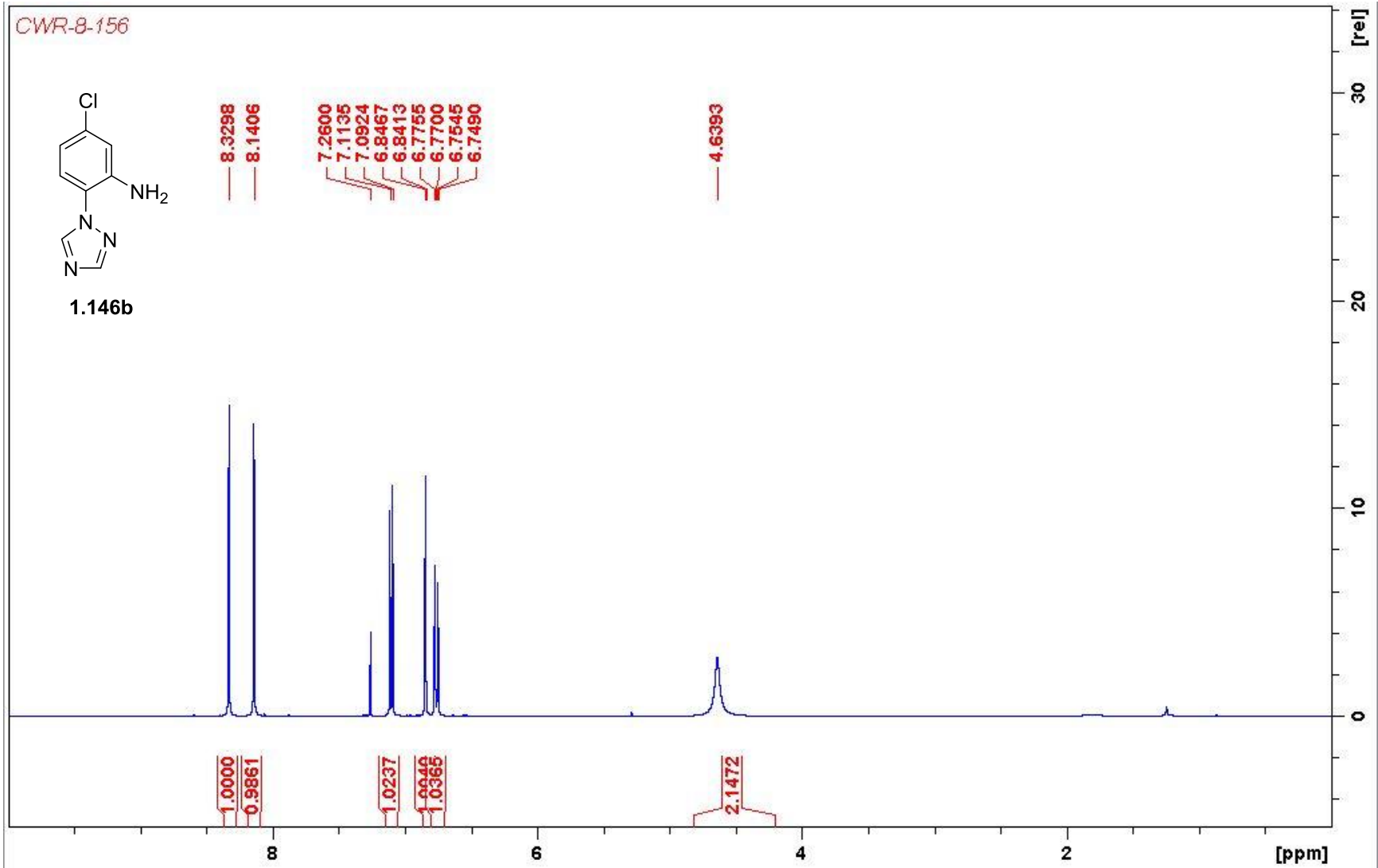




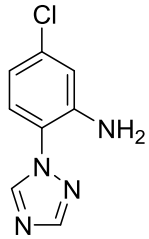
CWR-8-156



1.146b



CWR-8-156



1.146b

152.6967

143.4858
142.1733

135.6581

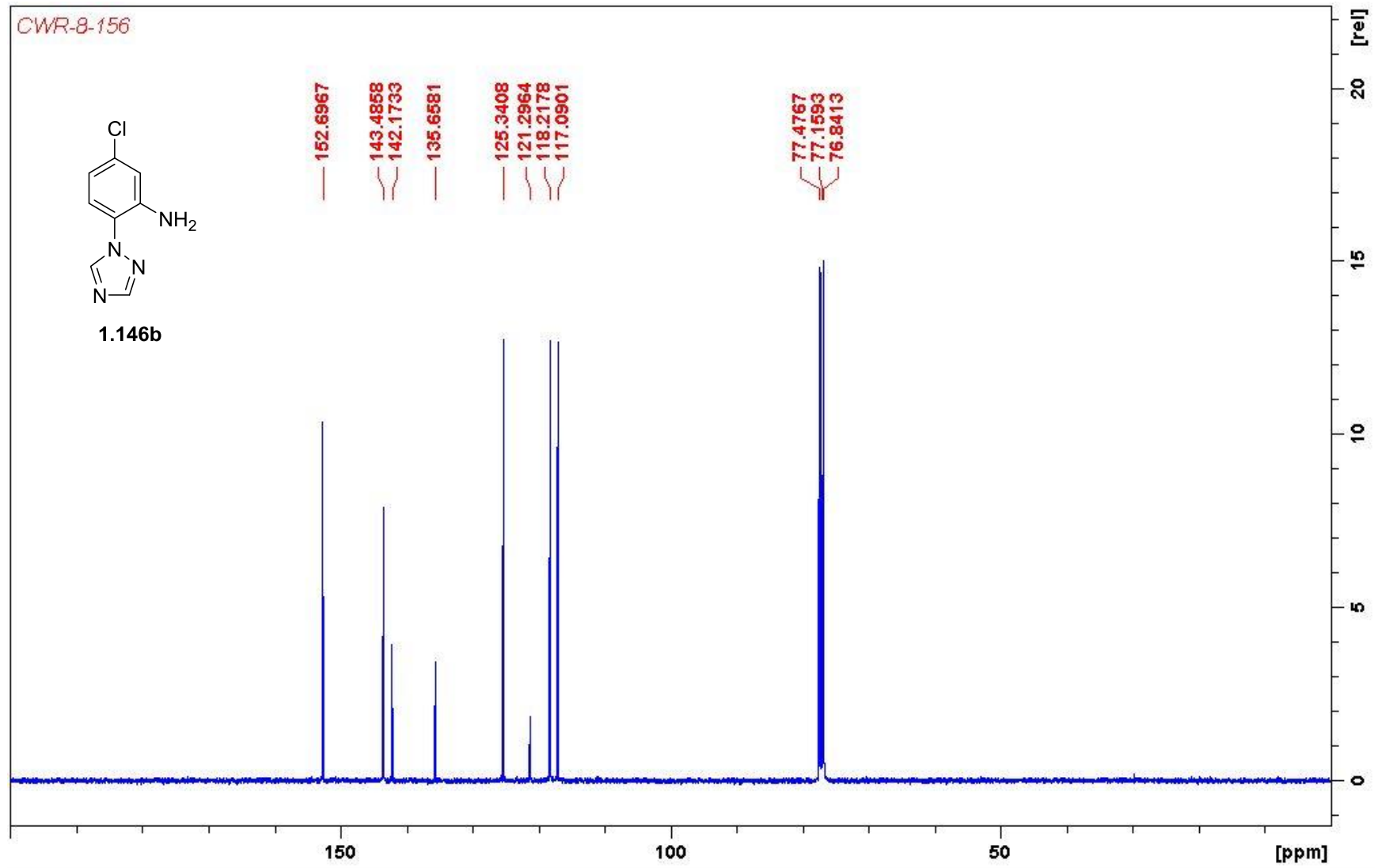
125.3408

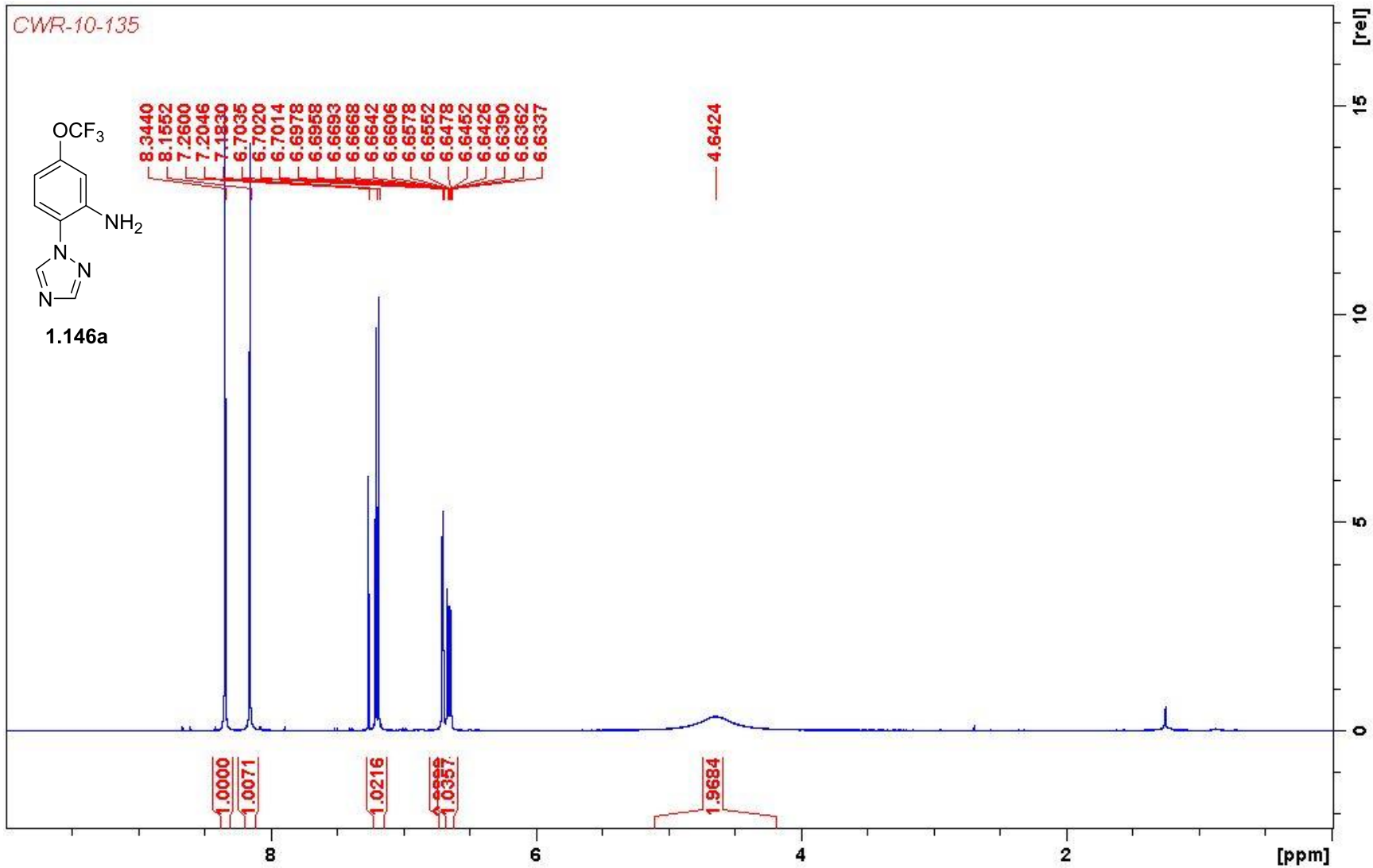
121.2964

118.2178

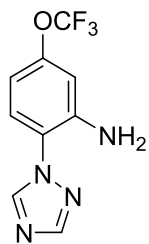
117.0901

77.4767
77.1593
76.8413





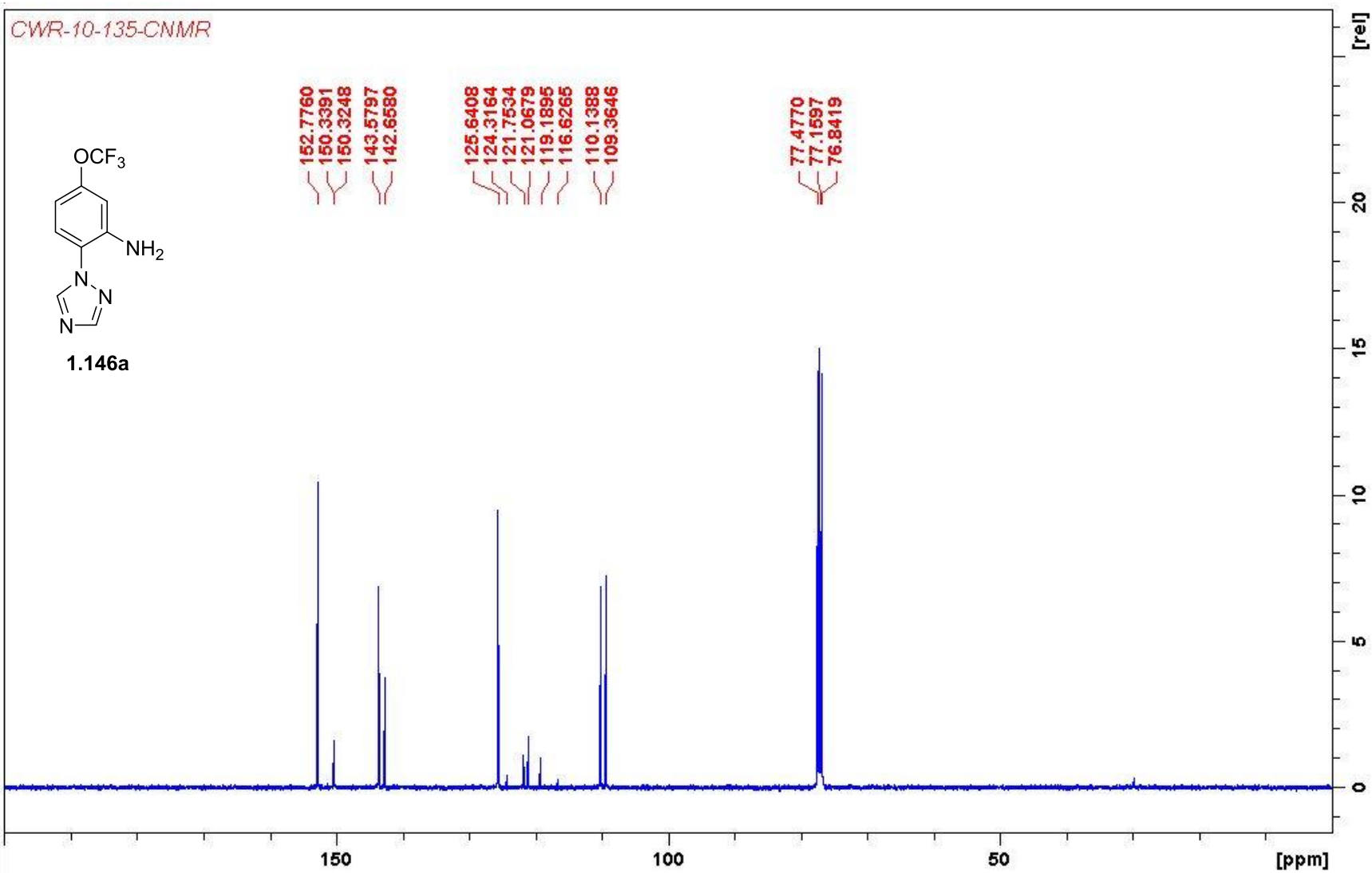
CWR-10-135-CNMR



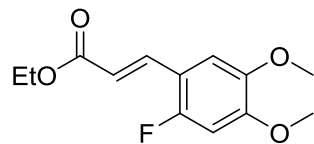
1.146a

152.7760
150.3391
150.3248
143.5797
142.6580
125.6408
124.3164
121.7534
121.0679
119.1895
116.6265
110.1388
109.3646

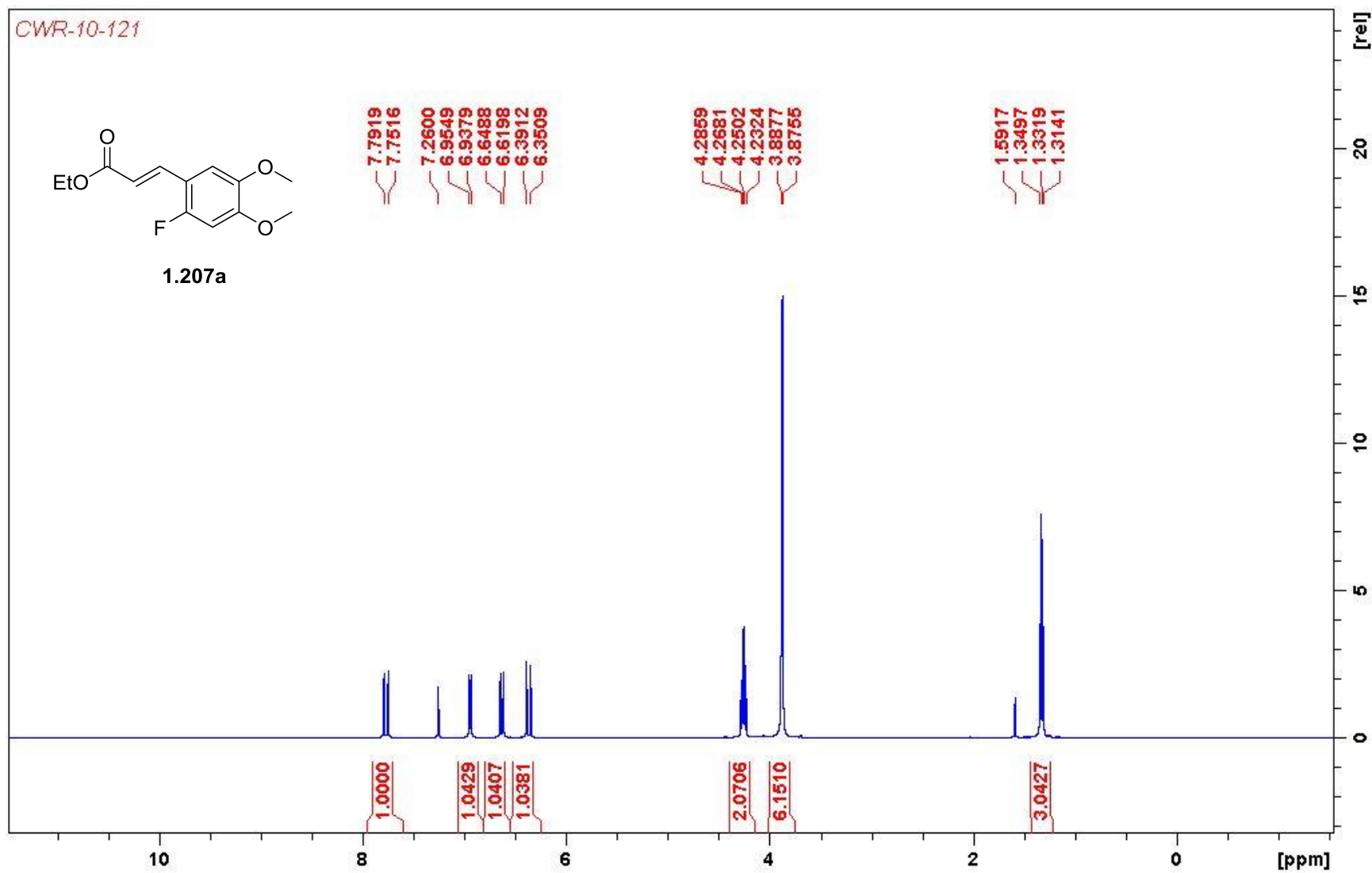
77.4770
77.1597
76.8419



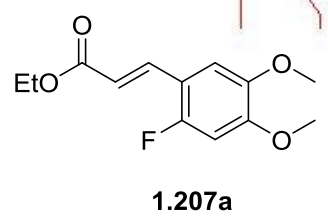
CWR-10-121



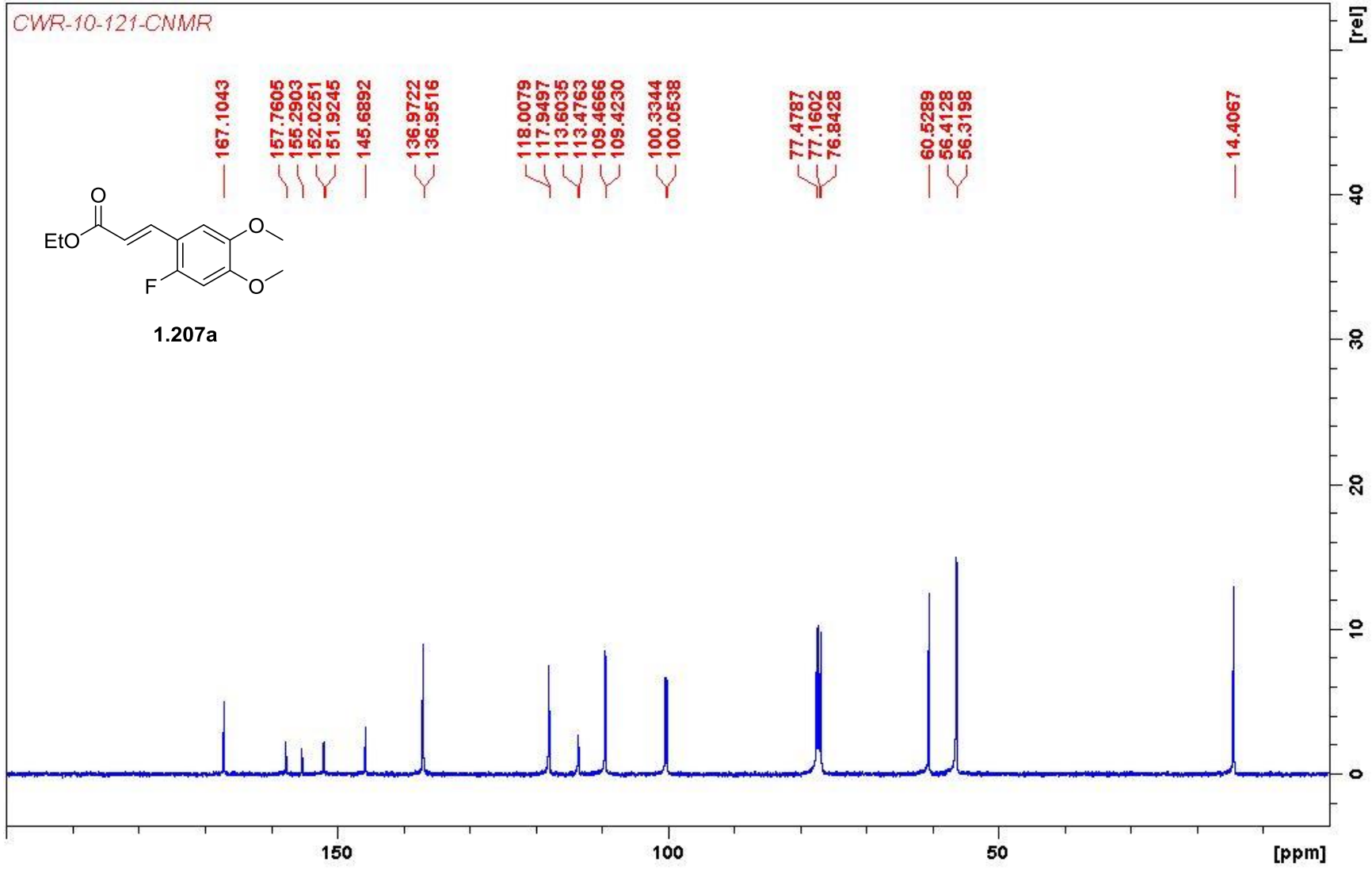
1.207a



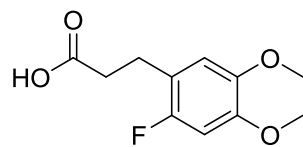
CWR-10-121-CNMR



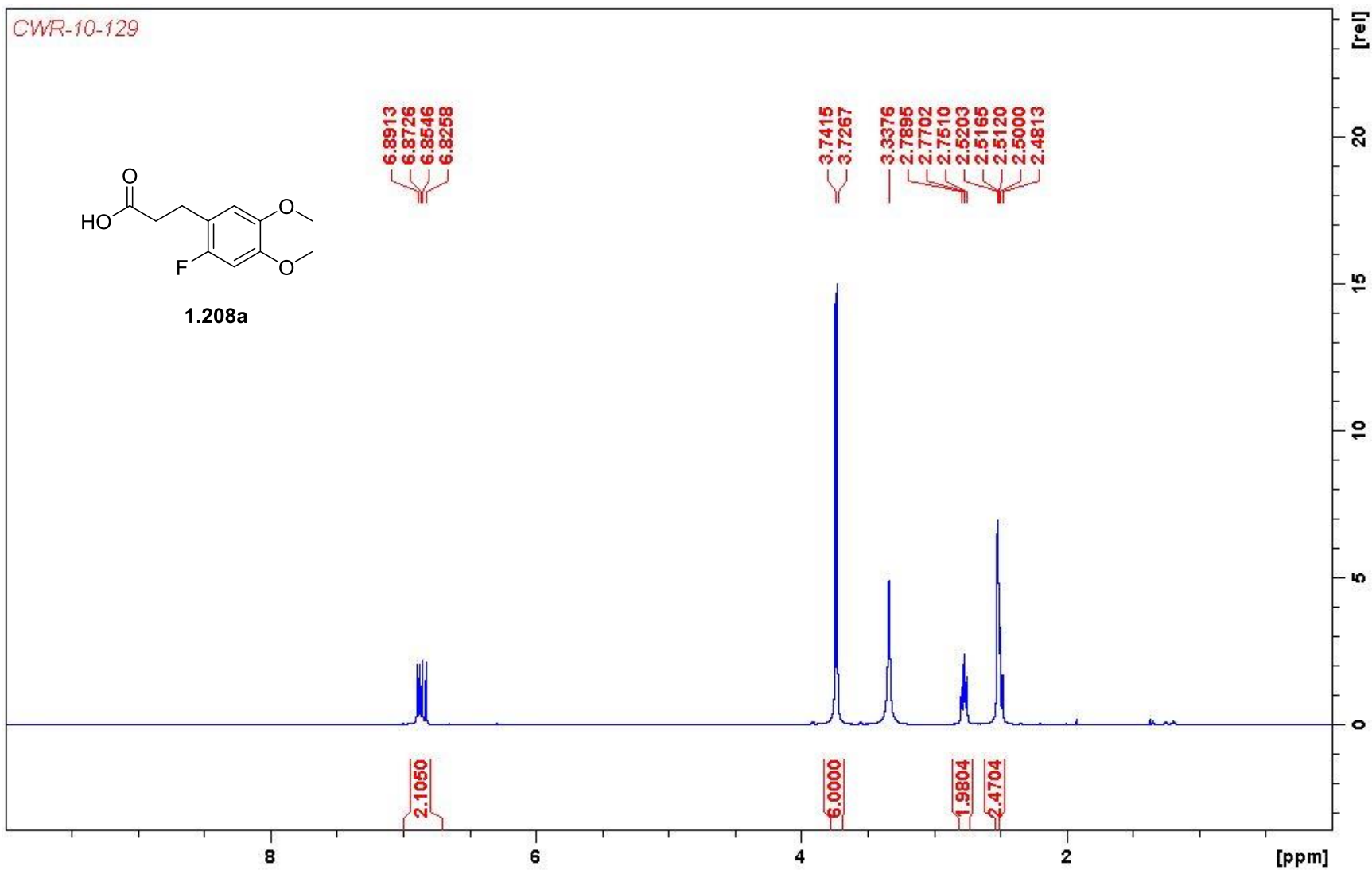
- 167.1043
- 157.7605
- 155.2903
- 152.0251
- 151.9245
- 145.6892
- 136.9722
- 136.9516
- 118.0079
- 117.9497
- 113.6035
- 113.4763
- 109.4666
- 109.4230
- 100.3344
- 100.0538
- 77.4787
- 77.1602
- 76.8428
- 60.5289
- 56.4128
- 56.3198
- 14.4067



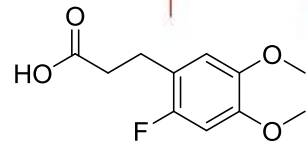
CWR-10-129



1.208a



CWR-10-129-CNMR



1.208a

173.6071

155.4229

153.0803

148.0678

147.9677

144.9265

144.9041

117.6513

117.4811

113.4781

113.4156

100.5898

100.3102

56.0426

55.8439

40.1476

39.9389

39.7302

39.5213

39.3127

39.1040

38.8956

34.2932

23.3768

150

100

50

[ppm]

[rel]

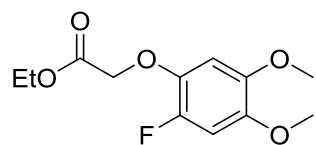
15

10

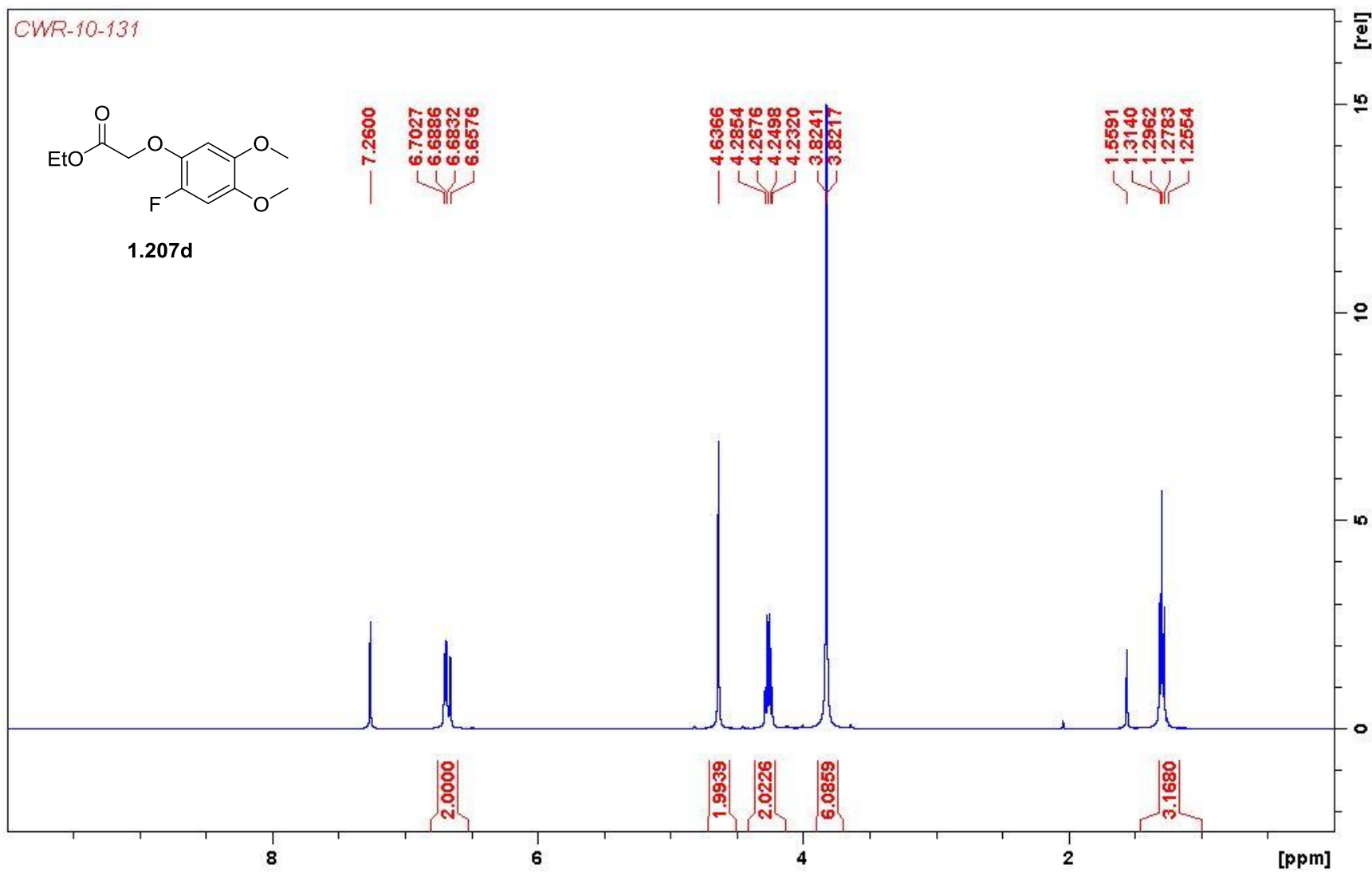
5

0

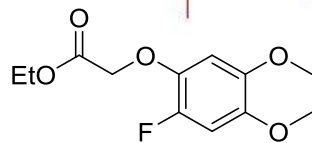
CWR-10-131



1.207d



CWR-10-131-CNMR



1.207d

169.1646

148.5954

146.2182

145.1163

145.0929

144.9228

144.8419

138.5961

138.4824

104.5312

104.5071

101.6025

101.3623

77.4787

77.1606

76.8431

69.0593

69.0272

61.3973

56.6372

56.5334

14.2785

150

100

50

[ppm]

20 [rel]

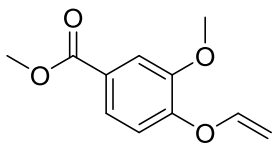
15

10

5

0

CWR-5-174



1.316

7.6572
7.6524
7.6365
7.6316
7.6087
7.6040
7.2599
7.0121
6.9913
6.6479
6.6328
6.6137
6.5986

4.8851
4.8802
4.8509
4.8460
4.5545
4.5496
4.5394
4.5345

3.9307
3.9038

1.5959

1.0258

1.0045

0.9484

0.9518

0.9686

6.3180

8

6

4

2

[ppm]

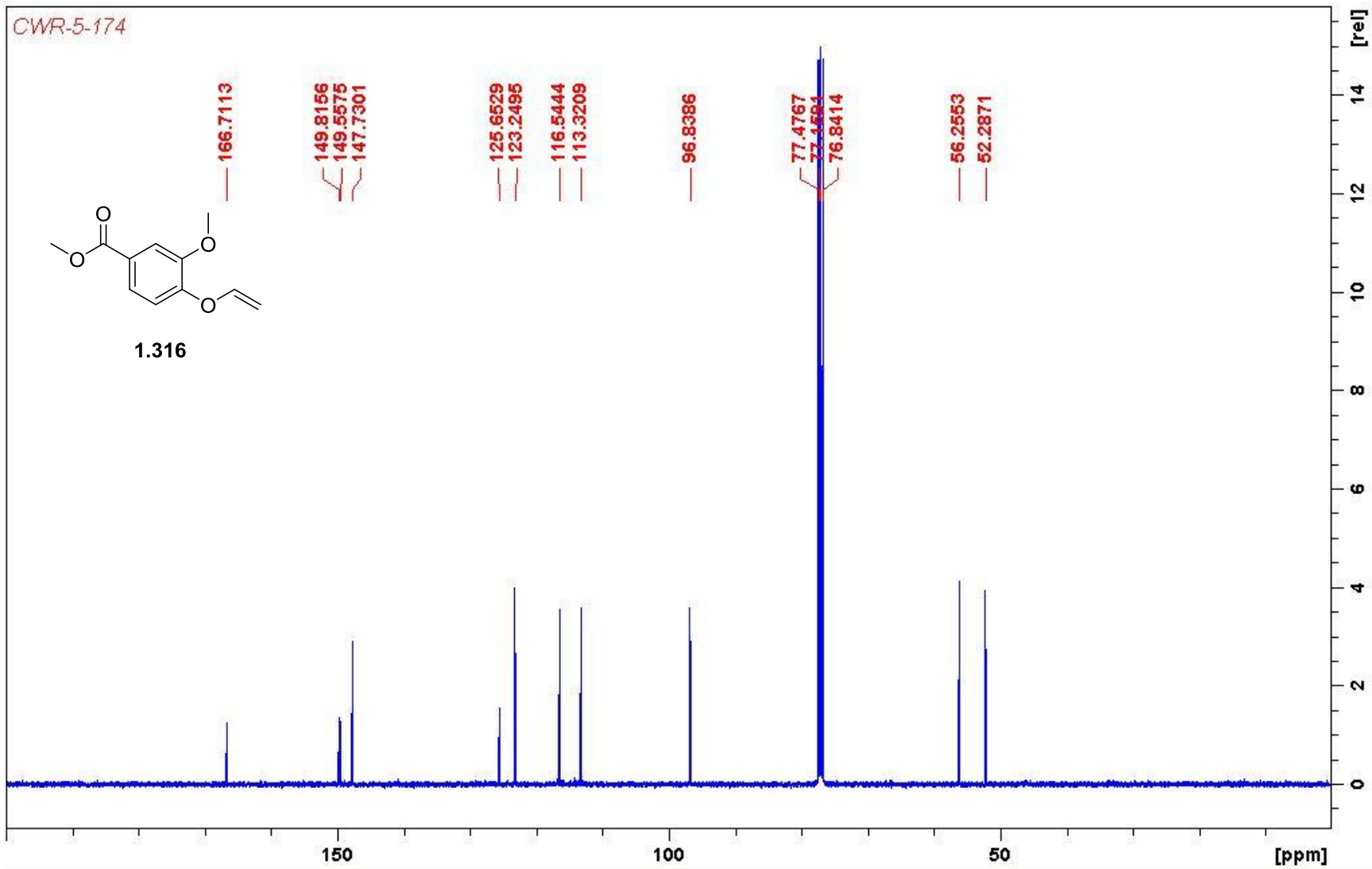
[rel]

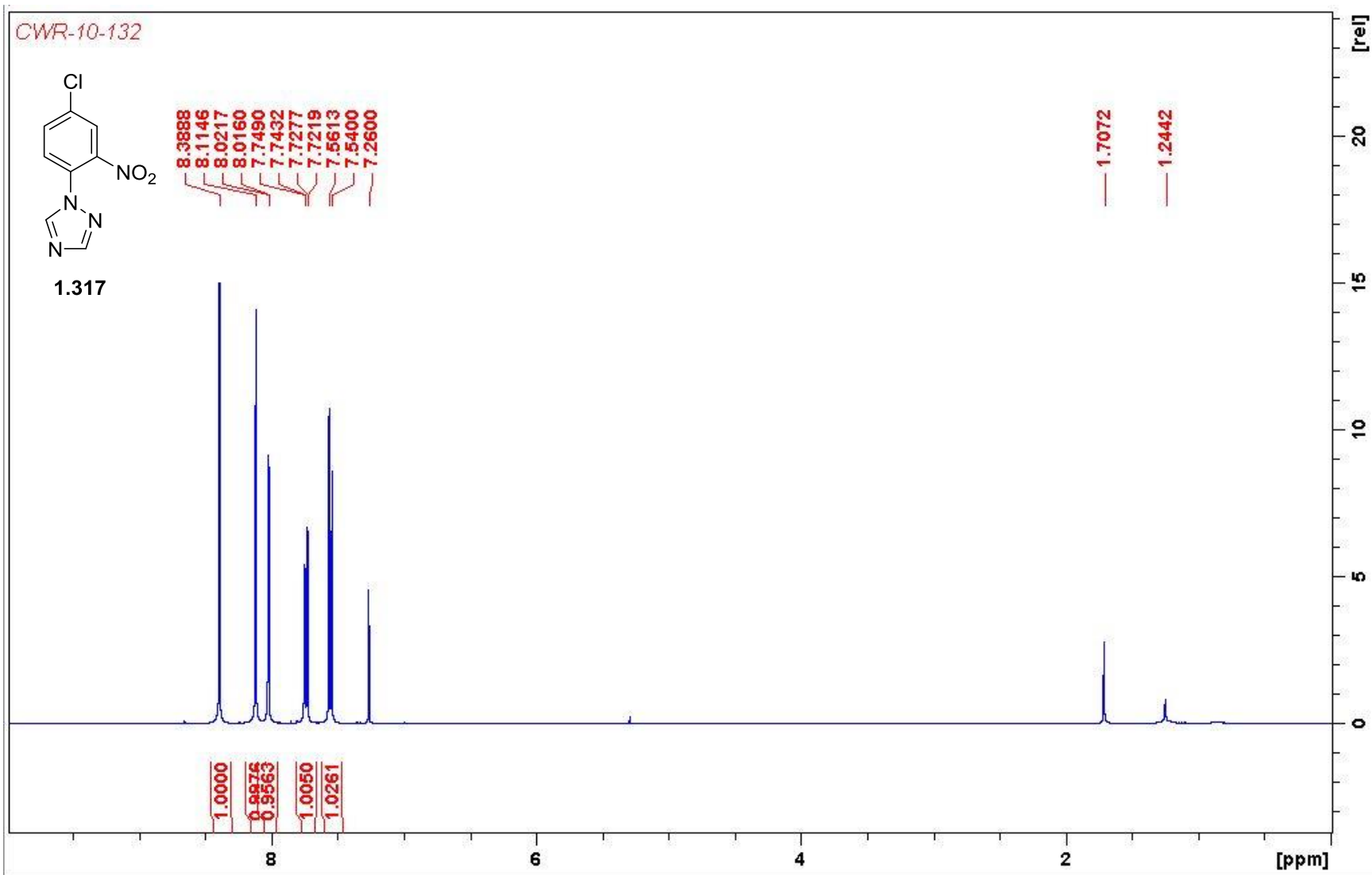
15

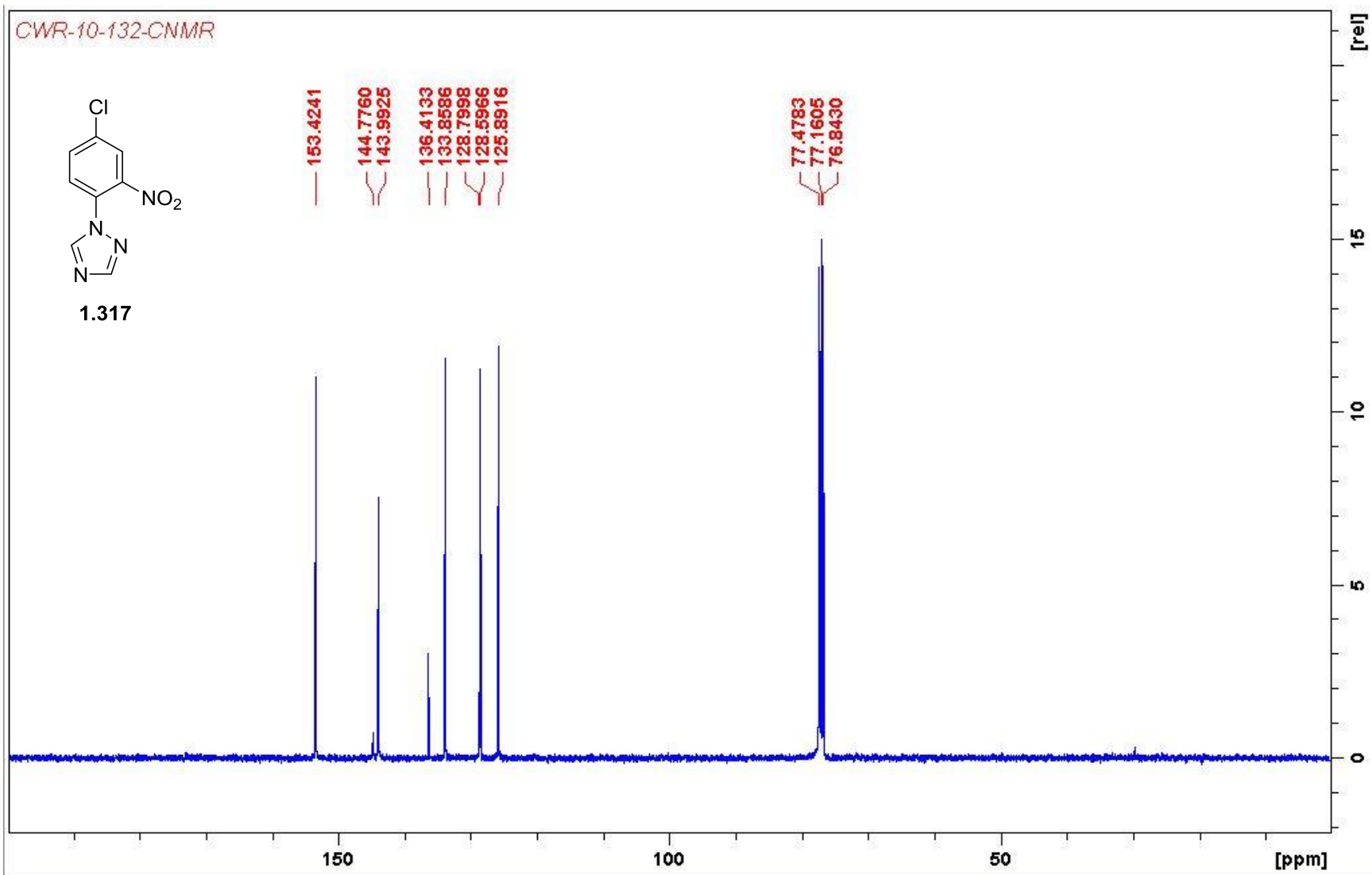
10

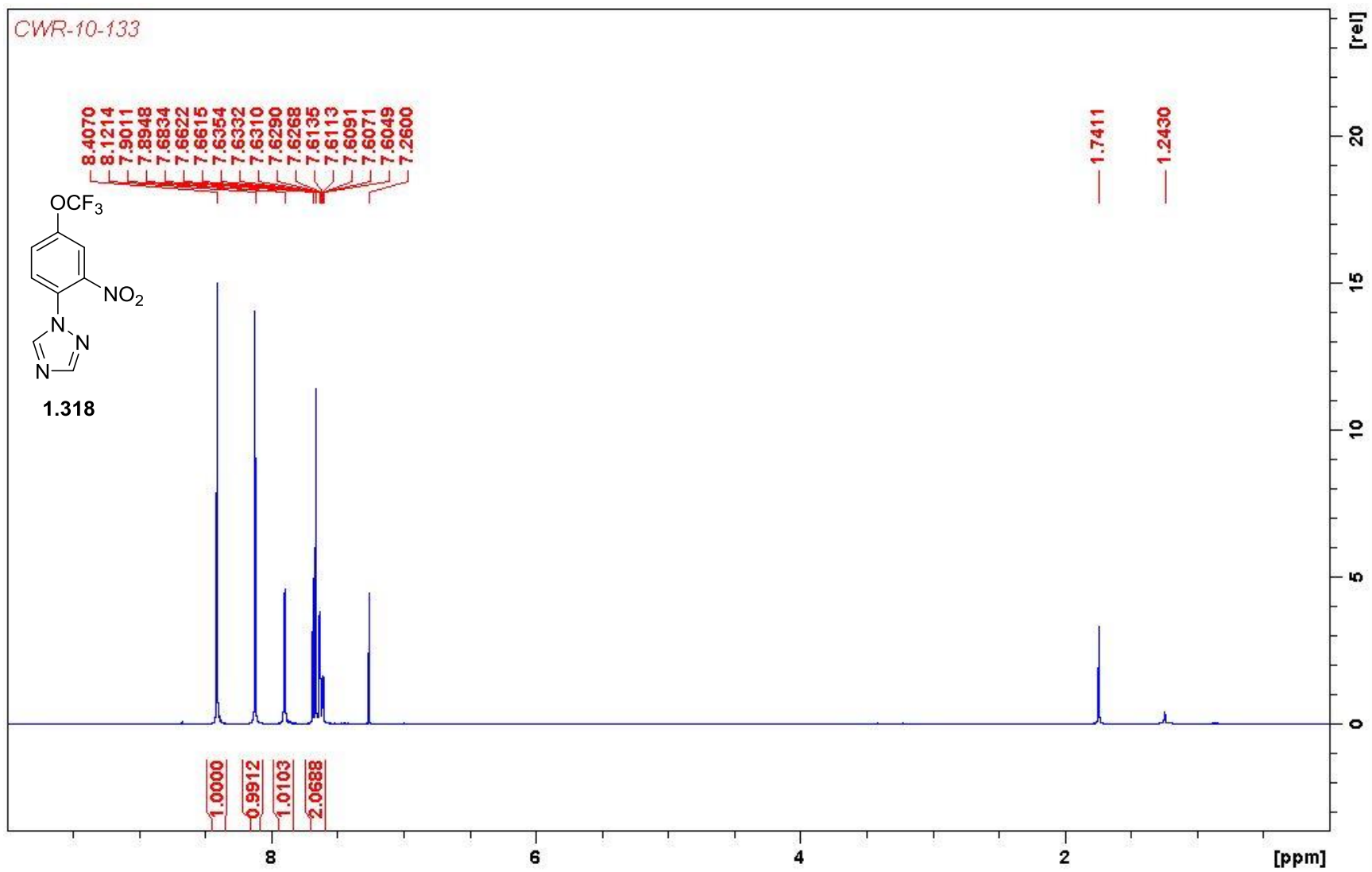
5

0

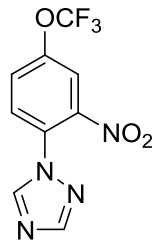






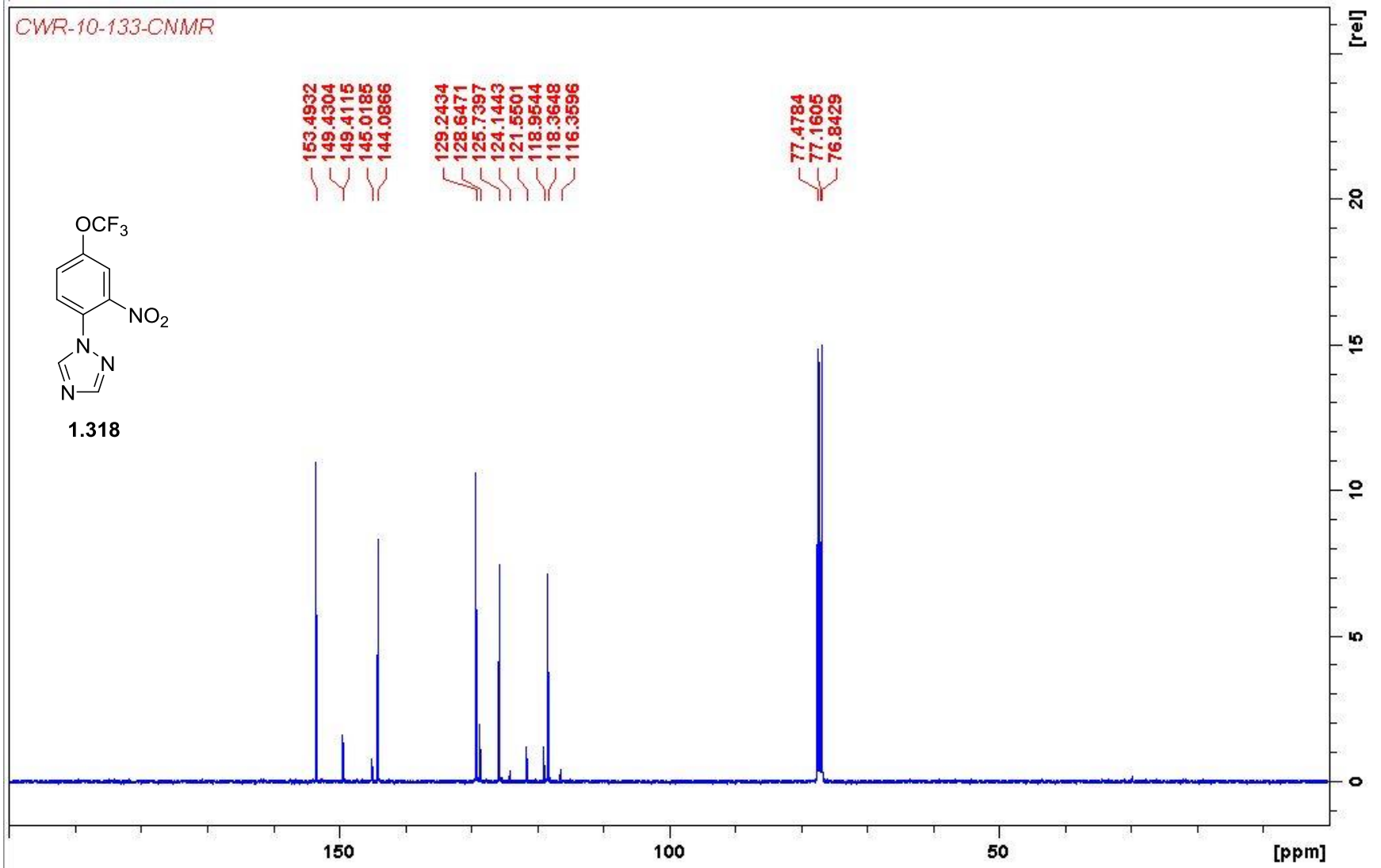


CWR-10-133-CNMR

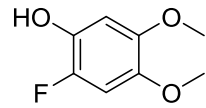


1.318

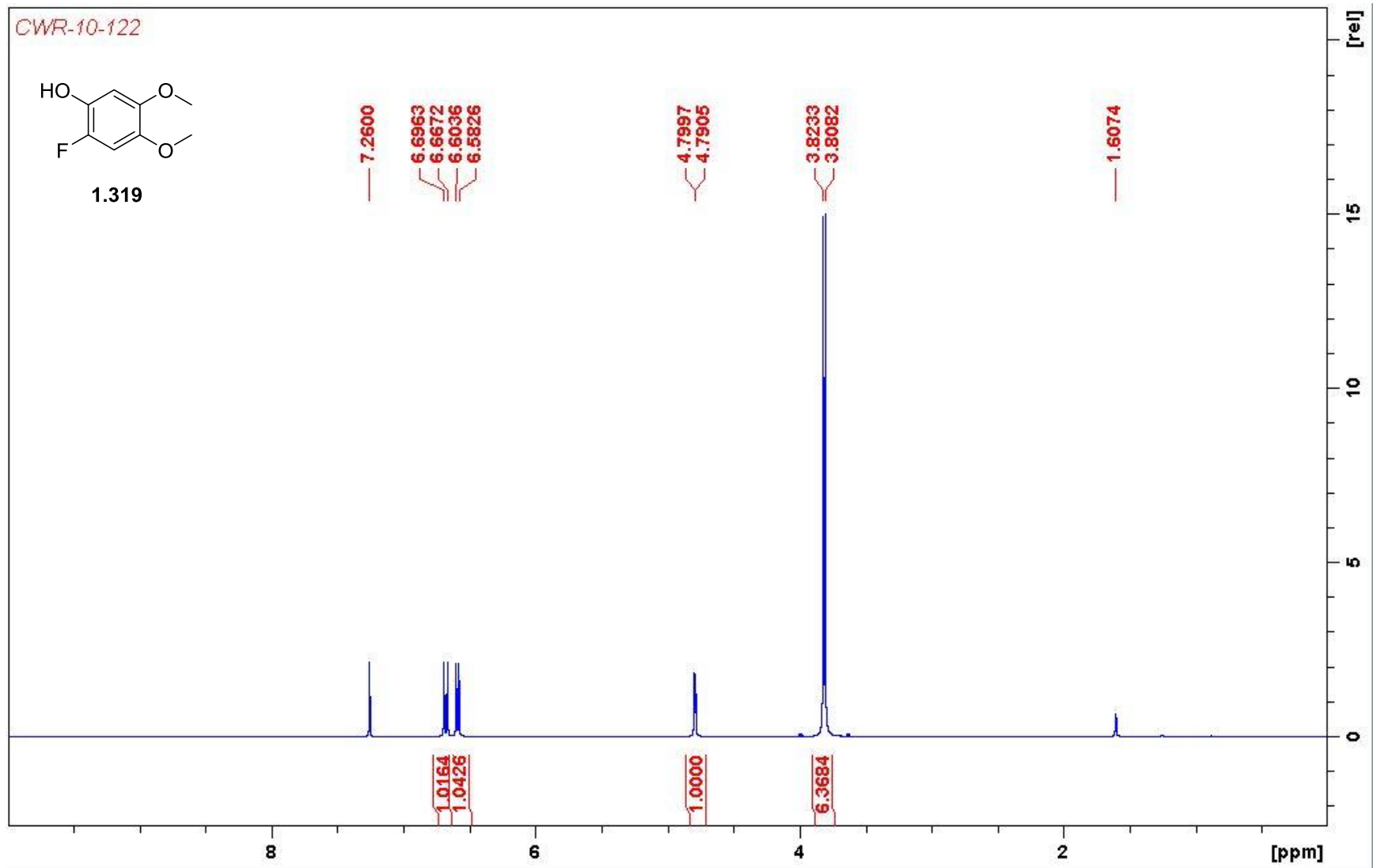
153.4932
149.4304
149.4115
145.0185
144.0866
129.2434
128.6471
125.7397
124.1443
121.5501
118.9544
118.3648
116.3596
77.4784
77.1605
76.8429



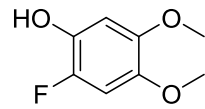
CWR-10-122



1.319



CWR-10-122-CNMR



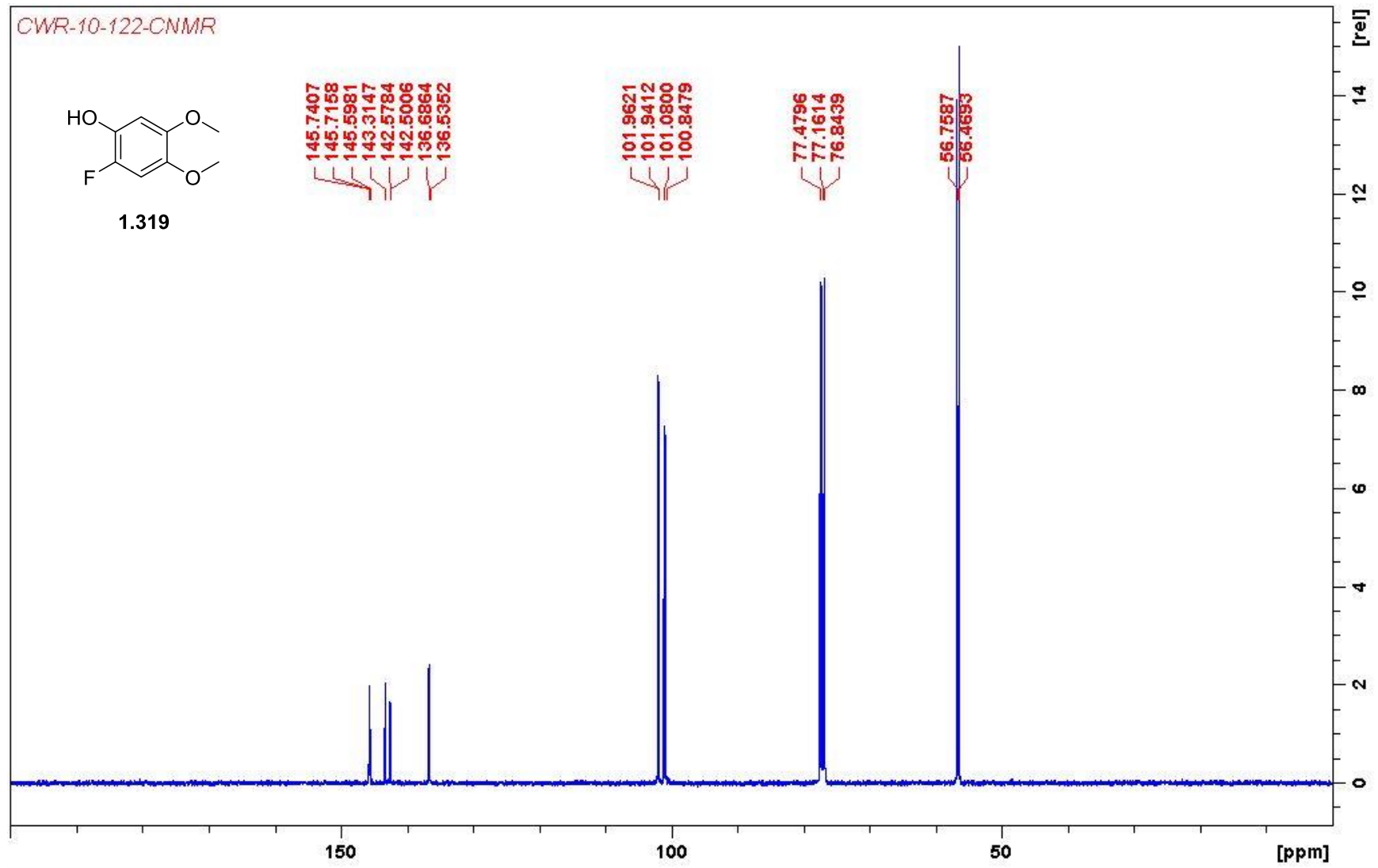
1.319

145.7407
145.7158
145.5981
143.3147
142.5784
142.5006
136.6864
136.5362

101.9621
101.9412
101.0800
100.8479

77.4796
77.1614
76.8439

56.7587
56.4693



CHAPTER II

PROGRESS TOWARDS THE DEVELOPMENT OF METABOTROPIC GLUTAMATE RECEPTOR 7 POSITIVE ALLOSTERIC MODULATORS

Background and Introduction

Known mGlu₇ Orthosteric and Allosteric Agonists, and Positive Allosteric Modulators

Unlike the development of small molecule negative allosteric modulators (NAMs) for mGlu₇, the development of selective positive allosteric modulators (PAMs) has been considerably more challenging.¹⁻² **Figure 2.1** summarizes the progress made in this area thus far.² While orthosteric agonists **2.1-2.4** show selectivity for the group III mGlu receptors, the highly conserved orthosteric binding site prevents obtaining selectivity amongst mGlu₄, mGlu₆, mGlu₇, and mGlu₈ receptors.³⁻⁷ Therefore, targeting an allosteric site as opposed to an orthosteric site (previously discussed in Chapter I) is paramount for achieving subtype selectivity for mGlu₇.⁸

In 2005, the first mGlu₇-specific tool compound, AMN082 (**2.5**), was reported in the literature (mGlu₇ EC₅₀ = 0.26 μM).⁹ **2.5**, an allosteric agonist, displayed an anxiolytic- and antidepressant-like profile in rat and mouse behavioral assays.⁹ However, conflicting results were observed with **2.5**; anxiogenic behavior was also observed in rat behavioral assays, resulting in a pharmacological paradox. To explain these conflicting data, **2.5** has been shown to induce desensitization of mGlu₇ via receptor internalization. Additionally, one of the major metabolites of **2.5** has considerable off-target activity at serotonin transporters (SERT) which confounds the

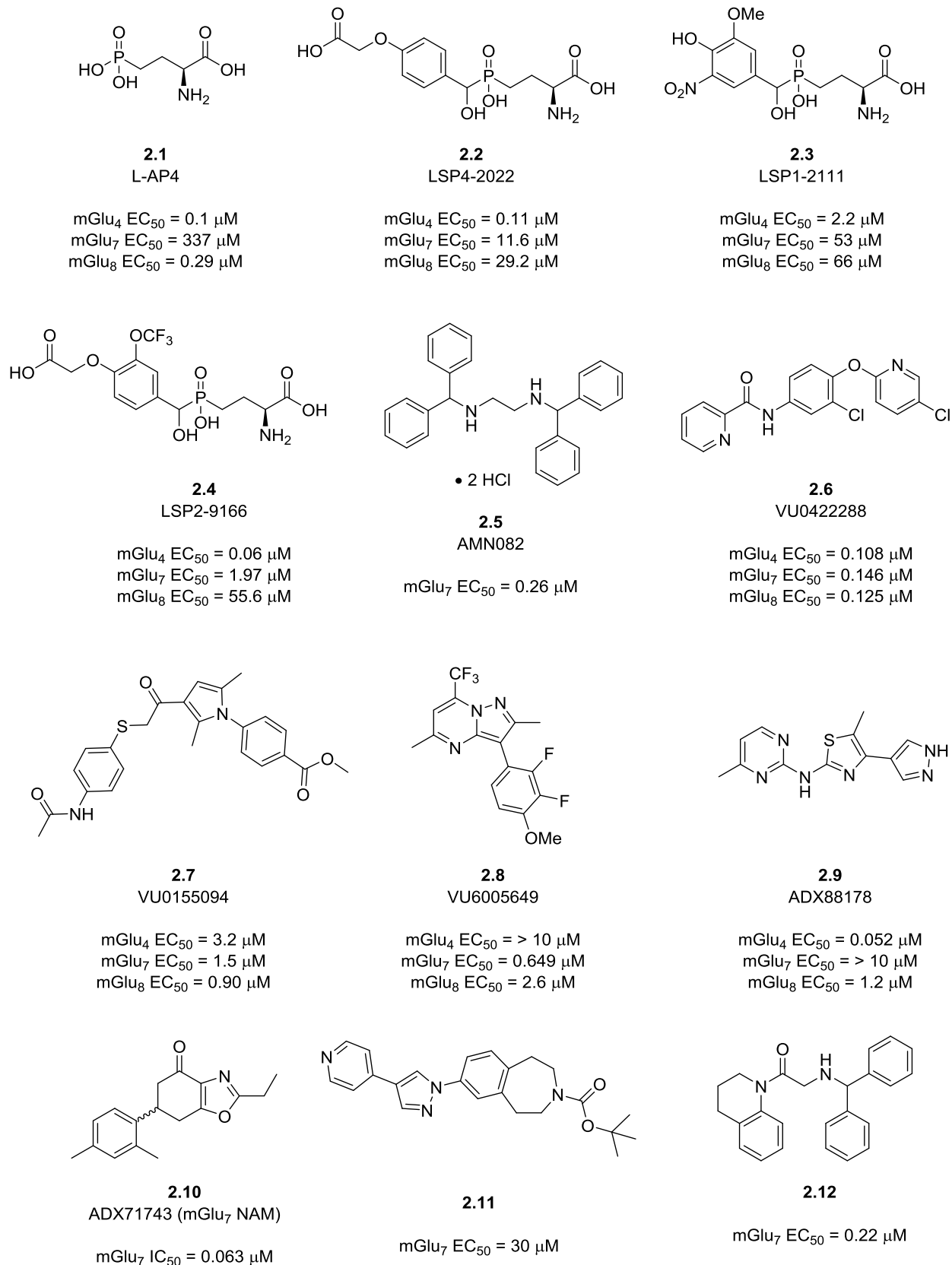


Figure 2.1: Known mGlu₇ orthosteric and allosteric agonists, and positive allosteric modulators

interpretation of *in vivo* data.¹⁰⁻¹³ Due to this complex pharmacology and off-target activity, efforts have shifted towards exploring selective positive allosteric modulators of mGlu₇. However, achieving selectivity for mGlu₇ through an allosteric modulation strategy has proven difficult. For example, VU0422288 (**2.6**), VU0155094 (**2.7**), and VU6005649 (**2.8**) were small molecules discovered through previous probe development campaigns, but these compounds were found to be either pan-group III PAMs (**2.6** and **2.7**) or a dual mGlu_{7/8} PAM (**2.8**).¹⁴⁻¹⁵ Additionally, **2.8** shows off-target activity at the neurokinin-1 receptor (NK1), which is believed to induce sedative effects and complicates the interpretation of *in vivo* experiments.¹⁵ Due to the lack of receptor selectivity of these small molecules, the concomitant use of additional tool compounds such as ADX88178 (**2.9**), a mGlu_{4/8} PAM, and ADX71743 (**2.10**), a mGlu₇ NAM previously discussed in Chapter I, is critical for confirming mGlu₇-mediated effects in both *in vitro* and *in vivo* experiments.¹⁶⁻¹⁸

Most recently, scientists from Janssen have reported their efforts on using proteochemometric modeling (PCM) techniques to identify novel mGlu₇ allosteric agonist chemotypes.¹⁹⁻²² In their computational modeling experiments, they have created a homology model for the seven-transmembrane (7-TM) domain of mGlu₇ based upon the known crystal structures of the 7-TM domains for mGlu₁ and mGlu₅ in combination with sequence alignment data associated with all of the mGlu receptors.²³⁻²⁵ They used this mGlu₇ 7-TM homology model to predict the binding mode of **2.5**.²¹ With this computationally determined allosteric site in hand, they virtually screened a small molecule library (~2800 compounds) for mGlu₇ allosteric binding and reported on the discovery of **2.11** and **2.12**.²¹⁻²² Both **2.11** and **2.12** were confirmed to be selective

mGlu₇ allosteric agonists in subsequent *in vitro* cell based assays, with mGlu₇ EC₅₀ values of 30 μM and 0.22 μM respectively. While **2.12** seems to be the superior choice with regards to potency, **2.12** was predicted to have high intrinsic clearance in humans and rats (both >346 μL/min/mg). Additionally, **2.12** contains the same benzhydryl motif as **2.5**, and as a result, it is unclear whether **2.12** would possess the same off-target effects as **2.5**.²¹⁻²²

Based on the limitations associated with these known mGlu₇ tool compounds, continued effort for the development of additional selective mGlu₇ PAMs is warranted. As stated previously, preliminary knockout experiments have associated mGlu₇ with neuropsychiatric disorders, neurodevelopmental disorders, and normal cognitive development.²⁶⁻³³ In particular, mGlu₇ has been implicated in Rett syndrome (RTT), and positive allosteric modulation of mGlu₇ may serve as a viable therapeutic avenue for this disorder.³⁴

Neurodevelopmental Disorders: Rett Syndrome (RTT)

Rett syndrome (RTT) is a rare X-linked neurodevelopmental disorder which affects approximately 1:10,000 females.³⁵⁻³⁹ Characteristic features of RTT are evident anywhere within 6-18 months of age.⁴⁰ At this stage, both normal development and cognitive development begin to regress. Patients diagnosed with RTT suffer from symptoms including repetitive hand claspings (stereotypic hand movements), limited speech, intellectual disabilities, motor impairment, apneas, epilepsy, scoliosis, gait ataxia, apraxia, and decreased growth.⁴¹⁻⁴⁴ Depending on the severity of the disease, the average life expectancy of patients suffering from this disease is approximately 14 years, where either epileptic seizures or aspiration pneumonia are the most common

causes of death.⁴⁵ However, patients suffering from mild forms of the disease can live well into adulthood.⁴⁵

Recently, it has been discovered that mutations in the *methyl CpG binding protein 2 (Mecp2)* gene are associated with the majority of incidences (~85-90%) of RTT.⁴⁶ Mecp2 belongs to the methyl-CpG-binding domain (MBD) family of proteins and plays an important role in regulating the epigenome.⁴⁷ In order to achieve this level of epigenetic regulation, Mecp2 contains three important protein domains that are required for activity: the aforementioned MBD, the transcription repression domain (TRD), and the C-terminal domain (CTD).⁴⁸⁻⁵⁰ The MBD of Mecp2 is responsible for binding to symmetrical methylated 5' CpG pairs.⁴⁸ It has been experimentally shown that Mecp2 prefers to bind to CpG islands with AT sequences (approximately 4 base pairs in length) within close proximity (approximately 6-9 base pairs away).⁵¹ This preferential binding led to the hypothesis that AT-hook domains were responsible for DNA binding as opposed to the MBD.⁵¹ However, further genetic analysis has revealed that while AT-hook domains exist within the *Mecp2* gene, their role is limited to secondary protein-protein interactions within the TRD. Specifically, upon binding of Mecp2 to DNA, it has been shown that the transcriptional co-repressor Sin3A and histone deacetylases 1 and 2 (HDAC1 and HDAC2) can be recruited through the TRD via interactions with these AT-hook domains.⁵³⁻⁵⁶ Activation of HDAC1 and HDAC2 results in DNA being wound more tightly around histones, resulting in an overall decrease in gene transcription.⁵³⁻⁵⁶ Although Mecp2 has been widely considered to be a transcriptional repressor through this mechanism, recent evidence has shown that Mecp2 can also serve as a transcriptional activator.⁵⁷ Through this mechanism, cAMP Responsive Element Binding

Protein 1 (CREB1) is recruited to the TRD of Mecp2 and is thought to serve as a transcriptional activator for certain genes.⁵⁷ For example, Zoghbi and coworkers were the first to show that Mecp2 activates transcription of genes encoding for neuropeptidic receptors (such as CNS GPCRs) and represses transcription of genes encoding for olfactory receptors.⁵⁷

Known Mutations of Mecp2 Gene Responsible for RTT

It has been established that mutations of the *Mecp2* gene are responsible for most cases of RTT.⁴⁶ While approximately 200 mutations have been identified as pathogenic, only 8 of these mutations are responsible for over 66% of RTT patients.⁵⁸⁻⁶¹ These 8 common mutations are either missense mutations (R106W, R133C, T158M, and R306C) or nonsense mutations (R168X, R255X, R270X, and R294X, where “X” represents a premature stop codon) and are depicted in **Figure 2.2**.⁵⁸⁻⁶¹ A missense mutation occurs when a single nucleotide point mutation results in a codon for a different amino acid, while a nonsense mutation occurs when a single nucleotide point

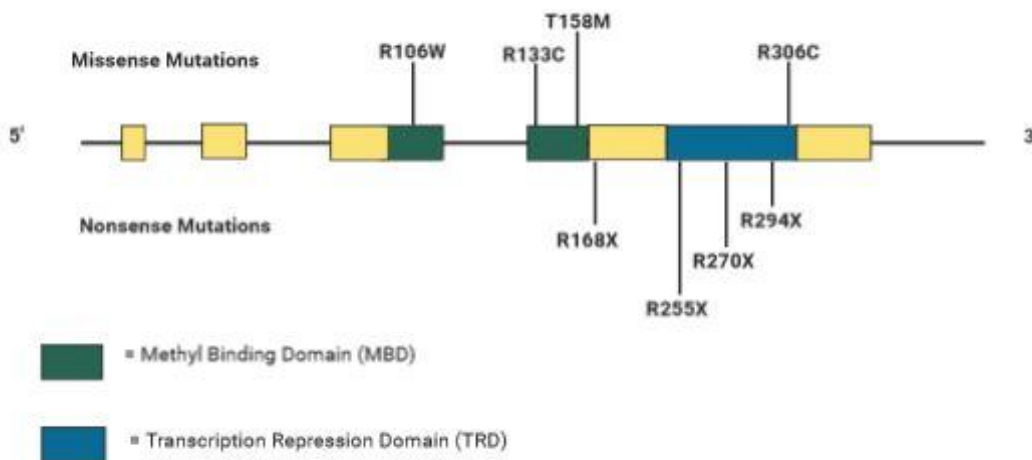


Figure 2.2: 8 common mutations of the *Mecp2* gene that lead to RTT

mutation results in a premature stop codon and leads to a truncated protein during translation.

Nonsense mutations have been shown to correlate with more severe disease phenotypes as opposed to the missense mutations in mouse models of RTT.⁵⁸ Nonsense mutations occurring at either the third or fourth exon of the *Mecp2* gene (**Figure 2.2**) have been shown to result in the formation of stable mRNA transcripts that are not targeted for degradation through the compensatory nonsense-mediated decay (NMD) pathway.⁶² These stable mRNA transcripts are then translated into their corresponding truncated *Mecp2* protein products (which do not contain the whole TRD necessary for activity), and as a result, the biological consequences are devastating. For example, the R270X mutation results in protein truncation before a critical AT-hook domain within the TRD that is responsible for mediating important protein-protein interactions. This mutation has been shown to result in severe neonatal encephalopathy and death.⁶¹ On the other hand, missense mutations (such as R106W and R133C) result in less severe disease phenotypes. These mutations occur within the MBD and destabilize the interaction between *Mecp2* and methylated CpG DNA segments.⁶³ The arginine residues R106 and R133 have been shown to form critical hydrogen bonds to methylated CpG DNA segments.⁶⁴⁻⁶⁵ Mutation of these arginine residues to either tryptophan or cysteine residues disrupts this critical hydrogen bonding interaction.⁶⁴⁻⁶⁵ However, both the R106W and R133C *Mecp2* proteins are still able to bind to DNA, albeit at much weaker binding affinities.⁶⁴⁻⁶⁵ DFT calculations infer that the binding of these mutated *Mecp2* proteins to DNA is approximately 100 times less stable than wild-type *Mecp2* DNA binding because the preferred hydrogen bond network is replaced by

less favorable Van der Waal interactions.⁶⁵ Since Mecp2 is still able to bind to DNA to a certain extent, both the R106W and R133C mutations are considered to result in milder phenotypes of RTT.⁶³⁻⁶⁵ Additionally, differing degrees of X-chromosomal inactivation in female patients has also been observed and can result in the variable severity of disease symptoms even amongst patients with the same genetic mutation.⁶³⁻⁶⁵

The Correlation Between mGlu₇ and RTT

mGlu₇ is primarily localized in the neocortex, prefrontal cortex, hippocampus, amygdala, and locus coeruleus of the brain and is believed to play an important role in learning, memory, and synaptic plasticity.²⁷ Although Mecp2 is expressed in all tissues, it is expressed primarily in the brain and at GABAergic interneurons. Additionally, Mecp2 has been found to be expressed at low levels during early stages of childhood development with increased expression observed as development progresses; this experimental observation is in accordance with the delayed presentation of RTT.⁶⁶⁻⁶⁷ Mouse models of RTT have shown cognitive deficits and altered hippocampal architecture which correspond to reduced synaptic transmission and attenuated LTP at hippocampal SC-CA1 synapses.⁶⁸⁻⁷³ Since it has been shown that activation of mGlu₇ is necessary for the induction of LTP at SC-CA1 synapses via a disinhibition mechanism of GABAergic interneurons,⁷⁴ Niswender and coworkers were interested to see if these RTT impairments correlated with deficits in mGlu₇ activity in this region of the brain.³⁴ By examining RTT brain autopsy samples compared to unaffected patient brain autopsy samples, it was found that mGlu₇ expression was significantly decreased in total cortex structures and hippocampal synapses. These data suggest that since Mecp2 deficits

lead to a decrease in mGlu₇ protein levels, *Mecp2* is a transcriptional activator for the *GRM7* gene (the gene that codes for the mGlu₇ protein).³⁴

To test whether this decrease in mGlu₇ expression contributes to any deficits in synaptic mGlu₇-mediated processes, Niswender and coworkers utilized *in vitro* electrophysiology experiments. Since it has been reported that agonism of mGlu₇ leads to a decrease in the slope of fEPSPs (field excitatory post-synaptic potentials) at SC-CA1 synapses, these electrophysiology experiments can be used to measure the ability of these neurons to participate in normal synaptic transmission.^{14,18,74} Application of the group III orthosteric agonist, LSP4-2022, (**2.2**) to hippocampal slices of *Mecp2*^{+/-} mice decreased the slope of fEPSPs, while administration of **2.2** to hippocampal slices of *Mecp2*^{-/-} mice did not lead to a change in slope of fEPSPs. These data suggest that the decreased levels of synaptic mGlu₇ in *Mecp2*^{-/-} mice lead to deficits in normal synaptic transmission across these synapses. Subsequently, it was observed that coapplication of pan group III PAMs (**2.6** and **2.7**) with **2.2** to hippocampal slices of *Mecp2*^{-/-} mice did lead to a decrease in the slope of fEPSPs. Since mGlu₇ has been shown to be the only mGlu receptor expressed presynaptically at these SC-CA1 synapses in adult mice, it can be deduced that positive allosteric modulation of mGlu₇ can reverse deficits in synaptic transmission in mouse models of RTT.³⁴

Since activation of mGlu₇ is necessary for the induction of LTP at SC-CA1 synapses, Niswender and coworkers hypothesized that the deficits in LTP observed in both *Mecp2*^{-/-} and *Mecp2*^{+/-} hippocampal slices were due to this decreased synaptic expression of hippocampal mGlu₇.³⁴ Indeed, high-frequency stimulation (HFS)-induced LTP was reduced in both *Mecp2*^{-/-} and *Mecp2*^{+/-} hippocampal slices when compared to

wild-type controls. Application of pan group III PAM **2.6** was able to restore HFS-induced LTP in these mouse models, which indicates that positive allosteric modulation of mGlu₇ is capable of reversing deficits in synaptic plasticity in mouse models of RTT.³⁴

With these hypotheses validated *in vitro*, Niswender and coworkers tested the ability of positive allosteric modulation of mGlu₇ in reversing cognitive deficits in mouse models of RTT using *in vivo* behavioral experiments.³⁴ Administration of the pan group III PAM **2.6** in *Mecp2*^{+/-} mice led to the correction of learning and memory deficits (compared to wild-type controls) in contextual fear conditioning, novel object recognition, elevated plus maze, and social recognition assays. To serve as a negative control, *Mecp2*^{+/-} mice were also dosed with the dual mGlu_{4/8} PAM ADX88178 (**2.9**). No reversal of these cognitive deficits was observed in these behavioral assays when compared to wild-type controls. Additionally, the co-administration of pan group III PAM **2.6** with the mGlu₇ NAM ADX71743 (**2.10**) in these behavioral assays resulted in the loss of any benefits observed in comparison to treatment with solely **2.6**. Treatment of *Mecp2*^{+/-} mice with the pan group III PAM **2.6** also led to a decrease in apneas when compared to wild-type controls. These data suggest that the social, cognitive, anxiety, and respiratory deficits of *Mecp2*^{+/-} mice are mGlu₇-mediated, and positive allosteric modulation of mGlu₇ is capable of restoring such deficits.³⁴

As a whole, Niswender and coworkers have established that several mutations of the *Mecp2* gene found in RTT patients lead to decreased expression of synaptic mGlu₇ in the hippocampus. This reduction of protein expression is responsible for deficits in normal synaptic transmission and synaptic plasticity in mouse models of RTT.

Furthermore, the abnormal social, cognitive, anxiety, and respiratory phenotypes of RTT

could be rescued via treatment with the pan group III PAM **2.6** *in vivo*. The use of control compounds **2.9** and **2.10** were carefully used to demonstrate that these effects are mGlu₇-mediated as opposed to other group III mGlu receptors, such as mGlu₄ and mGlu₈. These data suggest that the selective, positive allosteric modulation of mGlu₇ may serve as a potential therapeutic strategy for the treatment of RTT.³⁴

Therapeutic Strategies for Treating RTT

In 2007, Bird and coworkers were the first to demonstrate that RTT can be reversed in transgenic mouse models of the disease via restoration of *Mecp2* gene expression.⁷⁵ These data suggest that RTT is indeed a neurodevelopmental disorder and not a neurodegenerative disorder because neurological symptoms of the disease are reversible in both immature and mature animals.⁷⁵ The revocability of RTT symptoms in these mouse models has served as an inspiration for identifying viable therapeutic avenues for treating RTT. While our labs are interested in exploring mGlu₇ as a novel therapeutic target for RTT, other targets are also being explored for their efficacy in treating this disease, with a few of these alternatives entering clinical trials (**Figure 2.3**).⁷⁶

One of these additional targets is brain-derived neurotrophic factor (BDNF).⁷⁶ BDNF is responsible for activating tropomyosin receptor kinase B (TrkB) receptors and plays a crucial role in promoting neural growth and regulating synaptic plasticity.⁷⁷ Mutations in the *Mecp2* gene lead to decreased expression of BDNF, and restoration of BDNF expression in transgenic mice rescues neurological phenotypes of RTT.⁷⁸⁻⁸⁰ Since BDNF suffers from low blood-brain barrier (BBB) penetration, BDNF boosters and mimetics have been proposed as viable therapeutic alternatives.⁷⁶ For example,

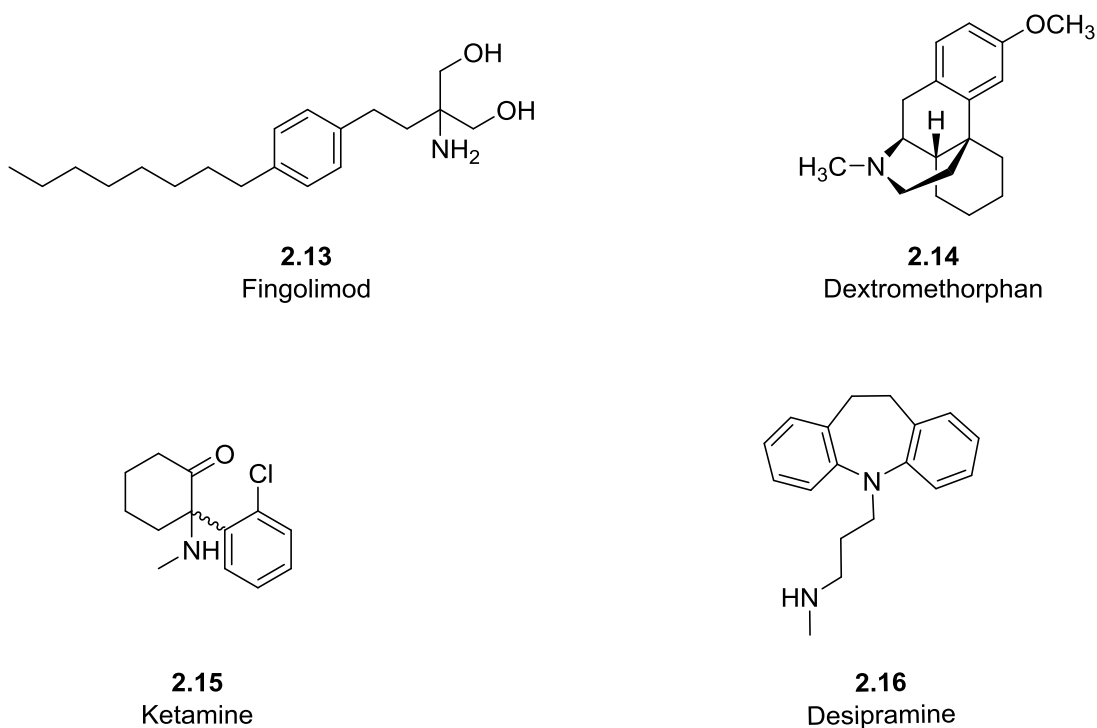


Figure 2.3: Current small molecules in ongoing clinical trials for the treatment of RTT

Fingolimod (**2.13**), a sphingosine-1 phosphate receptor modulator, increases BDNF levels via the mitogen-activated protein kinase pathway, while Glatiramer acetate is an immunomodulatory protein which increases BDNF levels via activation of autoreactive T cells.⁸¹⁻⁸² Additionally, other proteins such as insulin-like growth factor-1 (IGF-1) are able to cross the BBB and activate TrkB receptors in the same manner as BDNF.⁸³ Other compounds such as NMDA receptor antagonists (Dextromethorphan (**2.14**) and Ketamine (**2.15**)) and norepinephrine reuptake inhibitors (Desipramine (**2.16**)) have also been proposed as potential therapeutic avenues for targeting RTT.⁸⁴⁻⁸⁶ However, **2.14** and **2.16** have failed to show efficacy in clinical trials.⁸⁴⁻⁸⁶

Perhaps the most unique therapeutic strategy proposed is the use of gene therapy to reactivate *Mecp2* gene expression.⁷⁶ However, a therapeutic strategy based

on reactivation of *Mecp2* genes can be extremely risky. Neurological deficits have been observed as a result of overexpression of *Mecp2*.⁸⁷ Indeed, the overexpression of *Mecp2* (known as Mecp2 Duplication syndrome) has been known to lead to severe forms of intellectual disability in patients coupled with other complications such as recurrent respiratory infections, hypotonia, limited speech, intellectual-disabilities, autism-like behaviors, and epileptic seizures.⁸⁸⁻⁹¹ Additionally, the variable severity of RTT due to different *Mecp2* mutations, coupled with the process of X-chromosome inactivation in female patients, would need to confine gene therapy strategies to a patient-by-patient basis in order to avoid potential toxicity caused by an overexpression of *Mecp2*. Therefore, this therapeutic approach should be approached with extreme caution.

Conclusion

In conclusion, the seminal work of Niswender and coworkers has shown that mGlu₇ protein levels are diminished in RTT brain autopsy samples. Mouse models of RTT show deficits in normal synaptic transmission and the regulation/induction of synaptic plasticity mechanisms, and these deficits have been hypothesized to be a result of decreased mGlu₇ expression. Indeed, positive allosteric modulation of mGlu₇ is capable of restoring social, cognitive, anxiety, and respiratory phenotypes in mouse models of RTT. These data are important because they provide a novel glutamatergic mechanism that may be a reliable therapeutic avenue for treating RTT. Furthermore, depending on the severity and underlying mutation of the disease, either full-PAMs or partial PAMs could be used to restore mGlu₇ activity to basal levels. However, the lack of selective mGlu₇ PAM tool compounds impedes further investigation into this

receptor's therapeutic potential and warrants additional effort in the field. Therefore, the following sections of this chapter will detail our efforts and progress made towards the development of a novel class of selective mGlu₇ PAMs.

Materials and Methods

General Synthetic Methods and Instrumentation

All NMR spectra were recorded on a 400 MHz AMX Bruker NMR spectrometer. ¹H and ¹³C chemical shifts are reported in δ values in ppm downfield with the deuterated solvent as the internal standard. Data are reported as follows: chemical shift, multiplicity (s = singlet, d = doublet, t = triplet, q = quartet, b = broad, m = multiplet), integration, coupling constant (Hz). Low resolution mass spectra were obtained on an Agilent 6120 or 6150 with ESI source. MS parameters were as follows: fragmentor: 70, capillary voltage: 3000 V, nebulizer pressure: 30 psig, drying gas flow: 13 L/min, drying gas temperature: 350 °C. Samples were introduced via an Agilent 1290 UHPLC comprised of a G4220A binary pump, G4226A ALS, G1316C TCC, and G4212A DAD with ULD flow cell. UV absorption was generally observed at 215 nm and 254 nm with a 4 nm bandwidth. Column: Waters Acquity BEH C18, 1.0 x 50 mm, 1.7 μm. Gradient conditions: 5% to 95% CH₃CN in H₂O (0.1% TFA) over 1.4 min, hold at 95% CH₃CN for 0.1 min, 0.5 mL/min, 55 °C. High resolution mass spectra were obtained on an Agilent 6540 UHD Q-TOF with ESI source. MS parameters were as follows: fragmentor: 150, capillary voltage: 3500 V, nebulizer pressure: 60 psig, drying gas flow: 13 L/min, drying gas temperature: 275 °C. Samples were introduced via an Agilent 1200 UHPLC

comprised of a G4220A binary pump, G4226A ALS, G1316C TCC, and G4212A DAD with ULD flow cell. UV absorption was observed at 215 nm and 254 nm with a 4 nm bandwidth. Column: Agilent Zorbax Extend C18, 1.8 μm , 2.1 x 50 mm. Gradient conditions: 5% to 95% CH_3CN in H_2O (0.1% formic acid) over 1 min, hold at 95% CH_3CN for 0.1 min, 0.5 mL/min, 40 $^\circ\text{C}$. For compounds that were purified on a Gilson preparative reversed-phase HPLC, the system comprised of a 333 aqueous pump with solvent-selection valve, 334 organic pump, GX-271 or GX-281 liquid handler, two column switching valves, and a 155 UV detector. UV wavelength for fraction collection was user-defined, with absorbance at 254 nm always monitored. Method 1: Phenomenex Axia-packed Luna C18, 30 x 50 mm, 5 μm column. Mobile phase: CH_3CN in H_2O (0.1% TFA). Gradient conditions: 0.75 min equilibration, followed by user defined gradient (starting organic percentage, ending organic percentage, duration), hold at 95% CH_3CN in H_2O (0.1% TFA) for 1 min, 50 mL/min, 23 $^\circ\text{C}$. Method 2: Phenomenex Axia-packed Gemini C18, 50 x 250 mm, 10 μm column. Mobile phase: CH_3CN in H_2O (0.1% TFA). Gradient conditions: 7 min equilibration, followed by user defined gradient (starting organic percentage, ending organic percentage, duration), hold at 95% CH_3CN in H_2O (0.1% TFA) for 7 min, 120 mL/min, 23 $^\circ\text{C}$. All reagents were purchased from Aldrich Chemical Co. and were used without purification. All final compounds were >98% pure by LCMS (254 nm, 214 nM and ELSD). Following these purification protocols, final compounds were transferred to a barcode vial and diluted to a concentration of 10 μM using molecular biology grade dimethylsulfoxide (DMSO). These compounds were registered into Dotmatics and assigned a VU identification number before being tested in the primary screening assay.

Primary Screening (Calcium Mobilization) Assay

Human mGlu₄/G_{q15}/CHO cells (30,000 cells/20 µL/well), rat mGlu₇/G_{a15}/HEK cells (15,000 cells/20 µL/well), and rat mGlu₈/G_{a15}/HEK cells (15,000 cells/20 µL/well) were plated in black-walled, clear-bottomed, TC treated, 384 well plates (Greiner Bio-One, Monroe, NC) in DMEM containing 10% dialyzed FBS, 20 mM HEPES, 100 units/mL penicillin/streptomycin, and 1 mM sodium pyruvate (Plating Medium). The cells were grown overnight at 37 °C in the presence of 5% CO₂. The next day, the medium was removed and replaced with 20 µL of 1 µM Fluo-4, AM (Life Technologies, Thermo Fisher Scientific, Grand Island, NY) prepared as a 2.3 mM stock in DMSO and mixed in a 1:1 ratio with 10% (w/v) pluronic acid F-127 and diluted in Assay Buffer (Hank's balanced salt solution, 20 mM HEPES and 2.5 mM Probenecid (Sigma-Aldrich, St. Louis, MO)) for 45 minutes at 37 °C. Dye was removed and replaced with 20 µL of Assay Buffer. For concentration-response curve experiments, compounds were serially diluted 1:3 into 10 point concentration response curves in DMSO, transferred to daughter plates using an Echo acoustic plate reformatter (Labcyte, Sunnyvale, CA) Echo, and diluted in Assay Buffer to a 2X final concentration. Calcium flux was measured using the Functional Drug Screening System 6000 or 7000 (FDSS6000/7000, Hamamatsu, Japan). After establishment of a fluorescence baseline for 4 seconds (4 images at 1 Hz; excitation, 470 ± 20 nm; emission, 540 ± 30 nm), 20 µL of test compounds were added to the cells, and the response was measured. 142 seconds later, 10 µL (5X) of an EC₂₀ concentration of glutamate was added to the cells, and the response of the cells was measured; after an additional 120 seconds, 12 µL (5X) of an EC₈₀ concentration of agonist was added and readings taken for an additional 40 seconds. Calcium fluorescence was recorded as fold over basal fluorescence and raw

data were normalized to the maximal response to glutamate. Potency (EC₅₀) and maximum response (% Glu or L-AP4 Max) for compounds were determined using a four parameter logistical equation in GraphPad Prism (La Jolla, CA) or Dotmatics (XX.XX) software. For efficacy and selectivity experiments, a constant amount of compound was applied prior to the addition of a full glutamate concentration-response curve and the shift of the EC₅₀ of the curves was calculated as “fold shift”. mGlu receptor selectivity profiling, and GIRK assay were performed as previously reported^{84-85, 45}.

In Vitro DMPK Methods: Intrinsic Clearance in Murine and Rat Liver Microsomes

Murine or rat liver microsomes (0.5 mg/mL) and 1 μM test compound were incubated in 100 mM potassium phosphate pH 7.4 buffer with 3 mM MgCl₂ at 37 °C with constant shaking. After a 5 min preincubation, the reaction was initiated by addition of NADPH (1 mM). At selected time intervals (0, 3, 7, 15, 25, and 45 min), 50 μL aliquots were taken and subsequently placed into a 96-well plate containing 150 μL of cold acetonitrile with internal standard (50 ng/mL carbamazepine). Plates were then centrifuged at 3000 rcf (4 °C) for 10 min, and the supernatant was transferred to a separate 96-well plate and diluted 1:1 with water for LC/MS/MS analysis. The *in vitro* half-life (T_{1/2}, min, Eq. 1), intrinsic clearance (CL_{INT}, mL/min/kg, Eq. 2) and subsequent predicted hepatic clearance (CL_{HEP}, mL/min/kg, Eq. 3) were determined employing the following equations:

$$(1) \quad T_{1/2} = \frac{\text{Ln}(2)}{k}$$

where k represents the slope from linear regression analysis of the natural log percent remaining of test compound as a function of incubation time

$$(2) \quad CL_{int} = \frac{0.693}{in\ vitro T_{1/2}} \times \frac{mL\ incubation}{mg\ microsomes} \times \frac{45\ mg\ microsomes}{gram\ liver} \times \frac{45^a\ gram\ liver}{kg\ body\ wt}$$

^a scale-up factor that is species specific

$$(3) \quad CL_{hep} = \frac{Q_h \cdot CL_{int}}{Q_h + CL_{int}}$$

where Q_h (hepatic blood flow) is species specific.

Mouse and Rat Plasma Protein Binding

The protein binding of each compound was determined in rat or mouse plasma via equilibrium dialysis employing HTDialysis Teflon dialysis chamber and cellulose membranes (MWCO 12-14 K) (HTDialysis LLC, Gales Ferry, CT). Plasma was added to the 96-well plate containing test compound and mixed thoroughly for a final concentration of 5 μ M. Subsequently, 150 μ L of the plasma-compound mixture was transferred to the dialysis chamber, with an accompanying 150 μ L of phosphate buffer (25 mM, pH 7.4) on the other side of the membrane. The device plate was sealed and incubated for 4 hours at 37 °C with shaking. At completion, aliquots from each chamber were diluted 1:1 with either plasma (for the buffer sample) or buffer (for the plasma sample) and transferred to a new 96-well plate, at which time ice-cold acetonitrile containing internal standard (50 ng/mL carbamazepine) (2 volumes) was added to extract the matrices. The plate was centrifuged (3000 rcf, 10 min) and supernatants transferred and diluted 1:1 (supernatant: water) into a new 96 well plate, which was then sealed in preparation for LC/MS/MS analysis. Each compound was assayed in triplicate within the same 96-well plate. Fraction unbound was determined using the following equation:

$$F_u = \frac{Conc_{buffer}}{Conc_{plasma}}$$

Mouse and Rat Brain Homogenate Binding

The brain homogenate binding of each compound was determined in brain homogenate via equilibrium dialysis employing HTDialysis Teflon dialysis chamber and cellulose membranes (MWCO 12-14 K) (HTDialysis LLC, Gales Ferry, CT). Brain tissue homogenate was prepared by diluting one volume whole mouse or rat brain tissue with one to three volumes (species specific) of phosphate buffer (25 mM, pH 7.4). The mixture was then subjected to mechanical homogenization employing a Mini-Beadbeater™ and 1.0 mm Zirconia/Silica Beads (BioSpec Products). Brain homogenate spiked with test compound and mixed thoroughly for a final concentration of 5 µM. Subsequently, 150 µL of the brain homogenate-compound mixture was transferred to the dialysis chamber with an accompanying 150 µL of phosphate buffer (25 mM, pH 7.4) on the other side of the membrane. The block was sealed and incubated for 6 hours at 37 °C with shaking. At completion, aliquots from each side of the chamber were diluted 1:1 with either brain homogenate (to the buffer side) or buffer (to the brain homogenate side) in a new 96 well plate, at which time ice-cold acetonitrile containing internal standard (50 ng/mL carbamazepine) was added to extract the matrices. The plate was centrifuged (3000 rcf, 10 min) and supernatants transferred and diluted 1:1 (supernatant: water) into a new 96 well plate, which was then sealed in preparation for LC/MS/MS analysis. Each compound was assayed in triplicate within the same 96-well plate. Fraction unbound was determined using the following equation:

$$F_{u,tissue} = \frac{1/D_f}{(1/F_{u,hom} - 1) + 1/D_f}$$

Where $F_{u,hom}$ represent the measured fraction unbound in the diluted homogenate and D_f represents dilution factor.

LC/MS/MS Analysis of Samples from In Vitro Assays

Samples were analyzed via electrospray ionization (ESI) on an AB Sciex API-4000 (Foster City, CA) triple-quadrupole instrument that was coupled with Shimadzu LC-10AD pumps (Columbia, MD) and a Leap Technologies CTC PAL auto-sampler (Carrboro, NC). Analytes were separated by gradient elution using a Fortis C18 3.0 x 50 mm, 3 μ m column (Fortis Technologies Ltd, Cheshire, UK) thermostated at 40 °C. HPLC mobile phase A was 0.1% formic acid in water (pH unadjusted), mobile phase B was 0.1% formic acid in acetonitrile (pH unadjusted). The gradient started at 10% B after a 0.2 min hold and was linearly increased to 90% B over 1.2 min; held at 90% B for 0.1 min and returned to 10% B in 0.1 min followed by a re-equilibration (0.9 min). The total run time was 2.5 min and the HPLC flow rate was 0.5 mL/min. The source temperature was set at 500 °C and mass spectral analyses were performed using multiple reaction monitoring (MRM), with transitions specific for each compound utilizing a Turbo-Ionspray® source in positive ionization mode (5.0 kV spray voltage).

In Vivo PK Methods

All rodent PK experiments were conducted in accordance with the National Institute of Health regulations of animal care covered in Principles of Laboratory Animal Care (National Institutes of Health publication 85-23, revised 1985) and were approved by the Institutional Animal Care and Use Committee.

Time Course PK and Single Time Point Tissue Distribution Studies

IV cassette PK experiments in rats were carried out according to methods described previously.⁸⁶ Briefly, a cassette of compounds (n = 4–5/cassette) were formulated from 10 mM solutions of compounds in DMSO. In order to reduce the absolute volume of DMSO that was administered, the compounds were combined and diluted with ethanol and PEG 400 to achieve a final concentration of 0.4–0.5 mg/mL for each compound (2 mg/mL total) administered in each cassette. The final dosing solutions consisted of approximately 10% ethanol, 40% PEG400, and 50% DMSO (v/v). For time course PK studies, each cassette dose was administered IV via the jugular vein to two dual-cannulated (carotid artery and jugular vein) adult male Sprague–Dawley rats, each weighing between 250 and 350 g (Harlan, Indianapolis, IN) for a final dose of 0.2–0.25 mg/kg per compound. Whole blood collections via the carotid artery were performed at 0.033, 0.117, 0.25, 0.5, 1, 2, 4, 7, and 24 hours post dose and plasma samples prepared for bioanalysis. For single time point tissue distribution studies, compounds were formulated as described above (in cassette format) and dosed to male Sprague-Dawley rats for a final dose of 0.2–0.25 mg/kg per compound. Brain dissection and blood collections via the carotid artery were performed 0.25 hr post dose. The brain samples were rinsed in PBS, snap frozen and stored at -80 °C. Prior to LC/MS/MS analysis, brain samples were thawed to room temperature and subjected to mechanical homogenation employing a Mini-Beadbeater™ and 1.0 mm Zirconia/Silica Beads (BioSpec Products).

Mouse Tissue Distribution Studies

Tissue distribution studies with compound-in mice were performed by formulating the compound in 20% BCD and dosing via intraperitoneal injection to 20 week old male C57/Bl6 mice (3-4 per time point). At 0.5 hours post dose, animals were euthanized and decapitated, blood was collected via cardiac puncture and the brains were removed, thoroughly washed in cold phosphate-buffered saline, and immediately frozen on dry ice.

Plasma and Brain Sample Preparation

Plasma was separated by centrifugation (4000 rcf, 4 °C) and stored at –80 °C until analysis. On the day of analysis, frozen whole brains were weighed and diluted with 1:3 (w/w) parts of 70:30 isopropanol:water. The mixture was then subjected to mechanical homogenation employing a Mini-Beadbeater™ and 1.0 mm Zirconia/Silica Beads (BioSpec Products) followed by centrifugation. The sample extraction of plasma (20 µL) or brain homogenate (20 µL) was performed by a method based on protein precipitation using three volumes of ice-cold acetonitrile containing an internal standard (50 ng/mL carbamazepine). The samples were centrifuged (3000 rcf, 5 min) and supernatants transferred and diluted 1:1 (supernatant: water) into a new 96-well plate, which was then sealed in preparation for LC/MS/MS analysis.

LC/MS/MS Bioanalysis of Samples from In Vivo Assays

In vivo samples were analyzed via electrospray ionization (ESI) on an AB Sciex API-4000 (Foster City, CA) triple-quadrupole instrument that was coupled with Shimadzu LC-10AD pumps (Columbia, MD) and a Leap Technologies CTC PAL auto-sampler (Carrboro, NC). Analytes were separated by gradient elution using a Fortis C18 3.0 x 50 mm, 3 µm column (Fortis Technologies Ltd, Cheshire, UK) thermostated at 40

°C. HPLC mobile phase A was 0.1% formic acid in water (pH unadjusted), mobile phase B was 0.1% formic acid in acetonitrile (pH unadjusted). The source temperature was set at 500 °C and mass spectral analyses were performed using multiple reaction monitoring (MRM), with transitions specific for each compound utilizing a Turbo-Ionspray® source in positive ionization mode (5.0 kV spray voltage). The calibration curves were constructed, and linear response was obtained by spiking known amounts of test compound in blank brain homogenate or plasma. All data were analyzed using AB Sciex Analyst software v1.5.1. The final PK parameters were calculated by noncompartmental analysis using Phoenix (version 6.2) (Pharsight Inc., Mountain View, CA).

Eurofins Lead Profiling Data

A radioligand binding panel of 68 targets (GPCRs, ion channels, transporters, and nuclear hormones) with data reported as % inhibition of radioligand binding at a 10 µM concentration of compounds from two independent determinations.

Progress Towards the Development of Metabotropic Glutamate Receptor 7

Positive Allosteric Modulators

Identification of Molecular Switch: Discovery of VU6014181

In the process of our medicinal chemistry efforts for identifying novel, small molecule mGlu₇ NAM tool compounds, the optimization of multiple mGlu₇ NAM scaffolds was initiated. Scientists in our Cool Springs facility focused on the optimization of VU6009339 (**2.17**), a weak mGlu₇ NAM (**Figure 2.4**). Through their efforts, it was discovered that the replacement of the ethyl ester functionality of **2.17** for a nitrile group at the 3-position of the quinoline ring resulted in the formation of an mGlu₇ PAM, VU6014181 (**2.18**) (**Figure 2.4**). Subtle chemical modifications to a ligand that change the mode of pharmacology are known as ‘molecular switches’ and have been reported in the literature for other mGlu receptors.⁹² These molecular switches are thought to change a ligand’s mode of binding to a receptor’s allosteric site and stabilize different conformations of the receptor. In this case, binding of the mGlu₇ PAM stabilizes a conformation of mGlu₇ that potentiates the effect of glutamate on this receptor. **2.18** was

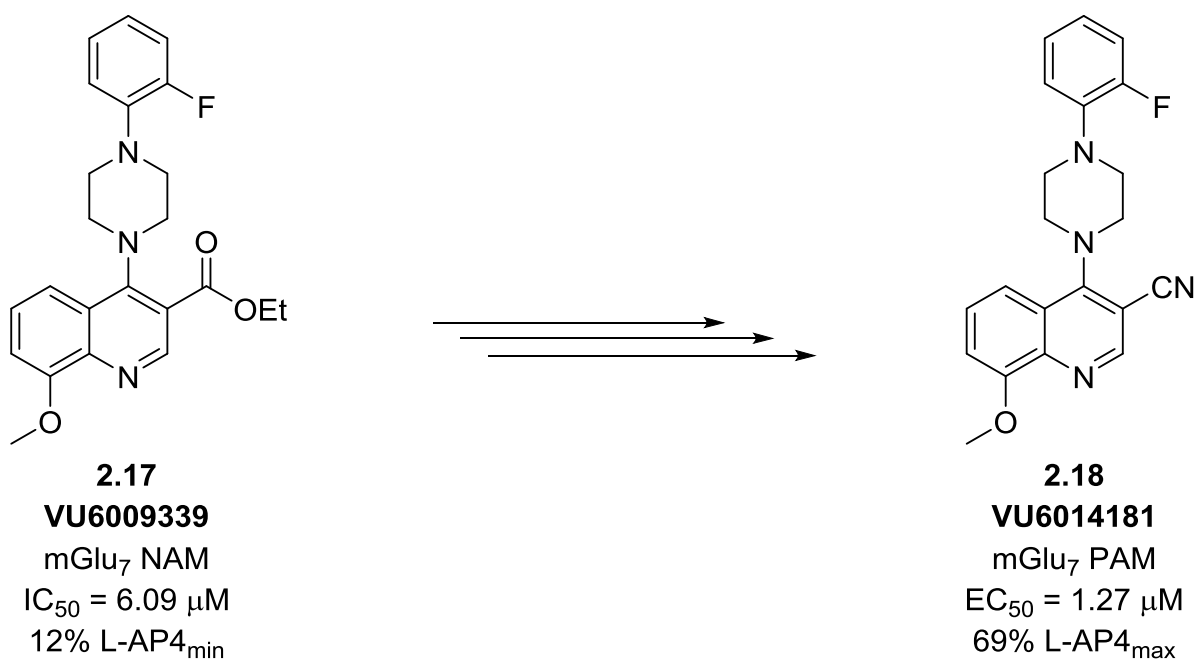


Figure 2.4: Structures of the mGlu₇ NAM VU6009339 (**2.17**) and the molecular switch mGlu₇ PAM VU6014181 (**2.18**)

found to be highly selective for mGlu₇ (mGlu_{1,2,3,4,5,6,8} EC₅₀ > 10 μM). However, in a Eurofins lead profiling panel, **2.18** was found to significantly inhibit the human dopamine transporter (DAT) with an IC₅₀ = 0.54 μM (**Table 2.1**).

Target/Protein	Species	% Inhibition
Adenosine A ₁	Human	34
Adenosine A _{2A}	Human	34
Adenosine A ₃	Human	39
Adrenergic α _{1A}	Rat	40
Adrenergic α _{1B}	Rat	13
Adrenergic α _{1D}	Human	13
Adrenergic α _{2A}	Human	20
Adrenergic β ₁	Human	7
Adrenergic β ₂	Human	2
Androgen (Testosterone)	Human	8
Bradykinin B ₁	Human	19
Bradykinin B ₂	Human	9
Calcium Channel L-Type, Benzothiazepine	Rat	16
Calcium Channel L-Type, Dihydropyridine	Rat	-5
Calcium Channel N-Type	Rat	19
Cannabinoid CB ₁	Human	19
Dopamine D ₁	Human	17
Dopamine D _{2S}	Human	10
Dopamine D ₃	Human	-3
Dopamine D _{4.2}	Human	6
Endothelin ET _A	Human	4
Endothelin ET _B	Human	3
Epidermal Growth Factor (EGF)	Human	-5
Estrogen Era	Human	9
GABA _A , Flunitrazepam, Central	Rat	-1
GABA _A , Muscimol, Central	Rat	5
GABA _{B1A}	Human	1
Glucocorticoid	Human	15
Glutamate, Kainate	Rat	-8
Glutamate, NMDA, Agonism	Rat	3
Glutamate, NMDA, Glycine	Rat	6
Glutamate, NMDA, Phencyclidine	Rat	21
Histamine H ₁	Human	4
Histamine H ₂	Human	-10

Histamine H ₃	Human	-14
Imidazoline I ₂ , Central	Rat	34
Interleukin IL-1	Mouse	-20
Leukotriene, Cysteinyl CysLT ₁	Human	0
Melatonin MT ₁	Human	43
Muscarinic M ₁	Human	13
Muscarinic M ₂	Human	6
Muscarinic M ₃	Human	-4
Neuropeptide Y Y ₁	Human	0
Neuropeptide Y Y ₂	Human	-2
Nicotinic Acetylcholine	Human	0
Nicotinic Acetylcholine α 1, Bungarotoxin	Human	-5
Opiate δ ₁ (OP1, DOP)	Human	-1
Opiate κ (OP2, KOP)	Human	14
Opiate μ (OP3, MOP)	Human	9
Phorbol Ester	Mouse	12
Platelet Activating Factor (PAF)	Human	-4
Potassium Channel [K _{ATP}]	Hamster	4
Potassium Channel hERG	Human	-3
Prostanoid EP ₄	Human	15
Purinergic P2X	Rabbit	-14
Rolipram	Rat	16
Serotonin (5-HT _{1A})	Human	2
Serotonin (5-HT _{2B})	Human	36
Serotonin (5-HT ₃)	Human	-5
Sigma σ ₁	Human	31
Sodium Channel, Site 2	Rat	42
Tachykinin NK ₁	Human	12
Thyroid Hormone	Rat	13
Transporter, Dopamine (DAT)	Human	85
Transporter, GABA	Rat	8
Transporter, Norepinephrine (NET)	Human	18
Transporter, Serotonin (SERT)	Human	-6

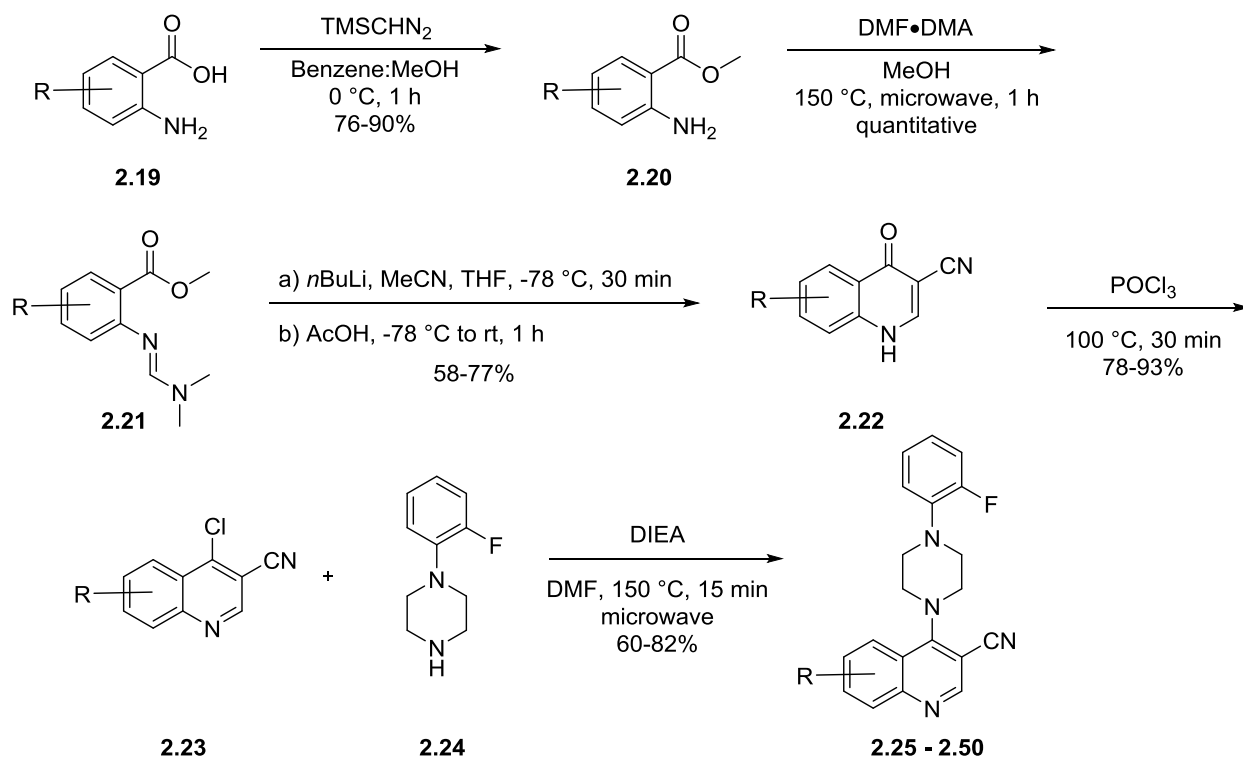
Table 2.1: Eurofins lead profiling panel of VU6014181 (**2.18**). Significant activity is defined as >50% inhibition at a 10 μ M concentration of **2.18**. Data courtesy of Eurofins.

Even though **2.18** showed off-target activity at the DAT, we wanted to further explore this quinoline PAM scaffold, as this was the first mGlu₇ PAM chemotype with full

mGlu receptor selectivity. Through our optimization efforts, we hope to not only improve the potency and efficacy of related analogs, but we also hoped to engender selectivity against human DAT. Therefore, the remaining sections of this chapter will summarize the optimization efforts that both myself and Jacob Kalbfleisch have achieved thus far.

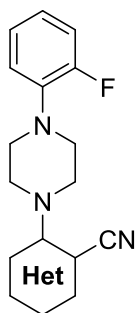
SAR of Western Heterocyclic Ring

To begin our optimization campaign, we elected to first observe what effects different substituted heterocycles would have on mGlu₇ activity. The synthesis of analogs of this nature is depicted below in **Scheme 2.1**. Anthranilic acids **2.19** are reacted with TMS diazomethane to form methyl esters **2.20** in 76-90% yield. Treatment of **2.20** with DMF•DMA under microwave irradiation resulted in the formation of amidines **2.21**. Crude amidines **2.21** are reacted with the conjugate base of acetonitrile



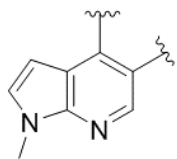
Scheme 2.1: SAR of western heterocyclic ring: synthesis of analogs **2.25-2.50**

(formed from the deprotonation of acetonitrile with *n*-BuLi) followed by subsequent treatment with acetic acid to form quinolones **2.22** in moderate to good yields (58-77%).⁹³ Quinolones **2.22** are then heated to 100 °C in neat POCl₃ to form chloroquinolines **2.23** in 78-93% yield. An S_NAr reaction between **2.23** and substituted piperazine **2.24** yielded analogs **2.25-2.50** in good yields (60-82%). The results of this SAR campaign are shown below in **Table 2.2**.



2.25 - 2.50

Het	Compound Number	VOID	mGlu ₇ EC ₅₀ (μM)	mGlu ₇ % L-AP ₄ _{max}
	2.25	VU6026235	Inactive	N/A
	2.26	VU6026236	Inactive	N/A
	2.27	VU6026237	Inactive	N/A

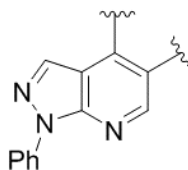


2.28

VU6026238

> 10

30%

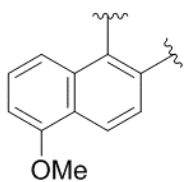


2.29

VU6026500

Inactive

N/A

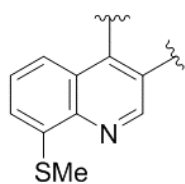


2.30

VU6026510

Inactive

N/A

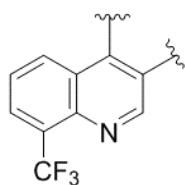


2.31

VU6026502

Inactive

N/A

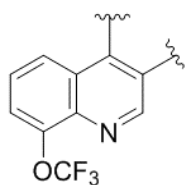


2.32

VU6026498

Inactive

N/A

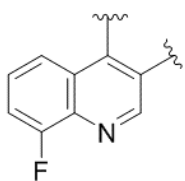


2.33

VU6026499

> 10

48%

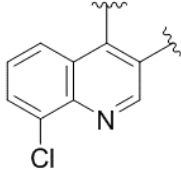
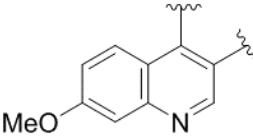
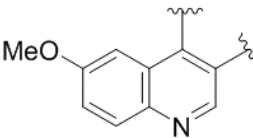
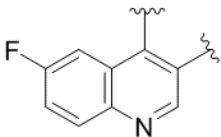
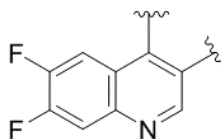
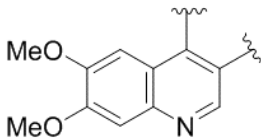
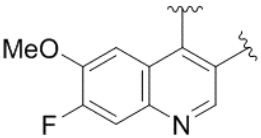


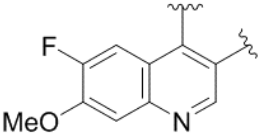
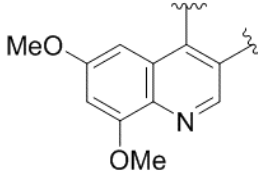
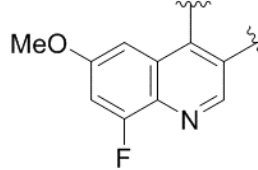
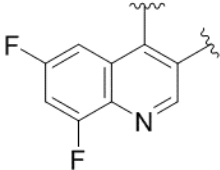
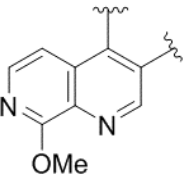
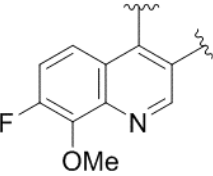
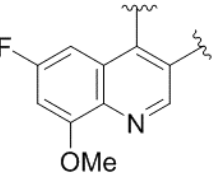
2.34

VU6026503

4.02

29%

	2.35	VU6026507	> 10	42%
	2.36	VU6026505	> 10	64%
	2.37	VU6026508	Inactive	N/A
	2.38	VU6027580	> 10	80%
	2.39	VU6027581	Inactive	N/A
	2.40	VU6027578	> 10	38%
	2.41	VU6027579	Inactive	N/A

	2.42	VU6027582	Inactive	N/A
	2.43	VU6027445	> 10	67%
	2.44	VU6027449	Inactive	N/A
	2.45	VU6027461	Inactive	N/A
	2.46	VU6027260	Inactive	N/A
	2.47	VU6026241	1.79	53%
	2.48	VU6026243	1.4	99%

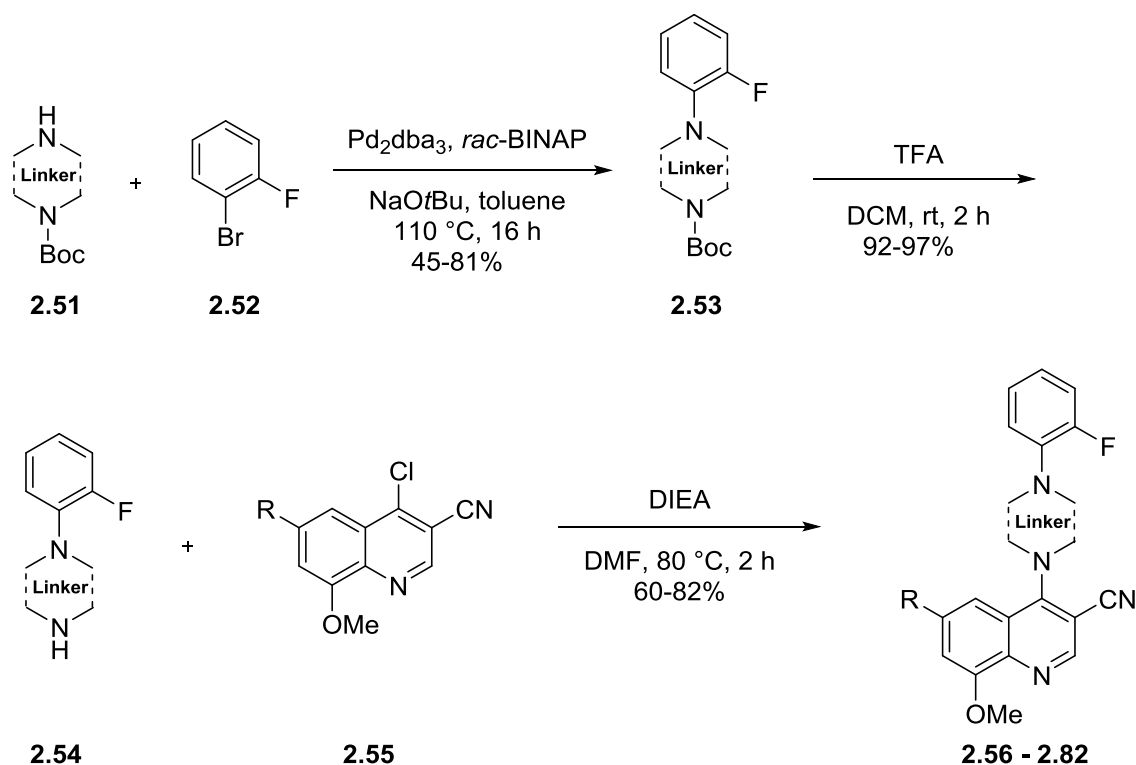
	2.49	VU6026242	> 10	35%
	2.50	VU6027447	1.11	62%

Table 2.2: SAR of western heterocyclic ring: analogs **2.25-2.50**

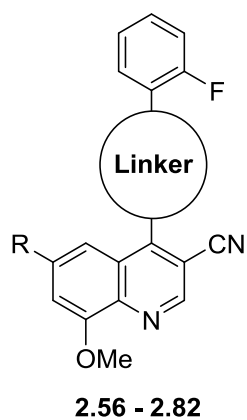
Unfortunately, steep SAR was observed in analogs **2.25-2.50**. The incorporation of quinoline bioisosteres (analog **2.25-2.29**) led to total loss of mGlu₇ activity. The nitrogen atom of the quinoline was found to be essential, as the anthracene analog **2.30** was inactive. The incorporation of electron withdrawing substituents at the 8-position of the quinoline ring (analog **2.31-2.35**) was not conducive for potency. A survey of alternative substituent patterns around the quinoline ring (analog **2.36-2.45**) led to either inactive or low potency compounds. Even the incorporation of azaheterocycles (analog **2.46**) was not tolerated. Fortunately, a fluorine walk around the quinoline ring was productive. We observed that the incorporation of a fluorine atom was tolerated in both the 7-position (analog **2.47**) and the 6-position (analog **2.48**) of the quinoline ring, while fluorine atom incorporation at the 5-position (analog **2.49**) led to a dramatic loss in potency. Due to the increased efficacy of **2.48** (99% L-AP₄_{max}), we decided that the incorporation of a fluorine atom at the 6-position was beneficial, and we would elect to pursue both 6-fluoro and des-fluoro analogs within our future SAR campaigns.

SAR of Piperazine Linkers

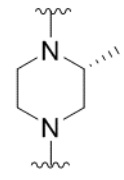
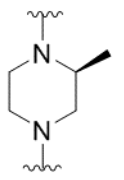
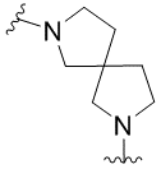
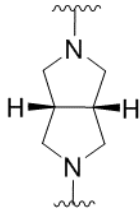
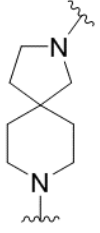
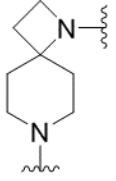
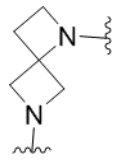
Next, we wanted to see if piperazine isosteres or alternative amine linkers were tolerated within this chemotype. Therefore, we initiated the synthesis of analogs of this nature, as shown in **Scheme 2.2**. Buchwald-Hartwig coupling of amines **2.51** with 2-fluorobromobenzene **2.52** yielded aryl amines **2.53** in 45-81% yield. Boc-deprotection of **2.53** with trifluoroacetic acid formed amines **2.54**, which underwent a subsequent S_NAr reaction with chloroquinolines **2.55** to afford analogs **2.56-2.82** in good yield. The results of this SAR campaign are shown below in **Table 2.3**.


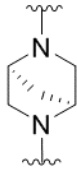
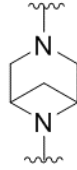
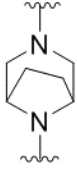
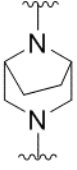
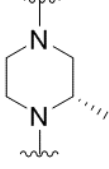
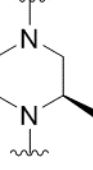
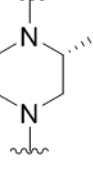


Scheme 2.2: SAR of piperazine linkers: analogs **2.56-2.82**



R	Linker	Compound Number	VOID	mGlu ₇ EC ₅₀ (μM)	mGlu ₇ % L-AP ₄ _{max}
H		2.56	VU6026239	Inactive	N/A
H		2.57	VU6026240	Inactive	N/A
H		2.58	VU6027456	Inactive	N/A
H		2.59	VU6026504	Inactive	N/A
H		2.60	VU6026511	> 10	33%

H		2.61	VU6026509	Inactive	N/A
H		2.62	VU6026506	3.11	50%
H		2.63	VU6026493	Inactive	N/A
H		2.64	VU6026494	Inactive	N/A
H		2.65	VU6026495	Inactive	N/A
H		2.66	VU6026496	> 10	35%
H		2.67	VU6026497	Inactive	N/A

H		2.68	VU6027448	Inactive	N/A
H		2.69	VU6027466	Inactive	N/A
H		2.70	VU6027465	Inactive	N/A
H		2.71	VU6027453	Inactive	N/A
H		2.72	VU6027468	Inactive	N/A
F		2.73	VU6027269	Inactive	N/A
F		2.74	VU6027277	> 10	36%
F		2.75	VU6027274	Inactive	N/A

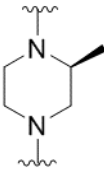
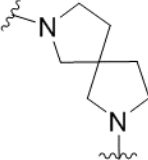
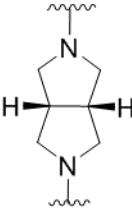
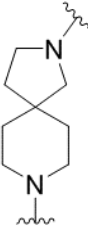
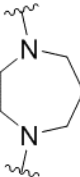

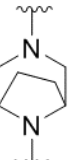
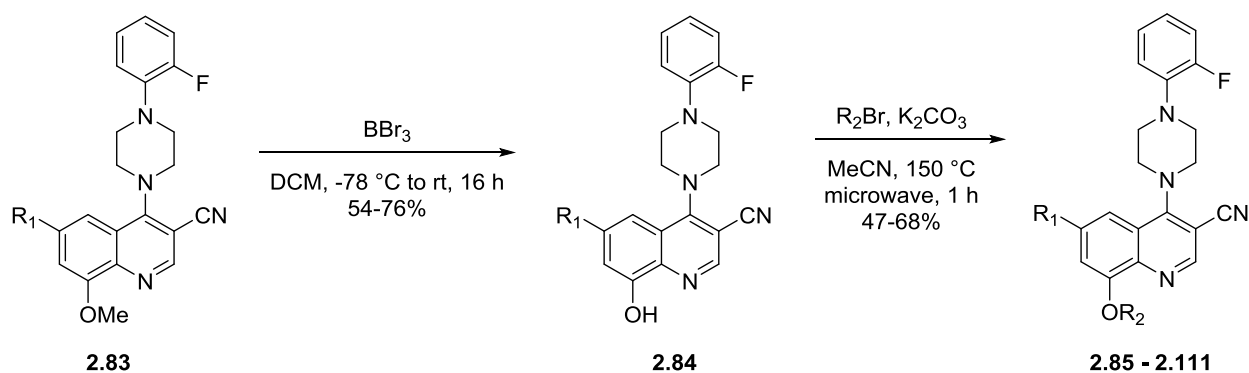
F		2.76	VU6027267	1.89	63%
F		2.77	VU6027462	Inactive	N/A
F		2.78	VU6027463	Inactive	N/A
F		2.79	VU6027464	Inactive	N/A
F		2.80	VU6027458	Inactive	N/A
F		2.81	VU6027451	> 10	48%
F		2.82	VU6027455	Inactive	N/A

Table 2.3: SAR of piperazine linkers: analogs **2.56-2.82**

As observed before with the SAR of the western heterocyclic motif, we encountered steep SAR. The incorporation of azetidine, piperazine, and diazepane heterocycles (analogs **2.56-2.58**) led to complete loss of mGlu₇ activity. The presence of chiral methyl groups on the piperazine ring (analogs **2.59-2.62**) were not conducive for potency. Even the use of piperazine isosteres such as spirocyclic congeners (analogs **2.63-2.67**) and bicyclic congeners (analogs **2.68-2.72**) did not lead to any benefits in potency and/or efficacy. The same linkers as described above were also applied to the 6-fluoro-8-methoxyquinoline congener, which we previously identified as the best alternative substitution pattern (analogs **2.73-2.82**); however, none of these modifications led to any appreciable improvements in potency and/or efficacy.

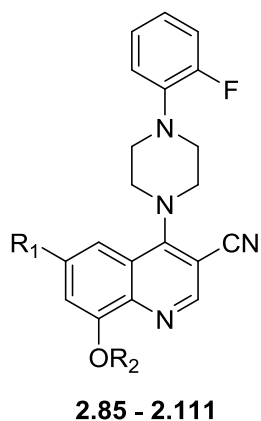
SAR of Alternative Alkoxy Groups

Similar to the optimization approach that we used for the mGlu₇ NAMs, we also investigated the incorporation of different alkoxy groups at the 8-position of the quinoline ring. In doing so, we could extend the length of our analogs in hopes of achieving a tighter fit into the allosteric site of the mGlu₇ receptor. Additionally, we were excited to test the possibility of any enantioference that the mGlu₇ receptor may possess with


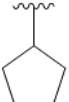
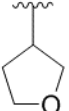
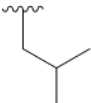
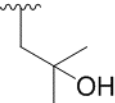

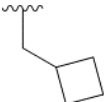
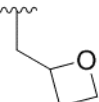
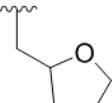
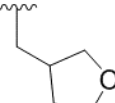
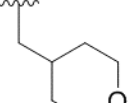



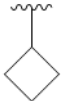
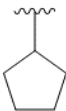
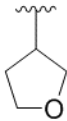
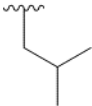

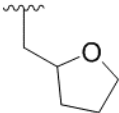
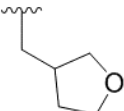
Scheme 2.3: SAR of alternative alkoxy groups: synthesis of analogs **2.85-2.111**

the incorporation of chiral alkoxy groups. Therefore, we initiated a synthetic strategy in order to arrive at compounds of this nature (**Scheme 2.3**). Methoxy-substituted quinolines **2.83** were demethylated upon treatment with boron tribromide, forming phenols **2.84** in 54-76% yield. Phenols **2.84** were then alkylated under microwave conditions using alkyl bromides to form alkoxy-substituted quinolines **2.85-2.111** in moderate to good yields (47-68% yield). The results from this SAR campaign are summarized below in **Table 2.4**.



R ₁	R ₂	Compound Number	UUID	mGlu ₇ EC ₅₀ (μM)	mGlu ₇ % L-AP ₄ _{max}
H	H	2.85	VU6027261	> 10	90%
H	CD ₃	2.86	VU6027264	1.51	73%
H	CF ₂ H	2.87	VU6027259	> 10	68%
H		2.88	VU6027254	1.25	67%

H		2.89	VU6027255	1.82	67%
H		2.90	VU6027253	7.63	80%
H		2.91	VU6027271	1.3	74%
H		2.92	VU6027266	6.74	66%
H		2.93	VU6027268	> 10	73%
H		2.94	VU6026501	> 10	56%
H		2.95	VU6027252	> 10	55%
H		2.96	VU6028183	2.28	84%
H		2.97	VU6027257	4.93	80%
H		2.98	VU6027256	1.35	88%
H		2.99	VU6027258	Inactive	N/A

F	H	2.100	VU6027262	> 10	90%
F	CD ₃	2.101	VU6027459	1.13	98%
F	CF ₂ H	2.102	VU6027460	3.84	98%
F		2.103	VU6027446	0.69	88%
F		2.104	VU6027272	> 10	23%
F		2.105	VU6027273	Inactive	N/A
F		2.106	VU6027275	0.51	71%
F		2.107	VU6027695	Inactive	N/A
F		2.108	VU6027694	> 10	31%
F		2.109	VU6027583	Inactive	N/A
F		2.110	VU6027584	0.65	76%

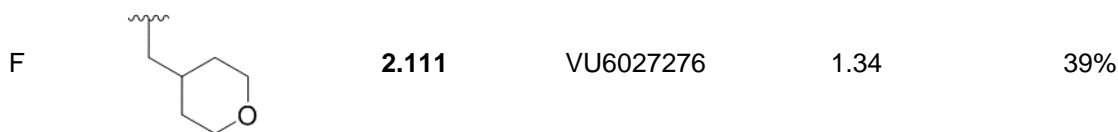
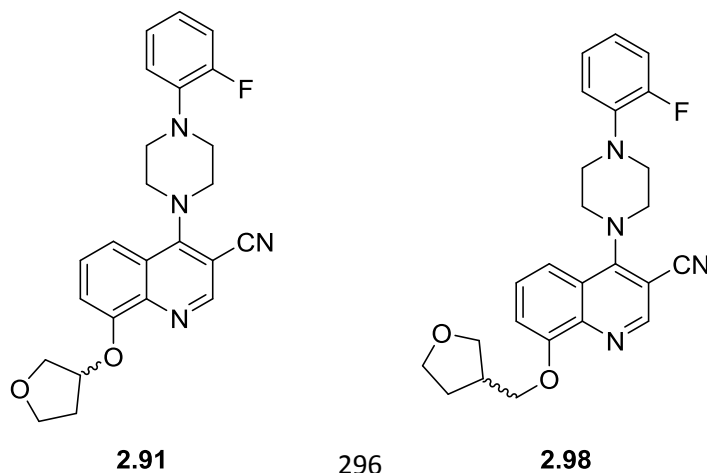


Table 2.4: SAR of alternative alkoxy groups: analogs **2.85-2.111**

To our delight, alternative alkoxy groups at the 8-position of the quinoline ring were well tolerated for both the 6-fluoro and des-fluoro quinoline motifs. In particular, we were excited about the further evaluation of **2.91** (mGlu₇ EC₅₀ = 1.30 μM, 74% L-AP4_{max}), **2.98** (mGlu₇ EC₅₀ = 1.35 μM, 88% L-AP4_{max}), **2.101** (mGlu₇ EC₅₀ = 1.13 μM, 98% L-AP4_{max}), and **2.103** (mGlu₇ EC₅₀ = 0.69 μM, 88% L-AP4_{max}). Due to their limited solubility, we decided to delay the investigation of **2.106** and **2.110** in favor of the aforementioned soluble compounds.

Since both analogs **2.91** and **2.98** possess chiral alkoxy groups, we were eager to test our enantiopreference hypothesis. The enantiomers of both **2.91** and **2.98** were separated via chiral supercritical fluid chromatography (SFC) in order to test both the (+)- and (-)-enantiomers in our cell based assays. Unfortunately, both the (+)- and (-)-enantiomers for **2.91** and **2.98** possessed comparable potency and efficacy values (**Table 2.5**). These data indicate that an enantiopreference does not exist for **2.91** and **2.98**.

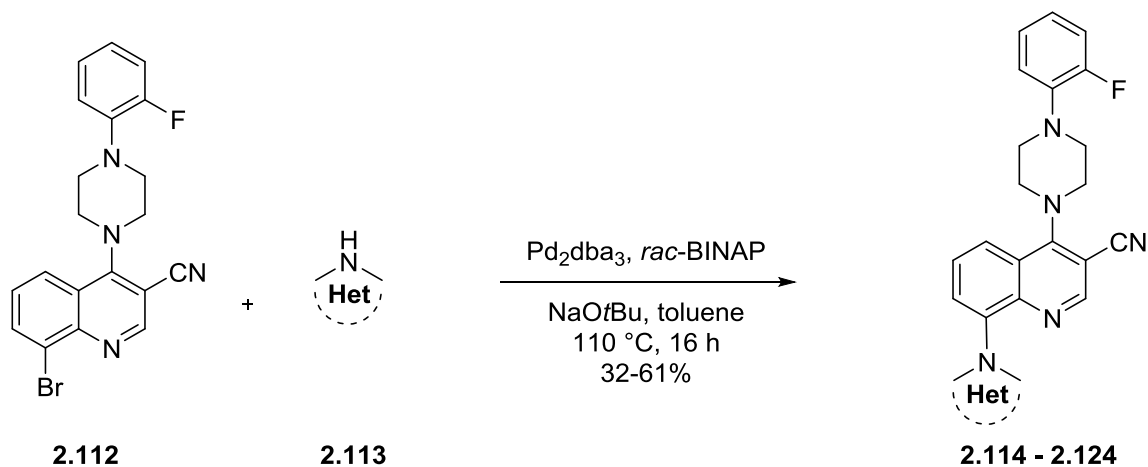


Parent Compound	Stereoisomer	VOID	mGlu ₇ EC ₅₀ (μM)	mGlu ₇ % L-AP ₄ _{max}
2.91	(+)	VU6028358	1.11	85%
2.91	(-)	VU6028359	1.17	70%
2.98	(+)	VU6028357	1.99	77%
2.98	(-)	VU6028356	1.33	89%

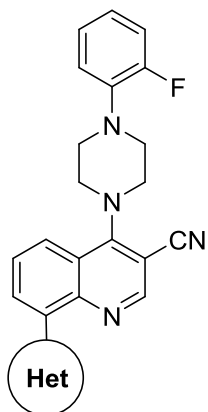
Table 2.5: SAR of enantiomers of both **2.91** and **2.98**

SAR of Buchwald-Hartwig Library

Given the success of examining alternative alkoxy groups at the 8-position of the quinoline ring, we also wanted to explore incorporating different amino groups at this 8-position. In order to synthesize analogs of this nature, we developed the synthetic route as shown in **Scheme 2.4**. 8-bromoquinoline **2.112** was reacted with azaheterocycles **2.113** in a Buchwald-Hartwig coupling reaction to form analogs **2.114-2.124**. The results of this SAR campaign are summarized below in **Table 2.6**.



Scheme 2.4: Synthesis of alternative 8-aminoquinoline analogs **2.114-2.124**



2.114 - 2.124

Het	Compound Number	VOID	mGlu ₇ EC ₅₀ (μM)	mGlu ₇ % L-AP ₄ _{max}
	2.114	VU6028180	Inactive	N/A
	2.115	VU6028179	6.73	81%
	2.116	VU6028182	Inactive	N/A
	2.117	VU6027467	Inactive	N/A
	2.118	VU6027588	Inactive	N/A

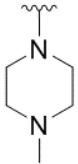
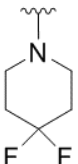
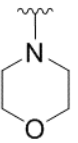
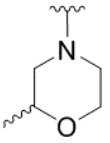
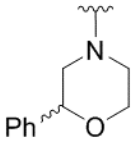
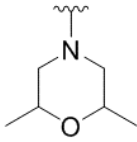
	2.119	VU6027592	> 10	70%
	2.120	VU6028195	Inactive	N/A
	2.121	VU6027452	1.31	74%
	2.122	VU6028192	7.14	84%
	2.123	VU6028193	Inactive	N/A
	2.124	VU6027707	9.31	74%

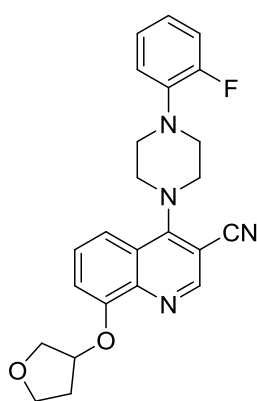
Table 2.6: SAR of 8-aminoquinoline analogs **2.114-2.124**

We found that the incorporation of unsaturated azacines such as pyrazole, imidazole, and 1,2,4-triazole heterocycles led to either loss of activity at mGlu₇ or a dramatic loss of potency (analog **2.114-2.116**). The incorporation of saturated

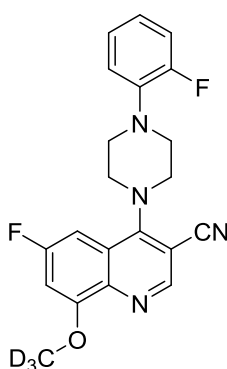
heterocycles such as pyrrolidine, piperidine, *N*-Me piperazine, and geminal-difluoropiperidine heterocycles (analogs **2.117-2.120**) were not conducive for potency. Surprisingly, the morpholino analog **2.121** possessed comparable potency and efficacy to our initial molecular switch lead **2.18**. Unfortunately, substitutions on the morpholine ring appeared to hinder the potency of these compounds (analogs **2.122-2.124**).

Identification of Potential *In Vivo* Tool Compounds

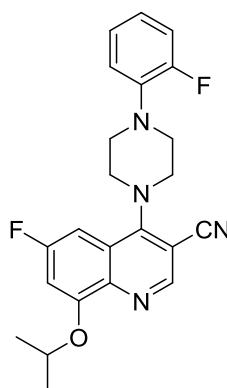
Given the SAR data we have collected thus far, we chose four of our most potent compounds (**2.91**, **2.101**, **2.103**, and **2.121**) to examine further. We hypothesized that through our SAR efforts, we would be able to eliminate the off-target activity at human DAT. To our delight, we were pleased to find that these compounds did not show off-target activity at human DAT, based on radioligand binding assays performed by Eurofins. In order to select viable options for an *in vivo* tool compound, we also wanted to examine the rat *in vivo* PK properties of these molecules (summarized in **Table 2.7**).



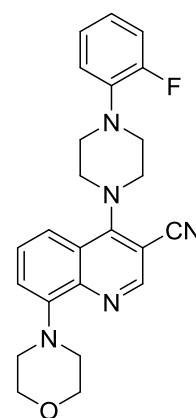
2.91
VU6027271
EC₅₀ = 1.30 μM
74% L-AP₄_{max}



2.101
VU6027459
EC₅₀ = 1.13 μM
98% L-AP₄_{max}



2.103
VU6027446
EC₅₀ = 0.69 μM
88% L-AP₄_{max}



2.121
VU6027452
EC₅₀ = 1.31 μM
74% L-AP₄_{max}

DMPK Parameter	2.91	2.101	2.103	2.121
plasma f_u	0.033	0.010	0.005	0.011
brain f_u	0.006	0.002	0.001	0.002
CL _p (mL/min/kg)	209	79.3	105	85.1
$t_{1/2}$ (min)	31.2	126	149	126
V _{ss} (L/kg)	8.54	8.34	11.5	8.10
K _p	4.36	4.78	4.99	6.84
K _{p_{uu}}	0.79	0.96	1.00	1.24

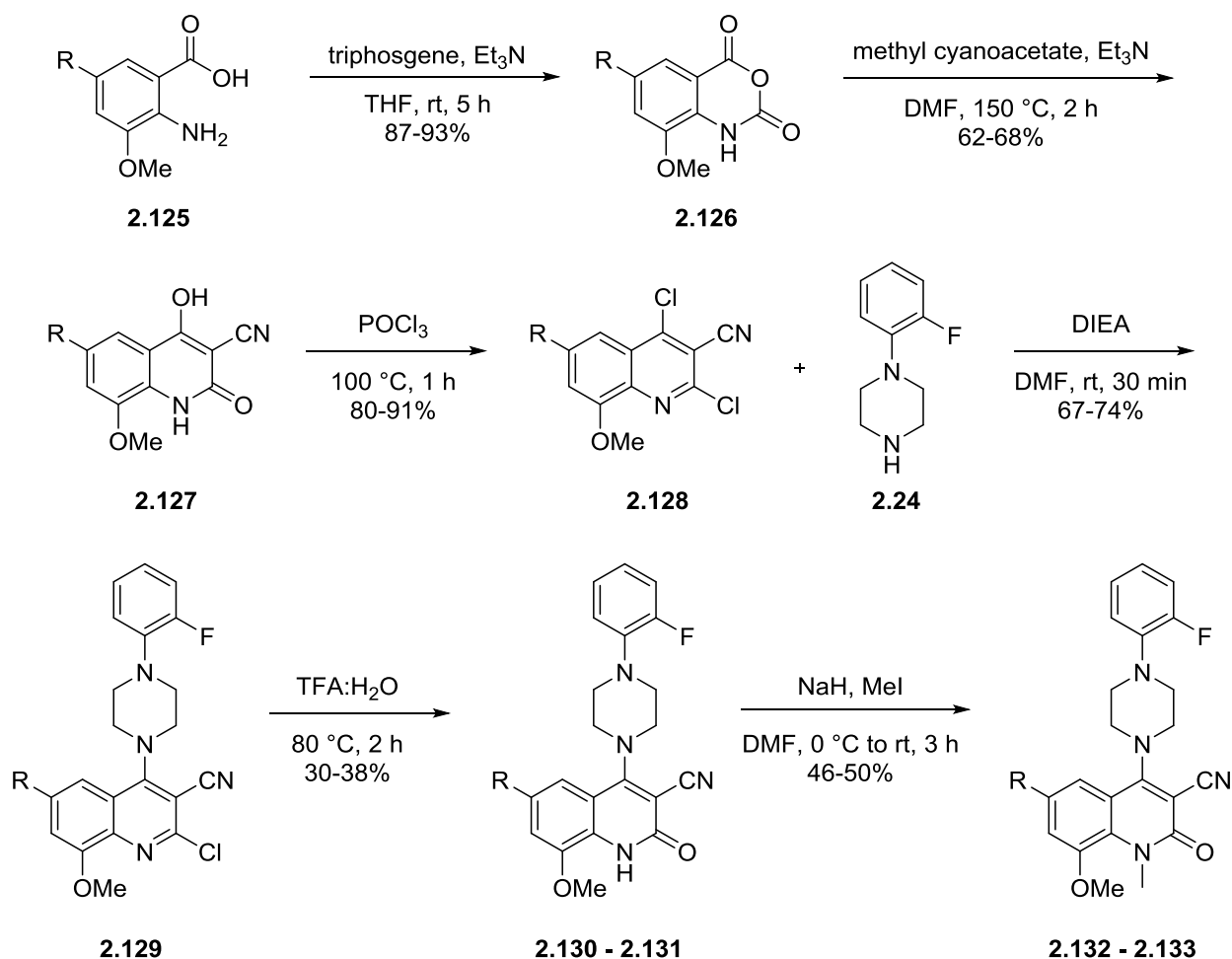
Table 2.7: Rat *in vivo* PK parameters for potential tool compounds **2.91**, **2.101**, **2.103**, and **2.121**

Although these compounds show high clearance in rats, they readily cross the blood brain barrier ($K_p > 4$ for all compounds) and possess large volumes of distribution at steady state ($V_{ss} > 8$ L/kg for all compounds). Therefore, even though oral administration is ruled out, intraperitoneal administration for these compounds should be sufficient for achieving concentrations within their respective *in vitro* EC₅₀ values. Additional mGlu selectivity assays for these compounds are underway and will be disclosed in future reports.

Addressing Potential Metabolic Sites of Quinoline Scaffold

Given the high *in vivo* clearance of **2.91**, **2.101**, **2.103**, and **2.121**, we wanted to mitigate this by examining the potential sites of metabolism for this quinoline scaffold en route to improved tool compounds. To name a few, we hypothesized that potential AO (aldehyde oxidase) metabolism may include oxidation of either the 2-position of the quinoline ring or oxidation of the quinoline nitrogen atom. While metabolic identification studies are currently underway for these compounds, we wanted to test out our metabolic hypotheses.

First, we wanted to investigate the potential oxidation at the 2-position of the quinoline ring to form substituted quinolone derivatives. To aid in the future identification of potential metabolites, the synthesis of these quinolones is paramount for validation of the metabolic ID studies. Analogs of this nature were synthesized according to **Scheme 2.5**. Anthranilic acids **2.125** were treated with triphosgene to form isatoic anhydrides **2.126** in excellent yield. Subsequent reaction with methyl cyanoacetate and triethylamine yielded quinolones **2.127**, which upon treatment with POCl₃ formed dichloroquinolines **2.128**. A regioselective S_NAr reaction of **2.128** with aryl piperazine **2.24** resulted in the formation of chloroquinolines **2.129**. Acidic hydrolysis of **2.129** with



Scheme 2.5: Synthesis of quinolone analogs **2.130-2.131** and *N*-methyl quinolones **2.132-2.133**

aqueous trifluoroacetic acid yielded the desired quinolones **2.130-2.131**. Additionally, we wanted to explore whether *N*-methyl quinolone derivatives would show activity at mGlu₇. Therefore, subsequent chemoselective *N*-methylation was accomplished with sodium hydride and methyl iodide to form the *N*-methyl quinolones **2.132-2.133**. Results for these compounds are shown below in **Table 2.8**. Unfortunately, none of these compounds displayed activity at the mGlu₇ receptor.

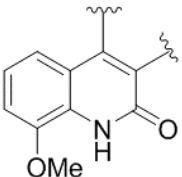
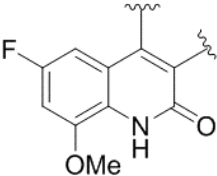
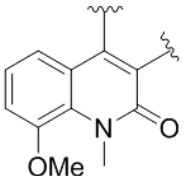
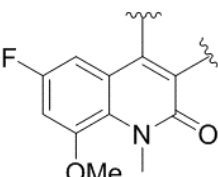
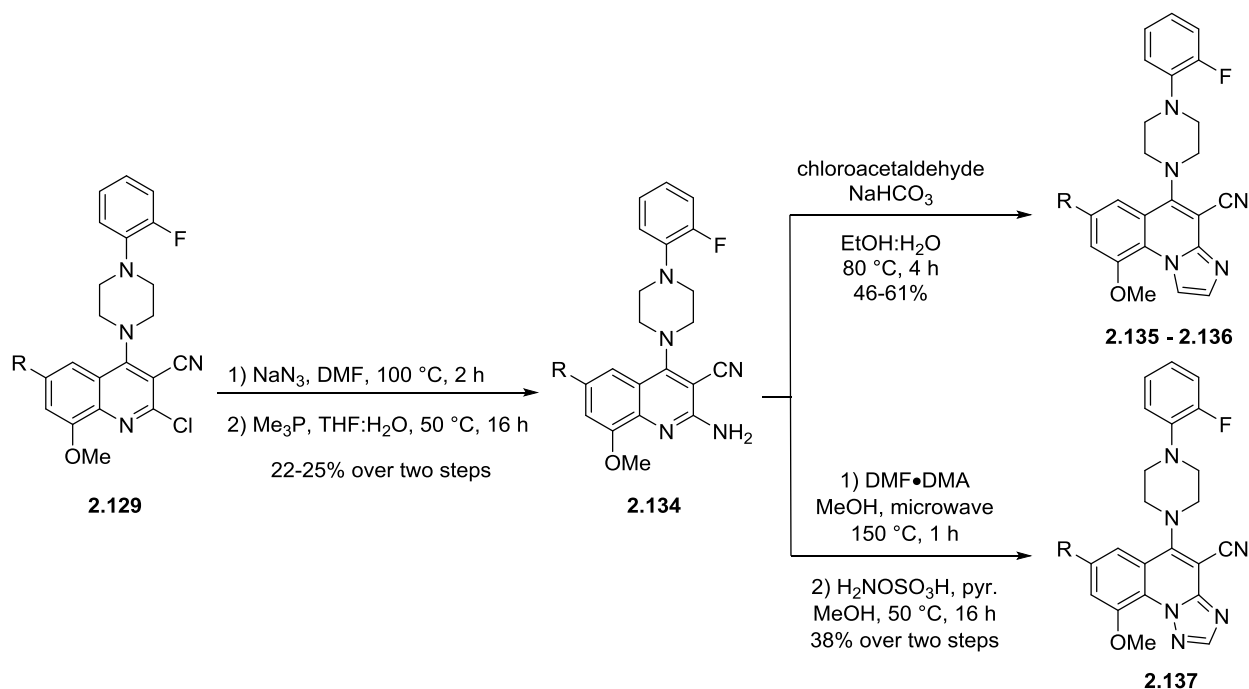
Het	Compound Number	VID	mGlu ₇ EC ₅₀ (μM)	mGlu ₇ % L-AP _{4max}
	2.130	VU6029264	Inactive	N/A
	2.131	VU6029268	Inactive	N/A
	2.132	VU6029269	Inactive	N/A
	2.133	VU6029270	Inactive	N/A

Table 2.8: SAR of quinolones **2.130-2.131** and *N*-methyl quinolones **2.132-2.133**

Next, we wanted to examine whether we could block the potential oxidation of the quinoline nitrogen atom via fusing imidazo- and triazolo-heterocycles between the nitrogen atom and the 2-position of the quinoline ring. Previous efforts within the VCND D have shown this to be a viable method for blocking such a mode of metabolism; therefore, the synthesis of such analogs was prioritized.⁹⁴ Analogs of this nature were synthesized according to **Scheme 2.6**. A S_NAr reaction between chloroquinolines **2.129** and sodium azide followed by Staudinger reduction with trimethylphosphine yielded aminoquinolines **2.134**. Aminoquinolines **2.134** were either reacted with chloroacetaldehyde and sodium bicarbonate to form fused imidazo-analogs **2.135-2.136** or reacted with dimethylformamide dimethylacetal and hydroxylamine O-sulfonic acid to form the fused triazolo-analog **2.137**. Results for these compounds are



Scheme 2.6: Synthesis of fused imidazo- and triazolo-heterocycles **2.135-2.137**

shown below in **Table 2.9**. Unfortunately, none of these compounds showed activity at the mGlu₇ receptor.

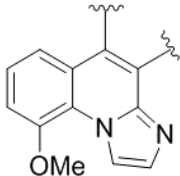
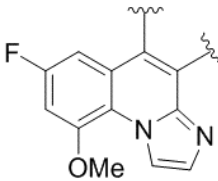
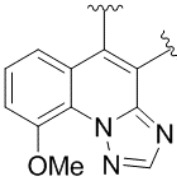
Het	Compound Number	VUID	mGlu ₇ EC ₅₀ (μM)	mGlu ₇ % L-AP ₄ _{max}
	2.135	VU6028361	Inactive	N/A
	2.136	VU6028364	Inactive	N/A
	2.137	VU6028363	Inactive	N/A

Table 2.9: SAR of fused imidazo- and triazolo-heterocycles **2.135-2.137**

Conclusions/Future Directions

Given these data, further exploration into the potential metabolites of our quinoline scaffold is warranted. In particular, we are interested in incorporating a deuterium atom at the 2-position of our quinoline scaffold. By doing so, we can hopefully improve upon the high clearance of first-generation analogs (**2.91**, **2.101**, **2.103**, and **2.121**) via slowing down potential oxidation of the quinoline heterocycle at this position. Additional mGlu selectivity assays and mouse *in vivo* PK experiments are still needed

for **2.91**, **2.101**, **2.103**, and **2.121** before selecting a suitable tool compound for use in either *in vitro* electrophysiology validation experiments or *in vivo* mouse models of RTT. These chemistry efforts will be pioneered by graduate student Jacob Kalbfleisch and will be disclosed in future reports.

Experimental Methods

General Synthetic Methods and Instrumentation

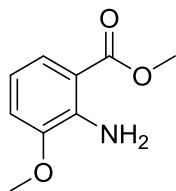
All NMR spectra were recorded on a 400 MHz AMX Bruker NMR spectrometer. ¹H and ¹³C chemical shifts are reported in δ values in ppm downfield with the deuterated solvent as the internal standard. Data are reported as follows: chemical shift, multiplicity (s = singlet, d = doublet, t = triplet, q = quartet, b = broad, m = multiplet), integration, coupling constant (Hz). Low resolution mass spectra were obtained on an Agilent 6120 or 6150 with ESI source. MS parameters were as follows: fragmentor: 70, capillary voltage: 3000 V, nebulizer pressure: 30 psig, drying gas flow: 13 L/min, drying gas temperature: 350 °C. Samples were introduced via an Agilent 1290 UHPLC comprised of a G4220A binary pump, G4226A ALS, G1316C TCC, and G4212A DAD with ULD flow cell. UV absorption was generally observed at 215 nm and 254 nm with a 4 nm bandwidth. Column: Waters Acquity BEH C18, 1.0 x 50 mm, 1.7 μ m. Gradient conditions: 5% to 95% CH₃CN in H₂O (0.1% TFA) over 1.4 min, hold at 95% CH₃CN for 0.1 min, 0.5 mL/min, 55 °C. High resolution mass spectra were obtained on an Agilent 6540 UHD Q-TOF with ESI source. MS parameters were as follows: fragmentor: 150, capillary voltage: 3500 V, nebulizer pressure: 60 psig, drying gas flow: 13 L/min, drying

gas temperature: 275 °C. Samples were introduced via an Agilent 1200 UHPLC comprised of a G4220A binary pump, G4226A ALS, G1316C TCC, and G4212A DAD with ULD flow cell. UV absorption was observed at 215 nm and 254 nm with a 4 nm bandwidth. Column: Agilent Zorbax Extend C18, 1.8 µm, 2.1 x 50 mm. Gradient conditions: 5% to 95% CH₃CN in H₂O (0.1% formic acid) over 1 min, hold at 95% CH₃CN for 0.1 min, 0.5 mL/min, 40 °C. For compounds that were purified on a Gilson preparative reversed-phase HPLC, the system comprised of a 333 aqueous pump with solvent-selection valve, 334 organic pump, GX-271 or GX-281 liquid handler, two column switching valves, and a 155 UV detector. UV wavelength for fraction collection was user-defined, with absorbance at 254 nm always monitored. Method 1: Phenomenex Axia-packed Luna C18, 30 x 50 mm, 5 µm column. Mobile phase: CH₃CN in H₂O (0.1% TFA). Gradient conditions: 0.75 min equilibration, followed by user defined gradient (starting organic percentage, ending organic percentage, duration), hold at 95% CH₃CN in H₂O (0.1% TFA) for 1 min, 50 mL/min, 23 °C. Method 2: Phenomenex Axia-packed Gemini C18, 50 x 250 mm, 10 µm column. Mobile phase: CH₃CN in H₂O (0.1% TFA). Gradient conditions: 7 min equilibration, followed by user defined gradient (starting organic percentage, ending organic percentage, duration), hold at 95% CH₃CN in H₂O (0.1% TFA) for 7 min, 120 mL/min, 23 °C. All reagents were purchased from Aldrich Chemical Co. and were used without purification. All final compounds were >98% pure by LCMS (254 nm, 214 nM and ELSD). Following these purification protocols, final compounds were transferred to a barcode vial and diluted to a concentration of 10 µM using molecular biology grade dimethylsulfoxide (DMSO). These

compounds were registered into Dotmatics and assigned a VU identification number before being tested in the primary screening assay.

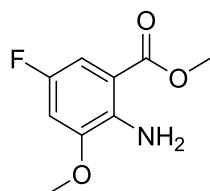
General Procedure 1: Synthesis of Methyl Esters 2.20

To a solution of the corresponding anthranilic acid (1.0 eq) in benzene (0.45 M) and methanol (1.0 M) cooled to 0 °C was added (trimethylsilyl)diazomethane (1.3 eq) (2.0 M solution in hexanes) dropwise. Upon completion of addition, the reaction was warmed to room temperature and stirred for 1 hr before being quenched with the dropwise addition of glacial acetic acid (4.0 eq). The crude reaction mixture was concentrated and purified via flash chromatography (Teledyne ISCO flash purification system; silica gel column; hexanes:EtOAc; 0-15% EtOAc gradient) to afford the desired products.



Synthesis of methyl 2-amino-3-methoxybenzoate (2.20a)

This compound was synthesized according to general procedure 1. White solid (1.07 g, 82% yield). ¹H NMR (400 MHz, CDCl₃) δ 7.48 (dd, *J* = 8.2 Hz and 1.2 Hz, 1H), 6.86 (dd, *J* = 7.8 Hz and 1.1 Hz, 1H), 6.59 (t, 1H), 5.88 (bs, 2H), 3.87 (s, 6H); ¹³C NMR (100 MHz, CDCl₃) δ = 168.8, 147.3, 141.5, 122.6, 115.0, 113.1, 110.5, 55.9, 51.6. LCMS (TOF, ES+) for C₉H₁₂NO₃ [M+H]⁺; 182.1.

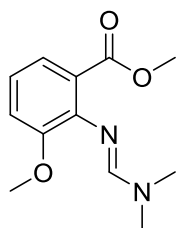


Synthesis of methyl 2-amino-5-fluoro-3-methoxybenzoate (**2.20b**)

This compound was synthesized according to general procedure 1. White solid (1.18 g, 76% yield). ^1H NMR (400 MHz, CDCl_3) δ 7.14 (dd, $J = 9.8$ Hz and 2.8 Hz, 1H), 6.65 (dd, $J = 9.6$ Hz and 2.8 Hz, 1H), 5.71 (bs, 2H), 3.86 (s, 3H), 3.85 (s, 3H); ^{13}C NMR (100 MHz, CDCl_3) $\delta = 168.1$ (d, $J_{\text{CF}} = 3.3$ Hz), 153.2 (d, $J_{\text{CF}} = 232.0$ Hz), 148.0 (d, $J_{\text{CF}} = 9.4$ Hz), 138.5, 109.0 (d, $J_{\text{CF}} = 8.7$ Hz), 106.4 (d, $J_{\text{CF}} = 23.0$ Hz), 102.9 (d, $J_{\text{CF}} = 28.0$ Hz), 56.1, 51.8. LCMS (TOF, ES+) for $\text{C}_9\text{H}_{11}\text{FNO}_3$ [M+H] $^+$; 199.9.

General Procedure 2: Synthesis of amidines **2.21**

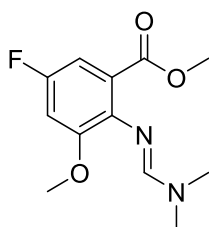
To a solution of the corresponding methyl ester **2.20** (1.0 eq) in methanol (0.55 M) in a Biotage microwave vial was added *N,N*-dimethylformamide dimethyl acetal (13.6 eq). The vial was sealed and heated to 150 °C for 1 hr using a Biotage microwave reactor. Upon cooling to room temperature, the crude reaction mixture was concentrated and dried on high vacuum overnight to afford the desired products in quantitative yields, which could be carried forward to the next step without further purification.



Synthesis of methyl (*E*)-2-(((dimethylamino)methylene)amino)-3-methoxybenzoate (**2.21a**)

This compound was synthesized according to general procedure 2. Crude yellow oil (1.40 g, quantitative yield). For characterization purposes, an aliquot of this material was

purified via flash chromatography (Teledyne ISCO flash purification system; hexanes with 1% Et₃N:EtOAc; 10-70% EtOAc gradient) to afford the desired product as a colorless oil. ¹H NMR (400 MHz, CDCl₃) δ 7.33 (s, 1H), 7.30 (dd, *J* = 6.8 Hz and 2.5 Hz, 1H), 6.94-6.92 (m, 2H), 3.79 (s, 3H), 3.78 (s, 3H), 3.00 (bs, 6H); ¹³C NMR (100 MHz, CDCl₃) δ = 168.8, 154.6, 152.8, 142.6, 125.2, 122.3, 121.8, 114.3, 56.2, 51.7, 40.1, 34.3. LCMS (TOF, ES+) for C₁₂H₁₇N₂O₃ [M+H]⁺; 237.1.

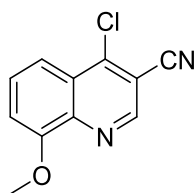


Synthesis of methyl (*E*)-2-(((dimethylamino)methylene)amino)-5-fluoro-3-methoxybenzoate (2.21b)

This compound was synthesized according to general procedure 2. Crude yellow oil (1.506 g, quantitative yield). For characterization purposes, an aliquot of this material was purified via flash chromatography (Teledyne ISCO flash purification system; hexanes:EtOAc; 0-60% EtOAc gradient) to afford the desired product as a colorless oil. ¹H NMR (400 MHz, CDCl₃) δ 7.28 (s, 1H), 7.01 (dd, *J* = 9.0 Hz and 2.6 Hz, 1H), 6.69 (dd, *J* = 10.0 Hz and 2.6 Hz, 1H), 3.79 (s, 3H), 3.77 (s, 3H), 3.00 (bs, 6H); ¹³C NMR (100 MHz, CDCl₃) δ = 167.5 (d, *J*_{CF} = 2.1 Hz), 157.6 (d, *J*_{CF} = 238.4 Hz), 155.0, 153.7 (d, *J*_{CF} = 9.6 Hz), 139.3, 124.7 (d, *J*_{CF} = 8.7 Hz), 107.6 (d, *J*_{CF} = 23.4 Hz), 102.7 (d, *J*_{CF} = 26.5 Hz), 56.4, 52.0, 40.2, 34.3. LCMS (TOF, ES+) for C₁₂H₁₆FN₂O₃ [M+H]⁺; 255.0.

General Procedure 3: Synthesis of Chloroquinolines (2.23)

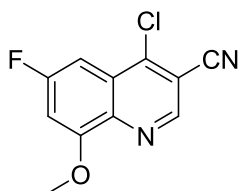
To a RBF charged with THF (2.65 M with respect to **2.21**) cooled to -78 °C was sequentially added *n*-BuLi (2.7 eq) (2.5 M solution in hexanes) and then a solution of acetonitrile (2.8 eq) in THF (1.77 M with respect to **2.21**) dropwise. The reaction was stirred for 30 min at -78 °C before the dropwise addition of a solution of the corresponding amidine **2.21** (1.0 eq) in THF (0.48 M with respect to **2.21**). After 1 hr of stirring at -78 °C, acetic acid (6.0 eq) was added, and the reaction was warmed to room temperature and stirred for an additional 30 min. Volatiles were removed *in vacuo*, and water was added to the crude residue. The resulting precipitate was isolated via vacuum filtration, washing with cold water to afford intermediate quinolones **2.22** which were immediately carried forward to the next step. **2.22a** was obtained as a beige solid (865 mg, 75% yield), while **2.22b** was obtained as a beige solid (960 mg, 77% yield). Intermediate quinolones **2.22** were treated with POCl₃ (28.0 eq) and heated to 100 °C for 30 min. Volatiles were removed *in vacuo*, and the resulting residue was diluted with DCM and quenched with the addition of sat. NaHCO₃. The layers were separated, and the aqueous layer was washed with DCM x 3. The combined organic material was passed through a phase separator and concentrated to afford the desired products, which could be carried forward to the next step without further purification.



Synthesis of 4-chloro-8-methoxyquinoline-3-carbonitrile (**2.23a**)

This compound was synthesized according to general procedure 3. Beige solid (787 mg, 83% yield from quinolone intermediate **2.22a**). For characterization purposes, a

small aliquot of this material was purified via flash chromatography (Teledyne ISCO flash purification system; silica gel column; hexanes:EtOAc; 0-50% EtOAc gradient). ^1H NMR (400 MHz, CDCl_3) δ 8.95 (s, 1H), 7.86 (dd, J = 8.6 Hz and 0.9 Hz, 1H), 7.70 (t, 1H), 7.27 (d, 1H), 4.12 (s, 3H); ^{13}C NMR (100 MHz, CDCl_3) δ = 155.8, 148.5, 147.3, 141.2, 129.9, 126.4, 116.4, 114.9, 111.6, 108.4, 56.7. LCMS (TOF, ES+) for $\text{C}_{11}\text{H}_8\text{ClN}_2\text{O}$ $[\text{M}+\text{H}]^+$; 219.0.



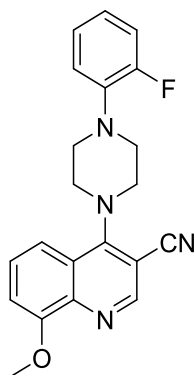
Synthesis of 4-chloro-6-fluoro-8-methoxyquinoline-3-carbonitrile (2.23b)

This compound was synthesized according to general procedure 3. Beige solid (926 mg, 89% yield from quinolone intermediate **2.22b**). For characterization purposes, a small aliquot of this material was purified via flash chromatography (Teledyne ISCO flash purification system; silica gel column; hexanes:EtOAc; 0-50% EtOAc gradient). ^1H NMR (400 MHz, CDCl_3) δ 8.90 (s, 1H), 7.48 (dd, J = 9.0 Hz and 2.5 Hz, 1H), 7.03 (dd, J = 10.2 Hz and 2.4 Hz, 1H), 4.12 (s, 3H); ^{13}C NMR (100 MHz, CDCl_3) δ = 162.8 (d, J_{CF} = 250.8 Hz), 157.9 (d, J_{CF} = 11.7 Hz), 147.8 (d, J_{CF} = 2.8 Hz), 146.5 (d, J_{CF} = 6.7 Hz), 138.8, 127.1 (d, J_{CF} = 12.6 Hz), 114.6, 109.4, 102.8 (d, J_{CF} = 29.8 Hz), 100.1 (d, J_{CF} = 25.3 Hz), 57.1. LCMS (TOF, ES+) for $\text{C}_{11}\text{H}_7\text{ClFN}_2\text{O}$ $[\text{M}+\text{H}]^+$; 236.9.

General Procedure 4: Synthesis of Quinolines (2.25-2.50)

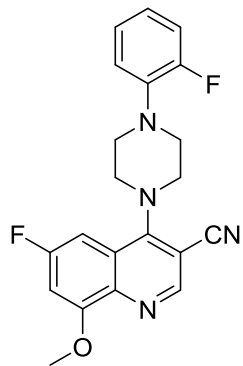
To a solution of the corresponding chloroquinoline **2.23** (1.0 eq) in DMF (0.2 M) in a Biotage microwave vial was sequentially added *N,N*-diisopropylethylamine (3.0 eq) and

aryl piperazine **2.24** (1.2 eq). The vial was sealed and heated to 150 °C for 15 min using a Biotage microwave reactor. Upon cooling to room temperature, the reaction was diluted with EtOAc and water. The layers were separated, and the aqueous layer was washed with EtOAc x 3. The combined organic material was passed through a phase separator, concentrated, and purified via flash chromatography (Teledyne ISCO flash purification system; silica gel column; hexanes:EtOAc; 0-100% EtOAc gradient) to afford the desired products.



Synthesis of 4-(4-(2-fluorophenyl)piperazin-1-yl)-8-methoxyquinoline-3-carbonitrile (**2.18**)

This compound was synthesized according to general procedure 4. Light orange solid (919 mg, 73% yield). ^1H NMR (400 MHz, CDCl_3) δ 8.78 (s, 1H), 7.63 (dd, $J = 8.7$ Hz and 0.8 Hz, 1H), 7.49 (t, 1H), 7.15-6.97 (m, 5H), 4.08 (s, 3H), 3.88 (m, 4H), 3.37 (m, 4H); ^{13}C NMR (100 MHz, CDCl_3) $\delta = 159.5, 156.1, 156.0$ (d, $J_{\text{CF}} = 244.9$ Hz), 151.5, 141.9, 139.7 (d, $J_{\text{CF}} = 8.5$ Hz), 127.1, 124.7 (d, $J_{\text{CF}} = 3.4$ Hz), 124.3, 123.4 (d, $J_{\text{CF}} = 7.9$ Hz), 119.5 (d, $J_{\text{CF}} = 2.6$ Hz), 118.6, 116.5 (d, $J_{\text{CF}} = 20.5$ Hz), 116.3, 110.4, 97.2, 56.4, 52.9, 51.33, 51.30. LCMS (TOF, ES+) for $\text{C}_{21}\text{H}_{20}\text{FN}_4\text{O}$ $[\text{M}+\text{H}]^+$; 363.0.



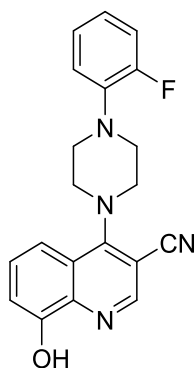
Synthesis of 6-fluoro-4-(4-(2-fluorophenyl)piperazin-1-yl)-8-methoxyquinoline-3-carbonitrile (2.48)

This compound was synthesized according to general procedure 4. Light orange solid (1.11 g, 77% yield). ^1H NMR (400 MHz, CDCl_3) δ 8.73 (s, 1H), 7.24 (dd, $J = 10.1$ Hz and 2.4 Hz, 1H), 7.12-6.97 (m, 4H), 6.91 (dd, $J = 10.1$ Hz and 2.4 Hz, 1H), 4.08 (s, 3H), 3.82 (m, 4H), 3.37 (m, 4H); ^{13}C NMR (100 MHz, CDCl_3) $\delta = 161.2$ (d, $J_{\text{CF}} = 246.2$ Hz), 158.9 (d, $J_{\text{CF}} = 5.5$ Hz), 158.1 (d, $J_{\text{CF}} = 11.5$ Hz), 156.0 (d, $J_{\text{CF}} = 244.8$ Hz), 150.8 (d, $J_{\text{CF}} = 2.2$ Hz), 139.6 (d, $J_{\text{CF}} = 8.6$ Hz), 139.5, 124.9 (d, $J_{\text{CF}} = 10.9$ Hz), 124.7 (d, $J_{\text{CF}} = 3.5$ Hz), 123.4 (d, $J_{\text{CF}} = 7.9$ Hz), 119.5 (d, $J_{\text{CF}} = 2.6$ Hz), 118.1, 116.5 (d, $J_{\text{CF}} = 20.5$ Hz), 101.4 (d, $J_{\text{CF}} = 29.5$ Hz), 99.9 (d, $J_{\text{CF}} = 24.2$ Hz), 98.5, 56.8, 52.5, 51.3, 51.2. LCMS (TOF, ES+) for $\text{C}_{21}\text{H}_{19}\text{F}_2\text{N}_4\text{O}$ $[\text{M}+\text{H}]^+$; 380.8.

General Procedure 5: Synthesis of Phenols 2.84

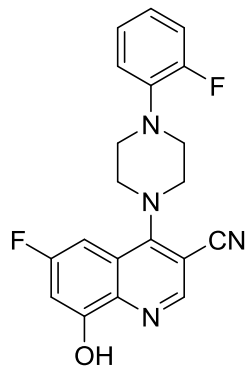
To a solution of the corresponding quinoline **2.83** (1.0 eq) in DCM (0.1 M) cooled to -78 °C was added BBr_3 solution (6.5 eq) (1.0 M solution in DCM) dropwise. Upon completion of addition, the reaction was stirred for 30 min at -78 °C before warming to room temperature and stirring for an additional 16 hr. The reaction was diluted with DCM and quenched with the careful addition of water, stirring vigorously. Upon formation of two distinct layers, the layers were separated, and the aqueous layer was

washed with DCM x 3. The combined organic material was washed with brine, passed through a phase separator, concentrated, and purified via flash chromatography (Teledyne ISCO flash purification system; silica gel column; hexanes:EtOAc; 0-80% EtOAc gradient) to afford the desired products.



Synthesis of 4-(4-(2-fluorophenyl)piperazin-1-yl)-8-hydroxyquinoline-3-carbonitrile (2.84a)

This compound was synthesized according to general procedure 5. Yellow solid (510 mg, 59% yield). ^1H NMR (400 MHz, CDCl_3) δ 8.63 (s, 1H), 8.20 (bs, 1H), 7.52 (dd, $J = 8.6$ Hz and 0.6 Hz, 1H), 7.46 (t, 1H), 7.24 (dd, $J = 7.5$ Hz and 0.8 Hz, 1H), 7.14-6.98 (m, 4H), 3.94 (m, 4H), 3.38 (m, 4H); ^{13}C NMR (100 MHz, CDCl_3) $\delta = 159.7$, 156.0 (d, $J_{\text{CF}} = 244.7$ Hz), 153.2, 150.6, 140.0, 139.7 (d, $J_{\text{CF}} = 8.4$ Hz), 127.9, 124.7 (d, $J_{\text{CF}} = 3.5$ Hz), 123.4 (d, $J_{\text{CF}} = 7.9$ Hz), 123.2, 119.5 (d, $J_{\text{CF}} = 2.5$ Hz), 118.7, 116.5 (d, $J_{\text{CF}} = 20.5$ Hz), 115.1, 113.0, 96.7, 52.9, 51.4, 51.3. LCMS (TOF, ES+) for $\text{C}_{20}\text{H}_{18}\text{FN}_4\text{O}$ $[\text{M}+\text{H}]^+$; 349.0.



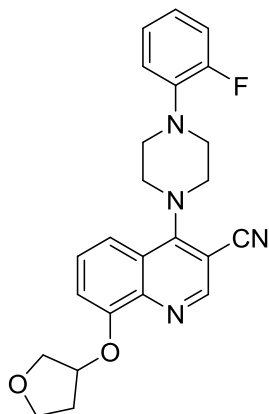
Synthesis of 6-fluoro-4-(4-(2-fluorophenyl)piperazin-1-yl)-8-hydroxyquinoline-3-carbonitrile (2.84b)

This compound was synthesized according to general procedure 5. Yellow solid (748 mg, 70% yield). ^1H NMR (400 MHz, DMSO- d_6) δ 10.66 (bs, 1H), 8.74 (s, 1H), 7.24-7.01 (m, 6H), 3.76 (m, 4H), 3.31 (m, 4H); ^{13}C NMR (100 MHz, DMSO- d_6) δ = 160.7 (d, J_{CF} = 242.4 Hz), 158.6 (d, J_{CF} = 5.3 Hz), 156.5 (d, J_{CF} = 14.0 Hz), 155.0 (d, J_{CF} = 242.9 Hz), 149.4, 139.5 (d, J_{CF} = 8.1 Hz), 137.8, 124.9 (d, J_{CF} = 3.2 Hz), 124.0 (d, J_{CF} = 11.6 Hz), 122.9 (d, J_{CF} = 7.8 Hz), 119.7, 118.2, 116.1 (d, J_{CF} = 20.4 Hz), 104.1 (d, J_{CF} = 27.7 Hz), 98.7 (d, J_{CF} = 24.6 Hz), 97.4, 51.8, 50.70, 50.68. LCMS (TOF, ES+) for $\text{C}_{20}\text{H}_{17}\text{F}_2\text{N}_4\text{O}$ $[\text{M}+\text{H}]^+$; 366.8.

General Procedure 6: Synthesis of Alkoxy-Substituted Quinolines 2.85-2.111

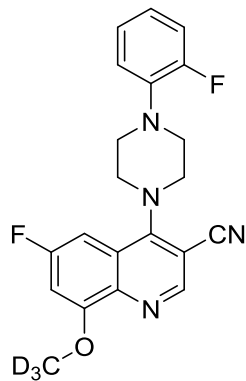
To a solution of the corresponding phenol **2.84** (1.0 eq) in MeCN (0.15 M) in a Biotage microwave vial was added potassium carbonate (2.0 eq) and the corresponding alkyl halide (1.0 eq). The vial was sealed and heated to either 80 °C for 2 hr under conventional heating (general procedure 6A) or to 150 °C for 1 hr using a Biotage microwave reactor (general procedure 6B). Upon cooling to room temperature, the reaction was diluted with EtOAc, filtered, concentrated, and purified via flash

chromatography (Teledyne ISCO flash purification system; silica gel column; hexanes:EtOAc; 0-80% EtOAc gradient) to afford the desired products.



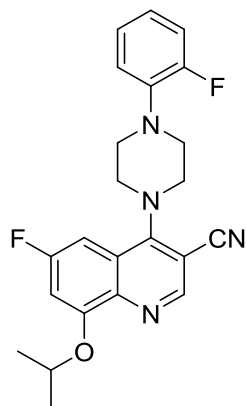
Synthesis of 4-(4-(2-fluorophenyl)piperazin-1-yl)-8-((tetrahydrofuran-3-yl)oxy)quinoline-3-carbonitrile (2.91)

This compound was synthesized according to general procedure 6B. Beige solid (35 mg, 58% yield). ^1H NMR (400 MHz, CDCl_3) δ 8.79 (s, 1H), 7.66 (d, $J = 8.5$ Hz, 1H), 7.47 (t, 1H), 7.12-6.97 (m, 5H), 5.18 (m, 1H), 4.14 (d, $J = 3.7$ Hz, 2H), 4.13-4.07 (m, 1H), 3.97-3.92 (m, 1H), 3.88 (m, 4H), 3.37 (m, 4H), 2.38-2.29 (m, 2H); ^{13}C NMR (100 MHz, CDCl_3) $\delta = 159.5, 156.0$ (d, $J_{\text{CF}} = 244.8$ Hz), 154.2, 151.6, 142.5, 139.6 (d, $J_{\text{CF}} = 8.5$ Hz), 126.9, 124.7 (d, $J_{\text{CF}} = 3.4$ Hz), 124.6, 123.4 (d, $J_{\text{CF}} = 7.9$ Hz), 119.4 (d, $J_{\text{CF}} = 2.5$ Hz), 118.5, 117.0, 116.5 (d, $J_{\text{CF}} = 20.5$ Hz), 113.6, 97.1, 79.2, 72.9, 67.4, 52.9, 51.29, 51.27, 33.2. LCMS (TOF, ES+) for $\text{C}_{24}\text{H}_{24}\text{FN}_4\text{O}_2$ $[\text{M}+\text{H}]^+$; 419.0.



Synthesis of 6-fluoro-4-(4-(2-fluorophenyl)piperazin-1-yl)-8-(methoxy-d₃)quinoline-3-carbonitrile (2.101)

This compound was synthesized according to general procedure 6A. White solid (18 mg, 68% yield). ¹H NMR (600 MHz, CDCl₃) δ 8.74 (s, 1H), 7.25 (dd, *J* = 9.9 Hz and 2.4 Hz, 1H), 7.12-6.98 (m, 4H), 6.91 (dd, *J* = 10.0 Hz and 2.3 Hz, 1H), 3.83 (m, 4H), 3.37 (m, 4H); ¹³C NMR (150 MHz, CDCl₃) δ = 161.2 (d, *J*_{CF} = 246.4 Hz), 159.0 (d, *J*_{CF} = 5.3 Hz), 158.0 (d, *J*_{CF} = 11.3 Hz), 156.0 (d, *J*_{CF} = 244.8 Hz), 150.7, 139.6 (d, *J*_{CF} = 8.5 Hz), 139.2, 124.9 (d, *J*_{CF} = 10.9 Hz), 124.7 (d, *J*_{CF} = 3.3 Hz), 123.5 (d, *J*_{CF} = 7.8 Hz), 119.5 (d, *J*_{CF} = 2.0 Hz), 118.1, 116.5 (d, *J*_{CF} = 20.6 Hz), 101.4 (d, *J*_{CF} = 29.4 Hz), 99.9 (d, *J*_{CF} = 24.2 Hz), 98.4, 56.1 (m, *J*_{CD} = 22.0 Hz), 52.6, 51.27, 51.26. LCMS (TOF, ES+) for C₂₁H₁₆[²H₃]F₂N₄O [M+H]⁺; 384.0.



Synthesis of 6-fluoro-4-(4-(2-fluorophenyl)piperazin-1-yl)-8-isopropoxyquinoline-3-carbonitrile (2.103)

This compound was synthesized according to general procedure 6B. White solid (15 mg, 54% yield). ¹H NMR (400 MHz, CDCl₃) δ 8.76 (s, 1H), 7.22 (dd, *J* = 9.9 Hz and 2.6 Hz, 1H), 7.13-6.97 (m, 4H), 6.92 (dd, *J* = 10.6 Hz and 2.5 Hz, 1H), 4.77 (m, 1H), 3.82 (m, 4H), 3.37 (m, 4H), 1.53 (d, 6H); ¹³C NMR (100 MHz, CDCl₃) δ = 161.2 (d, *J*_{CF} = 245.4 Hz), 159.0 (d, *J*_{CF} = 5.6 Hz), 156.5 (d, *J*_{CF} = 11.5 Hz), 156.0 (d, *J*_{CF} = 244.7 Hz), 150.6 (d, *J*_{CF} = 1.8 Hz), 140.1, 139.6 (d, *J*_{CF} = 8.5 Hz), 125.2 (d, *J*_{CF} = 11.1 Hz), 124.7 (d, *J*_{CF} = 3.5 Hz), 123.4 (d, *J*_{CF} = 7.8 Hz), 119.5 (d, *J*_{CF} = 2.3 Hz), 118.2, 116.5 (d, *J*_{CF} = 20.4 Hz), 103.3 (d, *J*_{CF} = 29.1 Hz), 99.5 (d, *J*_{CF} = 24.3 Hz), 98.3, 72.3, 52.5, 51.3, 51.2, 21.8. LCMS (TOF, ES+) for C₂₃H₂₃F₂N₄O [M+H]⁺; 409.0.

References for Chapter II

1. Vazquez-Villa, H.; Trabanco, A. A. Progress toward allosteric ligands of metabotropic glutamate 7 (mGlu7) receptor: 2008-present. *Med. Chem. Commun.* **2019**, *10*, 193-199.
2. Fisher, N. M.; Seto, M.; Lindsley, C. W.; Niswender, C. M. Metabotropic glutamate receptor 7: a new therapeutic target in neurodevelopmental disorders. *Front. Mol. Neurosci.* **2018**, *11*, 387, doi: 10.3389/fnmol.2018.00387.
3. Acher, F.; Pin, J-P. Goudet, C.; Eschalier, A.; Busserolles, J.; Rigault, D.; Lemasson, I.; Cesarini, S.; Commare, B. Hypophosphorous acid derivatives having antihyperalgetic activity and biological applications thereof. US Patent 2012: WO2012156931A1.
4. Selvam, C.; Lemasson, I. A.; Brabet, I.; Oueslati, N.; Karaman, B.; Cabaye, A.; Tore, A. S.; Commare, B.; Courtiol, T.; Cesarini, S.; McCort-Trancheoain, I.; Rigault, D.; Mony, L.; Bessiron, T.; McLean, H.; Leroux, F. R.; Colobert, F.; Daniel, H.; Goupil-Lamy, A.; Bertrand, H-O.; Goudet, C.; Pin, J-P.; Acher, F. C. Increased potency and selectivity for group III metabotropic glutamate receptor agonists binding at dual sites. *J. Med. Chem.* **2018**, *61*, 1969-1989.
5. Goudet, C.; Vilar, B.; Courtiol, T.; Deltheil, T.; Bessiron, T.; Brabet, I.; Oueslati, N.; Rigault, D.; Bertrand, H-O.; McLean, H.; Daniel, H.; Amalric, M.; Acher, F.; Pin, J-P. A novel selective metabotropic glutamate receptor 4 agonist reveals new possibilities for developing subtype selective ligands with therapeutic potential. *FASEB J.* **2012**, *26*, 1682-1693.
6. Hajasova, Z.; Canestrelli, C.; Acher, F.; Noble, F.; Marie, N. Role of mGlu7 receptor in morphine rewarding effects is uncovered by a novel orthosteric agonist. *Neuropharmacology* **2018**, *131*, 424-430.
7. Lebourgeois, S.; Vilpoux, C.; Jeanblanc, J.; Acher, F.; Marie, N.; Noble, F.; Naassila, M. Pharmacological activation of mGlu4 and mGlu7 receptors, by LSP2-9166, reduces ethanol consumption and relapse in rat. *Neuropharmacology* **2018**, *133*, 163-170.
8. Conn, P. J.; Christopoulos, A.; Lindsley, C. W. Allosteric modulators of GPCRs: a novel approach for the treatment of CNS disorders. *Nat. Rev. Drug Discovery* **2009**, *8*, 41-54.
9. Mitsukawa, K.; Yamamoto, R.; Ofner, S.; Nozulak, J.; Pescott, O.; Lukic, S.; Stoehr, N.; Mombereau, C.; Kuhn, R.; McAllister, K. H.; van der Putten, H.; Cryan, J. F.; Flor, P. J. A selective metabotropic glutamate receptor 7 agonist: activation of receptor signaling via an allosteric site modulates stress parameters *in vivo*. *Proc. Natl. Acad. Sci.* **2005**, *102*, 18712-18717.
10. Sukoff Rizzo, S. J.; Leonard, S. K.; Gilbert, A.; Dollings, P.; Smith, D. L.; Zhang, M-Y.; Di, L.; Platt, B. J.; Neal, S.; Dwyer, J. M.; Bender, C. N.; Zhang, J.; Lock, T.; Kowal, D.; Kramer, A.; Randall, A.; Huselton, C.; Vishwanathan, K.; Tse, S. Y.; Butera, J.; Ring, R. H.; Rosenzweig-Lipson, S.; Hughes, Z. A.; Dunlop, J. The metabotropic glutamate receptor 7 allosteric modulator AMN082: a monoaminergic agent in disguise? *J. Pharmacol. Exp. Ther.* **2011**, *338*, 345-352.

11. Ahnaou, A.; Raeyemaekers, L.; Huysmans, H.; Drinkenburg, W. H. I. M. Off-target potential of AMN082 on sleep EEG and related physiological variables: evidence from mGluR7(-/-) mice. *Behav. Brain Res.* **2016**, *311*, 287-297.
12. Conn, P. J.; Niswender, C. M. mGluR7's lucky number. *Proc. Natl. Acad. Sci.* **2006**, *103*, 251-252.
13. Suzuki, G.; Tsukamoto, N.; Fushiki, H.; Kawagishi, A.; Nakamura, M.; Kurihara, H.; Mitsuya, M.; Ohkubo, M.; Ohta, H. *In vitro* pharmacological characterization of novel isoxazolopyridone derivatives as allosteric metabotropic glutamate receptor 7 antagonists. *J. Pharmacol. Exp. Ther.* **2007**, *323*, 147-156.
14. Jalan-Sakrikar, N.; Field, J. R.; Klar, R.; Mattmann, M. E.; Gregory, K. J.; Zamorano, R.; Engers, D. W.; Bollinger, S. R.; Weaver, C. D.; Days, E. L.; Lewis, L. M.; Utley, T. J.; Hurtado, M.; Rigault, D.; Acher, F.; Walker, A. G.; Melancon, B. J.; Wood, M. R.; Lindsley, C. W.; Conn, P. J.; Xiang, Z.; Hopkins, C. R.; Niswender, C. M. Identification of positive allosteric modulators VU0155094 (ML397) and VU0422288 (ML396) reveals new insights into the biology of metabotropic glutamate receptor 7. *ACS Chem. Neurosci.* **2014**, *5*, 1221-1237.
15. Abe, M.; Seto, M.; Gogliotti, R. G.; Loch, M. T.; Bollinger, K. A.; Chang, S.; Engelberg, E. M.; Luscombe, V. B.; Harp, J. M.; Bubser, M.; Engers, D. W.; Jones, C. K.; Rodrigues, A. L.; Blobaum, A. L.; Conn, P. J.; Niswender, C. M.; Lindsley, C. W. Discovery of VU6005649, a CNS penetrant mGlu_{7/8} receptor PAM derived from a series of pyrazolo[1,5-a]pyrimidines. *ACS Med. Chem. Lett.* **2017**, *8*, 1110-1115.
16. Le Poul, E.; Bolea, C.; Girard, F.; Poli, S.; Charvin, D.; Campo, B.; Bortoli, J.; Bessif, A.; Luo, B.; Koser, A. J.; Hodge, L. M.; Smith, K. M.; DiLella, A. G.; Liverton, N.; Hess, F.; Browne, S. E.; Reynolds, I. J. A potent and selective metabotropic glutamate receptor 4 positive allosteric modulator improves movement in rodent models of Parkinson's disease. *J. Pharmacol. Exp. Ther.* **2012**, *343*, 167-177.
17. Kalinichev, M.; Le Poul, E.; Bolea, C.; Girard, F.; Campo, B.; Fonsi, M.; Royer-Urios, I.; Browne, S. E.; Uslaner, J. M.; Davis, M. J.; Raber, J.; Duvoisin, R.; Bate, S. T.; Reynolds, I. J.; Poli, S.; Celanire, S. Characterization of the novel positive allosteric modulator of the metabotropic glutamate receptor 4 ADX88178 in rodent models of neuropsychiatric disorders. *J. Pharmacol. Exp. Ther.* **2014**, *350*, 495-505.
18. Kalinichev, M.; Rouillier, M.; Girard, F.; Royer-Urios, I.; Bournique, B.; Finn, T.; Charvin, D.; Campo, B.; Le Poul, E.; Mutel, V.; Poli, S.; Neale, S. A.; Salt, T. E.; Lütjens, R. ADX71743, a potent and selective negative allosteric modulator of metabotropic glutamate receptor 7: *in vitro* and *in vivo* characterization. *J. Pharmacol. Exp. Ther.* **2013**, *344*, 626-636.
19. Lapinsh, M.; Prusis, P.; Guitcaits, A.; Lundstedt, T.; Wikberg, J. E. Development of proteo-chemometrics: a novel technology for the analysis of drug-receptor interactions. *Biochim. Biophys. Acta, Gen. Subj.* **2001**, *1525*, 180-190.
20. Van Westen, G. J. P.; Wegner, J. K.; Ijzerman, A. P.; Van Vlijmen, H. W. T.; Bender, A. Proteochemometric modeling as a tool for designing selective compounds and extrapolating to novel targets. *Med. Chem. Commun.* **2011**, *2*, 16-30.

21. Tresadern, G.; Trabanco, A. A.; Perez-Benito, L.; Overington, J. P.; van Vlijmen, H. W. T.; van Westen, G. J. P. Identification of allosteric modulators of metabotropic glutamate 7 receptor using proteochemometric modeling. *J. Chem. Inf. Model* **2017**, *57*, 2976-2985.
22. Cid, J. M.; Lavreysen, H.; Tresadern, G.; Perez-Benito, L.; Tovar, F.; Fontana, A.; Trabanco, A. A. Computationally guided identification of allosteric agonists of the metabotropic glutamate 7 receptor. *ACS Chem. Neurosci.* **2019**, *10*, 1043-1054.
23. Dore, A-S.; Okrasa, K.; Patel, J-C.; Serrano-Vega, M.; Bennett, K.; Cooke, R-M.; Errey, J-C.; Jazayeri, A.; Khan, S.; Tehan, B.; Weir, M.; Wiggin, G. R.; Marshall, F. H. Structure of class C GPCR metabotropic glutamate receptor 5 transmembrane domain. *Nature* **2014**, *511*, 557-562.
24. Wu, H.; Wang, C.; Gregory, K-J.; Han, G-W.; Cho, H-P.; Xia, Y.; Niswender, C. M.; Katritch, V.; Meiler, J.; Cherezov, V.; Conn, P. J.; Stevens, R. C. Structure of a class C GPCR metabotropic glutamate receptor 1 bound to an allosteric modulator. *Science* **2014**, *344*, 58-64.
25. Rasmussen, S. G. F.; DeVree, B. T.; Zou, Y.; Kruse, A. C.; Chung, K. Y.; Kobilka, T. S.; Thian, F. S.; Chae, P. S.; Pardon, E.; Calinski, D.; Mathiesen, J. M.; Shah, S. T.; Lyons, J. A.; Caffrey, M.; Gellmann, S. H.; Steyaert, J.; Skiniotis, G.; Weis, W. I.; Sunahara, R. K.; Kobilka, B. K. Crystal structure of the β_2 adrenergic receptor-Gs protein complex. *Nature* **2011**, *477*, 549-555.
26. Sansig, G.; Bushell, T. J.; Clarke, V. R. J.; Rozov, A.; Burnashev, N.; Portet, C.; Gasparini, F.; Schmutz, M.; Klebs, K.; Shigemoto, R.; Flor, P. J.; Kuhn, R.; Knoepfel, T.; Schroeder, M.; Hampson, D. R.; Collett, V. J.; Zhang, C.; Duvoisin, R. M.; Collingridge, G. L.; van der Putten, H. Increased seizure susceptibility in mice lacking metabotropic glutamate receptor 7. *J. Neurosci.* **2001**, *21*, 8734-8745.
27. Goddyn, H.; Callaerts-Vegh, Z.; Stroobants, S.; Dirikx, T.; Vansteenwegen, D.; Hermans, D.; van der Putten, H.; D'Hooge, R. Deficits in acquisition and extinction of conditioned responses in mGluR7 knockout mice. *Neurobiology of Learning and Memory* **2008**, *90*, 103-111.
28. Palucha, A.; Klak, K.; Branski, P.; van der Putten, H.; Flor, P.; Pilc, A. Activation of the mGlu₇ receptor elicits antidepressant-like effects in mice. *Psychopharmacology* **2007**, *194*, 555-562.
29. Callaerts-Vegh, Z.; Beckers, T.; Ball, S. M.; Baeyens, F.; Callaerts, P. F.; Cryan, J. F.; Molnar, E.; D'Hooge, R. Concomitant deficits in working memory and fear extinction are functionally dissociated from reduced anxiety in metabotropic glutamate receptor 7-deficient mice. *J. Neurosci.* **2006**, *26*, 6573-6582.
30. Mitsukawa, K.; Mombereau, C.; Lötscher, E.; Uzunov, D. P.; van der Putten, H.; Flor, P. J.; Cryan, J. F. Metabotropic glutamate receptor subtype 7 ablation causes dysregulation of the HPA axis and increases hippocampal BDNF protein levels: implications for stress-related psychiatric disorders. *Neuropsychopharmacology* **2006**, *31*, 1112-1122.
31. Hölscher, C.; Schmid, S.; Pilz, P. K. D.; Sansig, G.; van der Putten, H.; Plappert, C. F. Lack of the metabotropic glutamate receptor subtype 7 selectively impairs short-term working memory but not long-term memory. *Behavioral Brain Research* **2004**, *154*, 473-481.

32. Bushell, T. J.; Sansig, G.; Collett, V. J.; van der Putten, H.; Collingridge, G. L. Altered short-term synaptic plasticity in mice lacking the metabotropic glutamate receptor mGlu₇. *The Scientific World Journal* **2002**, *2*, 730-737.
33. Masugi, M.; Yokoi, M.; Shigemoto, R.; Muguruma, K.; Watanabe, Y.; Sansig, G.; van der Putten, H.; Nakanishi, S. Metabotropic glutamate receptor subtype 7 ablation causes deficit in fear response and conditioned taste aversion. *J. Neurosci.* **1999**, *19*, 955-963.
34. Gogliotti, R. G., Senter, R. K., Fisher, N. M., Adams, J., Zamorano, R., Walker, A. G., Blobaum, A. L., Engers, D. W., Hopkins, C. R., Daniels, J. S., Jones, C. K., Lindsley, C. W., Xiang, Z., Conn, P. J., Niswender, C. M. mGlu₇ potentiation rescues cognitive, social, and respiratory phenotypes in a mouse model of Rett syndrome. *Sci. Transl. Med.* **2017**, *9*, eaai7459.
35. Armstrong, D. D. The neuropathology of Rett syndrome – overview 1994. *Neuropediatrics* **1995**, *26*, 100-104.
36. Hagberg, B. Clinical manifestations and stages of Rett syndrome. *Mental Retardation and Developmental Disabilities Research Reviews* **2002**, *8*, 61-65.
37. Naidu, S. B. Rett syndrome. *Indian Journal of Pediatrics* **1997**, *64*, 651-659.
38. Hagberg, B. A. Rett syndrome: clinical peculiarities, diagnostic approach, and possible cause. *Pediatric Neurology* **1989**, *5*, 75-83.
39. Hendrich, B.; Bickmore, W. Human diseases with underlying defects in chromatin structure and modification. *Human Molecular Genetics* **2001**, *10*, 2233-2242.
40. Dunn, H. G. Importance of Rett syndrome in child neurology. *Brain and Development* **2001**, *23*, supplement 1, S38-S43.
41. Neul, J. L.; Kaufmann, W. E.; Glaze, D. G.; Christodoulou, J.; Clarke, A. J.; Bahi-Buisson, N.; Leonard, H.; Bailey, M. E. S.; Schanen, N. C.; Zappella, M.; Renieri, A.; Huppke, P.; Percy, A. K. Rett syndrome: revised diagnostic criteria and nomenclature. *Ann. Neurol.* **2010**, *68*, 944-950.
42. Dunn, H. G.; MacLeod, P. M. Rett syndrome: review of biological abnormalities. *Canadian Journal of Neurological Sciences* **2001**, *28*, 16-29.
43. Akbarian, S. The neurobiology of Rett syndrome. *Neuroscientist* **2003**, *9*, 57-63.
44. Armstrong, D. D. Review of Rett syndrome. *Journal of Neuropathology and Experimental Neurology* **1997**, *56*, 843-849.
45. Freilinger, M.; Bebbington, A.; Lanator, I.; De Klerk, N.; Dunkler, D.; Seidl, R.; Leonard, H.; Ronen, G. M. Survival with Rett syndrome: comparing Rett's original sample with data from the Australian Rett syndrome database. *Developmental Medicine and Child Neurology* **2010**, 962-965, doi: 10.1111/j.1469-8749.2010.03716.x
46. Amir, R. E.; Van den Veyver, I. B.; Wan, M.; Tran, C. Q.; Francke, U.; Zoghbi, H. Y. Rett syndrome is caused by mutations in X-linked MECP2, encoding methyl-CpG-binding protein 2. *Nat. Genet.* **1999**, *23*, 185-188.
47. Lewis, J. D.; Meehan, R. R.; Henzel, W. J.; Maurer-Fogy, I.; Jeppesen, P.; Klein, F.; Bird, A. Purification, sequence, and cellular localization of a novel chromosomal protein that binds to methylated DNA. *Cell* **1992**, *69*, 905-914.
48. Nan, X.; Meehan, R. R.; Bird, A. Dissection of the methyl-CpG-binding domain from the chromosomal protein MeCP2. *Nucleic Acids Res.* **1993**, *21*, 4886-4892.

49. Nan, X.; Ng, H. H.; Johnson, C. A.; Laherty, C. D.; Turner, B. M.; Eisenman, R. N.; Bird, A. Transcriptional repression by the methyl-CpG-binding protein MeCP2 involves a histone deacetylase complex. *Nature* **1998**, *393*, 386-389.
50. Jones, P. L.; Veenstra, G. J.; Wade, P. A.; Vermaak, D.; Kass, S. U.; Landsberger, N.; Strouboulis, J.; Wolffe, A. P. Methylated DNA and MeCP2 recruit histone deacetylase to repress transcription. *Nature Genet.* **1998**, *19*, 187-191.
51. Klose, R. J.; Sarraf, S. A.; Schmiedeberg, L.; McDermott, S. M.; Stancheva, I.; Bird, A. P. DNA binding selectivity of MeCP2 due to a requirement for A/T sequences adjacent to methyl-CpG. *Mol. Cell* **2005**, *19*, 667-678.
52. Horike, S.; Cai, S.; Miyano, M.; Cheng, J. F.; Kohwi-Shigematsu, T. Loss of silent-chromatin looping and impaired imprinting of DLX5 in Rett syndrome. *Nat. Genet.* **2005**, *37*, 31-40.
53. Jones, P. L.; Wolffe, A. P. Relationships between chromatin organization and DNA methylation in determining gene expression. *Semin. Cancer Biol.* **1999**, *9*, 339-347.
54. Nan, X.; Cross, S.; Bird, A. Gene silencing by methyl-CpG-binding proteins. *Novartis Found. Symp.* **1998**, *214*, 6-16.
55. Kass, S. U.; Wolffe, A. P. DNA methylation, nucleosomes, and the inheritance of chromatin structure and function. *Novartis Found. Symp.* **1998**, *214*, 22-35.
56. Wolffe, A. P.; Guschin, D. Chromatin structural features and targets that regulate transcription. *J. Struct. Biol.* **2000**, *129*, 102-122.
57. Chahrour, M.; Jung, S. Y.; Shaw, C.; Zhou, X.; Wong, S. T. C.; Qin, J.; Zoghbi, H. Y. MeCP2, a key contributor to neurological disease, activates and represses transcription. *Science* **2008**, *320*, 1224-1229.
58. Dragich, J.; Houwink-Manville, I.; Schanen, C. Rett syndrome: a surprising result of mutation in MECP2. *Human Molecular Genetics* **2000**, *9*, 2365-2375.
59. Bienvenu, T.; Chelly, J. Molecular genetics of Rett syndrome: when DNA methylation goes unrecognized. *Nat. Rev. Genet.* **2006**, *7*, 415-426.
60. Lawson-Yuen, A.; Liu, D.; Han, L.; Jiang, Z. I.; Tsai, G. E.; Basu, A. C.; Picker, J.; Feng, J.; Coyle, J. T. Ube3a mRNA and protein expression are not decreased in MeCP2R168X mutant mice. *Brain Res.* **2007**, *1180*, 1-6.
61. Baker, S. A.; Chen, L.; Wilkins, A. D.; Yu, P.; Lichtarge, O.; Zoghbi, H. Y. An AT-hook domain in MeCP2 determines the clinical course of Rett syndrome and related disorders. *Cell* **2013**, *152*, 984-996.
62. Zhang, J.; Sun, X.; Qian, Y.; Maquat, L. E. Intron function in the nonsense-mediated decay of beta-globin mRNA: indications that pre-mRNA splicing in the nucleus can influence mRNA translation in the cytoplasm. *RNA* **1998**, *4*, 801-815.
63. Ballestar, E.; Yusufzai, T. M.; Wolffe, A. P. Effects of Rett syndrome mutations of the methyl-CpG binding domain of the transcriptional repressor MeCP2 on selectivity for association with methylated DNA. *Biochemistry* **2000**, *39*, 7100-7106.
64. Leonard, H.; Colvin, L.; Christodoulou, J.; Schiavello, T.; Williamson, S.; Davis, M.; Ravine, D.; Fyfe, S.; de Klerk, N.; Matsuishi, T.; Kondo, I.; Clarke, A.; Hackwell, S.; Yamashita, Y. Patients with the R133C mutation: is their phenotype

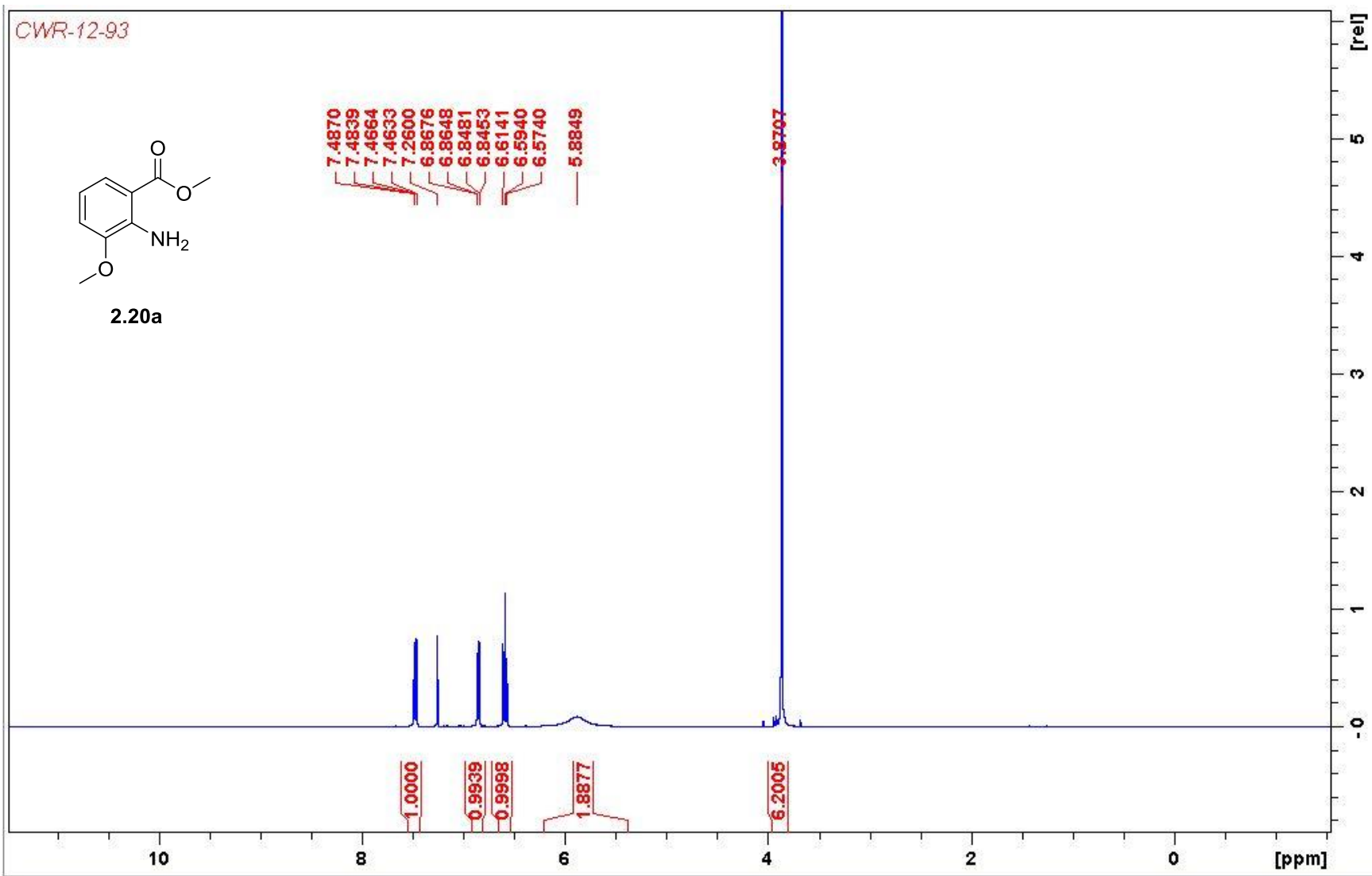
- different from patients with Rett syndrome with other mutations? *J. Med. Genet.* **2003**, *40*, e52.
65. Kucukkal, T. G.; Alexov, E. Structural, dynamical, and energetical consequences of Rett syndrome mutation R133C in MeCP2. *Computational and Mathematical Methods in Medicine* **2015**, article ID 746157.
 66. Skene, P. J.; Illingworth, R. S.; Webb, S.; Kerr, A. R.; James, K. D.; Turner, D. J.; Andrews, R.; Bird, A. P. Neuronal MeCP2 is expressed at near histone-octamer levels and globally alters the chromatin state. *Mol. Cell* **2010**, *37*, 457-468.
 67. Chao, H. T.; Chen, H.; Samaco, R. C.; Xue, M.; Chahrour, M.; Yoo, J.; Neul, J. L.; Gong, S.; Lu, H. C.; Heintz, N.; Ekker, M.; Rubenstein, J. L.; Noebels, J. L.; Rosenmund, C.; Zoghbi, H. Y. Dysfunction in GABA signaling mediates autism-like stereotypies and Rett syndrome phenotypes. *Nature* **2010**, *468*, 263-269.
 68. Asaka, Y.; Jugloff, D. G. M.; Zhang, L.; Eubanks, J. H.; Fitzsimonds, R. M. Hippocampal synaptic plasticity is impaired in the *Mecp2*-null mouse model of Rett syndrome. *Neurobiol. Dis.* **2006**, *21*, 217-227.
 69. Moretti, P.; Levenson, J. M.; Battaglia, F.; Atkinson, R.; Teague, R.; Antalffy, B.; Armstrong, D.; Aranio, O. Sweatt, J. D.; Zoghbi, H. Y. Learning and memory and synaptic plasticity are impaired in a mouse model of Rett syndrome. *J. Neurosci.* **2006**, *26*, 319-327.
 70. Weng, S-M.; McLeod, F.; Bailey, M. E. S.; Cobb, S. R. Synaptic plasticity deficits in an experimental model of Rett syndrome: long term potentiation saturation and its pharmacological reversal. *Neuroscience* **2011**, *180*, 314-321.
 71. Armstrong, D. D. Rett syndrome neuropathology review. *Brain Dev.* **2000**, *23*, Suppl 1: S72-76.
 72. Chen, R. Z.; Akbarian, S.; Tudor, M.; Jaenisch, R. Deficiency of methyl-CpG binding protein-2 in CNS neurons results in a Rett-like phenotype in mice. *Nat. Genet.* **2001**, *27*, 327-331.
 73. Na, E. S.; Nelson, S. D.; Kavalali, E. T.; Monteggia, L. M. The impact of MeCP2 loss- or gain-of-function on synaptic plasticity. *Neuropsychopharmacology* **2013**, *38*, 212-219.
 74. Klar, R.; Walker, A. G.; Ghose, D.; Grueter, B. A.; Engers, D. W.; Hopkins, C. R.; Lindsley, C. W.; Xiang, Z.; Conn, P. J.; Niswender, C. M. Activation of metabotropic glutamate receptor 7 is required for induction of long-term potentiation at SC-CA1 synapses in the hippocampus. *J. Neurosci.* **2015**, *35*, 7600-7615.
 75. Guy, J.; Gan, J.; Selfridge, J.; Cobb, S.; Bird, A. Reversal of neurological defects in a mouse model of Rett syndrome. *Science* **2007**, *315*, 1143-1147.
 76. Pozzo-Miller, L.; Pati, S.; Percy, A. K. Rett syndrome: reaching for clinical trials. *Neurotherapeutics* **2015**, *12*, 631-640.
 77. Park, H.; Poo, M. M. Neurotrophin regulation of neural circuit development and function. *Nat. Rev. Neurosci.* **2013**, *14*, 7-23.
 78. Katz, D. M. Brain-derived neurotrophic factor and Rett syndrome. *Handb. Exp. Pharmacol.* **2014**, *220*, 481-495.
 79. Li, W.; Pozzo-Miller, L. BDNF deregulation in Rett syndrome. *Neuropharmacology* **2014**, *76*, 737-746.

80. Chang, Q.; Khare, G.; Dani, V.; Nelson, S.; Jaenisch, R. The disease progression of *Mecp2* mutant mice is affected by the level of BDNF expression. *Neuron* **2006**, *49*, 341-348.
81. Deogracias, R.; Yazdani, M.; Dekkers, M. P. J.; Guy, J.; Ionescu, M. C. S.; Vogt, K. E.; Barde, Y-A. Fingolimod, a sphingosine-1 phosphate receptor modulator, increases BDNF levels and improves symptoms of a mouse model of Rett syndrome. *Proc. Natl. Acad. Sci.* **2012**, *109*, 14230-14235.
82. Ziemssen, T.; Kumpfel, T.; Linkert, W. E.; Neuhaus, O.; Hohlfeld, R. Glatiramer acetate-specific T-helper 1- and 2-type cell lines produce BDNF: implications for multiple sclerosis therapy: brain-derived neurotrophic factor. *Brain* **2002**, *125*, 2381-2391.
83. Zheng, W. H.; Quirion, R. Comparative signaling pathways of insulin-like growth factor-1 and brain-derived neurotrophic factor in hippocampal neurons and the role of the PI3 kinase pathway in cell survival. *J. Neurochem.* **2004**, *89*, 844-852.
84. Roux, J. C.; Dura, E.; Moncla, A.; Mancini, J.; Villard, L. Treatment with desipramine improves breathing and survival in a mouse model for Rett syndrome. *Eur. J. Neurosci.* **2007**, *25*, 1915-1922.
85. Zanella, S.; Mebarek, S.; Lajard, A. M.; Picard, N.; Dutschmann, M.; Hilaire, G. Oral treatment with desipramine improves breathing and life span in Rett syndrome mouse model. *Respir. Physiol. Neurobiol.* **2008**, *160*, 116-121.
86. Kron, M.; Howell, C. J.; Adams, I. T.; Ransbottom, M.; Christian, D.; Ogier, M.; Katz, D. M. Brain activity mapping in *Mecp2* mutant mice reveals functional deficits in forebrain circuits, including key nodes in the default mode network, that are reversed with ketamine treatment. *J. Neurosci.* **2012**, *32*, 13860-13872.
87. Collins, A. L.; Levenson, J. M.; Vilaythong, A. P.; Richman, R.; Armstrong, D. L.; Noebels, J. L.; Sweatt, J. D.; Zoghbi, H. Y. Mild overexpression of *Mecp2* causes a progressive neurological disorder in mice. *Hum. Mol. Genet.* **2004**, *13*, 2679-2689.
88. Moretti, P.; Zoghbi, H. Y. *Mecp2* dysfunction in Rett syndrome and related disorders. *Curr. Opin. Genet. Dev.* **2006**, *16*, 276-281.
89. Van Esch, H.; Bauters, M.; Ignatius, J.; Jansen, M.; Raynaud, M.; Hollanders, K.; Lugtenberg, D.; Bienvenu, T.; Jensen, L. R.; Gecz, J.; Moraine, C.; Marynen, P.; Fryns, J-P.; Froyen, G. Duplication of the MECP2 region is a frequent cause of severe mental retardation and progressive neurological symptoms in males. *Am. J. Hum. Genet.* **2005**, *77*, 442-453.
90. Del Gaudio, D.; Fang, P.; Scaglia, F.; Ward, P. A.; Craigen, W. J.; Glaze, D. G.; Neul, J. L.; Patel, A.; Lee, J. A.; Irons, M.; Berry, S. A.; Pursley, A. A.; Grebe, T. A.; Freedenberg, D.; Martin, R. A.; Hsich, G. E.; Khera, J. R.; Friedman, N. R.; Zoghbi, H. Y.; Eng, C. M.; Lupski, J. R.; Beaudet, A. L. Cheung, S. W.; Roa, B. B. Increased MECP2 gene copy number as the result of genomic duplication in neurodevelopmentally delayed males. *Genet. Med.* **2006**, *8*, 784-792.
91. Fisher, N. M.; Gogliotti, R. G.; Vermudez, S. A. D.; Stansley, B. J.; Conn, P. J.; Niswender, C. M. Genetic reduction or negative modulation of mGlu₇ does not impact anxiety and fear learning phenotypes in a mouse model of MECP2 duplication syndrome. *ACS Chem. Neurosci.* **2018**, *9*, 2210-2217.

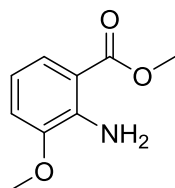
92. Wood, M. R.; Hopkins, C. R.; Brogan, J. T.; Conn, P. J.; Lindsley, C. W. "Molecular switches" on mGluR allosteric ligands that modulate modes of pharmacology. *Biochemistry* **2011**, *50*, 2403-2410.
93. Boschelli, D. H.; Wu, B.; Ye, F.; Durutlic, H.; Golas, J. M.; Lucas, J.; Boschelli, F. Facile preparation of new 4-phenylamino-3-quinolinecarbonitrile Src kinase inhibitors via 7-fluoro intermediates: identification of potent 7-amino analogs. *Bioorg. Med. Chem. Lett.* **2008**, *16*, 405-412.
94. Chopko, T. C.; Han, C.; Gregro, A. R.; Engers, D. W.; Felts, A. S.; Poslusney, M. S.; Bollinger, K. A.; Morrison, R. D.; Bubser, M.; Lamsal, A.; Luscombe, V. B.; Cho, H. P.; Schnetz-Boutaud, N. C.; Rodriguez, A. L.; Chang, S.; Daniels, J. S.; Stec, D. F.; Niswender, C. M.; Jones, C. K.; Wood, M. R.; Wood, M. W.; Duggan, M. E.; Brandon, N. J.; Conn, P. J.; Bridges, T. M.; Lindsley, C. W.; Melancon, B. J. SAR inspired by aldehyde oxidase (AO) metabolism: discovery of novel, CNS penetrant tricyclic M₄ PAMs. *Bioorg. Med. Chem. Lett.* **2019**, *29*, 2224-2228.

Appendix B

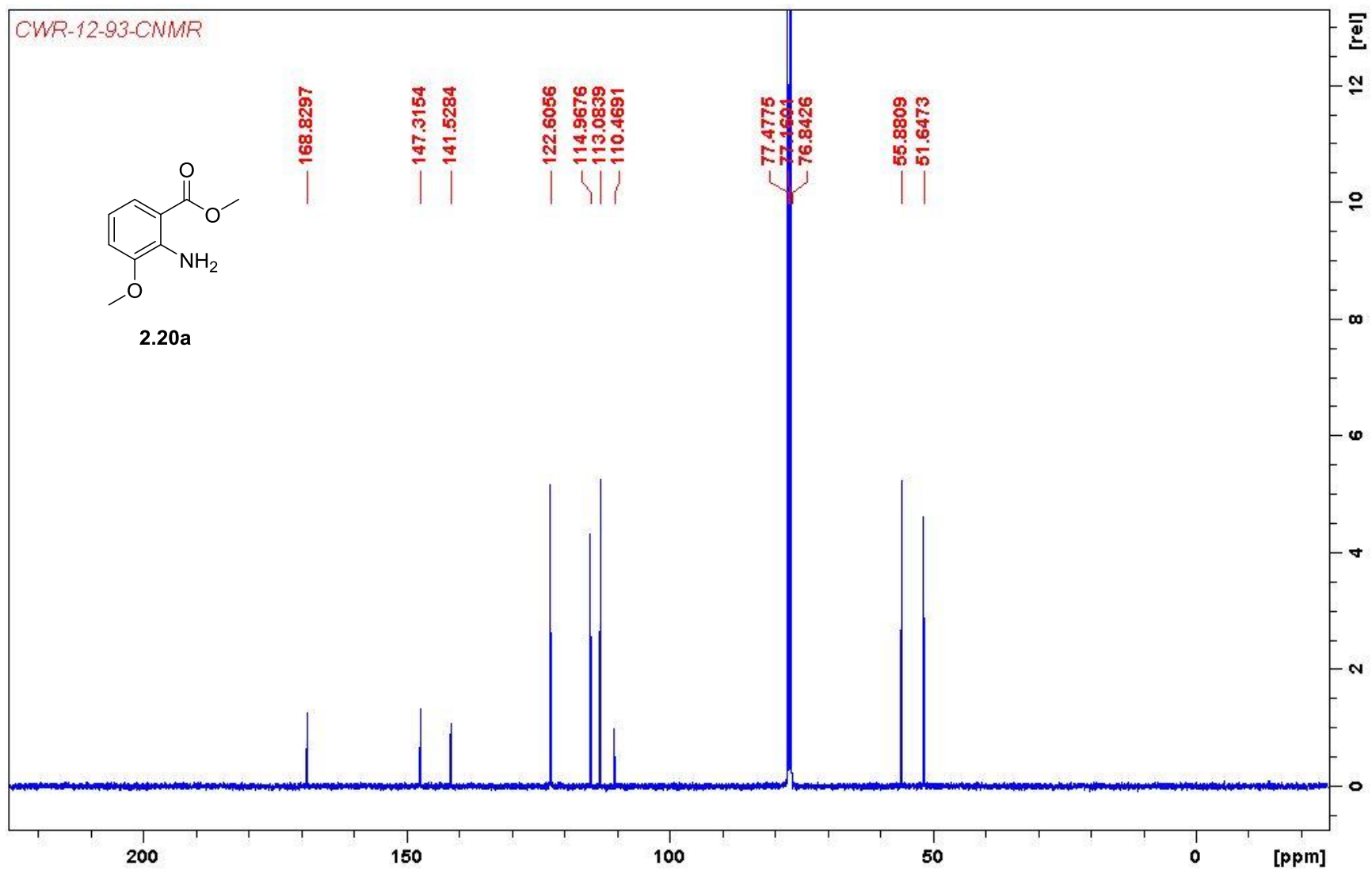
Relevant Spectra for Chapter II

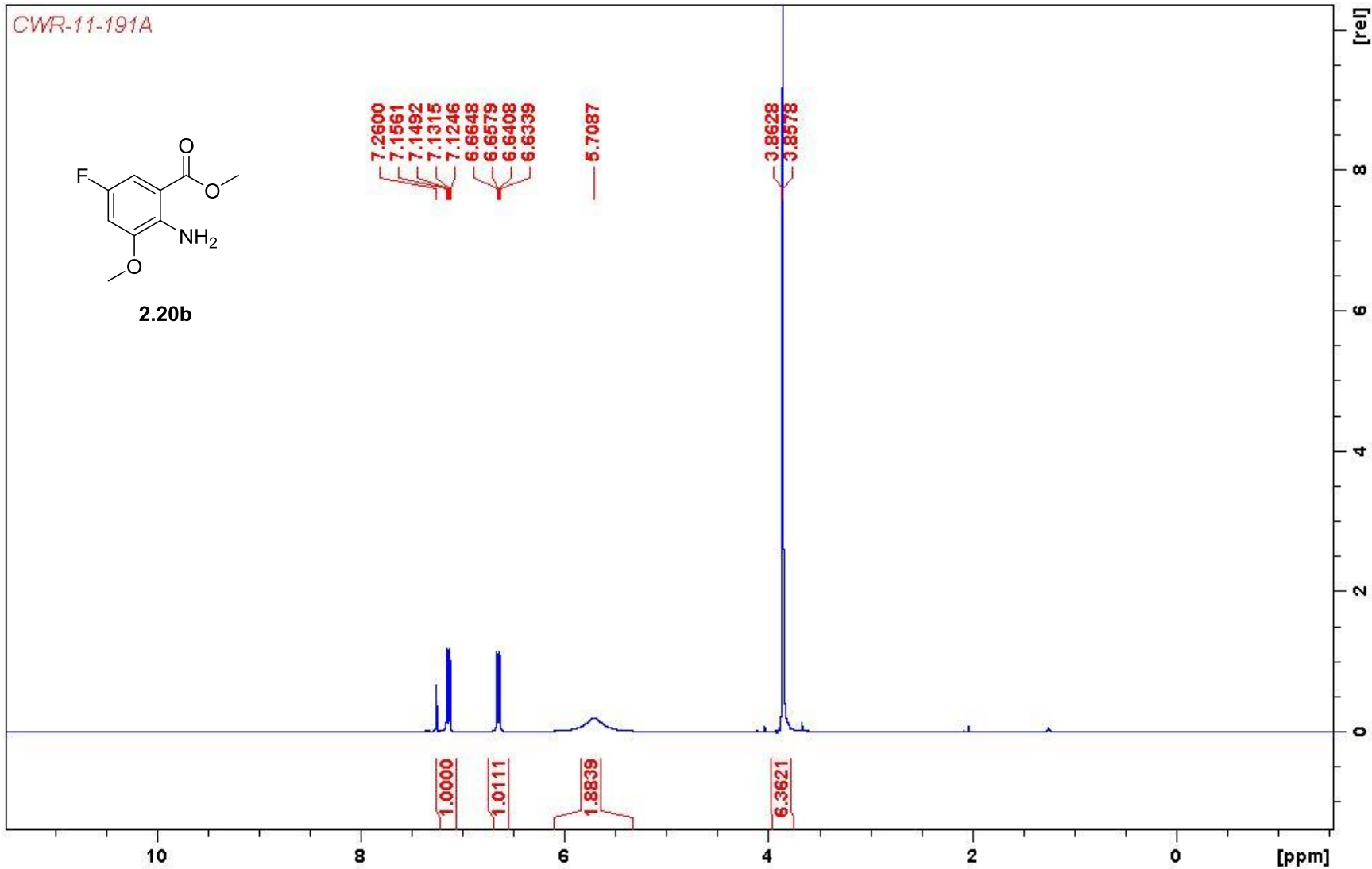


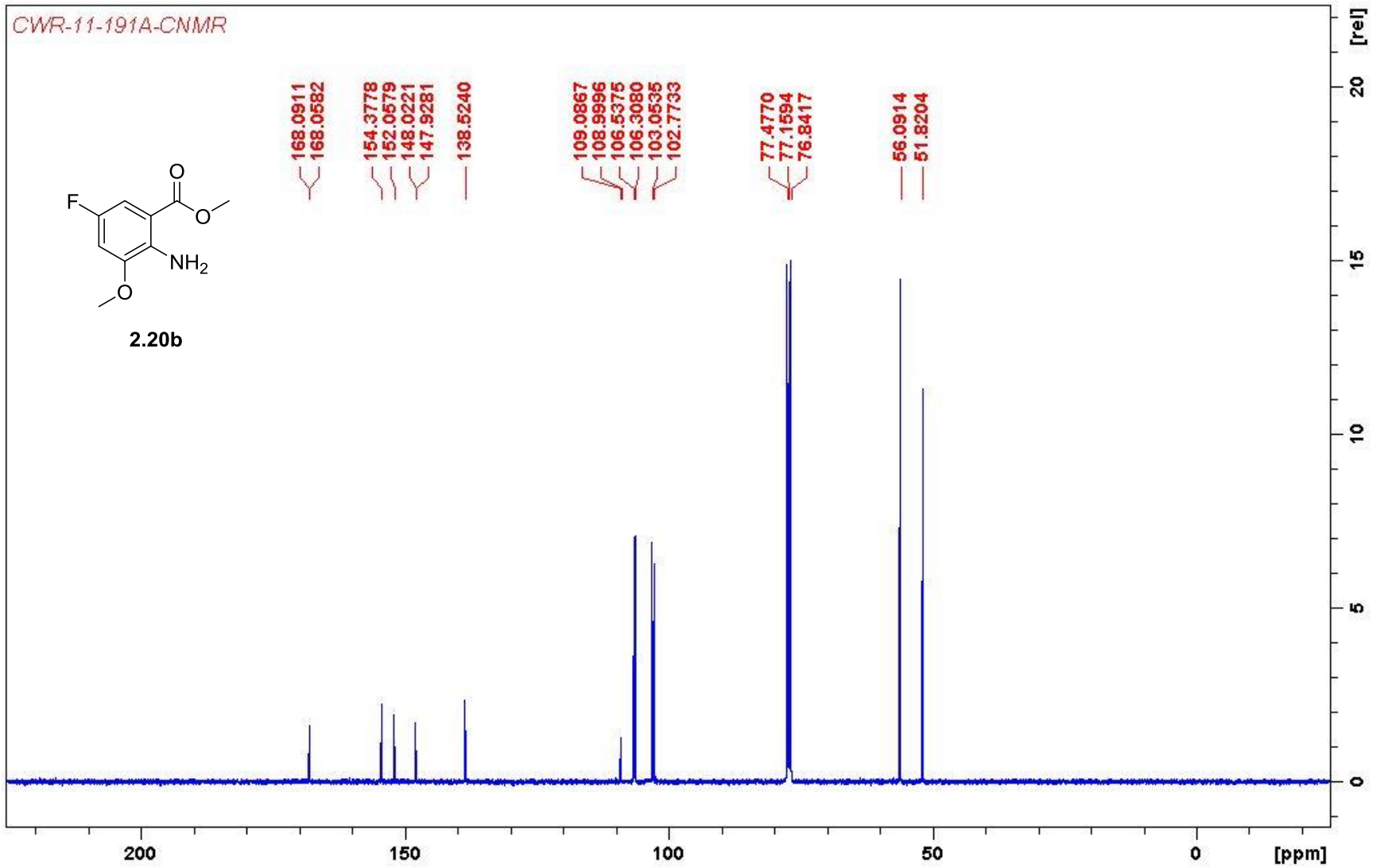
CWR-12-93-CNMR



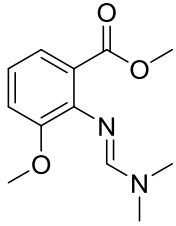
2.20a



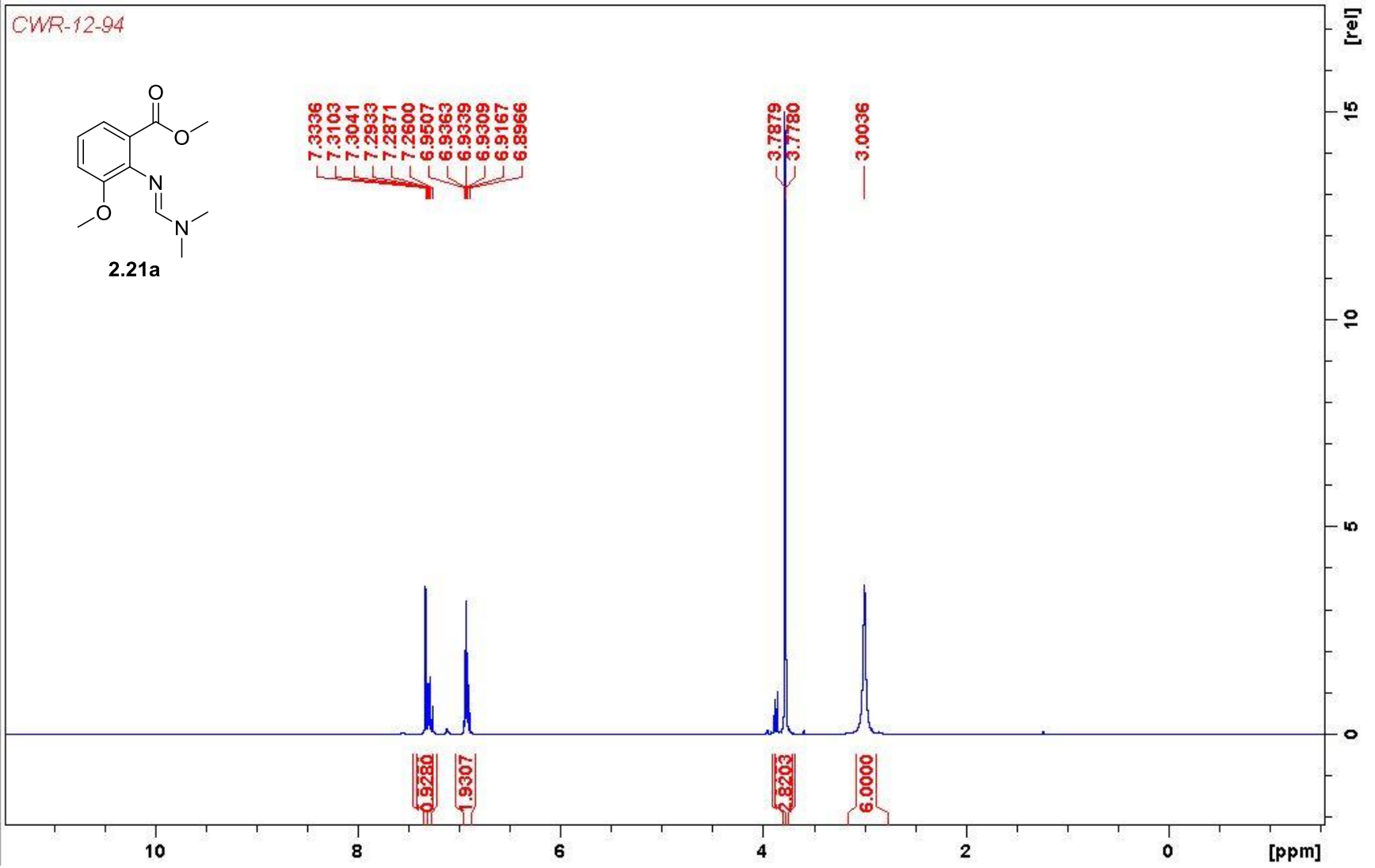




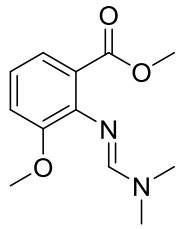
CWR-12-94



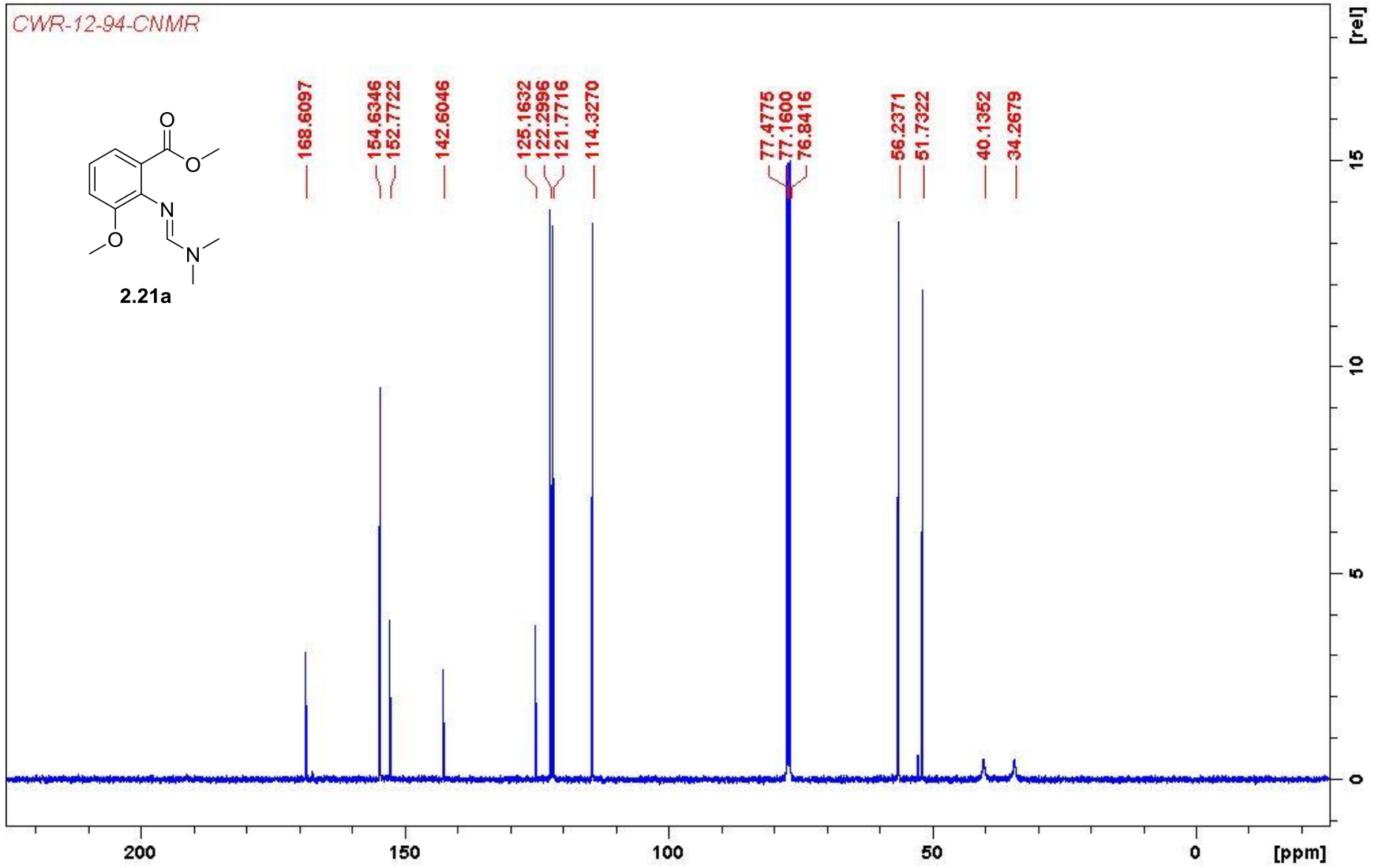
2.21a



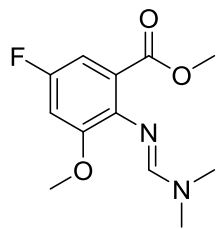
CWR-12-94-CNMR



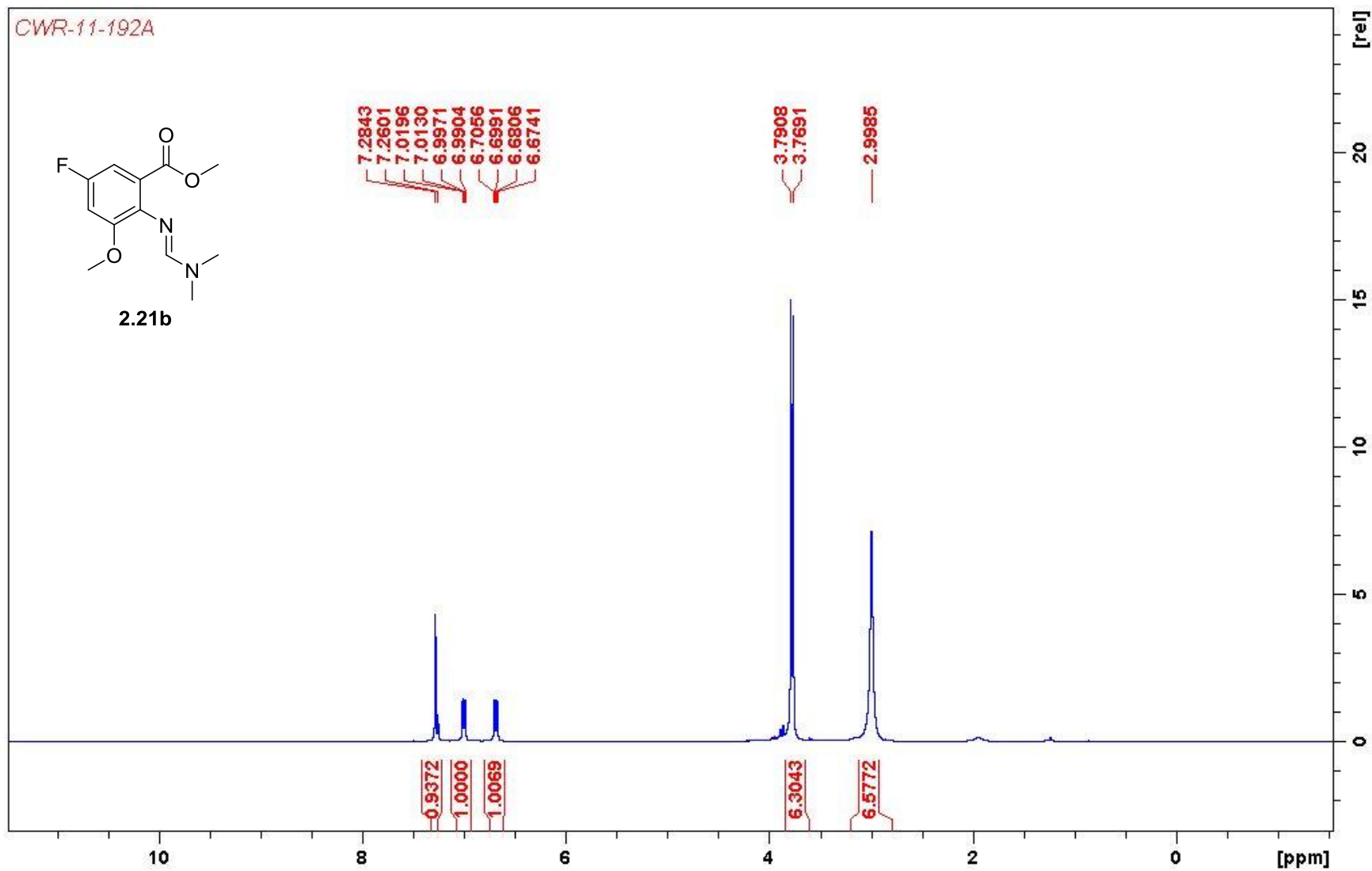
2.21a



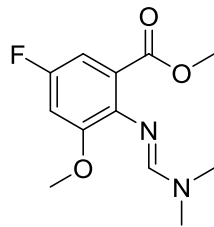
CWR-11-192A



2.21b

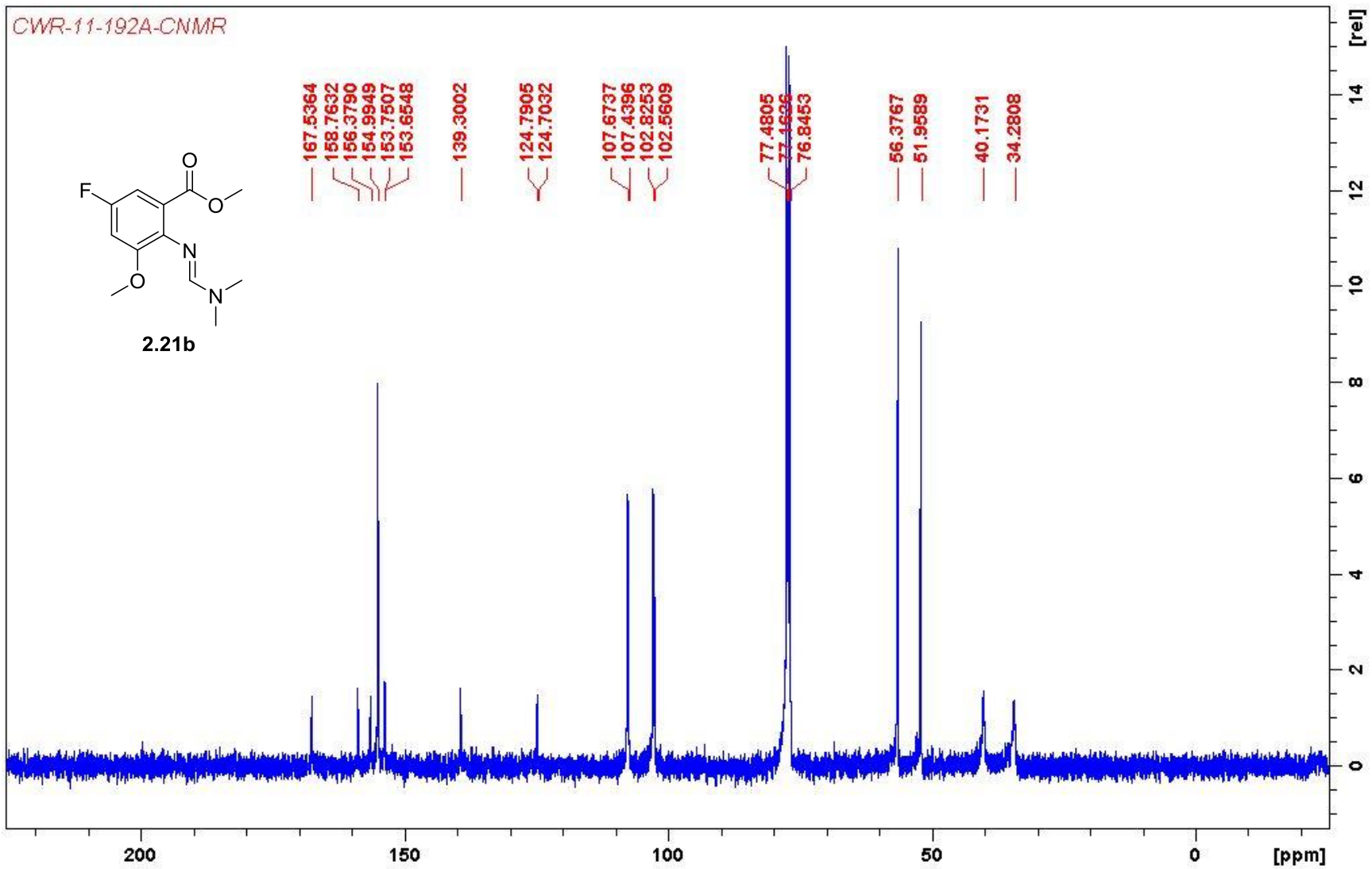


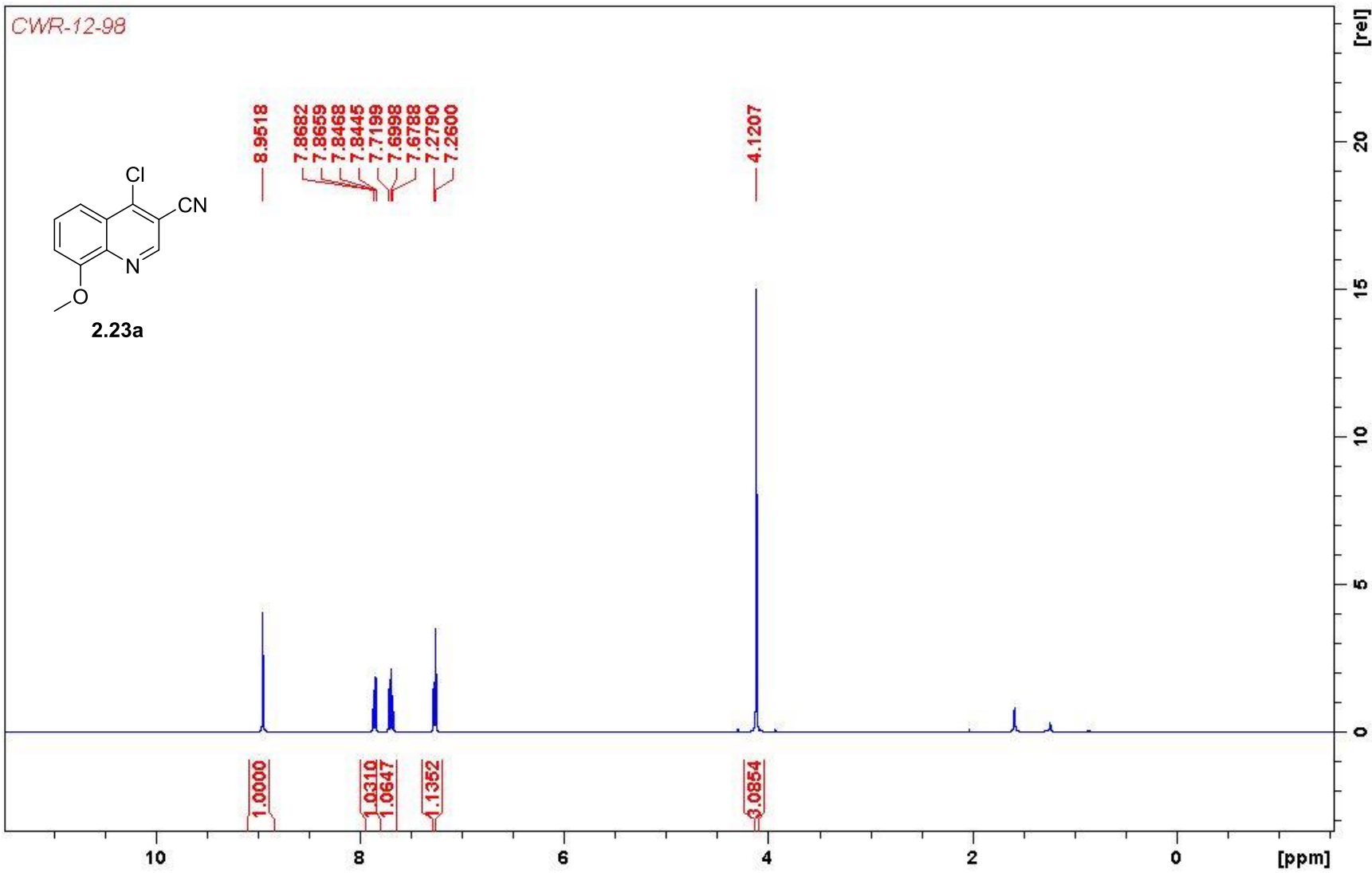
CWR-11-192A-CNMR



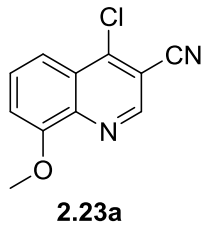
2.21b

- 167.5364
- 158.7632
- 156.3790
- 154.9949
- 153.7507
- 153.6548
- 139.3002
- 124.7905
- 124.7032
- 107.6737
- 107.4396
- 102.8253
- 102.5609
- 77.4805
- 77.4626
- 76.8453
- 56.3767
- 51.9589
- 40.1731
- 34.2808





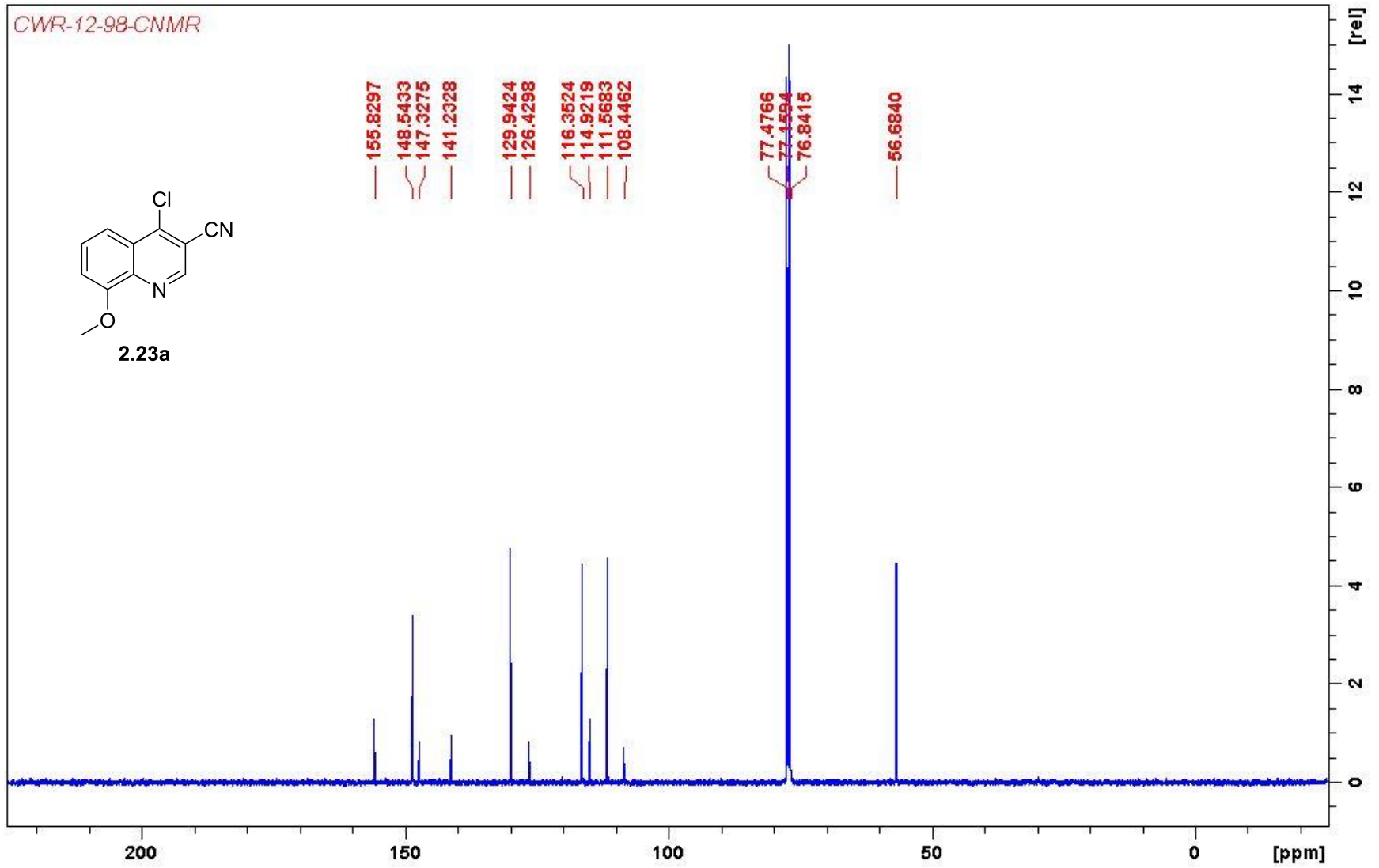
CWR-12-98-CNMR



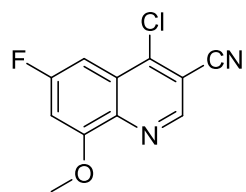
- 155.8297
- 148.5433
- 147.3275
- 141.2328
- 129.9424
- 126.4298
- 116.3624
- 114.9219
- 111.5683
- 108.4462

- 77.4766
- 77.4594
- 76.8415

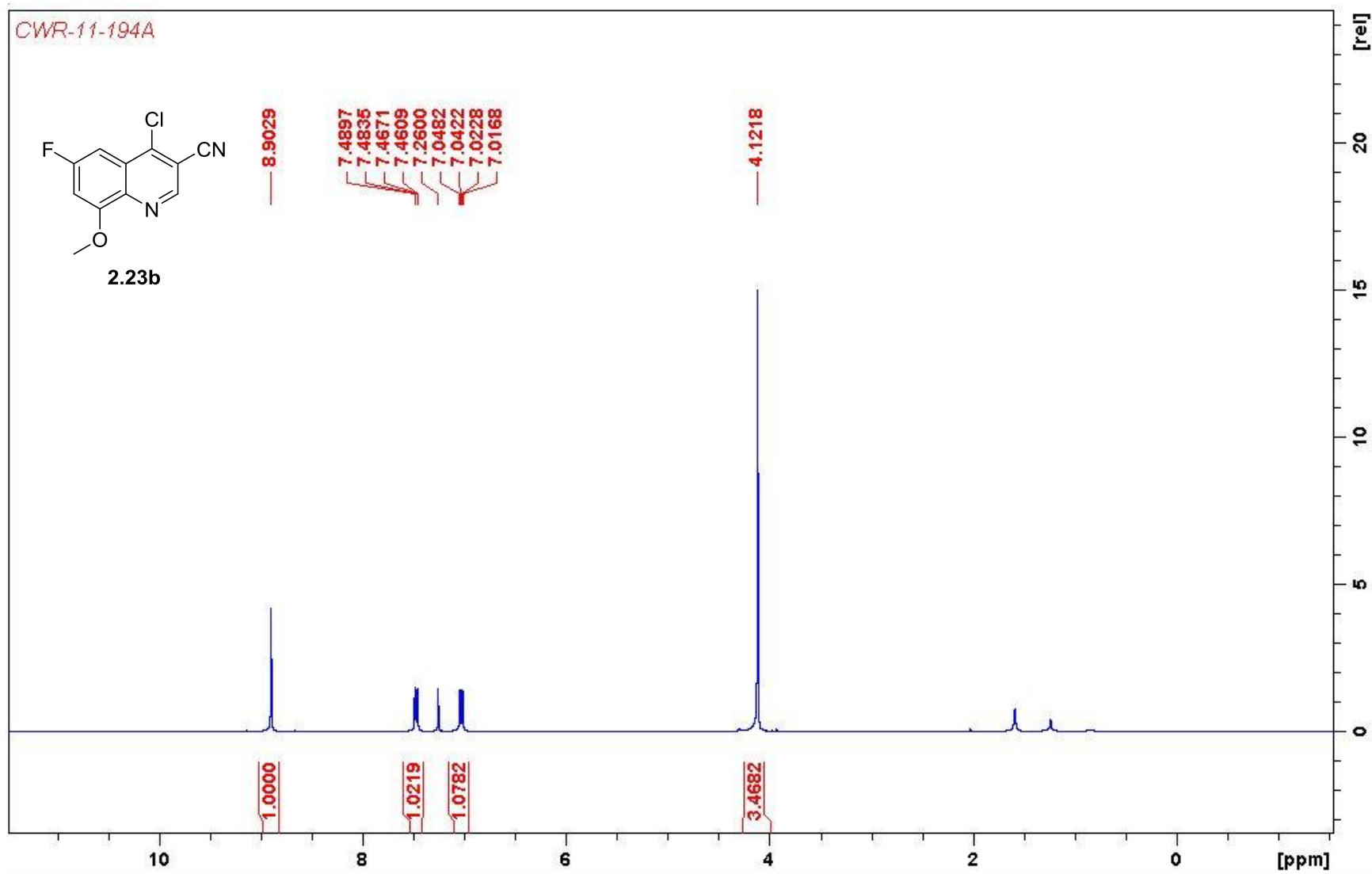
- 56.6840



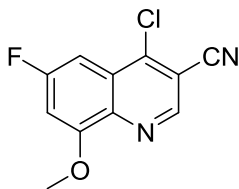
CWR-11-194A



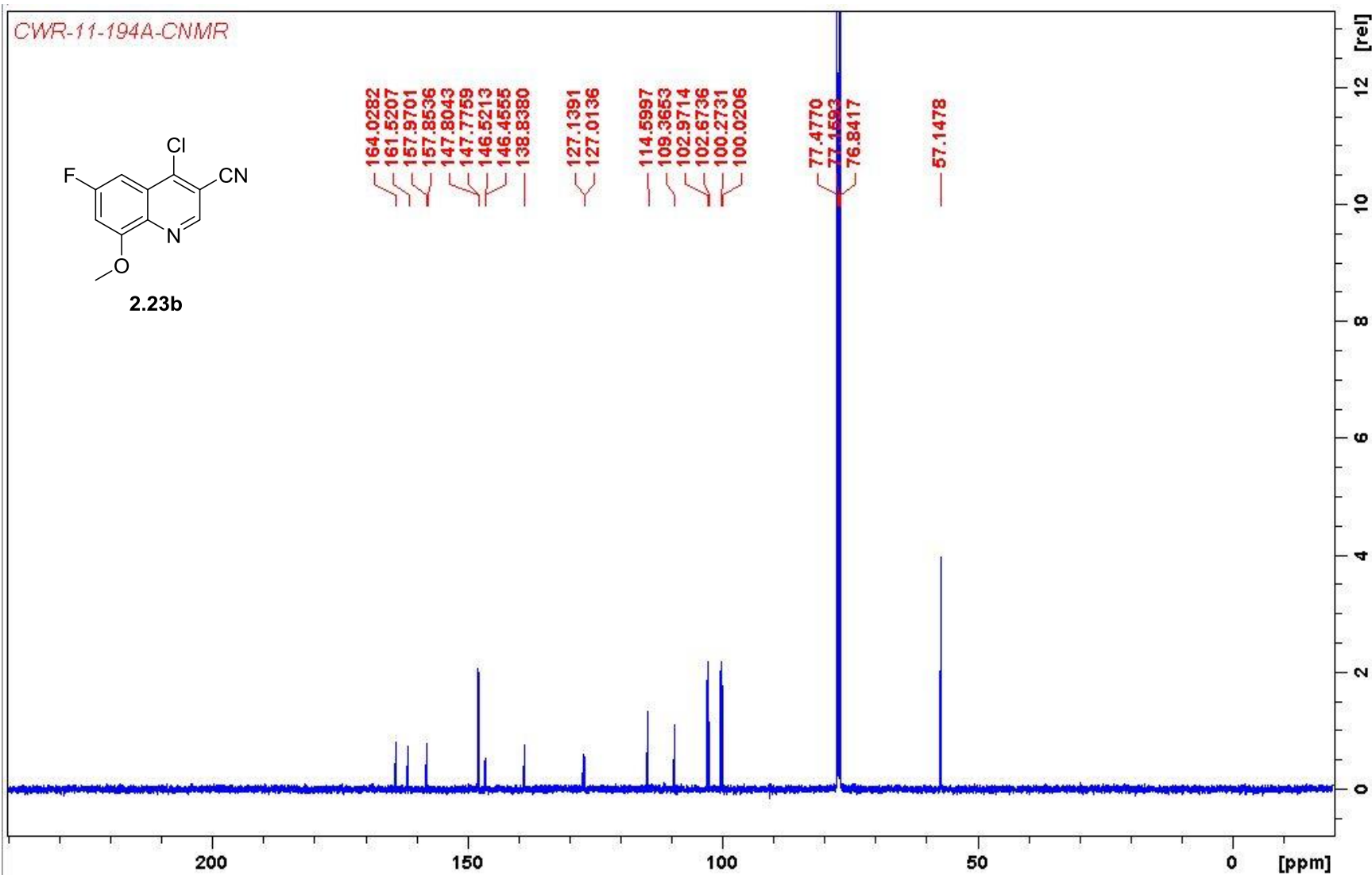
2.23b

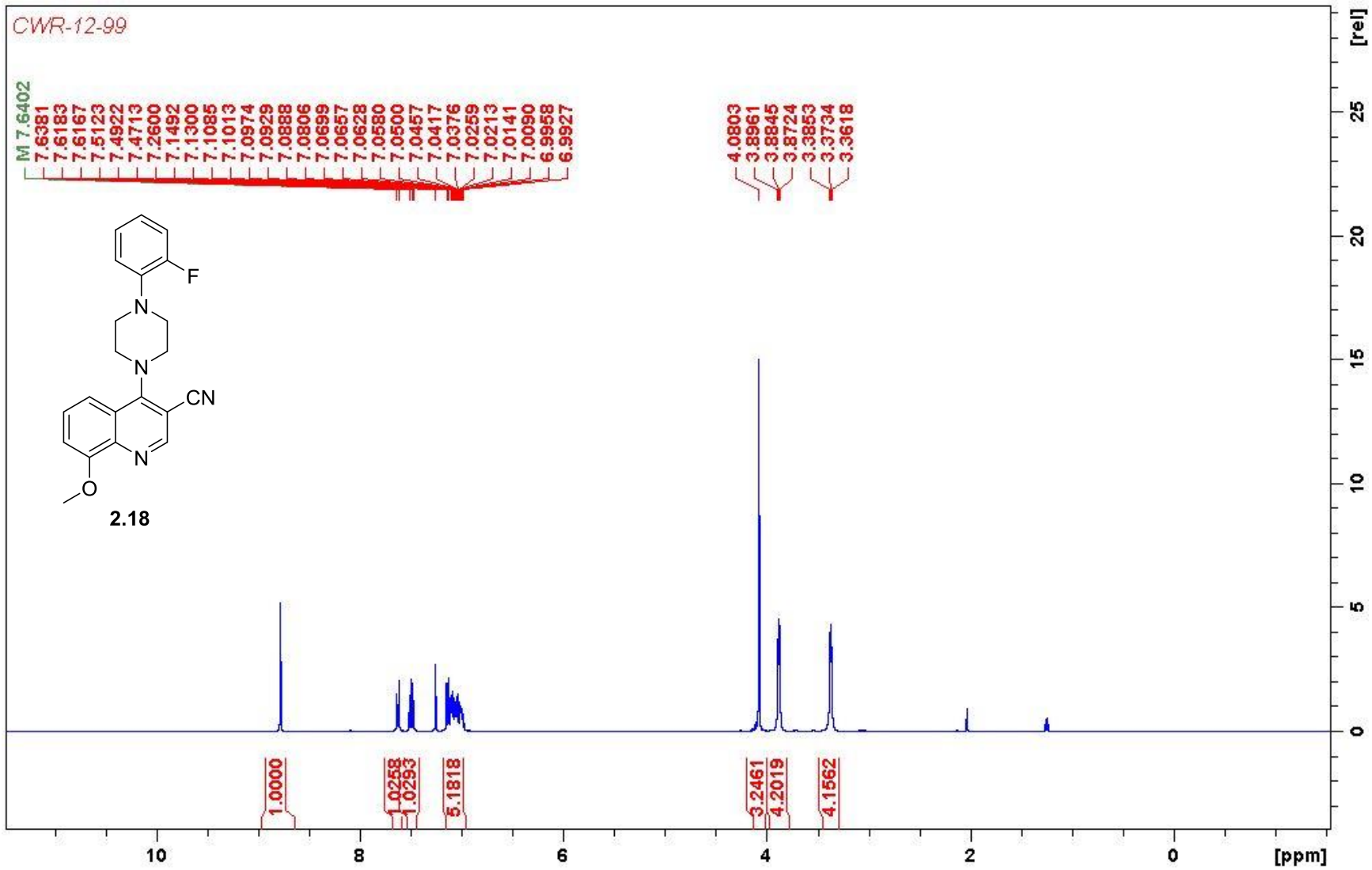


CWR-11-194A-CNMR

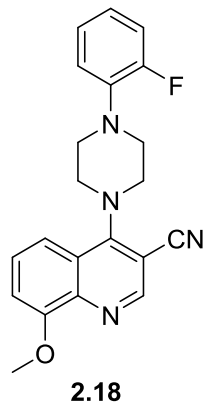


2.23b

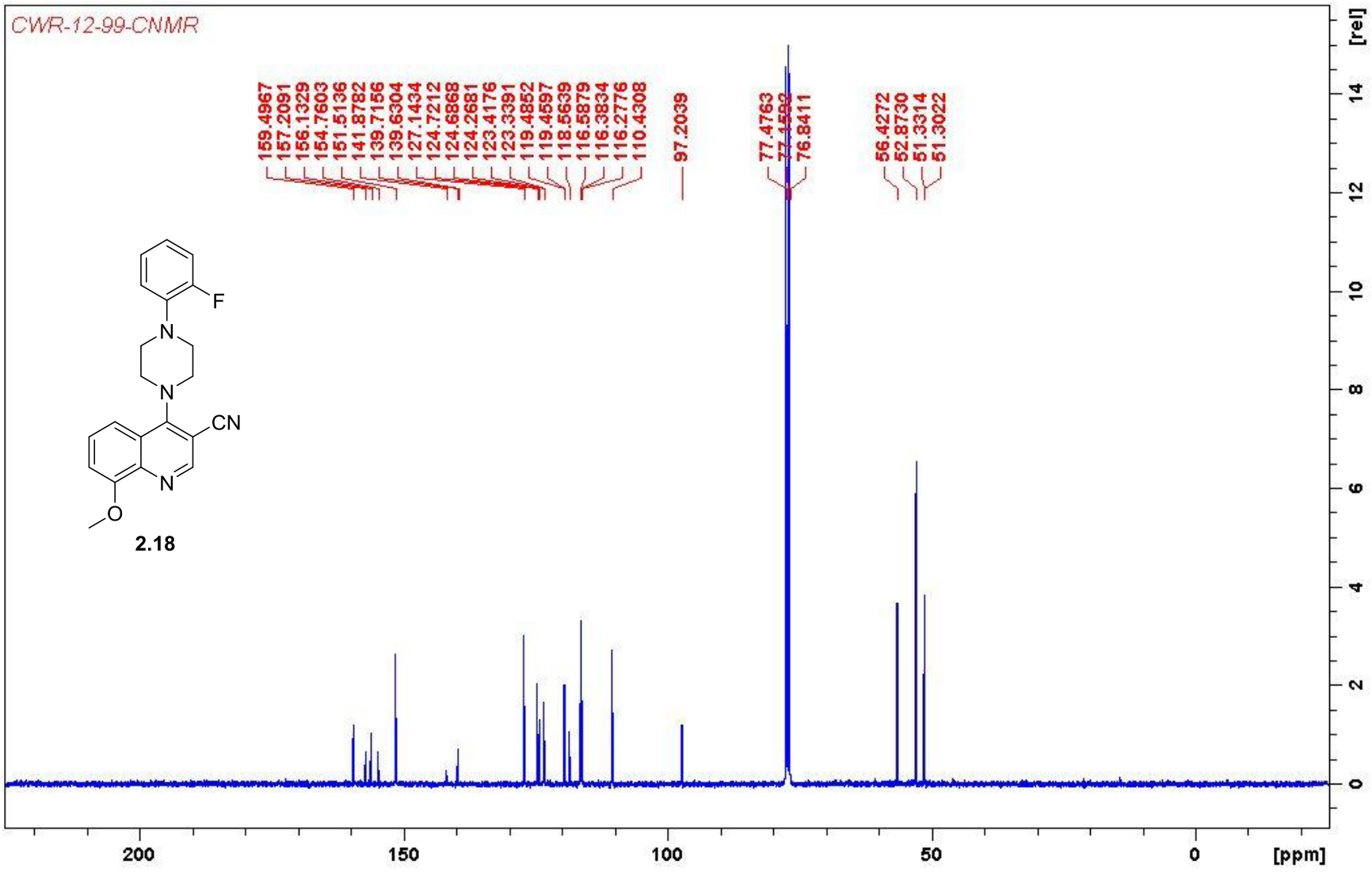


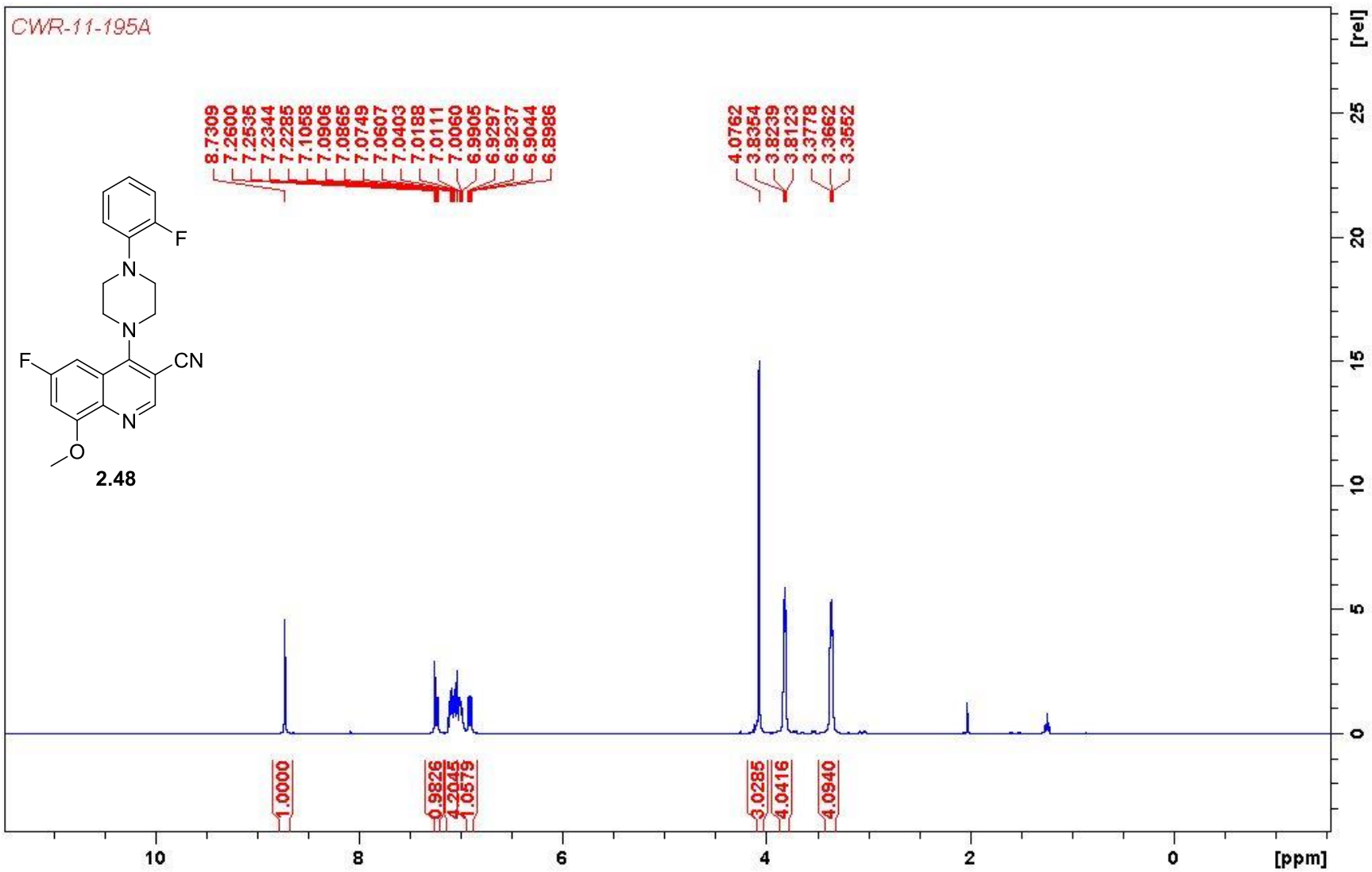


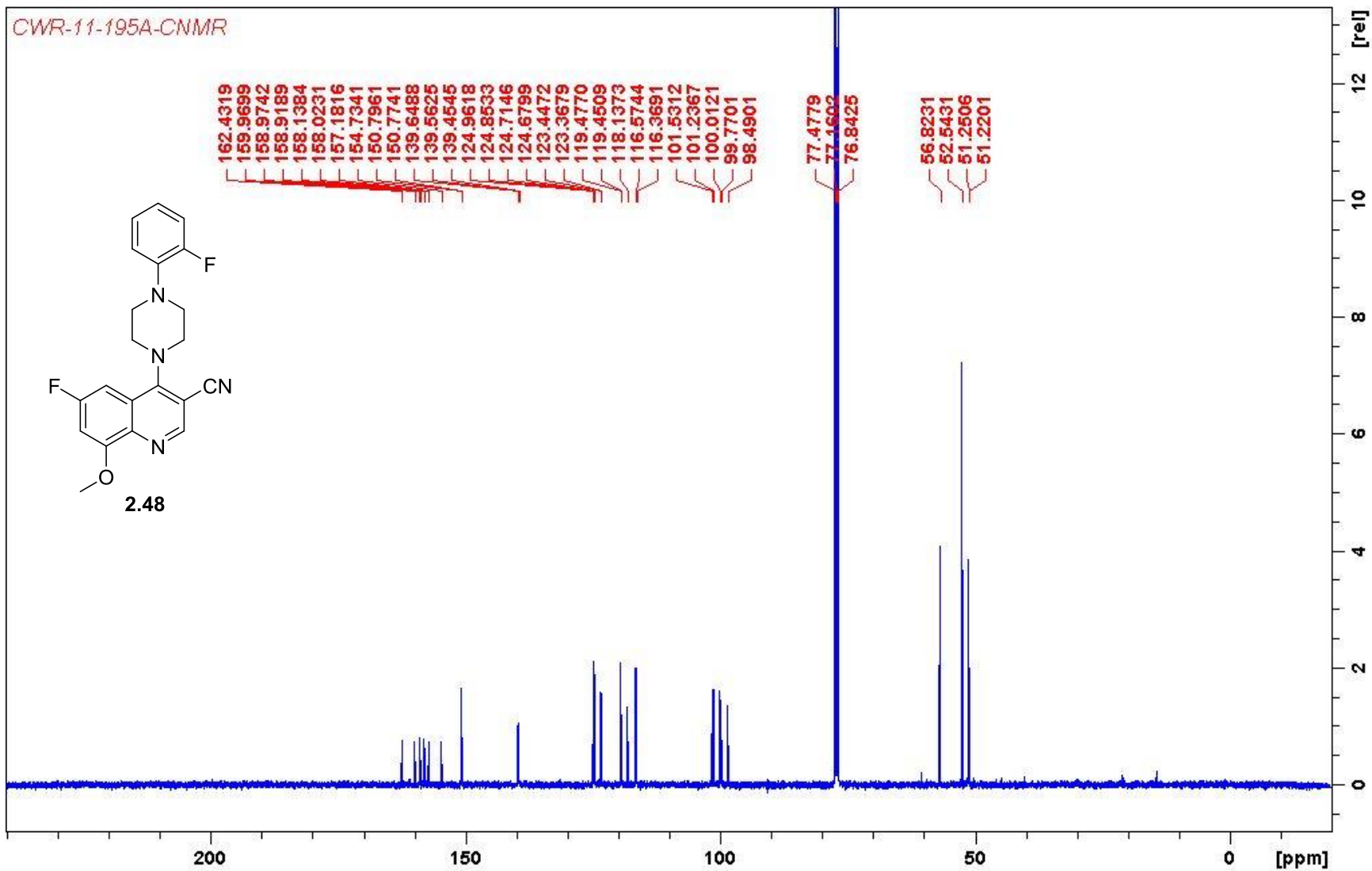
CWR-12-99-CNMR



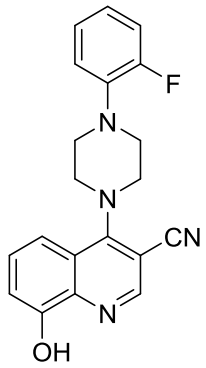
- 159.4967
- 157.2091
- 156.1329
- 154.7603
- 151.5136
- 141.8782
- 139.7156
- 139.6304
- 127.1434
- 124.7212
- 124.6868
- 124.2681
- 123.4176
- 123.3391
- 119.4852
- 119.4597
- 118.5639
- 116.5879
- 116.3834
- 116.2776
- 110.4308
- 97.2039
- 77.4763
- 77.4592
- 76.8411
- 56.4272
- 52.8730
- 51.3314
- 51.3022



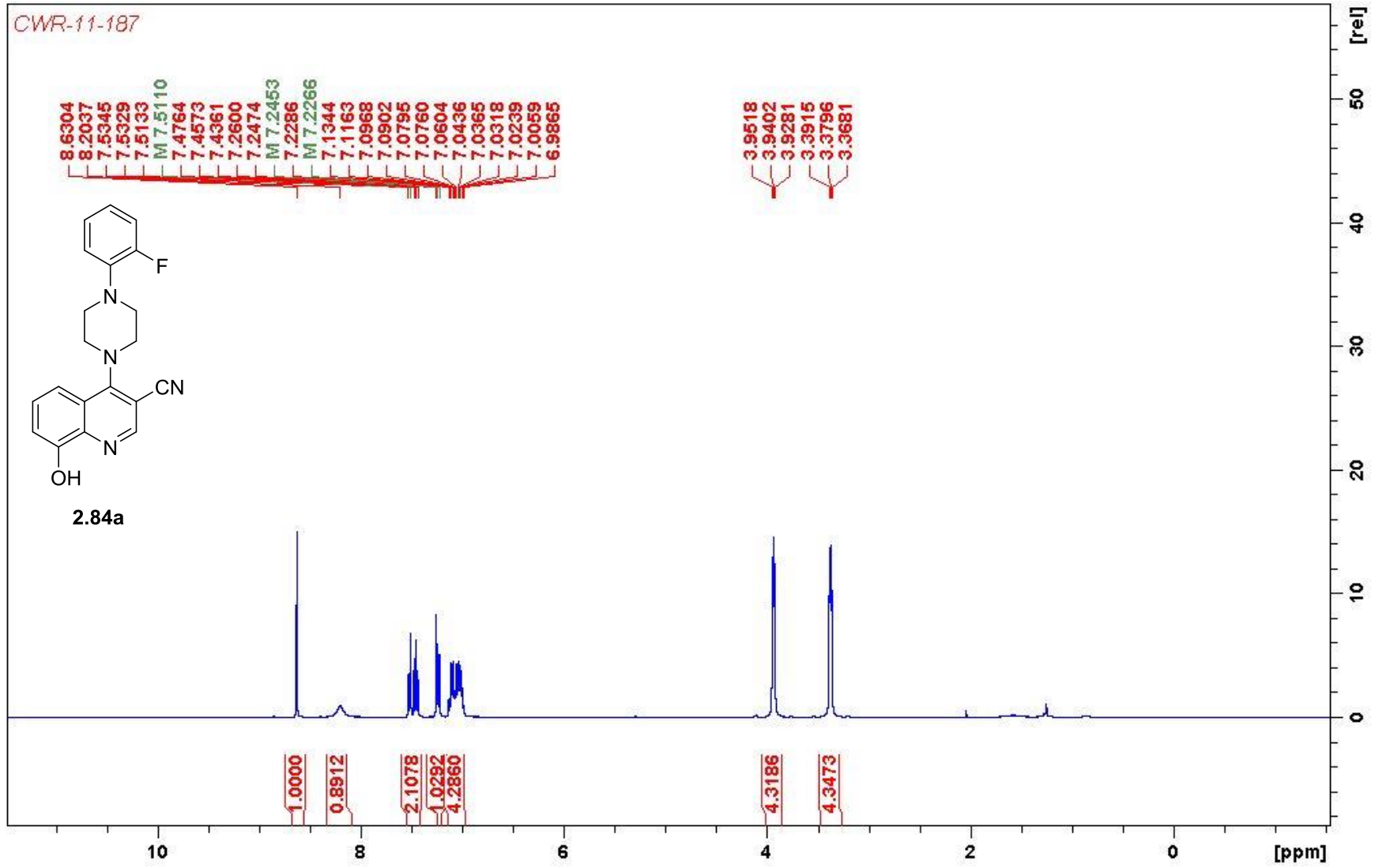




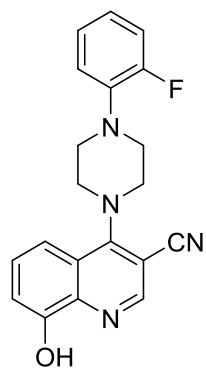
CWR-11-187



2.84a

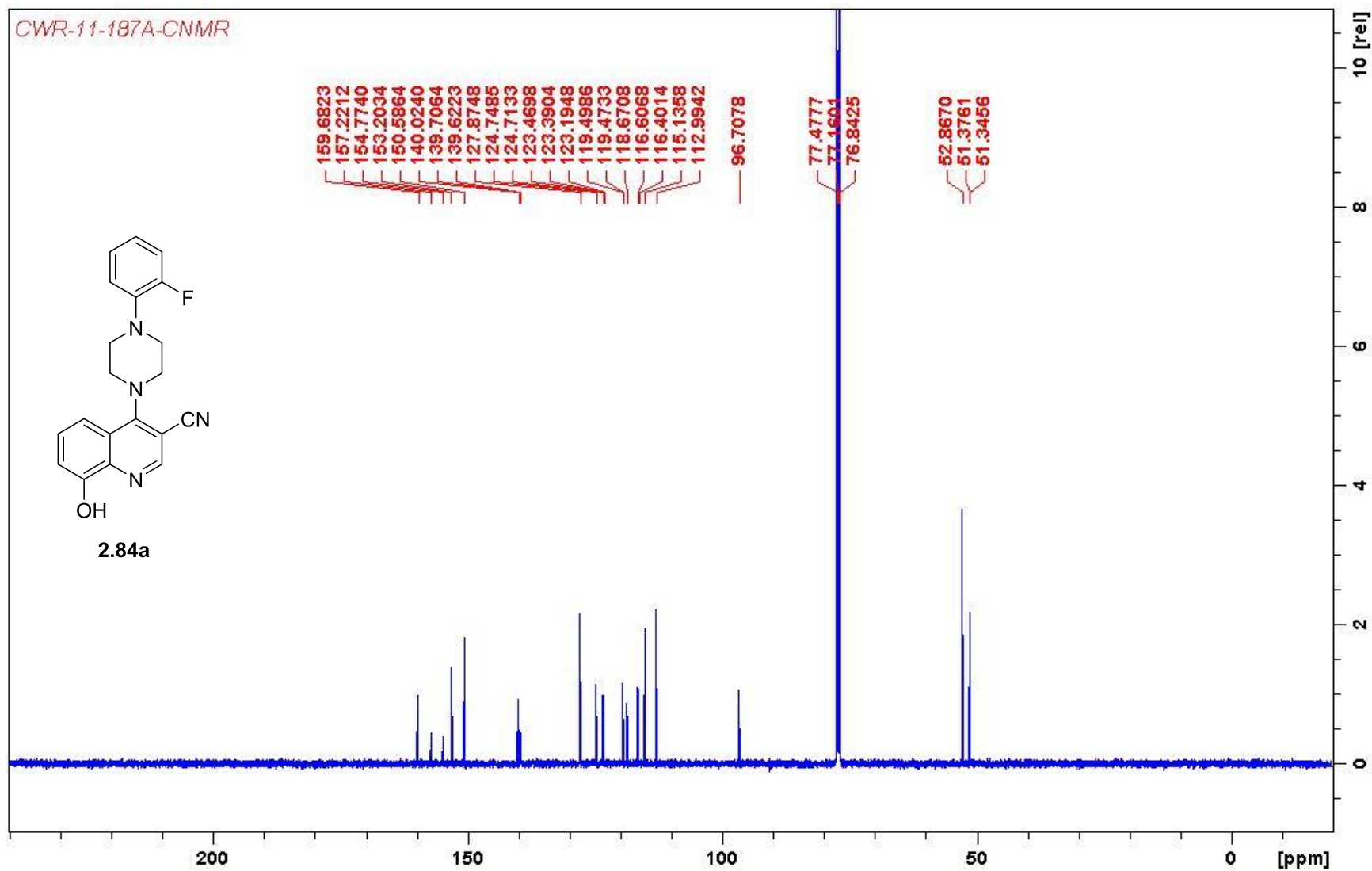


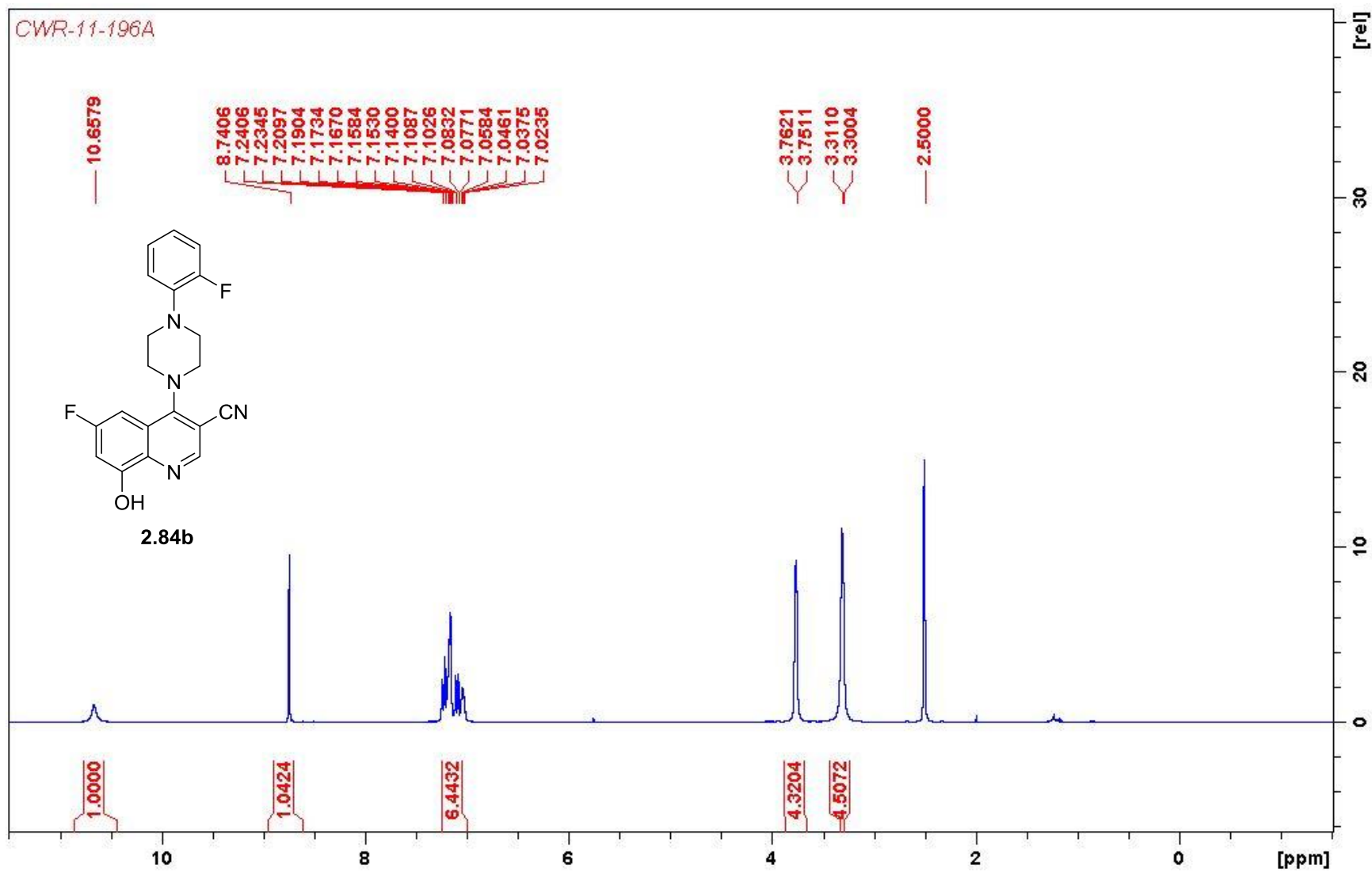
CWR-11-187A-CNMR



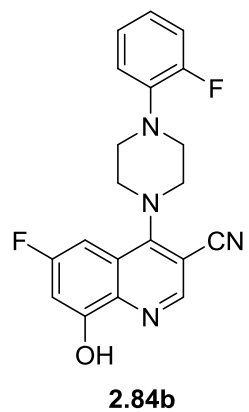
2.84a

159.6823
157.2212
154.7740
153.2034
150.5864
140.0240
139.7064
139.6223
127.8748
124.7485
124.7133
123.4698
123.3904
123.1948
119.4986
119.4733
118.6708
116.6068
116.4014
115.1358
112.9942
— 96.7078
77.4777
77.1604
76.8425
52.8670
51.3761
51.3456



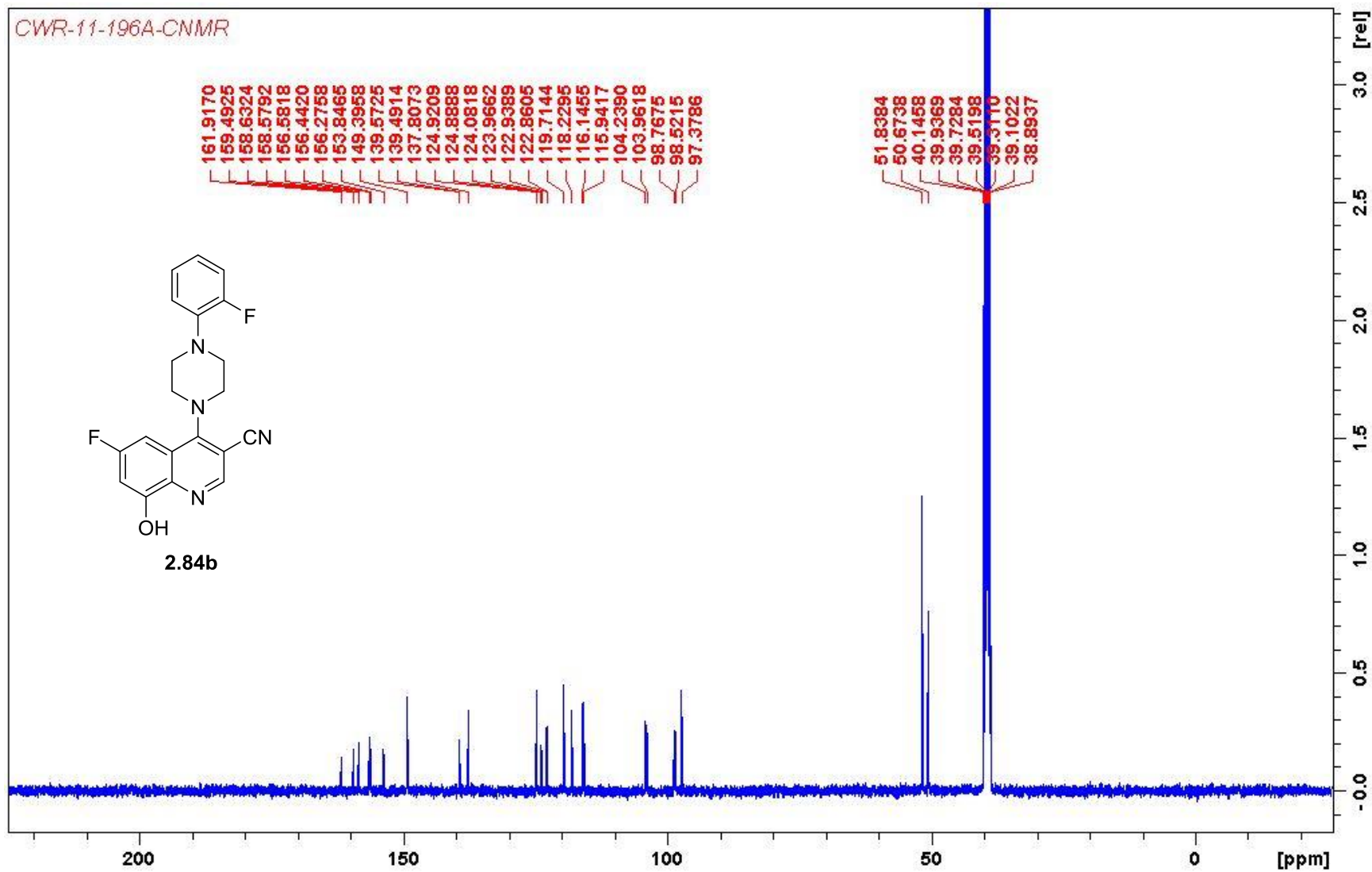


CWR-11-196A-CNMR

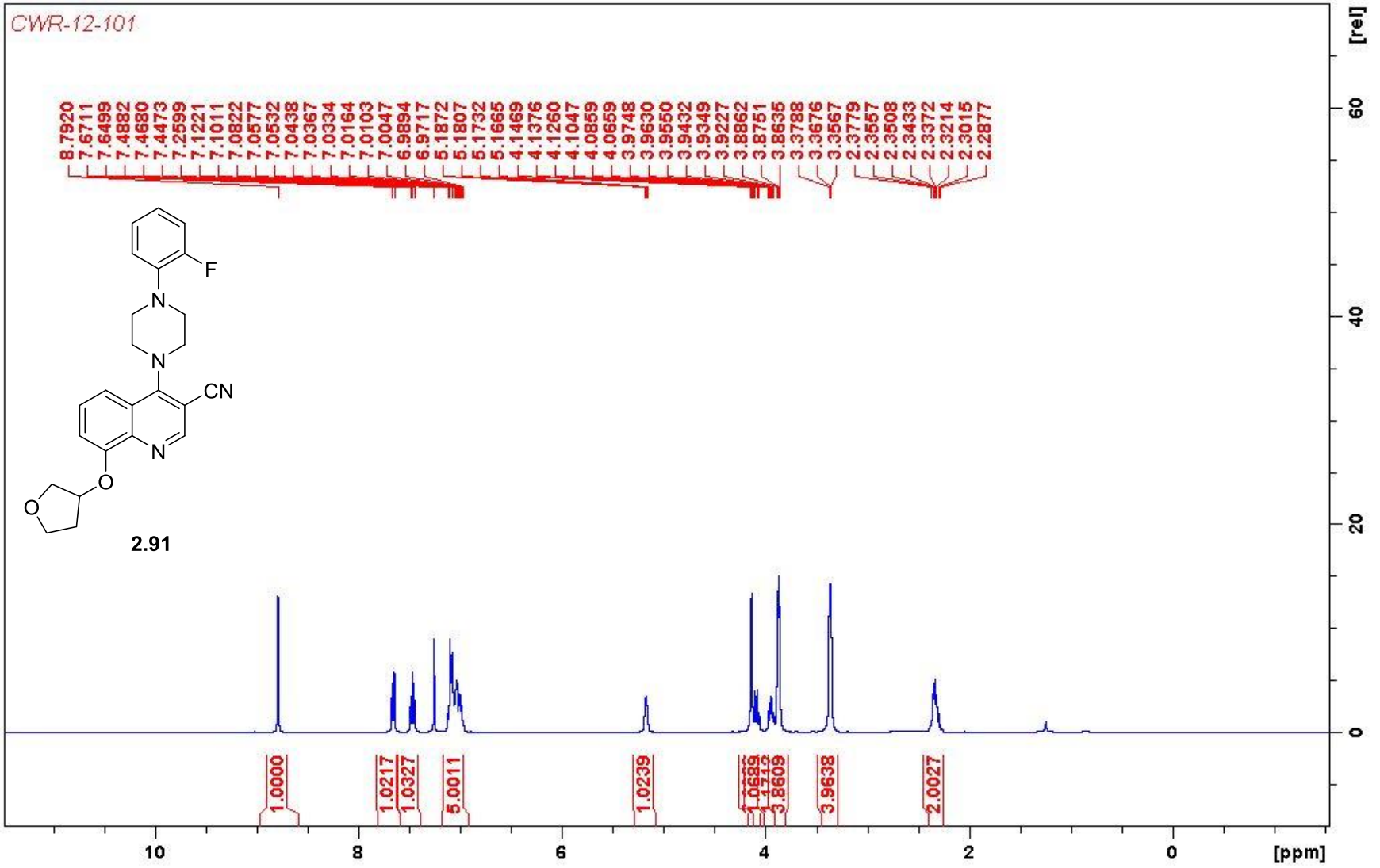


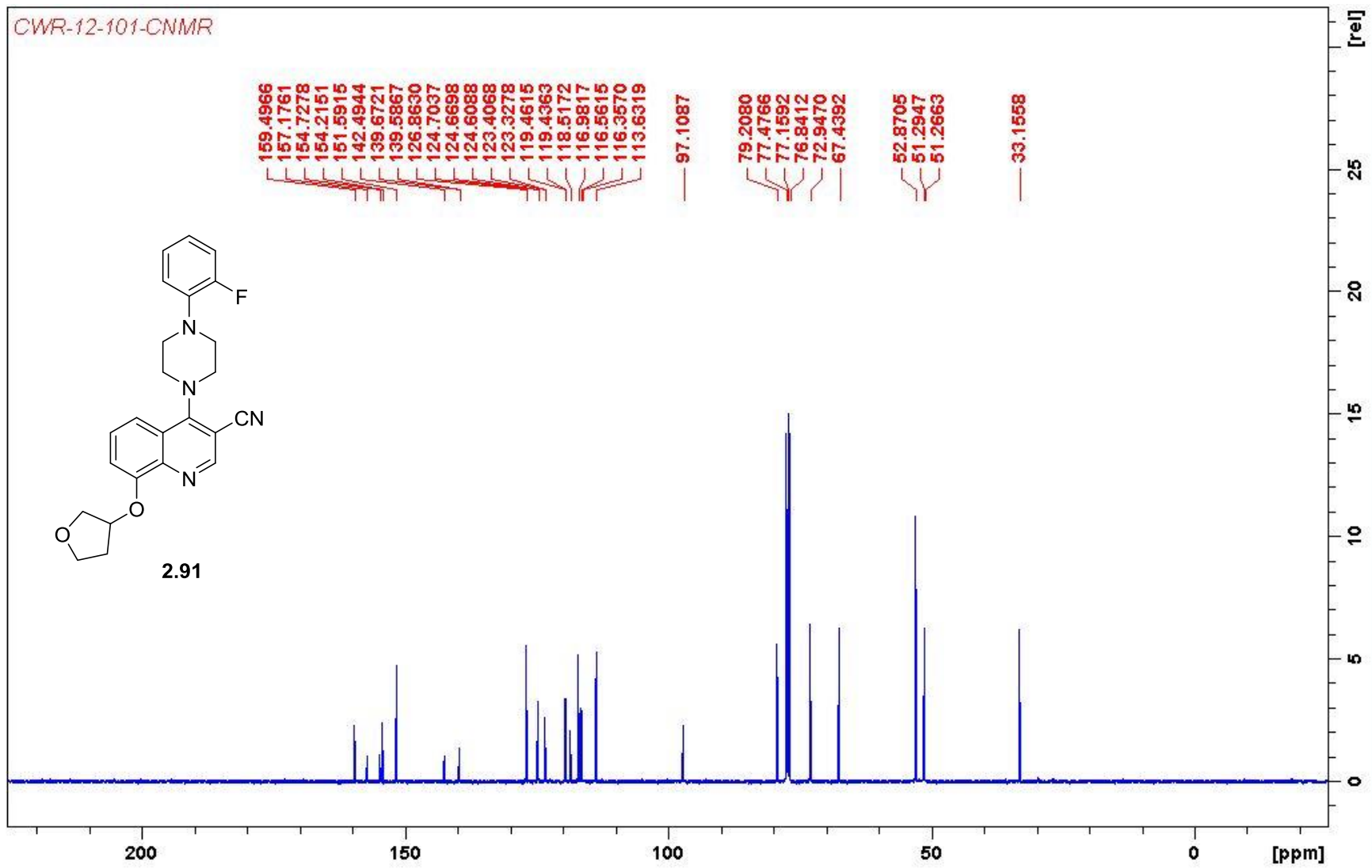
161.9170
159.4925
158.6324
158.5792
156.5818
156.4420
156.2758
153.8465
149.3958
139.5725
139.4914
137.8073
124.9209
124.8888
124.0818
123.9662
122.9389
122.8605
119.7144
118.2295
116.1455
115.9417
104.2390
103.9618
98.7675
98.5215
97.3786

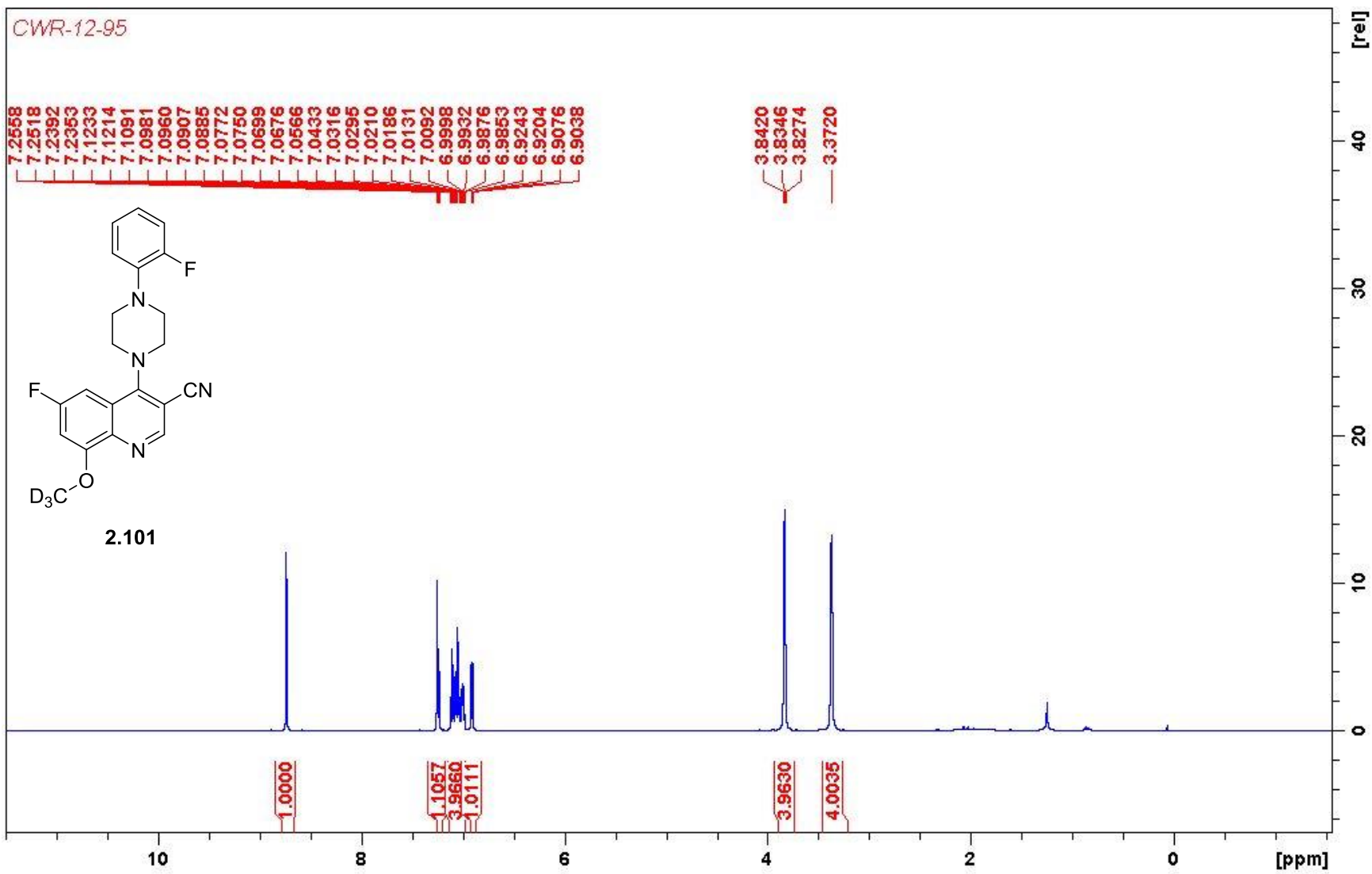
51.8384
50.6738
40.1458
39.9369
39.7284
39.5198
39.3110
39.1022
38.8937

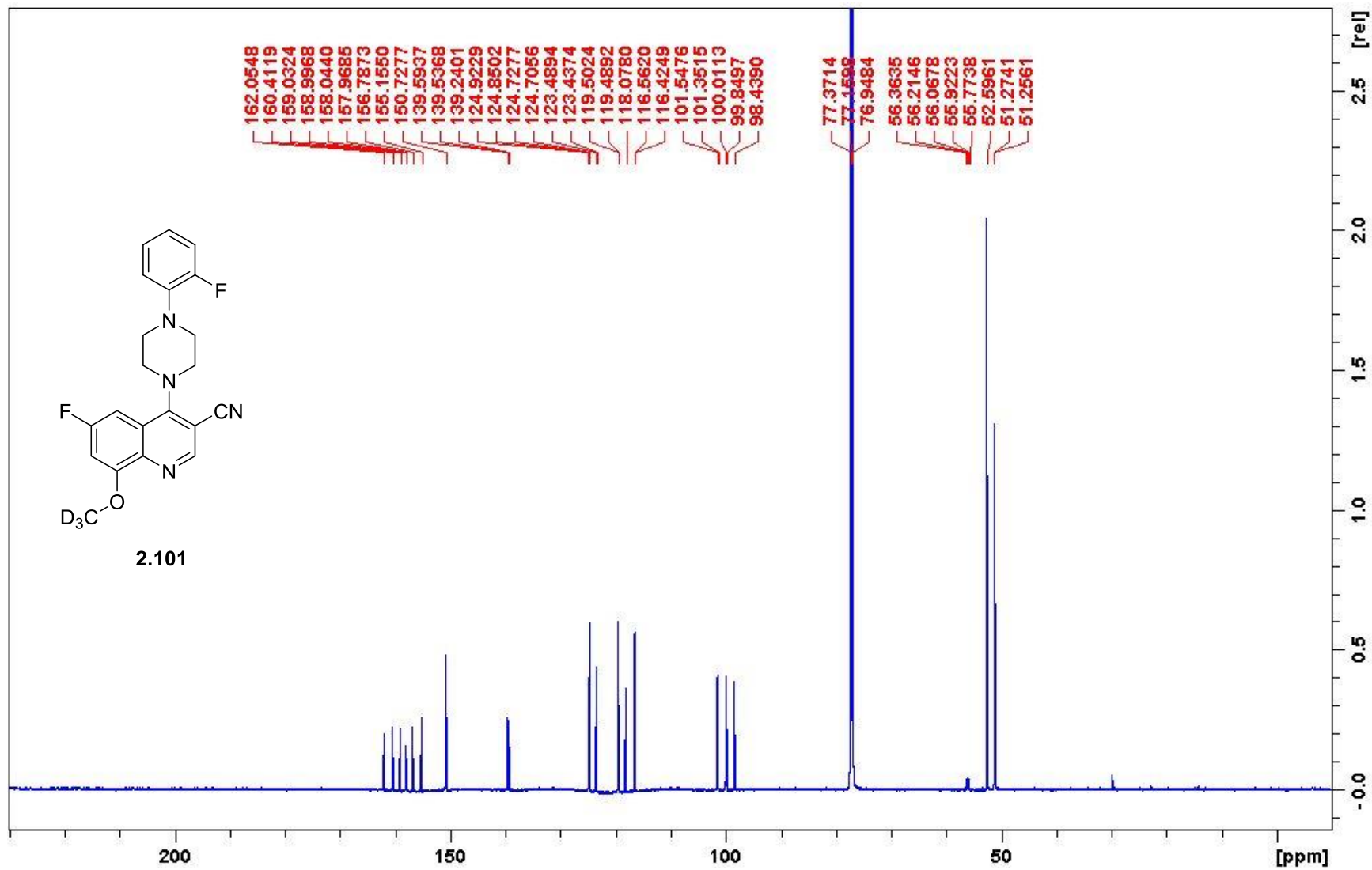


CWR-12-101

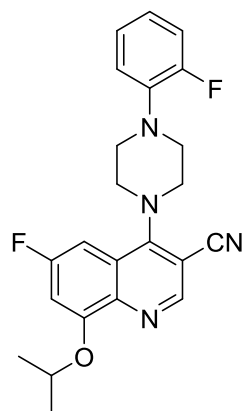








CWR-12-96



2.103

8.7629
7.2600
7.2395
7.2331
7.2148
7.2084
7.1320
7.1283
7.1106
7.1008
7.0954
7.0908
7.0804
7.0660
7.0619
7.0495
7.0456
7.0415
7.0253
7.0224
7.0150
7.0102
6.9971
6.9941
6.9346
6.9284
6.9081
6.9019

4.7988
4.7836
4.7684
4.7532
4.7380
3.8280
3.8166
3.8045
3.3797
3.3680
3.3565

1.5427
1.5276

1.0000

1.0696
4.2879
1.0312

1.0966

4.3661

4.2164

6.4605

10

8

6

4

2

0

[ppm]

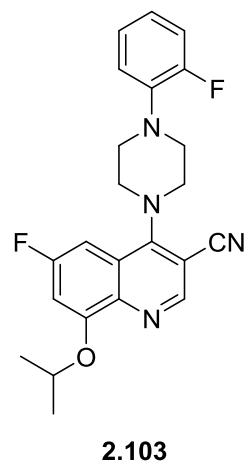
[rel]

20

10

0

CWR-12-96-CNMR



162.4524
159.9983
159.0401
158.9844
157.2061
156.5672
156.4523
154.7589
150.6430
150.6253
140.0700
139.6886
139.6035
125.2398
125.1286
124.7241
124.6892
123.4420
123.3636
119.4964
119.4731
118.2314
116.5882
116.3839
103.4033
103.1124
99.6501
99.4067
98.3184

77.4766
77.1592
76.8413
72.3219

52.5470
51.2781
51.2493

21.7746

[rel]

[ppm]

CHAPTER III

A GENERAL, ENANTIOSELECTIVE SYNTHESIS OF 2-SUBSTITUTED THIOMORPHOLINES AND THIOMORPHOLINE 1,1-DIOXIDES

Background and Introduction

Importance of Saturated Azaheterocycles

Azaheterocycles are perhaps the most important motif within agrochemical products and are also extensively explored pharmacophores within medicinal chemistry programs.¹⁻² In comparison to their unsaturated, aromatic counterparts, saturated azaheterocycles are preferable for lead optimization due to their improved solubility and

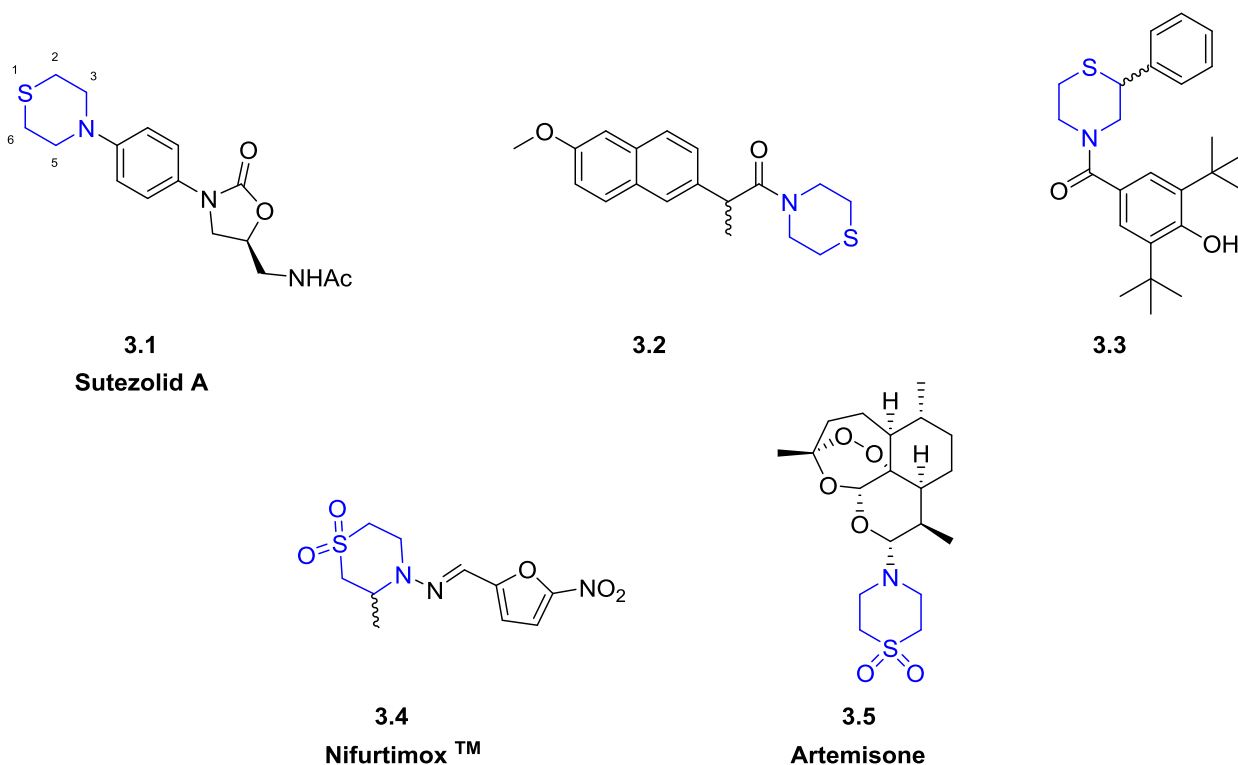


Figure 3.1. Examples of pharmaceutically relevant thiomorpholines **3.1-3.3** and their oxidized congeners (thiomorpholine 1,1-dioxides) **3.4-3.5**.

favorable metabolic and pharmacokinetic profiles.²⁻⁴ Of the saturated azaheterocycles, the thiomorpholine ring is an example of a privileged medicinal chemistry scaffold and has attracted more attention in recent years in comparison to its related morpholine counterpart.²⁻⁴ The presence of the sulfur atom in lieu of the oxygen atom not only increases this heterocycle's lipophilicity but also allows access to related heterocycles with differing oxidation states (chiral thiomorpholine 1-oxides, chiral sulfoximines, and achiral thiomorpholine 1,1-dioxides), which provides more opportunities for substrate derivatization.³

Figure 3.1 shows a few examples of biologically active compounds containing such functionalities. For example, Sutezolid A (**3.1**), an oxazolidinone antibiotic, is used to treat drug resistant strains of *Mycobacterium tuberculosis*.⁵⁻⁸ Compound **3.2**, a thiomorpholine amide derivative of the non-steroidal anti-inflammatory drug (NSAID) Naproxen, retains the anti-inflammatory properties of Naproxen while also displaying hypolipidemic activity in a rat model of hyperlipidemia.⁹⁻¹¹ In addition, the thiomorpholine amide in compound **3.3** was conducive for both hypolipidemic and antioxidant activity in Triton WR-1339-induced hyperlipidemic rats.¹¹ Unique biological activity is not solely limited to thiomorpholine analogs; thiomorpholine 1,1-dioxides are also privileged pharmacophores. For example, Nifurtimox (**3.4**) is FDA-approved for the treatment of chronic Chagas disease, while Artemisone (**3.5**) is effective in the treatment of malaria in patients infected with artemisinin resistant *Plasmodium falciparum*.¹²⁻¹⁴

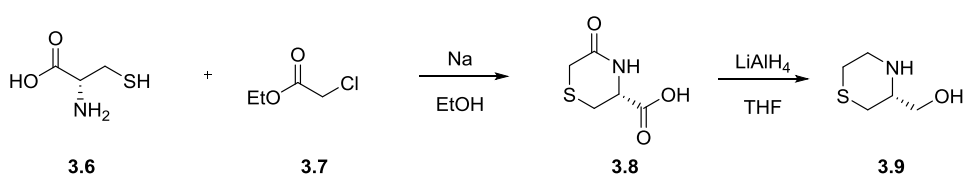
Traditional Methods for Synthesizing Substituted Thiomorpholine Heterocycles

Despite their prevalence and interesting biological activity, the various synthetic strategies for accessing 2- or 3-substituted chiral thiomorpholines are lacking.¹⁵⁻¹⁸

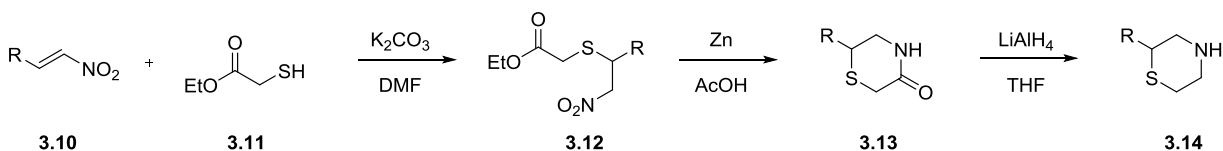
Scheme 3.1 describes the most common traditional approaches for synthesizing substituted thiomorpholines. 3-substituted thiomorpholines are made in a two-step protocol, starting with *L*-cysteine **3.6**.¹⁹ **3.6** is first deprotonated and reacted with ethyl chloroacetate **3.7** in a S_N2 reaction followed by intramolecular cyclization to form acid **3.8**. Treatment of **3.8** with an excess of lithium aluminum hydride results in the desired chiral thiomorpholine **3.9**. Unfortunately, this synthetic route relies heavily on the use of the chiral pool (cysteine amino acids) or would rely on the development of an asymmetric Strecker reaction to obtain chiral cysteine analogs.²⁰⁻²¹ Furthermore, this route does not present easy opportunities for derivatization with regards to analog development.

Scheme 3.1 also describes the traditional strategy for accessing 2-substituted thiomorpholines, which are made in a three-step protocol.²² Michael addition of ethyl thioglycolate **3.11** with α,β -unsaturated nitro compounds **3.10** affords esters **3.12**. Nitro reduction followed by intramolecular cyclization gives amides **3.13**, which can be

A: Access to Chiral 3-Substituted Thiomorpholines



B: Access to Racemic 2-Substituted Thiomorpholines



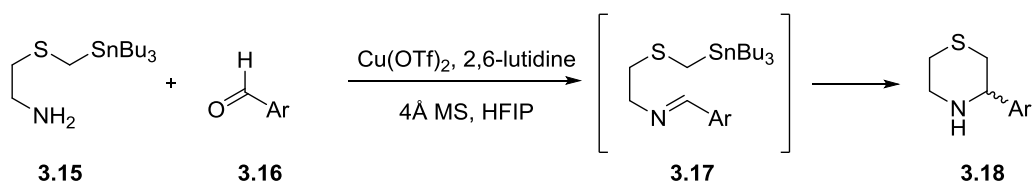
Scheme 3.1: Synthetic strategies for accessing both 3- and 2-substituted thiomorpholines.

reduced with an excess of lithium aluminum hydride to racemic thiomorpholines **3.14**. Unfortunately, with this approach, chiral HPLC/SFC is required to access enantioenriched products.

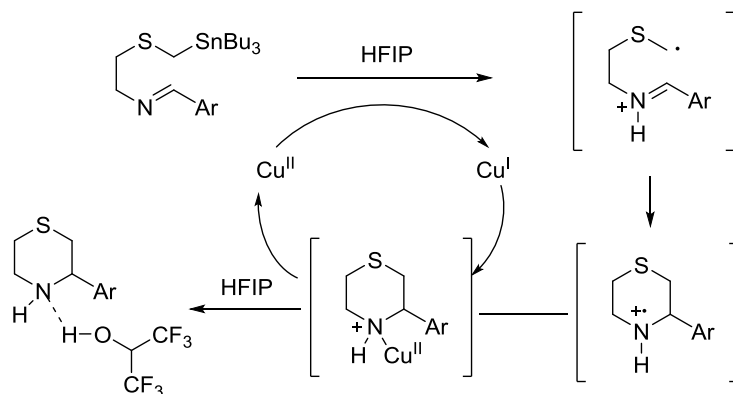
Recent Thiomorpholine Synthetic Strategies Using Transition Metals

Given these pitfalls, recent work has been devoted to improving access to both 2- and 3- chiral substituted thiomorpholines. Most notably, in 2013, the Bode group developed a facile, one-step SnAP (Stannyl Amine Protocol) reaction to access 3-aryl substituted morpholine, piperazine, and thiomorpholine heterocycles (**Scheme 3.2**).²³⁻²⁴

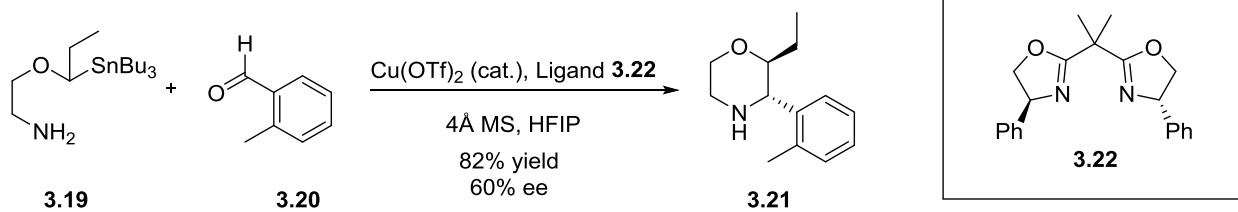
A: Initial Reaction Development Involving Stoichiometric Copper



B: Proposed Catalytic Cycle



C: Improved Catalytic Reaction Conditions

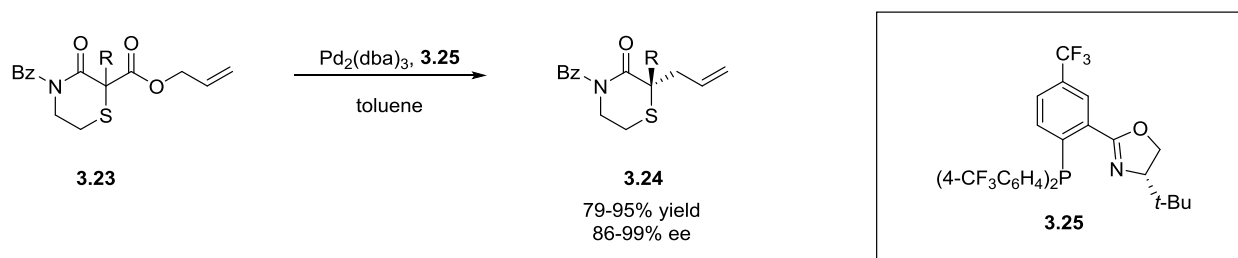


Scheme 3.2. Synthetic strategy developed by Bode and coworkers to obtain 3-aryl substituted thiomorpholines

In this protocol, organostannane **3.15** is condensed with benzaldehydes **3.16** to form intermediate imines **3.17**. Intramolecular cyclization then occurs to afford desired thiomorpholine heterocycles **3.18**.²³ Initial reports required stoichiometric amounts of Cu(OTf)₂ in order for the reaction to proceed at a reasonable rate, which led the authors to putatively assign the mechanistic role of Cu(OTf)₂ solely as a Lewis acid, activating imine **3.17** for nucleophilic attack.²³⁻²⁴ However, further mechanistic investigation utilizing radical trap experiments with TEMPO confirmed the hypothesis that the reaction does indeed involve a radical pathway, and Cu^I/Cu^{II} species would serve as electron donor/acceptor pairs in an overall redox neutral reaction (**Scheme 3.2**).²⁵ Therefore, Bode and coworkers hypothesized that the use of ligands to stabilize the Cu^I/Cu^{II} species throughout the catalytic cycle would decrease catalyst inactivation and obviate the need for stoichiometric Cu(OTf)₂. Refinement of the reaction conditions utilizing racemic PhBox ligands allowed for the incorporation of catalytic amounts (as low as 5 mol%) of Cu(OTf)₂ and the synthesis of heteroatom-substituted thiomorpholines, which were elusive under the seminal reaction conditions.²³ Given these results, the use of chiral ligand **3.22** ((S)-PhBox)) was further investigated for its utility in the enantioselective formation of these heterocycles. SnAP reagent **3.19** was condensed with benzaldehyde **3.20**, and intramolecular cyclization afforded morpholine **3.21** in excellent yield, albeit with low enantioselectivity (60% ee).²⁵ Interestingly, the application of these reaction conditions were not applied/reported towards the thiomorpholine congeners.²⁵ However, even though the improved catalytic reaction conditions are a considerable improvement, the reliance on transition metal catalyzed reactions and the use of toxic organostannane reagents are of concern. Additionally, the

SnAP strategy for synthesizing morpholine, piperazine, or thiomorpholine heterocycles only allows for the incorporation of aryl groups and not alkyl groups at the 3-position. By analyzing the proposed mechanism in **Scheme 3.2**, it is evident that the success of the reaction entails formation of imine **3.17**. Since alkyl substitutions would allow for imine/enamine tautomerization, the desired intramolecular radical cyclization would not occur. Indeed, Bode and coworkers observed only protodestannylated side products for alkyl substituted aldehydes in their reaction methodology.²⁵ Given these issues and the low enantioselectivity observed for the synthesis of morpholine **3.21**, considerable effort is still needed to access heterocycles of this nature.

In 2015, Stoltz and coworkers reported their efforts towards the enantioselective synthesis of 2,2-disubstituted thiomorpholin-3-ones, as shown in **Scheme 3.3**.²⁶⁻²⁷ In this work, thiomorpholine-3-ones **3.23** were treated with Pd₂(dba)₃ and (*S*)-*t*-BuPHOX ligand **3.25** to initiate a palladium-catalyzed decarboxylative allylation reaction to afford 2,2-disubstituted thiomorpholine-3-ones **3.24** in high yields (79-95%) and excellent enantioselectivities (86-99% ee). Various R groups (alkyl groups, benzyl groups, benzyl ethers, methyl esters, and aliphatic nitriles) were well tolerated for this reaction.²⁶⁻²⁷ However, this methodology also requires transition metal catalysis and involves lengthy synthetic routes to obtain the starting materials **3.23**, which would complicate efforts for diversification in a medicinal chemistry program.



Scheme 3.3: Synthetic strategy developed by Stoltz and coworkers to obtain 2,2-disubstituted thiomorpholine-3-ones **3.24**

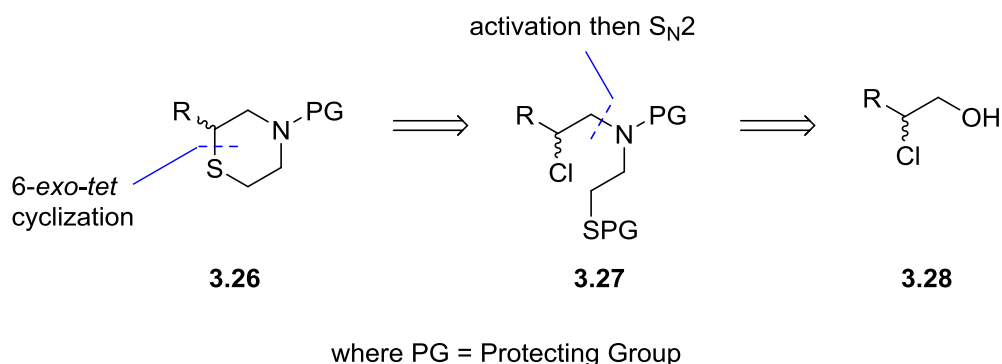


Figure 3.2: Key bond disconnections used to access β -chloro alcohols **3.28**

Proposed Synthetic Strategy for Accessing Chiral 2-Substituted Thiomorpholines Using Organocatalysis

In light of these current synthetic strategies, we sought to develop a robust synthetic approach for synthesizing chiral 2-substituted thiomorpholines **3.26**, where **Figure 3.2** highlights the key bond disconnections and our retrosynthetic analysis towards these compounds. β -chloro alcohols **3.28** were identified as ideal synthetic precursors en route to thiomorpholines **3.26**. Since we did not want to rely on the preexisting chiral pool for defining the stereochemistry at the β -position, we wanted to utilize robust asymmetric induction strategies to access both enantiomers of **3.28** for a diverse substrate scope. In order to achieve this level of asymmetric induction, chemists have relied heavily on the use of C_2 -symmetric organocatalysts.²⁸ Utilizing organocatalysis with C_2 -symmetric amines is a very powerful synthetic strategy for inducing asymmetry within a scaffold, since the unique steric environment introduced by these chiral auxiliaries reduces the number of competing, diastereomeric transition states for a given chemical transformation.²⁸ Both Whitesell and Katsuki have previously demonstrated the synthetic utility of C_2 -symmetric pyrrolidine chiral auxiliaries in a

variety of asymmetric reactions including the alkylation of enamides and amides, aldol reactions, [2,3]-Wittig rearrangements, and Diels-Alder reactions.²⁹⁻³⁸

In 2004, Jørgensen and coworkers published their efforts towards the asymmetric α -chlorination of aldehydes utilizing different C_2 -symmetric amine organocatalysts.³⁹ In this methodology, reaction of aldehydes **3.29** with the C_2 -symmetric (2*R*,5*R*)-diphenylpyrrolidine organocatalyst **3.31** and *N*-chlorosuccinimide (NCS) as an electrophilic chlorine source afforded α -chloro aldehydes **3.30** in high yields (up to 99% yield) and excellent enantioselectivities (up to 95% ee) (**Figure 3.3**)³⁹. While the substrate scope was limited to simple aliphatic systems, we decided that Jørgensen's efforts would serve as an excellent starting point for our methodology en route to β -chloro alcohols **3.28**.

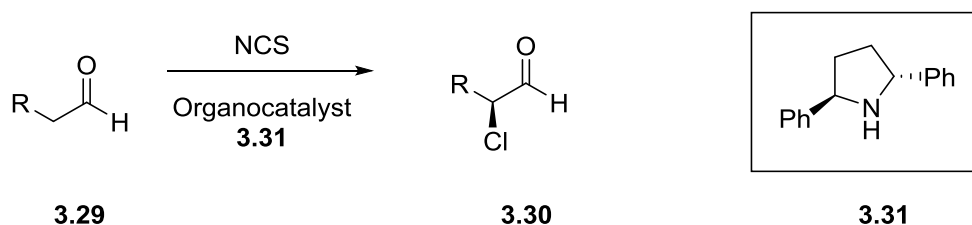


Figure 3.3: Jørgensen's asymmetric α -chlorination of aldehydes methodology

In order to explain the diastereofacial selectivity observed in these reactions, we propose **Figure 3.4** as a putative rationale. Reaction of organocatalyst **3.31** with aldehydes **3.29** results in the formation of the thermodynamically favored (*E*)-enamines **3.33**, avoiding $A^{1,3}$ strain, which would be a consequence of (*Z*)-enamine formation. Steric congestion about the Re-face of enamines **3.33** favors the electrophilic chlorine source to approach from the Si-face. Following nucleophilic addition of enamines **3.33**

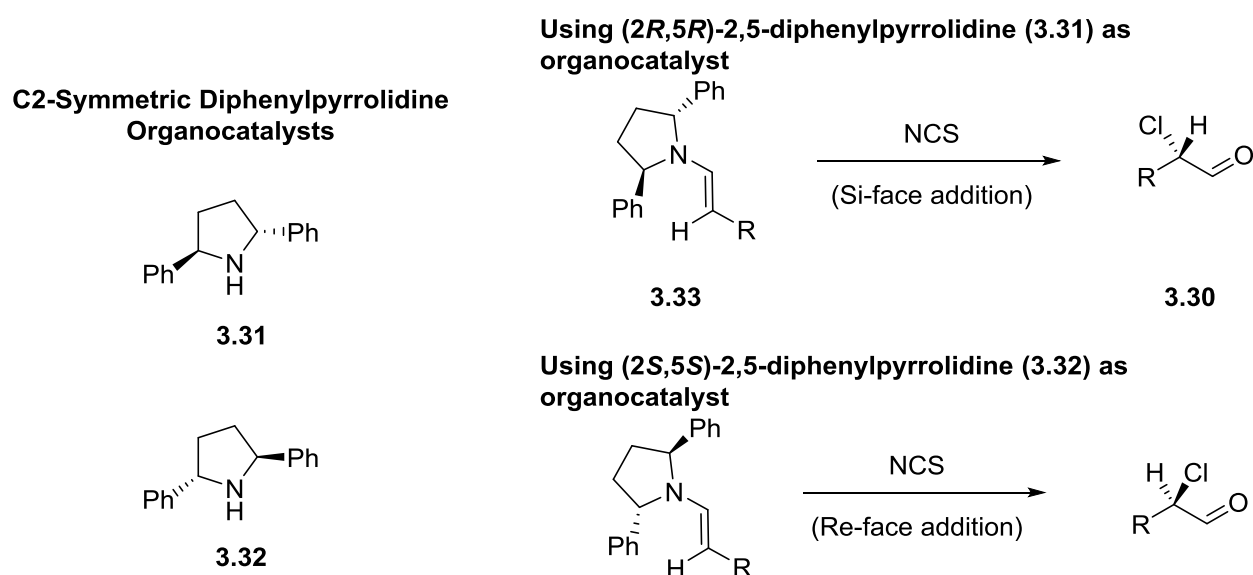


Figure 3.4: Putative rationale for diastereofacial selectivity observed in α -chlorination reaction

with NCS, hydrolysis of the resulting imine provides α -chloro aldehydes **3.30**. Although it was not used in Jørgensen's seminal methodology, we propose that the enantiomer of **3.31**, (2*S*,5*S*)-diphenylpyrrolidine **3.32**, could also be used in a similar manner. In this case, steric congestion around the Si-face of enamines **3.34** would result in the electrophile approaching from the Re-face, allowing access to aldehydes **3.35**.

By using both enantiomers of the diphenylpyrrolidine organocatalyst (**3.31** and **3.32**), we plan to develop a method for accessing either enantiomer of 2-alkyl substituted thiomorpholine heterocycles from key β -chloro alcohol intermediates **3.28**, which can be synthesized from commercially available aldehydes **3.29**. To lend credence to our ideology, previous effort in our lab has also demonstrated the synthetic utility of intermediates **3.28** in the enantioselective synthesis of other saturated azaheterocycles including aziridines, azetidines, morpholines, and piperazines.⁴⁰⁻⁴³

Materials and Methods

General Synthetic Methods and Instrumentation

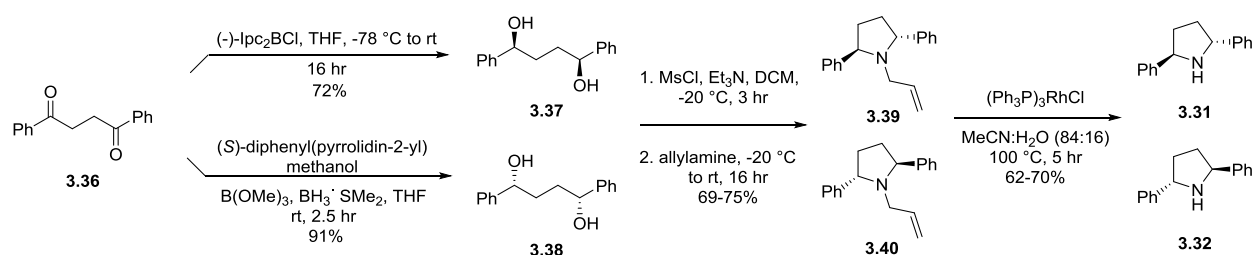
Unless otherwise stated, all reactions were conducted in flame-dried or oven-dried glassware under inert atmospheres of argon. All commercially available reagents and reaction solvents were used as received, unless otherwise noted. All NMR spectra were recorded on a 400 MHz AMX Bruker NMR spectrometer. ^1H and ^{13}C chemical shifts are reported in δ values in ppm downfield with the deuterated solvent as the internal standard. Data are reported as follows: chemical shift, multiplicity (s = singlet, d = doublet, t = triplet, q = quartet, b = broad, m = multiplet), integration, coupling constant (Hz). Low resolution mass spectra were obtained on an Agilent 6120 or 6150 with ESI source. MS parameters were as follows: fragmentor: 70, capillary voltage: 3000 V, nebulizer pressure: 30 psig, drying gas flow: 13 L/min, drying gas temperature: 350 °C. Samples were introduced via an Agilent 1290 UHPLC comprised of a G4220A binary pump, G4226A ALS, G1316C TCC, and G4212A DAD with ULD flow cell. UV absorption was generally observed at 215 nm and 254 nm with a 4 nm bandwidth. Column: Waters Acquity BEH C18, 1.0 x 50 mm, 1.7 μm . Gradient conditions: 5% to 95% CH_3CN in H_2O (0.1% TFA) over 1.4 min, hold at 95% CH_3CN for 0.1 min, 0.5 mL/min, 55 °C. High resolution mass spectra were obtained on an Agilent 6540 UHD Q-TOF with ESI source. MS parameters were as follows: fragmentor: 150, capillary voltage: 3500 V, nebulizer pressure: 60 psig, drying gas flow: 13 L/min, drying gas temperature: 275 °C. Samples were introduced via an Agilent 1200 UHPLC comprised of a G4220A binary pump, G4226A ALS, G1316C TCC, and G4212A DAD with ULD flow cell. UV absorption was observed at 215 nm and 254 nm with a 4 nm bandwidth.

Column: Agilent Zorbax Extend C18, 1.8 μm , 2.1 x 50 mm. Gradient conditions: 5% to 95% CH_3CN in H_2O (0.1% formic acid) over 1 min, hold at 95% CH_3CN for 0.1 min, 0.5 mL/min, 40 $^\circ\text{C}$. For compounds that were purified on a Gilson preparative reversed-phase HPLC, the system comprised of a 333 aqueous pump with solvent-selection valve, 334 organic pump, GX-271 or GX-281 liquid handler, two column switching valves, and a 155 UV detector. UV wavelength for fraction collection was user-defined, with absorbance at 254 nm always monitored. Method 1: Phenomenex Axiapacked Luna C18, 30 x 50 mm, 5 μm column. Mobile phase: CH_3CN in H_2O (0.1% TFA). Gradient conditions: 0.75 min equilibration, followed by user defined gradient (starting organic percentage, ending S3 organic percentage, duration), hold at 95% CH_3CN in H_2O (0.1% TFA) for 1 min, 50 mL/min, 23 $^\circ\text{C}$. Method 2: Phenomenex Axia-packed Gemini C18, 50 x 250 mm, 10 μm column. Mobile phase: CH_3CN in H_2O (0.1% TFA). Gradient conditions: 7 min equilibration, followed by user defined gradient (starting organic percentage, ending organic percentage, duration), hold at 95% CH_3CN in H_2O (0.1% TFA) for 7 min, 120 mL/min, 23 $^\circ\text{C}$. All reagents were purchased from Aldrich Chemical Co. and were used without purification. Sure-Seal solvents were purchased from Sigma Aldrich. Analytical thin layer chromatography was performed on 250 μM silica gel 60 F₂₅₄ plates. Visualization was accomplished with UV light, and/or the use of potassium permanganate or Seebach stain followed by development with a heat gun. Chiral SFC was performed using either an Agilent 1260 Series SFC or Waters Corporation SFC utilizing a Chiralpak IE column (4.6 x 250 mm); co-solvent = methanol (0.1% DEA); 5-50% gradient/5min, hold for 5 min.

General Enantioselective Synthesis of 2-Substituted Thiomorpholines and Thiomorpholine 1,1-Dioxides

Synthesis of C2-Symmetric Organocatalysts **3.31** and **3.32**

Our methodology begins with the synthesis of both enantiomers of our diphenylpyrrolidine organocatalyst (**3.31** and **3.32**) following literature precedent, as shown in **Scheme 3.4**⁴⁴⁻⁴⁶. Diketone **3.36** is first stereoselectively reduced to the corresponding *syn*-1,4-diols; **3.37** was formed via (-)-DIP-Chloride reduction⁴⁷, while **3.38** was formed via Corey-Bakshi-Shibata (CBS) reduction⁴⁸. Both **3.37** and **3.38** were treated with an excess of mesyl chloride to form the bis-mesylates and subsequently reacted with allylamine in a S_N2 reaction/cyclization to form *N*-allyl pyrrolidines **3.39** and **3.40**. Treatment of **3.39** and **3.40** with Wilkinson's catalyst in aqueous acetonitrile resulted in olefin isomerization followed by hydrolysis of the corresponding imines to afford (*2R,5R*)-diphenylpyrrolidine **3.31** and (*2S,5S*)-diphenylpyrrolidine **3.32**.

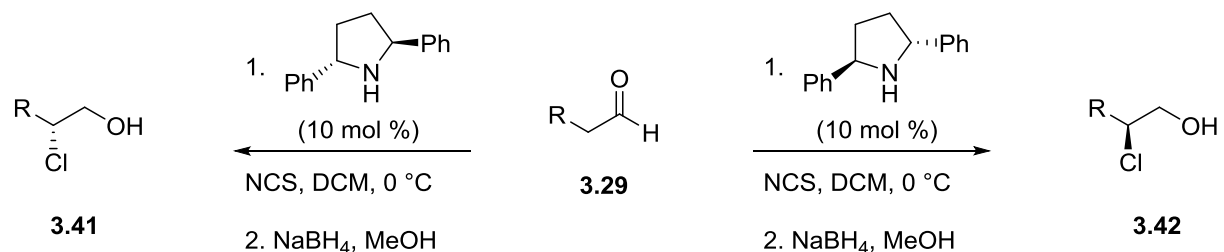


Scheme 3.4: Synthesis of diphenylpyrrolidine organocatalysts **3.31** and **3.32**.

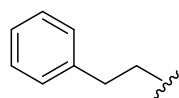
Synthesis of β -Chloro Alcohols (*R*)-**3.41a-h** and (*S*)-**3.42a-h**

With our organocatalysts **3.31** and **3.32** in hand, we were ready to apply Jørgensen's methodology to synthesize optically active β -chloro alcohols (**Scheme 3.5**). Commercially available aldehydes **3.29** were treated with a catalytic amount (10 mol %)

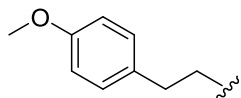
of either **3.31** or **3.32** followed by the addition of NCS at 0 °C. Upon completion of the reaction via TLC, the intermediate chiral α -chloro aldehydes were reduced via sodium borohydride in methanol in the same pot to obtain β -chloro alcohols (*R*)-**3.41a-h** and (*S*)-**3.42a-h** in good yields (60-86%).⁵¹ It was crucial that the intermediate chiral α -chloro aldehydes be reduced in the same pot immediately upon formation, as they were found to readily decompose even with storage at -20 °C. In addition, previous efforts within our lab involving the synthesis of morpholine and piperazine heterocycles have noted that these α -chloro aldehyde intermediates are prone to racemization under mild, basic reaction conditions, which ruled out the feasibility of direct reductive amination strategies to install the amine functionality in **3.27**.⁴³



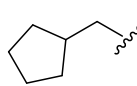
R =



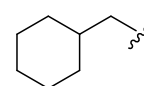
3.41a, 70%
3.42a, 74%



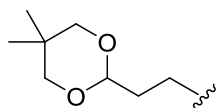
3.41b, 86%
3.42b, 72%



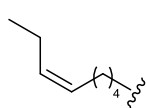
3.41c, 66%
3.42c, 69%



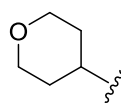
3.41d, 67%
3.42d, 73%



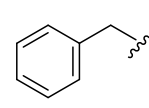
3.41e, 60%
3.42e, 65%



3.41f, 70%
3.42f, 70%



3.41g, 79%
3.42g, 62%

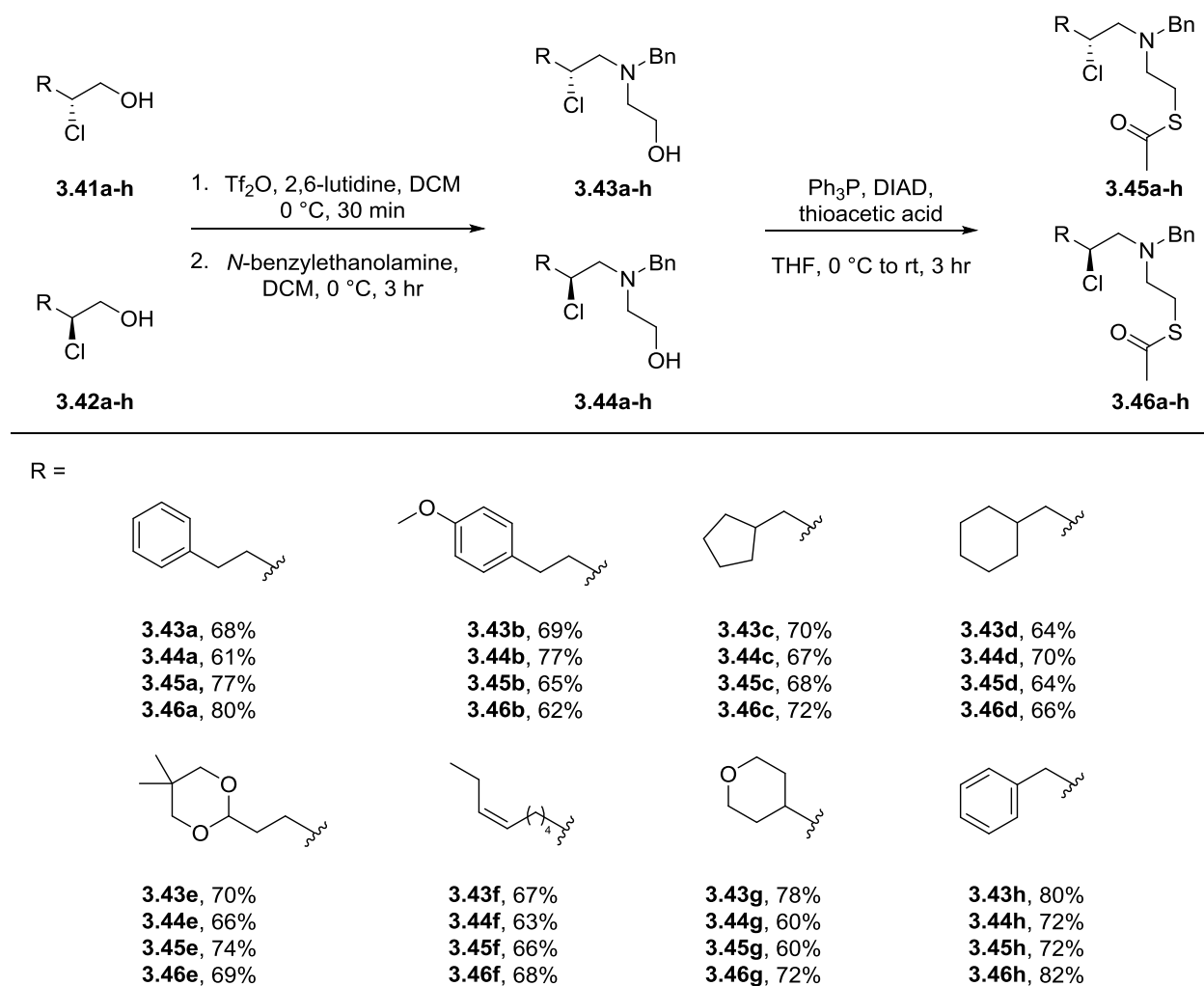


3.41h, 68%
3.42h, 66%

Scheme 3.5: Synthesis of β -chloro alcohols (*R*)-**3.41a-h** and (*S*)-**3.42a-h**.

Synthesis of Cyclization Precursors: Thioesters **3.45a-h** and **3.46a-h**

Since the direct reductive amination strategy for installing the amine functionality in **3.27** was not a viable synthetic approach, the chemoselective functionalization of alcohols **3.41a-h** and **3.42a-h** was achieved as shown in **Scheme 3.6**. Alcohols **3.41a-h** and **3.42a-h** were reacted with triflic anhydride in the presence of 2,6-lutidine to form the corresponding triflates. Subsequent treatment of these triflates with *N*-benzylethanolamine resulted in a chemoselective S_N2 reaction to afford amino alcohols **3.43a-h** and **3.44a-h** in 60-78% yield.⁵¹ With the presence of the alcohol functional

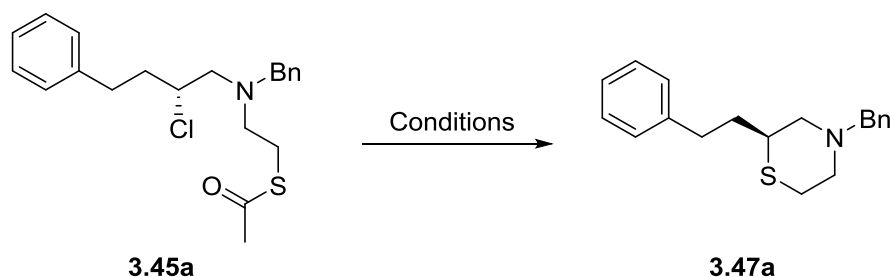


Scheme 3.6: Synthesis of cyclization precursors: thioesters **3.45a-h** and **3.46a-h**.

group, we envisioned that a Mitsunobu reaction with a protected thiol moiety would grant us access to suitable cyclization precursors. Gratifyingly, Mitsunobu reaction of amino alcohols **3.43a-h** and **3.44a-h** with thioacetic acid afforded thioesters **3.45a-h** and **3.46a-h** in good yields (60-80%).⁵¹

*Optimization of the Deprotection/Cyclization Cascade: Synthesis of Chiral C2-Substituted Thiomorpholines **3.47a-h** and **3.48a-h***

With thioesters **3.45a-h** and **3.46a-h** in hand, we wanted to test the feasibility of a one-pot deprotection/cyclization cascade sequence. Upon orthogonal removal of the acetyl protecting group, the nucleophilic thiolate anion should engage in a favorable 6-*exo-tet* cyclization to afford the desired thiomorpholine heterocycles.⁴⁹ We chose to use substrate **3.45a** as a model system to test different reaction conditions in pursuit of achieving this transformation (**Table 3.1**).⁵¹

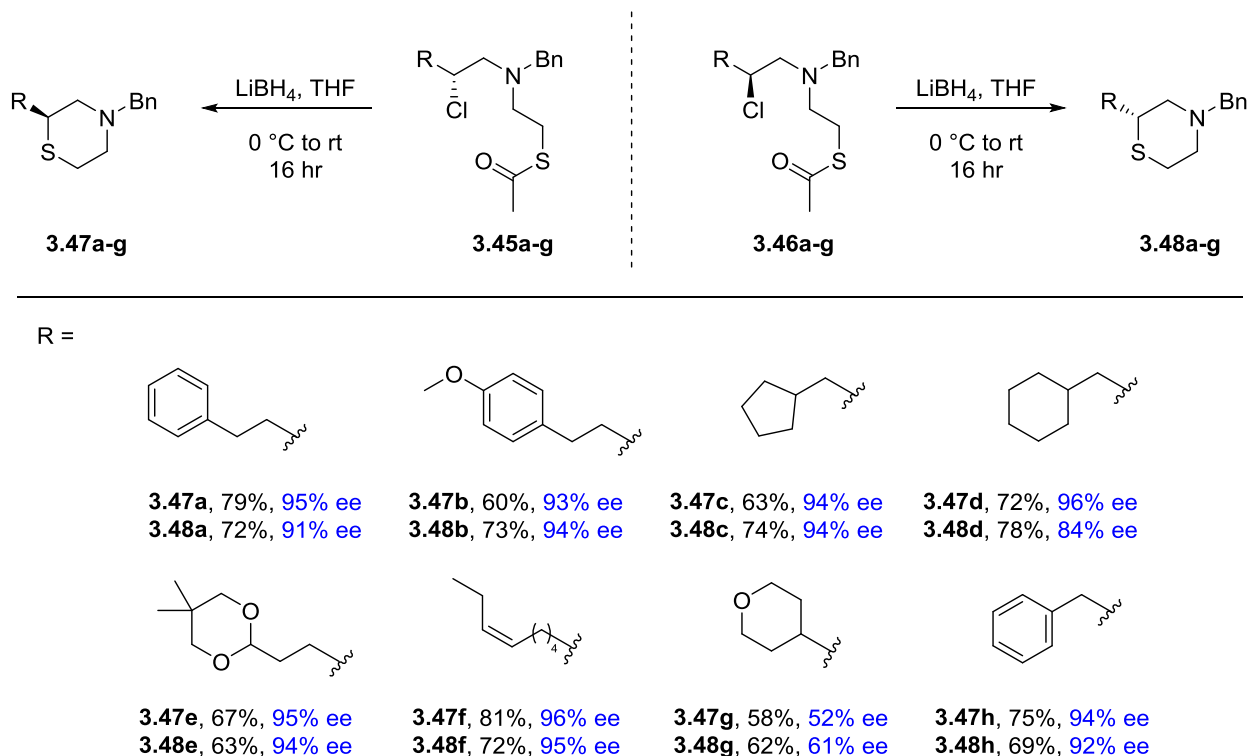


Entry	Reaction Conditions	Conversion
1	NaOMe, 0 °C, THF	complex mixture by LCMS
2	NaOMe, -20 °C, THF	complex mixture by LCMS
3	<i>t</i> BuOK, 0 °C, DMF	complex mixture by LCMS
4	<i>t</i> BuOK, -20 °C, DMF	complex mixture by LCMS
5	LiBH ₄ , 0 °C to rt, THF	> 95%

Table 3.1: Reaction optimization of the deprotection/cyclization cascade.

Attempts at cleaving the acetyl protecting group of **3.45a** under a variety of basic conditions (entries 1-4) led to formation of complex reaction mixtures devoid of the desired thiomorpholine **3.47a** as determined by LCMS. However, treatment of **3.45a** under reductive conditions using lithium borohydride resulted in the successful removal of the thiol protecting group followed by concomitant cyclization to thiomorpholine **3.47a** in excellent conversion. Upon workup and purification via flash chromatography, **3.47a** was isolated in 79% yield with 95% ee.⁵¹ Enantioselectivity was determined by chiral SFC analysis with comparison to a racemic thiomorpholine sample synthesized in the same manner, but using *DL*-proline as the organocatalyst for the α -chlorination step.

These reaction conditions were applied to the remainder of the thioester substrates to afford thiomorpholines (*S*)-**3.47a-h** and (*R*)-**3.48a-h**, as shown in **Scheme 3.7**. Overall, the deprotection/cyclization was determined to be a robust method for

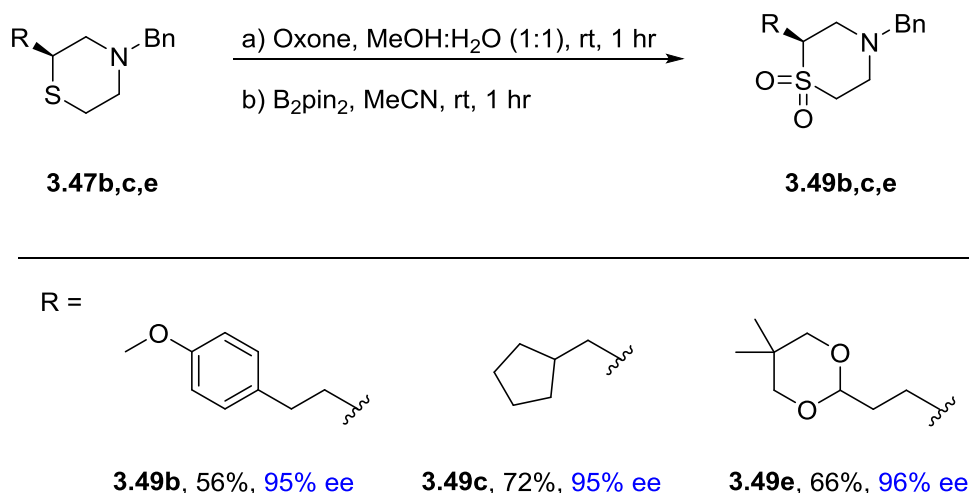


Scheme 3.7: Synthesis of chiral C2-substituted thiomorpholines **3.47a-h** and **3.48a-h**.

achieving this transformation in good yields (58-79%) amongst all the different substrates in this study. Additionally, all of the thiomorpholine products are accessible in high enantioselectivities (84-96% ee) except for the sterically hindered pyranyl analogs **3.47g** and **3.48g**, which were found to have 52% ee and 61% ee respectively.⁵¹

Synthesis of Chiral C2-Substituted Thiomorpholine 1,1-Dioxides **3.49**

With the synthesis of chiral C2-substituted thiomorpholines completed, we wanted to focus our attention to the related thiomorpholine 1,1-dioxide heterocycle, another high demand pharmacophore. The synthesis of these oxidized congeners is shown in **Scheme 3.8**. Attempts at the chemoselective oxidation of the sulfur atom of thiomorpholines **3.47** were not trivial. Mixtures of the desired product and formation of an undesired tertiary amine-*N*-oxide were always obtained. Therefore, to circumvent this issue of selectivity, exhaustive oxidation of **3.47** using an excess of oxone followed by treatment with bis(pinacolato)diboron (B_2pin_2) in the same pot, which has been shown to chemoselectively reduce amine-*N*-oxides, afforded the desired thiomorpholine 1,1-dioxides **3.49** in 56-72% yield without a loss of enantioselectivity (95-96% ee).⁵⁰⁻⁵¹



Scheme 3.8: Synthesis of chiral C2-substituted thiomorpholine 1,1-dioxides **3.49**

Conclusion

Herein, we have reported a robust, enantioselective synthetic strategy for accessing C2-substituted thiomorpholine and thiomorpholine 1,1-dioxide heterocycles, which are often high demand pharmacophores for drug discovery programs. The abundance of commercially available aldehydes is an attractive feature for high-throughput medicinal chemistry campaigns. Additionally, our method utilizes organocatalysis as opposed to transition metal catalyzed approaches, and it does not rely on the chiral pool or chiral chromatography to access enantioenriched products.⁵¹

Experimental Methods

General Synthetic Methods and Instrumentation

Unless otherwise stated, all reactions were conducted in flame-dried or oven-dried glassware under inert atmospheres of argon. All commercially available reagents and reaction solvents were used as received, unless otherwise noted. All NMR spectra were recorded on a 400 MHz AMX Bruker NMR spectrometer. ¹H and ¹³C chemical shifts are reported in δ values in ppm downfield with the deuterated solvent as the internal standard. Data are reported as follows: chemical shift, multiplicity (s = singlet, d = doublet, t = triplet, q = quartet, b = broad, m = multiplet), integration, coupling constant (Hz). Low resolution mass spectra were obtained on an Agilent 6120 or 6150 with ESI source. MS parameters were as follows: fragmentor: 70, capillary voltage: 3000 V, nebulizer pressure: 30 psig, drying gas flow: 13 L/min, drying gas temperature: 350 °C. Samples were introduced via an Agilent 1290 UHPLC comprised of a G4220A binary pump, G4226A ALS, G1316C TCC, and G4212A DAD with ULD flow cell. UV

absorption was generally observed at 215 nm and 254 nm with a 4 nm bandwidth. Column: Waters Acquity BEH C18, 1.0 x 50 mm, 1.7 μ m. Gradient conditions: 5% to 95% CH₃CN in H₂O (0.1% TFA) over 1.4 min, hold at 95% CH₃CN for 0.1 min, 0.5 mL/min, 55 °C. High resolution mass spectra were obtained on an Agilent 6540 UHD Q-TOF with ESI source. MS parameters were as follows: fragmentor: 150, capillary voltage: 3500 V, nebulizer pressure: 60 psig, drying gas flow: 13 L/min, drying gas temperature: 275 °C. Samples were introduced via an Agilent 1200 UHPLC comprised of a G4220A binary pump, G4226A ALS, G1316C TCC, and G4212A DAD with ULD flow cell. UV absorption was observed at 215 nm and 254 nm with a 4 nm bandwidth. Column: Agilent Zorbax Extend C18, 1.8 μ m, 2.1 x 50 mm. Gradient conditions: 5% to 95% CH₃CN in H₂O (0.1% formic acid) over 1 min, hold at 95% CH₃CN for 0.1 min, 0.5 mL/min, 40 °C. For compounds that were purified on a Gilson preparative reversed-phase HPLC, the system comprised of a 333 aqueous pump with solvent-selection valve, 334 organic pump, GX-271 or GX-281 liquid handler, two column switching valves, and a 155 UV detector. UV wavelength for fraction collection was user-defined, with absorbance at 254 nm always monitored. Method 1: Phenomenex Axiapacked Luna C18, 30 x 50 mm, 5 μ m column. Mobile phase: CH₃CN in H₂O (0.1% TFA). Gradient conditions: 0.75 min equilibration, followed by user defined gradient (starting organic percentage, ending S3 organic percentage, duration), hold at 95% CH₃CN in H₂O (0.1% TFA) for 1 min, 50 mL/min, 23 °C. Method 2: Phenomenex Axia-packed Gemini C18, 50 x 250 mm, 10 μ m column. Mobile phase: CH₃CN in H₂O (0.1% TFA). Gradient conditions: 7 min equilibration, followed by user defined gradient (starting organic percentage, ending organic percentage, duration), hold at 95% CH₃CN in H₂O

(0.1% TFA) for 7 min, 120 mL/min, 23 °C. All reagents were purchased from Aldrich Chemical Co. and were used without purification. Sure-Seal solvents were purchased from Sigma Aldrich. Analytical thin layer chromatography was performed on 250 μ M silica gel 60 F₂₅₄ plates. Visualization was accomplished with UV light, and/or the use of potassium permanganate or Seebach stain followed by development with a heat gun. Chiral SFC was performed using either an Agilent 1260 Series SFC or Waters Corporation SFC utilizing a Chiralpak IE column (4.6 x 250 mm); co-solvent = methanol (0.1% DEA); 5-50% gradient/5min, hold for 5 min.

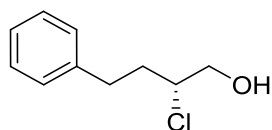
General Procedure 1A: Synthesis of β -chloro alcohols 3.41

To a solution of the requisite aldehyde (1.0 eq) in DCM (0.50 M) cooled to 0 °C was subsequently added (2*S*, 5*S*)-2,5-diphenylpyrrolidine (0.1 eq) and *N*-chlorosuccinimide (1.3 eq). The reaction was allowed to stir at 0 °C for 1 hr before being allowed to slowly warm to room temperature and stir for an additional 16 hr. The reaction was then cooled to 0 °C for the addition of methanol (0.18 M) and sodium borohydride (5.0 eq) portionwise. After an additional 30 min of stirring at 0 °C, the reaction was quenched with the addition of water and diluted with EtOAc. The layers were separated, and the aqueous layer was extracted with EtOAc x 3. The combined organic material was washed with brine, dried over MgSO₄, filtered, concentrated, and purified via flash chromatography (Teledyne ISCO flash purification system; silica gel column; hexanes:EtOAc) to afford the desired products.

General Procedure 1B: Synthesis of β -chloro alcohols 3.42

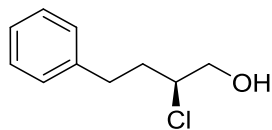
This general procedure is identical to General Procedure 1A, but (2*R*, 5*R*)-2,5-diphenylpyrrolidine is used as the organocatalyst.

Note: Racemic samples were also prepared, with a procedure identical to General Procedure 1A, but using DL-proline as the organocatalyst. These racemic samples were carried forward throughout the rest of the route (procedures described below) in order to determine %ee for enantioenriched samples.



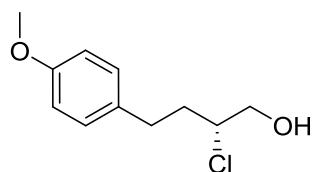
Synthesis of (*R*)-2-chloro-4-phenylbutan-1-ol (**3.41a**)

This compound was synthesized according to general procedure 1A and purified via flash chromatography (0-20% EtOAc gradient) to afford the product as a colorless oil (163 mg, 70% yield). ¹H NMR (400 MHz, CDCl₃): 7.32-7.29 (m, 2H), 7.23-7.20 (m, 3H), 4.01-3.95 (m, 1H), 3.80-3.76 (m, 1H), 3.72-3.67 (m, 1H), 2.94-2.87 (m, 1H), 2.80-2.73 (m, 1H), 2.09-2.00 (m, 3H). ¹³C NMR (100 MHz, CDCl₃): 140.7, 128.7, 128.6, 126.4, 67.1, 64.3, 35.9, 32.5. HRMS (TOF, ES⁺) calcd for C₁₀H₁₂Cl [M-OH]⁺, 167.0622; found, 167.0620. [α]_D²⁵ = +60.6 (c = 2.76, CHCl₃).



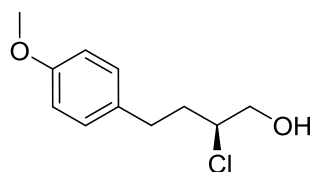
Synthesis of (*S*)-2-chloro-4-phenylbutan-1-ol (**3.42a**)

This compound was synthesized according to general procedure 1B and purified via flash chromatography (0-20% EtOAc gradient) to afford the product as a colorless oil (185 mg, 74% yield). Spectral data matched that of **3.41a**, but [α]_D²⁵ = -55.8 (c = 1.23, CHCl₃).



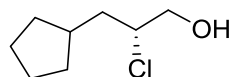
Synthesis of (*R*)-2-chloro-4-(4-methoxyphenyl)butan-1-ol (**3.41b**)

This compound was synthesized according to general procedure 1A and purified via flash chromatography (0-20% EtOAc gradient) to afford the product as a colorless oil (165 mg, 86% yield). ¹H NMR (400 MHz, CDCl₃): 7.12 (d, *J* = 8.6 Hz, 2H), 6.84 (d, *J* = 8.6 Hz, 2H), 3.99-3.93 (m, 1H), 3.79 (s, 3H), 3.79-3.75 (m, 1H), 3.71-3.66 (m, 1H), 2.87-2.80 (m, 1H), 2.74-2.67 (m, 1H), 2.05-1.99 (m, 3H). ¹³C NMR (100 MHz, CDCl₃): 158.2, 132.8, 129.6, 114.1, 67.2, 64.3, 55.4, 36.1, 31.5. HRMS (TOF, ES⁺) calcd for C₁₁H₁₄ClO [M-OH]⁺, 197.0728; found, 197.0727. [α]_D²⁵ = +64.0 (c = 1.21, CHCl₃).



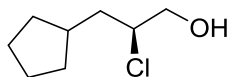
Synthesis of (*S*)-2-chloro-4-(4-methoxyphenyl)butan-1-ol (**3.42b**)

This compound was synthesized according to general procedure 1B and purified via flash chromatography (0-20% EtOAc gradient) to afford the product as a colorless oil (150 mg, 72% yield). Spectral data matched that of **3.41b**, but [α]_D²⁵ = -58.4 (c = 1.06, CHCl₃).



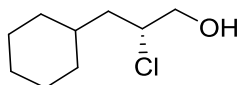
Synthesis of (*R*)-2-chloro-3-cyclopentylpropan-1-ol (**3.41c**)

This compound was synthesized according to general procedure 1A and purified via flash chromatography (0-20% EtOAc gradient) to afford the product as a colorless oil (146 mg, 66% yield). ^1H NMR (400 MHz, CDCl_3): 4.06-4.03 (m, 1H), 3.82-3.78 (m, 1H), 3.68-3.63 (m, 1H), 2.09-1.99 (m, 2H), 1.87-1.78 (m, 3H), 1.70-1.50 (m, 5H), 1.18-1.02 (m, 2H). ^{13}C NMR (100 MHz, CDCl_3): 67.4, 65.1, 40.6, 37.2, 32.9, 32.2, 25.2, 25.1. HRMS (TOF, ES+) calcd for $\text{C}_8\text{H}_{14}\text{Cl}$ $[\text{M}-\text{OH}]^+$, 145.0779; found, 145.0776. $[\alpha]_D^{25} = +35.8$ ($c = 1.03$, CHCl_3).



Synthesis of (S)-2-chloro-3-cyclopentylpropan-1-ol (3.42c)

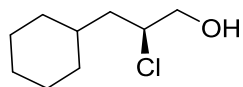
This compound was synthesized according to general procedure 1B and purified via flash chromatography (0-20% EtOAc gradient) to afford the product as a colorless oil (134 mg, 69% yield). Spectral data matched that of **3.41c**, but $[\alpha]_D^{25} = -31.9$ ($c = 1.11$, CHCl_3).



Synthesis of (R)-2-chloro-3-cyclohexylpropan-1-ol (3.41d)

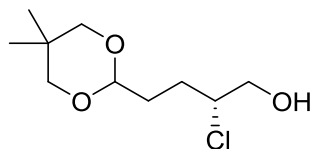
This compound was synthesized according to general procedure 1A and purified via flash chromatography (0-20% EtOAc gradient) to afford the product as a colorless oil (168 mg, 67% yield). ^1H NMR (400 MHz, CDCl_3): 4.16-4.10 (m, 1H), 3.79-3.75 (m, 1H), 3.66-3.61 (m, 1H), 2.06 (bs, 1H), 1.81-1.49 (m, 8H), 1.32-1.09 (m, 3H), 1.02-0.80 (m, 2H). ^{13}C NMR (100 MHz, CDCl_3): 67.6, 63.3, 41.8, 34.5, 33.9, 32.3, 26.6, 26.3, 26.1.

HRMS (TOF, ES+) calcd for C₉H₁₆Cl [M-OH]⁺, 159.0935; found, 159.0934. $[\alpha]_D^{25} = +29.5$ (c = 1.20, CHCl₃).



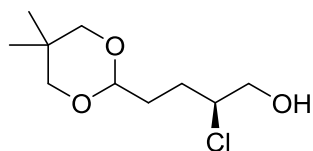
Synthesis of (S)-2-chloro-3-cyclohexylpropan-1-ol (3.42d)

This compound was synthesized according to general procedure 1B and purified via flash chromatography (0-20% EtOAc gradient) to afford the product as a colorless oil (156 mg, 73% yield). Spectral data matched that of **3.41d**, but $[\alpha]_D^{25} = -28.7$ (c = 1.06, CHCl₃).



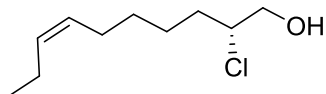
Synthesis of (R)-2-chloro-4-(5,5-dimethyl-1,3-dioxan-2-yl)butan-1-ol (3.41e)

This compound was synthesized according to general procedure 1A and purified via flash chromatography (3:1 hexanes:EtOAc) to afford the product as a colorless oil (165 mg, 60% yield). ¹H NMR (400 MHz, CDCl₃): 4.47 (t, 1H), 4.10-4.04 (m, 1H), 3.79 (dd, *J* = 12.0, 4.0 Hz, 1H), 3.67 (dd, *J* = 12.0, 6.9 Hz, 1H), 3.59 (d, 2H), 3.41 (d, 2H), 2.02-1.74 (m, 5H), 1.17 (s, 3H), 0.72 (s, 3H). ¹³C NMR (100 MHz, CDCl₃): 101.4, 77.3, 67.0, 65.0, 31.4, 30.3, 28.5, 23.1, 21.9. HRMS (TOF, ES+) calcd for C₁₀H₁₉ClO₃Na [M+Na]⁺, 245.0915; found, 245.0917. $[\alpha]_D^{25} = +15.2$ (c = 1.11, CHCl₃).



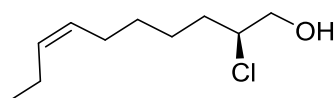
Synthesis of (S)-2-chloro-4-(5,5-dimethyl-1,3-dioxan-2-yl)butan-1-ol (3.42e)

This compound was synthesized according to general procedure 1B and purified via flash chromatography (3:1 hexanes:EtOAc) to afford the product as a colorless oil (172 mg, 65% yield). Spectral data matched that of **3.41e**, but $[\alpha]_D^{25} = -14.7$ ($c = 1.01$, CHCl_3).



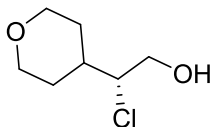
Synthesis of (R,Z)-2-chlorodec-7-en-1-ol (3.41f)

This compound was synthesized according to general procedure 1A and purified via flash chromatography (0-20% EtOAc gradient) to afford the product as a colorless oil (172 mg, 70% yield). ^1H NMR (400 MHz, CDCl_3): 5.41-5.28 (m, 2H), 4.05-3.99 (m, 1H), 3.81-3.77 (m, 1H), 3.69-3.64 (m, 1H), 2.07-2.00 (m, 4H), 1.92 (bs, 1H), 1.83-1.67 (m, 2H), 1.58-1.51 (m, 1H), 1.47-1.32 (m, 3H), 0.96 (t, 3H). ^{13}C NMR (100 MHz, CDCl_3): 132.2, 128.8, 67.2, 65.5, 34.3, 29.3, 27.0, 26.1, 20.7, 14.5. HRMS (TOF, ES^+) calcd for $\text{C}_{10}\text{H}_{20}\text{ClO}$ $[\text{M}+\text{H}]^+$, 191.1197; found, 191.1199. $[\alpha]_D^{25} = +20.2$ ($c = 1.05$, CHCl_3).



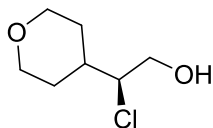
Synthesis of (S,Z)-2-chlorodec-7-en-1-ol (3.42f)

This compound was synthesized according to general procedure 1B and purified via flash chromatography (0-20% EtOAc gradient) to afford the product as a colorless oil (160 mg, 70% yield). Spectral data matched that of **3.41f**, but $[\alpha]_D^{25} = -24.1$ ($c = 3.48$, CHCl_3).



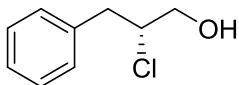
Synthesis of (*R*)-2-chloro-2-(tetrahydro-2H-pyran-4-yl)ethan-1-ol (**3.41g**)

This compound was synthesized according to general procedure 1A and purified via flash chromatography (0-50% EtOAc gradient) to afford the product as a colorless oil (203 mg, 79% yield). ¹H NMR (400 MHz, CDCl₃): 4.03-3.97 (m, 2H), 3.88-3.75 (m, 3H), 3.41-3.34 (m, 2H), 2.17 (bs, 1H), 2.04-1.94 (m, 1H), 1.83-1.78 (m, 1H), 1.66-1.59 (m, 1H), 1.57-1.44 (m, 2H). ¹³C NMR (100 MHz, CDCl₃): 69.7, 67.8, 67.5, 64.5, 38.5, 30.1, 29.6. HRMS (TOF, ES+) calcd for C₇H₁₄ClO₂ [M+H]⁺, 165.0677; found, 165.0676. [α]_D²⁵ = +14.8 (c = 1.27, CHCl₃).



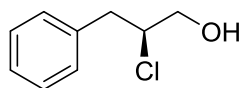
Synthesis of (*S*)-2-chloro-2-(tetrahydro-2H-pyran-4-yl)ethan-1-ol (**3.42g**)

This compound was synthesized according to general procedure 1B and purified via flash chromatography (0-50% EtOAc gradient) to afford the product as a colorless oil (200 mg, 62% yield). Spectral data matched that of **3.41g**, but [α]_D²⁵ = -13.5 (c = 1.03, CHCl₃).



Synthesis of (*R*)-2-chloro-3-phenylpropan-1-ol (**3.41h**)

This compound was synthesized according to general procedure 1A and purified via flash chromatography (0-20% EtOAc gradient) to afford the product as a colorless oil (260 mg, 68% yield). ¹H NMR (400 MHz, CDCl₃): 7.34-7.21 (m, 5H), 4.25-4.19 (m, 1H), 3.82-3.78 (m, 1H), 3.71-3.66 (m, 1H), 3.17-3.11 (m, 1H), 3.07-3.02 (m, 1H), 2.15 (bs, 1H). ¹³C NMR (100 MHz, CDCl₃): 137.2, 129.4, 128.7, 127.1, 66.0, 64.9, 40.8. LCMS: m/z = 153.0 [M-OH]⁺. [α]_D²⁵ = +14.6 (c = 1.97, CHCl₃).



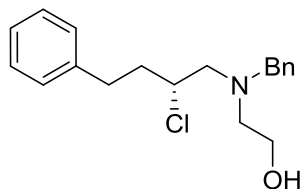
Synthesis of (S)-2-chloro-3-phenylpropan-1-ol (3.42h)

This compound was synthesized according to general procedure 1B and purified via flash chromatography (0-20% EtOAc gradient) to afford the product as a colorless oil (250 mg, 66% yield). Spectral data matched that of **3.41h**, but [α]_D²⁵ = -15.7 (c = 1.98, CHCl₃).

General Procedure 2: Synthesis of amino alcohols 3.43 and 3.44

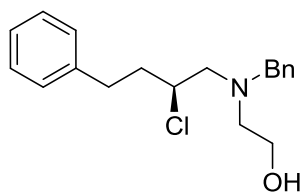
To a solution of the requisite β-chloro alcohol (1.0 eq) in DCM (0.18 M) cooled to 0 °C was sequentially added 2,6-lutidine (5.0 eq) and trifluoromethanesulfonic anhydride (1.2 eq, 1.0 M solution in DCM) dropwise. The resulting solution was stirred for 30 min at 0 °C before being transferred to a syringe and added dropwise to a solution of *N*-benzylethanolamine (10.0 eq) in DCM (7.0 M, with respect to *N*-benzylethanolamine) cooled to 0 °C. The reaction was allowed to stir for an additional 3 hr before being diluted with DCM and quenched with sat. NaHCO₃. The layers were separated, and the aqueous layer was extracted with DCM x 3. The combined organic material was washed with brine, dried over MgSO₄, filtered, concentrated, and purified via flash

chromatography (Teledyne ISCO flash purification system; silica gel column; hexanes:EtOAc) to afford the desired products.



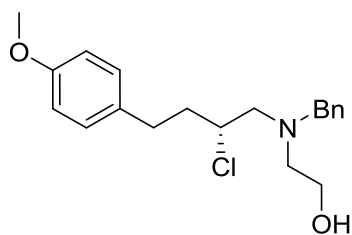
Synthesis of (*R*)-2-(benzyl(2-chloro-4-phenylbutyl)amino)ethan-1-ol (**3.43a**)

This compound was synthesized according to general procedure 2 and purified via flash chromatography (0-20% EtOAc gradient) to afford the product as a yellow oil (166 mg, 68% yield). ¹H NMR (400 MHz, CDCl₃): 7.33-7.17 (m, 10H), 3.91 (bs, 1H), 3.72-3.55 (m, 4H), 2.90-2.60 (m, 7H), 2.13-2.02 (m, 1H), 1.93-1.84 (m, 1H). ¹³C NMR (100 MHz, CDCl₃): 141.0, 138.3, 129.2, 128.7, 128.6, 127.6, 126.3, 61.3, 60.4, 59.5, 58.9, 56.5, 37.8, 32.4. HRMS (TOF, ES+) calcd for C₁₉H₂₅ClNO [M+H]⁺, 318.1619; found, 318.1618. [α]_D²⁵ = -9.38 (c = 0.93, CHCl₃).



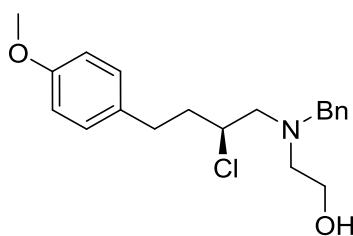
Synthesis of (*S*)-2-(benzyl(2-chloro-4-phenylbutyl)amino)ethan-1-ol (**3.44a**)

This compound was synthesized according to general procedure 2 and purified via flash chromatography (0-20% EtOAc gradient) to afford the product as a yellow oil (200 mg, 77% yield). Spectral data matched that of **3.43a**, but [α]_D²⁵ = +10.4 (c = 1.29, CHCl₃).



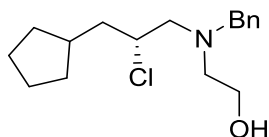
Synthesis of (*R*)-2-(benzyl(2-chloro-4-(4-methoxyphenyl)butyl)amino)ethan-1-ol (**3.43b**)

This compound was synthesized according to general procedure 2 and purified via flash chromatography (0-20% EtOAc gradient) to afford the product as a yellow oil (200 mg, 69% yield). ¹H NMR (400 MHz, CDCl₃): 7.34-7.27 (m, 5H), 7.10 (d, *J* = 8.6 Hz, 2H), 6.85 (d, *J* = 8.6 Hz, 2H), 3.91 (bs, 1H), 3.80 (s, 3H), 3.73-3.56 (m, 4H), 2.85-2.63 (m, 7H), 2.09-2.00 (m, 1H), 1.92-1.82 (m, 1H). ¹³C NMR (100 MHz, CDCl₃): 158.1, 138.3, 133.0, 129.5, 129.2, 128.6, 127.6, 114.1, 61.3, 60.4, 59.5, 58.9, 56.4, 55.4, 38.0, 31.5. HRMS (TOF, ES⁺) calcd for C₂₀H₂₇ClNO₂ [M+H]⁺, 348.1725; found, 348.1725. [α]_D²⁵ = -9.42 (*c* = 1.03, CHCl₃).



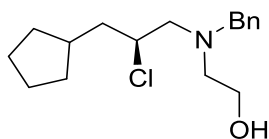
Synthesis of (*S*)-2-(benzyl(2-chloro-4-(4-methoxyphenyl)butyl)amino)ethan-1-ol (**3.44b**)

This compound was synthesized according to general procedure 2 and purified via flash chromatography (0-20% EtOAc gradient) to afford the product as a yellow oil (95 mg, 65% yield). Spectral data matched that of **3.43b**, but [α]_D²⁵ = +10.8 (*c* = 0.46, CHCl₃).



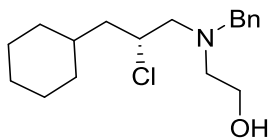
Synthesis of (*R*)-2-(benzyl(2-chloro-3-cyclopentylpropyl)amino)ethan-1-ol (**3.43c**)

This compound was synthesized according to general procedure 2 and purified via flash chromatography (0-20% EtOAc gradient) to afford the product as a yellow oil (136 mg, 70% yield). ¹H NMR (400 MHz, CDCl₃): 7.34-7.25 (m, 5H), 3.93 (bs, 1H), 3.77-3.56 (m, 4H), 2.77-2.68 (m, 5H), 2.11-1.98 (m, 1H), 1.80-1.48 (m, 8H), 1.13-1.04 (m, 1H), 1.01-0.91 (m, 1H). ¹³C NMR (100 MHz, CDCl₃): 138.4, 129.2, 128.6, 127.6, 61.8, 61.0, 59.7, 58.9, 56.6, 42.7, 37.2, 33.0, 32.0, 25.13, 25.08. HRMS (TOF, ES+) calcd for C₁₇H₂₇ClNO [M+H]⁺, 296.1776; found, 296.1777. $[\alpha]_D^{25} = -25.7$ (c = 1.10, CHCl₃).



Synthesis of (*S*)-2-(benzyl(2-chloro-3-cyclopentylpropyl)amino)ethan-1-ol (**3.44c**)

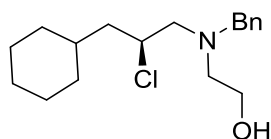
This compound was synthesized according to general procedure 2 and purified via flash chromatography (0-20% EtOAc gradient) to afford the product as a yellow oil (127 mg, 68% yield). Spectral data matched that of **3.43c**, but $[\alpha]_D^{25} = +27.4$ (c = 1.01, CHCl₃).



Synthesis of (*R*)-2-(benzyl(2-chloro-3-cyclohexylpropyl)amino)ethan-1-ol (**3.43d**)

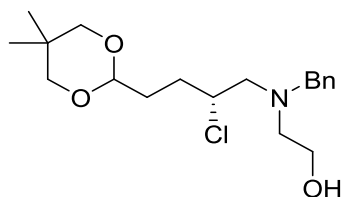
This compound was synthesized according to general procedure 2 and purified via flash chromatography (0-20% EtOAc gradient) to afford the product as a yellow oil (145 mg,

64% yield). ^1H NMR (400 MHz, CDCl_3): 7.38-7.27 (m, 5H), 4.00 (bs, 1H), 3.80-3.50 (m, 4H), 2.86-2.63 (m, 4H), 1.73-1.52 (m, 9H), 1.30-1.07 (m, 3H), 0.98-0.88 (m, 1H), 0.82-0.72 (m, 1H). ^{13}C NMR (100 MHz, CDCl_3): 138.4, 129.1, 128.5, 127.5, 61.9, 59.6, 59.1, 58.9, 56.5, 43.9, 34.5, 33.9, 32.1, 26.5, 26.3, 26.0. HRMS (TOF, ES+) calcd for $\text{C}_{18}\text{H}_{29}\text{ClNO}$, 310.1932; found, 310.1937. $[\alpha]_D^{25} = -18.5$ (c = 1.12, CHCl_3).



Synthesis of (S)-2-(benzyl(2-chloro-3-cyclohexylpropyl)amino)ethan-1-ol (3.44d)

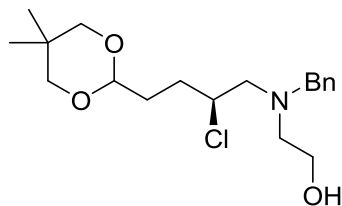
This compound was synthesized according to general procedure 2 and purified via flash chromatography (0-20% EtOAc gradient) to afford the product as a yellow oil (153 mg, 64% yield). Spectral data matched that of **3.43d**, but $[\alpha]_D^{25} = +17.0$ (c = 0.91, CHCl_3).



Synthesis of (R)-2-(benzyl(2-chloro-4-(5,5-dimethyl-1,3-dioxan-2-yl)butyl)amino)ethan-1-ol (3.43e)

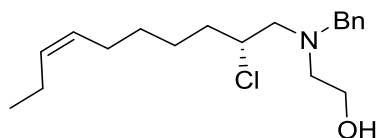
This compound was synthesized according to general procedure 2 and purified via flash chromatography (0-30% EtOAc gradient) to afford the product as a yellow oil (157 mg, 70% yield). ^1H NMR (400 MHz, CDCl_3): 7.34-7.28 (m, 5H), 4.44 (t, 1H), 4.04 (m, 1H), 3.75 (m, 4H), 3.59 (d, 2H), 3.41 (d, 2H), 2.80 (m, 5H), 2.01-1.95 (m, 1H), 1.90-1.81 (m, 1H), 1.80-1.72 (m, 2H), 1.17 (s, 3H), 0.71 (s, 3H). ^{13}C NMR (100 MHz, CDCl_3): 138.1, 129.1, 128.4, 127.4, 101.2, 77.1, 61.0, 59.4, 58.8, 56.3, 31.2, 30.10, 30.08, 23.0, 21.8.

HRMS (TOF, ES+) calcd for C₁₉H₃₁ClNO₃ [M+H]⁺, 356.1987; found, 356.1995. $[\alpha]_D^{25} = -24.4$ (c = 0.66, CHCl₃).



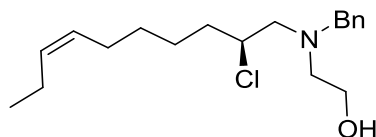
Synthesis of (S)-2-(benzyl(2-chloro-4-(5,5-dimethyl-1,3-dioxan-2-yl)butyl)amino)ethan-1-ol (3.44e)

This compound was synthesized according to general procedure 2 and purified via flash chromatography (0-30% EtOAc gradient) to afford the product as a yellow oil (145 mg, 74% yield). Spectral data matched that of **3.43e**, but $[\alpha]_D^{25} = +24.9$ (c = 0.64, CHCl₃).



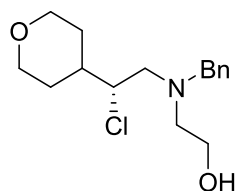
Synthesis of (R,Z)-2-(benzyl(2-chlorodec-7-en-1-yl)amino)ethan-1-ol (3.43f)

This compound was synthesized according to general procedure 2 and purified via flash chromatography (0-20% EtOAc gradient) to afford the product as a yellow oil (183 mg, 67% yield). ¹H NMR (400 MHz, CDCl₃): 7.33-7.24 (m, 5H), 5.41-5.27 (m, 2H), 3.93 (bs, 1H), 3.76-3.55 (m, 4H), 2.76-2.64 (m, 5H), 2.07-1.98 (m, 4H), 1.78-1.70 (m, 1H), 1.63-1.45 (m, 2H), 1.43-1.25 (m, 3H), 0.96 (t, 3H). ¹³C NMR (100 MHz, CDCl₃): 138.3, 132.1, 129.3, 128.8, 128.7, 127.7, 61.3, 59.6, 58.8, 56.5, 36.2, 29.3, 27.0, 25.9, 20.7, 14.5. HRMS (TOF, ES+) calcd for C₁₉H₃₁ClNO [M+H]⁺, 324.2089; found, 324.2092. $[\alpha]_D^{25} = -29.2$ (c = 1.16, CHCl₃).



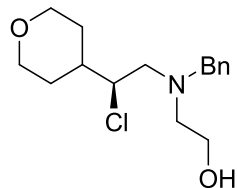
Synthesis of (S,Z)-2-(benzyl(2-chlorodec-7-en-1-yl)amino)ethan-1-ol (3.44f)

This compound was synthesized according to general procedure 2 and purified via flash chromatography (0-20% EtOAc gradient) to afford the product as a yellow oil (135 mg, 66% yield). Spectral data matched that of **3.43f**, but $[\alpha]_D^{25} = +28.2$ ($c = 1.07$, CHCl_3).



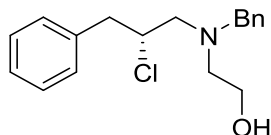
Synthesis of (R)-2-(benzyl(2-chloro-2-(tetrahydro-2H-pyran-4-yl)ethyl)amino)ethan-1-ol (3.43g)

This compound was synthesized according to general procedure 2 and purified via flash chromatography (0-35% EtOAc gradient) to afford the product as a yellow oil (148 mg, 78% yield). ^1H NMR (400 MHz, CDCl_3): 7.44-7.29 (m, 5H), 3.96-3.91 (m, 2H), 3.88-3.79 (m, 1H), 3.73-3.53 (m, 3H), 3.38-3.29 (m, 3H), 2.84-2.75 (m, 3H), 1.88 (bs, 1H), 1.62-1.35 (m, 6H). ^{13}C NMR (100 MHz, CDCl_3): 138.3, 129.0, 128.3, 127.3, 67.5, 65.5, 59.3, 58.9, 58.1, 56.4, 38.9, 30.1, 27.3. HRMS (TOF, ES+) calcd for $\text{C}_{16}\text{H}_{25}\text{ClNO}_2$ $[\text{M}+\text{H}]^+$, 298.1568; found, 298.1574. $[\alpha]_D^{25} = -22.3$ ($c = 0.96$, CHCl_3).



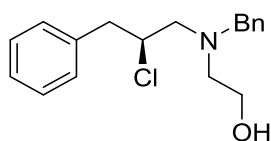
Synthesis of (S)-2-(benzyl(2-chloro-2-(tetrahydro-2H-pyran-4-yl)ethyl)amino)ethan-1-ol (3.44g)

This compound was synthesized according to general procedure 2 and purified via flash chromatography (0-35% EtOAc gradient) to afford the product as a yellow oil (168 mg, 60% yield). Spectral data matched that of **3.43g**, but $[\alpha]_D^{25} = +21.8$ ($c = 1.28$, CHCl_3).



Synthesis of (R)-2-(benzyl(2-chloro-3-phenylpropyl)amino)ethan-1-ol (3.43h)

This compound was synthesized according to general procedure 2 and purified via flash chromatography (0-25% EtOAc gradient) to afford the product as a yellow oil (300 mg, 80% yield). ^1H NMR (400 MHz, CDCl_3): 7.35-7.24 (m, 8H), 7.17-7.15 (m, 2H), 4.16-4.09 (m, 1H), 3.69 (q, 2H), 3.64-3.53 (m, 2H), 3.11-3.06 (m, 1H), 2.93-2.86 (m, 1H), 2.84-2.73 (m, 4H), 2.68-2.62 (m, 1H). ^{13}C NMR (100 MHz, CDCl_3): 138.3, 137.7, 129.3, 129.2, 128.59, 128.58, 127.5, 126.9, 61.7, 60.8, 59.6, 59.0, 56.6, 42.8. LCMS: $m/z = 303.9$ $[\text{M}+\text{H}]^+$. $[\alpha]_D^{25} = -47.3$ ($c = 1.74$, CHCl_3).

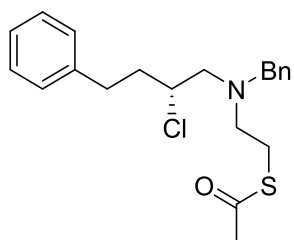


Synthesis of (S)-2-(benzyl(2-chloro-3-phenylpropyl)amino)ethan-1-ol (3.44h)

This compound was synthesized according to general procedure 2 and purified via flash chromatography (0-25% EtOAc gradient) to afford the product as a yellow oil (230 mg, 72% yield). Spectral data matched that of **3.43h**, but $[\alpha]_D^{25} = +47.3$ ($c = 1.75$, CHCl_3).

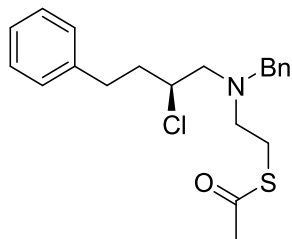
General Procedure 3: Synthesis of thioesters 3.45 and 3.46

To a solution of triphenylphosphine (1.2 eq) in THF (0.25 M) cooled to 0 °C was added diisopropyl azodicarboxylate (1.2 eq) dropwise. The reaction was stirred at this temperature for 30 min before the addition of a solution of the requisite amino alcohol (1.0 eq) and thioacetic acid (1.0 eq) in THF (0.52 M). The resulting suspension was warmed to room temperature and stirred for an additional 2 hr. The crude reaction mixture was condensed directly onto silica gel and purified via flash chromatography (Teledyne ISCO flash purification system; silica gel column; hexanes:EtOAc) to afford the desired products.



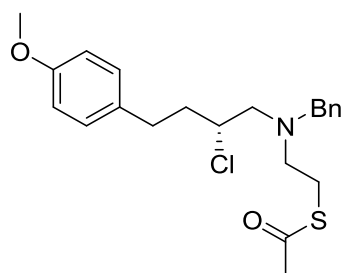
Synthesis of (*R*)-*S*-(2-(benzyl(2-chloro-4-phenylbutyl)amino)ethyl) ethanethioate (3.45a)

This compound was synthesized according to general procedure 3 and purified via flash chromatography (0-5% EtOAc gradient) to afford the product as a colorless oil (102 mg, 61% yield). ¹H NMR (400 MHz, CDCl₃): 7.31-7.18 (m, 10H), 3.83 (m, 1H), 3.69, 3.59 (ABq, 2H, *J*_{AB} = 13.7 Hz), 2.99-2.90 (m, 2H), 2.88-2.74 (m, 3H), 2.72-2.63 (m, 3H), 2.29 (s, 3H), 2.29-2.22 (m, 1H), 1.87-1.77 (m, 1H). ¹³C NMR (100 MHz, CDCl₃): 195.6, 141.2, 138.7, 128.9, 128.6, 128.5, 128.3, 127.2, 126.0, 61.2, 60.1, 59.2, 54.0, 37.3, 32.3, 30.6, 27.1. HRMS (TOF, ES⁺) calcd for C₂₁H₂₇ClNOS [M+H]⁺, 376.1496; found, 376.1499. [α]_D²⁵ = +28.0 (c = 3.61, CHCl₃).



Synthesis of (*S*)-S-(2-(benzyl(2-chloro-4-phenylbutyl)amino)ethyl) ethanethioate (3.46a)

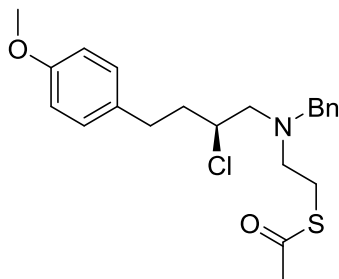
This compound was synthesized according to general procedure 3 and purified via flash chromatography (0-5% EtOAc gradient) to afford the product as a colorless oil (156 mg, 80% yield). Spectral data matched that of **3.45a**, but $[\alpha]_D^{25} = -27.6$ ($c = 1.29$, CHCl_3).



Synthesis of (*R*)-S-(2-(benzyl(2-chloro-4-(4-methoxyphenyl)butyl)amino)ethyl) ethanethioate (3.45b)

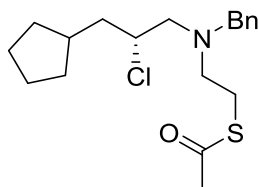
This compound was synthesized according to general procedure 3 and purified via flash chromatography (0-5% EtOAc gradient) to afford the product as a colorless oil (175 mg, 77% yield). ^1H NMR (400 MHz, CDCl_3): 7.32-7.30 (m, 5H), 7.12 (d, $J = 8.5$ Hz, 2H), 6.84 (d, $J = 8.5$ Hz, 2H), 3.85-3.79 (m, 1H), 3.80 (s, 3H), 3.69, 3.60 (ABq, 2H, $J_{AB} = 13.7$ Hz), 2.99-2.91 (m, 2H), 2.87-2.75 (m, 3H), 2.69-2.60 (m, 3H), 2.30 (s, 3H), 2.29-2.19 (m, 1H), 1.85-1.75 (m, 1H). ^{13}C NMR (100 MHz, CDCl_3): 195.8, 158.0, 138.8, 133.3, 129.6, 129.0, 128.4, 127.3, 114.0, 61.3, 60.2, 59.3, 55.4, 54.1, 37.7, 31.5, 30.7, 27.2. HRMS

(TOF, ES+) calcd for C₂₂H₂₉ClNO₂S [M+H]⁺, 406.1602; found, 406.1601. $[\alpha]_D^{25} = +26.5$ (c = 1.13, CHCl₃).



Synthesis of (S)-S-(2-(benzyl(2-chloro-4-(4-methoxyphenyl)butyl)amino)ethyl)ethanethioate (3.46b)

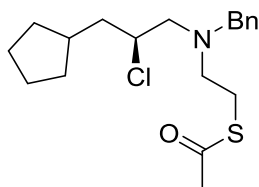
This compound was synthesized according to general procedure 3 and purified via flash chromatography (0-5% EtOAc gradient) to afford the product as a colorless oil (47 mg, 62% yield). Spectral data matched that of **3.45b**, but $[\alpha]_D^{25} = -23.5$ (c = 2.89, CHCl₃).



Synthesis of (R)-S-(2-(benzyl(2-chloro-3-cyclopentylpropyl)amino)ethyl)ethanethioate (3.45c)

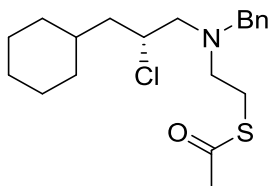
This compound was synthesized according to general procedure 3 and purified via flash chromatography (0-5% EtOAc gradient) to afford the product as a colorless oil (84 mg, 67% yield). ¹H NMR (400 MHz, CDCl₃): 7.33-7.24 (m, 5H), 3.90-3.83 (m, 1H), 3.74, 3.64 (ABq, 2H, $J_{AB} = 13.7$ Hz), 3.00-2.97 (m, 2H), 2.85-2.69 (m, 4H), 2.31 (s, 3H), 2.09-1.99 (m, 1H), 1.85-1.72 (m, 3H), 1.66-1.48 (m, 5H), 1.15-1.05 (m, 1H), 1.04-0.96 (m, 1H). ¹³C

NMR (100 MHz, CDCl₃): 195.9, 139.0, 129.0, 128.4, 127.3, 62.0, 60.9, 59.4, 54.3, 42.5, 37.3, 33.2, 31.8, 30.7, 27.3, 25.2, 25.1. HRMS (TOF, ES+) calcd for C₁₉H₂₉ClNOS [M+H]⁺, 354.1653; found, 354.1654. $[\alpha]_D^{25} = +27.7$ (c = 0.91, CHCl₃).



Synthesis of (S)-S-(2-(benzyl(2-chloro-3-cyclopentylpropyl)amino)ethyl) ethanethioate (3.46c)

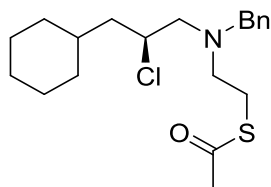
This compound was synthesized according to general procedure 3 and purified via flash chromatography (0-5% EtOAc gradient) to afford the product as a colorless oil (81 mg, 72% yield). Spectral data matched that of **3.45c**, but $[\alpha]_D^{25} = -25.3$ (c = 1.16, CHCl₃).



Synthesis of (R)-S-(2-(benzyl(2-chloro-3-cyclohexylpropyl)amino)ethyl) ethanethioate (3.45d)

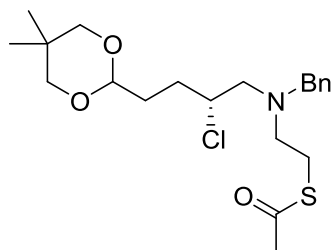
This compound was synthesized according to general procedure 3 and purified via flash chromatography (0-5% EtOAc gradient) to afford the product as a colorless oil (91 mg, 70% yield). ¹H NMR (400 MHz, CDCl₃): 7.34-7.29 (m, 5H), 3.98-3.91 (m, 1H), 3.73, 3.64 (ABq, 2H, $J_{AB} = 13.5$ Hz), 3.00-2.94 (m, 2H), 2.85-2.79 (m, 1H), 2.75-2.66 (m, 3H), 2.31 (s, 3H), 1.75-1.51 (m, 7H), 1.44-1.36 (m, 1H), 1.31-1.09 (m, 3H), 0.99-0.90 (m, 1H), 0.84-0.76 (m, 1H). ¹³C NMR (100 MHz, CDCl₃): 195.9, 139.0, 129.0, 128.4, 127.3, 62.0,

59.4, 58.9, 54.3, 43.9, 34.6, 32.0, 30.7, 27.3, 26.7, 26.4, 26.1. HRMS (TOF, ES+) calcd for C₂₀H₃₁ClNOS [M+H]⁺, 368.1809; found, 368.1812. $[\alpha]_D^{25} = +26.1$ (c = 1.09, CHCl₃).



Synthesis of (S)-S-(2-(benzyl(2-chloro-3-cyclohexylpropyl)amino)ethyl) ethanethioate (3.46d)

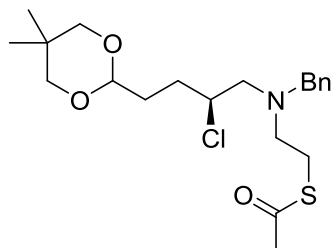
This compound was synthesized according to general procedure 3 and purified via flash chromatography (0-5% EtOAc gradient) to afford the product as a colorless oil (105 mg, 66% yield). Spectral data matched that of **3.45d**, but $[\alpha]_D^{25} = -23.2$ (c = 1.03, CHCl₃).



Synthesis of (R)-S-(2-(benzyl(2-chloro-4-(5,5-dimethyl-1,3-dioxan-2-yl)butyl)amino)ethyl) ethanethioate (3.45e)

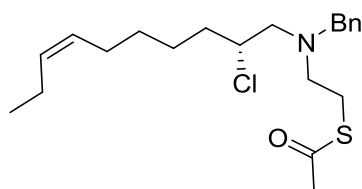
This compound was synthesized according to general procedure 3 and purified via flash chromatography (0-8% EtOAc gradient) to afford the product as a colorless oil (96 mg, 66% yield). ¹H NMR (400 MHz, CDCl₃): 7.34-7.24 (m, 5H), 4.44 (t, 1H), 3.93 (m, 1H), 3.69 (q, 2H), 3.59 (d, 2H), 3.41 (d, 2H), 2.97 (m, 2H), 2.85-2.66 (m, 3H), 2.31 (s, 3H), 2.14-2.07 (m, 1H), 1.91-1.82 (m, 1H), 1.77-1.59 (m, 3H), 1.18 (s, 3H), 0.71 (s, 3H). ¹³C NMR (100 MHz, CDCl₃): 195.9, 138.9, 129.1, 128.4, 127.3, 101.6, 77.3, 61.3, 61.1,

59.3, 54.0, 31.5, 30.7, 30.34, 30.26, 27.2, 23.2, 22.0. HRMS (TOF, ES+) calcd for $C_{21}H_{33}ClNO_3S$ $[M+H]^+$, 414.1864; found, 414.1866. $[\alpha]_D^{25} = +6.02$ (c = 0.84, $CHCl_3$).



Synthesis of (S)-S-(2-(benzyl(2-chloro-4-(5,5-dimethyl-1,3-dioxan-2-yl)butyl)amino)ethyl) ethanethioate (3.46e)

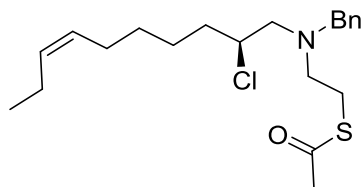
This compound was synthesized according to general procedure 3 and purified via flash chromatography (0-8% EtOAc gradient) to afford the product as a colorless oil (78 mg, 69% yield). Spectral data matched that of **3.45e**, but $[\alpha]_D^{25} = -6.94$ (c = 0.73, $CHCl_3$).



Synthesis of (R,Z)-S-(2-(benzyl(2-chlorodec-7-en-1-yl)amino)ethyl) ethanethioate (3.45f)

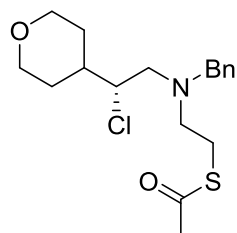
This compound was synthesized according to general procedure 3 and purified via flash chromatography (0-5% EtOAc gradient) to afford the product as a colorless oil (115 mg, 63% yield). 1H NMR (400 MHz, $CDCl_3$): 7.33-7.24 (m, 5H), 5.41-5.29 (m, 2H), 3.90-3.84 (m, 1H), 3.73, 3.64 (ABq, 2H, $J_{AB} = 13.8$ Hz), 3.03-2.93 (m, 2H), 2.84-2.69 (m, 4H), 2.31 (s, 3H), 2.08-1.87 (m, 5H), 1.58-1.45 (m, 2H), 1.40-1.29 (m, 3H), 0.96 (t, 3H). ^{13}C NMR (100 MHz, $CDCl_3$): 195.9, 139.0, 132.0, 129.0, 128.4, 127.3, 61.35, 61.25, 59.4, 54.2,

35.8, 30.7, 29.4, 27.3, 27.1, 25.9, 20.7, 14.5. HRMS (TOF, ES+) calcd for C₂₁H₃₃ClNOS [M+H]⁺, 382.1966; found, 382.1974. $[\alpha]_D^{25} = +19.8$ (c = 1.29, CHCl₃).



Synthesis of (S,Z)-S-(2-(benzyl(2-chlorodec-7-en-1-yl)amino)ethyl) ethanethioate (3.46f)

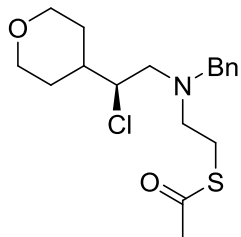
This compound was synthesized according to general procedure 3 and purified via flash chromatography (0-5% EtOAc gradient) to afford the product as a colorless oil (68 mg, 68% yield). Spectral data matched that of **3.45f**, but $[\alpha]_D^{25} = -19.1$ (c = 1.22, CHCl₃).



Synthesis of (R)-S-(2-(benzyl(2-chloro-2-(tetrahydro-2H-pyran-4-yl)ethyl)amino)ethyl) ethanethioate (3.45g)

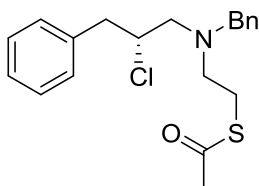
This compound was synthesized according to general procedure 3 and purified via flash chromatography (0-8% EtOAc gradient) to afford the product as a colorless oil (87 mg, 60% yield). ¹H NMR (400 MHz, CDCl₃): 7.32-7.25 (m, 5H), 3.99-3.95 (m, 1H), 3.90-3.73 (m, 3H), 3.57-3.54 (m, 1H), 3.40-3.33 (m, 1H), 3.27-3.21 (m, 1H), 3.03-2.99 (m, 2H), 2.88-2.83 (m, 1H), 2.74-2.69 (m, 3H), 2.33 (s, 3H), 2.09-2.01 (m, 1H), 1.72-1.62 (m, 1H), 1.50-1.38 (m, 2H), 1.12-1.09 (m, 1H). ¹³C NMR (100 MHz, CDCl₃): 195.8, 138.9, 129.2, 128.5, 127.4, 67.9, 67.8, 65.2, 59.2, 57.8, 54.3, 38.0, 30.7, 30.6, 27.4, 26.6.

HRMS (TOF, ES+) calcd for C₁₈H₂₇ClNO₂S [M+H]⁺, 356.1446; found, 356.1453. $[\alpha]_D^{25} = +16.6$ (c = 0.67, CHCl₃).



Synthesis of (S)-S-(2-(benzyl(2-chloro-2-(tetrahydro-2H-pyran-4-yl)ethyl)amino)ethyl) ethanethioate (3.46g)

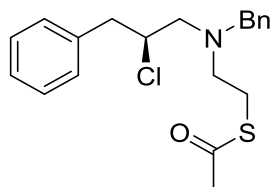
This compound was synthesized according to general procedure 3 and purified via flash chromatography (0-8% EtOAc gradient) to afford the product as a colorless oil (150 mg, 72% yield). Spectral data matched that of **3.45g**, but $[\alpha]_D^{25} = -16.2$ (c = 1.24, CHCl₃).



Synthesis of (R)-S-(2-(benzyl(2-chloro-3-phenylpropyl)amino)ethyl) ethanethioate (3.45h)

This compound was synthesized according to general procedure 3 and purified via flash chromatography (0-4% EtOAc gradient) to afford the product as a colorless oil (245 mg, 72% yield). ¹H NMR (400 MHz, CDCl₃): 7.34-7.18 (m, 10H), 4.08-4.01 (m, 1H), 3.77, 3.65 (ABq, 2H, *J*_{AB} = 13.7 Hz), 3.35 (dd, 1H, *J* = 14.3 Hz, 4.2 Hz), 3.04-2.98 (m, 2H), 2.91-2.81 (m, 2H), 2.78-2.74 (m, 2H), 2.71-2.68 (m, 1H), 2.33 (s, 3H). ¹³C NMR (100 MHz, CDCl₃): 195.9, 138.8, 138.4, 129.4, 129.1, 128.50, 128.46, 127.4, 126.7, 61.5,

61.2, 59.4, 54.3, 42.4, 30.8, 27.4. LCMS: $m/z = 361.9 [M+H]^+$. $[\alpha]_D^{25} = +8.9$ ($c = 1.83$, CHCl_3).

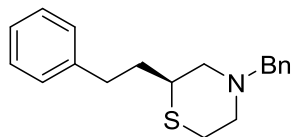


Synthesis of (S)-S-(2-(benzyl(2-chloro-3-phenylpropyl)amino)ethyl) ethanethioate (3.46h)

This compound was synthesized according to general procedure 3 and purified via flash chromatography (0-4% EtOAc gradient) to afford the product as a colorless oil (177 mg, 82% yield). Spectral data matched that of **3.45h**, but $[\alpha]_D^{25} = -7.3$ ($c = 1.98$, CHCl_3).

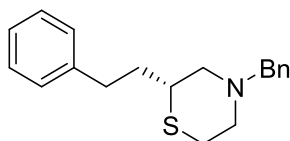
General Procedure 4: Synthesis of thiomorpholines 3.47 and 3.48

To a solution of the requisite thioester (1.0 eq) in THF (0.15 M) cooled to 0 °C was added lithium borohydride (10.0 eq, 2.0 M solution in THF) dropwise. Upon completion of addition, the reaction was allowed to slowly warm to room temperature and stir for 16 hr. The reaction mixture was then added dropwise to methanol (0.03 M) cooled to 0 °C. Upon completion of addition, the flask was warmed to room temperature and stirred for 4 hr to quench any unreacted lithium borohydride and borane adducts. Volatiles were removed *in vacuo*, and the resulting residue was suspended in 1:1 EtOAc:H₂O. The layers were separated, and the aqueous layer was extracted with EtOAc x 3. The combined organic material was washed with brine, dried over MgSO₄, filtered, concentrated, and purified via flash chromatography (Teledyne ISCO flash purification system; silica gel column; hexanes:EtOAc) to afford the desired products.



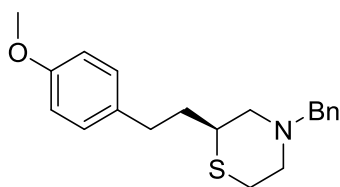
Synthesis of (*S*)-4-benzyl-2-phenethylthiomorpholine (**3.47a**)

This compound was synthesized according to general procedure 4 and purified via flash chromatography (0-15% EtOAc gradient) to afford the product as a colorless oil (47 mg, 79% yield). ¹H NMR (400 MHz, CDCl₃): 7.35-7.18 (m, 10H), 3.58, 3.53 (ABq, 2H, J_{AB} = 13.3 Hz), 3.02-2.96 (m, 2H), 2.94-2.61 (m, 5H), 2.48-2.41 (m, 1H), 2.30-2.23 (m, 1H), 1.89-1.83 (m, 2H). ¹³C NMR (100 MHz, CDCl₃): 141.7, 138.1, 129.1, 128.5, 128.4, 128.3, 127.2, 126.0, 63.6, 61.0, 54.8, 40.3, 35.2, 33.0, 27.6. HRMS (TOF, ES+) calcd for C₁₉H₂₄NS [M+H]⁺, 298.1624; found, 298.1630. $[\alpha]_D^{25}$ = -18.9 (c = 1.43, CHCl₃). This compound was determined to have 95% ee by chiral SFC analysis (Chiralpak IE, SFC traces shown in Appendix C).



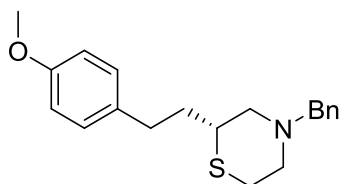
Synthesis of (*R*)-4-benzyl-2-phenethylthiomorpholine (**3.48a**)

This compound was synthesized according to general procedure 4 and purified via flash chromatography (0-15% EtOAc gradient) to afford the product as a colorless oil (66 mg, 72% yield). Spectral data matched that of **3.47a**, but $[\alpha]_D^{25}$ = +20.0 (c = 5.35, CHCl₃). This compound was determined to have 91% ee by chiral SFC analysis (Chiralpak IE, SFC traces shown in Appendix C).



Synthesis of (*S*)-4-benzyl-2-(4-methoxyphenethyl)thiomorpholine (**3.47b**)

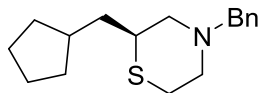
This compound was synthesized according to general procedure 4 and purified via flash chromatography (0-15% EtOAc gradient) to afford the product as a colorless oil (58 mg, 60% yield). ^1H NMR (400 MHz, CDCl_3): 7.35-7.27 (m, 5H), 7.07 (d, $J = 8.5$ Hz, 2H), 6.82 (d, $J = 8.5$ Hz, 2H), 3.79 (s, 3H), 3.56, 3.51 (ABq, 2H, $J_{AB} = 13.3$ Hz), 2.99-2.96 (m, 2H), 2.89-2.80 (m, 2H), 2.72-2.56 (m, 3H), 2.42 (m, 1H), 2.23 (m, 1H), 1.82-1.76 (m, 2H). ^{13}C NMR (100 MHz, CDCl_3): 157.9, 138.2, 133.8, 129.4, 129.2, 128.4, 127.3, 113.9, 63.6, 61.0, 55.4, 54.8, 40.3, 35.5, 32.1, 27.6. HRMS (TOF, ES+) calcd for $\text{C}_{20}\text{H}_{26}\text{NOS}$ $[\text{M}+\text{H}]^+$, 328.1730; found, 328.1735. $[\alpha]_D^{25} = -14.7$ ($c = 5.47$, CHCl_3). This compound was determined to have 93% ee by chiral SFC analysis (Chiralpak IE, SFC traces shown in Appendix C).



Synthesis of (*R*)-4-benzyl-2-(4-methoxyphenethyl)thiomorpholine (**3.48b**)

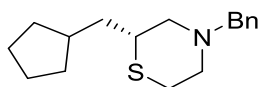
This compound was synthesized according to general procedure 4 and purified via flash chromatography (0-15% EtOAc gradient) to afford the product as a colorless oil (16 mg, 73% yield). Spectral data matched that of **3.47b**, but $[\alpha]_D^{25} = +12.9$ ($c = 0.27$, CHCl_3).

This compound was determined to have 94% ee by chiral SFC analysis (Chiralpak IE, SFC traces shown in Appendix C).



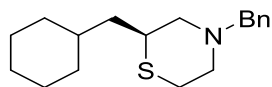
Synthesis of (S)-4-benzyl-2-(cyclopentylmethyl)thiomorpholine (3.47c)

This compound was synthesized according to general procedure 4 and purified via flash chromatography (0-15% EtOAc gradient) to afford the product as a colorless oil (31 mg, 63% yield). ^1H NMR (400 MHz, CDCl_3): 7.33-7.24 (m, 5H), 3.58, 3.51 (ABq, 2H, $J_{AB} = 13.7$ Hz), 3.03-2.83 (m, 4H), 2.57-2.52 (m, 1H), 2.36-2.31 (m, 1H), 2.17-2.12 (m, 1H), 1.96-1.89 (m, 1H), 1.83-1.71 (m, 2H), 1.63-1.40 (m, 6H), 1.12-1.02 (m, 2H). ^{13}C NMR (100 MHz, CDCl_3): 138.0, 129.2, 128.4, 127.3, 63.6, 61.7, 54.7, 40.4, 40.0, 37.3, 33.1, 32.6, 27.9, 25.2. HRMS (TOF, ES+) calcd for $\text{C}_{17}\text{H}_{26}\text{NS}$ $[\text{M}+\text{H}]^+$, 276.1780; found, 276.1785. $[\alpha]_D^{25} = -2.35$ ($c = 2.05$, CHCl_3). This compound was determined to have 94% ee by chiral SFC analysis (Chiralpak IE, SFC traces shown in Appendix C).



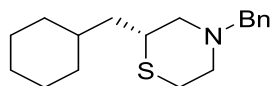
Synthesis of (R)-4-benzyl-2-(cyclopentylmethyl)thiomorpholine (3.48c)

This compound was synthesized according to general procedure 4 and purified via flash chromatography (0-15% EtOAc gradient) to afford the product as a colorless oil (35 mg, 74% yield). Spectral data matched that of **3.47c**, but $[\alpha]_D^{25} = +2.95$ ($c = 1.96$, CHCl_3). This compound was determined to have 94% ee by chiral SFC analysis (Chiralpak IE, SFC traces shown in Appendix C).



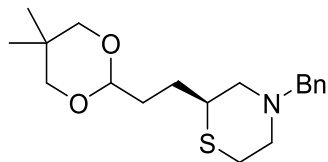
Synthesis of (S)-4-benzyl-2-(cyclohexylmethyl)thiomorpholine (3.47d)

This compound was synthesized according to general procedure 4 and purified via flash chromatography (0-15% EtOAc gradient) to afford the product as a colorless oil (40 mg, 72% yield). ^1H NMR (400 MHz, CDCl_3): 7.34-7.24 (m, 5H), 3.58, 3.50 (ABq, 2H, $J_{AB} = 13.3$ Hz), 3.04-2.95 (m, 3H), 2.88-2.82 (m, 1H), 2.56-2.51 (m, 1H), 2.35-2.30 (m, 1H), 2.15-2.10 (m, 1H), 1.79-1.61 (m, 5H), 1.43-1.09 (m, 6H), 0.94-0.77 (m, 2H). ^{13}C NMR (100 MHz, CDCl_3): 138.1, 129.2, 128.4, 127.3, 63.6, 61.9, 54.7, 41.2, 38.4, 34.5, 34.0, 32.9, 27.9, 26.7, 26.33, 26.27. HRMS (TOF, ES+) calcd for $\text{C}_{18}\text{H}_{28}\text{NS}$ $[\text{M}+\text{H}]^+$, 290.1937; found, 290.1943. $[\alpha]_D^{25} = -3.04$ ($c = 1.88$, CHCl_3). This compound was determined to have 96% ee by chiral SFC analysis (Chiralpak IE, SFC traces shown in Appendix C).



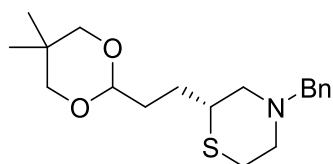
Synthesis of (R)-4-benzyl-2-(cyclohexylmethyl)thiomorpholine (3.48d)

This compound was synthesized according to general procedure 4 and purified via flash chromatography (0-15% EtOAc gradient) to afford the product as a colorless oil (52 mg, 78% yield). Spectral data matched that of **3.47d**, but $[\alpha]_D^{25} = +2.79$ ($c = 2.32$, CHCl_3). This compound was determined to have 84% ee by chiral SFC analysis (Chiralpak IE, SFC traces shown in Appendix C).



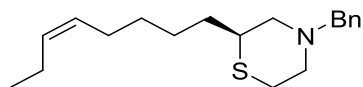
Synthesis of (*S*)-4-benzyl-2-(2-(5,5-dimethyl-1,3-dioxan-2-yl)ethyl)thiomorpholine (**3.47e**)

This compound was synthesized according to general procedure 4 and purified via flash chromatography (0-50% EtOAc gradient) to afford the product as a colorless oil (33 mg, 67% yield). ^1H NMR (400 MHz, CDCl_3): 7.33-7.24 (m, 5H), 4.41 (t, 1H), 3.56 (t, 4H), 3.39 (d, 2H), 3.00-2.80 (m, 4H), 2.58-2.54 (m, 1H), 2.37 (t, 1H), 2.17 (t, 1H), 1.82-1.55 (m, 4H), 1.17 (s, 3H), 0.70 (s, 3H). ^{13}C NMR (100 MHz, CDCl_3): 138.1, 129.2, 128.4, 127.3, 101.8, 77.3, 63.5, 61.2, 54.7, 40.8, 32.2, 30.3, 27.8, 23.1, 22.0. HRMS (TOF, ES+) calcd for $\text{C}_{19}\text{H}_{30}\text{NO}_2\text{S}$ $[\text{M}+\text{H}]^+$, 336.1992; found, 336.1998. $[\alpha]_D^{25} = -14.6$ ($c = 2.47$, CHCl_3). This compound was determined to have 95% ee by chiral SFC analysis (Chiralpak IE, SFC traces shown in Appendix C).



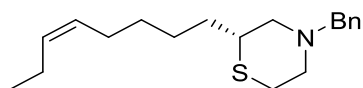
Synthesis of (*R*)-4-benzyl-2-(2-(5,5-dimethyl-1,3-dioxan-2-yl)ethyl)thiomorpholine (**3.48e**)

This compound was synthesized according to general procedure 4 and purified via flash chromatography (0-50% EtOAc gradient) to afford the product as a colorless oil (31 mg, 63% yield). Spectral data matched that of **3.47e**, but $[\alpha]_D^{25} = +13.9$ ($c = 2.30$, CHCl_3). This compound was determined to have 94% ee by chiral SFC analysis (Chiralpak IE, SFC traces shown in Appendix C).



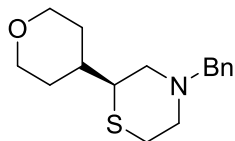
Synthesis of (*S,Z*)-4-benzyl-2-(oct-5-en-1-yl)thiomorpholine (**3.47f**)

This compound was synthesized according to general procedure 4 and purified via flash chromatography (0-15% EtOAc gradient) to afford the product as a colorless oil (32 mg, 81% yield). ¹H NMR (400 MHz, CDCl₃): 7.32-7.24 (m, 5H), 5.39-5.26 (m, 2H), 3.57, 3.51 (ABq, 2H, $J_{AB} = 13.4$ Hz), 3.01-2.98 (m, 2H), 2.92-2.82 (m, 2H), 2.58-2.53 (m, 1H), 2.38-2.32 (m, 1H), 2.18-2.13 (m, 1H), 2.06-1.99 (m, 4H), 1.54-1.26 (m, 6H), 0.95 (t, 3H). ¹³C NMR (100 MHz, CDCl₃): 138.2, 131.9, 129.2, 129.0, 128.4, 127.3, 63.6, 61.4, 54.8, 41.1, 33.5, 29.7, 27.9, 27.0, 26.6, 20.6, 14.5. HRMS (TOF, ES⁺) calcd for C₁₉H₃₀NS [M+H]⁺, 304.2093; found, 304.2102. $[\alpha]_D^{25} = -9.42$ (c = 1.21, CHCl₃). This compound was determined to have 96% ee by chiral SFC analysis (Chiralpak IE, SFC traces shown in Appendix C).



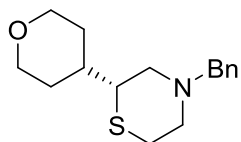
Synthesis of (*R,Z*)-4-benzyl-2-(oct-5-en-1-yl)thiomorpholine (**3.48f**)

This compound was synthesized according to general procedure 4 and purified via flash chromatography (0-15% EtOAc gradient) to afford the product as a colorless oil (23 mg, 72% yield). Spectral data matched that of **3.47f**, but $[\alpha]_D^{25} = +7.50$ (c = 0.64, CHCl₃). This compound was determined to have 95% ee by chiral SFC analysis (Chiralpak IE, SFC traces shown in Appendix C).



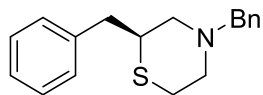
Synthesis of (S)-4-benzyl-2-(tetrahydro-2H-pyran-4-yl)thiomorpholine (3.47g)

This compound was synthesized according to general procedure 4 and purified via flash chromatography (0-50% EtOAc gradient) to afford the product as a colorless oil (25 mg, 52% yield). ¹H NMR (400 MHz, CDCl₃): 7.33-7.24 (m, 5H), 3.99-3.91 (m, 2H), 3.57, 3.50 (ABq, 2H, $J_{AB} = 13.2$ Hz), 3.37-3.29 (m, 2H), 3.01-2.92 (m, 2H), 2.79-2.70 (m, 2H), 2.65-2.60 (m, 1H), 2.45-2.32 (m, 2H), 1.81-1.68 (m, 2H), 1.55-1.52 (m, 1H), 1.45-1.31 (m, 2H). ¹³C NMR (100 MHz, CDCl₃): 138.0, 129.2, 128.6, 128.4, 127.3, 68.2, 67.9, 63.7, 58.1, 54.8, 46.4, 37.8, 30.9, 30.6, 27.4. HRMS (TOF, ES+) calcd for C₁₆H₂₄NOS [M+H]⁺, 278.1573; found, 278.1577. $[\alpha]_D^{25} = -16.2$ (c = 1.45, CHCl₃). This compound was determined to have 58% ee by chiral SFC analysis (Chiralpak IE, SFC traces shown in Appendix C).



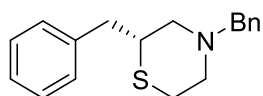
Synthesis of (R)-4-benzyl-2-(tetrahydro-2H-pyran-4-yl)thiomorpholine (3.48g)

This compound was synthesized according to general procedure 4 and purified via flash chromatography (0-50% EtOAc gradient) to afford the product as a colorless oil (63 mg, 61% yield). Spectral data matched that of **3.47g**, but $[\alpha]_D^{25} = +13.7$ (c = 5.94, CHCl₃). This compound was determined to have 62% ee by chiral SFC analysis (Chiralpak IE, SFC traces shown in Appendix C).



Synthesis of (S)-2,4-dibenzylthiomorpholine (3.47h)

This compound was synthesized according to general procedure 4 and purified via flash chromatography (0-15% EtOAc gradient) to afford the product as a colorless oil (123 mg, 75% yield). ^1H NMR (400 MHz, CDCl_3): 7.34-7.17 (m, 10H), 3.56, 3.46 (ABq, 2H, $J_{AB} = 13.3$ Hz), 3.17-3.11 (m, 1H), 3.00-2.95 (m, 1H), 2.94-2.86 (m, 2H), 2.83-2.75 (m, 2H), 2.65-2.59 (m, 1H), 2.44-2.38 (m, 1H), 2.32-2.27 (m, 1H). ^{13}C NMR (100 MHz, CDCl_3): 138.9, 138.1, 129.19, 129.18, 128.5, 128.4, 127.2, 126.6, 63.6, 60.6, 54.4, 42.3, 40.0, 27.8. LCMS: $m/z = 284.1$ $[\text{M}+\text{H}]^+$. $[\alpha]_D^{25} = +31.2$ ($c = 4.55$, CHCl_3). This compound was determined to have 94% ee by chiral SFC analysis (Chiralpak IF, SFC traces shown in Appendix C).

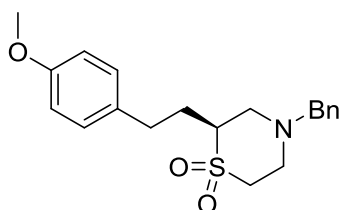


Synthesis of (R)-2,4-dibenzylthiomorpholine (3.48h)

This compound was synthesized according to general procedure 4 and purified via flash chromatography (0-15% EtOAc gradient) to afford the product as a colorless oil (80 mg, 69% yield). Spectral data matched that of **3.47h**, but $[\alpha]_D^{25} = -30.4$ ($c = 4.70$, CHCl_3). This compound was determined to have 92% ee by chiral SFC analysis (Chiralpak IF, SFC traces shown in Appendix C).

General Procedure 5: Synthesis of thiomorpholine 1,1-dioxides 3.49

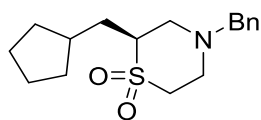
To a solution of the requisite thiomorpholine (1.0 eq) in MeOH:H₂O (1:1) (0.10 M) was added oxone (3.5 eq) at room temperature. The resulting suspension was allowed to stir at room temperature for 1 hr before being diluted with EtOAc. The layers were separated, and the aqueous layer was extracted with EtOAc x 3. The combined organic material was passed through a phase separator and concentrated to afford a crude, colorless oil. This crude material was dissolved in MeCN (0.12 M), and bis(pinacolato)diboron (1.1 eq) was added. The resulting reaction was stirred at room temperature for 1 hr before the dropwise addition of ethylenediamine (20.0 eq). After 30 min, the reaction was diluted with water and extracted with EtOAc x 3. The combined organic material was passed through a phase separator, concentrated, and purified via flash chromatography (Teledyne ISCO flash purification system; silica gel column; hexanes:EtOAc) to afford the desired products.



Synthesis of (S)-4-benzyl-2-(4-methoxyphenethyl)thiomorpholine 1,1-dioxide (3.49b)

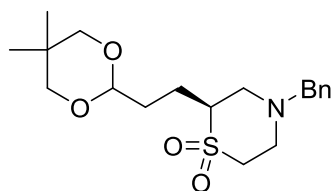
This compound was synthesized according to general procedure 5 and purified via flash chromatography (0-50% EtOAc gradient) to afford the product as a colorless oil (12 mg, 56% yield). ¹H NMR (600 MHz, CDCl₃): 7.38-7.33 (m, 5H), 7.01 (d, *J* = 8.5 Hz, 2H), 6.81 (d, *J* = 8.6 Hz, 2H), 3.79 (s, 3H), 3.76-3.66 (m, 2H), 3.21-2.99 (m, 5H), 2.72-2.63 (m, 3H), 2.35-2.30 (m, 1H), 1.78 (m, 1H), 1.25 (m, 1H). ¹³C NMR (150 MHz, CDCl₃): 158.3, 132.1, 129.4, 129.0, 114.2, 61.7, 59.2, 55.4, 55.0, 50.8, 31.6, 29.8, 25.9. HRMS (TOF,

ES+) calcd for C₂₀H₂₆NO₃S [M+H]⁺, 360.1628; found, 360.1636. $[\alpha]_D^{25} = -4.18$ (c = 2.90, CHCl₃). This compound was determined to have 95% ee by chiral SFC analysis (Chiralpak IE, SFC traces shown in Appendix C).



Synthesis of (S)-4-benzyl-2-(cyclopentylmethyl)thiomorpholine 1,1-dioxide (3.49c)

This compound was synthesized according to general procedure 5 and purified via flash chromatography (0-50% EtOAc gradient) to afford the product as a colorless oil (14 mg, 72% yield). ¹H NMR (400 MHz, CDCl₃): 7.36-7.29 (m, 5H), 3.69, 3.59 (ABq, 2H, $J_{AB} = 13.1$ Hz), 3.03 (m, 5H), 2.87-2.85 (m, 1H), 2.61 (m, 1H), 2.00-1.93 (m, 1H), 1.87-1.75 (m, 2H), 1.73-1.65 (m, 1H), 1.63-1.44 (m, 5H), 1.14-1.05 (m, 2H). ¹³C NMR (100 MHz, CDCl₃): 137.5, 128.9, 128.7, 127.8, 61.8, 60.3, 55.7, 50.9, 50.7, 36.9, 33.1, 32.2, 29.8, 25.2, 25.1. HRMS (TOF, ES+) calcd for C₁₇H₂₆NO₂S [M+H]⁺, 308.1679; found, 308.1687. $[\alpha]_D^{25} = -4.34$ (c = 0.95, CHCl₃). This compound was determined to have 95% ee by chiral SFC analysis (Chiralpak IE, SFC traces shown in Appendix C).



Synthesis of (S)-4-benzyl-2-(2-(5,5-dimethyl-1,3-dioxan-2-yl)ethyl)thiomorpholine 1,1-dioxide (3.49e)

This compound was synthesized according to general procedure 5 and purified via flash chromatography (0-75% EtOAc gradient) to afford the product as a colorless oil (13 mg,

66% yield). ^1H NMR (600 MHz, CDCl_3): 7.35-7.29 (m, 5H), 4.41 (t, 1H), 3.69-3.59 (m, 2H), 3.55 (d, 2H), 3.37 (d, 2H), 3.10-3.02 (m, 4H), 2.88 (m, 1H), 2.62 (m, 1H), 2.19-2.13 (m, 1H), 1.75-1.63 (m, 3H), 1.26-1.24 (m, 1H), 1.14 (s, 3H), 0.70 (s, 3H). ^{13}C NMR (150 MHz, CDCl_3): 137.5, 128.8, 127.9, 101.2, 77.25, 77.21, 61.7, 60.4, 55.4, 50.8, 31.5, 30.2, 29.8, 25.0, 23.1, 21.9, 18.6. HRMS (TOF, ES+) calcd for $\text{C}_{19}\text{H}_{30}\text{NO}_4\text{S}$ $[\text{M}+\text{H}]^+$, 368.1890; found, 368.1900. $[\alpha]_D^{25} = -10.7$ (c = 1.07, CHCl_3). This compound was determined to have 96% ee by chiral SFC analysis (Chiralpak IE, SFC traces shown in Appendix C).

References for Chapter III

1. Aitken, R.A.; Aitken, K.M. 1,4-Thiazines and their Benzo Derivatives. *Comprehensive Heterocyclic Chemistry III*, **2008**, *8*, 607-675.
2. Taylor, R.D.; MacCoss, M.; Lawson, A.D.G. Rings in Drugs. *J. Med. Chem.* **2014**, *14*, 5845-5859.
3. Vitaku, E.; Smith, D.T.; Njardson, J.T. Analysis of the Structural Diversity, Substitution Patterns, and Frequency of Nitrogen Heterocycles among U.S. FDA Approved Pharmaceuticals. *J. Med. Chem.* **2014**, *57*, 10257-10274.
4. Roughley, S.D.; Jordan, A.M. The Medicinal Chemist's Toolbox: An Analysis of Reactions Used in the Pursuit of Drug Candidates. *J. Med. Chem.* **2011**, *54*, 3451-3479.
5. Barbachyn, M.R.; Hutchinson, D.K.; Brickner, S.J.; Cynamon, M.H.; Kilburn, J.O.; Klemens, S.P.; Glickman, S.E.; Grega, K.C.; Hendges, S.K.; Toops, D.S.; Ford, C.W.; Zurenko, G.E. Identification of a novel oxazolidinone (U-100480) with potent antimycobacterial activity. *J. Med. Chem.* **1996**, *39*, 680-685.
6. Cynamon, M.H.; Klemens, S.P.; Sharpe, C.A.; Chase, S. Activities of several novel oxazolidinones against *Mycobacterium tuberculosis* in a murine model. *Antimicrob. Agents Chemother.* **1999**, *43*, 1189-1191.
7. Shaw, K.J.; Barbachyn, M.R. The oxazolidinones: past, present, and future. *Ann. N. Y. Acad. Sci.* **2011**, *1241*, 48-70.
8. Wallis, R.S.; Jakubiec, W.; Kumar, V.; Bedarida, G.; Silvia, A.; Paige, D.; Zhu, T.; Mitton-Fry, M.; Ladutko, L.; Campbell, S.; Miller, P.F. Biomarker-assisted dose selection for safety and efficacy in early development of PNU-100480 for tuberculosis. *Antimicrob. Agents Chemother.* **2011**, *55*, 567-574.
9. Theodosis-Nobelos, P.; Kourti, M.; Gavalas, A.; Rekka, E.A. Amides of non-steroidal anti-inflammatory drugs with thiomorpholine can yield hypolipidemic agents with improved anti-inflammatory activity. *Bioorg. Med. Chem. Lett.* **2016**, *26*, 910-913.
10. Rekka, E.A.; Kourounakis, P.N. Medicinal chemistry of 2,2,4-substituted morpholines. *Curr. Med. Chem.* **2010**, *17*, 3422-3430.
11. Tooulia, K.K.; Theodosis-Nobelos, P.; Rekka, E.A. Thiomorpholine Derivatives with Hypolipidemic and Antioxidant Activity. *Arch. Pharm. Chem. Life Sci.* **2015**, *348*, 629-634.
12. Bern, C.; Montgomery, S.P.; Herwaldt, B.L.; Rassi Jr, A.; Marin-Neto, J.A.; Dantas, R.O.; Maguire, J.H.; Acquatella, H.; Morillo, C.; Kirchoff, L.V.; Gilman, R.H.; Reyes, P.A.; Salvatella, R.; Moore, A.C. Evaluation and Treatment of Chagas Disease in the United States: A Systemic Review. *JAMA* **2007**, *298*, 2171-2181.
13. Coertzen, D.; Reader, J.; van der Watt, M.; Nondaba, S.H.; Gibhard, L.; Wiesner, L.; Smith, P.; D'Alessandro, S.; Taramelli, D.; Wong, H.N.; du Preez, J.L.; Wu, R.W.K.; Birkholtz, L-M; Haynes, R.K. Artemisone and artemiside are potent panreactive antimalarial agents that also synergize redox imbalance in *Plasmodium falciparum* transmissible gametocyte stages. *Antimicrob. Agents Chemother.* **2018**, *62*, 1-17.

14. Cinque, G.M.; Szajnman, S.H.; Zhong, L.; Docampo, R.; Schwartzapel, A.J.; Rodriguez, J.B.; Gros, E.G. Structure-Activity Relationship of New Growth Inhibitors of *Trypanosoma cruzi*. *J. Med. Chem.* **1998**, *41*, 1540-1554.
15. Metzner, P.; Thuillier, A. In *Sulfur Reagents in Organic Synthesis*; Katritzky, A.R.; Meth-Cohn, O.; Rees, C.W.; Eds.; Academic Press: London, 1994.
16. Teyssot, M-L.; Fayolle, M.; Philouze, C.; Dupuy, C. Bis-Heteronucleophilic Michael Addition to Divinyl Sulfone: A New Efficient Access to Macrocycles. *Eur. J. Org. Chem.* **2003**, 54-62.
17. Fishman, A.G.; Mallams, A.K.; Puar, M.S.; Rossman, R.R.; Stephens, R.L. Novel Semisynthetic Oxo and Alkyl Macrolide Antibacterials and Related Derivatives. *J. Chem. Soc. Perkin Trans. 1* **1987**, 1189-1209.
18. Fishman, A.G.; Mallams, A.K.; Rossman, R.R. Semisynthetic macrolide antibacterials derived from tylosin. Synthesis of 3-O-acetyl-23-O-demycinosyl-4"-O-isovaleryltylosin and related compounds, as well as the 12,13-epoxy derivatives. *J. Chem. Soc. Perkin Trans. 1* **1989**, 787-798.
19. Armilli, M.N. Nitrogen and sulfur-containing heterocycle derivatives. Patent WO2010025436A2.
20. Wang, J.; Liu, X.; Feng, X. Asymmetric Strecker Reactions. *Chem. Rev.* **2011**, *111*, 6947-6983.
21. Yan, H.; Oh, J.S.; Lee, J-W; Song, C.E. Scalable organocatalytic asymmetric Strecker reactions catalyzed by a chiral cyanide generator. *Nature Communications* **2012**, DOI: 10.1038/ncomms2216.
22. Bungard, C.J.; Converso, A.; De Leon, P.; Hanney, B.; Hartingh, T. J.; Manikowski, J.J.; Manley, P.J.; Meissner, R.; Meng, Z.; Perkins, J.J.; Rudd, M.T.; Shu, Y. Quinoline carboxamide and quinoline carbonitrile derivatives as mGluR2-negative allosteric modulators, compositions, and their use. Patent WO2013066736A1.
23. Vo, C-V.T.; Mikutis, G.; Bode, J.W. SnAP Reagents for the Transformation of Aldehydes into Substituted Thiomorpholines – An Alternative to Cross-Coupling with Saturated Heterocycles. *Angew. Chem. Int. Ed.* **2013**, *52*, 1705-1708.
24. Luescher, M.H.; Vo, C-V.T.; Bode, J.W. SnAP Reagents for the Synthesis of Piperazines and Morpholines. *Org. Lett.* **2014**, *16*, 1236-1239.
25. Luescher, M.U.; Bode, J.W. Catalytic Synthesis of N-Unprotected Piperazines, Morpholines, and Thiomorpholines from Aldehydes and SnAP Reagents. *Angew. Chem. Int. Ed.* **2015**, *54*, 10884-10888.
26. Behenna, D.C.; Liu, Y.; Yurino, T.; Kim, J.; White, D.E.; Virgil, S.C.; Stoltz, B.M. Enantioselective construction of quaternary N-heterocycles by palladium-catalyzed decarboxylative allylic alkylation of lactams. *Nature Chem.* **2012**, *4*, 130-133.
27. Numajiri, Y.; Jimenez-Oses, G.; Wang, B.; Houk, K.N.; Stoltz, B.M. Enantioselective synthesis of dialkylated N-Heterocycles by Palladium-Catalyzed Allylic Alkylation. *Org. Lett.* **2015**, *17*, 1082-1085.
28. Whitesell, J.K. C₂ Symmetry and Asymmetric Induction. *Chem. Rev.* **1989**, *89*, 1581-1590.
29. Whitesell, J.K.; Felman, S.W. Asymmetric Induction: Enantioselective Alkylation of Cyclohexanone via a Chiral Enamine. *J. Org. Chem.* **1977**, *42*, 1663-1664.

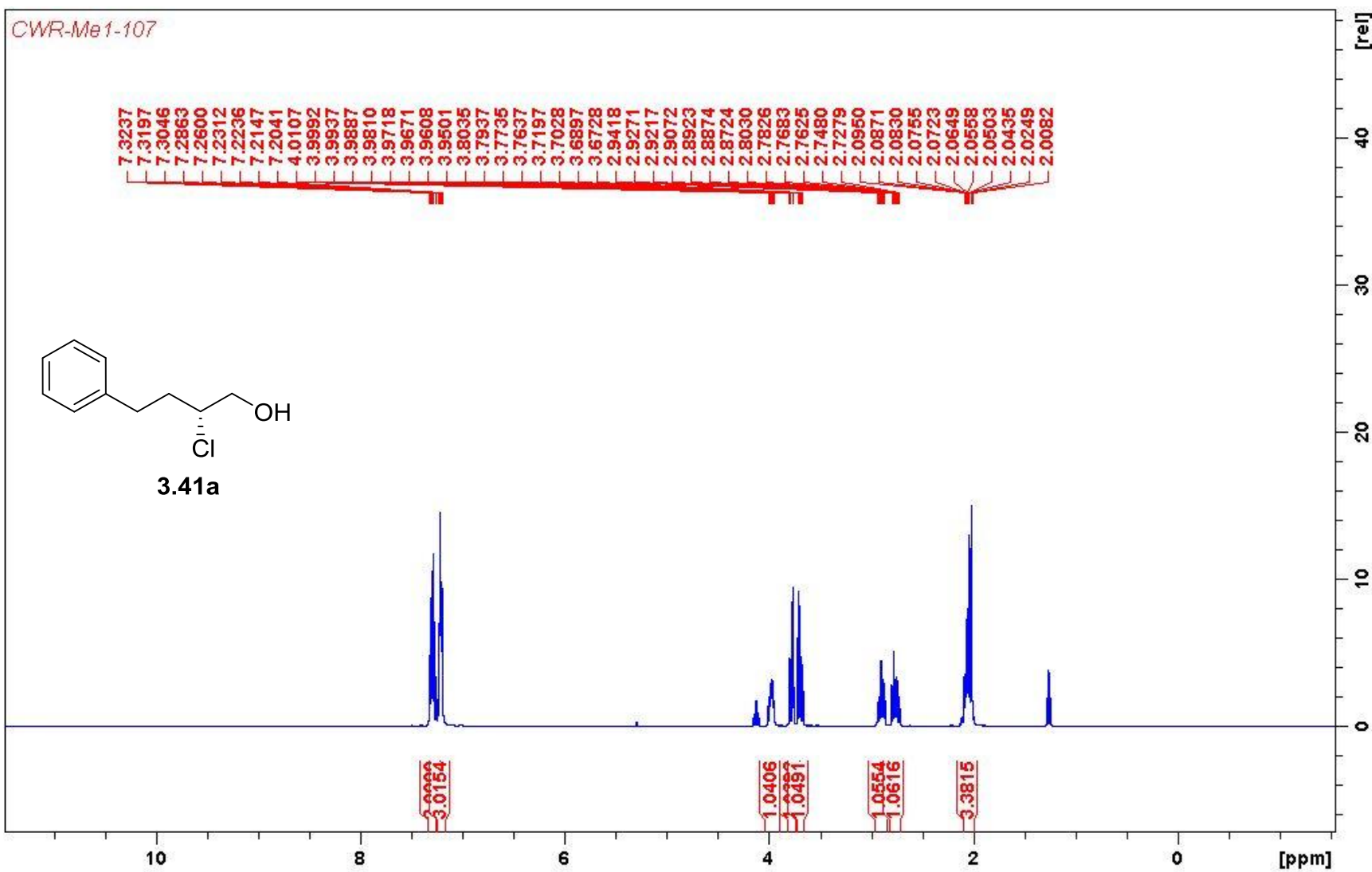
30. Whitesell, J.K. New Perspectives in Asymmetric Induction. *Acc. Chem. Res.* **1985**, *18*, 280-284.
31. Kawanami, Y.; Ito, Y.; Kitagawa, T.; Taniguchi, Y.; Katsuki, T.; Yamaguchi, M. Asymmetric alkylation of carboxyamides by using *trans*-2,5-disubstituted pyrrolidines as chiral auxiliaries. *Tetrahedron Letters* **1984**, *25*, 857-860.
32. Katsuki, T.; Yamaguchi, M. Asymmetric aldol reaction of amide enolates bearing *trans*-2,5-disubstituted pyrrolidines as chiral auxiliaries. *Tetrahedron Letters* **1985**, *26*, 5807-5810.
33. Uchikawa, M.; Hanamoto, T.; Katsuki, T.; Yamaguchi, M. Asymmetric [2,3] wittig rearrangement of 2'-alkenyloxyacetamide bearing *trans*-2,5-bis(methoxymethoxymethyl)pyrrolidine moiety as a chiral auxiliary. *Tetrahedron Letters* **1986**, *27*, 4577-4580.
34. Katsuki, T.; Yamaguchi, M. Synthesis of optically active insect pheromones, (2*R*,5*S*)-2-methyl-5-hexanolide, (3*S*,11*S*)-3,11-dimethyl-2-nonacosanone, and serricornin. *Tetrahedron Letters* **1987**, *28*, 651-654.
35. Ikegami, S.; Uchiyama, H.; Hayama, T.; Katsuki, T.; Yamaguchi, M. Asymmetric synthesis of α -amino acids by alkylation of *N*-[*N*-bis-(methylthio)methyleneglycyl]-2,5-bis(methoxymethoxymethyl)pyrrolidine and enantioselective synthesis of protected (2*S*,9*S*)-2-amino-8-oxo-9,10-epoxydecanoic acid. *Tetrahedron* **1988**, *44*, 5333-5342.
36. Kawanami, Y.; Fujita, I.; Asahara, S.; Katsuki, T.; Yamaguchi, M. Diastereoselective reduction of α -keto amides having *trans*-2,5-disubstituted pyrrolidine as a chiral auxiliary. *Bull. Chem. Soc. Jpn.* **1989**, *62*, 3598-3602.
37. Veit, A.; Lenz, R.; Seiler, M.E.; Neuburger, M.; Zehnder, M.; Giese, B. C₂-Symmetrical Pyrrolidine Derivatives as Chiral Auxiliaries in Radical Chemistry. *Helv. Chim. Acta.* **1993**, *76*, 441-450.
38. Marzi, M.; Misiti, D. Asymmetric synthesis of *trans*-(2*R*,5*R*)-bis(benzyloxymethyl)pyrrolidine. *Tetrahedron Letters* **1989**, *30*, 6075-6076.
39. Halland, N.; Braunton, A.; Bachmann, S. Marigo, M.; Jørgensen, K.A.; Direct organocatalytic asymmetric α -chlorination of aldehydes. *J. Am. Chem. Soc.* **2004**, *126*, 4790-4791.
40. Fadeyi, O.O.; Schulte, M.L.; Lindsley, C.W. General Access to Chiral *N*-Alkyl Terminal Aziridines via Organocatalysis. *Org. Lett.* **2010**, *12*, 3276-3278.
41. Senter, T.J.; O'Reilly, M.C.; Chong, K.M.; Sulikowski, G.A.; Lindsley, C.W. A general, enantioselective synthesis of *N*-alkyl terminal aziridines and C2-functionalized azetidines via organocatalysis. *Tetrahedron Letters* **2015**, *56*, 1276-1279.
42. O'Reilly, M.C.; Lindsley, C.W. Enantioselective synthesis of C2-functionalized, *N*-protected morpholines and orthogonally *N,N'*-protected piperazines via organocatalysis. *Tetrahedron Letters* **2012**, *53*, 1539-1542.
43. O'Reilly, M.C.; Lindsley, C.W. A General, Enantioselective Synthesis of Protected Morpholines and Piperazines. *Org. Lett.* **2012**, *14*, 2910-2913.
44. Kempainen, E.K.; Sahoo, G.; Valkonen, A.; Pihko, P.M. Mukaiyama-Michael Reactions with Acrolein and Methacrolein: A Catalytic Enantioselective Synthesis of the C17-C28 Fragment of Pectenotoxins. *Org. Lett.* **2012**, *14*, 1086-1089.

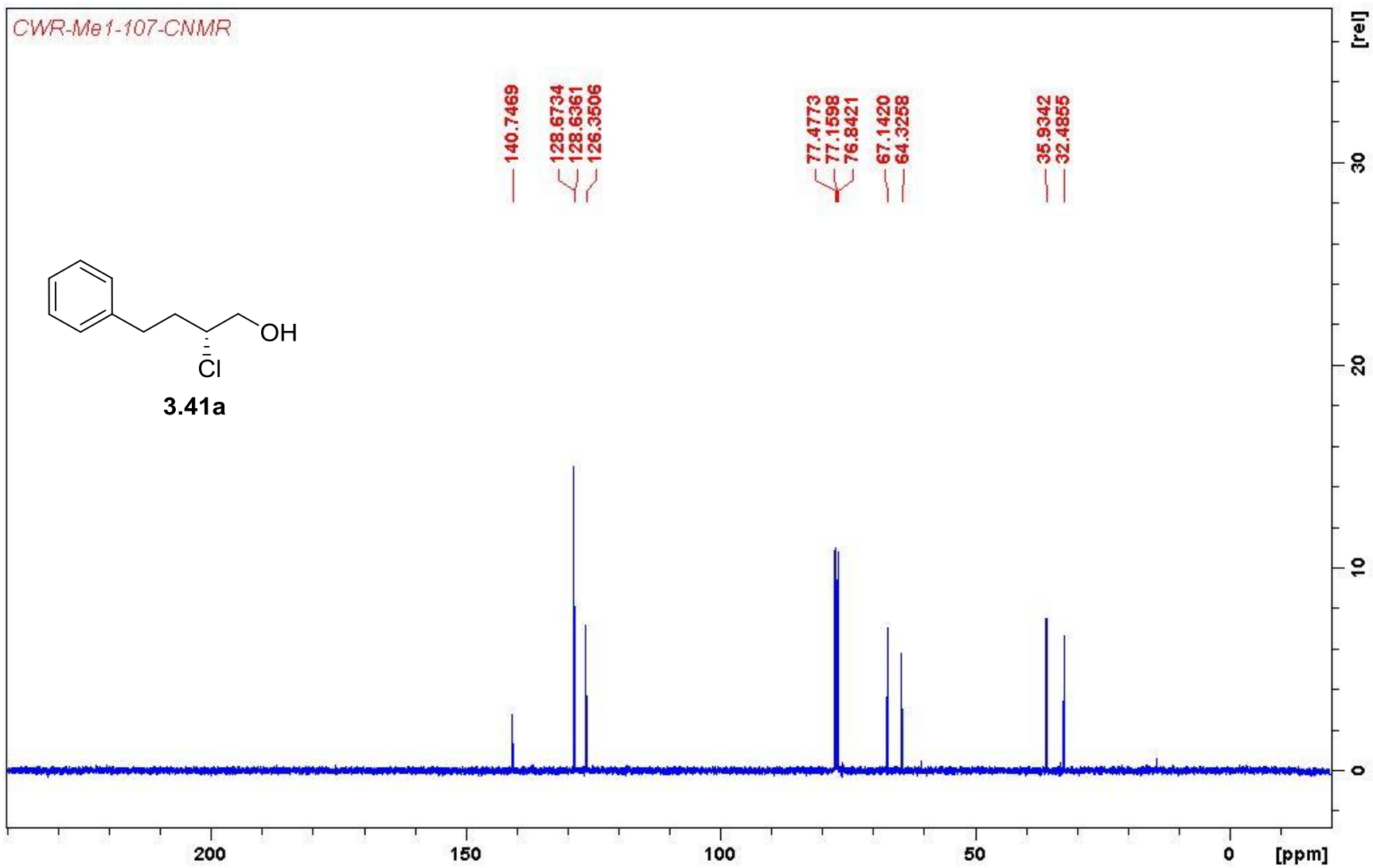
45. Chong, J.M.; Clarke, I.S.; Koch, I.; Olbach, P.C.; Taylor, N.J. Asymmetric synthesis of *trans*-2,5-diphenylpyrrolidine: A C₂-symmetric chiral amine. *Tetrahedron: Asymmetry* **1995**, *6*, 409-418.
46. Senter, T.J.; O'Reilly, M.C.; Chong, K.M.; Sulikowski, G.A.; Lindsley, C.W. A general, enantioselective synthesis of *N*-alkyl terminal aziridines and C2-functionalized azetidines via organocatalysis. *Tetrahedron Letters* **2015**, *56*, 1276-1279.
47. Brown, H.C.; Ramachandran, P.V. Asymmetric reduction with chiral organoboranes based on α -pinene. *Acc. Chem. Res.* **1992**, *25*, 16-24.
48. Corey, E.J.; Bakshi, R.K.; Shibata, S. Highly enantioselective borane reduction of ketones catalyzed by chiral oxazaborolidines: Mechanism and synthetic implications. *J. Am. Chem. Soc.* **1987**, *109*, 5551-5553.
49. Baldwin, J.E. Rules for ring closure. *J.C.S. Chem. Comm.* **1976**, 734-736.
50. Kokalta, H.P.; Thomson, P.F.; Bae, S.; Doddi, V.R.; Lakshman, M.K. Reduction of Amine *N*-Oxides by Diboron Reagents. *J. Org. Chem.* **2011**, *76*, 7842-7848.
51. Reed, C. W.; Lindsley, C. W. A general, enantioselective synthesis of 2-substituted thiomorpholines and thiomorpholine 1,1-dioxides. *Tetrahedron Letters* **2019**, *60*, 151104.

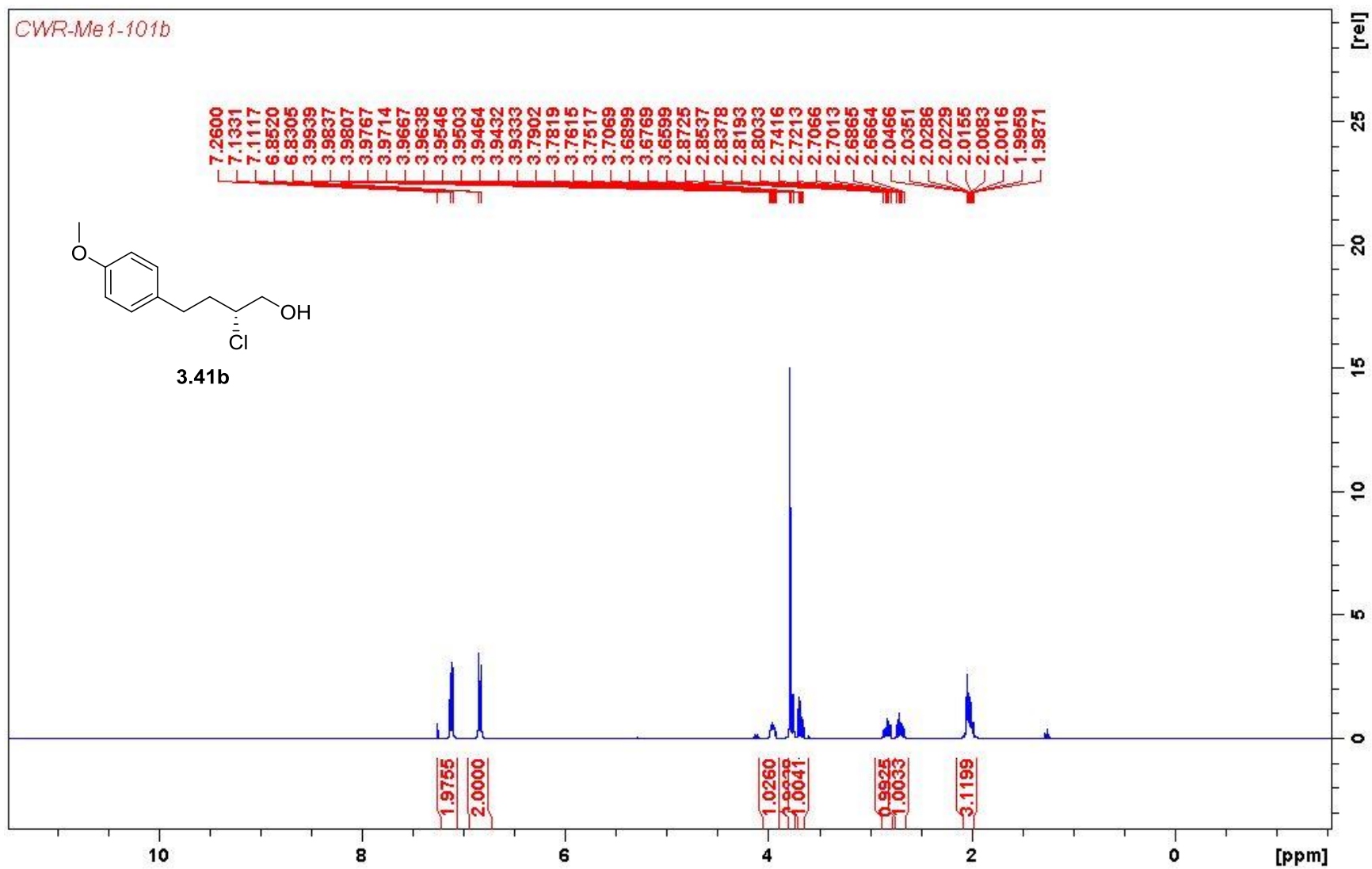
Appendix C

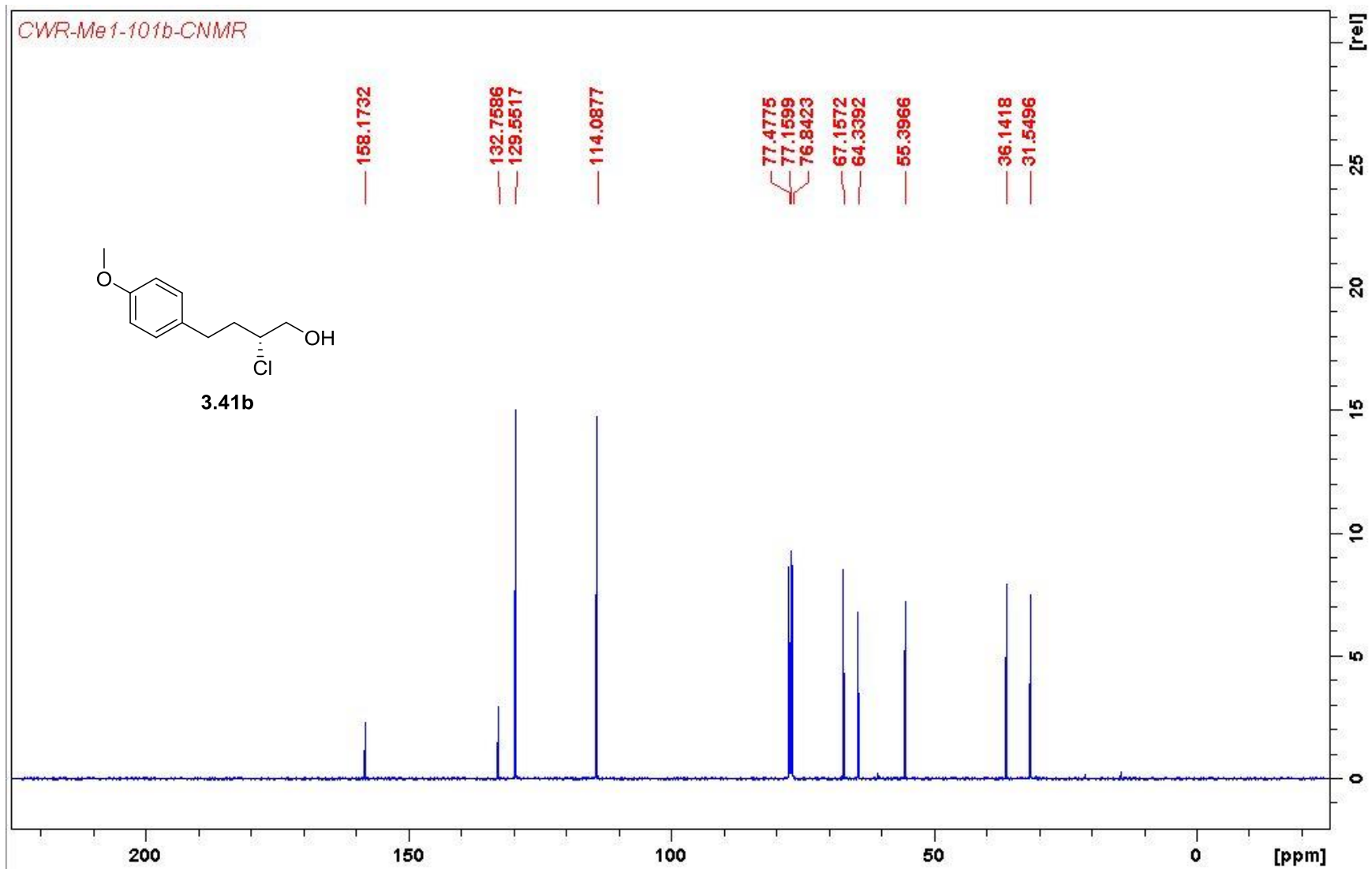
Relevant Spectra and Chiral SFC Traces for Chapter III

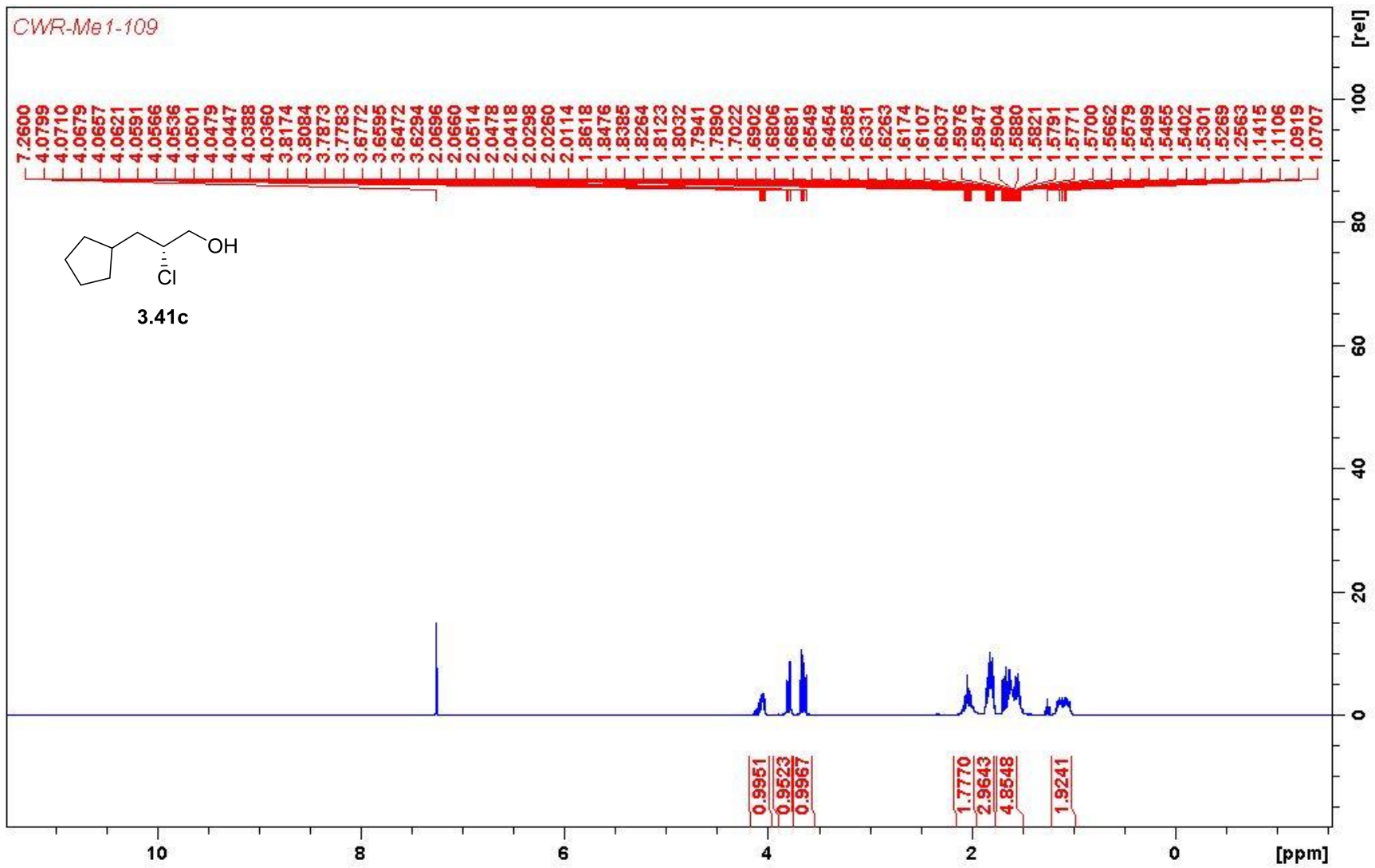
CWR-Me1-107

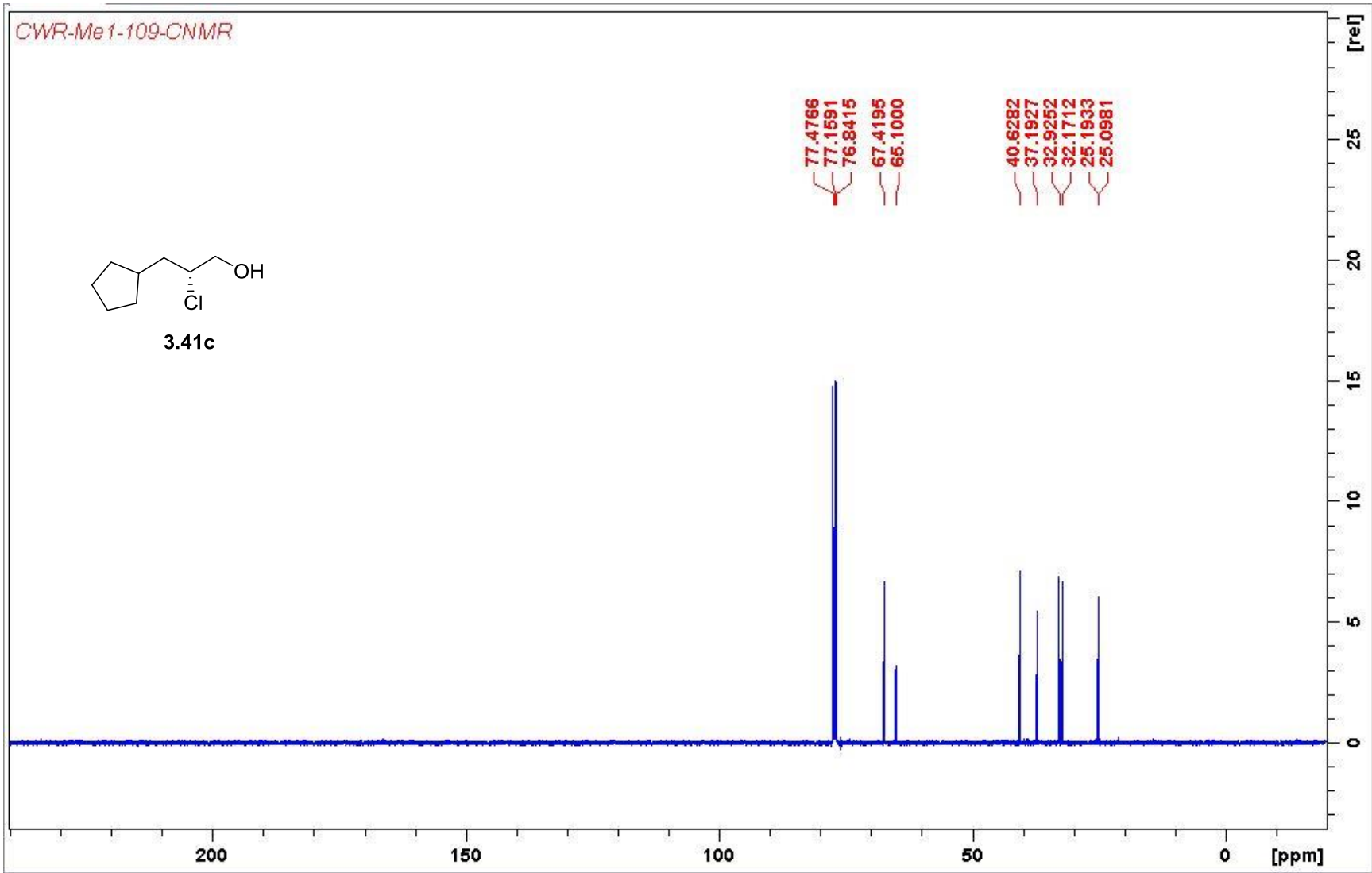


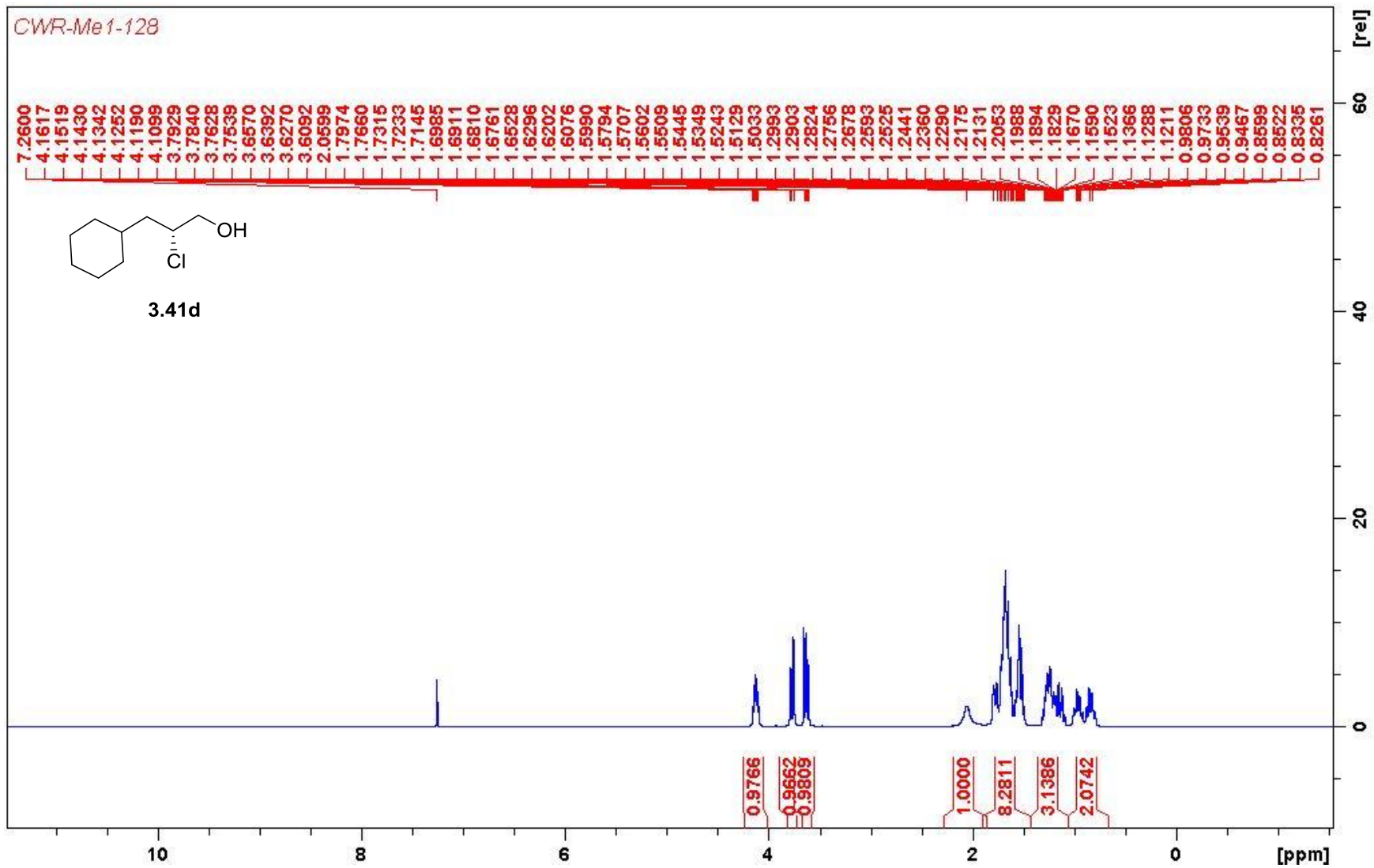




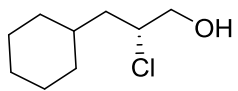




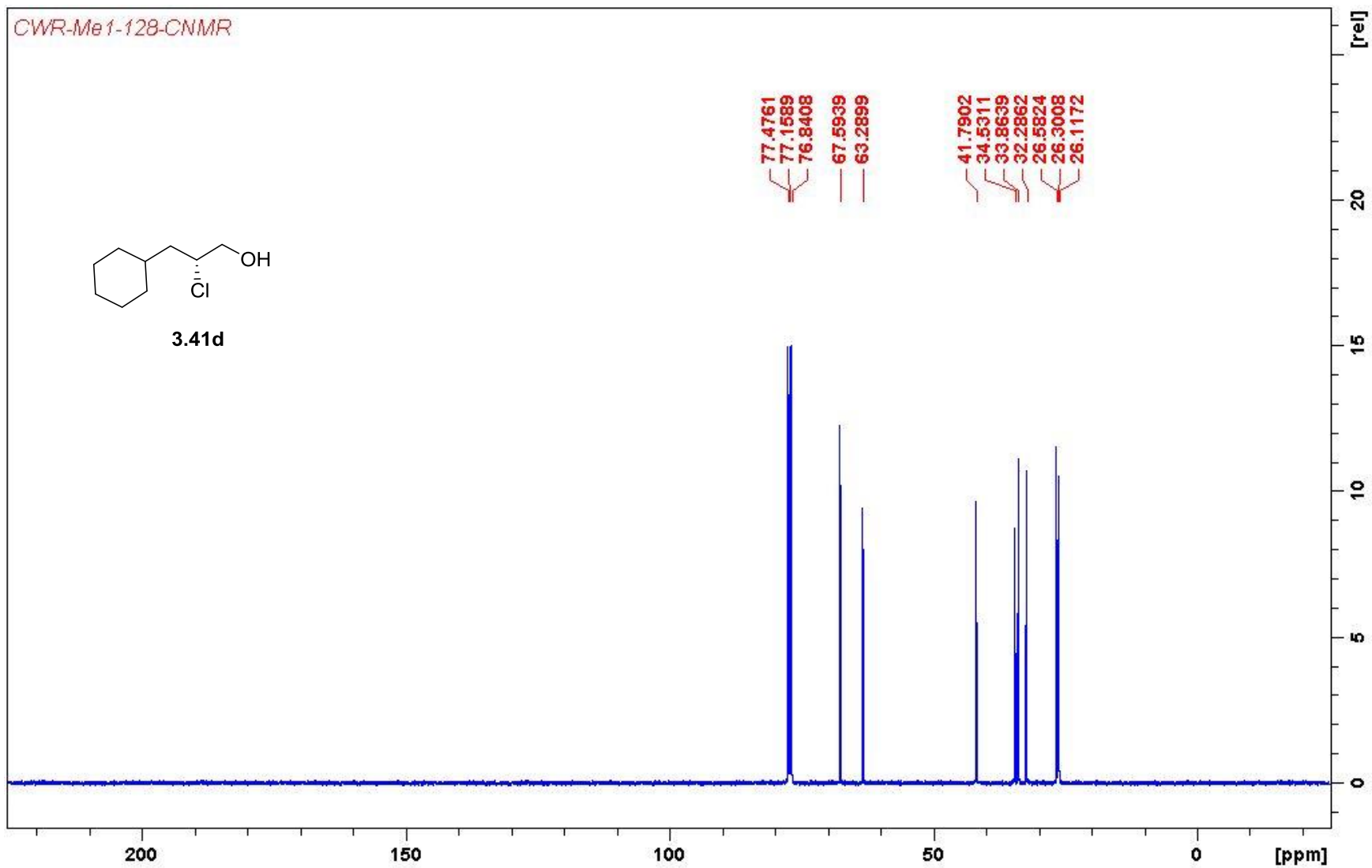


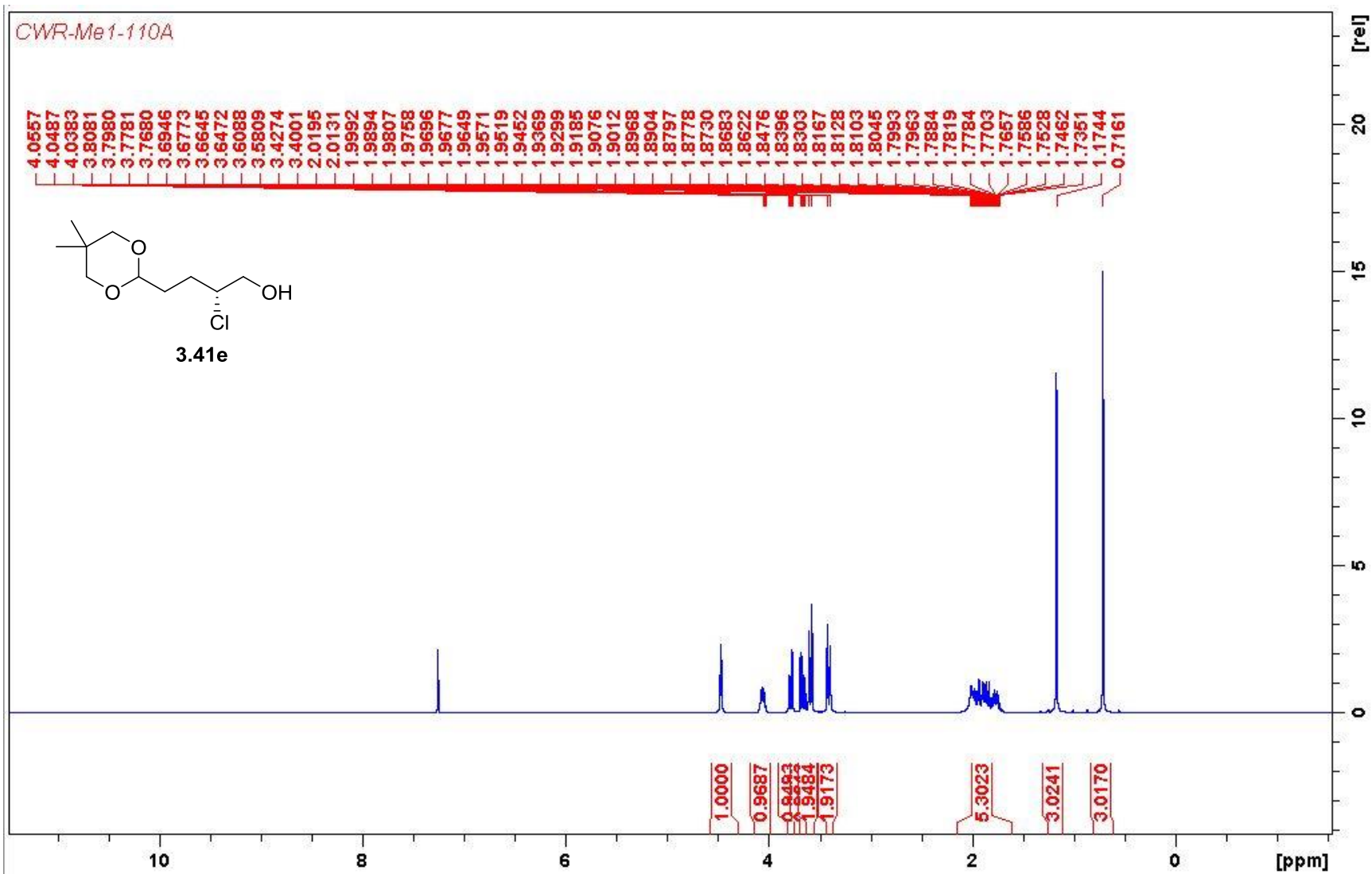


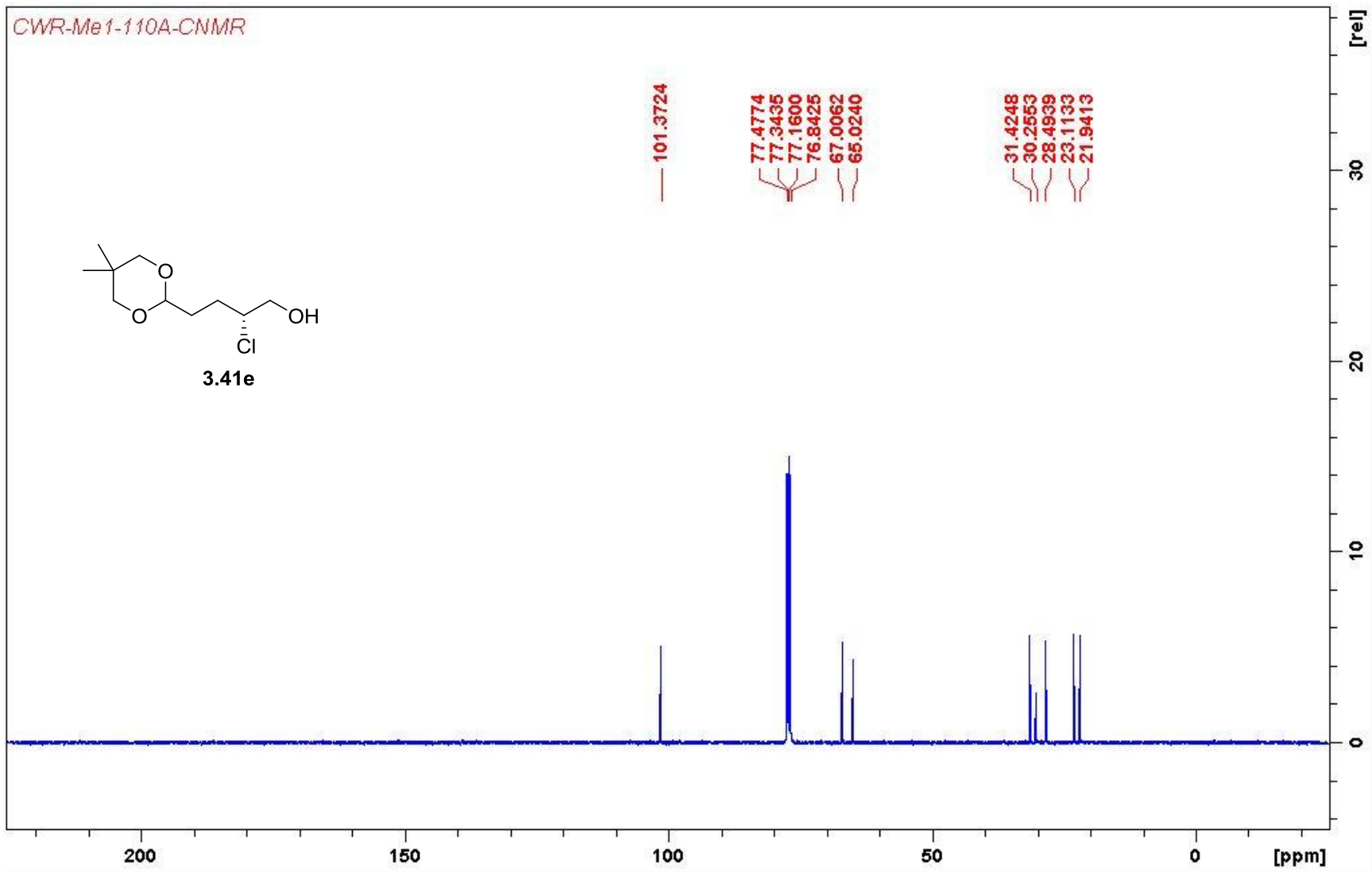
CWR-Me1-128-CNMR

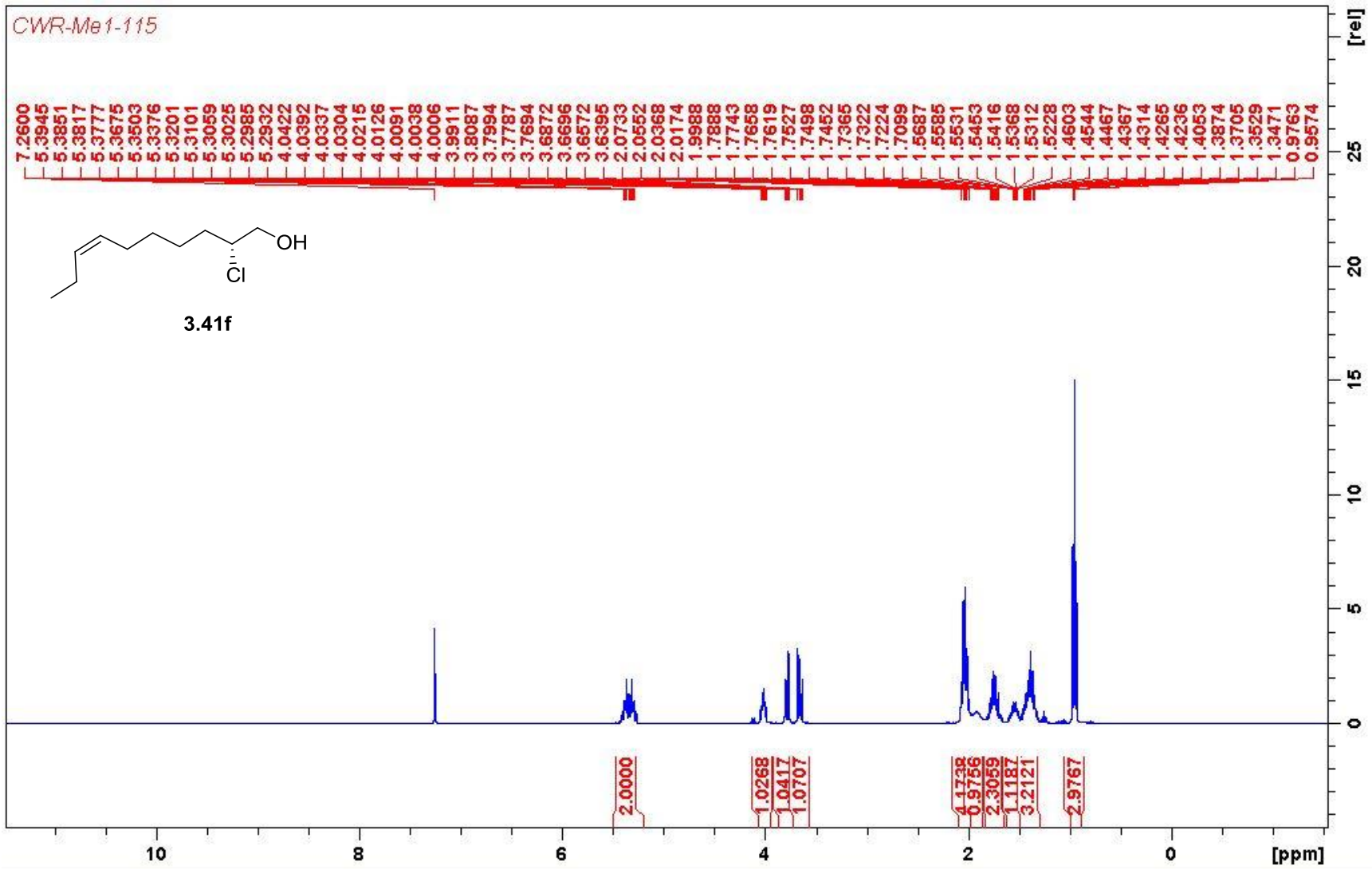


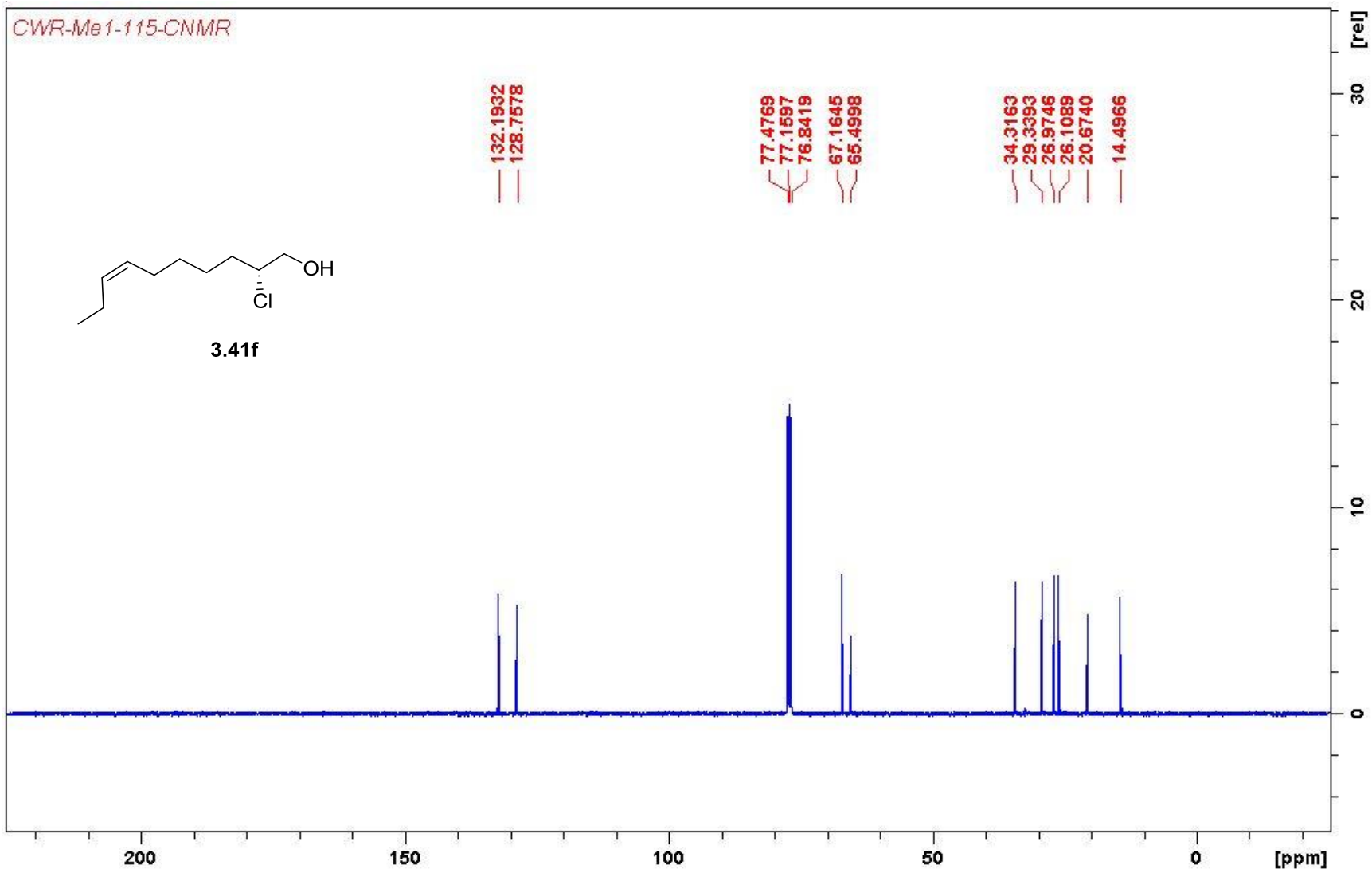
3.41d

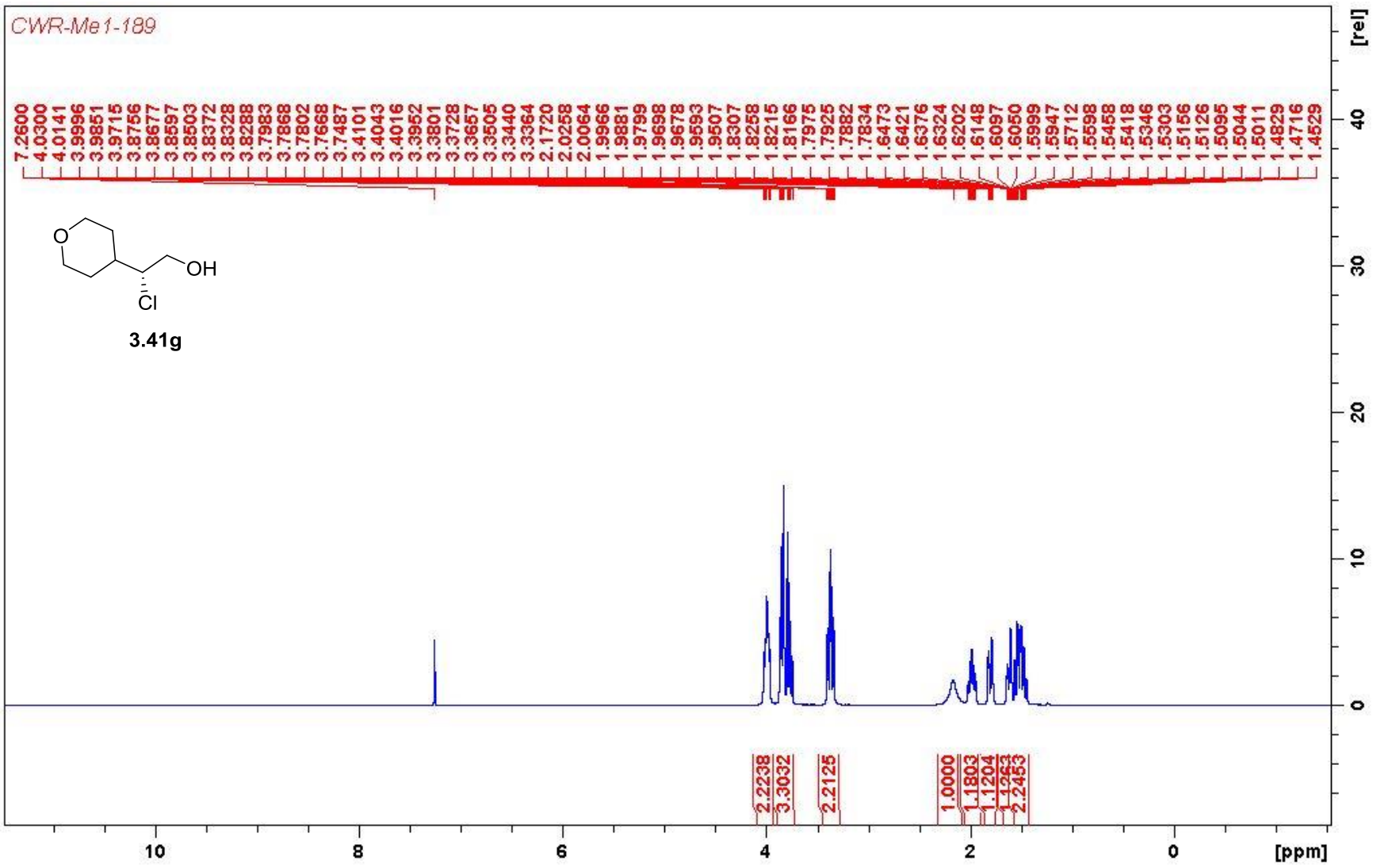




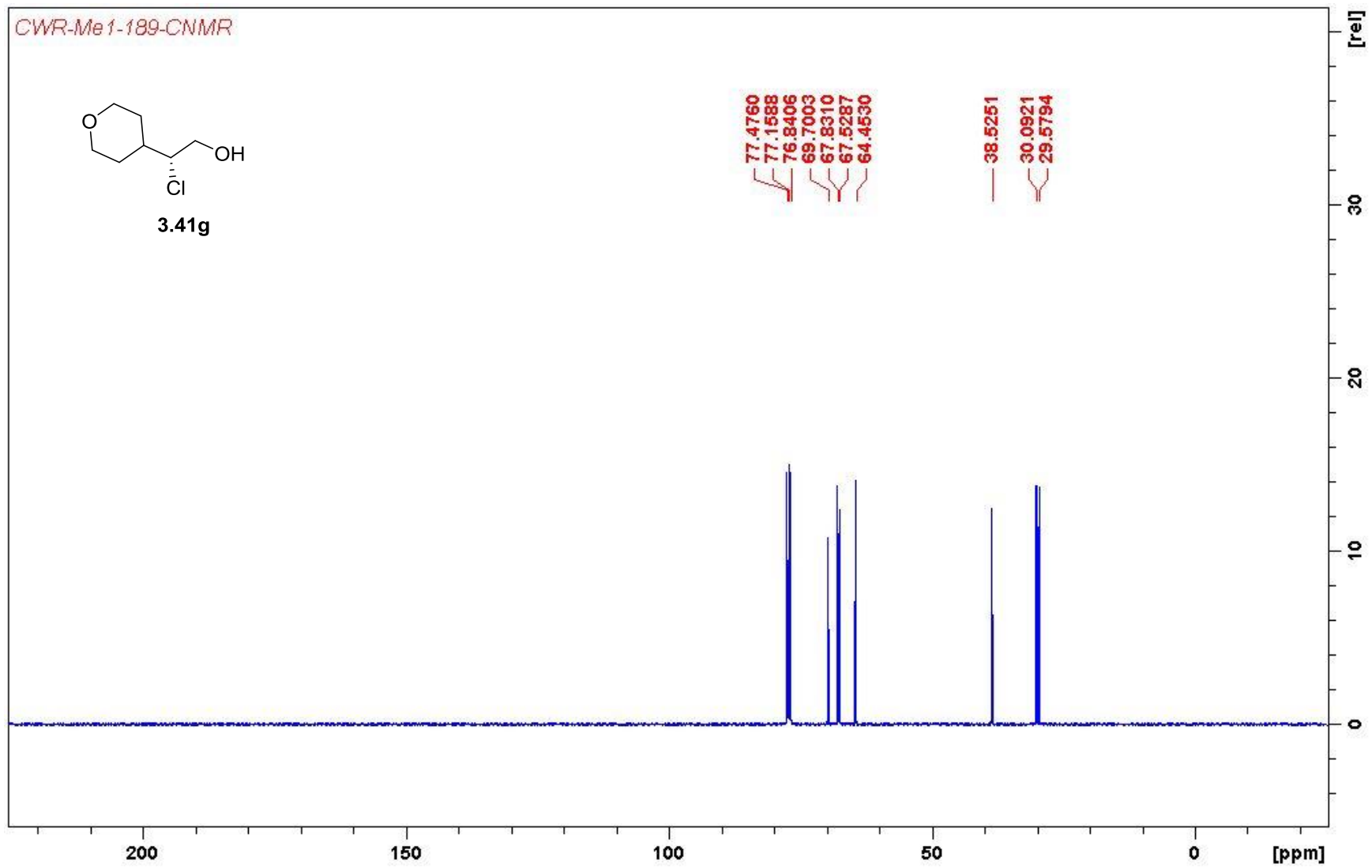
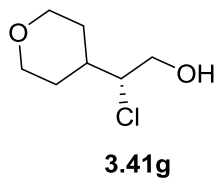


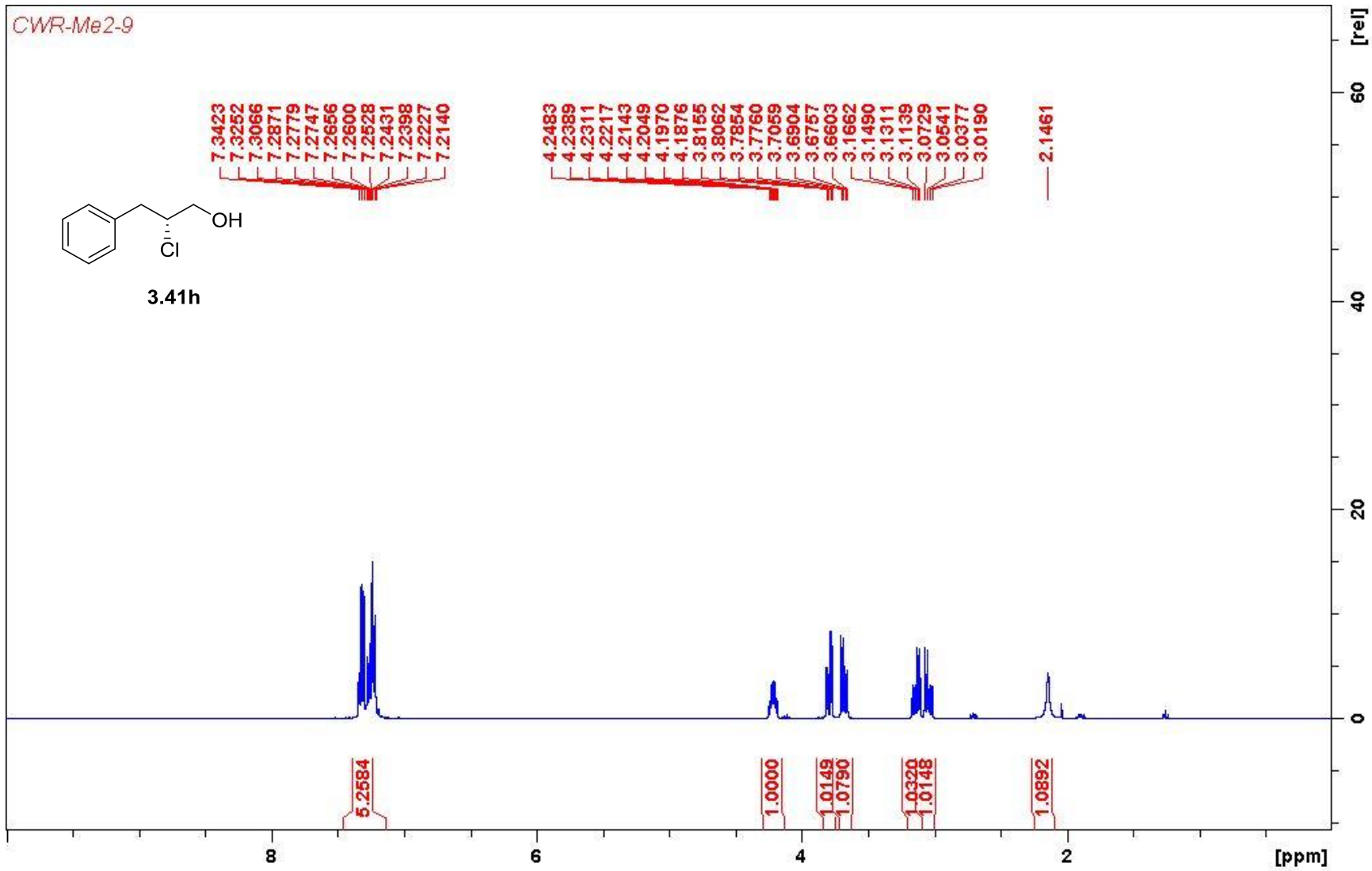




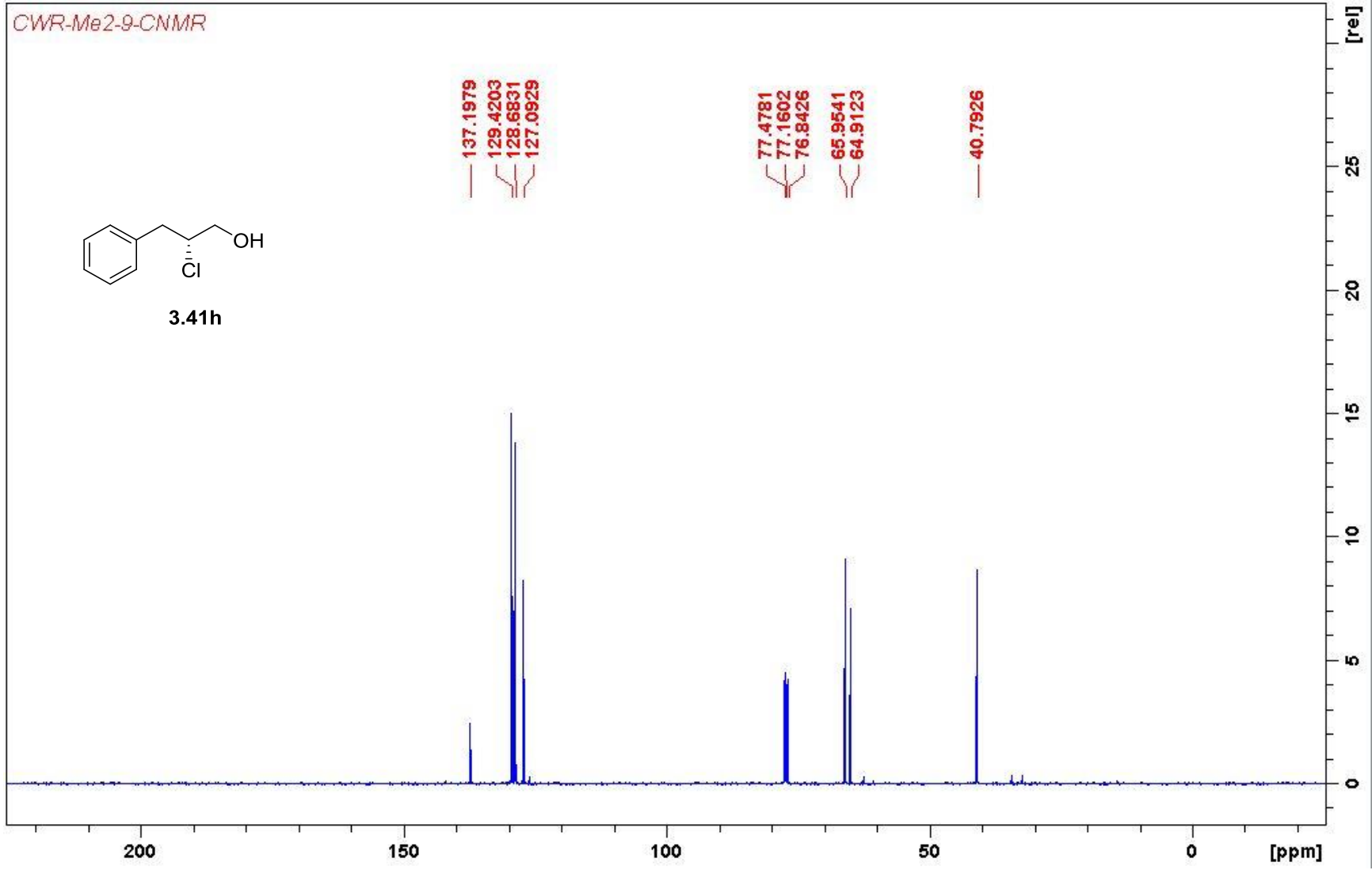
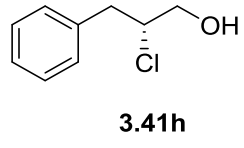


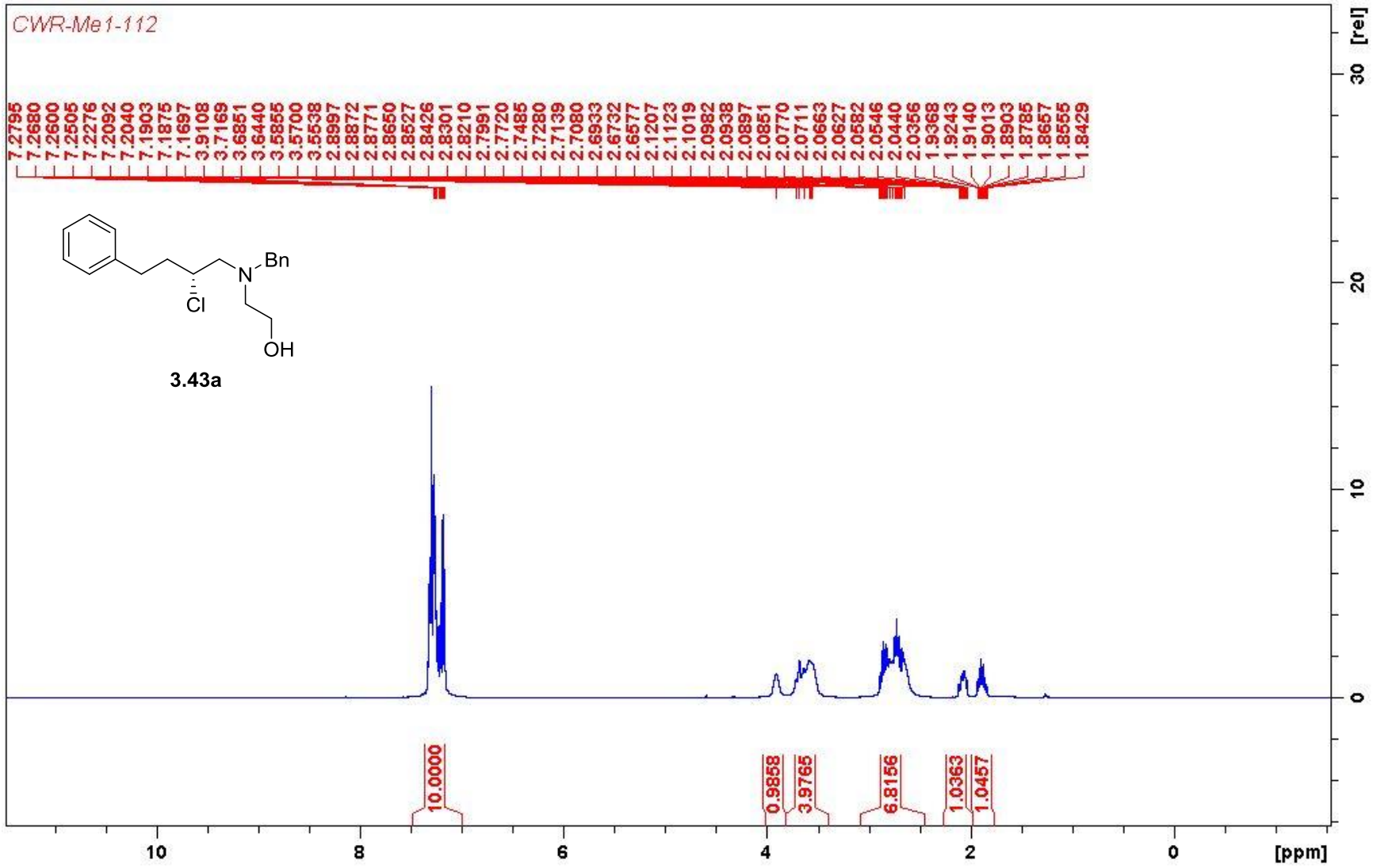
CWR-Me1-189-CNMR

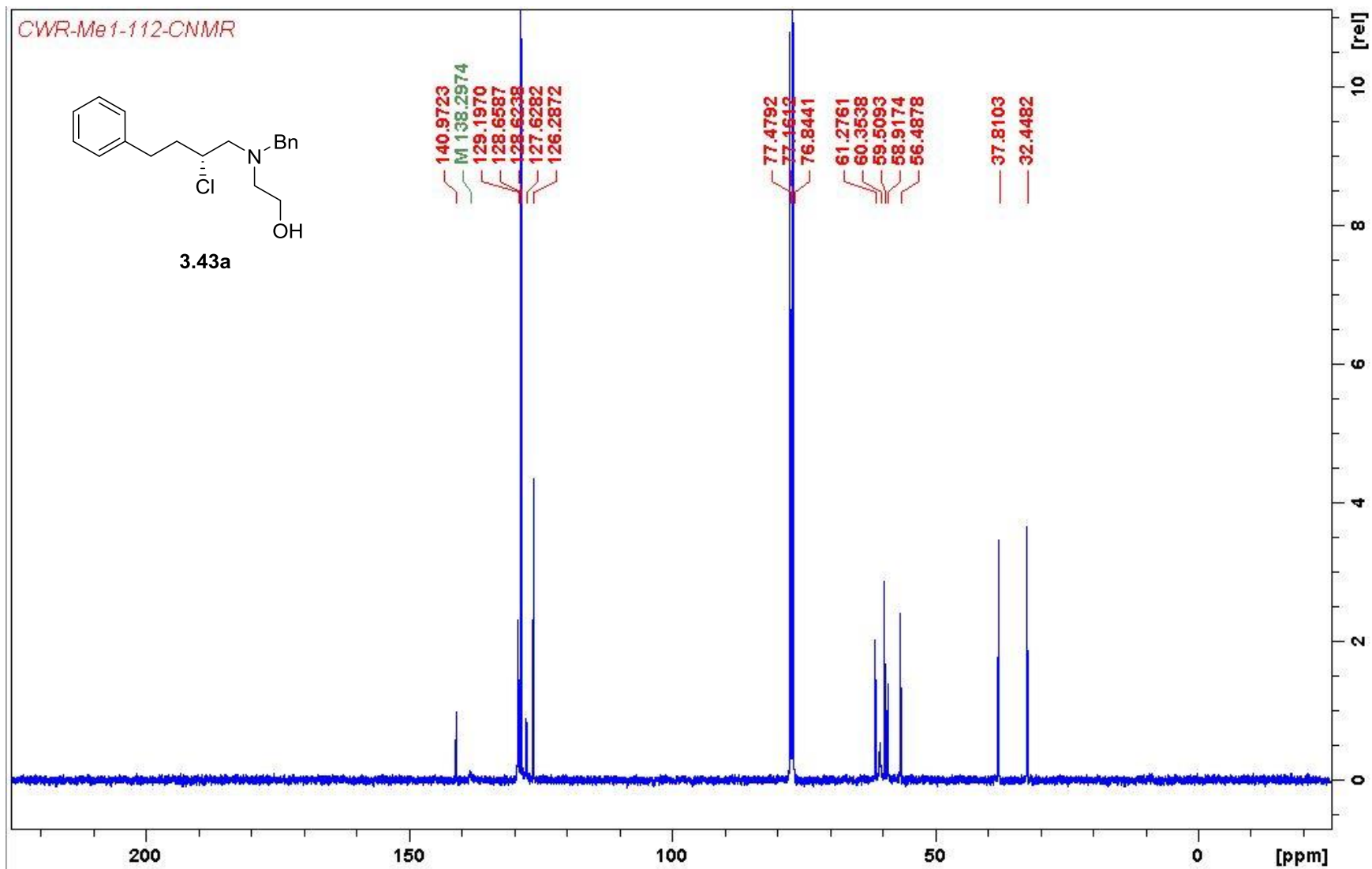


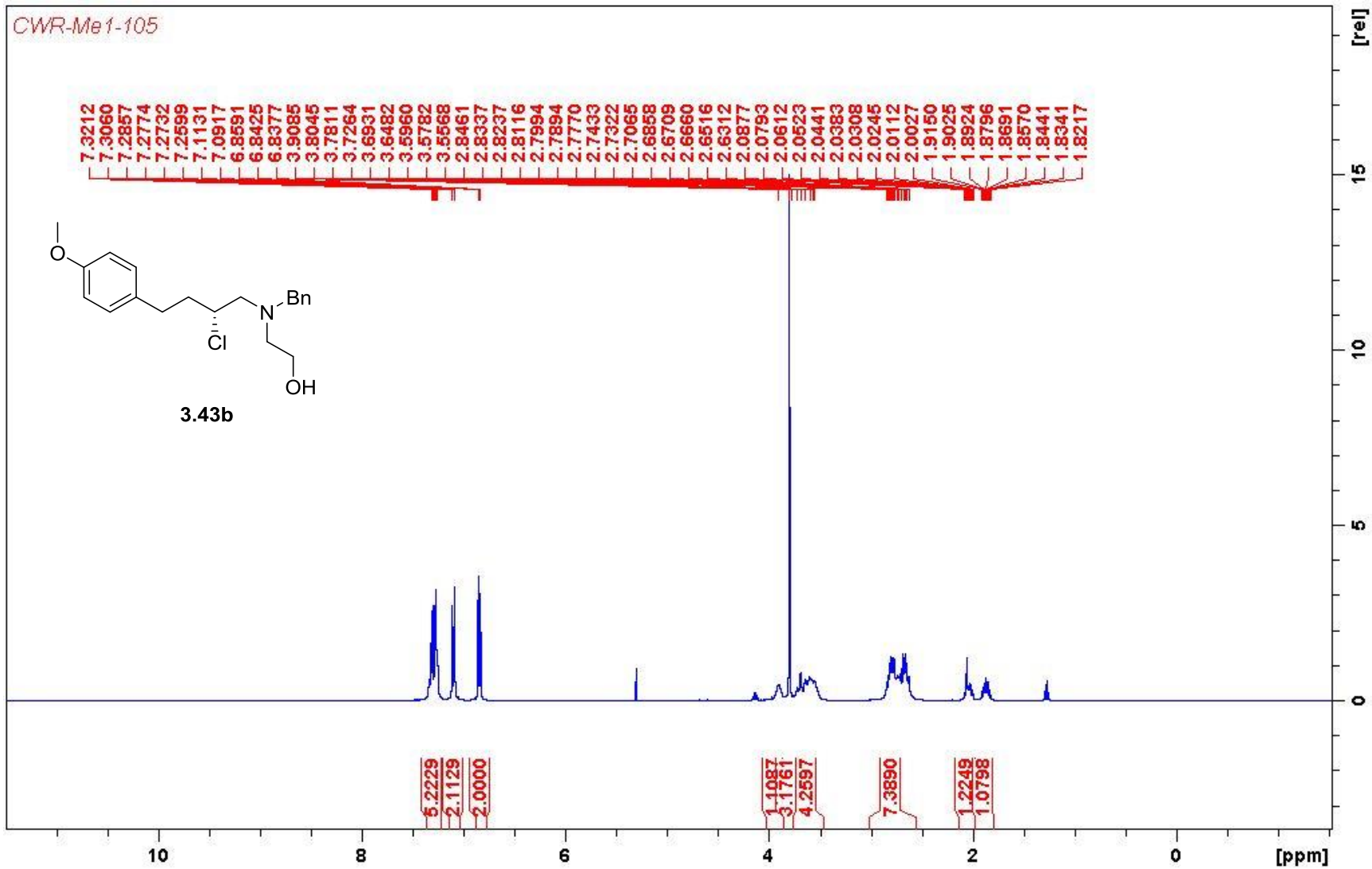


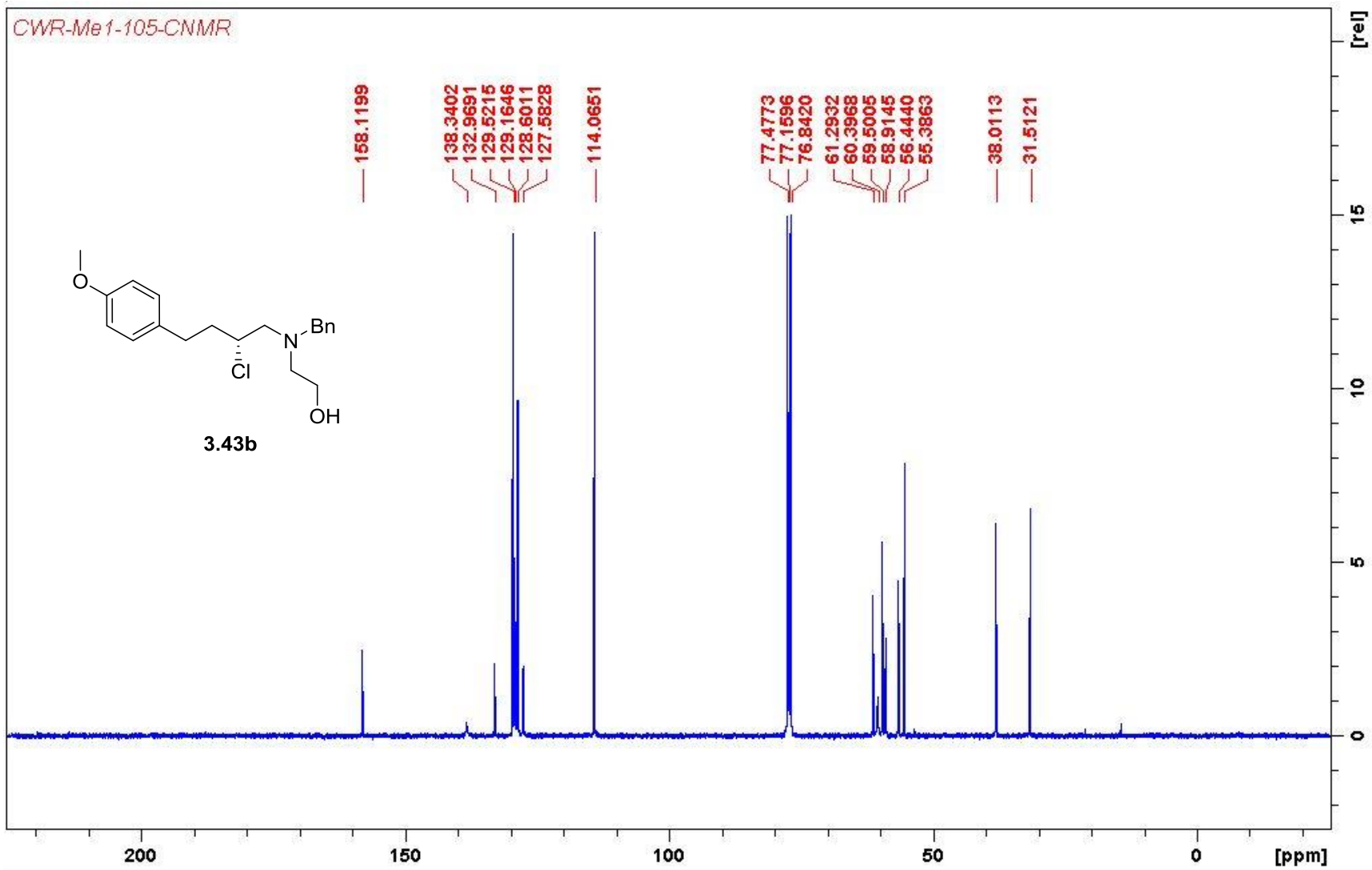
CWR-Me2-9-CNMR

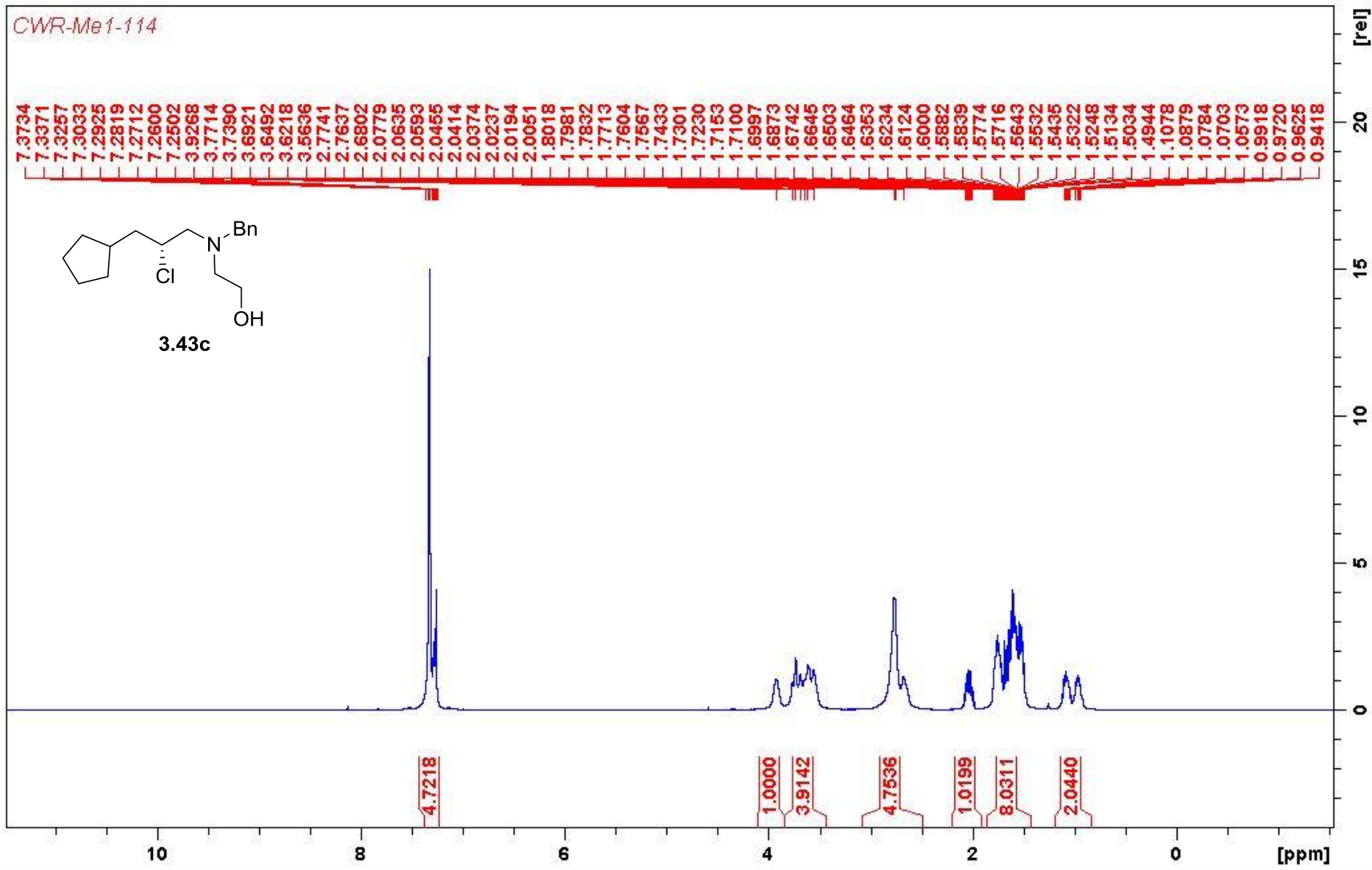




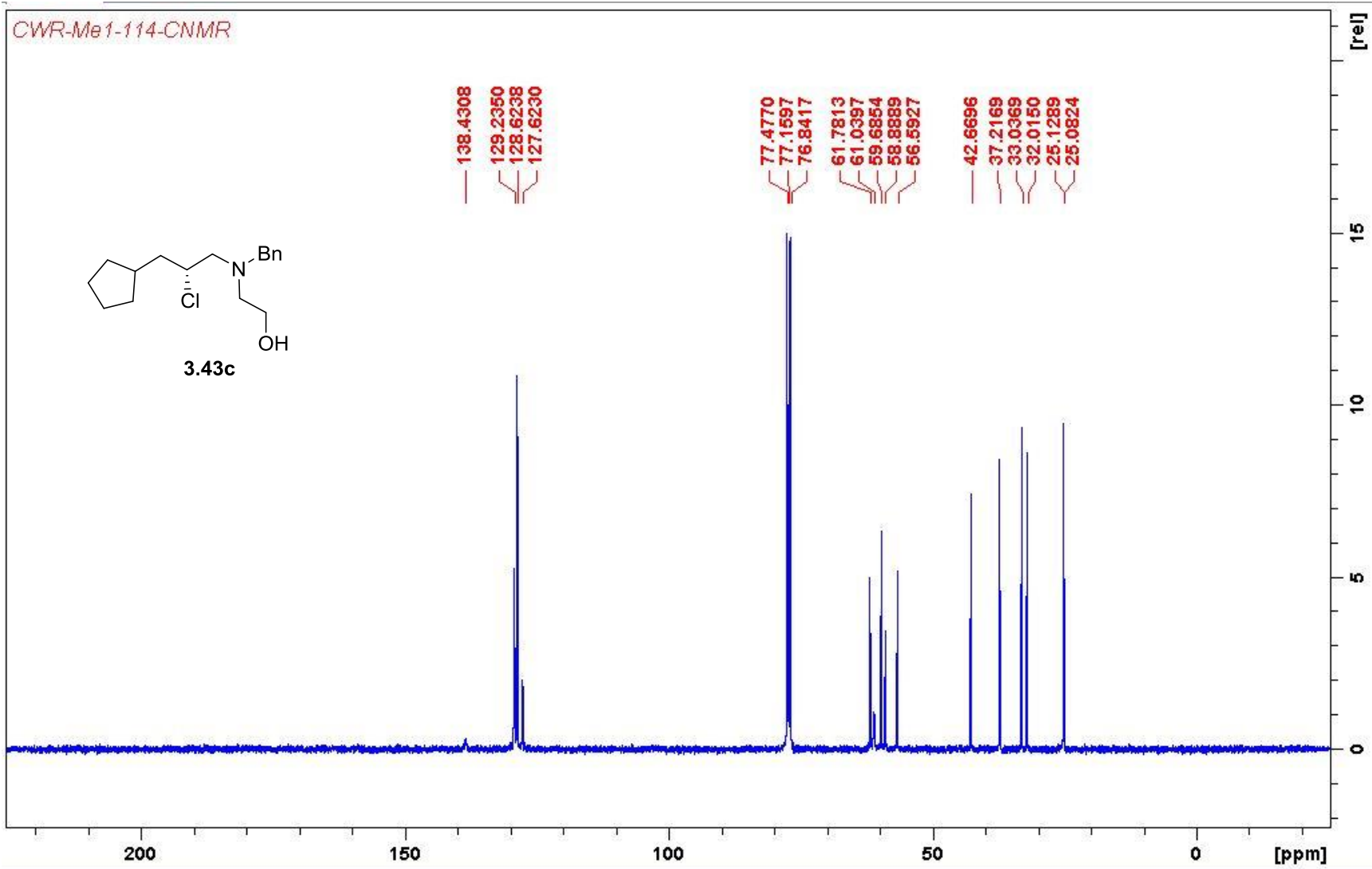
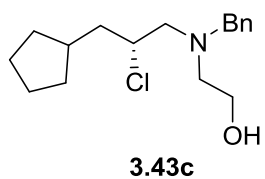


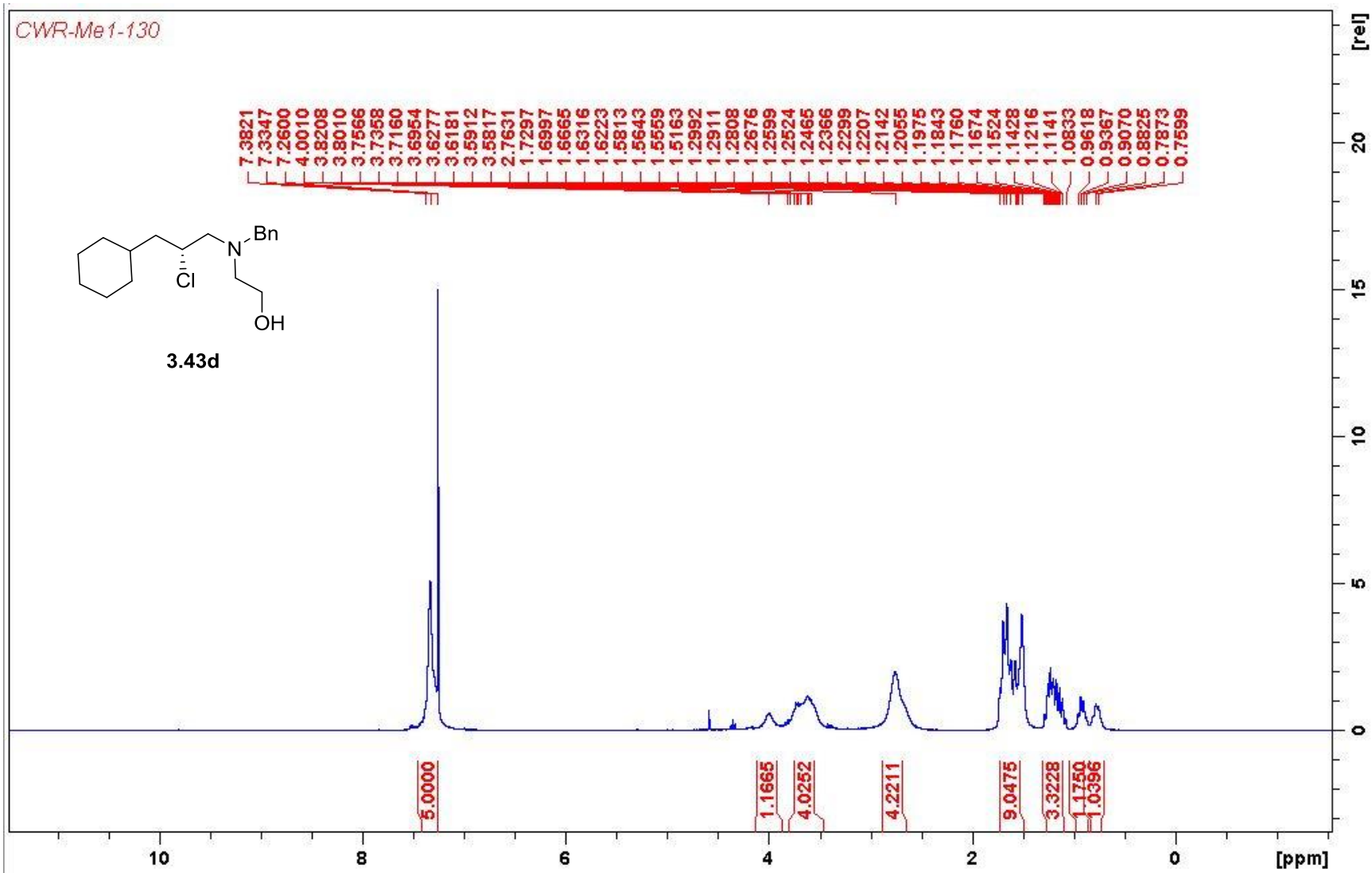


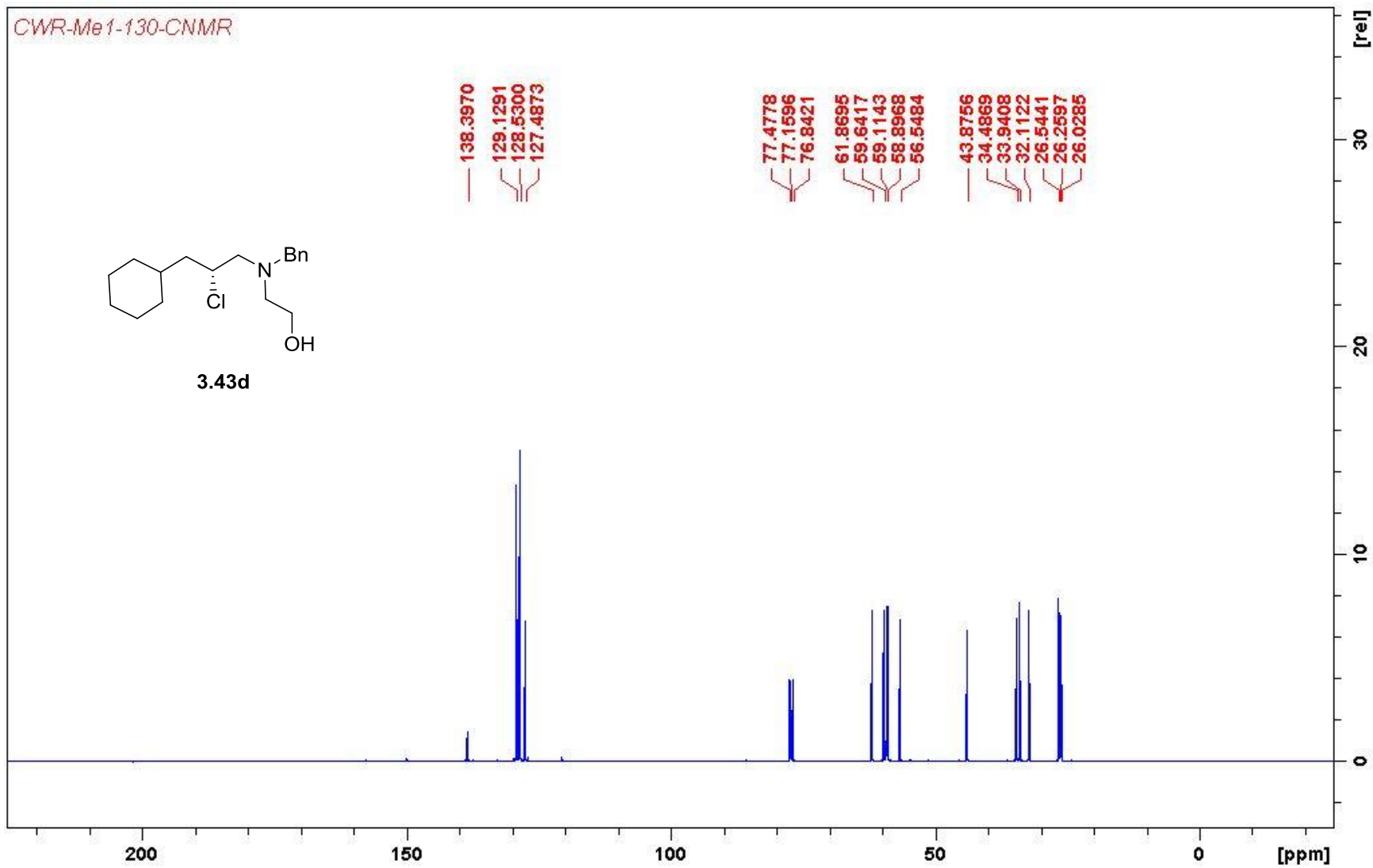




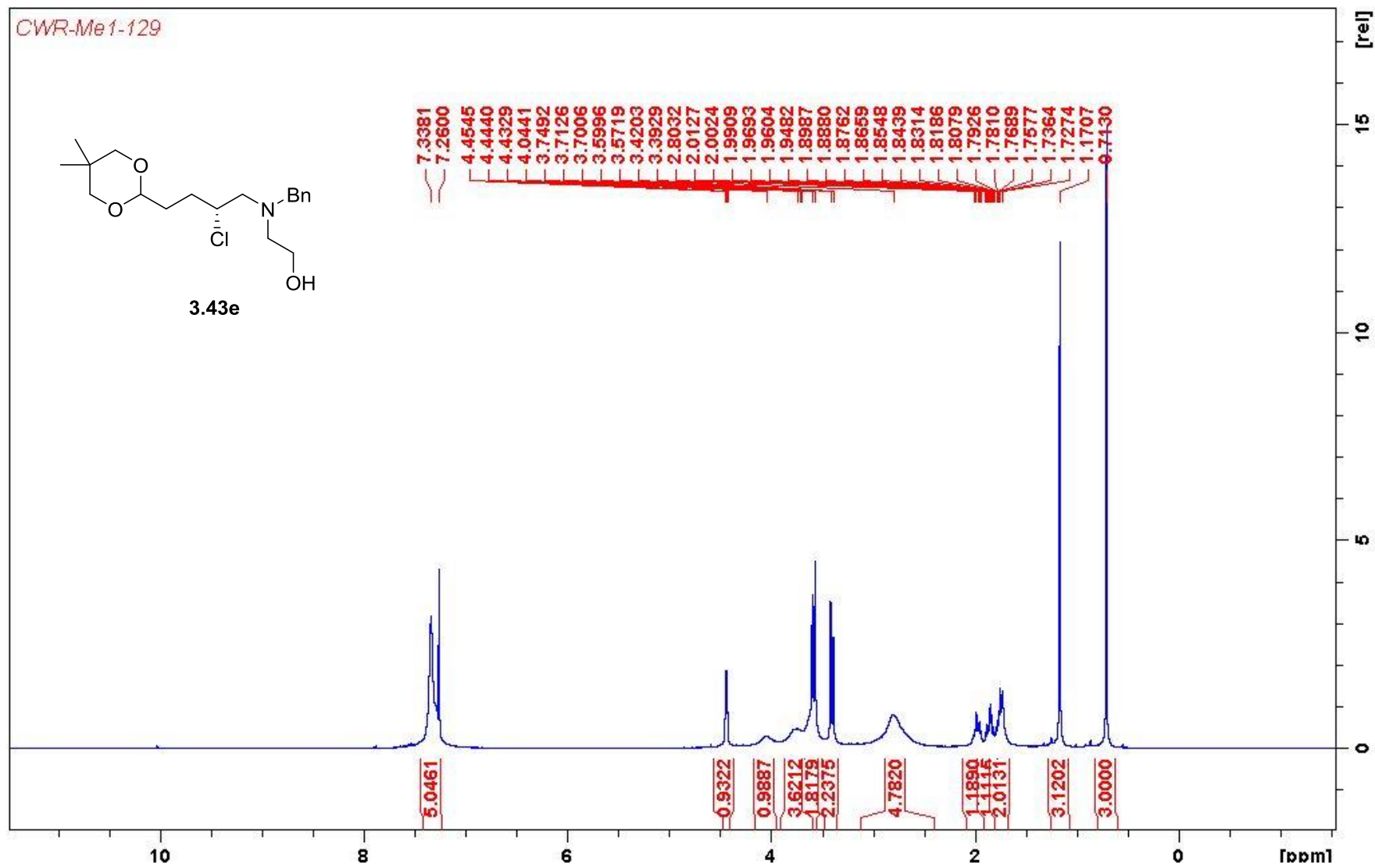
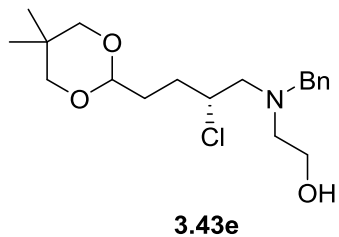
CWR-Me1-114-CNMR

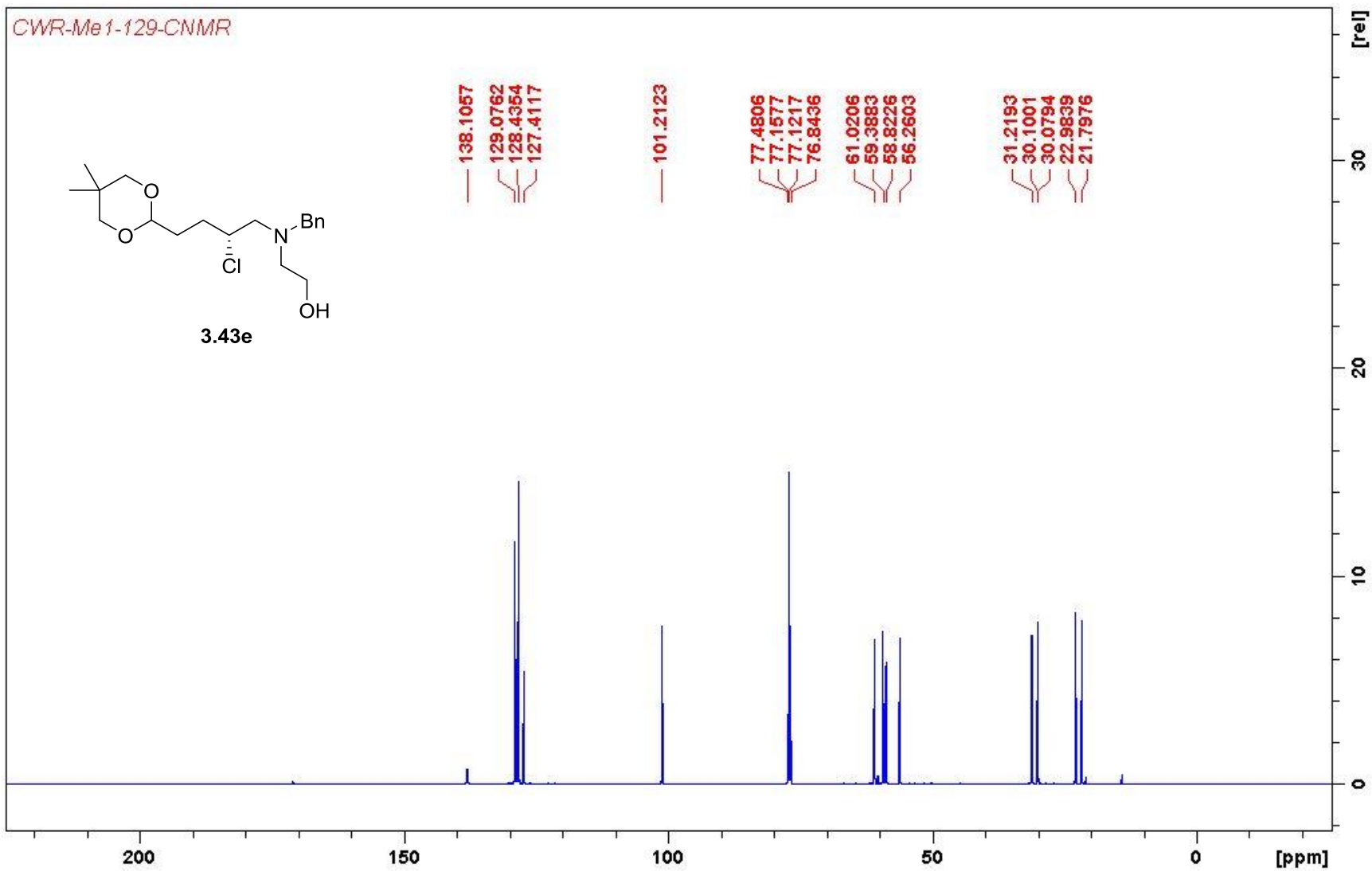


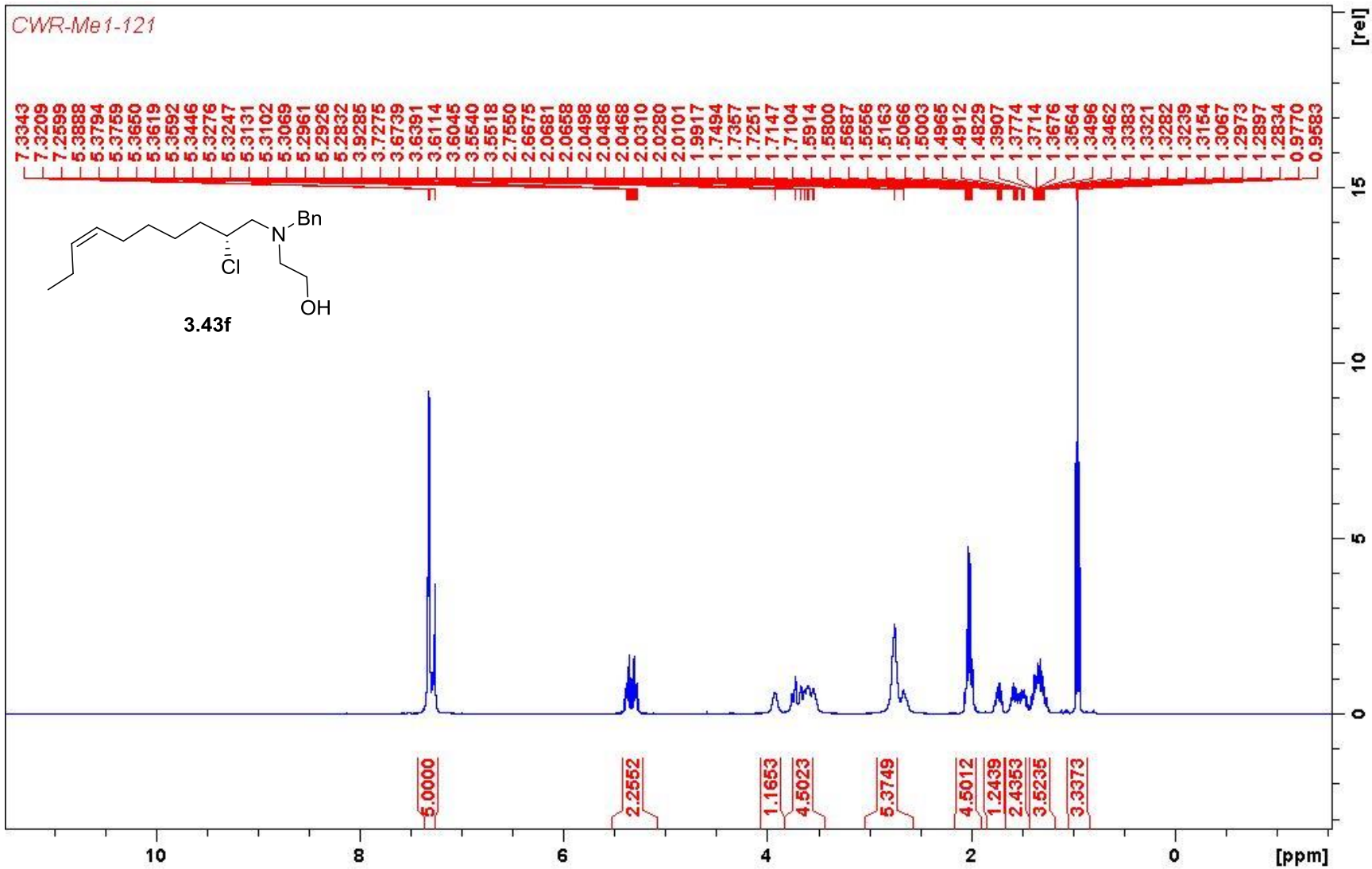




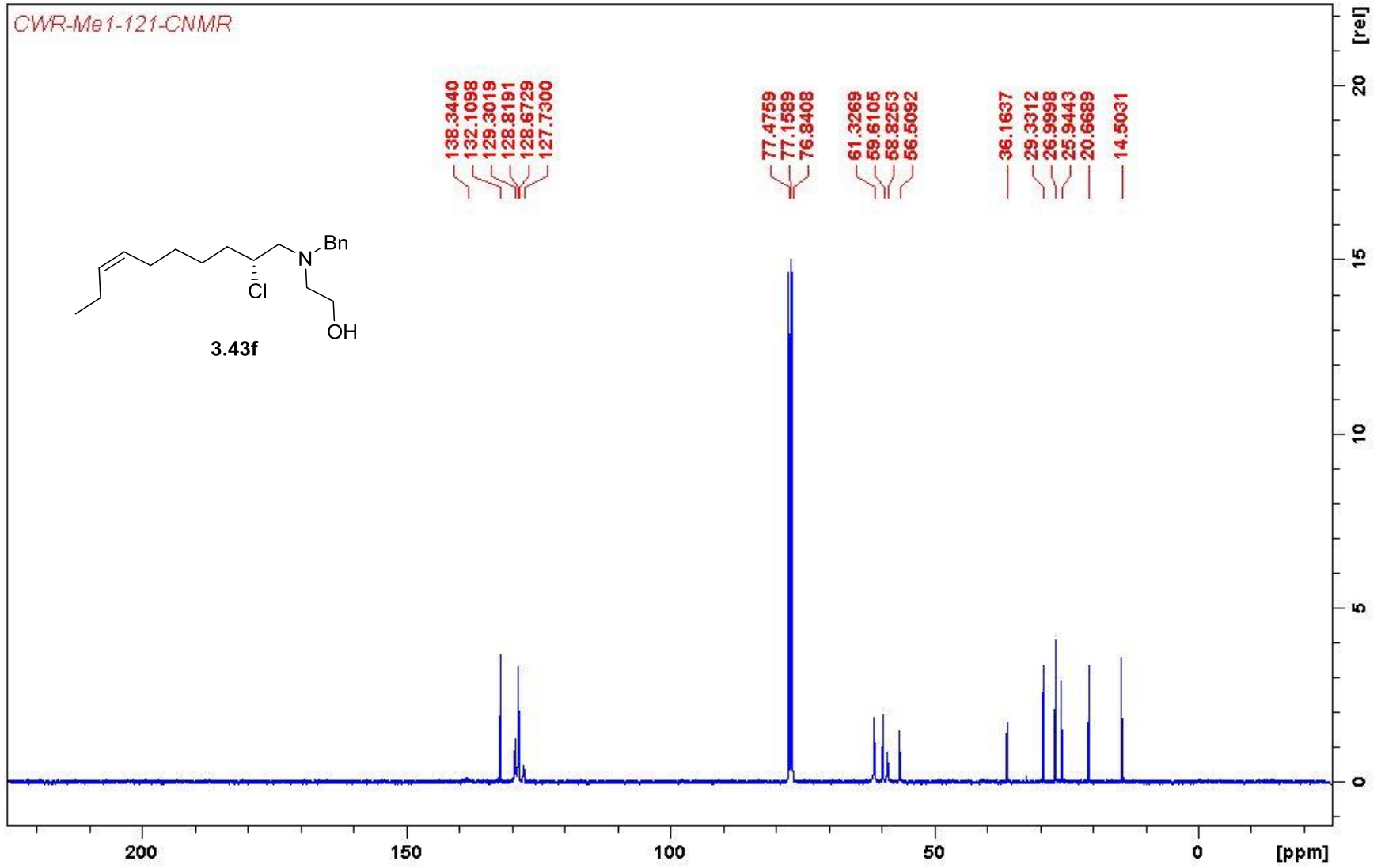
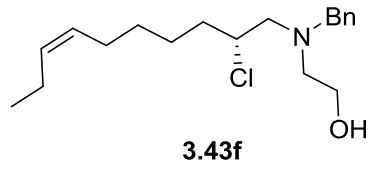
CWR-Me1-129



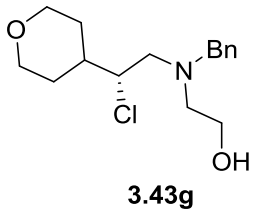




CWR-Me1-121-CNMR



CWR-Me1-190

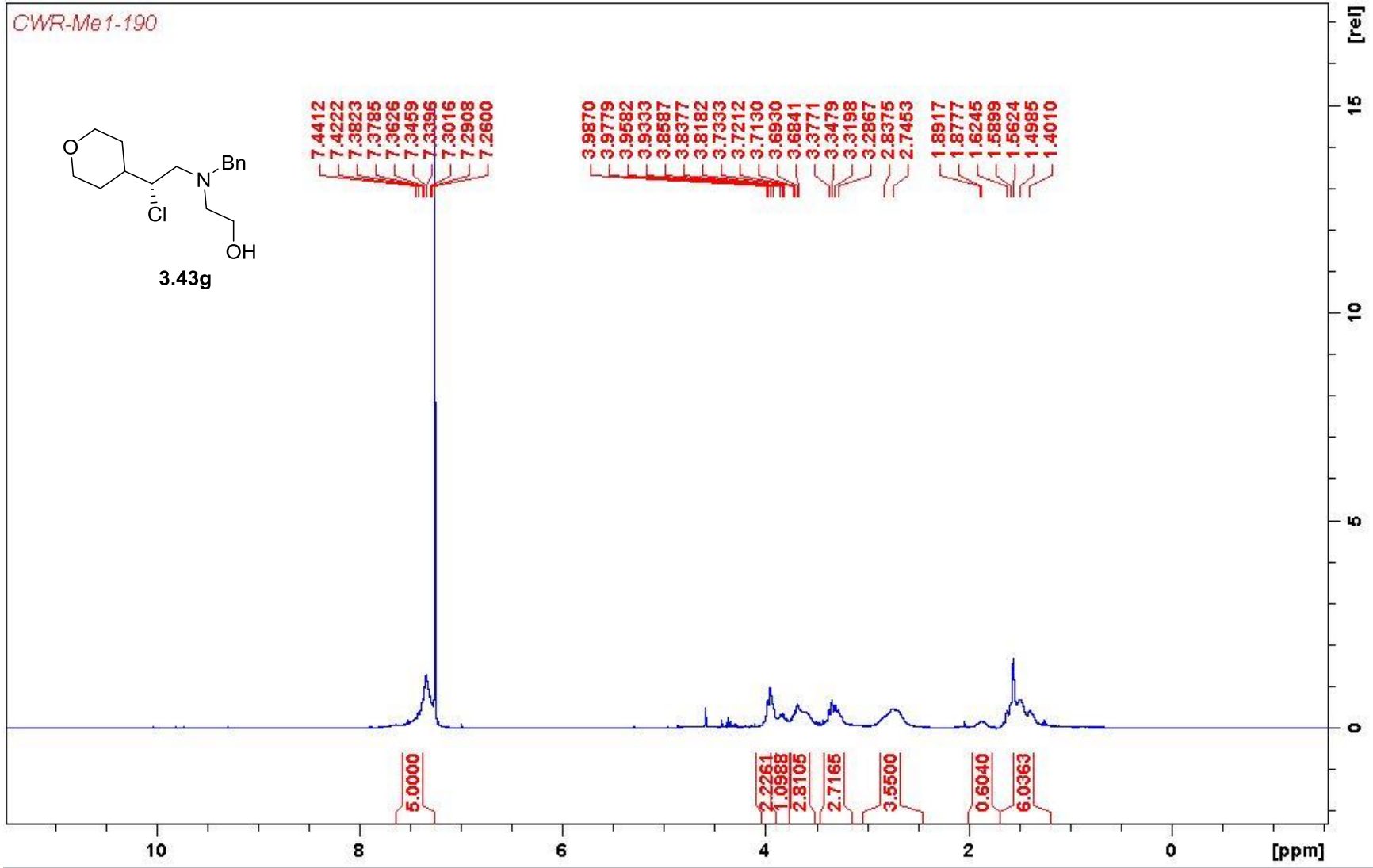


7.4412
7.4222
7.3823
7.3785
7.3626
7.3459
7.3396
7.3016
7.2908
7.2600

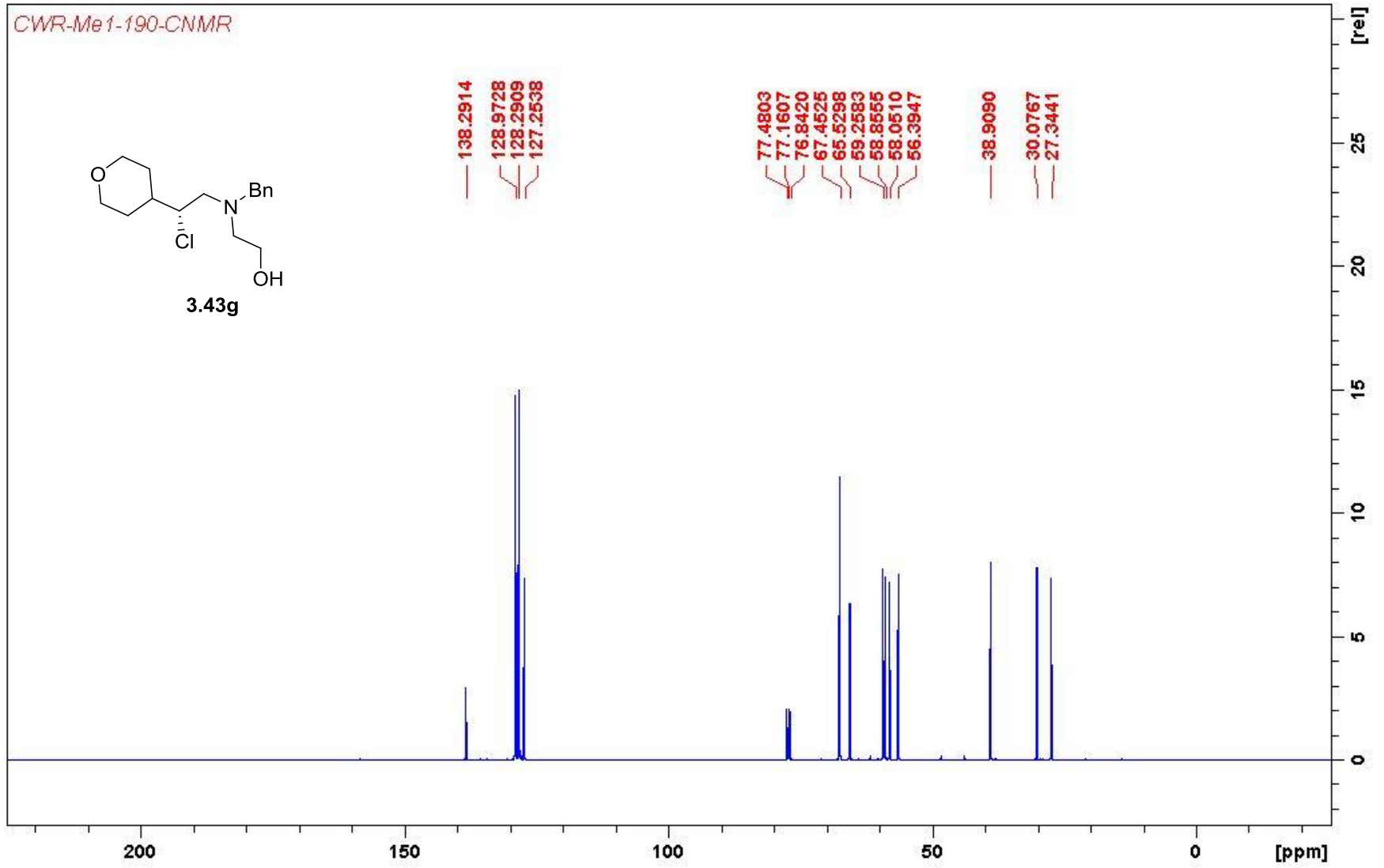
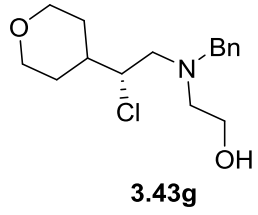
3.9870
3.9779
3.9582
3.9333
3.8587
3.8377
3.8182
3.7333
3.7212
3.7130
3.6930
3.6841
3.3771
3.3479
3.3198
3.2867
2.8375
2.7453

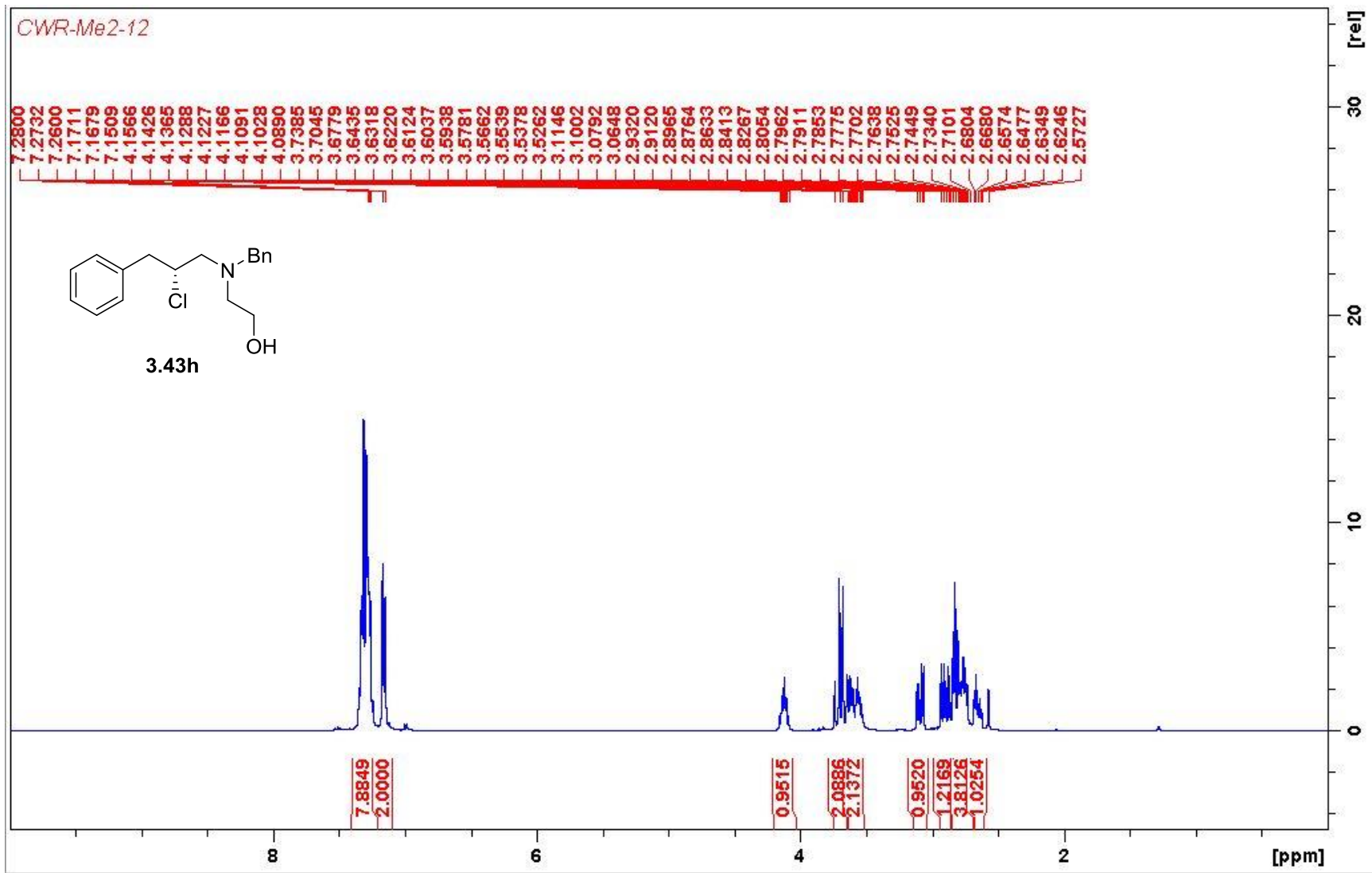
1.8917
1.8777
1.6245
1.5899
1.5624
1.4985
1.4010

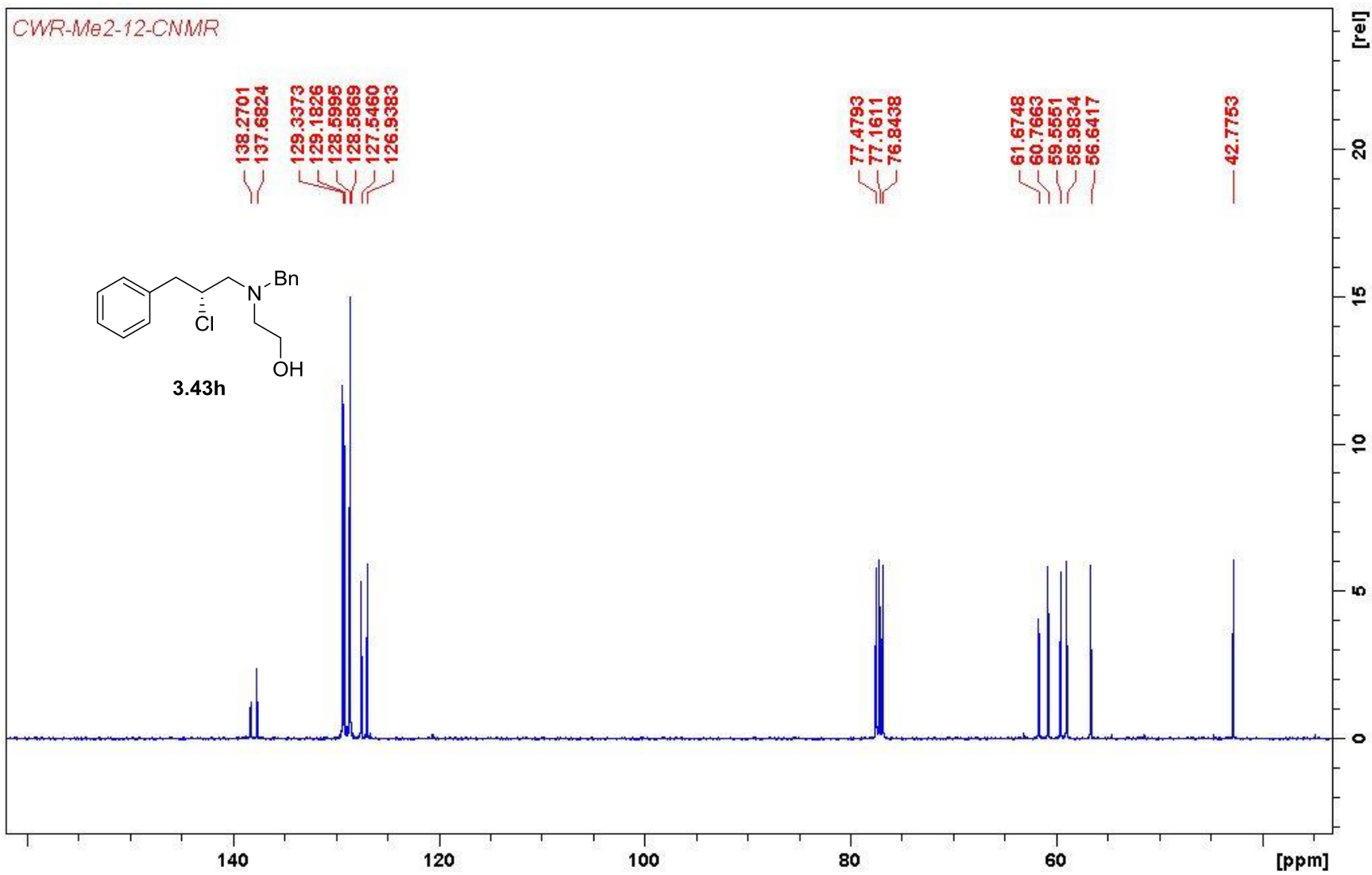
5.0000
2.2261
1.0988
2.8105
2.7165
3.5500
0.6040
6.0363

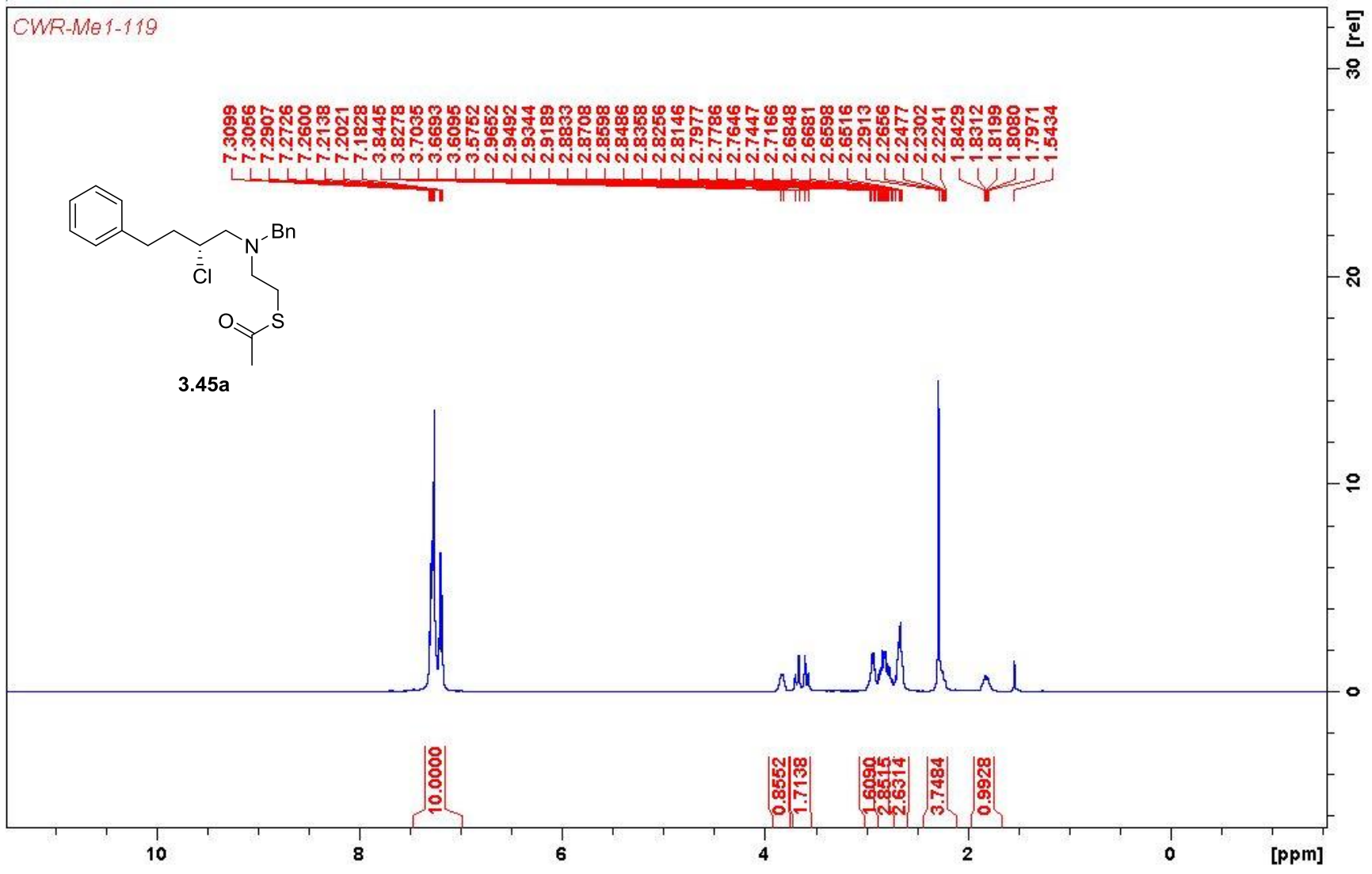


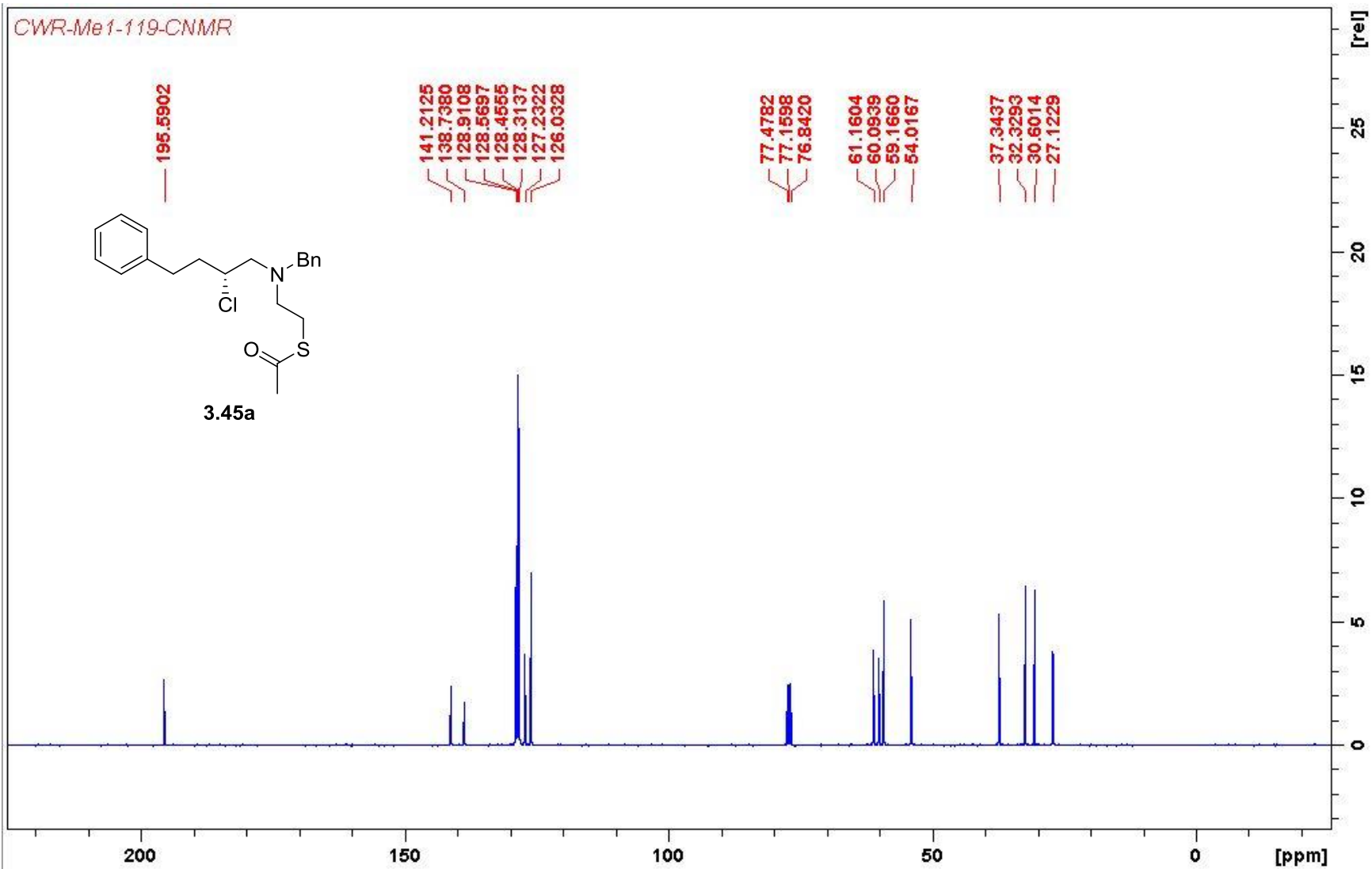
CWR-Me1-190-CNMR

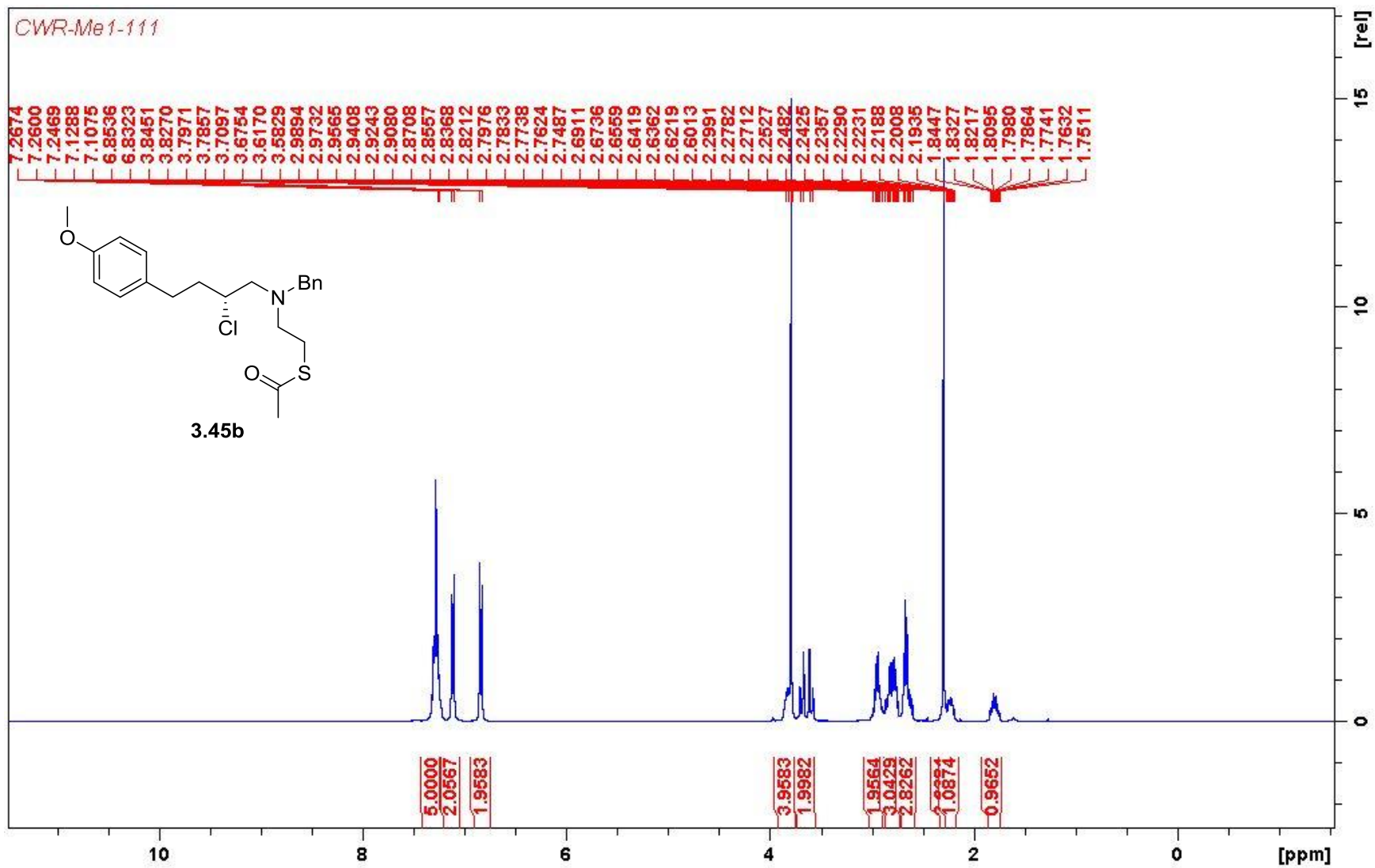


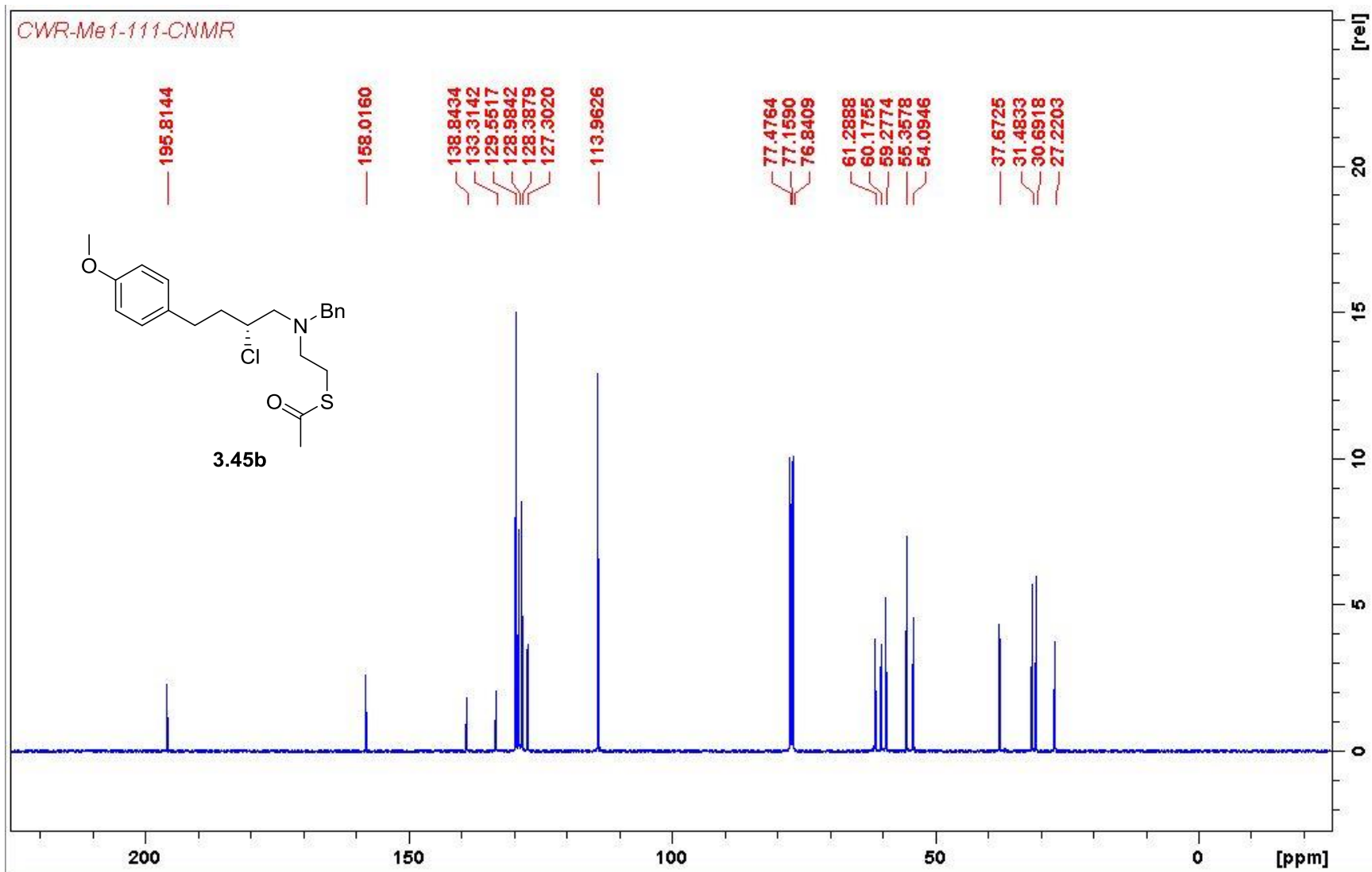


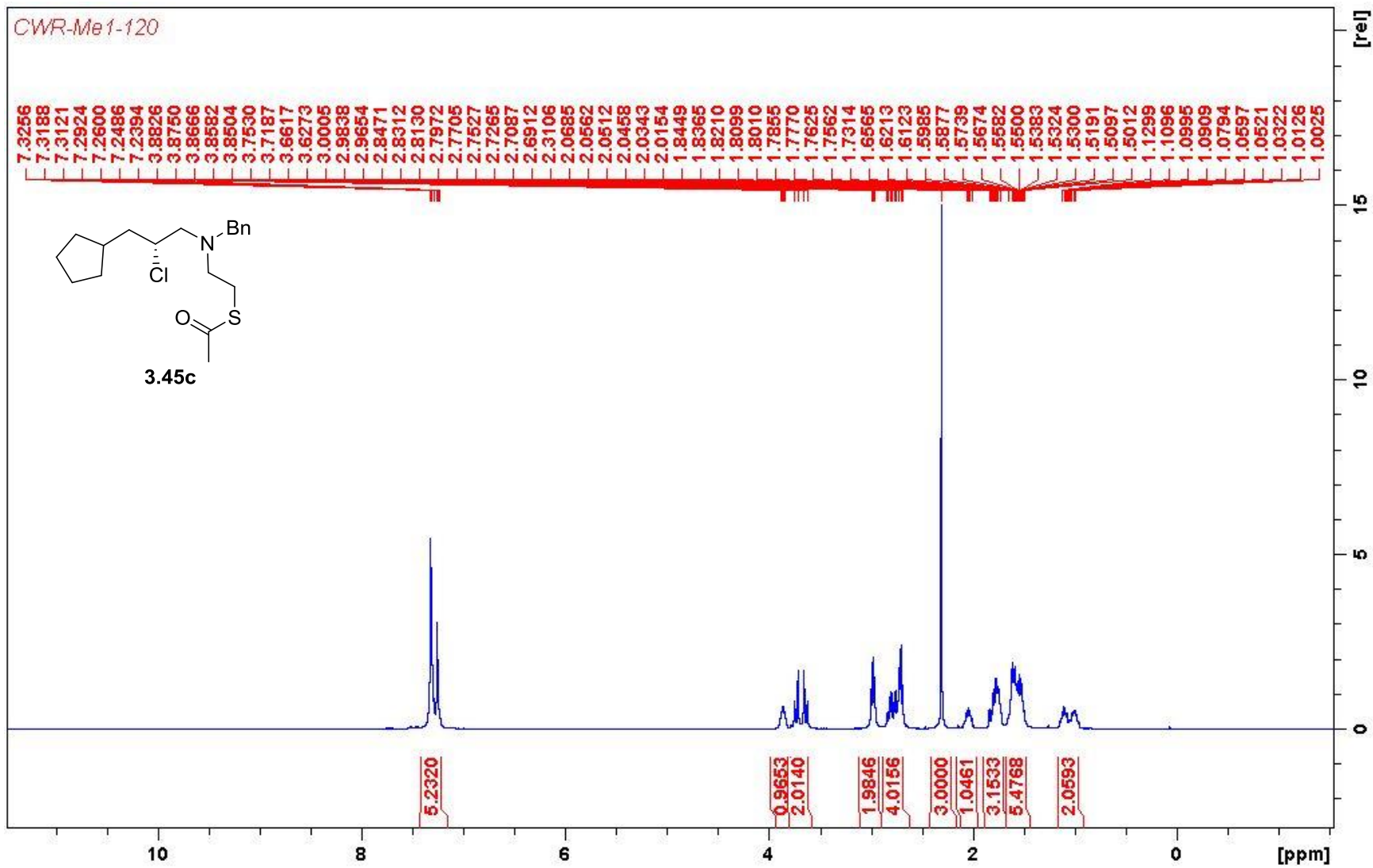


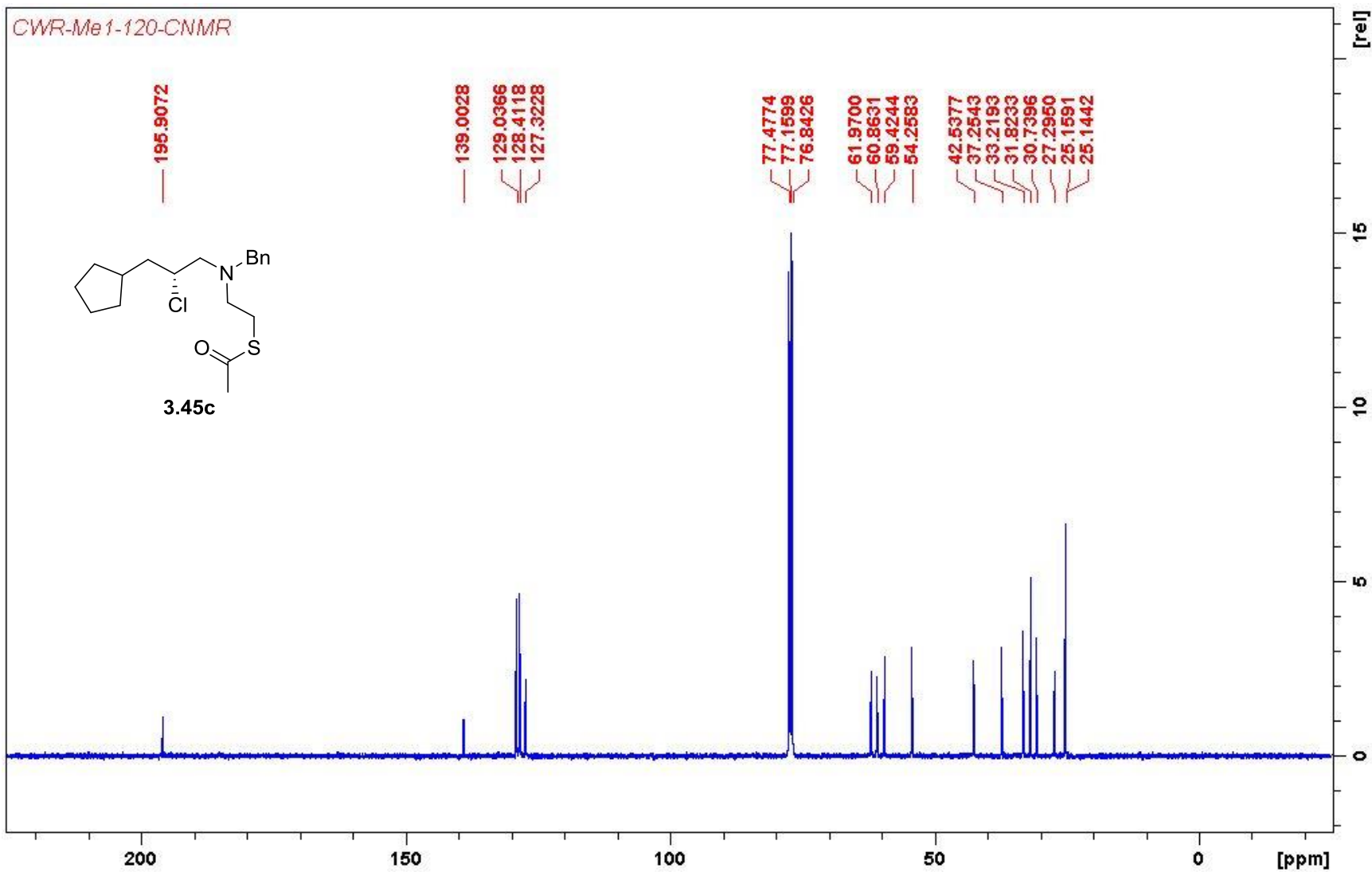


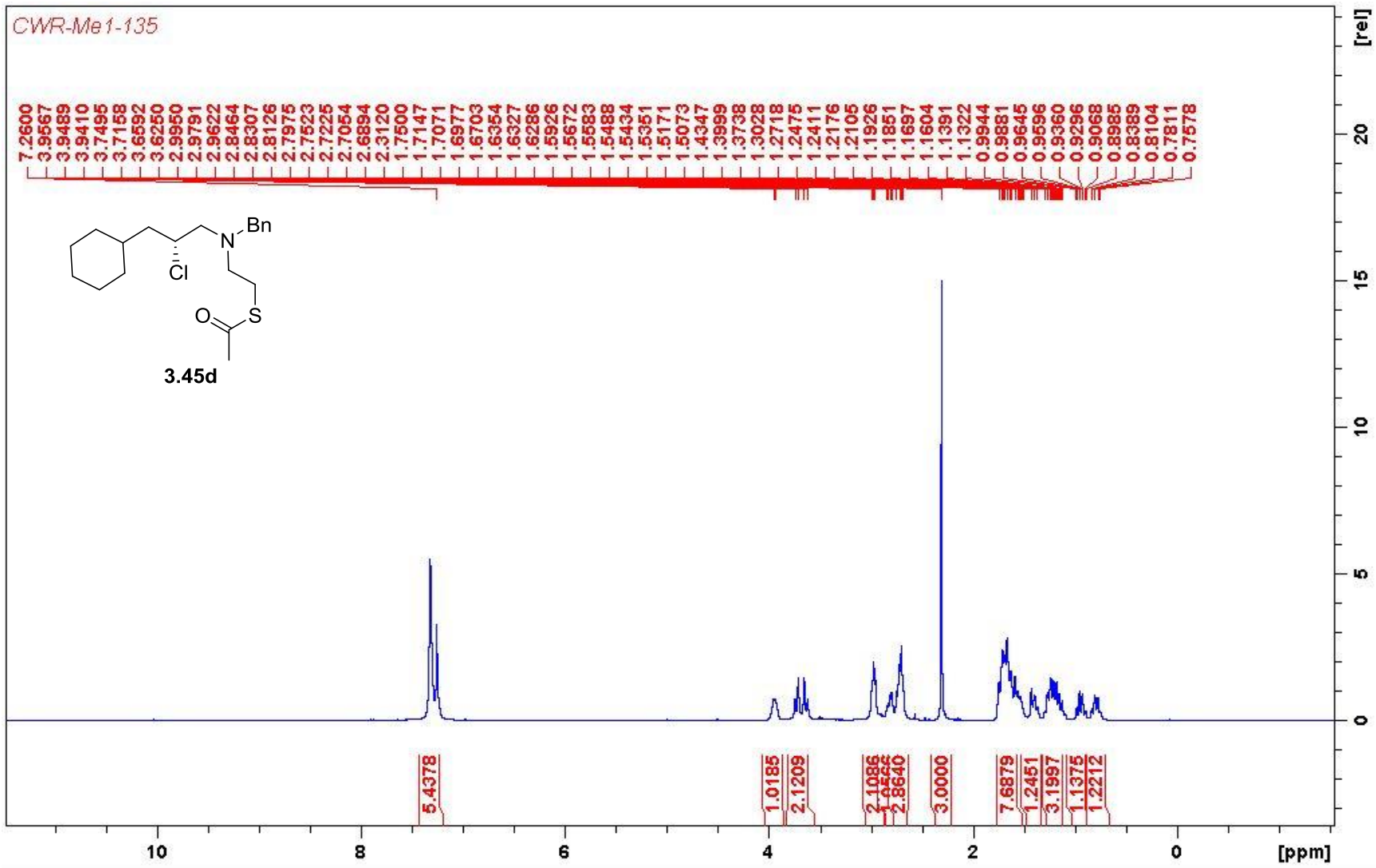


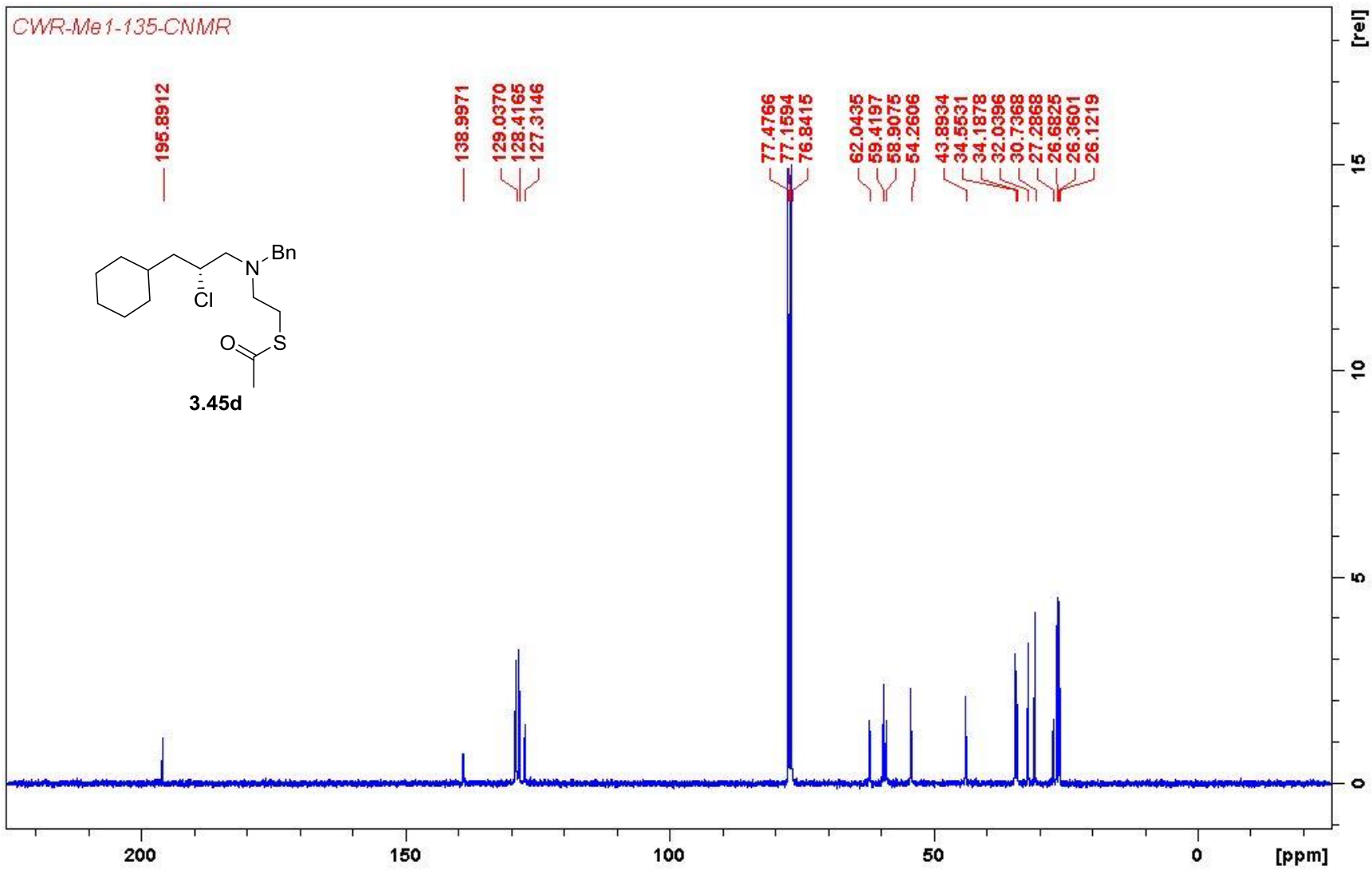




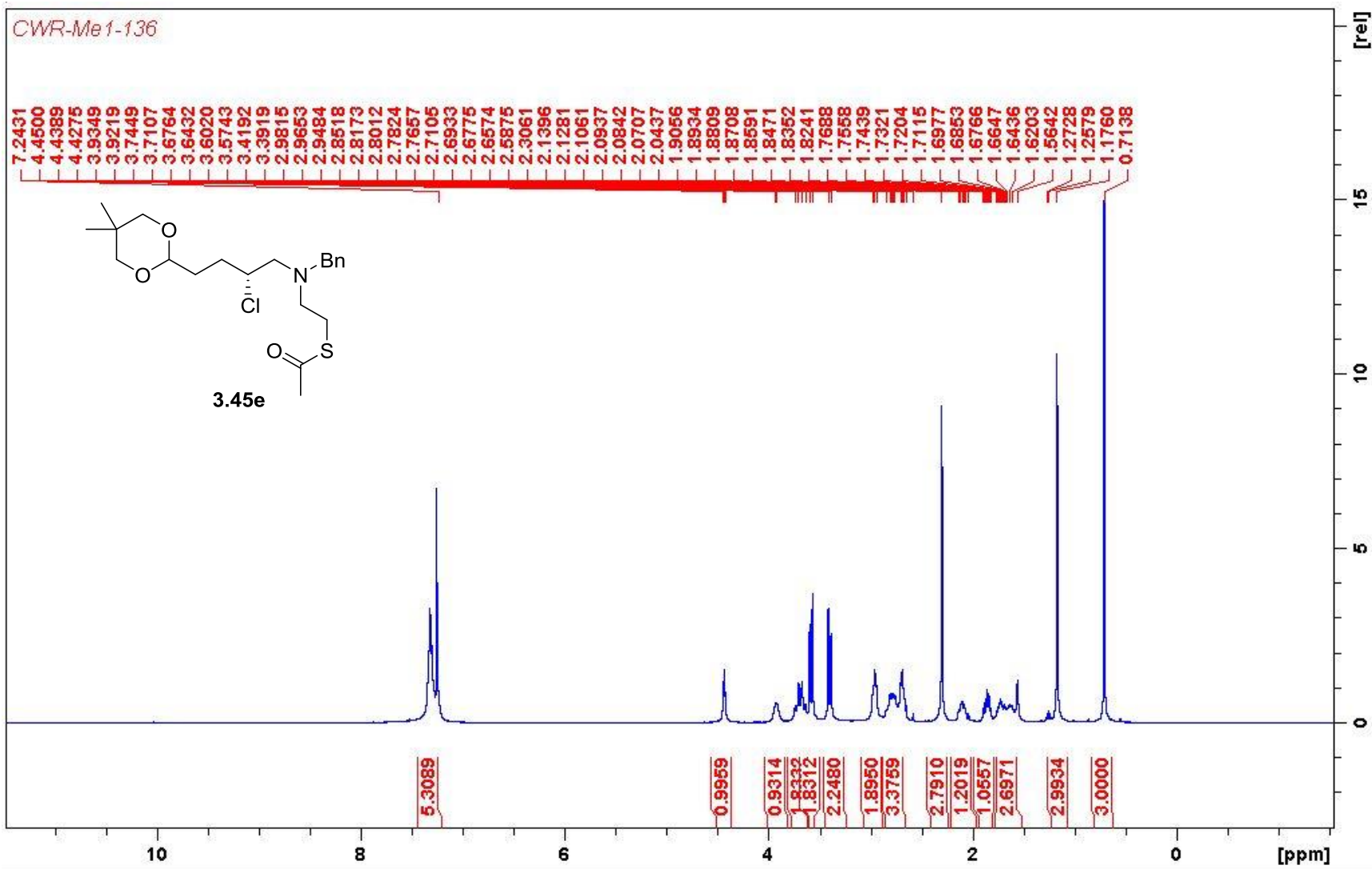


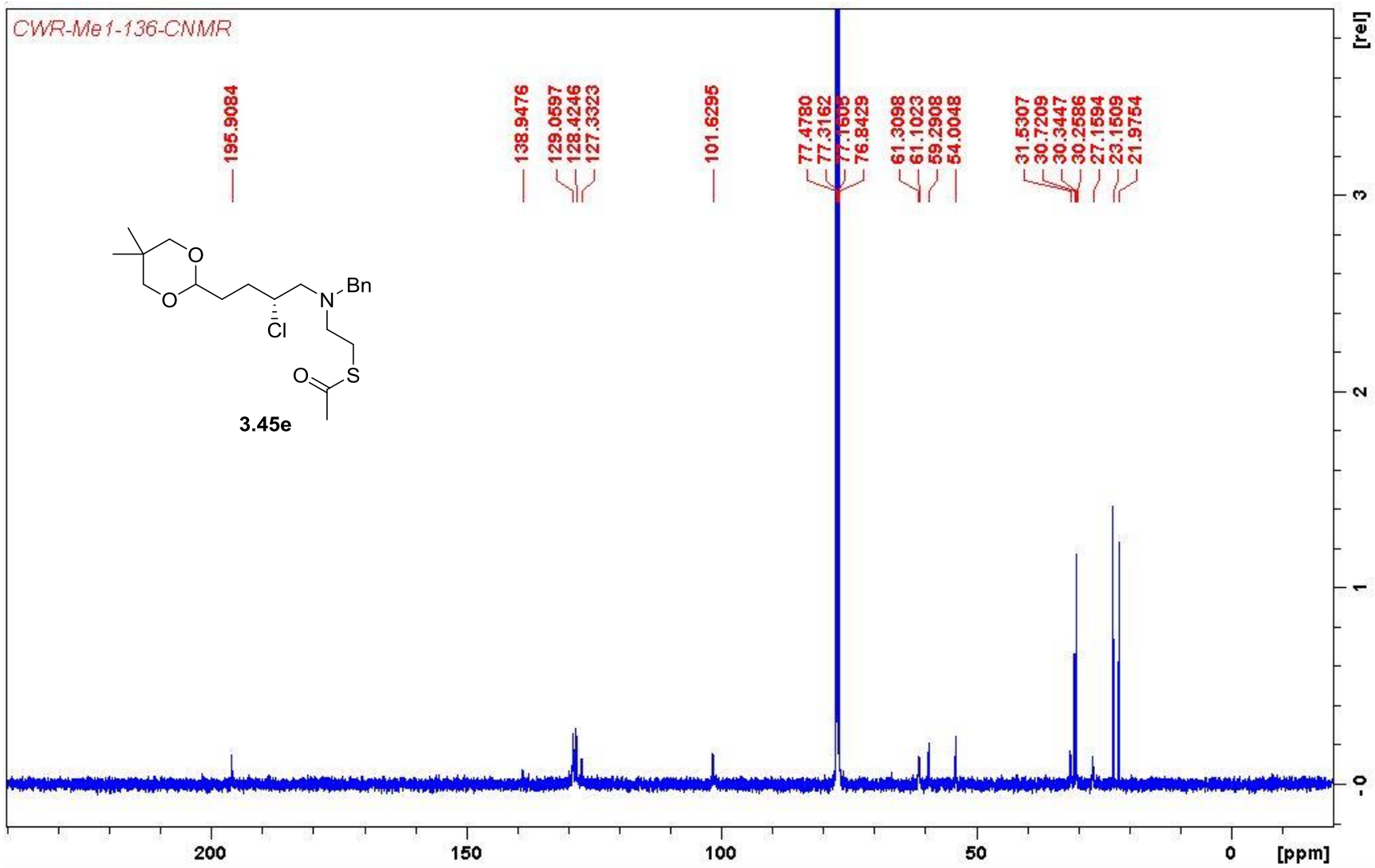


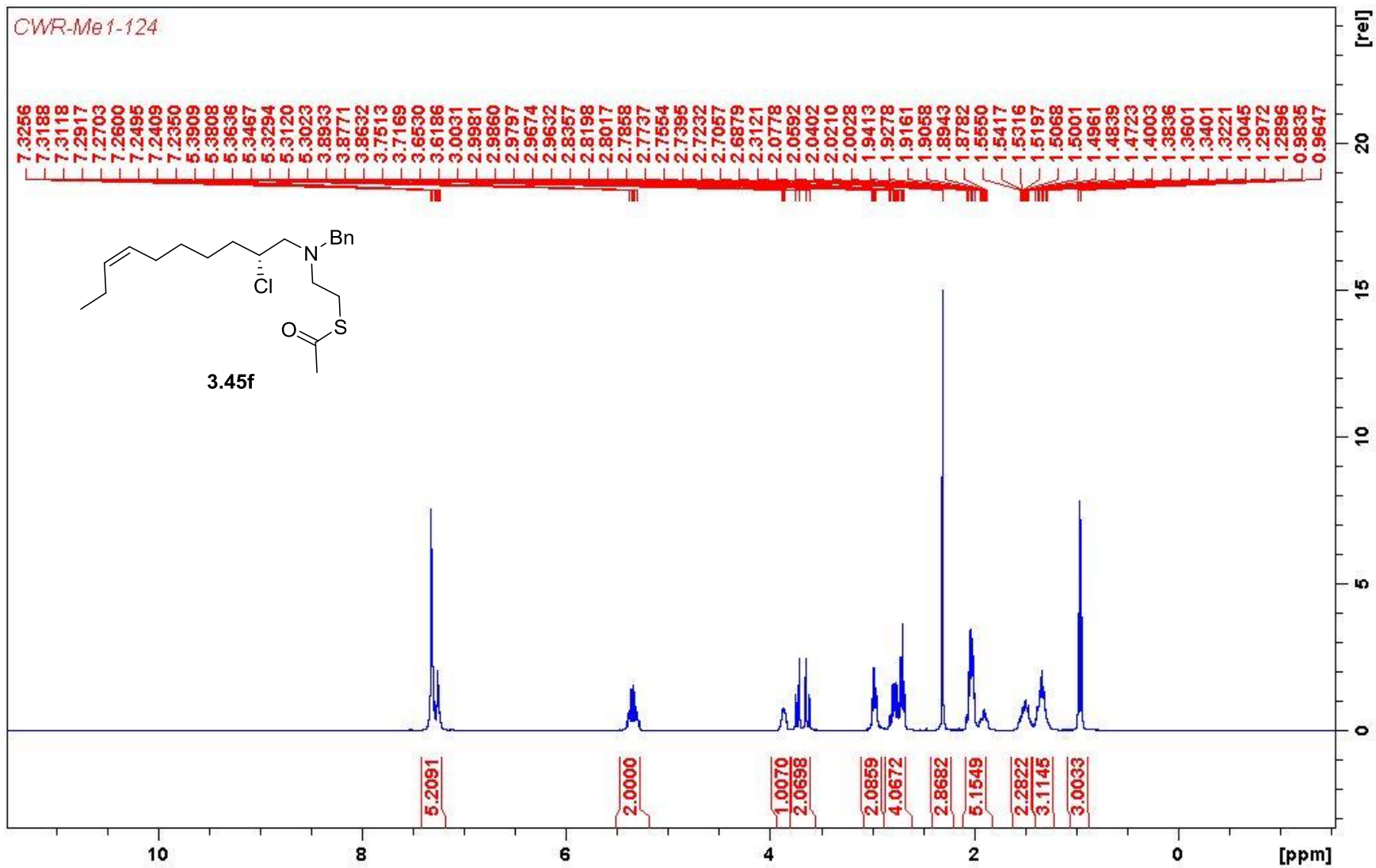


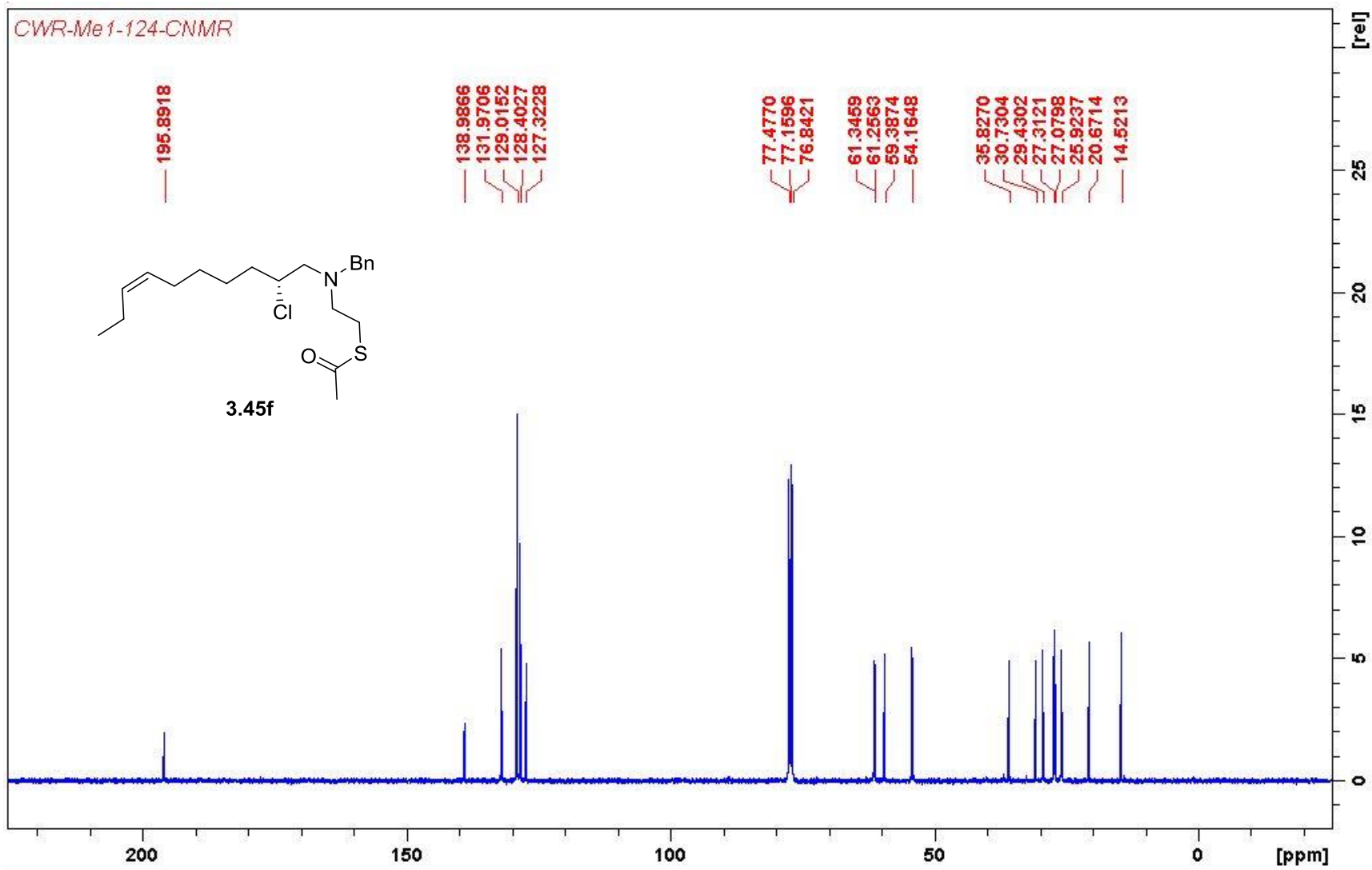


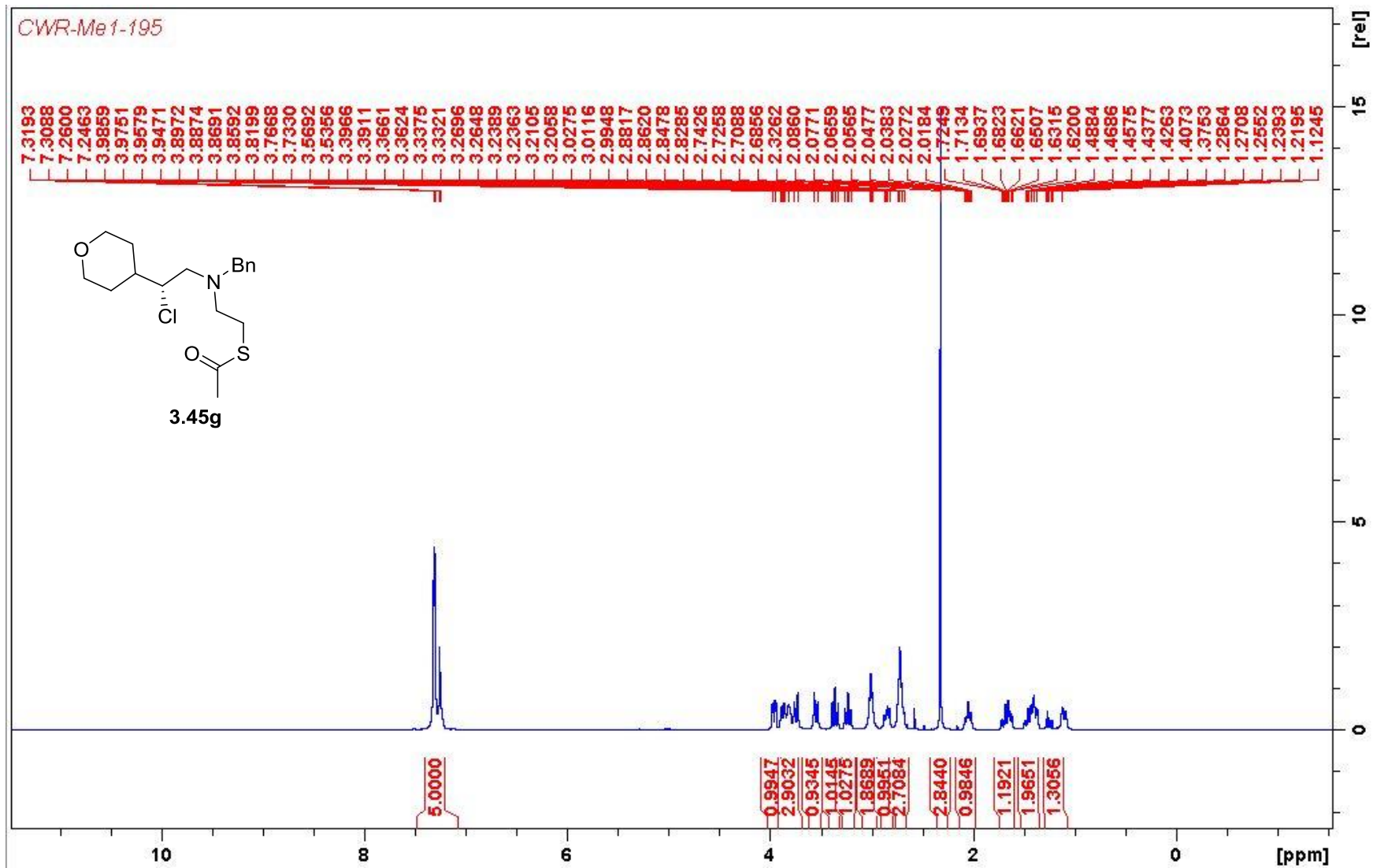
CWR-Me1-136

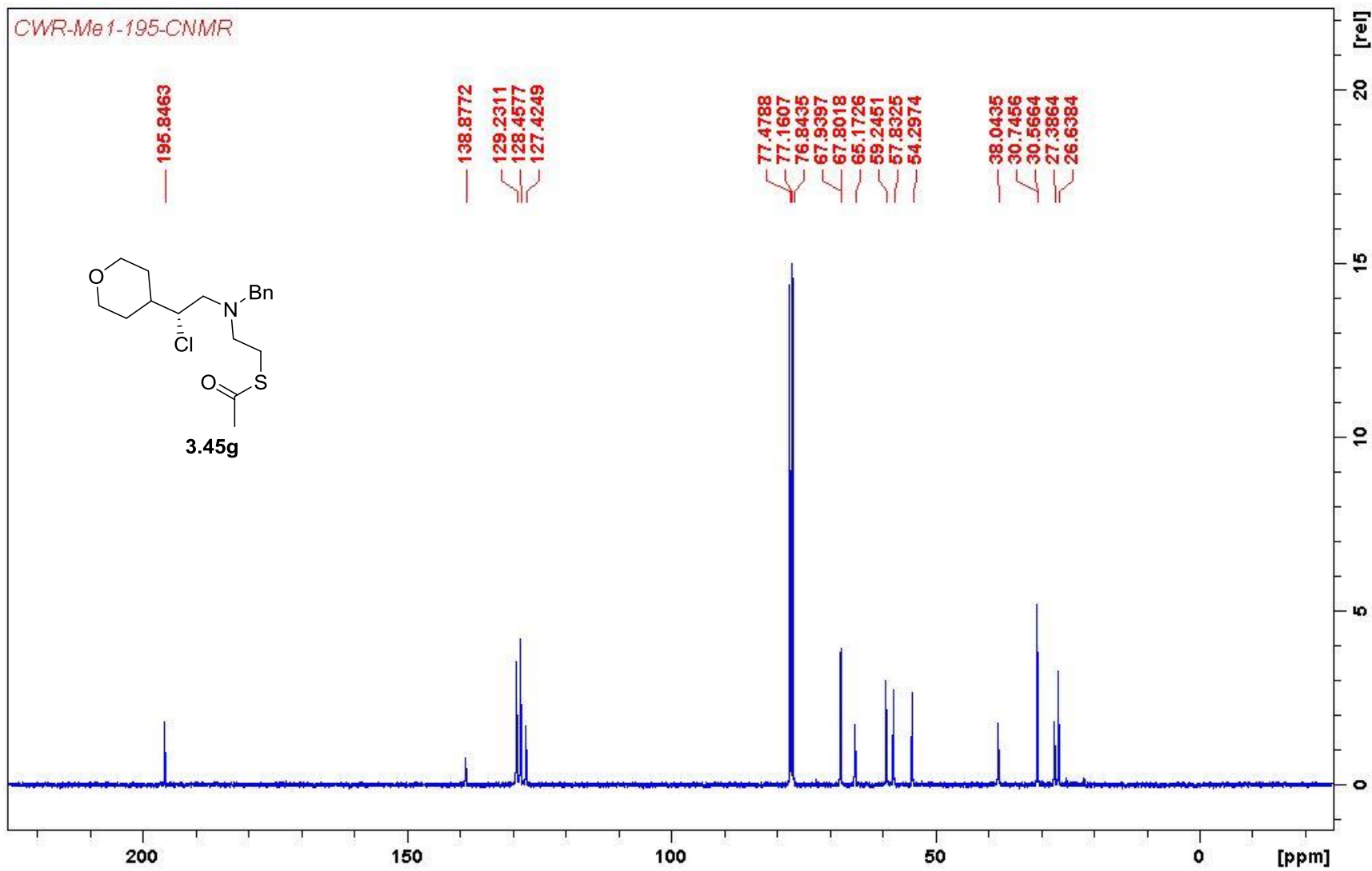


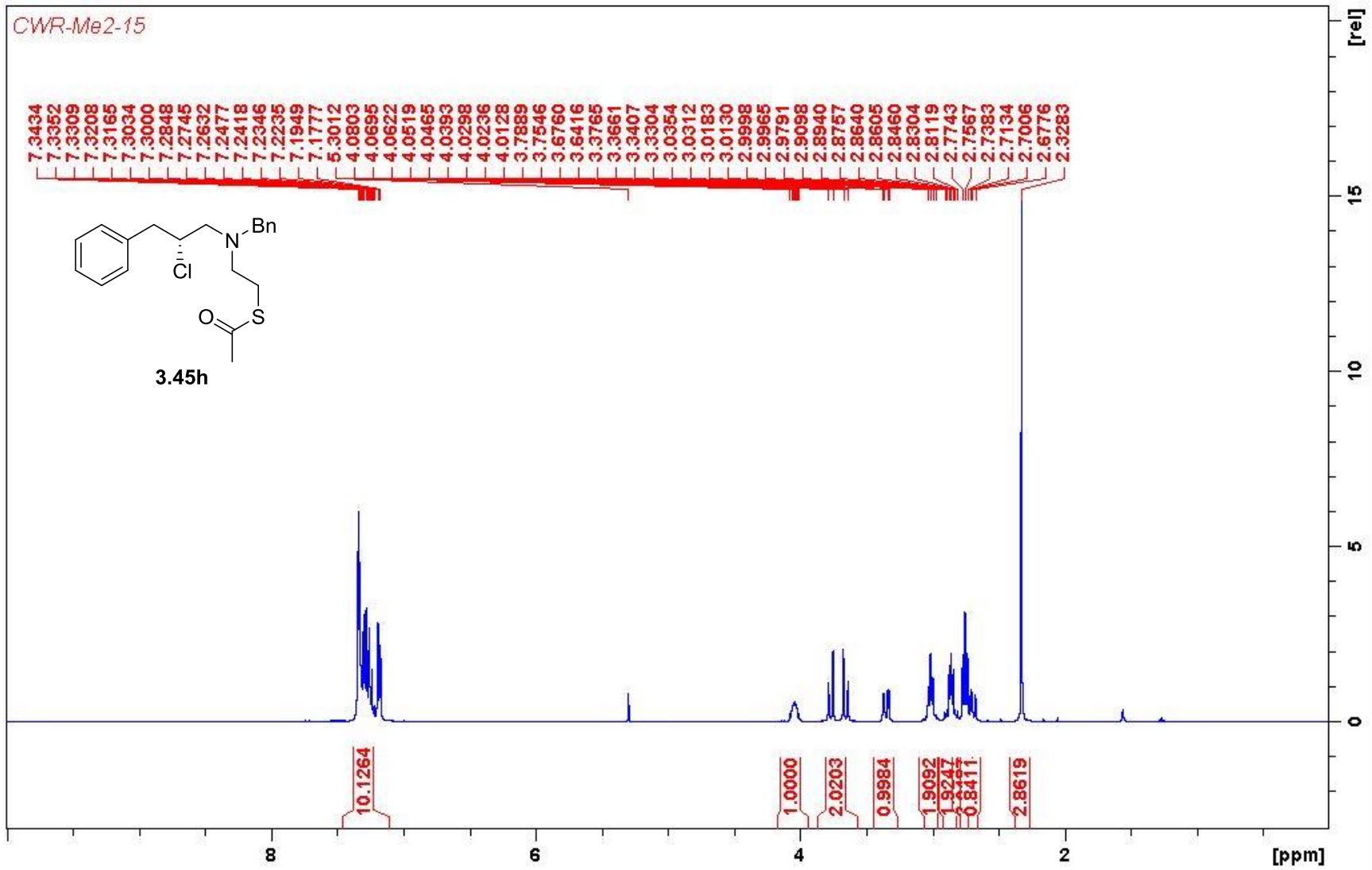


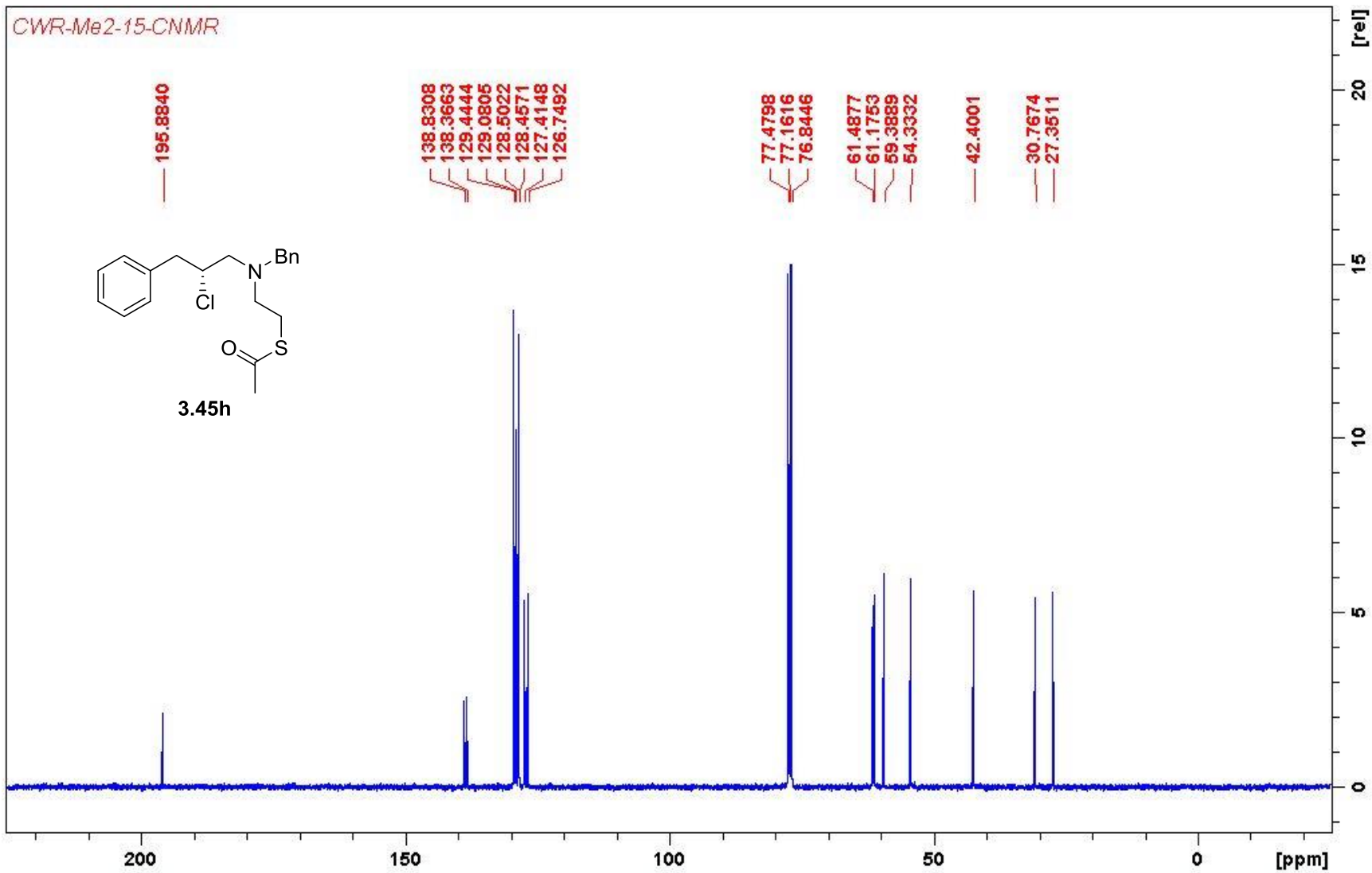


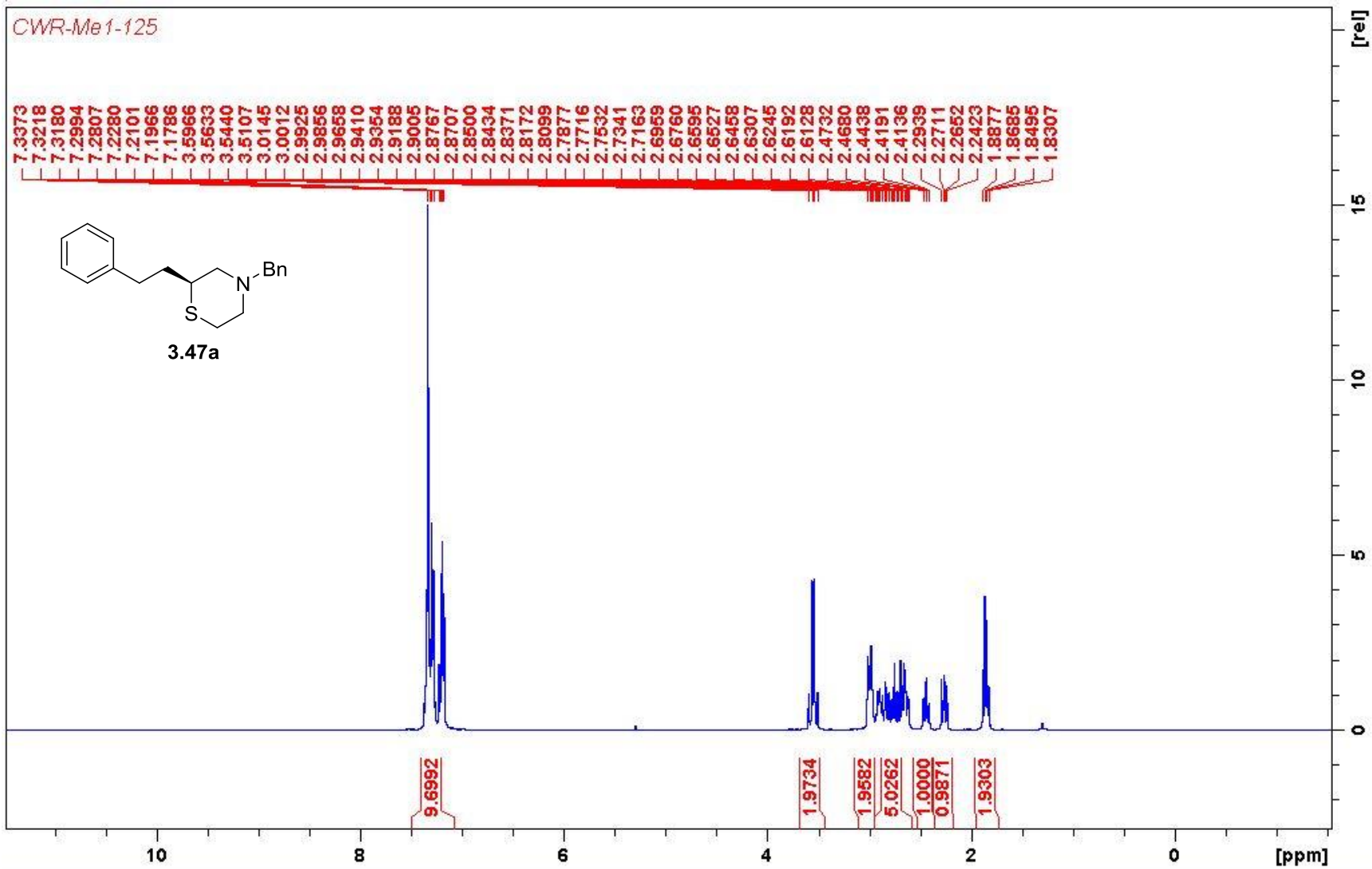


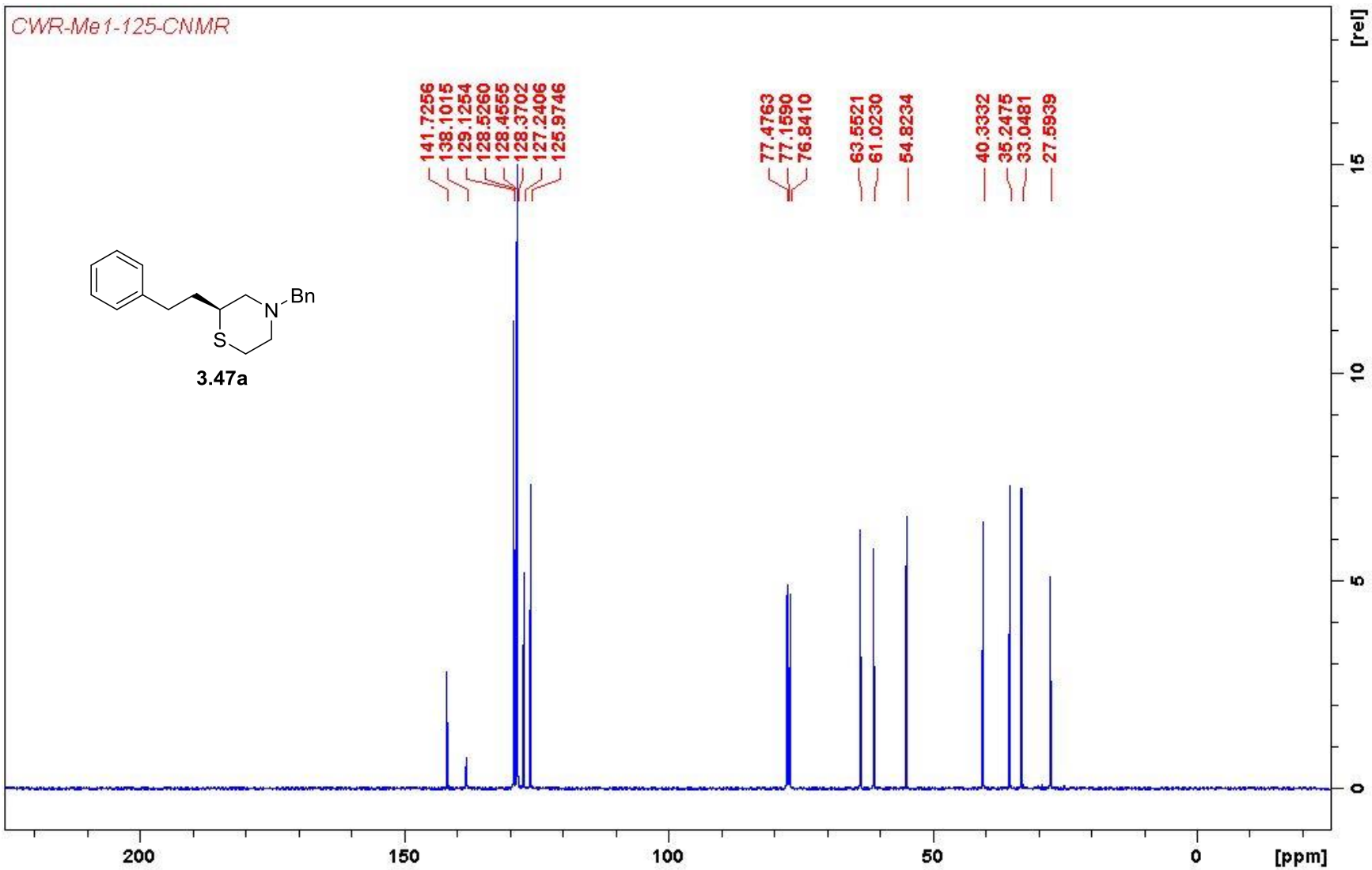


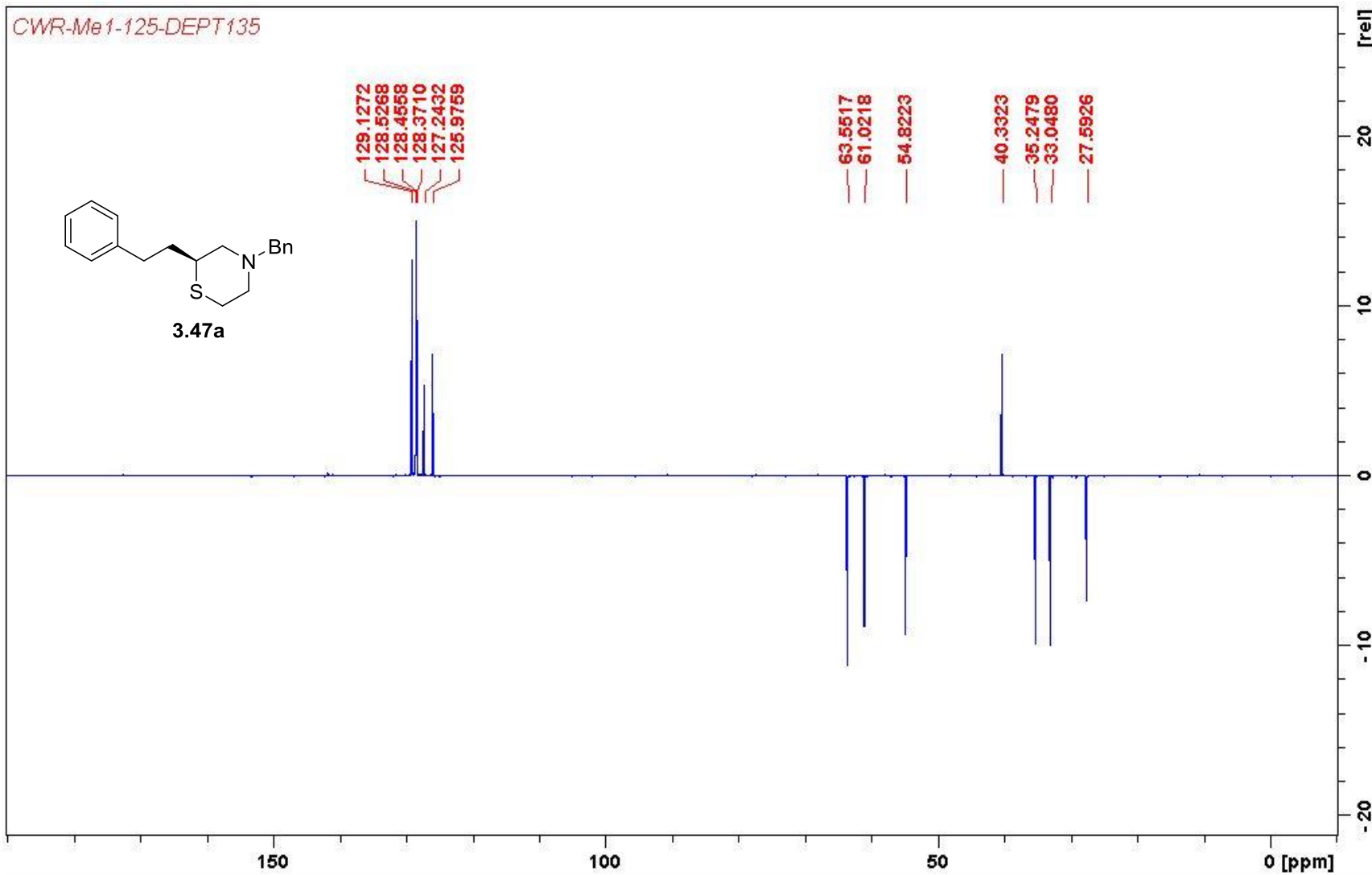


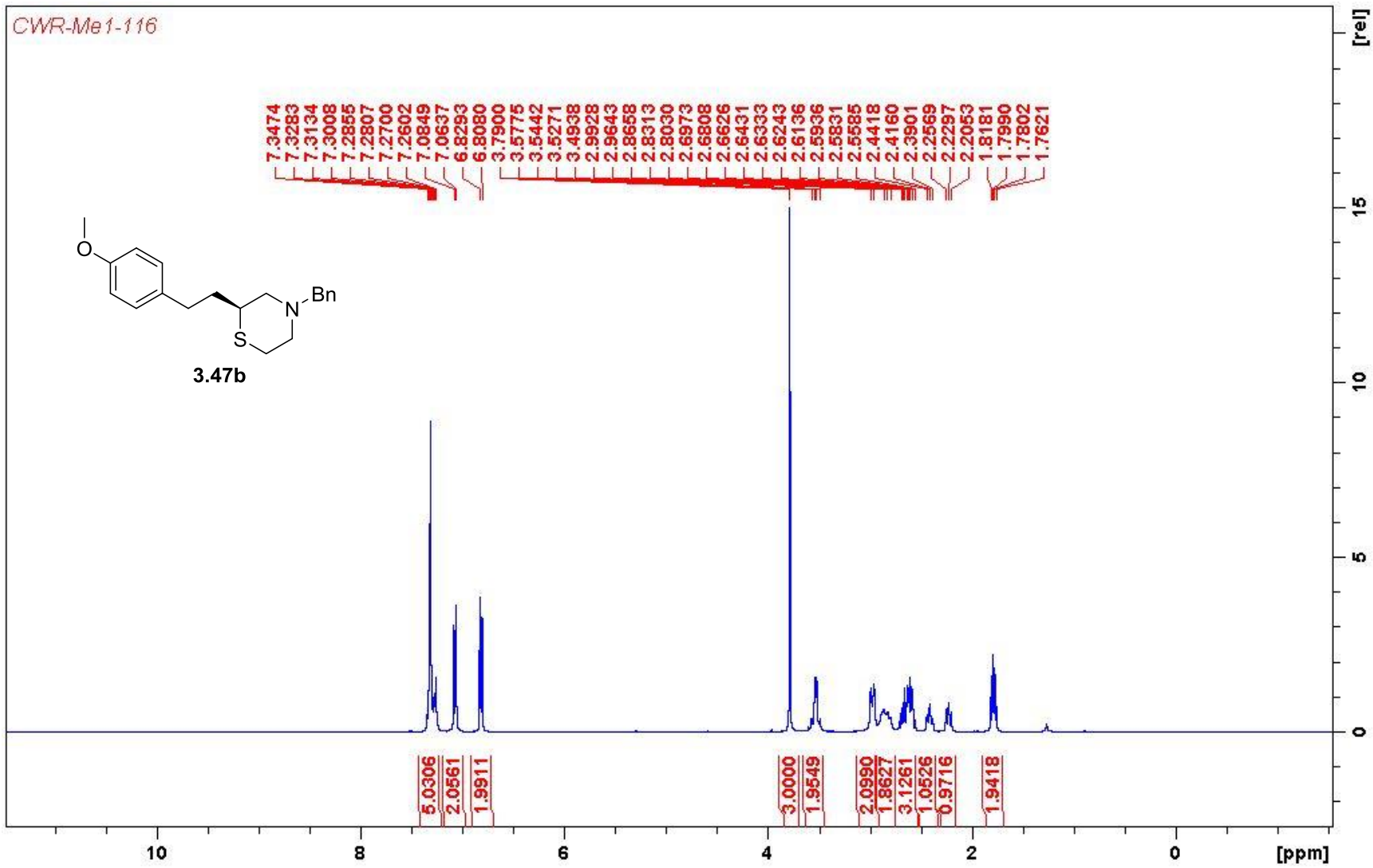


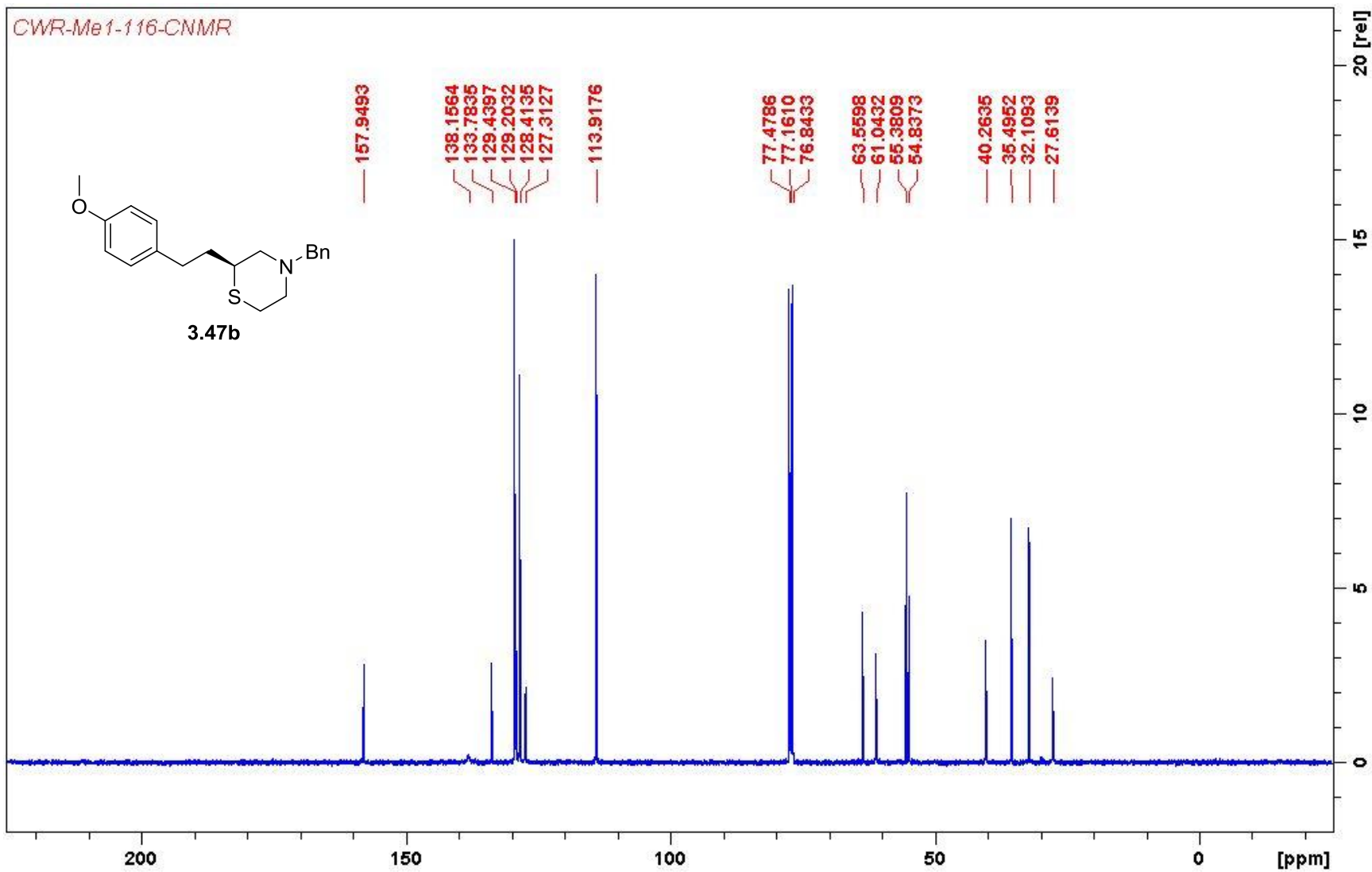


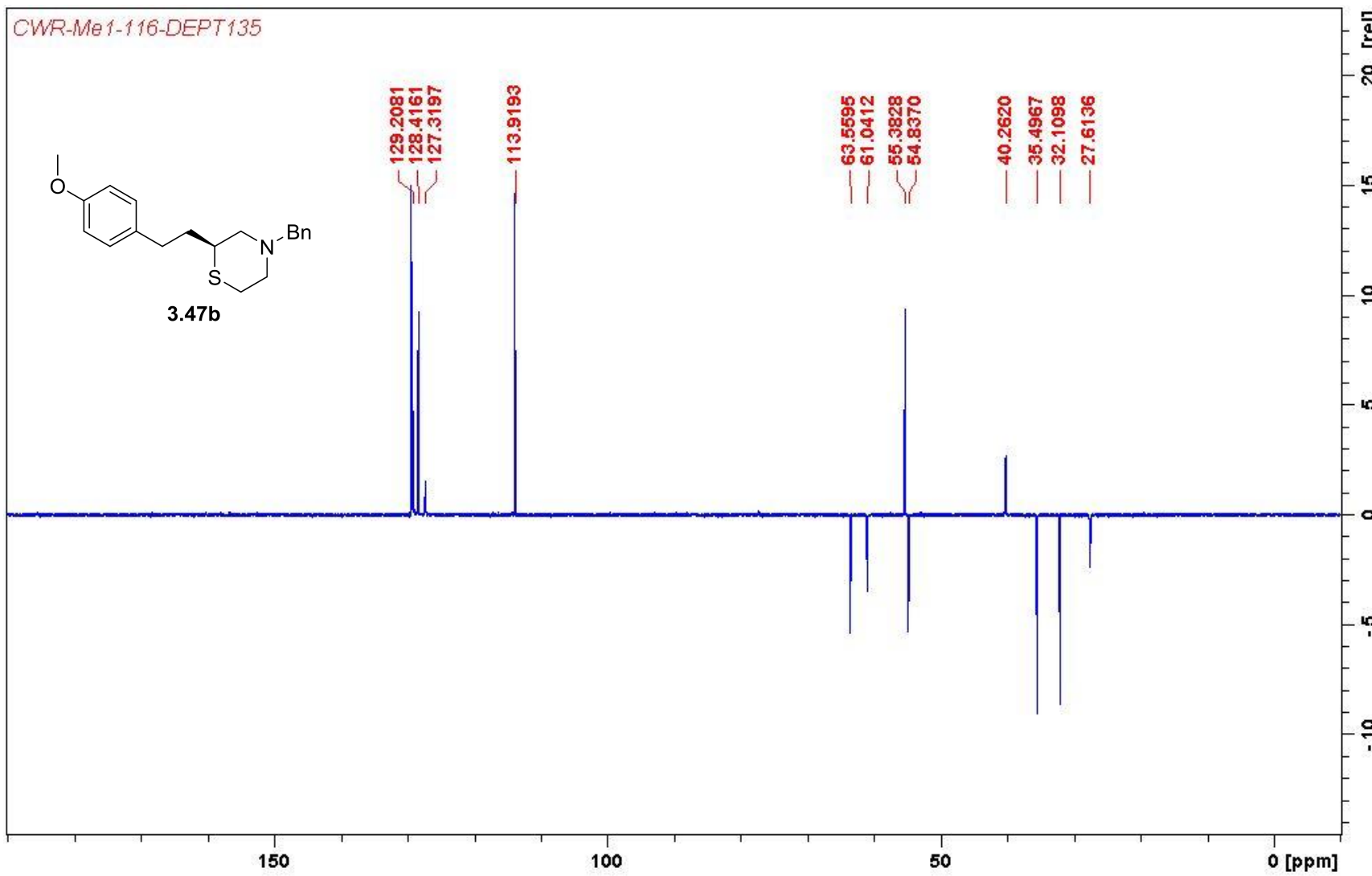




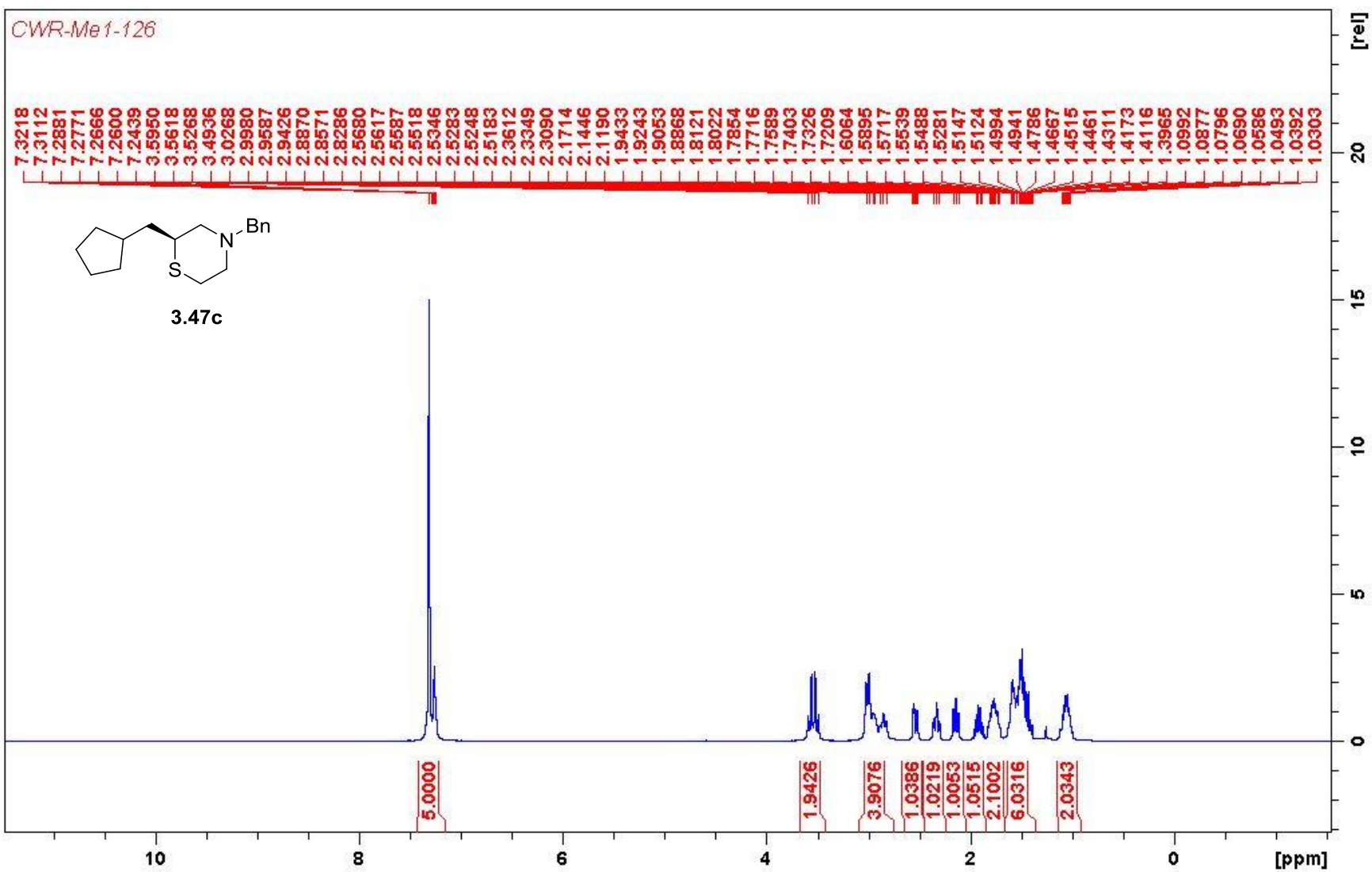


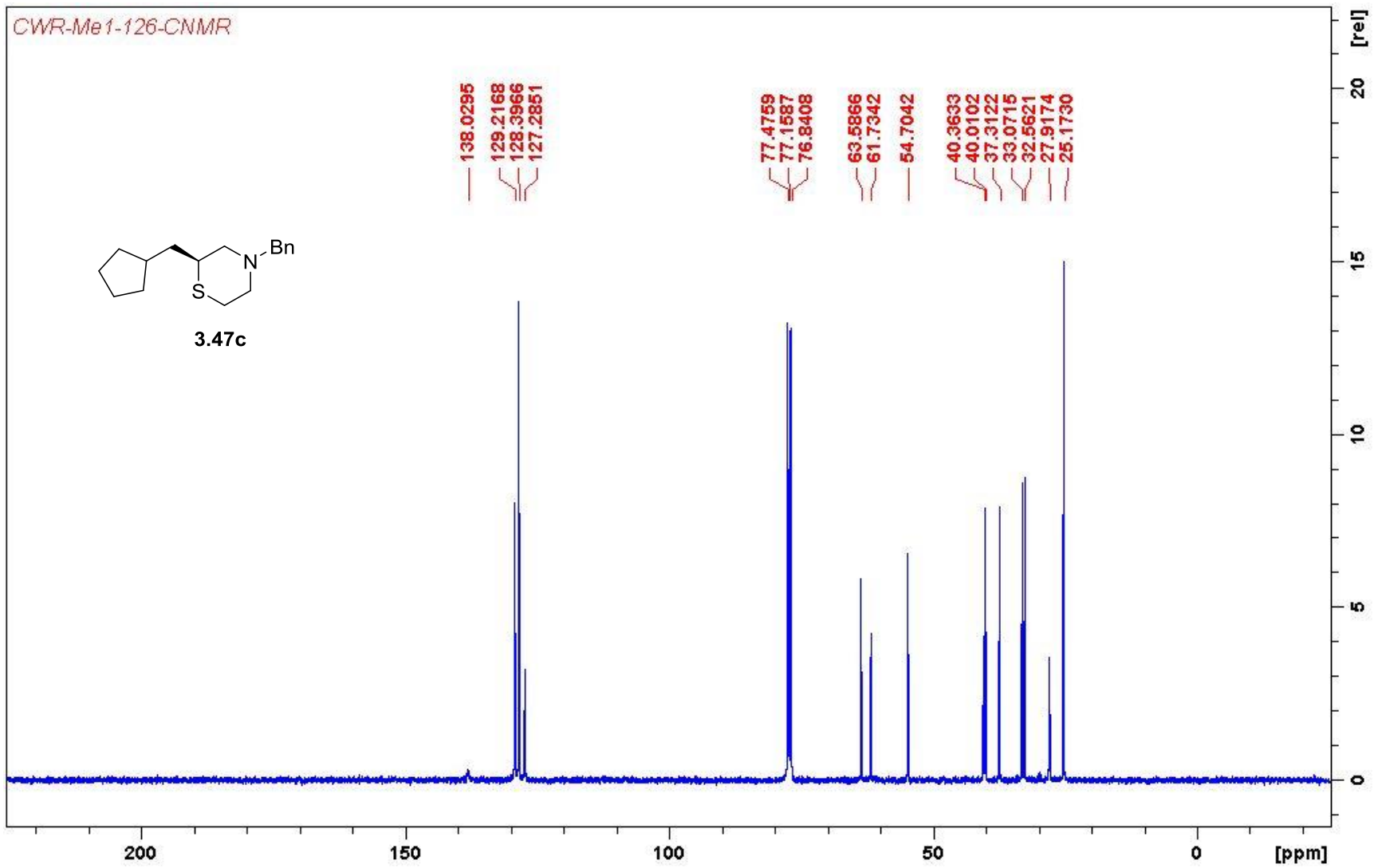


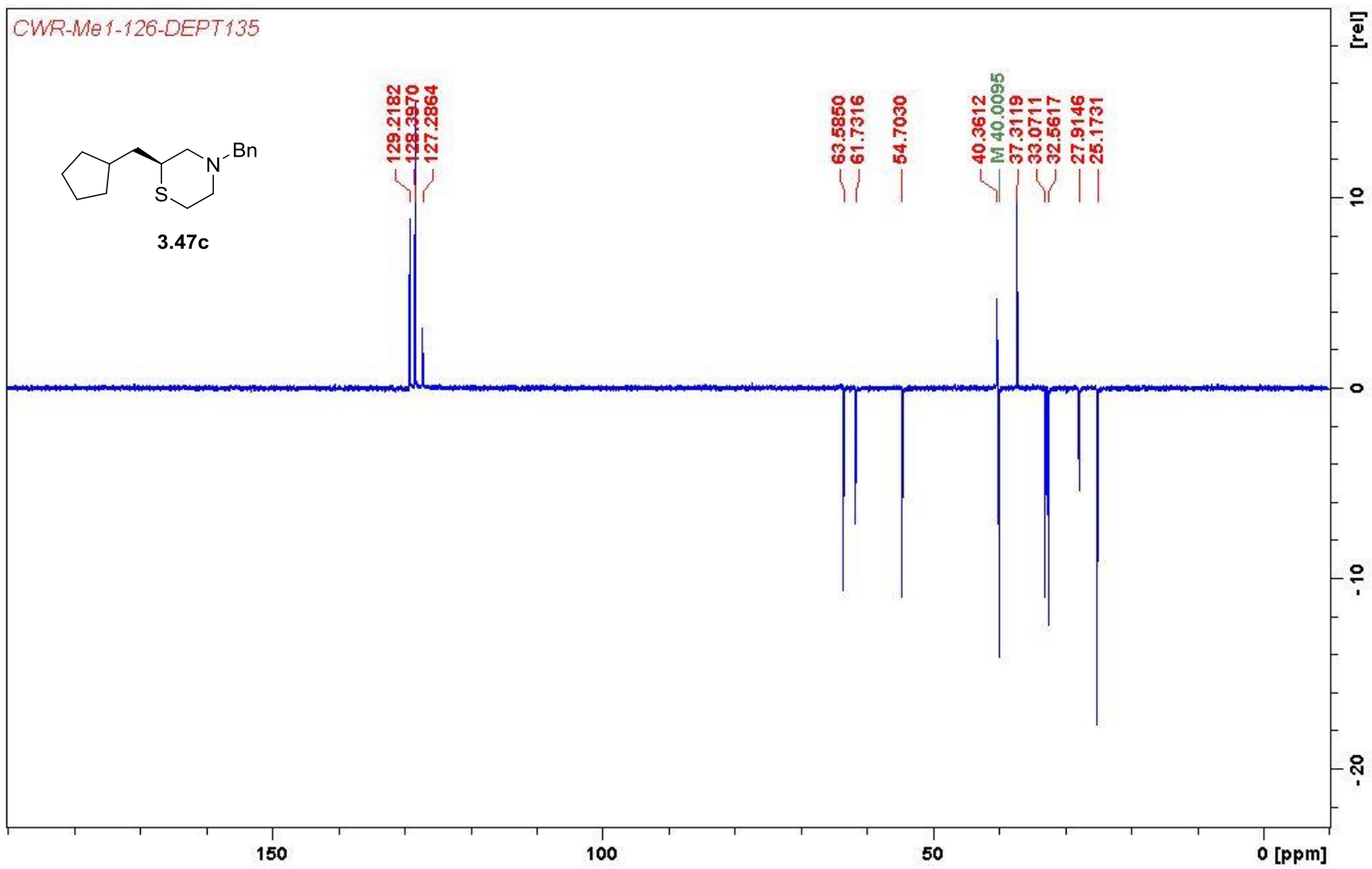


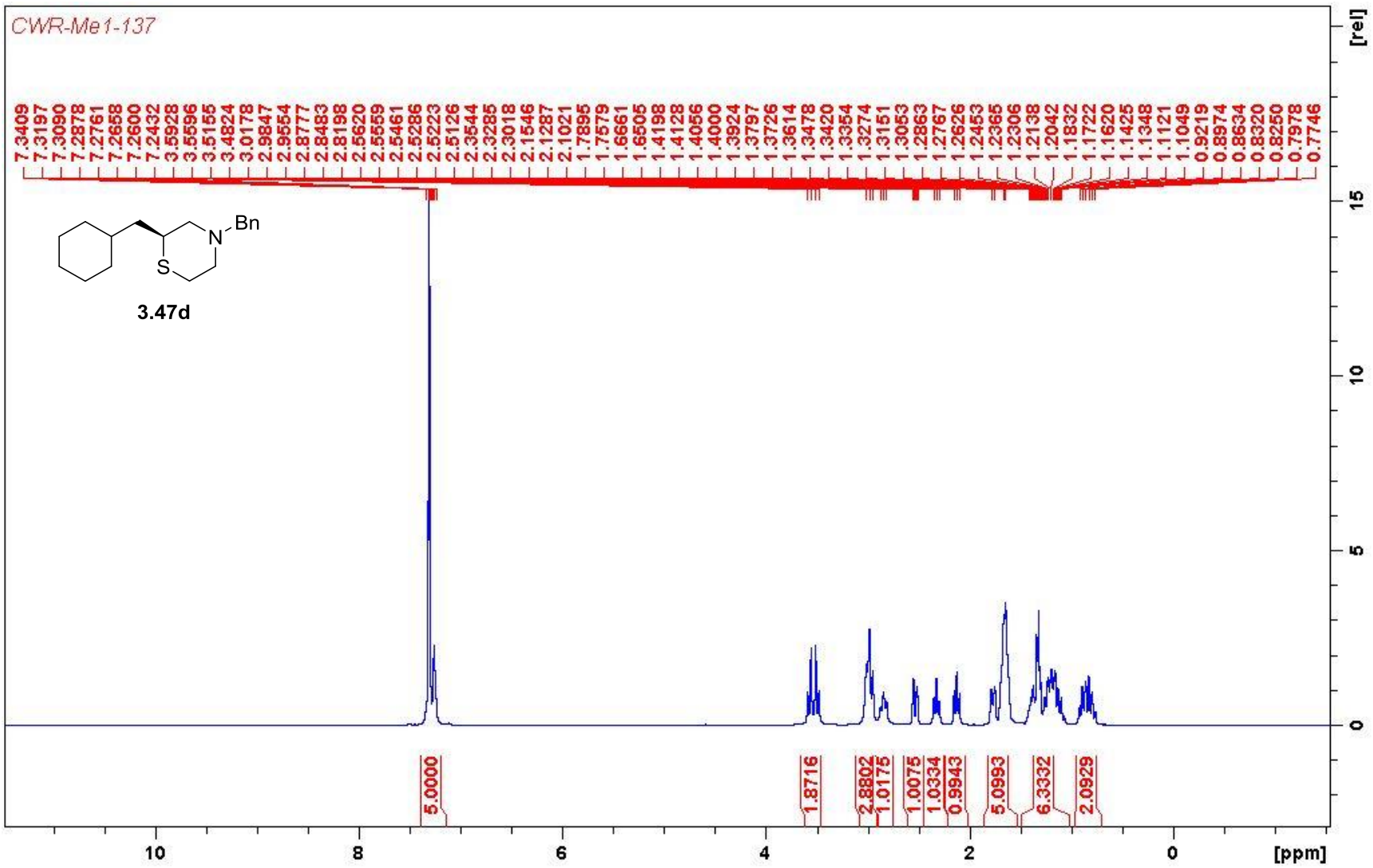


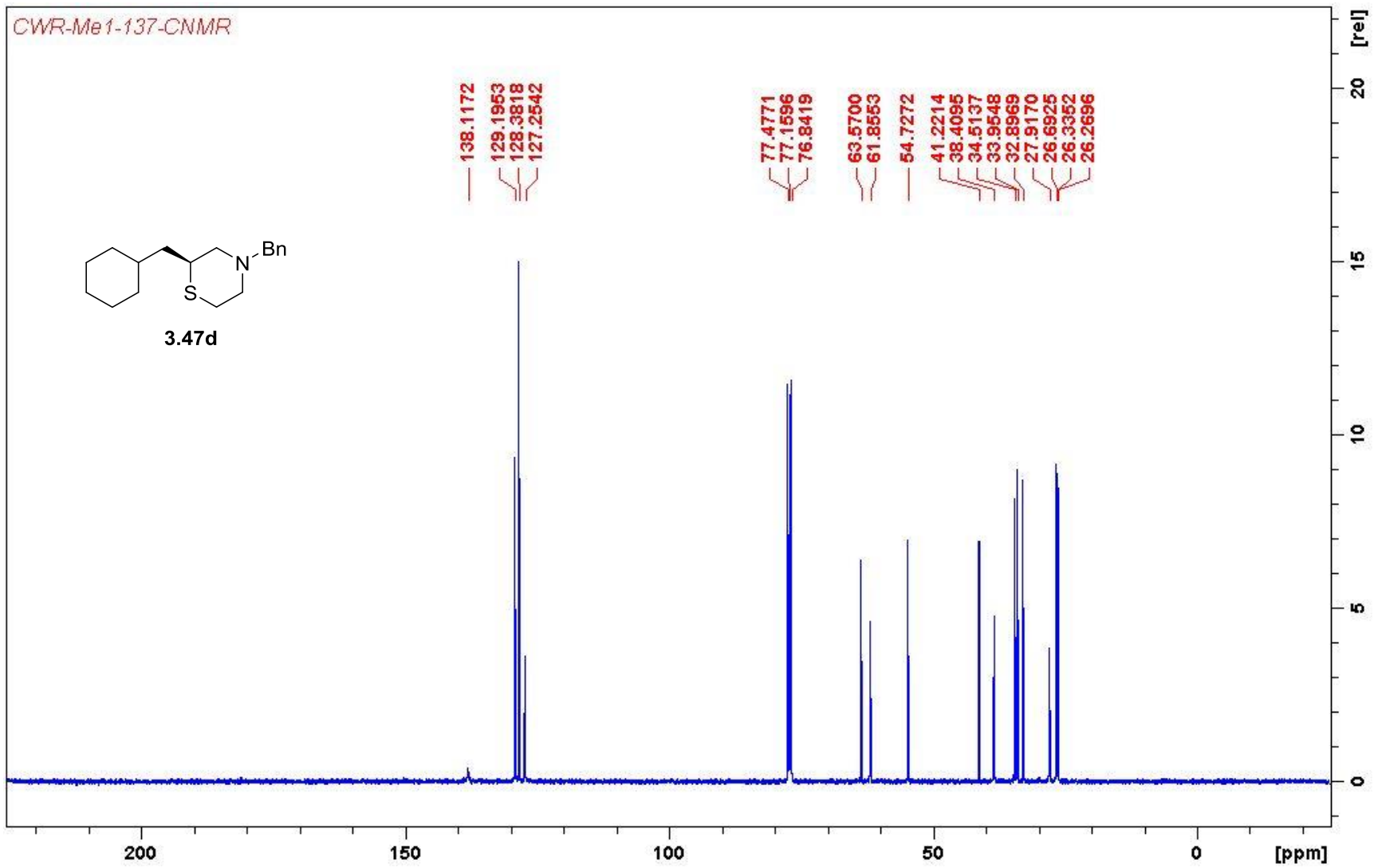
CWR-Me1-126

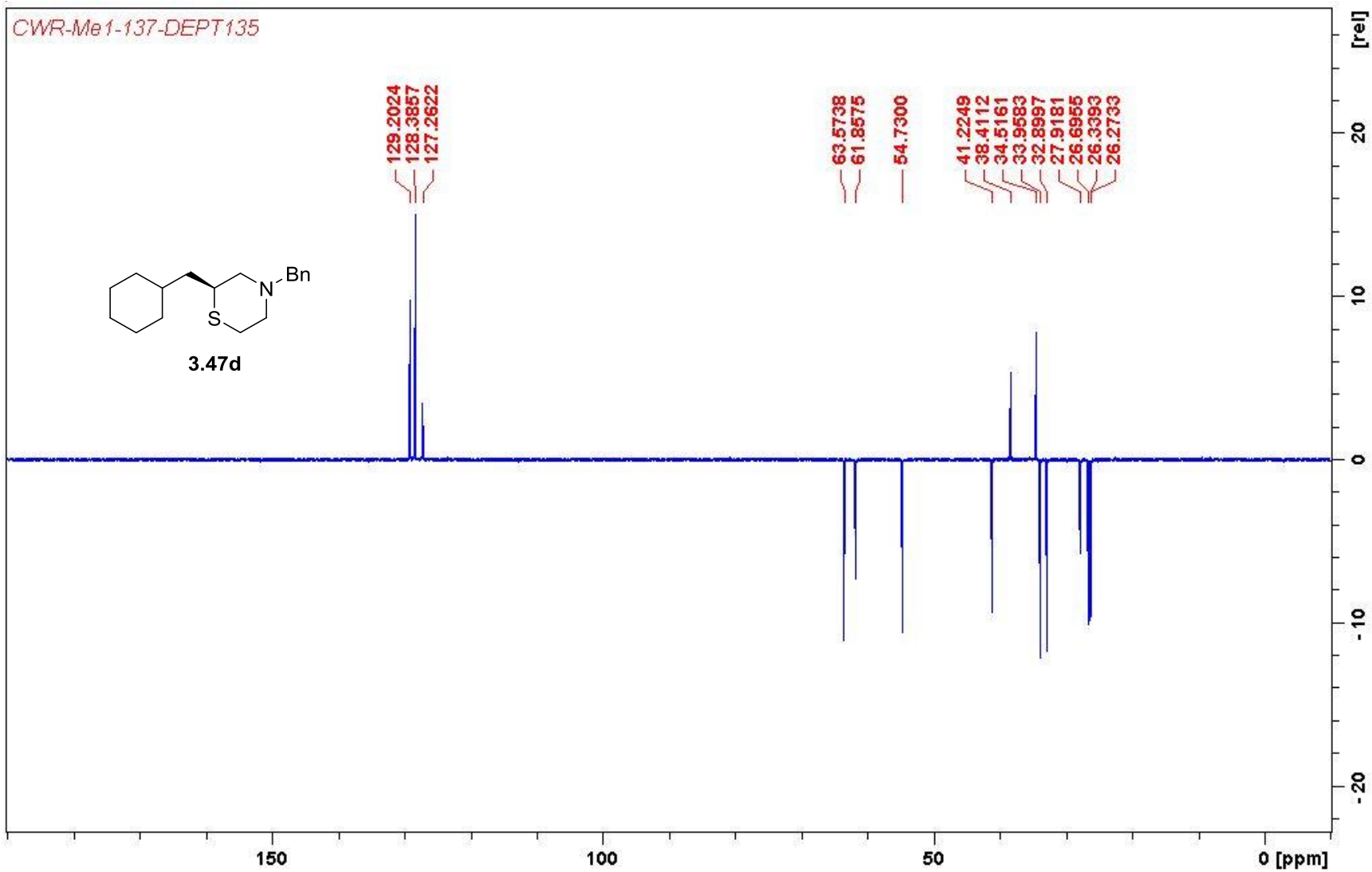




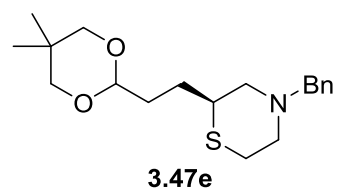








CWR-Me1-138



7.3066
7.2959
7.2760
7.2600
7.2434
7.2314
4.4163
4.4051
4.3932
3.5875
3.5600
3.5264
3.4028
3.3768
3.0000
2.9734
2.8670
2.8282
2.8006
2.5820
2.5783
2.5718
2.5542
2.5483
2.5384
2.3934
2.3670
2.3404
2.1924
2.1664
2.1405
1.8133
1.8006
1.7880
1.7742
1.7667
1.7552
1.7409
1.7284
1.7207
1.7075
1.6951
1.6824
1.6708
1.6615
1.6489
1.6377
1.6260
1.6103
1.5995
1.5922
1.5800
1.5732
1.5661
1.5453
1.1661
0.7037

10 8 6 4 2 0 [ppm]

5.0000
1.0147
3.8501
2.2117
3.8505
1.0361
0.9739
1.0186
4.0581
2.9470
2.9577

[rel]

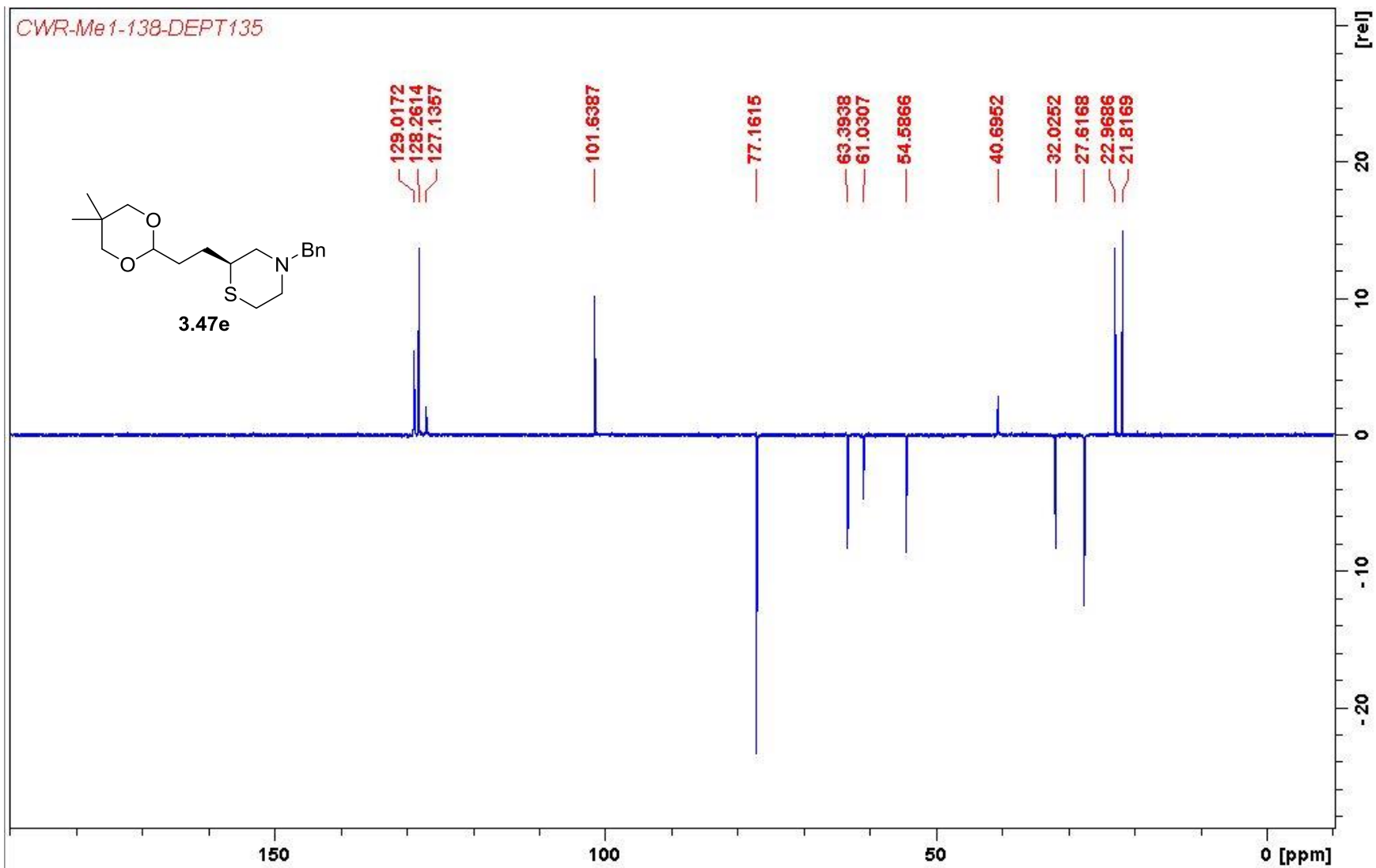
20

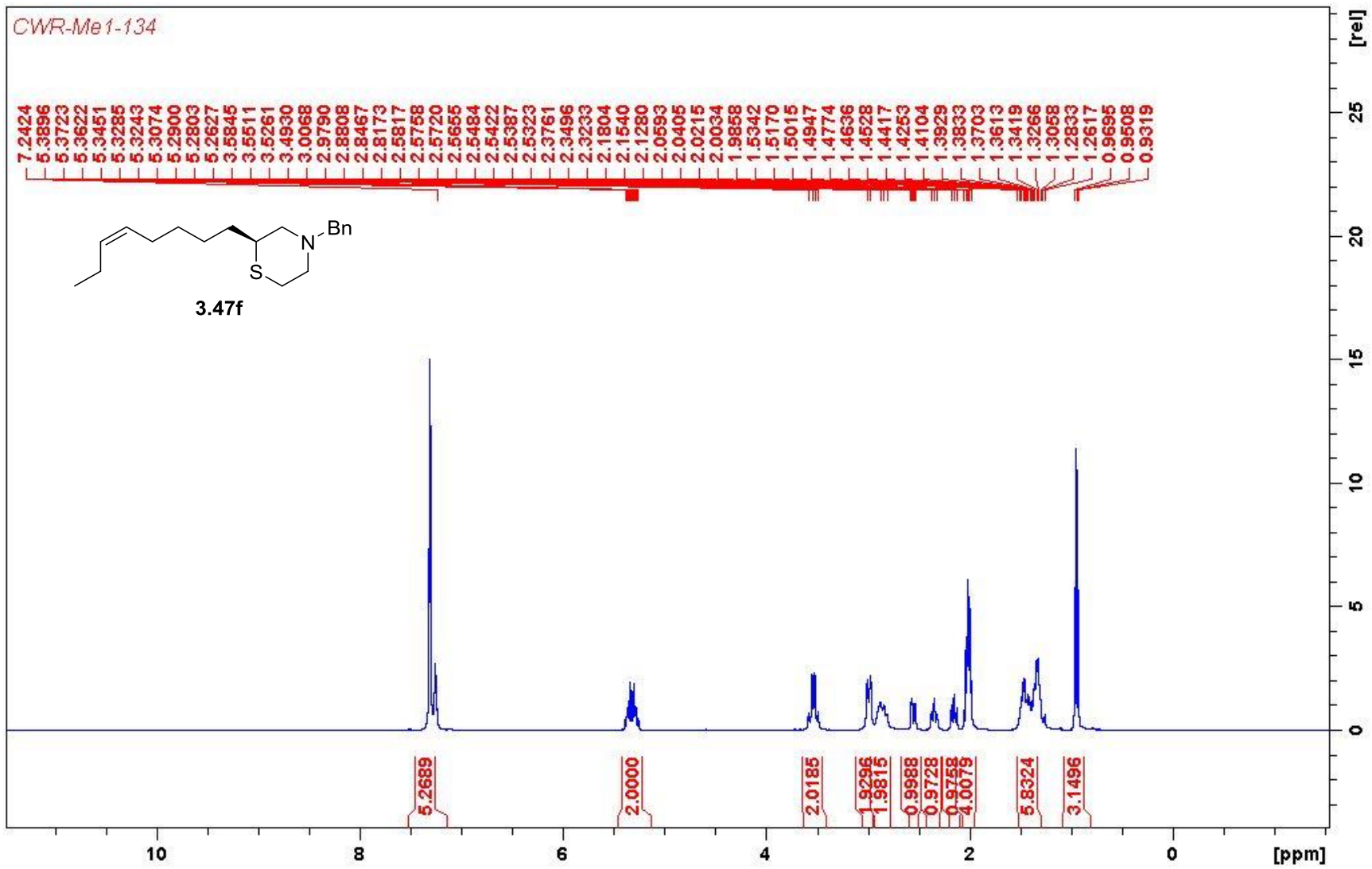
15

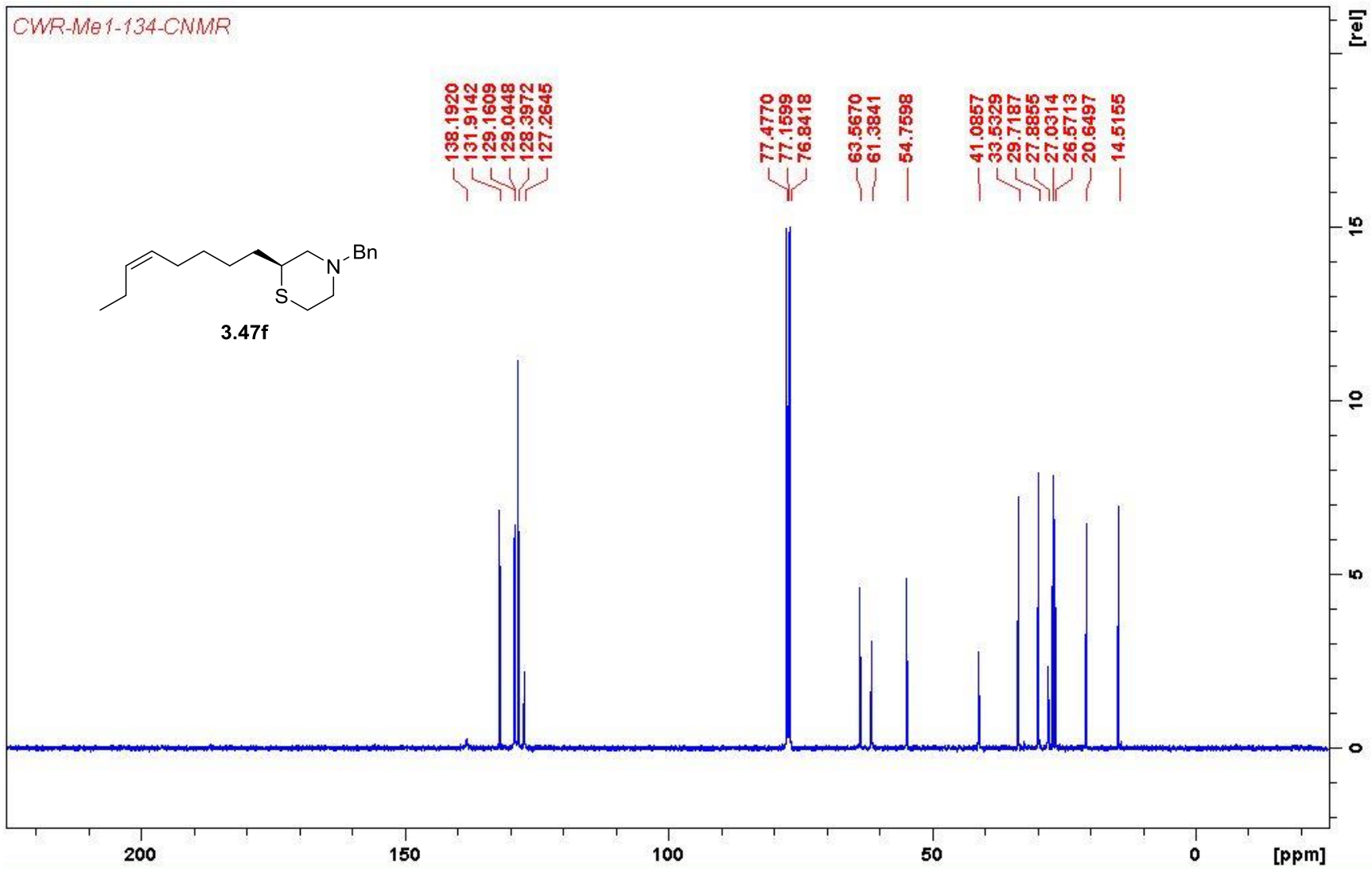
10

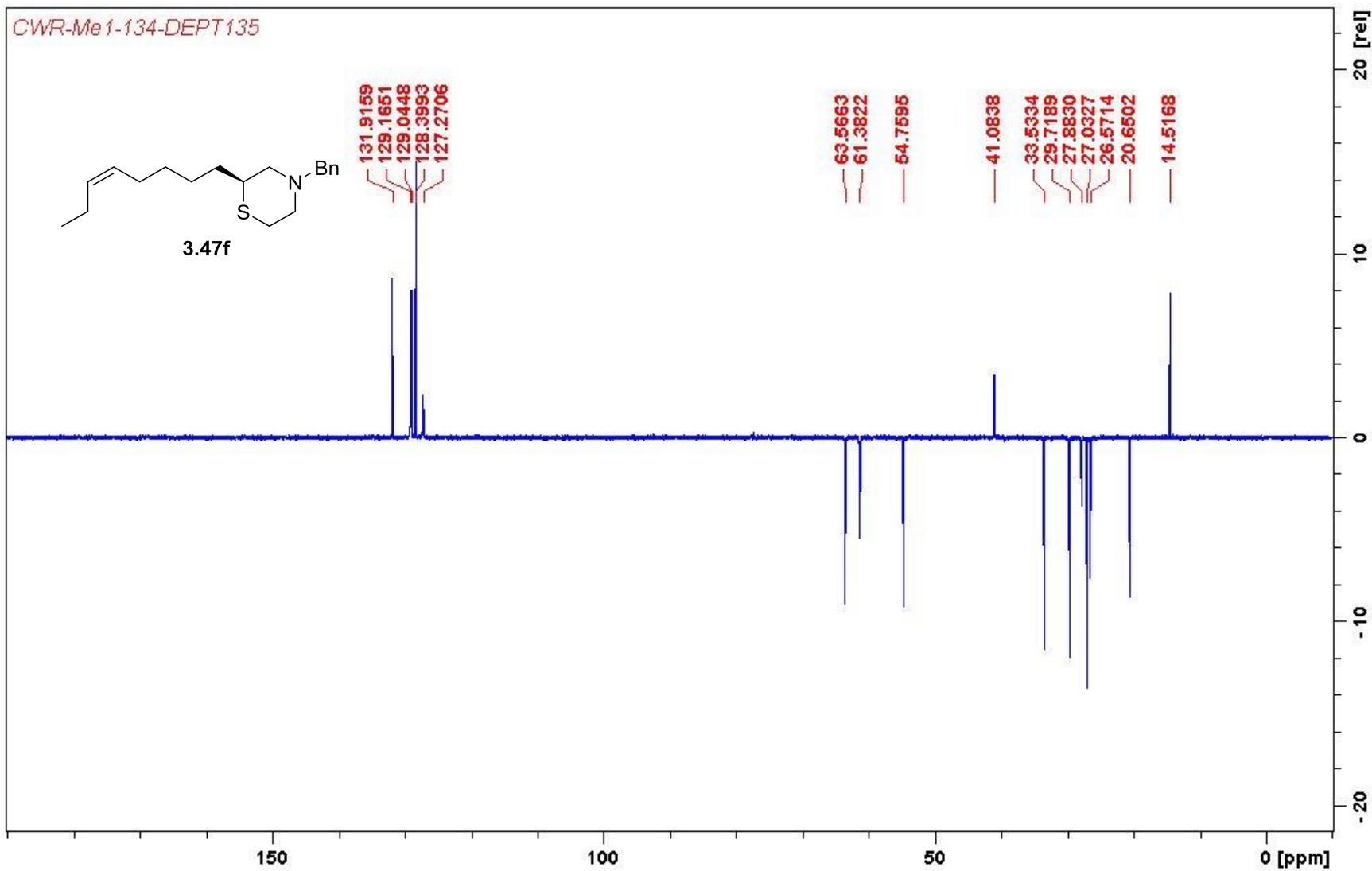
5

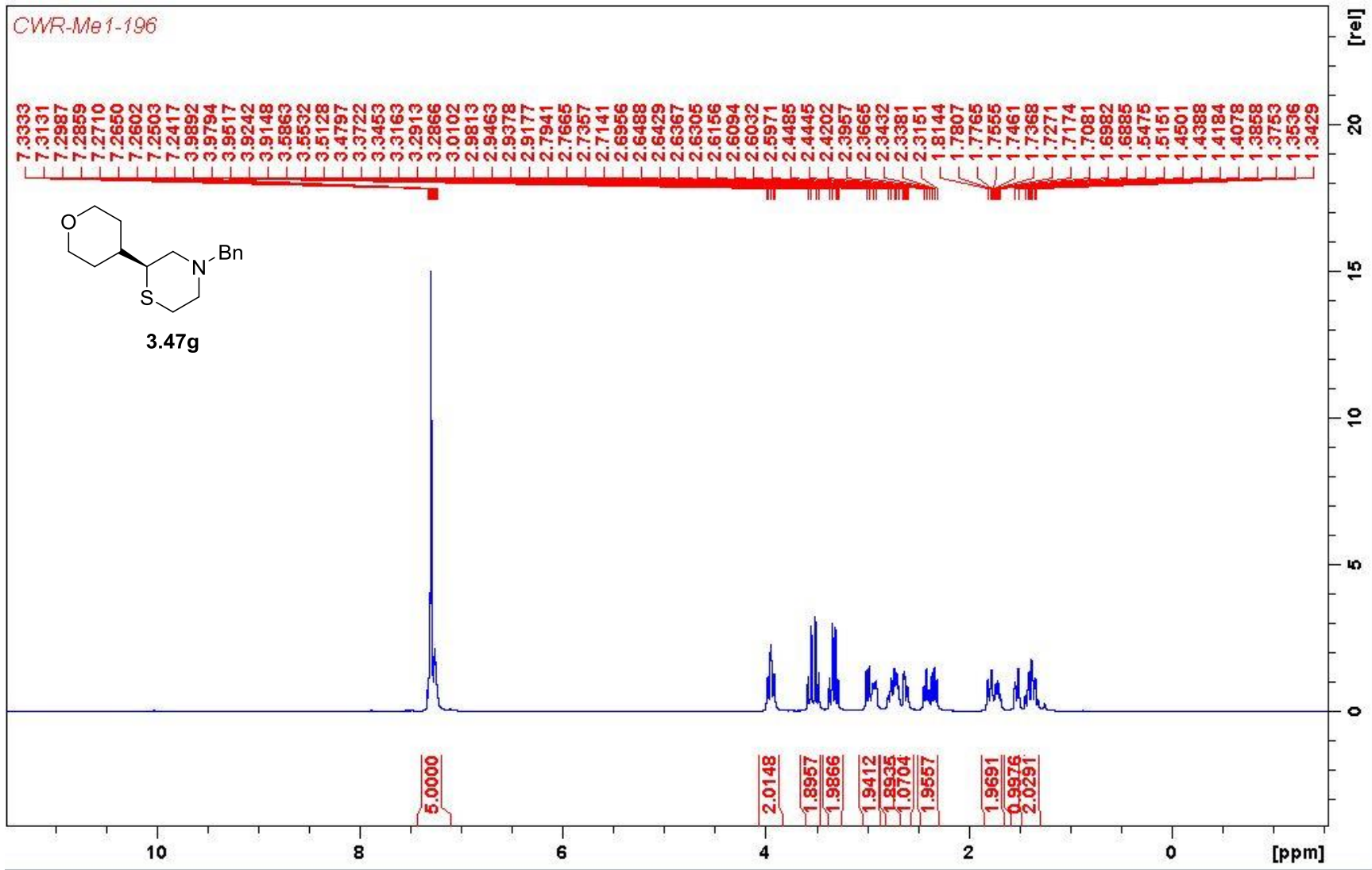
0

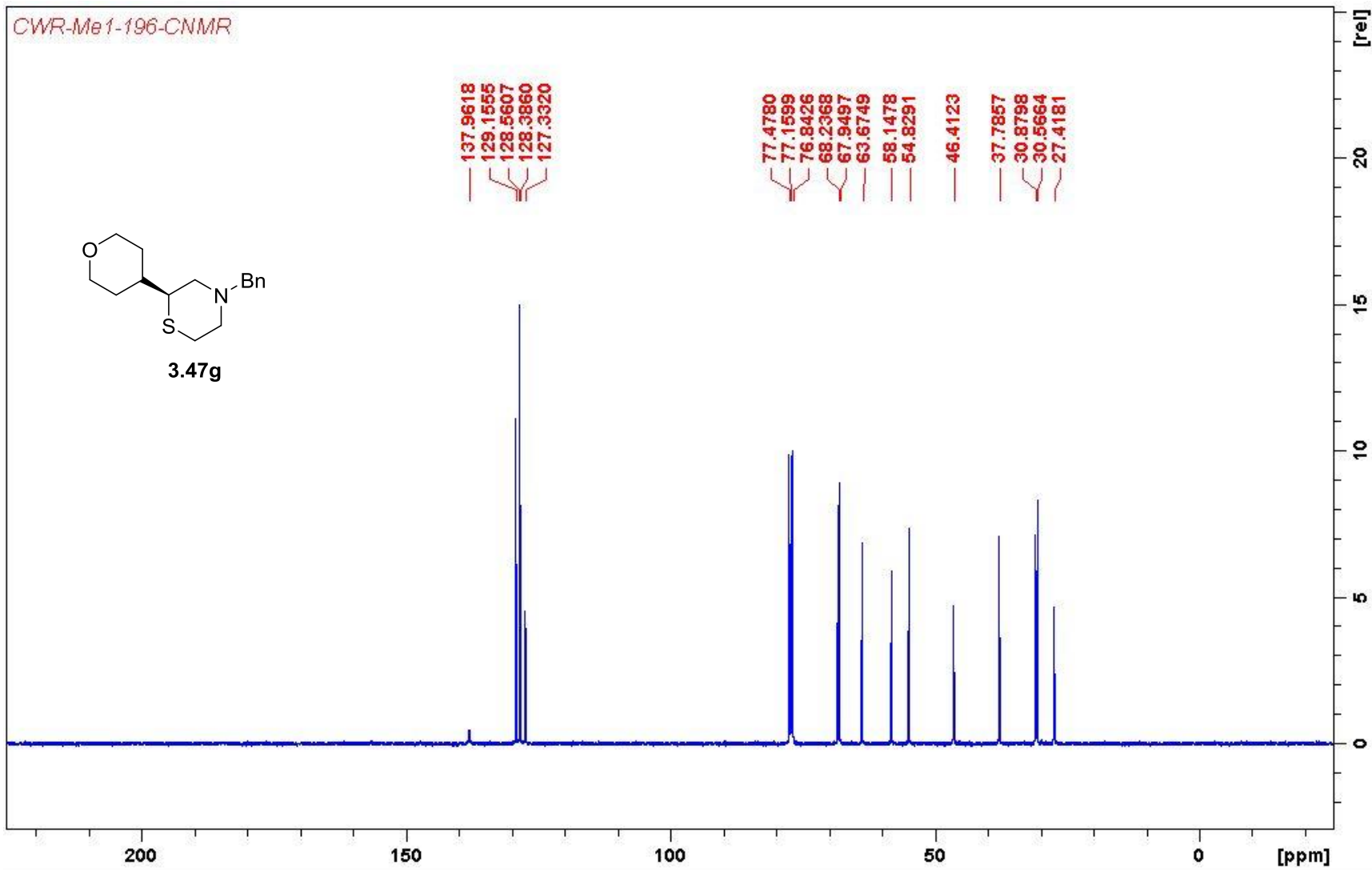


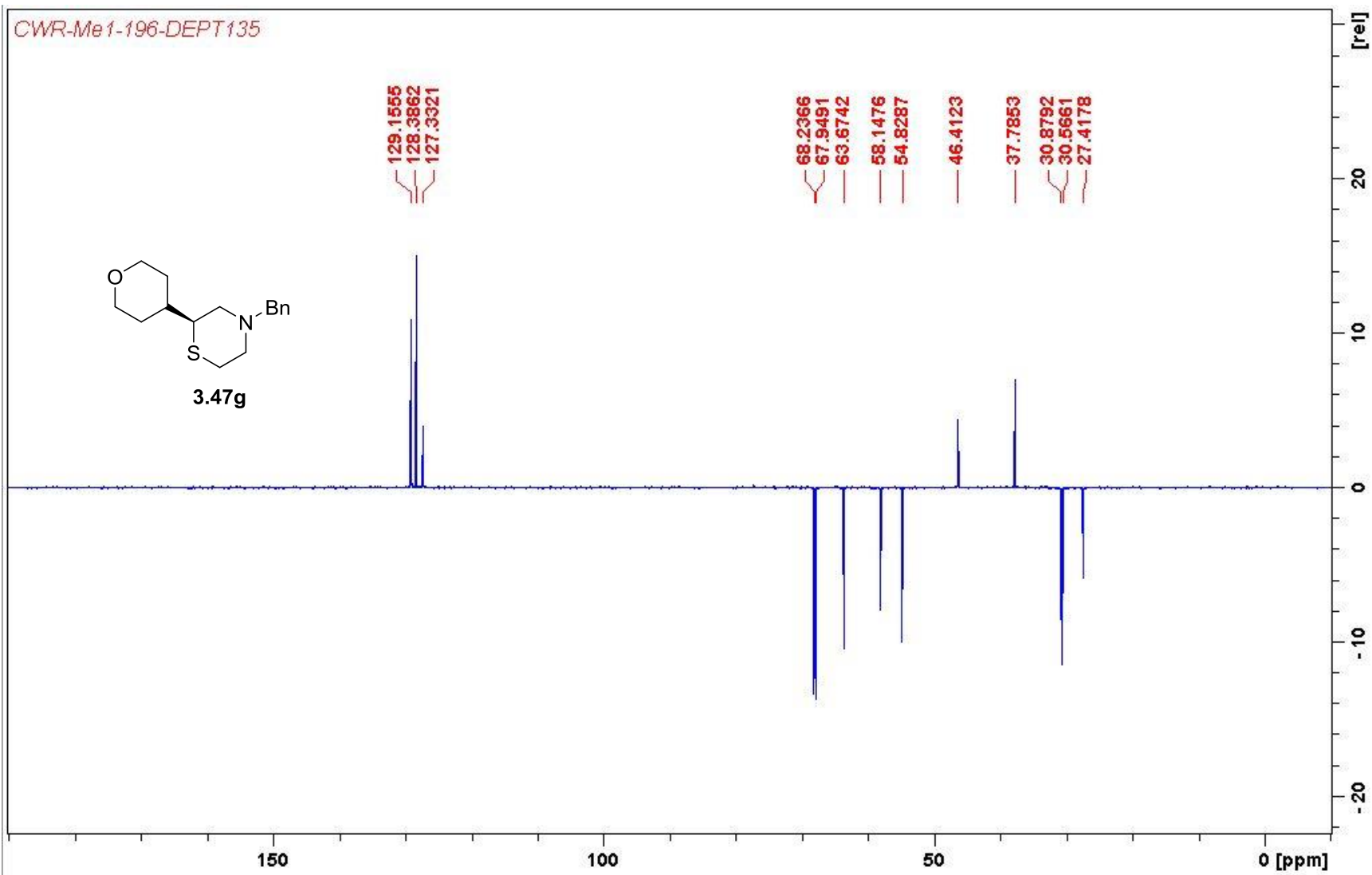




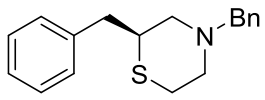




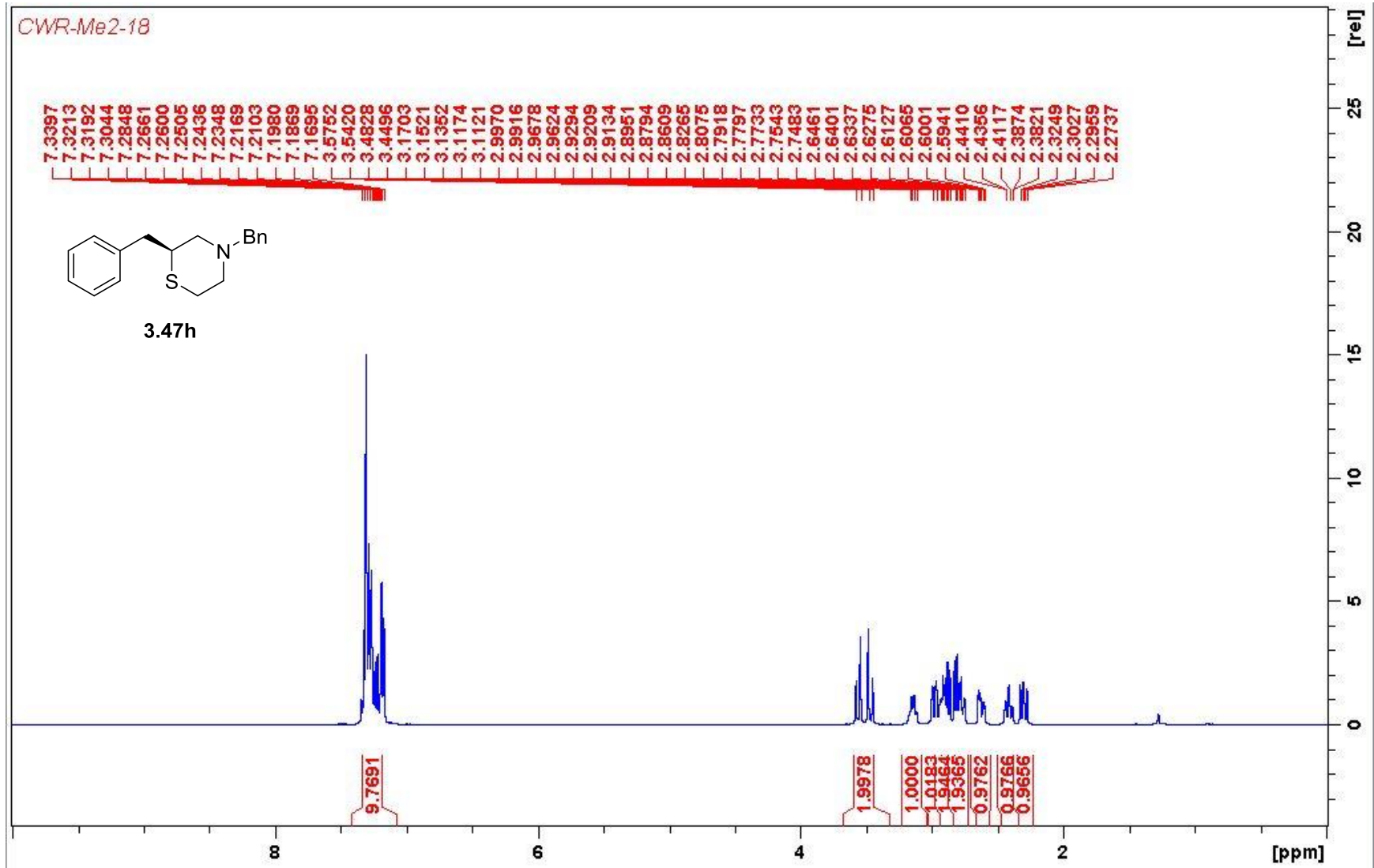


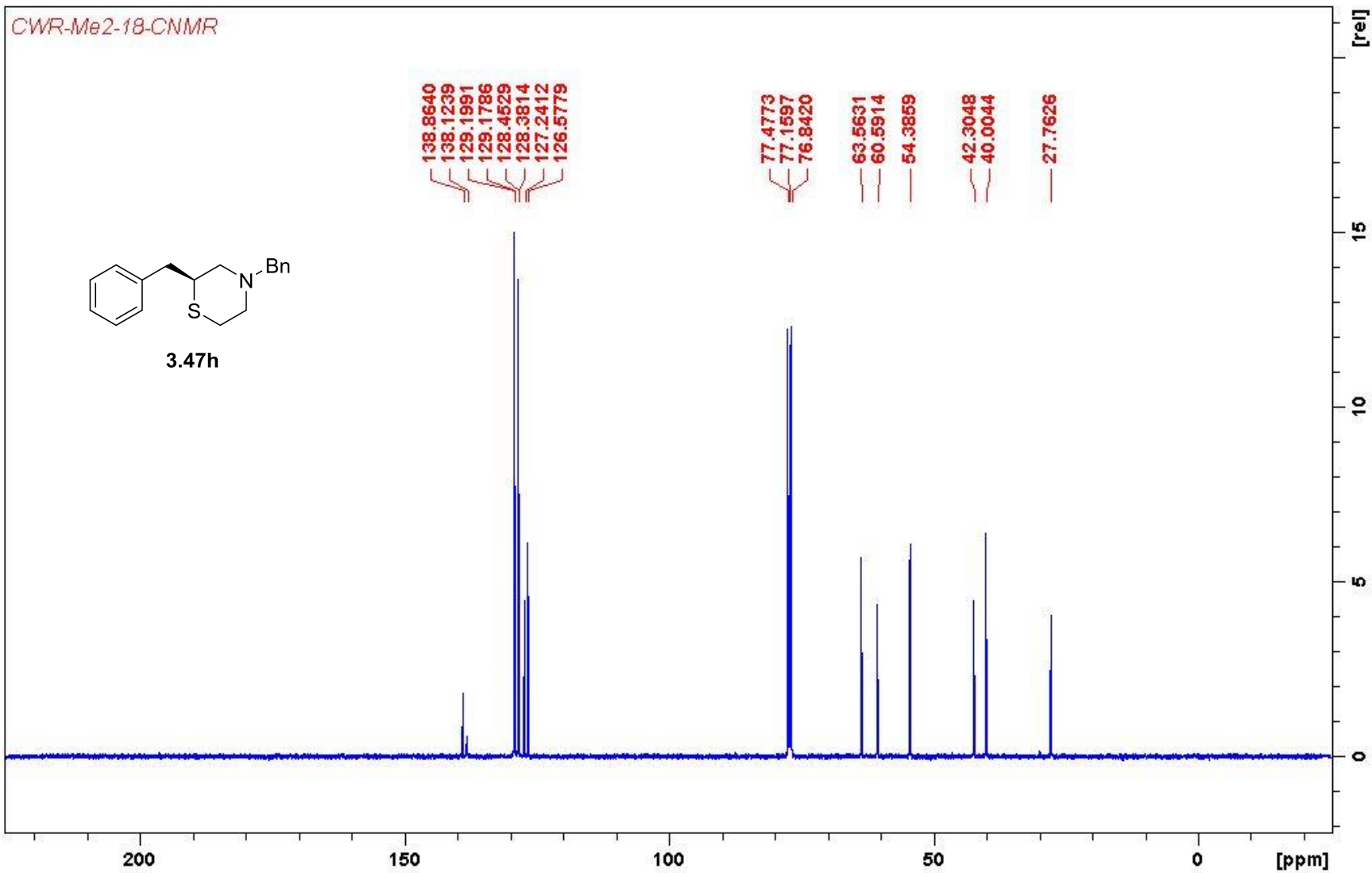


CWR-Me2-18

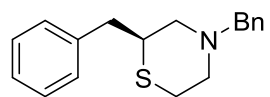


3.47h

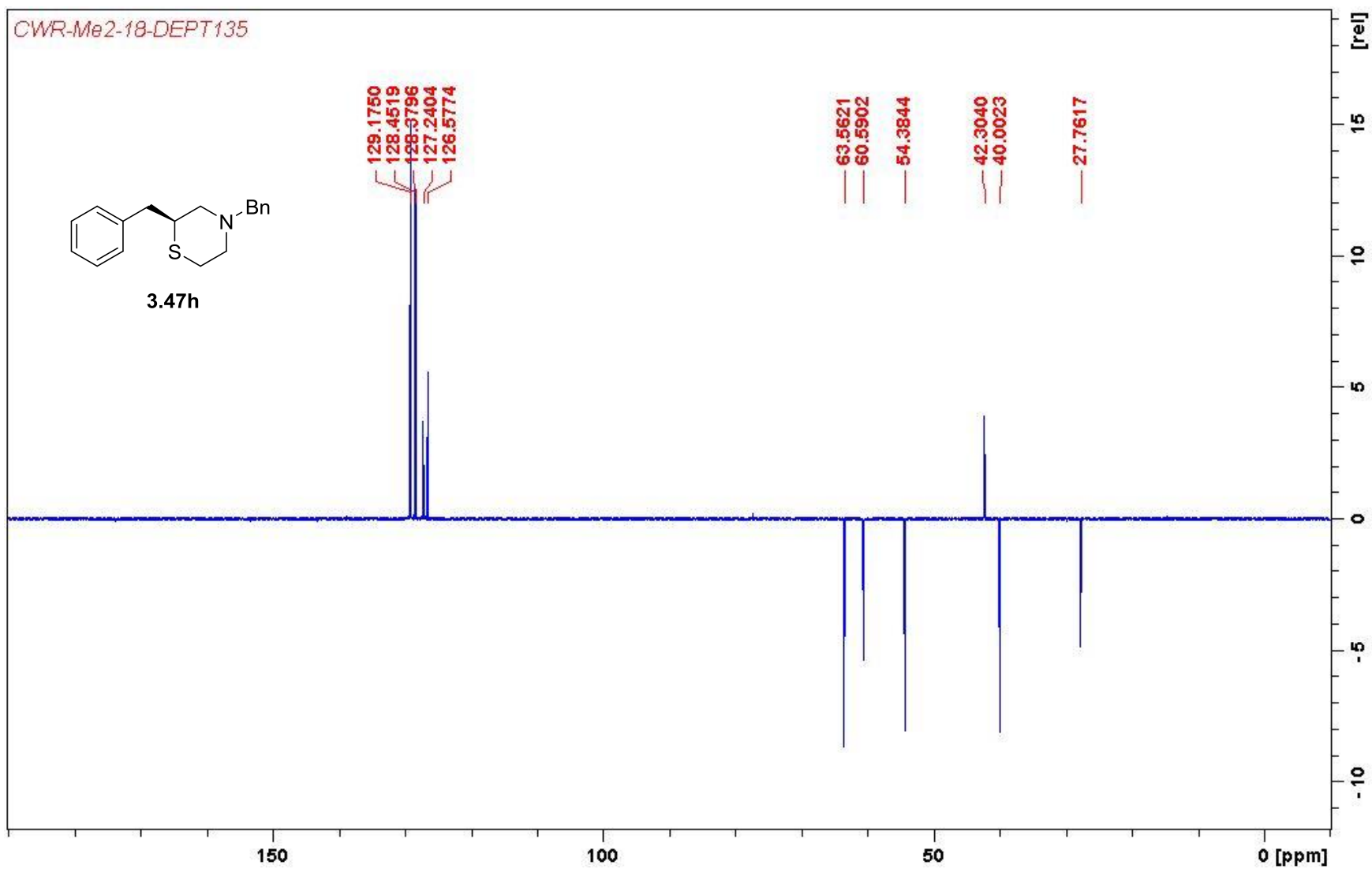


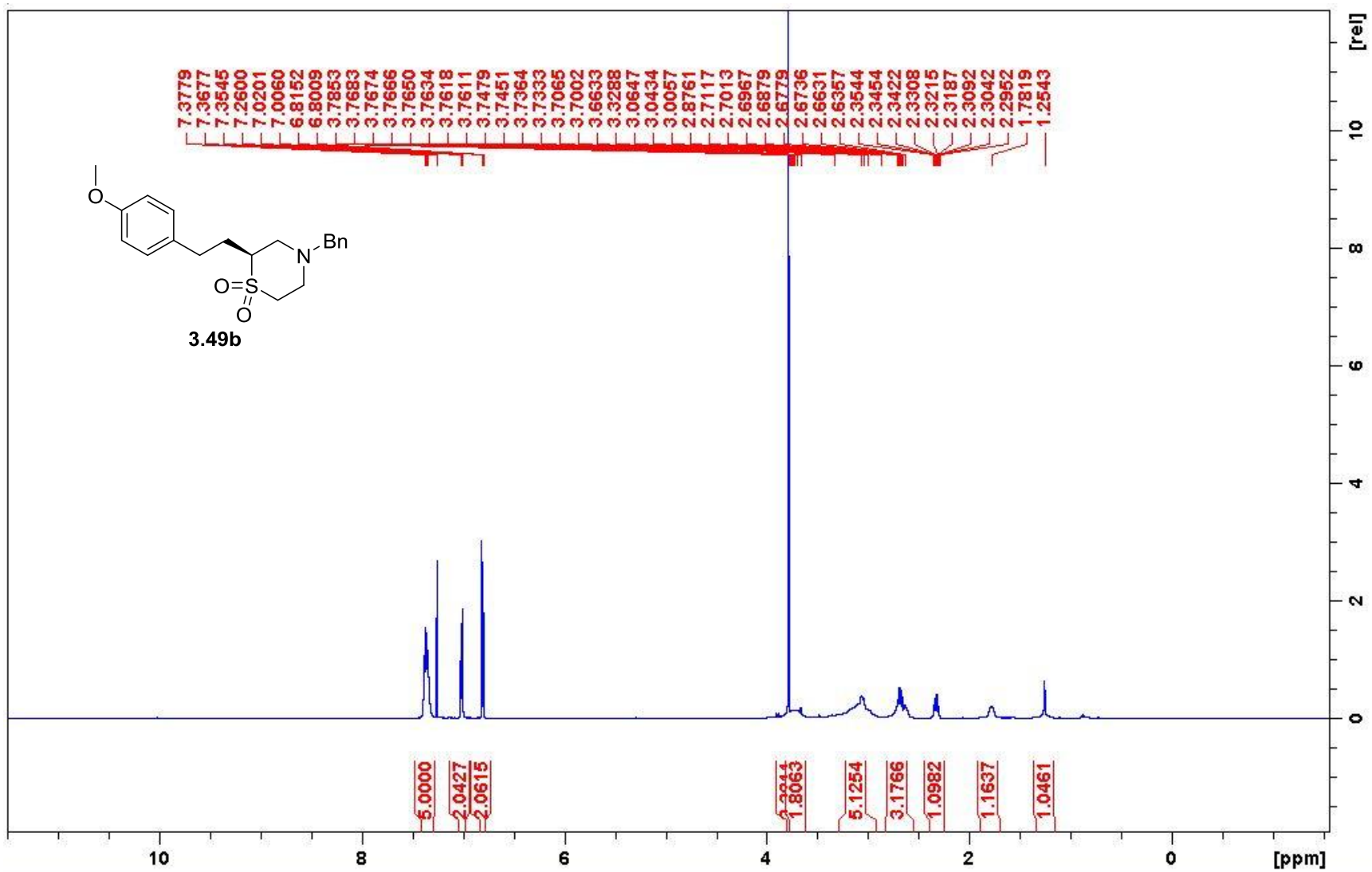


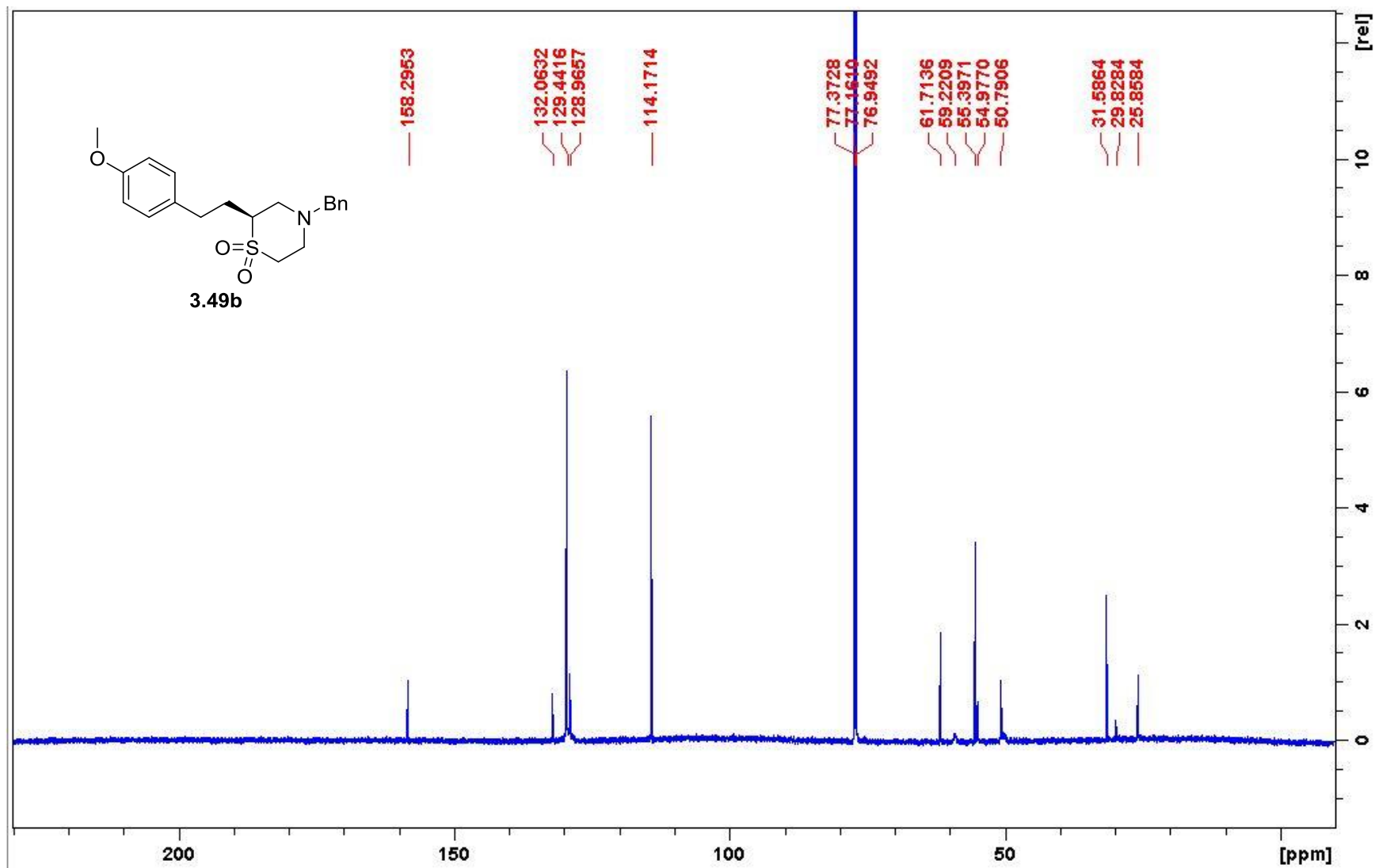
CWR-Me2-18-DEPT135

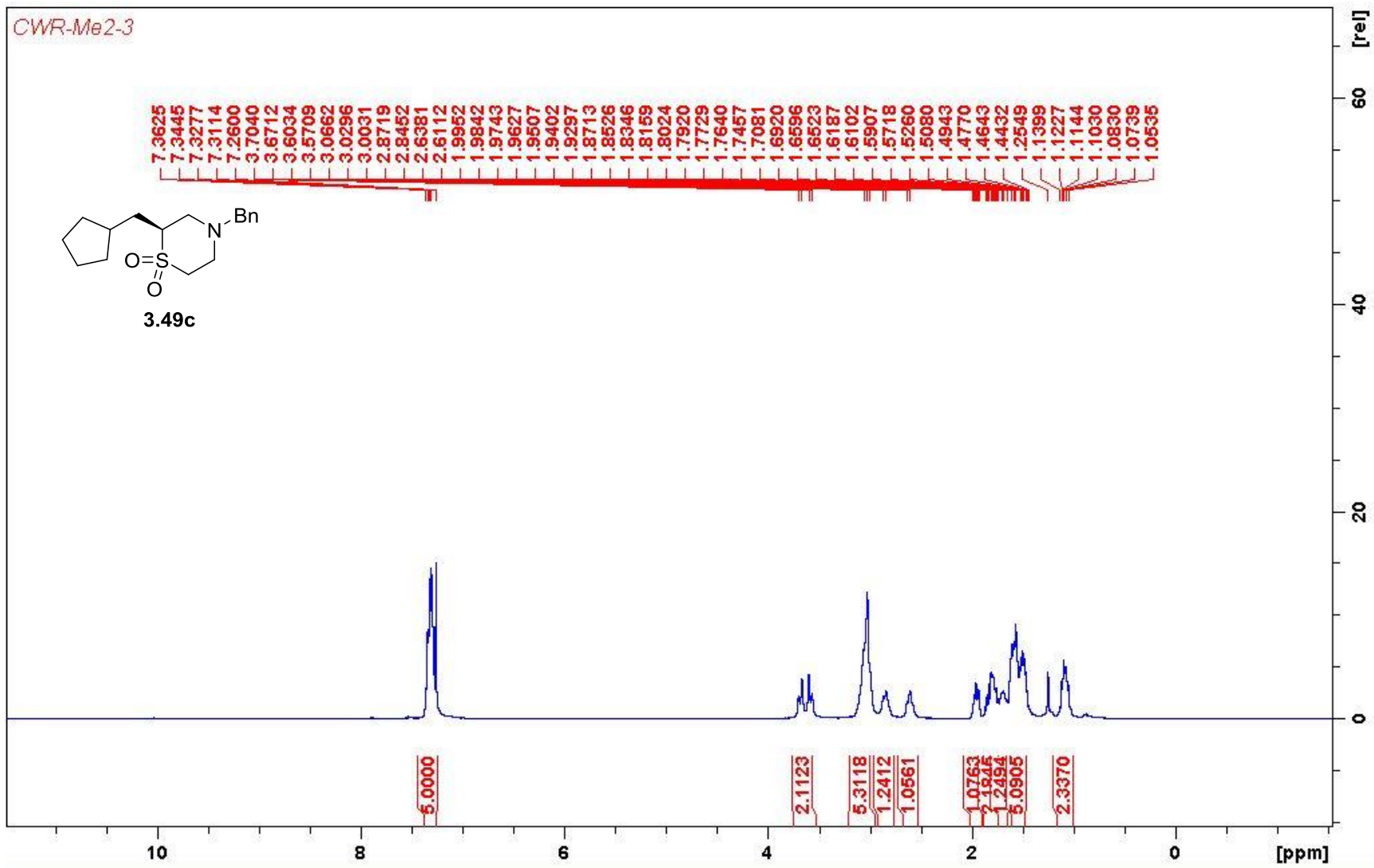


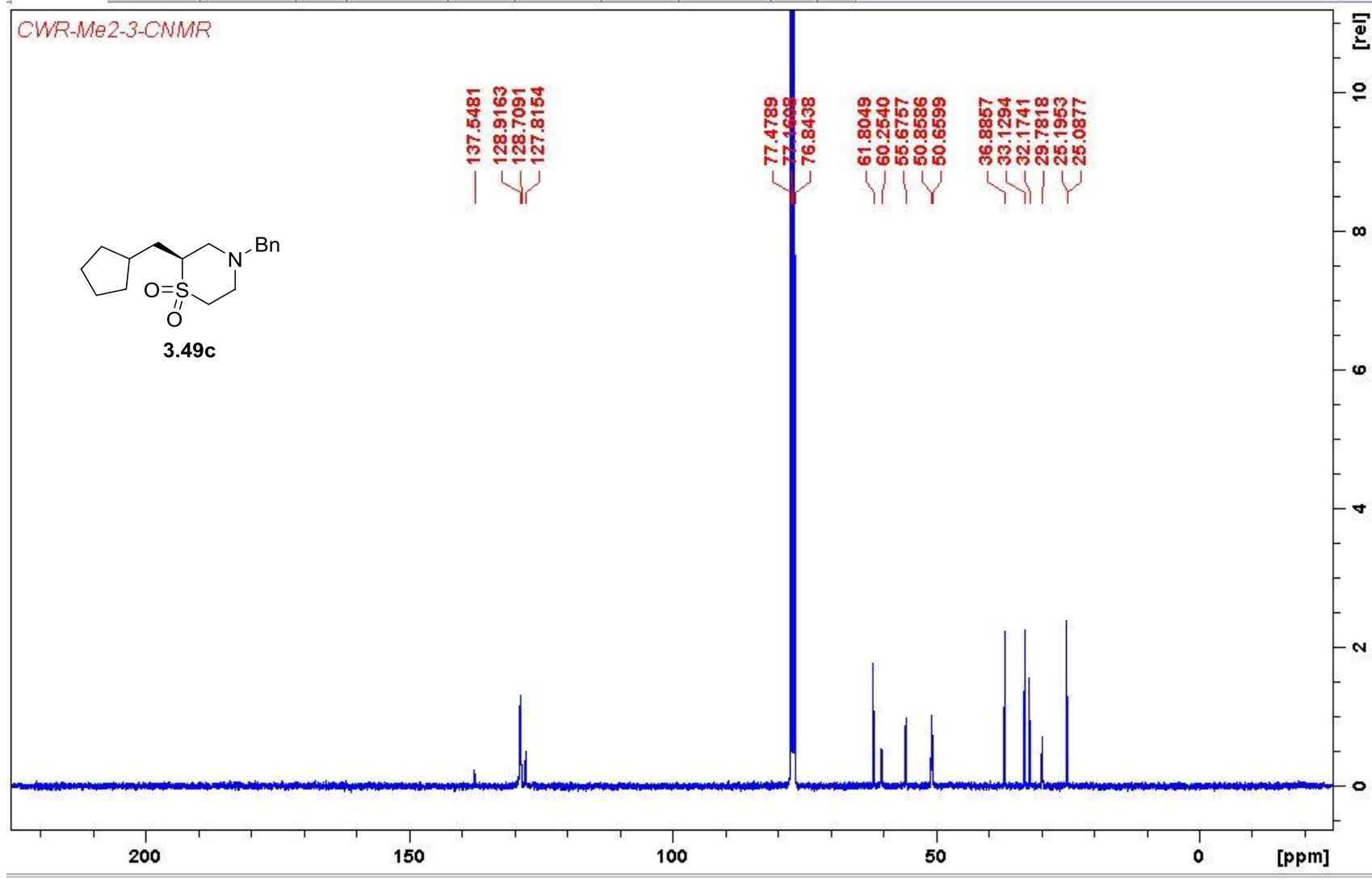
3.47h

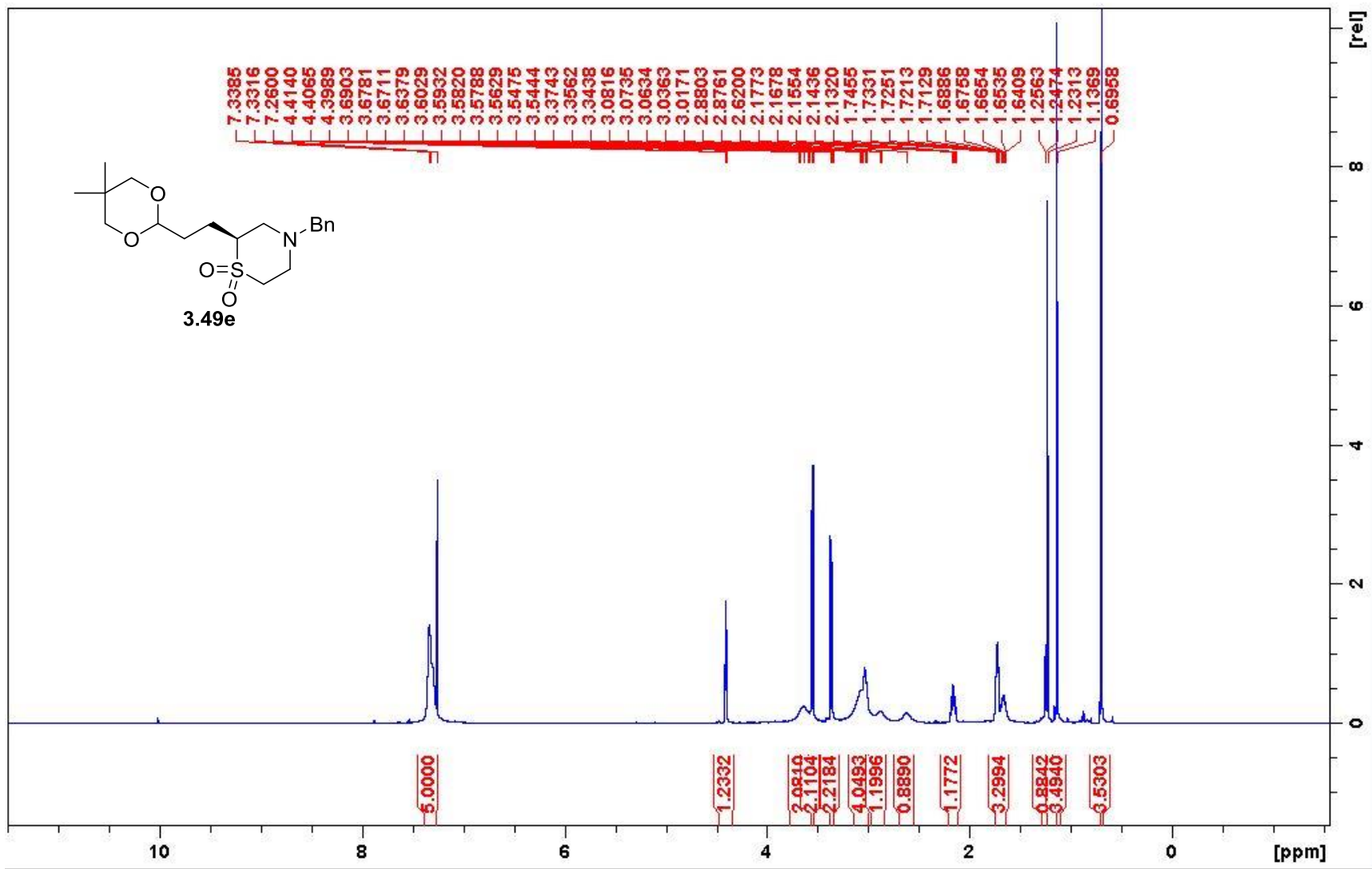


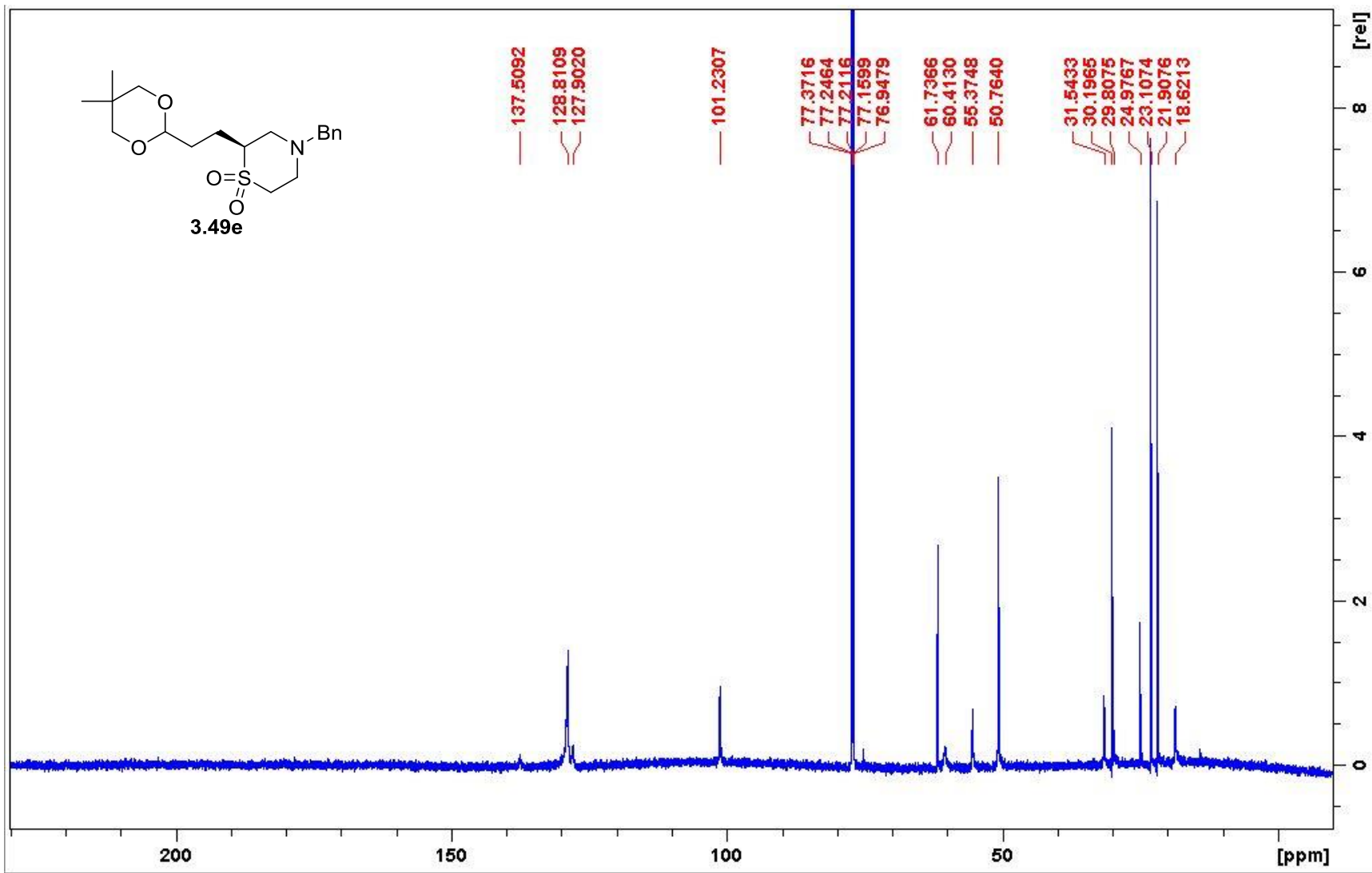




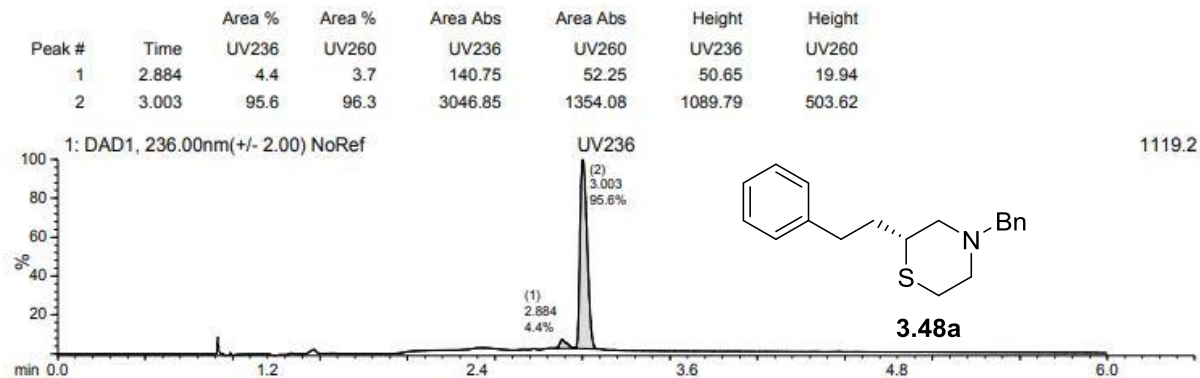
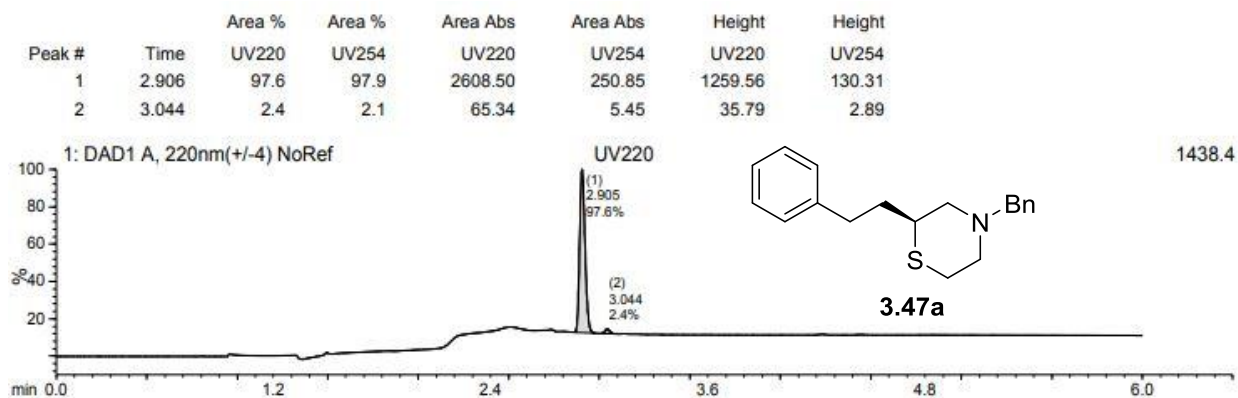
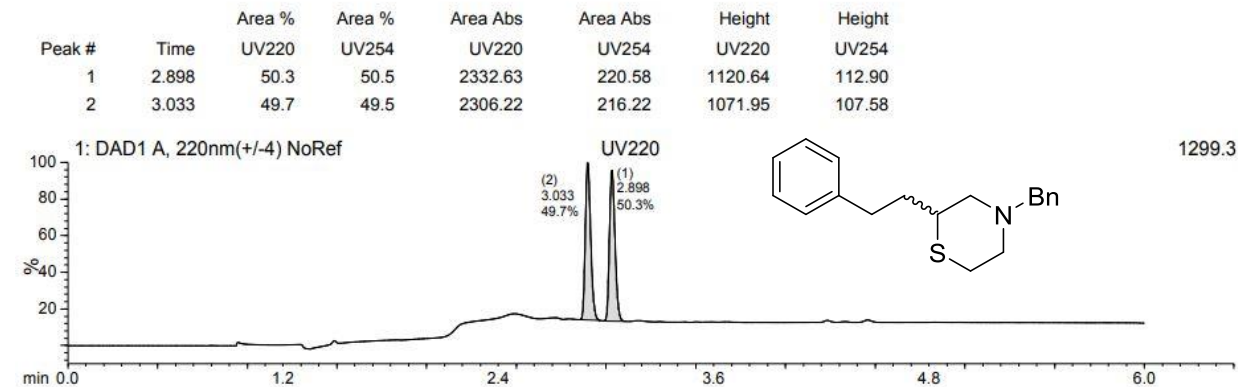




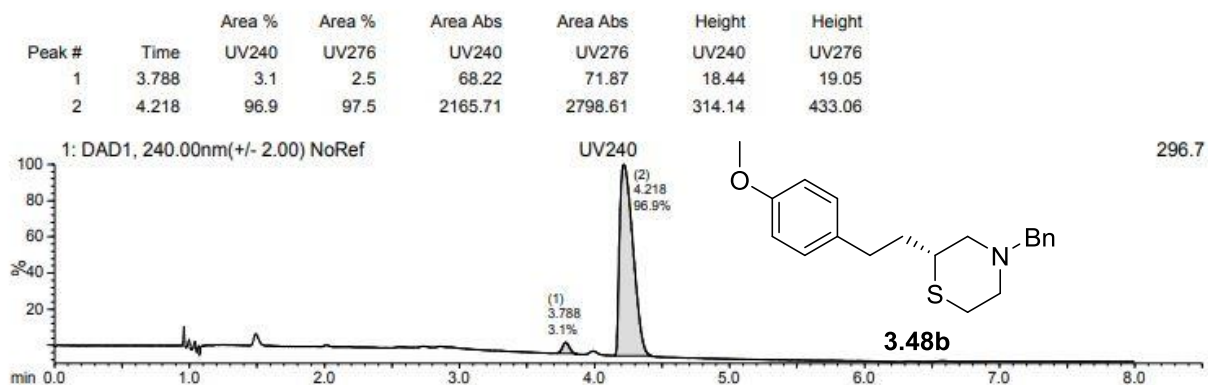
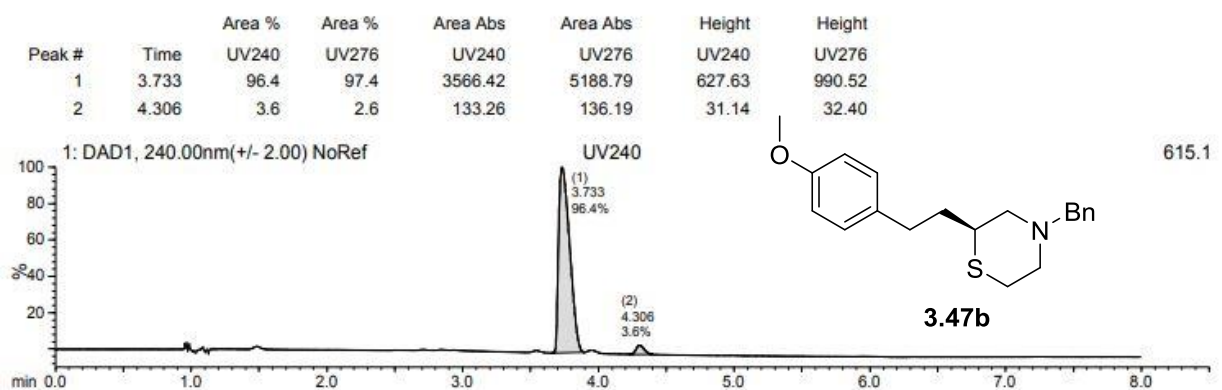
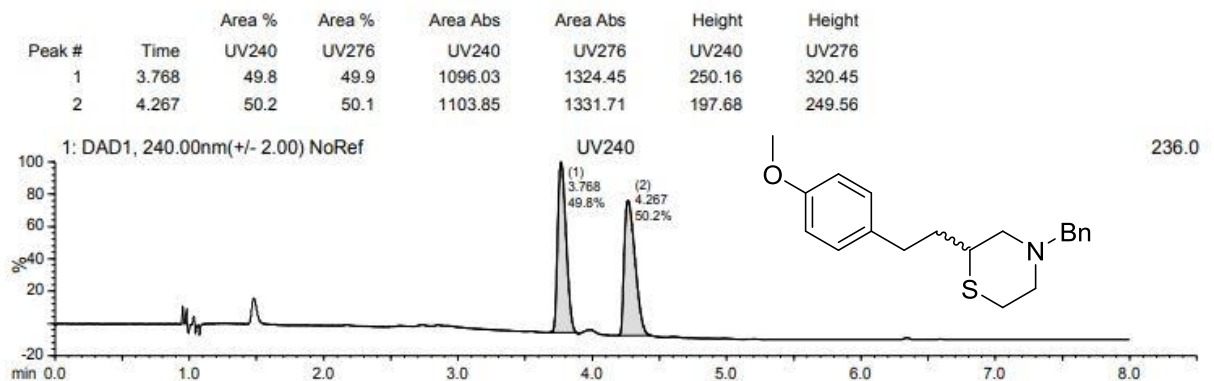




Chiral SFC Traces for Thiomorpholines 3.47a and 3.48a

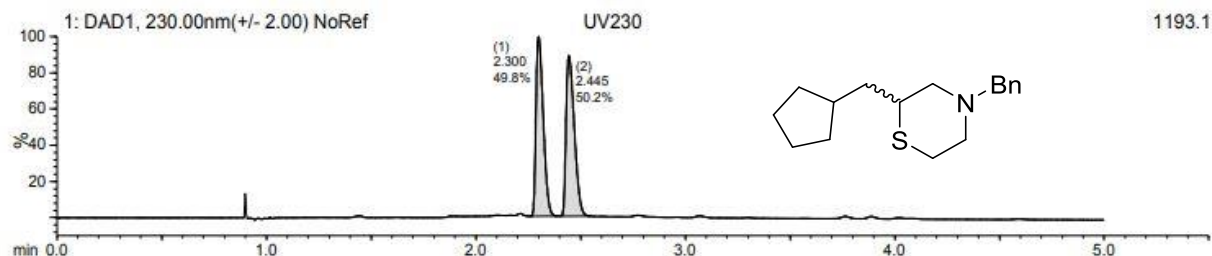


Chiral SFC Traces for Thiomorpholines 3.47b and 3.48b

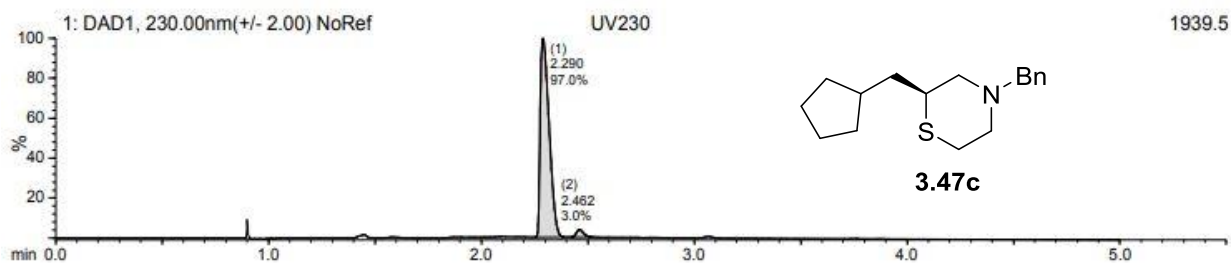


Chiral SFC Traces for Thiomorpholines 3.47c and 3.48c

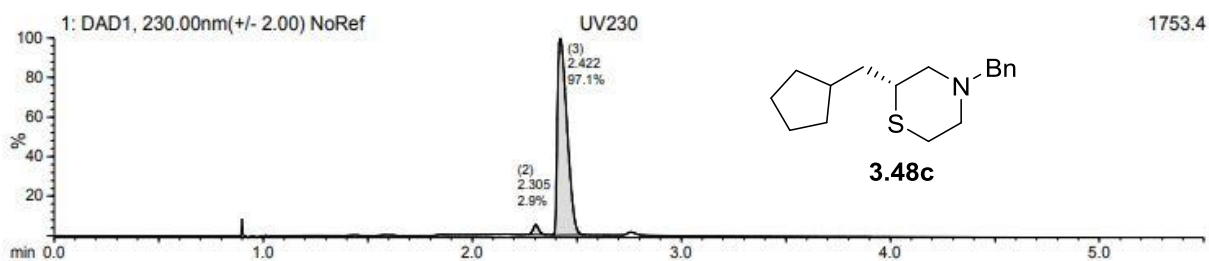
Peak #	Time	Area %		Area Abs		Height	
		UV230	UV260	UV230	UV260	UV230	UV260
1	2.300	49.8	49.8	2876.76	387.63	1184.30	168.76
2	2.445	50.2	50.2	2904.86	391.07	1057.59	149.48



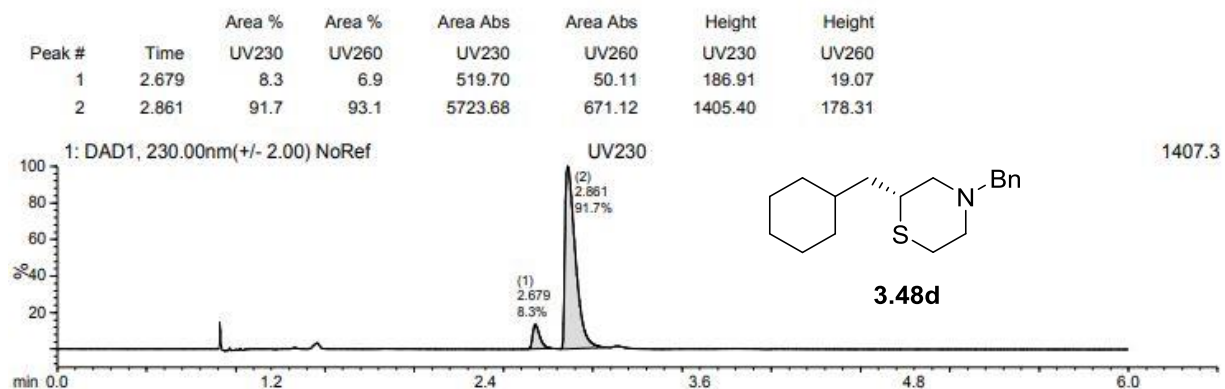
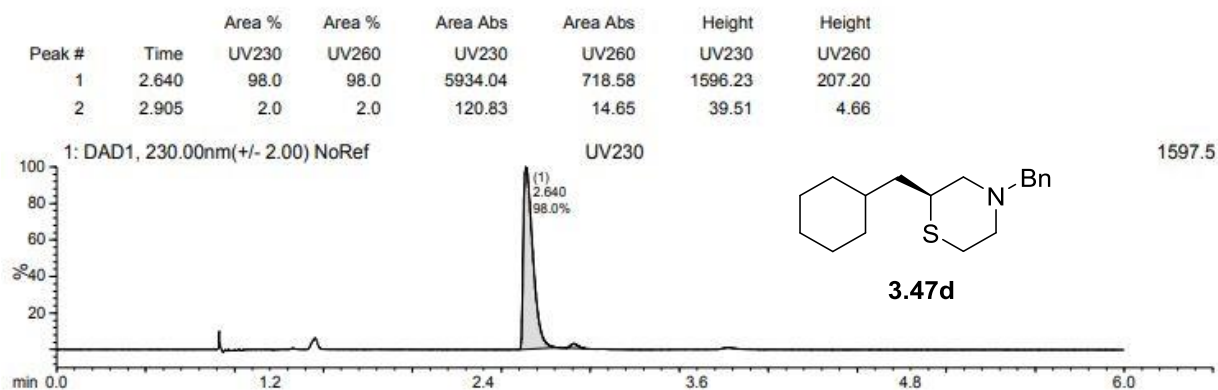
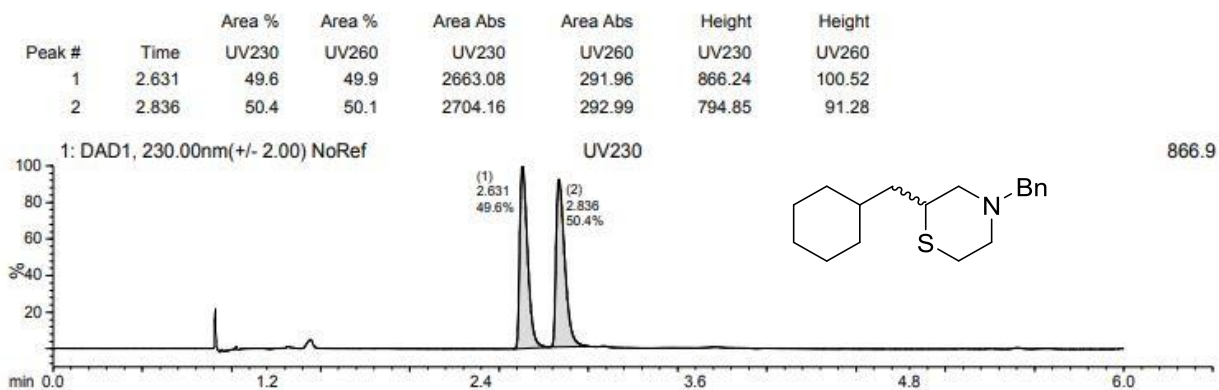
Peak #	Time	Area %		Area Abs		Height	
		UV230	UV260	UV230	UV260	UV230	UV260
1	2.290	97.0	97.7	5606.79	829.29	1932.36	307.70
2	2.462	3.0	2.3	174.85	19.93	73.99	8.83



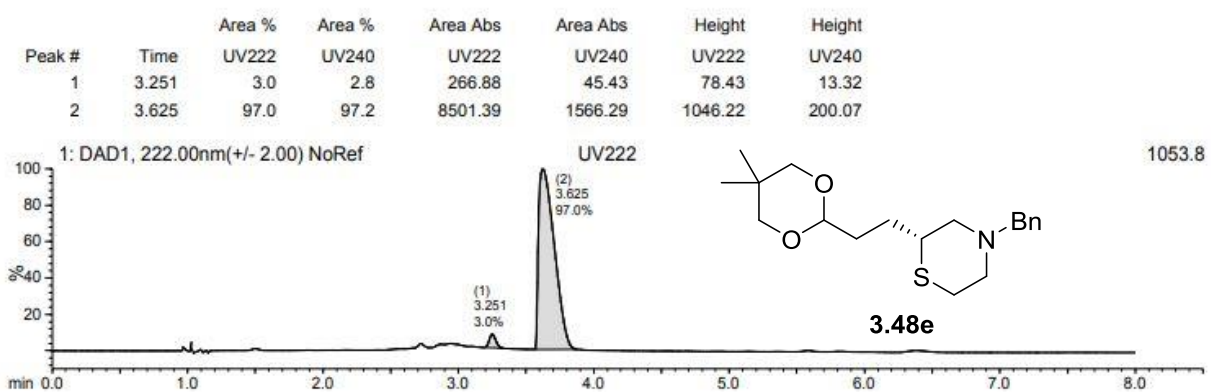
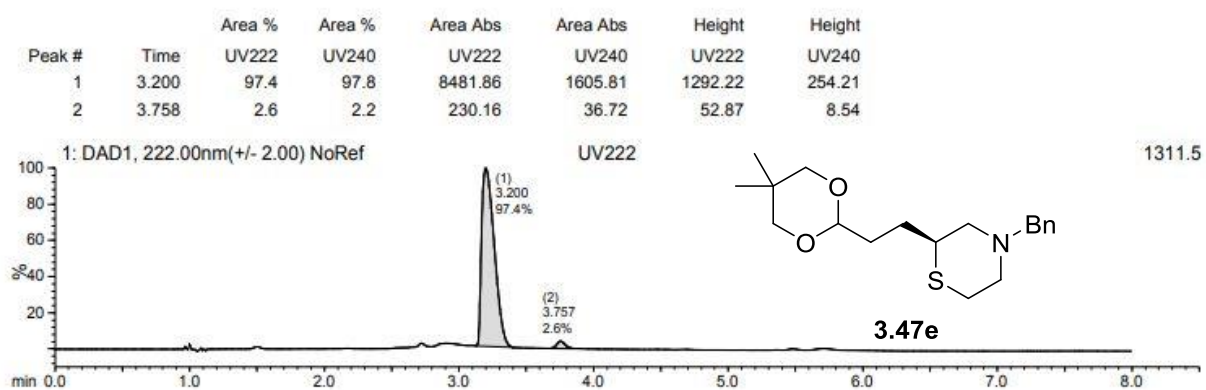
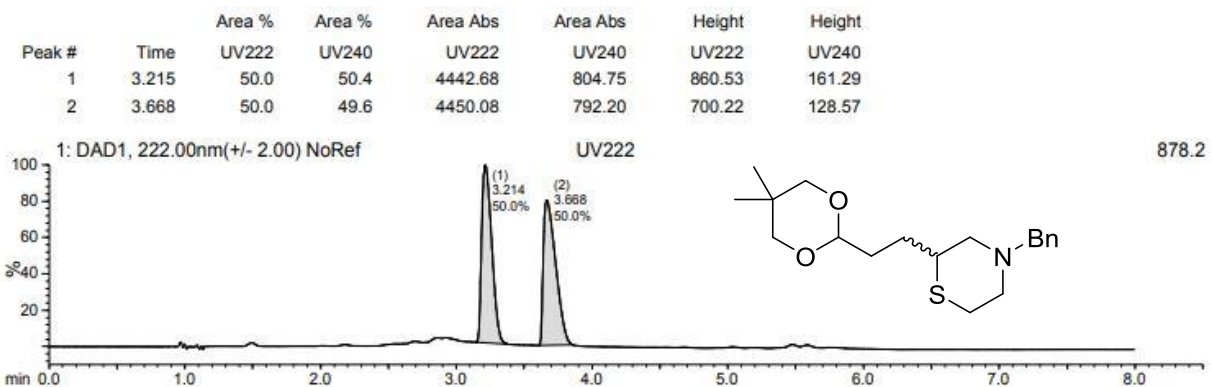
Peak #	Time	Area %		Area Abs		Height	
		UV230	UV260	UV230	UV260	UV230	UV260
1	2.267	0.0	1.3	0	11.16	0.00	6.58
2	2.305	2.9	2.4	165.73	20.30	86.47	10.52
3	2.422	97.1	96.3	5577.28	807.86	1748.65	271.54



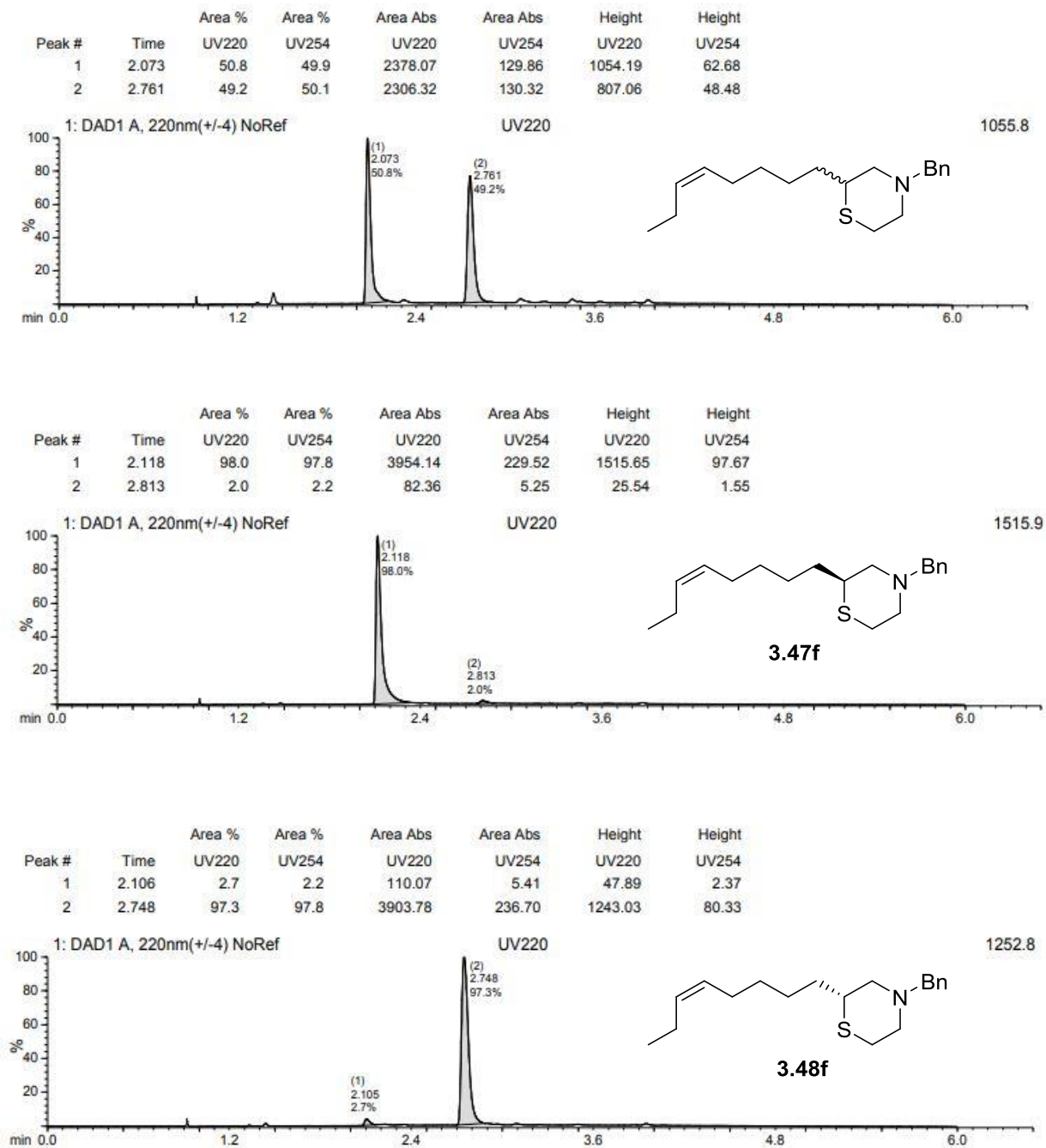
Chiral SFC Traces for Thiomorpholines 3.47d and 3.48d



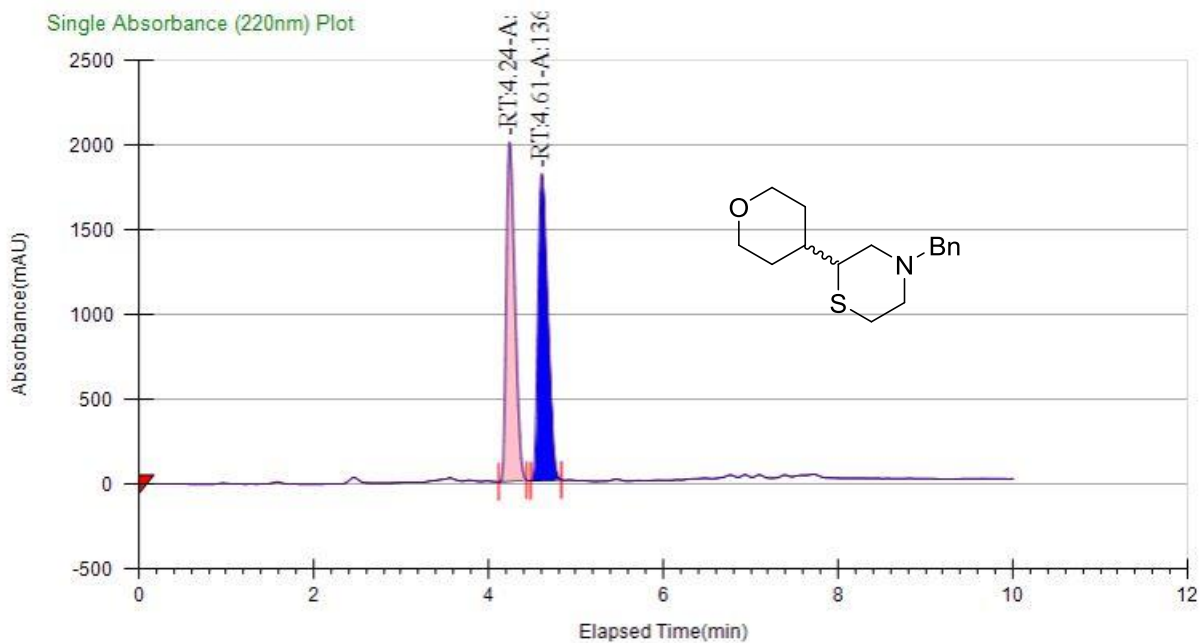
Chiral SFC Traces for Thiomorpholines 3.47e and 3.48e



Chiral SFC Traces for Thiomorpholines 3.47f and 3.48f

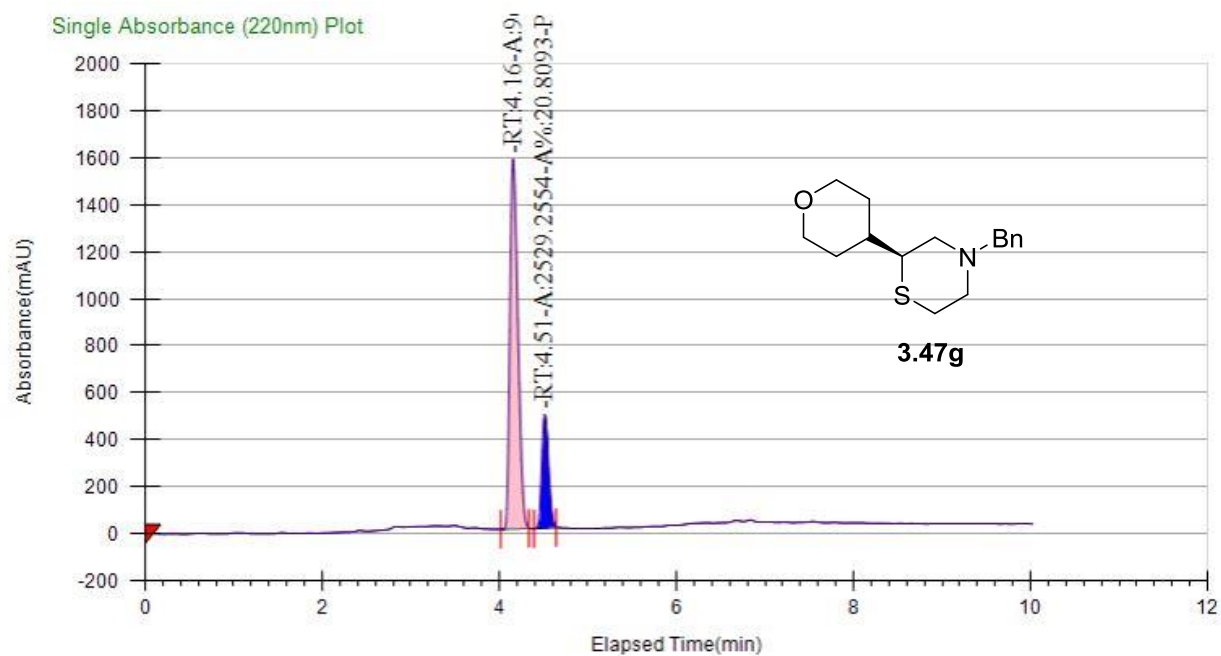


Chiral SFC Traces for Thiomorpholines 3.47g and 3.48g



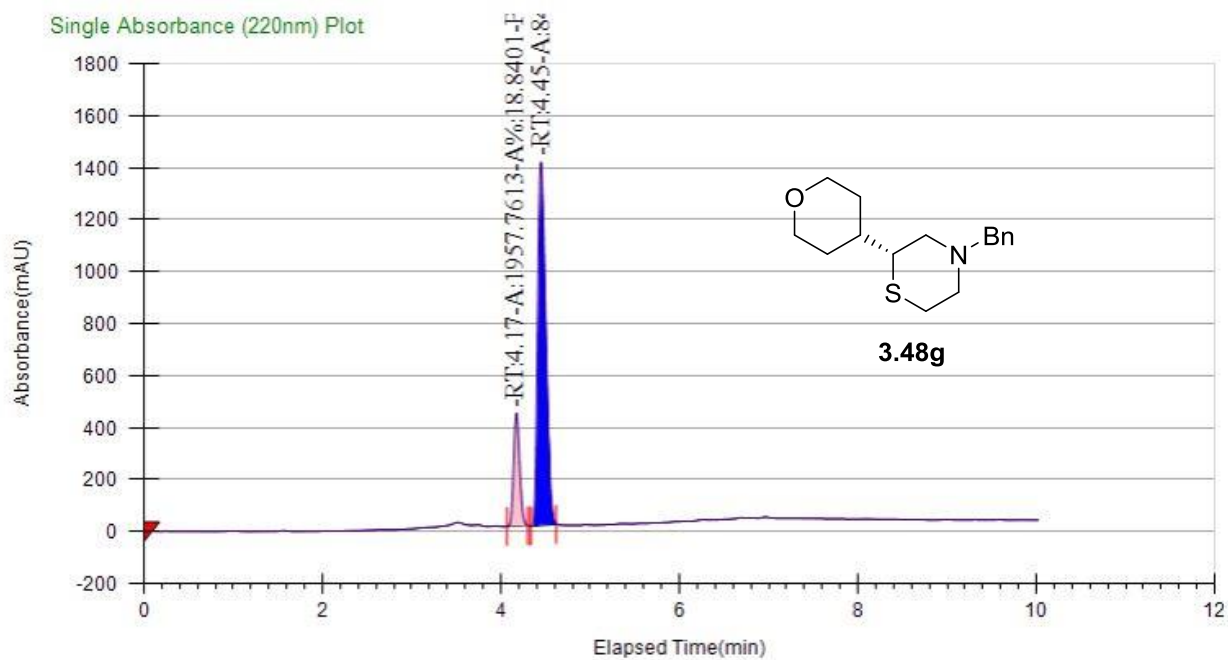
Peak Information

Peak No	% Area	Area	Ret. Time	Height	Cap. Factor
1	49.328	13290.725	4.24 min	1999.4332	0
2	50.672	13652.837	4.61 min	1808.7082	0



Peak Information

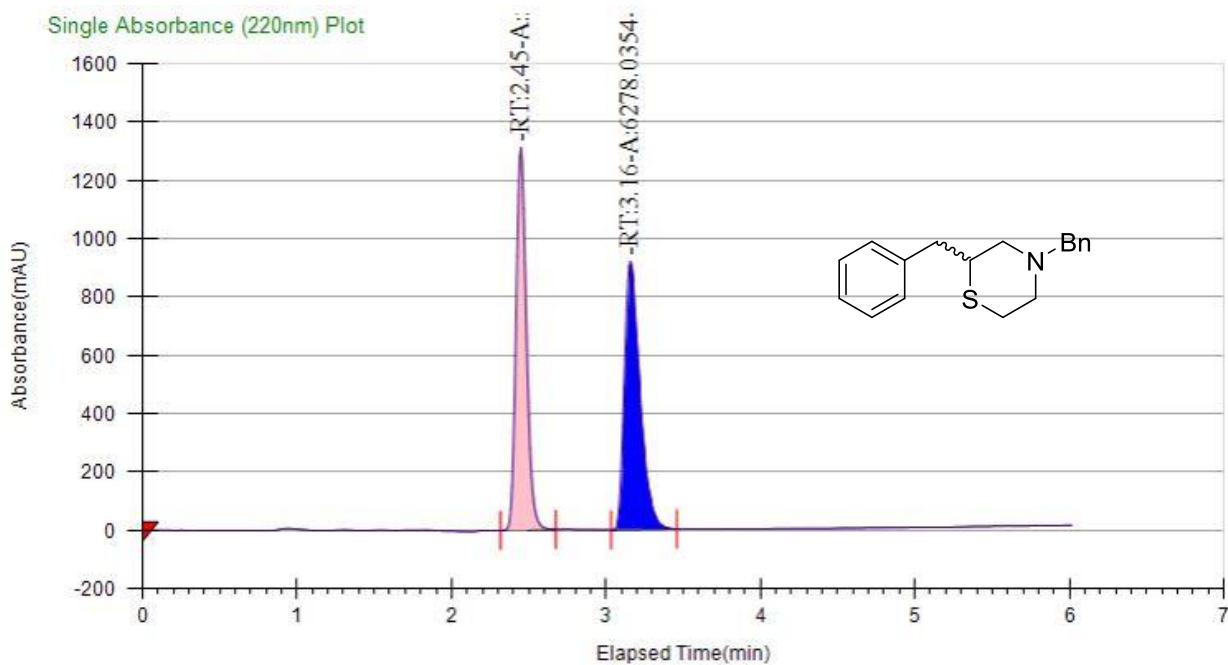
Peak No	% Area	Area	Ret. Time	Height	Cap. Factor
1	79.1907	9625.1856	4.16 min	1573.4516	0
2	20.8093	2529.2554	4.51 min	483.1733	0



Peak Information

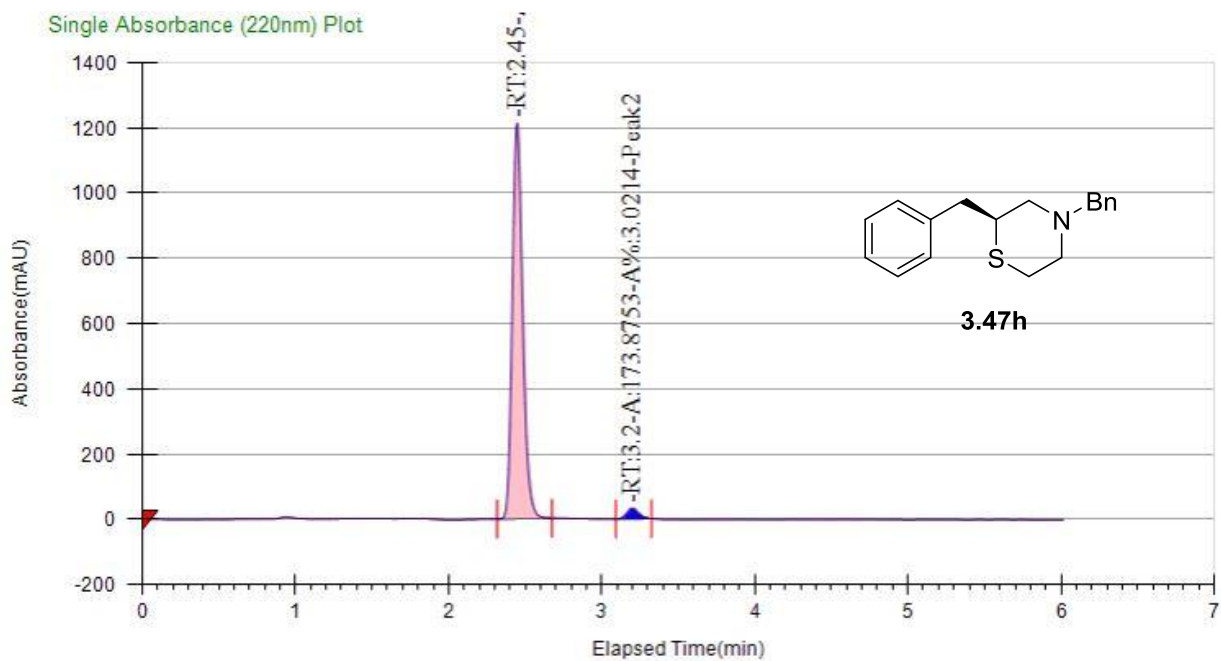
Peak No	% Area	Area	Ret. Time	Height	Cap. Factor
1	18.8401	1957.7613	4.17 min	434.9075	0
2	81.1599	8433.6981	4.45 min	1396.5819	0

Chiral SFC Traces for Thiomorpholines 3.47h and 3.48h



Peak Information

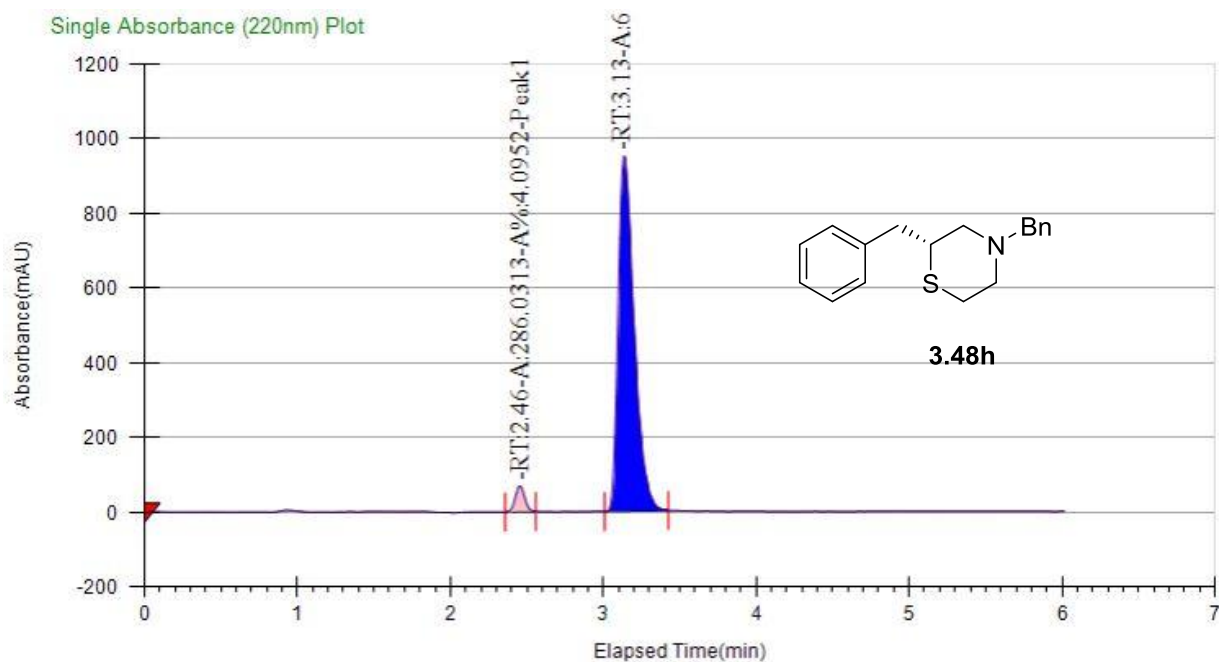
Peak No	% Area	Area	Ret. Time	Height	Cap. Factor
1	48.8512	5996.0354	2.45 min	1312.8927	0
2	51.1488	6278.0354	3.16 min	920.1496	0



Peak Information

Peak No	% Area	Area	Ret. Time	Height	Cap. Factor
1	96.9786	5580.9466	2.45 min	1214.0258	0
2	3.0214	173.8753	3.2 min	32.6525	0

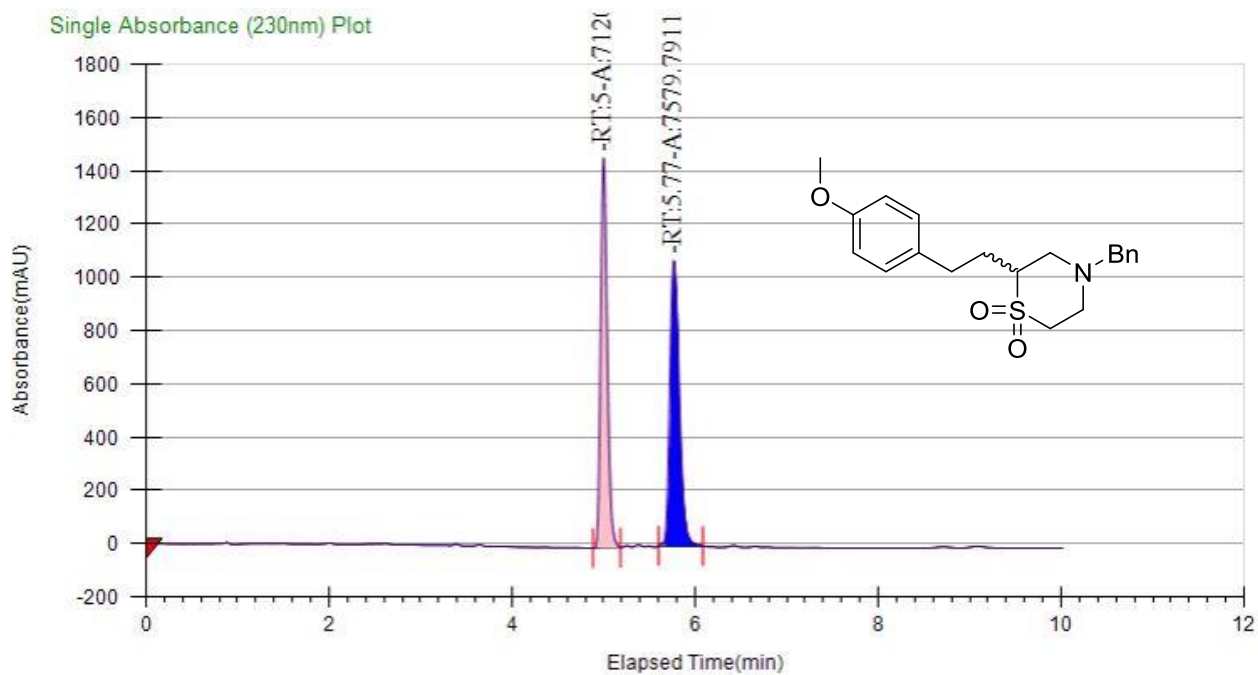
Single Absorbance (220nm) Plot



Peak Information

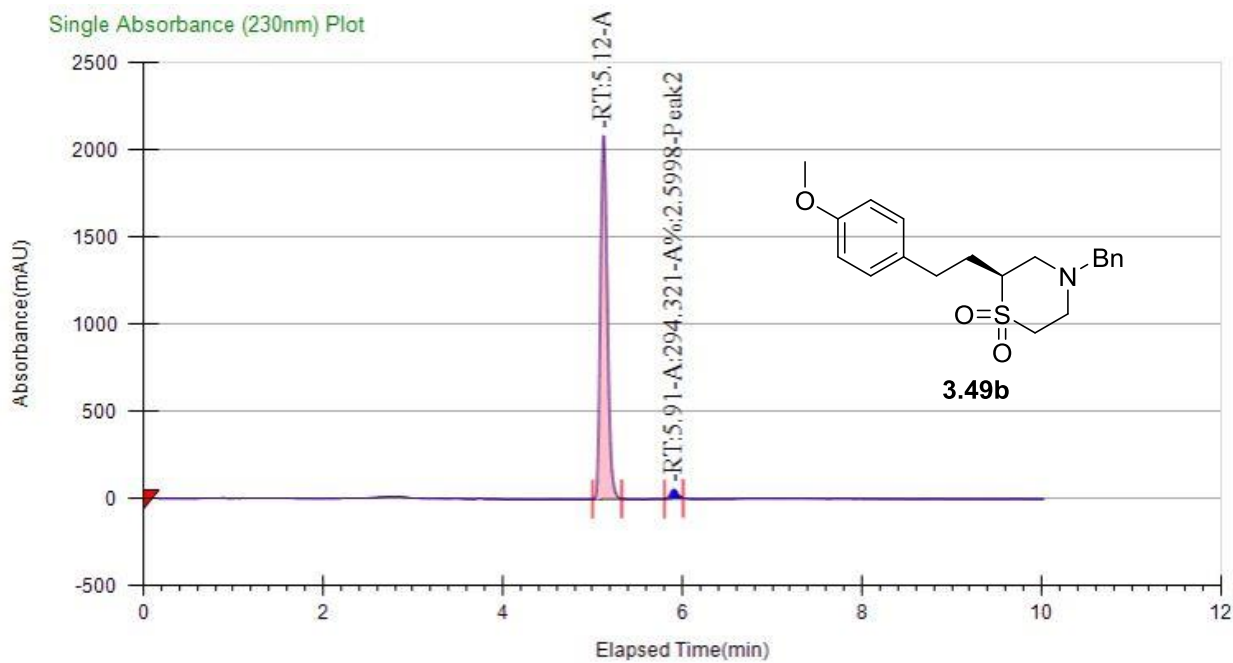
Peak No	% Area	Area	Ret. Time	Height	Cap. Factor
1	4.0952	286.0313	2.46 min	69.0589	0
2	95.9048	6698.5807	3.13 min	951.1033	0

Chiral SFC Traces for Thiomorpholine 1,1-dioxide 3.49b



Peak Information

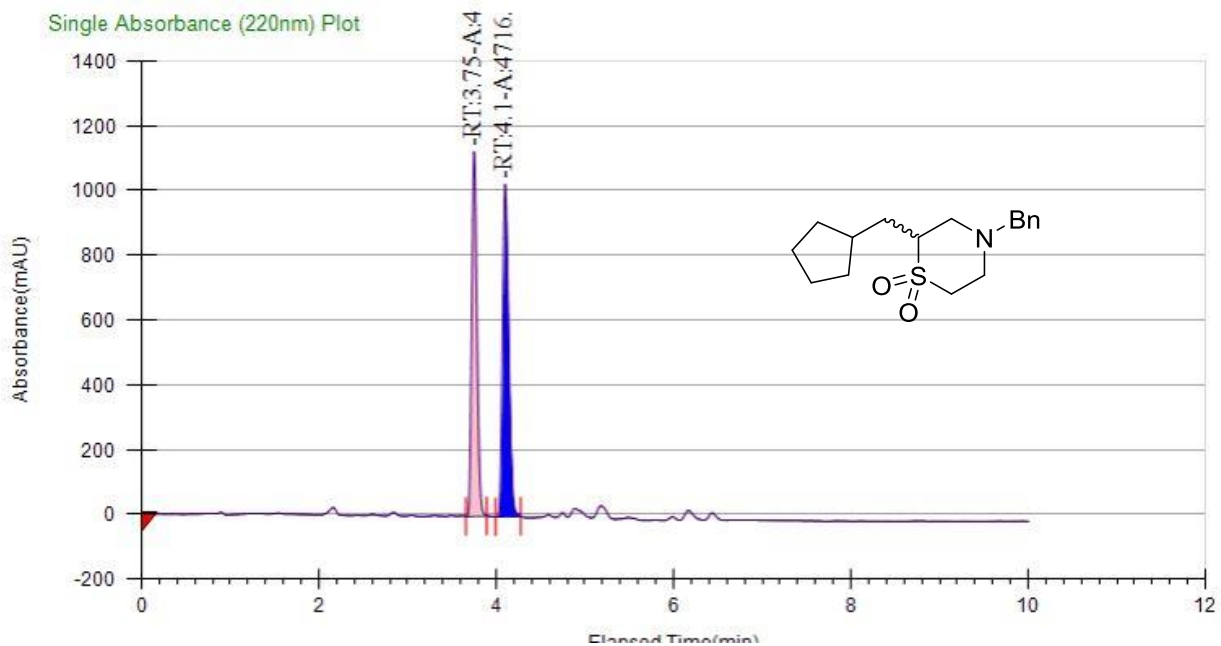
Peak No	% Area	Area	Ret. Time	Height	Cap. Factor
1	48.4384	7120.6653	5 min	1462.9986	4998.9333
2	51.5616	7579.7911	5.77 min	1071.18	5765.5833



Peak Information

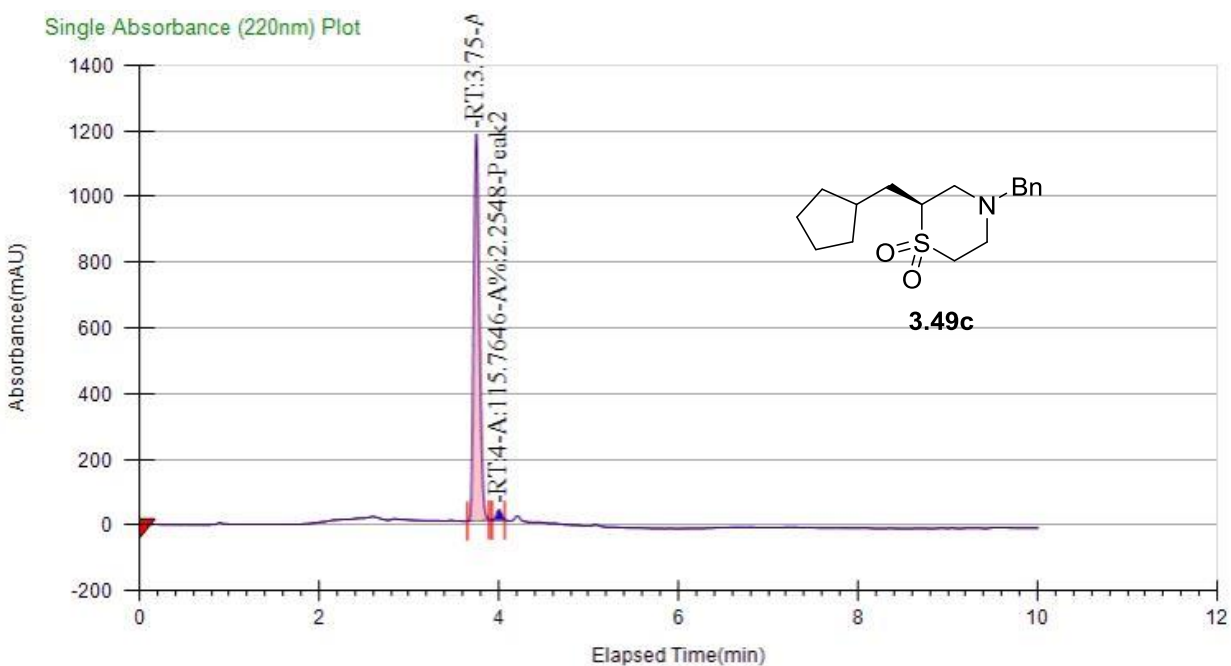
Peak No	% Area	Area	Ret. Time	Height	Cap. Factor
1	97.4002	11026.700 3	5.12 min	2085.4013	0
2	2.5998	294.321	5.91 min	54.1511	0

Chiral SFC Traces for Thiomorpholine 1,1-dioxide 3.49c



Peak Information

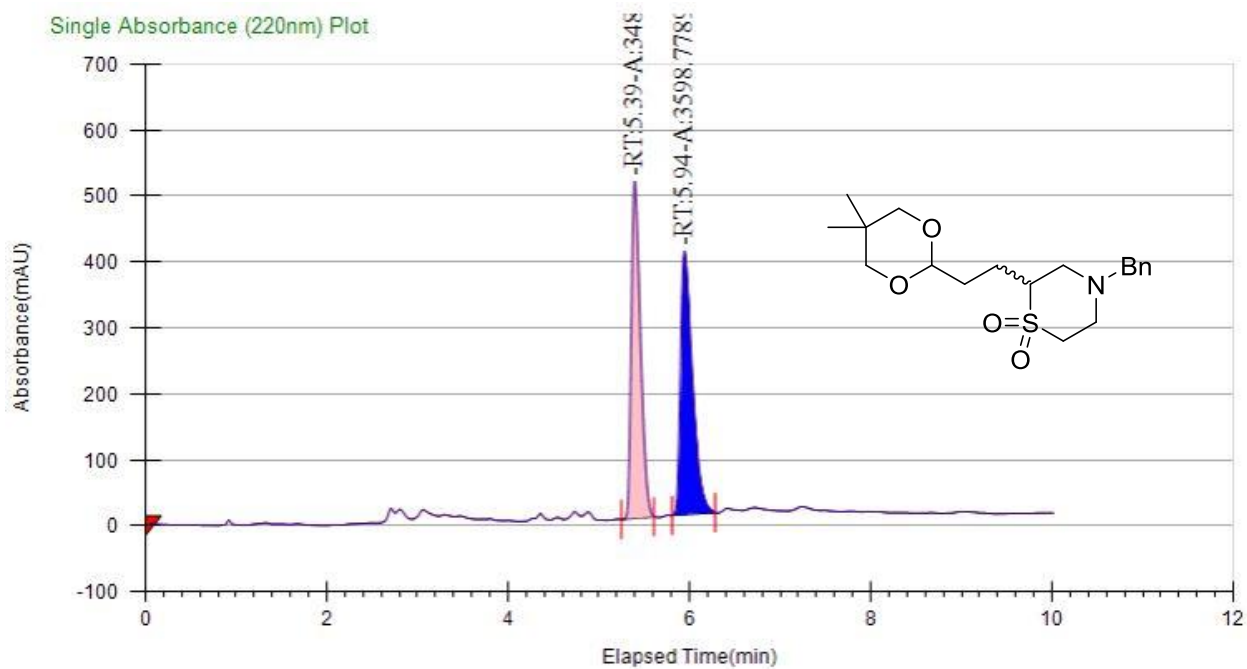
Peak No	% Area	Area	Ret. Time	Height	Cap. Factor
1	48.4615	4434.4859	3.75 min	1126.7358	3748.95
2	51.5385	4716.0533	4.1 min	1027.0817	4098.95



Peak Information

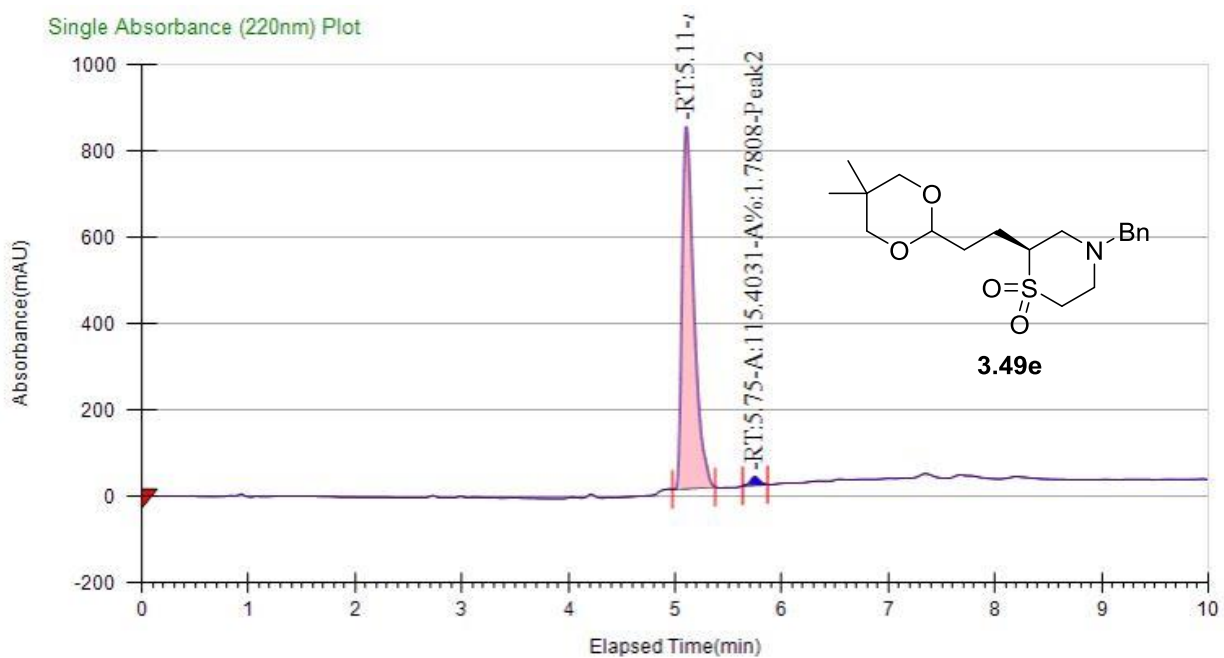
Peak No	% Area	Area	Ret. Time	Height	Cap. Factor
1	97.7452	5018.3273	3.75 min	1177.218	0
2	2.2548	115.7646	4 min	31.76	0

Chiral SFC Traces for Thiomorpholine 1,1-dioxide 3.49e



Peak Information

Peak No	% Area	Area	Ret. Time	Height	Cap. Factor
1	49.1969	3484.9924	5.39 min	510.8115	5390.5833
2	50.8031	3598.7789	5.94 min	399.9314	5940.5833



Peak Information

Peak No	% Area	Area	Ret. Time	Height	Cap. Factor
1	98.2192	6365.0898	5.11 min	838.5974	0
2	1.7808	115.4031	5.75 min	19.7947	0

CHAPTER IV

TOTAL SYNTHESIS OF NATURAL (-)- AND UNNATURAL (+)-MELEARORIDE A

Background and Introduction

Importance of Natural Products

The increasing demand for new pharmaceuticals has placed a significant challenge on both synthetic and medicinal chemists. The demand for novel drug chemotypes is important as the amount of evolutionary resistant organisms and adaptive cellular mechanisms are rising at an alarming rate.¹ Natural products provide novel chemotypes and scaffolds with structural diversity and biological pre-validation, and possess underutilized therapeutic potential.² The recent advances in natural product isolation and chemical biology techniques have allowed for easier access to complex natural products.³ Indeed, secondary metabolites isolated from both terrestrial and marine species are the targets of modern total synthesis campaigns due to their interesting biological activity and potential therapeutic utilization.⁴

Nevertheless, the unique pharmacophores presented by natural products have been exploited since early, traditional medicine.⁵⁻⁸ As early as the 4th century B.C., Hippocrates was the first to demonstrate that chewing on the leaves and the bark of willow trees resulted in pain relief for women in the process of childbirth. Much later, the active metabolite responsible for these analgesic effects would be identified as salicylic

acid.⁶ Additional therapeutic agents which have also shown their roots in early, traditional medicine include anticancer, antibiotic, antimalarial, hypolipidemic, anti-inflammatory, and CNS drugs such as taxol (4.1), penicillin G (4.2), lovastatin (4.3), morphine (4.4), colchicine (4.5), and artemisinin (4.6) (Figure 4.1).⁹⁻¹⁴

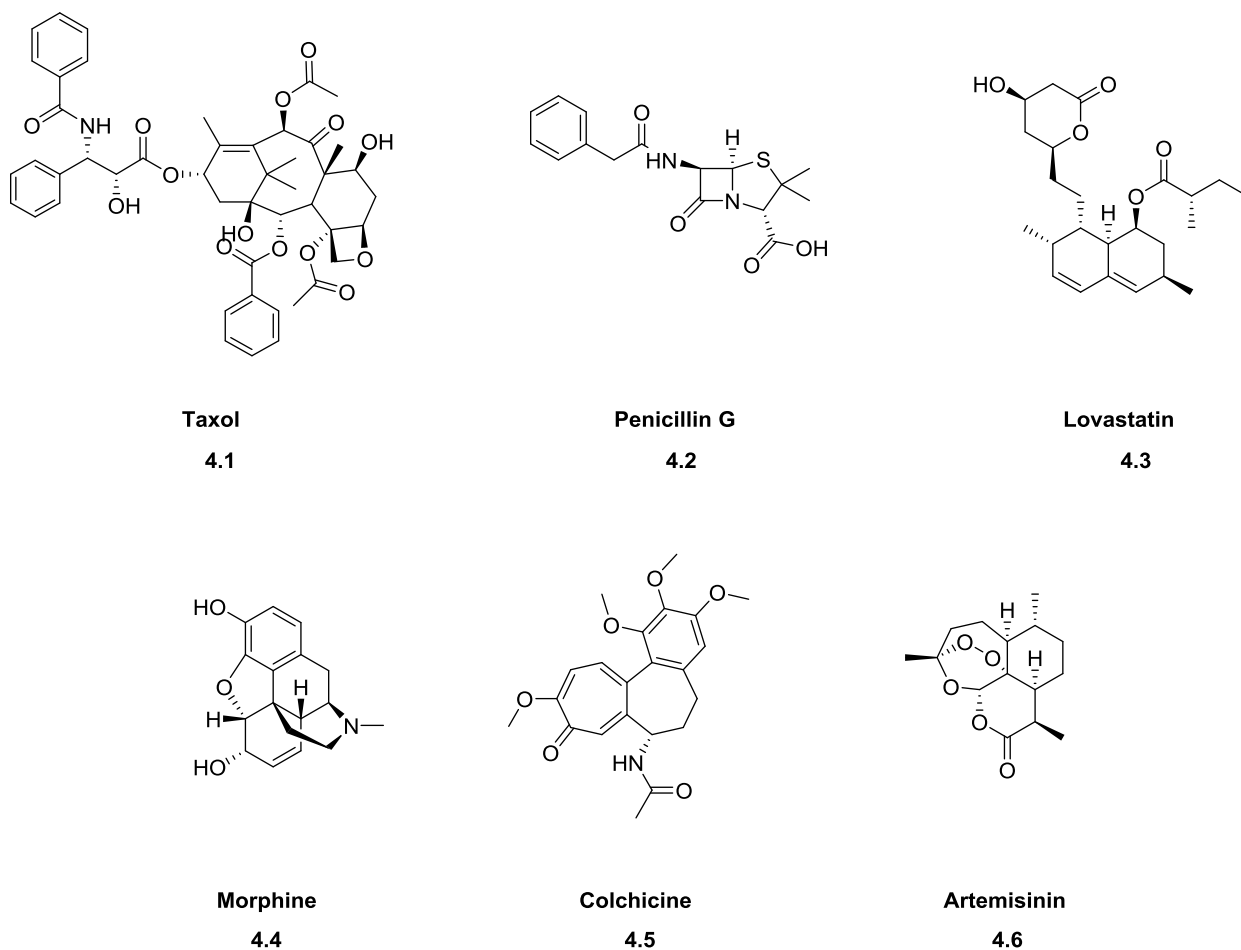


Figure 4.1: Representative natural product therapeutic agents 4.1-4.6

However, the introduction and use of natural products as therapeutic agents is not without its pitfalls. The advent of high-throughput screening technology and the simplicity associated with small molecule combinatorial chemistry has enabled scientists to screen large libraries of small molecules within a large, diverse chemical space.¹⁵⁻¹⁶ In comparison, the longer synthetic routes needed to access complex natural products

hinders the rate of production and diversification of such analogs. As a result, structurally-simpler small molecule drug development has become more popular. 35% of the FDA-approved drugs from 1981-2014 were derived from small molecules, while only 6% of the approved drugs were unmodified natural products.¹⁷⁻¹⁸ Additionally, natural products are often plagued with unfavorable ADMET (absorption, distribution, metabolism, excretion, and toxicity) properties, low solubility, and low oral bioavailability, which preclude their use in a pharmaceutical context.¹⁹

Nevertheless, this does not mean that natural product scaffolds are without merit. From 1981-2014, 59% of the FDA-approved drugs were small molecules which either contained pharmacophores of natural products or were small molecules derived from a structural simplification strategy.¹⁷⁻¹⁹ The structural simplification of natural products is perhaps the most important strategy for bypassing the inherent limitations of natural products (such as poor drug-like properties) and increasing the success rate of natural product drug development.¹⁹⁻²² This strategy can be exemplified through the HMG-CoA reductase inhibitor class of drugs. The hypolipidemic natural product lovastatin (**4.3**), isolated from *Aspergillus terreus*, was found to have undesirable *in vitro* pharmacokinetic (PK) properties; therefore, medicinal chemistry techniques were used to optimize these PK properties and to simplify the complexity of the natural product. As a result, atorvastatin (Lipitor®) (**4.7**) was discovered and is the most prescribed drug in the statin family (**Figure 4.2**).¹¹ Given the importance of natural product scaffolds within the drug discovery and development process, future effort still needs to be devoted to the both the isolation and synthesis of these natural products in order to gain a better understanding on their biological properties.

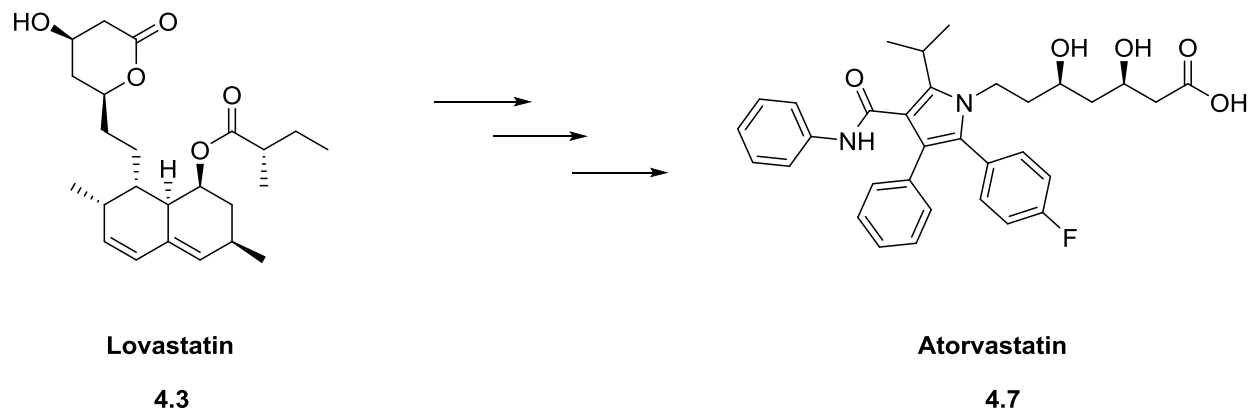


Figure 4.2: Structural simplification of the natural product lovastatin (**4.3**) leads to atorvastatin (**4.7**).

Isolation and Biological Activity of Melearoride A (4.8a)

In 2016, Koyama and coworkers reported on the isolation of two novel 13-membered macrolides (-)-Melearoride A (**4.8a**) and (-)-Melearoride B (**4.9**) from the marine fungus *Penicillium melearinum* var. *viridiflavum* (**Figure 4.3**).²³ These macrolides are structurally similar to the related family of natural products PF1163A (**4.10**), PF1163B (**4.11**), PF1163D (**4.12**), PF1163H (**4.13**), and PF1163F (**4.14**) (**Figure 4.3**). Both **4.10** and **4.11** were originally isolated in 1999 and found to inhibit ergosterol biosynthesis in *Saccharomyces cerevisiae*.²⁴⁻²⁶ Additional mechanistic studies have shown that **4.10** and **4.11** inhibit a different enzyme (C-4 sterol methyl oxidase) in the ergosterol biosynthetic pathway when compared to the azole class of antifungal drugs (such as fluconazole), which inhibit lanosterol 14 α -demethylase.²⁶⁻²⁷ Armed with this data involving related analogs **4.10** and **4.11**, Koyama and coworkers were curious to see if the newly discovered compound **4.8a** would show synergistic activity with fluconazole against azole-resistant strains of fungi. To their delight, they found that

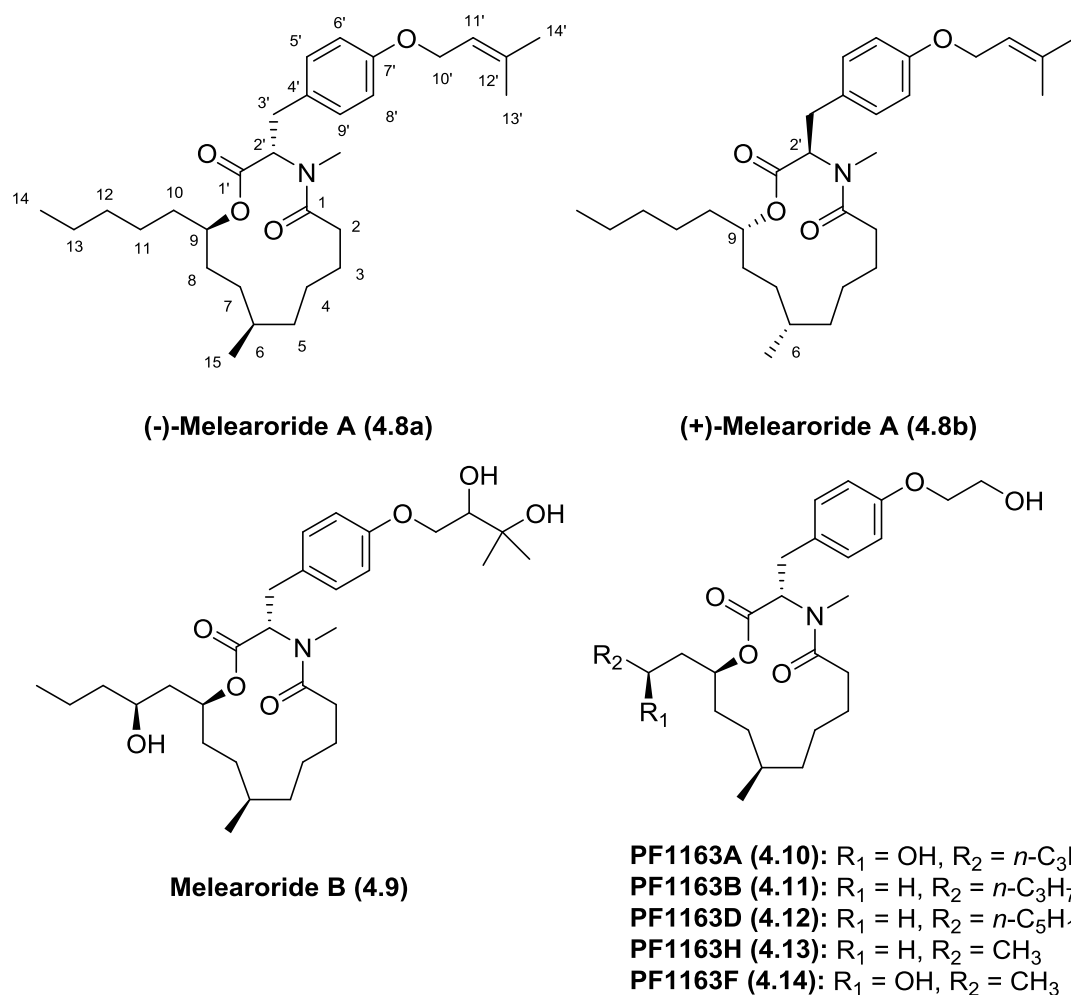


Figure 4.3: Structures of (-)-Melearoride A (**4.8a**), (+)-Melearoride A (**4.8b**), (-)-Melearoride B (**4.9**), and the PF1163 Family of Related Natural Products (**4.10-4.14**)

administration of **4.8a** in combination with fluconazole was effective at inhibiting the growth of azole-resistant *Candida albicans* ($\text{MIC}_{\text{combination}} = 1 \mu\text{g/mL}$ and $\text{FIC}_A = 0.031$).²³

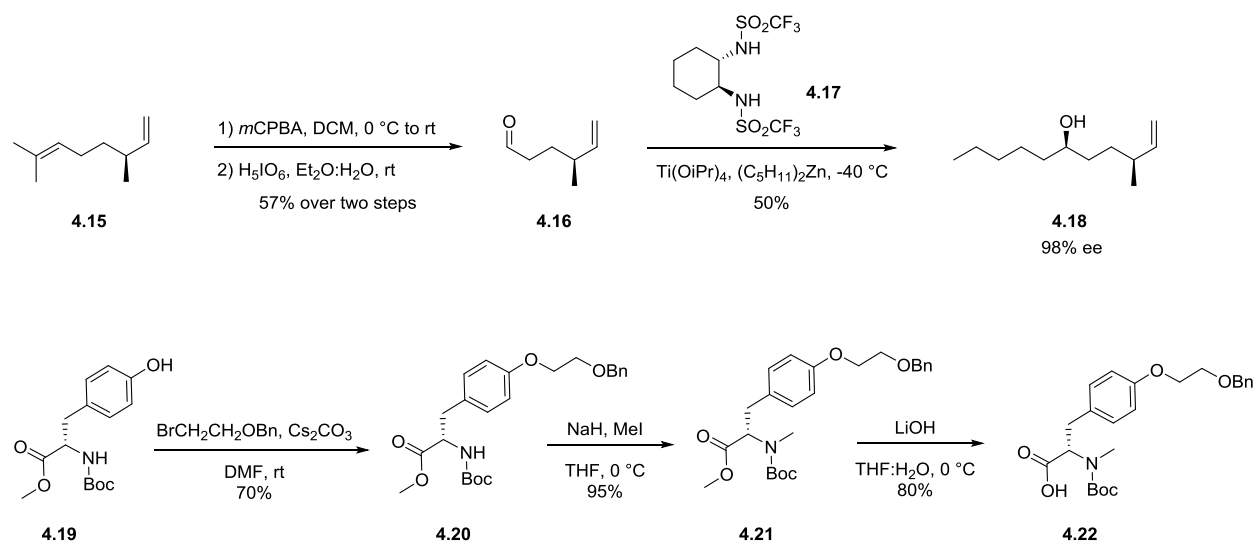
These data are important because the rate of antimycotic resistance is increasing at an exponential rate.²⁸ The azole class of drugs has been used as the primary line of defense for both superficial and deep-seated fungal infections, but the emergence of azole-resistant fungal strains has complicated treating these infections, especially for immuno-compromised patients.²⁸ Therefore, we hope that by accomplishing the total

synthesis of **4.8a** and analogs thereof, we can begin to gain a better understanding of the minimum pharmacophore needed for activity and to also delve into antifungal SAR.

Synthesis of PF1163B (**4.11**): A Related Natural Product

Although multiple syntheses have been reported for both PF1163A (**4.10**) and PF1163B (**4.11**),²⁹⁻³² the synthesis of **4.11** reported by Gesson and coworkers is perhaps the most straightforward route.³³ This synthesis relies on the formation of key intermediates **4.18** and **4.22** (Scheme 4.1).

Starting with commercially available (*S*)-citronellene **4.15**, regioselective epoxidation of the tri-substituted olefin was accomplished via the reaction with *meta*-chloroperoxybenzoic acid (*m*CPBA). Acidic hydrolysis followed by oxidative cleavage of the resulting 1,2-diol via treatment with periodic acid yielded aldehyde **4.16** in reasonable yield (57% over this two-step sequence). Following the precedent of Kobayashi and Knochel, reaction of disulfonamide organocatalyst **4.17** with Ti(O*i*Pr)₄ yielded a chiral titanium Lewis acid which enabled the diastereoselective addition of

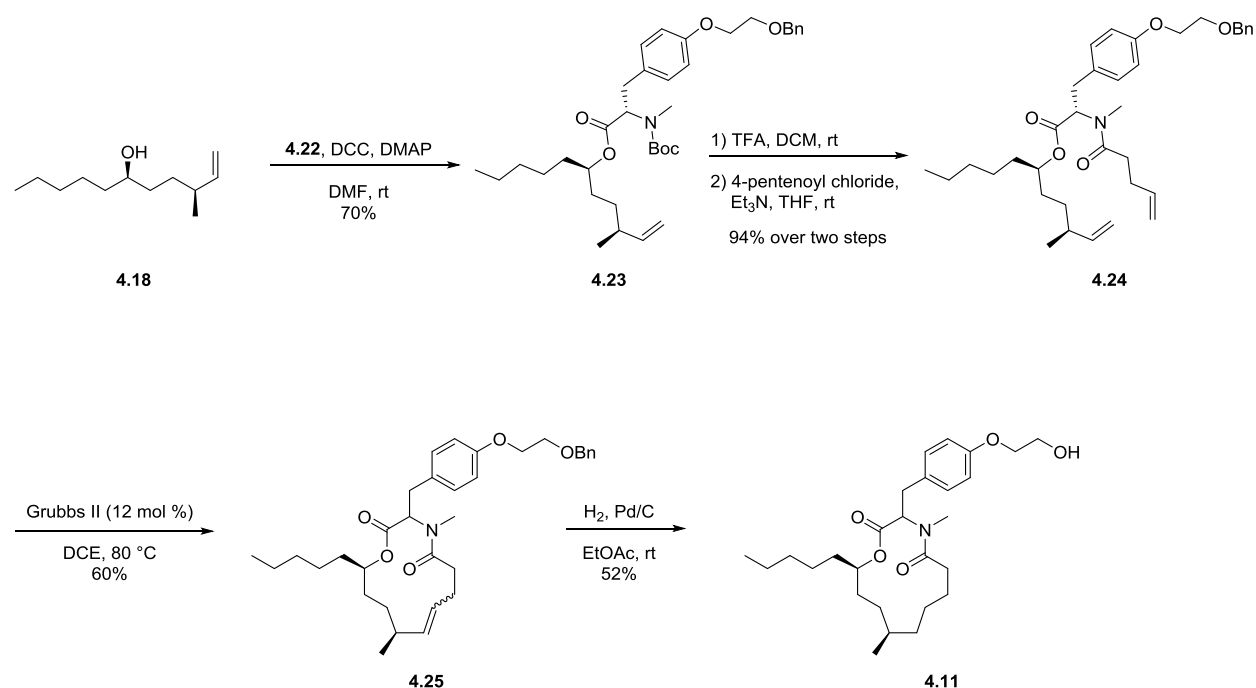


Scheme 4.1: Gesson and coworker's synthetic approach to versatile intermediates **4.18** and **4.22**

dipentyl zinc to aldehyde **4.16** to form alcohol **4.18** (50% yield with 98% ee).³⁴⁻³⁵

Additionally, the phenol functional group of *N*-Boc-L-tyrosine methyl ester **4.19** was chemoselectively alkylated with benzyl 2-bromoethyl ether using cesium carbonate in DMF to form methyl ester **4.20**. *N*-alkylation using sodium hydride and methyl iodide yielded **4.21**, which was hydrolyzed to the requisite carboxylic acid **4.22** under mild conditions (lithium hydroxide in THF:H₂O at 0 °C) in 76% yield over two-steps without significant racemization.³³

With intermediates **4.18** and **4.22** in hand, Gesson and coworkers were ready to proceed with their final synthetic operations (**Scheme 4.2**). Steglich esterification of alcohol **4.18** with carboxylic acid **4.22** using DCC and DMAP resulted in the formation of ester **4.23** in 70% yield. Boc-deprotection of **4.23** followed by reaction with 4-pentenoyl chloride and triethylamine yielded amide **4.24**. To form the desired 13-membered



Scheme 4.2: Endgame strategy utilized by Gesson and coworkers to synthesize PF1163B (**4.11**)

macrocyclic ring, a ring-closing metathesis reaction was then utilized. Treatment of amide **4.24** with Grubbs II catalyst in refluxing DCE resulted in the formation of the desired macrocycle **4.25** as a mixture of *E*- and *Z*-olefin isomers in moderate yield (60%). Hydrogenation of **4.25** resulted in reduction of the olefin and concomitant removal of the benzyl protecting group to afford PF1163B (**4.11**) in 11 total synthetic steps with a 3.1% overall yield.³³

Necessity of a Novel, Modular Synthetic Approach for Accessing Additional Analogs of This Family of Natural Products

By analysis of the first-generation synthetic approaches to PF1163A (**4.10**) and PF1163B (**4.11**), their success depends upon the use of diastereoselective additions into advanced aldehyde or lactal intermediates, or Sharpless kinetic resolution techniques to set the C9 stereocenter (using the numbering scheme introduced in **Figure 4.3**).²⁹⁻³³ While the diastereoselective nature of these transformations is a powerful tool for setting the requisite stereocenters of the parent target molecules, it can hinder additional analog development for analyzing structure-activity relationships (SAR). For example, in the case of Gesson's synthesis, the *cis*-stereochemical relationship between the newly formed alcohol functional group and the chiral methyl group of **4.18** impedes the formation of diastereomers of **4.18**. Additionally, given that the starting material is (*S*)-citronellene **4.15**, there are no opportunities for the incorporation of additional functional groups into the core of the target molecule.³³ Therefore, given the absence of strategies for analog development in the present syntheses and the fact that natural (-)-Melearoride A (**4.8a**) has yet to be synthesized, we set out to develop a modular synthesis strategy for accessing **4.8a** that would be

amenable for analog development. In doing so, additional antimycotic SAR can be explored against azole-resistant fungal strains.

Materials and Methods

General Synthetic Methods and Instrumentation

Unless otherwise stated, all reactions were conducted in flame-dried or oven-dried glassware under inert atmospheres of argon. All commercially available reagents and reaction solvents were used as received, unless otherwise noted. All NMR spectra were recorded on a 400 MHz AMX Bruker NMR spectrometer. ^1H and ^{13}C chemical shifts are reported in δ values in ppm downfield with the deuterated solvent as the internal standard. Data are reported as follows: chemical shift, multiplicity (s = singlet, d = doublet, t = triplet, q = quartet, b = broad, m = multiplet), integration, coupling constant (Hz). Low resolution mass spectra were obtained on an Agilent 6120 or 6150 with ESI source. MS parameters were as follows: fragmentor: 70, capillary voltage: 3000 V, nebulizer pressure: 30 psig, drying gas flow: 13 L/min, drying gas temperature: 350 °C. Samples were introduced via an Agilent 1290 UHPLC comprised of a G4220A binary pump, G4226A ALS, G1316C TCC, and G4212A DAD with ULD flow cell. UV absorption was generally observed at 215 nm and 254 nm with a 4 nm bandwidth. Column: Waters Acquity BEH C18, 1.0 x 50 mm, 1.7 μm . Gradient conditions: 5% to 95% CH_3CN in H_2O (0.1% TFA) over 1.4 min, hold at 95% CH_3CN for 0.1 min, 0.5 mL/min, 55 °C. High resolution mass spectra were obtained on an Agilent 6540 UHD Q-TOF with ESI source. MS parameters were as follows: fragmentor: 150, capillary

voltage: 3500 V, nebulizer pressure: 60 psig, drying gas flow: 13 L/min, drying gas temperature: 275 °C. Samples were introduced via an Agilent 1200 UHPLC comprised of a G4220A binary pump, G4226A ALS, G1316C TCC, and G4212A DAD with ULD flow cell. UV absorption was observed at 215 nm and 254 nm with a 4 nm bandwidth. Column: Agilent Zorbax Extend C18, 1.8 μm , 2.1 x 50 mm. Gradient conditions: 5% to 95% CH_3CN in H_2O (0.1% formic acid) over 1 min, hold at 95% CH_3CN for 0.1 min, 0.5 mL/min, 40 °C. For compounds that were purified on a Gilson preparative reversed-phase HPLC, the system comprised of a 333 aqueous pump with solvent-selection valve, 334 organic pump, GX-271 or GX-281 liquid handler, two column switching valves, and a 155 UV detector. UV wavelength for fraction collection was user-defined, with absorbance at 254 nm always monitored. Method 1: Phenomenex Axiapacked Luna C18, 30 x 50 mm, 5 μm column. Mobile phase: CH_3CN in H_2O (0.1% TFA). Gradient conditions: 0.75 min equilibration, followed by user defined gradient (starting organic percentage, ending S3 organic percentage, duration), hold at 95% CH_3CN in H_2O (0.1% TFA) for 1 min, 50 mL/min, 23 °C. Method 2: Phenomenex Axia-packed Gemini C18, 50 x 250 mm, 10 μm column. Mobile phase: CH_3CN in H_2O (0.1% TFA). Gradient conditions: 7 min equilibration, followed by user defined gradient (starting organic percentage, ending organic percentage, duration), hold at 95% CH_3CN in H_2O (0.1% TFA) for 7 min, 120 mL/min, 23 °C. All reagents were purchased from Aldrich Chemical Co. and were used without purification. Sure-Seal solvents were purchased from Sigma Aldrich. Analytical thin layer chromatography was performed on 250 μM silica gel 60 F₂₅₄ plates. Visualization was accomplished with UV light, and/or the use of potassium permanganate or Seebach stain followed by development with a heat gun.

Total Synthesis of Natural (-)- and Unnatural (+)-Melearoride A

Retrosynthetic Analysis for **4.8a** and **4.8b**

Our retrosynthetic approach for accessing natural (-)-Melearoride A (**4.8a**) is depicted in **Figure 4.4**.³⁶ We propose that the synthesis of **4.8a** can be achieved through the use of five key fragments (**4.26a**, **4.27**, **4.28**, **4.29a**, and **4.30a**) which are either commercially available or are readily accessible using chiral pool starting materials. The key features of this modular synthetic approach include an Evans asymmetric alkylation, the opening of a chiral epoxide using functionalized higher order cyanocuprates, ring-closing metathesis similar to that of Gesson³³ to access the desired 13-membered macrocyclic core, and late-stage O-alkylation using Mitsunobu conditions.³⁶

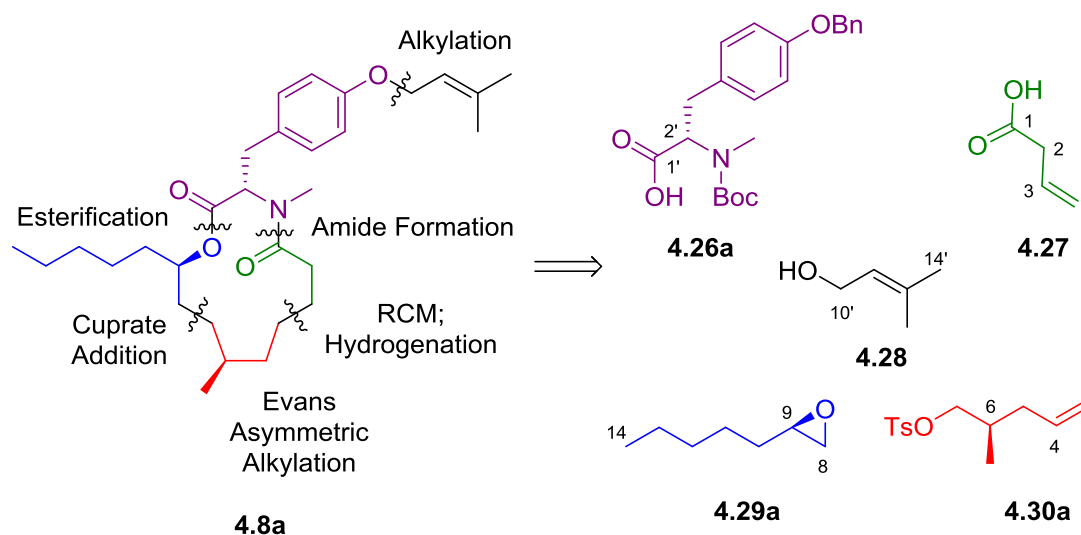


Figure 4.4: Retrosynthetic analysis for natural (-)-Melearoride A **4.8a**

It is interesting to note that none of the previous syntheses for PF1163B **4.11** have made an attempt to synthesize the unnatural enantiomer.³³ From a SAR perspective, the inclusion of the unnatural enantiomer for analog testing is important, as

these unnatural analogs often display superior bioactivity when compared to their natural counterparts.³⁷⁻³⁸ Therefore, to show the utility of our modular synthetic strategy, we also wanted to synthesize unnatural (+)-Melearoride A **4.8b**, which can be accessed using the enantiomers of the chiral building blocks (**4.26b**, **4.29b**, and **4.30b**) (Figure 4.5).

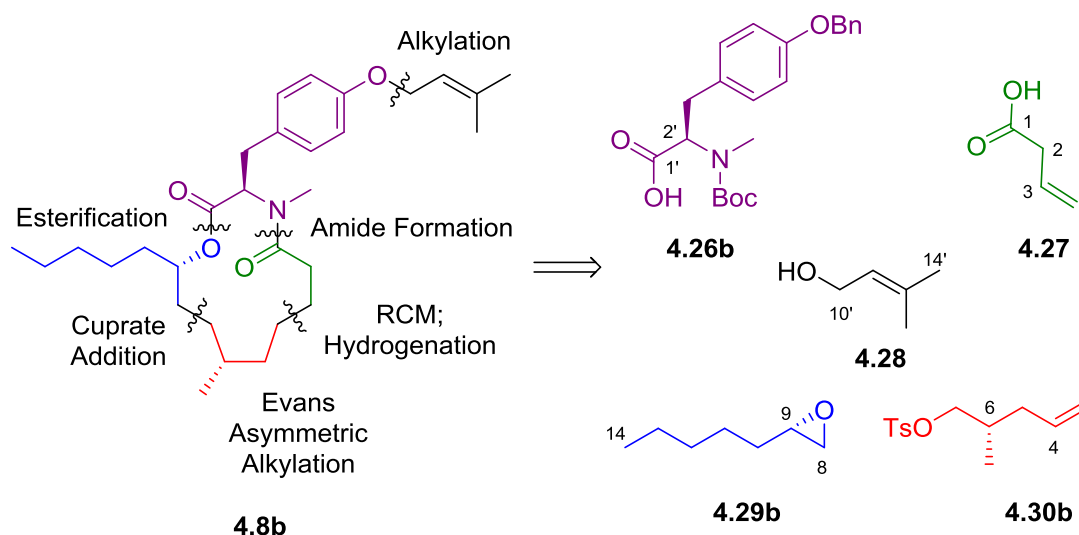
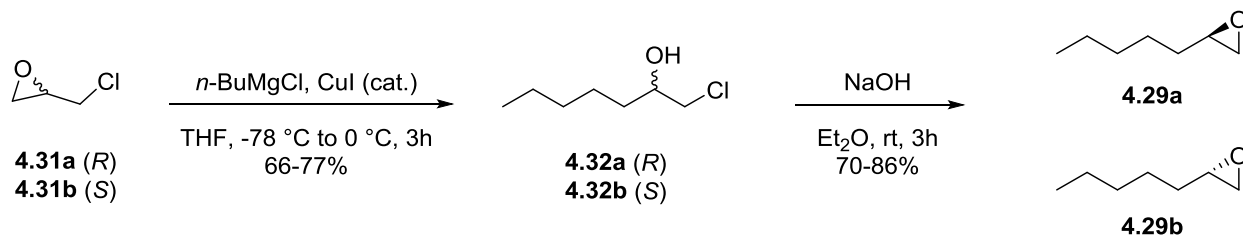


Figure 4.5: Retrosynthetic analysis for unnatural (+)-Melearoride A **4.8b**

Synthesis of Chiral Epoxides **4.29a** and **4.29b**

The synthesis of our chiral epoxide intermediates **4.29a** and **4.29b** was accomplished as shown in **Scheme 4.3**. (*R*)-epichlorohydrin **4.31a** and (*S*)-epichlorohydrin **4.31b** were treated with *n*-butylmagnesium chloride and catalytic copper(I) iodide to afford β -chloro alcohols **4.32a** and **4.32b**, respectively in good yield

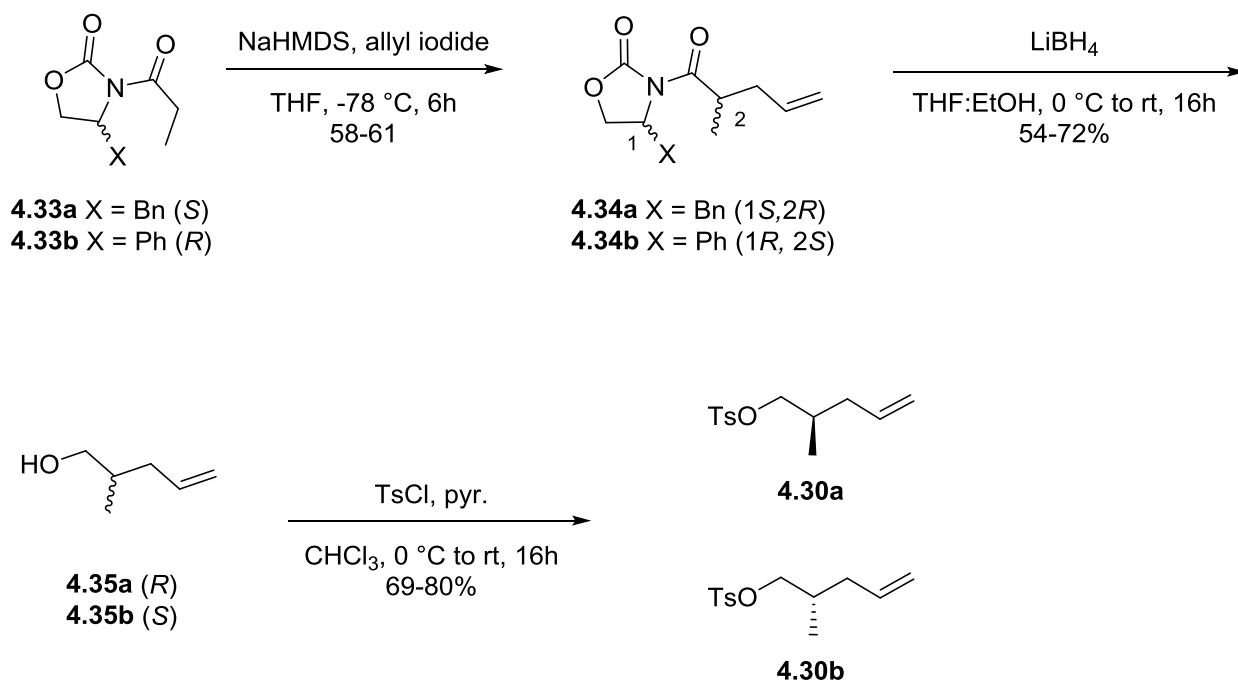


Scheme 4.3: Synthesis of chiral epoxides **4.29a** and **4.29b**

(66-77%). Reaction of β -chloro alcohols **4.32a** and **4.32b** with sodium hydroxide in diethyl ether resulted in an intramolecular cyclization to form chiral epoxide intermediates **4.29a** and **4.29b**, respectively in 70-86% yield.³⁹⁻⁴⁰

Synthesis of Chiral Tosylates **4.30a** and **4.30b**

The requisite chiral tosylate intermediates **4.30a** and **4.30b** were synthesized as shown in **Scheme 4.4**. Acylated oxazolidinones **4.33a** and **4.33b** were deprotonated with sodium hexamethyldisilazide (NaHMDS), and the corresponding sodium enolates were reacted with allyl iodide at -78 °C to afford the expected Evans asymmetric alkylation products **4.34a** and **4.34b** in 58-61% yield. Lithium borohydride reduction of these oxazolidinones yielded chiral alcohols **4.35a** and **4.35b**, which were subsequently treated with *p*-toluenesulfonyl chloride and pyridine to form the corresponding chiral tosylates **4.30a** and **4.30b**, respectively in 37-57% yield over a two-step sequence.⁴¹⁻⁴²

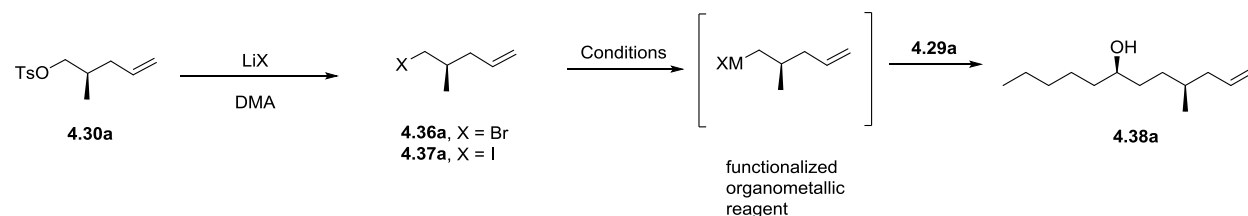


Scheme 4.4: Synthesis of chiral tosylates **4.30a** and **4.30b**

Optimizing the Formation of Alcohol **4.38a**

With requisite chiral intermediates **4.29a-b** and **4.30a-b** in hand, we needed to establish a method for uniting these fragments together to form the crucial C7-C8 bond (**Figure 4.3**). We envisioned that a S_N2 reaction between chiral tosylate **4.30a** and an appropriate metal halide salt would result in the formation of chiral alkyl halides (**4.36a** or **4.37a**). These alkyl halides would then serve as viable precursors for the formation of functionalized organometallic reagents, which could then react with epoxide **4.29a** to afford alcohol **4.38a**. Therefore, we chose to use **4.29a** and **4.30a** to test various reaction conditions for achieving these chemical transformations, as summarized in

Table 4.1.



Entry	Alkyl Halide	Conditions	Activating Agent or Additive	Results
1	4.36a	Mg turnings, THF, reflux	N/A	No rxn
2	4.36a	Mg turnings, THF, reflux	Dry stirring	No rxn
3	4.36a	Mg turnings, THF, reflux	I ₂ crystal	Wurtz coupling and starting material
4	4.36a	Mg turnings, THF, reflux	DIBAL-H	Wurtz coupling and starting material
5	4.36a	Rieke Mg, THF, 0 °C	N/A	Wurtz coupling and starting material
6	4.37a	Mg turnings, THF, reflux	I ₂ crystal	No rxn
7	4.37a	Mg turnings, THF, reflux	DIBAL-H	No rxn
8	4.37a	Rieke Mg, THF, 0 °C	N/A	Wurtz coupling exclusively
9	4.37a	<i>t</i> -BuLi, THF:Et ₂ O, -78 °C	N/A	Mixture of epoxide opening products
10	4.37a	<i>t</i> -BuLi, THF:Et ₂ O, -78 °C to rt	lithium 2-thienylcyanocuprate	56% isolated yield of desired 4.38a

Table 4.1: Optimization of our synthetic route en route to alcohol **4.38a**

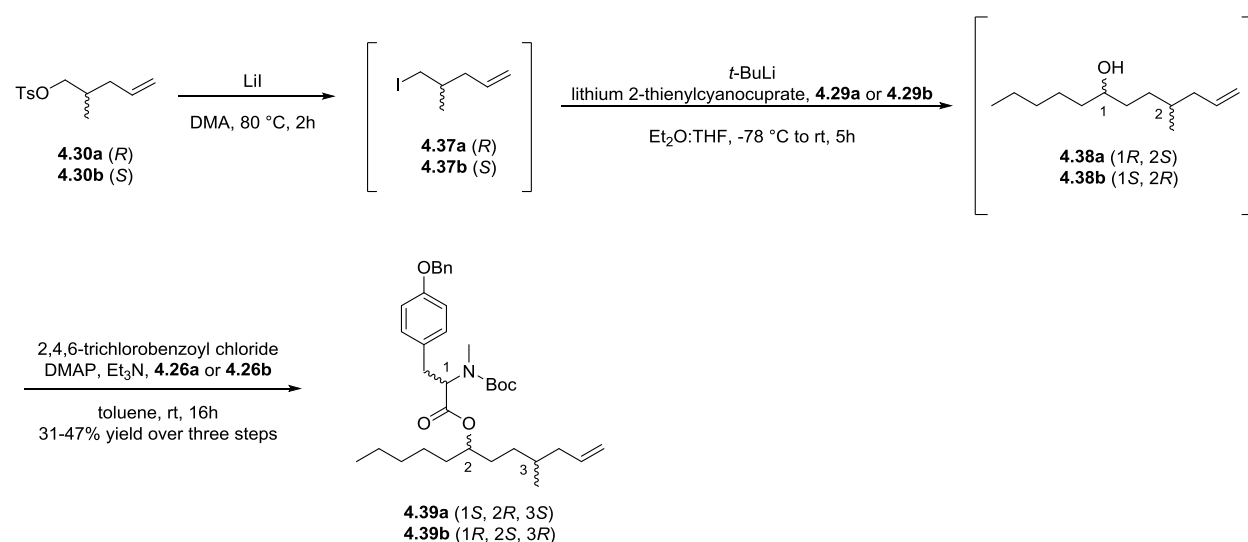
As seen in Table 4.1, conversion of **4.30a** to the corresponding alkyl bromide **4.36a** and attempts at forming the functionalized Grignard reagent via treatment with magnesium metal in THF at reflux (entry 1) resulted in no reaction. We initially thought that this lack of reactivity was due to the formation of an unreactive magnesium oxide layer on the metal surface, so the magnesium metal was pretreated with a variety of activating agents in an attempt to obtain a more reactive metal surface (entries 2-4).⁴³⁻⁴⁴ However, these efforts were futile as we either again observed no reaction (entry 2), or we observed significant amounts of the undesired Wurtz coupling product (entries 3-4). We hypothesized that the Wurtz coupling side-product was a result of a slow oxidative addition of the magnesium metal; therefore, we decided to use a more reactive form of magnesium metal (Rieke magnesium) (entry 5). However, we still observed significant amounts of Wurtz coupling at temperatures as low as 0 °C. Next, we tested whether or not the corresponding alkyl iodide **4.37a** would be a more suitable alkyl halide for ameliorating this slow oxidative addition step. However, utilization of **4.37a** under the same battery of conditions as described above (entries 6-8) was unsuccessful at providing access to the desired alcohol **4.38a**.

At this moment, we decided to abandon the strategy of forming the corresponding Grignard reagent in favor for alternative strategies. In particular, we wanted to test the reactivity of an alkyl lithium species derived from alkyl iodide **4.37a**. Therefore, **4.37a** was treated with *t*-BuLi at -78 °C for one hour before the addition of epoxide **4.29a** (entry 9). Crude ¹H NMR analysis indicated formation of a mixture of epoxide opening products. With this result, we were delighted to see that a lithium-halogen exchange reaction using alkyl iodide **4.37a** was possible, and the functionalized

organometallic species was capable of reacting with epoxide **4.29a**. In order to achieve the necessary selectivity of opening epoxide **4.29a** to alcohol **4.38a**, we envisioned that a functionalized higher order organocyanocuprate, as originally reported by Lipshutz and coworkers, would serve as both a reactive and selective reagent for this transformation.⁴⁵ Indeed, treatment of **4.37a** with *t*-BuLi at -78 °C for one hour resulted in a smooth lithium-halogen exchange reaction. Transmetalation of the resulting alkyl lithium reagent with lithium 2-thienylcyano cuprate resulted in the formation of the desired higher order organocuprate reagent which reacted with epoxide **4.29a** to form alcohol **4.38a** in 56% yield (entry 10).

Synthesis of Esters **4.39a** and **4.39b**

With a reliable method for obtaining alcohol **4.38a** in hand, we wanted to test the idea of telescoping these reactions en route to esters **4.39a** (Scheme 4.5). Tosylate **4.30a** was reacted with lithium iodide in DMA to afford alkyl iodide **4.37a**. Following the

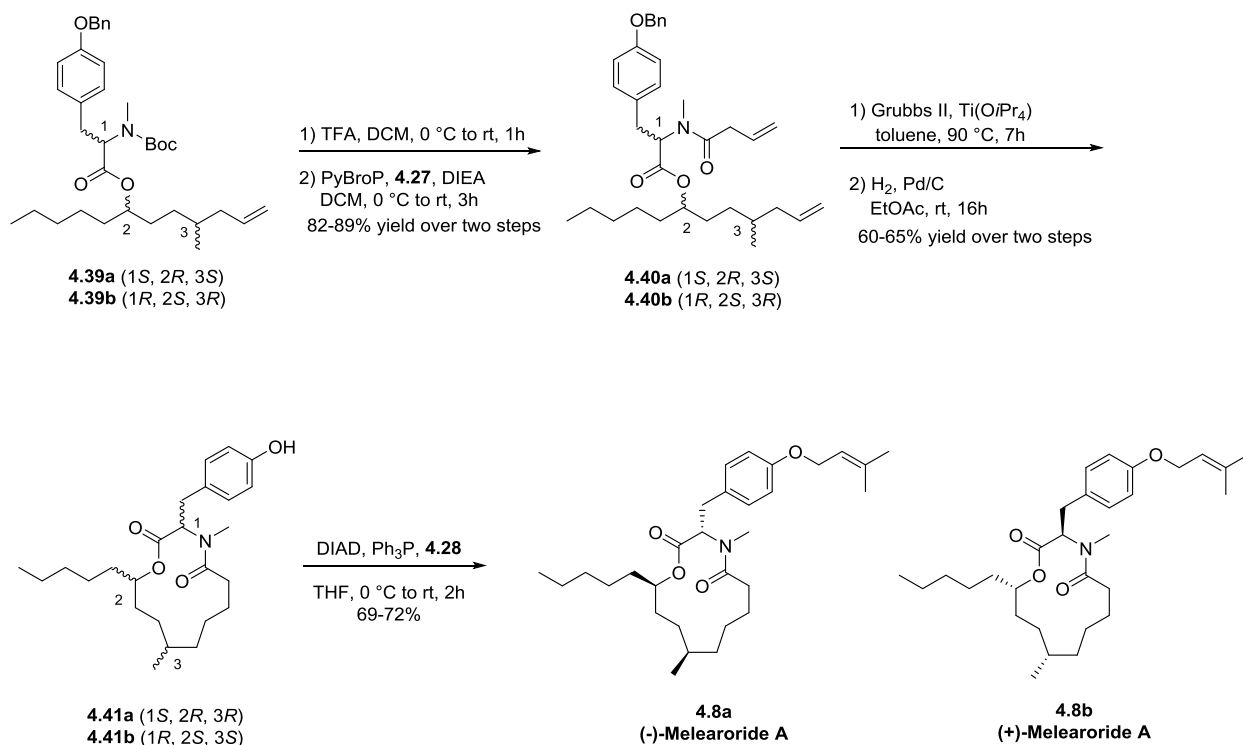


Scheme 4.5: Synthesis of esters **4.39a** and **4.39b**

same lithium-halogen exchange/transmetalation conditions as described above (**Table 4.1**, entry 10), alcohol **4.38a** was obtained, and this crude material was taken forward to the esterification reaction without using flash chromatography for purification. The use of the Steglich esterification conditions as reported by Gesson and coworkers resulted in a mixture of the desired ester **4.39a** with the dicyclohexylurea byproduct.³³ However, we found that crude alcohol **4.38a** can be efficiently transformed into ester **4.39a** via the utilization of Yamaguchi esterification conditions.⁴⁶ This sequence of reaction conditions was also applied to the enantiomeric substrates, resulting in the formation of ester **4.39b** (31-47% yield over this three step sequence).

*Synthesis of Natural (-)-Melearoride A **4.8a** and Unnatural (+)-Melearoride A **4.8b***

To complete our total synthesis, we chose an endgame strategy similar to that of Gesson (**Scheme 4.6**).³³ Boc deprotection of esters **4.39a-b** followed by PyBroP mediated amide coupling of the resulting *N*-Me amine with vinylacetic acid **4.27** resulted in the formation of amides **4.40a-b** in 82-89% yield over the two-step sequence. In order to form the desired 13-membered macrocyclic core, a ring-closing metathesis reaction was employed. However, treatment of amides **4.40a-b** with Grubbs II in toluene at 90 °C resulted in the formation of the desired macrocyclic olefins in low yield (~10%). We hypothesized that the presence of the β,γ -unsaturated amide in **4.40a-b** was the reason for these low yields. As shown in **Figure 4.6**, β,γ -unsaturated amides of this nature have been known to form stable 5-membered chelates **4.42** with RCM catalysts.⁴⁷ Formation of this stable chelated intermediate **4.42** would sequester the catalyst and could be the reason why we were observing low yields for our RCM reaction. Therefore, in order to prevent catalyst chelation, we tried the RCM reaction again using the Lewis acid



Scheme 4.6: Synthesis of natural (-)-Melearoride A **4.8a** and unnatural (+)-Melearoride A **4.8b**

additive Ti(*O*Pr₄).⁴⁸ To our delight, the desired RCM products were obtained in ~72% NMR yield under these Lewis acid assisted RCM reaction conditions. Hydrogenation of these crude products resulted in the formation of phenols **4.41a-b** in 60-65% over two steps. *O*-alkylation of phenols **4.41a-b** was accomplished using alcohol **4.28** under Mitsunobu conditions to afford both natural (-)-Melearoride A **4.8a** and unnatural (+)-Melearoride A **4.8b** in 69-72% yield.³⁶

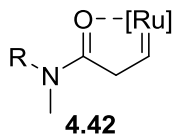


Figure 4.6: Structure of 5-membered chelate **4.42**

Conclusion

In conclusion, we present a novel, modular synthetic approach for synthesizing analogs of either the Melearoride or PF1163 family of natural products. Although the synthesis of some of these natural products have been previously reported, this synthetic approach is more amenable for analog development en route to studying antifungal SAR for azole-resistant fungal strains. To show the utility of this synthetic strategy, the first total synthesis of both natural (-)-Melearoride A **4.8a** and unnatural (+)-Melearoride A **4.8b** was accomplished in 13 total synthetic steps with overall yields of 4.3% and 1.0% respectively.³⁶

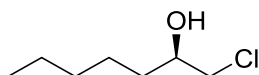
Experimental Methods

General Synthetic Methods and Instrumentation

Unless otherwise stated, all reactions were conducted in flame-dried or oven-dried glassware under inert atmospheres of argon. All commercially available reagents and reaction solvents were used as received, unless otherwise noted. All NMR spectra were recorded on a 400 MHz AMX Bruker NMR spectrometer. ¹H and ¹³C chemical shifts are reported in δ values in ppm downfield with the deuterated solvent as the internal standard. Data are reported as follows: chemical shift, multiplicity (s = singlet, d = doublet, t = triplet, q = quartet, b = broad, m = multiplet), integration, coupling constant (Hz). Low resolution mass spectra were obtained on an Agilent 6120 or 6150 with ESI source. MS parameters were as follows: fragmentor: 70, capillary voltage: 3000 V, nebulizer pressure: 30 psig, drying gas flow: 13 L/min, drying gas temperature: 350 °C. Samples were introduced via an Agilent 1290 UHPLC comprised of a G4220A binary

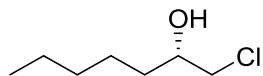
pump, G4226A ALS, G1316C TCC, and G4212A DAD with ULD flow cell. UV absorption was generally observed at 215 nm and 254 nm with a 4 nm bandwidth. Column: Waters Acquity BEH C18, 1.0 x 50 mm, 1.7 μ m. Gradient conditions: 5% to 95% CH₃CN in H₂O (0.1% TFA) over 1.4 min, hold at 95% CH₃CN for 0.1 min, 0.5 mL/min, 55 °C. High resolution mass spectra were obtained on an Agilent 6540 UHD Q-TOF with ESI source. MS parameters were as follows: fragmentor: 150, capillary voltage: 3500 V, nebulizer pressure: 60 psig, drying gas flow: 13 L/min, drying gas temperature: 275 °C. Samples were introduced via an Agilent 1200 UHPLC comprised of a G4220A binary pump, G4226A ALS, G1316C TCC, and G4212A DAD with ULD flow cell. UV absorption was observed at 215 nm and 254 nm with a 4 nm bandwidth. Column: Agilent Zorbax Extend C18, 1.8 μ m, 2.1 x 50 mm. Gradient conditions: 5% to 95% CH₃CN in H₂O (0.1% formic acid) over 1 min, hold at 95% CH₃CN for 0.1 min, 0.5 mL/min, 40 °C. For compounds that were purified on a Gilson preparative reversed-phase HPLC, the system comprised of a 333 aqueous pump with solvent-selection valve, 334 organic pump, GX-271 or GX-281 liquid handler, two column switching valves, and a 155 UV detector. UV wavelength for fraction collection was user-defined, with absorbance at 254 nm always monitored. Method 1: Phenomenex Axiapacked Luna C18, 30 x 50 mm, 5 μ m column. Mobile phase: CH₃CN in H₂O (0.1% TFA). Gradient conditions: 0.75 min equilibration, followed by user defined gradient (starting organic percentage, ending S3 organic percentage, duration), hold at 95% CH₃CN in H₂O (0.1% TFA) for 1 min, 50 mL/min, 23 °C. Method 2: Phenomenex Axia-packed Gemini C18, 50 x 250 mm, 10 μ m column. Mobile phase: CH₃CN in H₂O (0.1% TFA). Gradient conditions: 7 min equilibration, followed by user defined gradient (starting

organic percentage, ending organic percentage, duration), hold at 95% CH₃CN in H₂O (0.1% TFA) for 7 min, 120 mL/min, 23 °C. All reagents were purchased from Aldrich Chemical Co. and were used without purification. Sure-Seal solvents were purchased from Sigma Aldrich. Analytical thin layer chromatography was performed on 250 μM silica gel 60 F₂₅₄ plates. Visualization was accomplished with UV light, and/or the use of potassium permanganate or Seebach stain followed by development with a heat gun. Chiral SFC was performed using either an Agilent 1260 Series SFC or Waters Corporation SFC utilizing a Chiralpak IE column (4.6 x 250 mm); co-solvent = methanol (0.1% DEA); 5-50% gradient/5min, hold for 5 min.



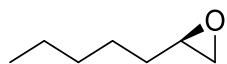
Synthesis of (R)-1-chloroheptan-2-ol (4.32a)

To a suspension of **4.31a** (0.85 mL, 10.8 mmol) and copper (I) iodide (206 mg, 1.08 mmol) in THF (11 mL) cooled to -78 °C was added butylmagnesium chloride (6.0 mL, 12.0 mmol, 2.0 M solution in THF) dropwise. The resulting reaction was stirred at -78 °C for 1 hr before warming to 0 °C. The reaction was stirred at this temperature for 2 hr whereupon TLC analysis showed complete consumption of starting material. The reaction was quenched with the addition of sat. NH₄Cl, and the layers were separated. The aqueous layer was washed with Et₂O x 3. The combined organic material was dried over MgSO₄, filtered, concentrated, and purified via flash chromatography (Teledyne ISCO flash purification system; silica gel column; hexanes:EtOAc; 0-15% EtOAc gradient) to afford the desired material as a colorless oil (1.25g, 77% yield). Spectral data were in accordance with reported literature values.³⁹



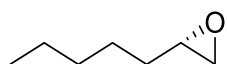
Synthesis of (S)-1-chloroheptan-2-ol (4.32b)

4.32b was synthesized as described above in 66% yield, using **4.31b** as the starting material. Spectral data were in accordance with reported literature values.³⁹



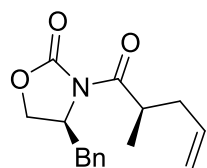
Synthesis of (R)-2-pentyloxirane (4.29a)

To a solution of **4.32a** (651 mg, 4.32 mmol) in Et₂O (16.3 mL) was added finely powdered sodium hydroxide (886 mg, 21.6 mmol) at room temperature. The resulting suspension was stirred for 3 hr whereupon TLC analysis showed complete consumption of starting material. The reaction was diluted with Et₂O and filtered. The filtrate was carefully concentrated, and the desired product was obtained as a colorless oil (423 mg, 86% yield) after distillation under reduced pressure. Spectral data were in accordance with reported literature values.⁴⁰



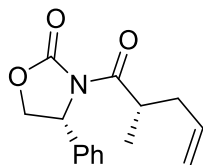
Synthesis of (S)-2-pentyloxirane (4.29b)

4.29b was synthesized as described above in 70% yield, using **4.32b** as the starting material. Spectral data were in accordance with reported literature values.⁴⁰



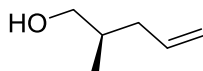
Synthesis of (S)-4-benzyl-3-((R)-2-methylpent-4-enoyl)oxazolidin-2-one (4.34a)

To a solution of **4.33a** (22.4 g, 96.0 mmol) in THF (300 mL) cooled to -78 °C was added NaHMDS (100 mL, 100 mmol, 1.0 M solution in THF) dropwise over 20 min. The reaction was stirred at -78 °C for an additional hour before the dropwise addition of allyl iodide (8.78 mL, 96.0 mmol) over 10 min. The reaction was stirred for an additional 5 hr at -78 °C before the cooling bath was removed and the reaction was quenched with the addition of sat. NH₄Cl. The layers were separated, and the aqueous layer was washed with Et₂O x 3. The combined organic material was washed with sat. Na₂S₂O₃, dried over MgSO₄, filtered, concentrated, and purified via flash chromatography (Teledyne ISCO flash chromatography system; silica gel column; 9:1 Hexane:EtOAc) to afford the desired product as a colorless oil (14.9 g, 58% yield). Spectral data were in accordance with reported literature values.⁴¹



Synthesis of (R)-3-((S)-2-methylpent-4-enoyl)-4-phenyloxazolidin-2-one (4.34b)

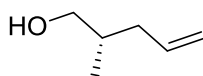
4.34b was synthesized as described above in 61% yield, using **4.33b** as the starting material. Spectral data were in accordance with reported literature values.⁵¹



Synthesis of (R)-2-methylpent-4-en-1-ol (4.35a)

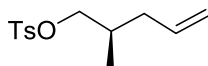
To a solution of **4.34a** (14.4 g, 52.7 mmol) in Et₂O (300 mL) cooled to 0 °C was sequentially added ethanol (3.72 mL, 63.7 mmol) and lithium borohydride (31.9 mL,

63.7 mmol, 2.0 M solution in THF) dropwise. The reaction was allowed to slowly warm to room temperature and stir for 16 hr. Upon cooling to 0 °C, the reaction was quenched with the addition of 1 M NaOH, and the resulting mixture was stirred at room temperature until it was free of particulates. The layers were separated, and the aqueous layer was washed with Et₂O x 3. The combined organic material was washed with brine, dried over MgSO₄, filtered, concentrated, and purified via flash chromatography (Teledyne ISCO flash purification system; silica gel column; hexanes:EtOAc; 0-30% EtOAc gradient) to afford the desired product as a colorless oil (2.86 g, 54% yield). Spectral data were in accordance with reported literature values.⁴¹



Synthesis of (S)-2-methylpent-4-en-1-ol (4.35b)

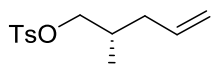
4.35b was synthesized as described above in 72% yield, using **4.34b** as the starting material. Spectral data were in accordance with reported literature values.⁴¹



Synthesis of (R)-2-methylpent-4-en-1-yl 4-methylbenzenesulfonate (4.30a)

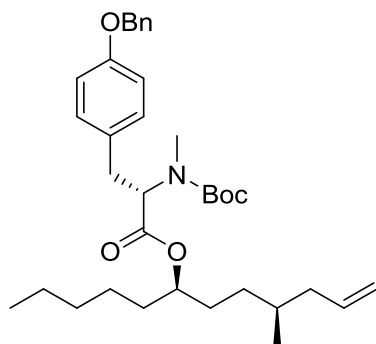
To a solution of **4.35a** (2.3 g, 23.0 mmol) and pyridine (3.71 mL, 45.9 mmol) in CHCl₃ (76.6 mL) cooled to 0 °C was added tosyl chloride (6.57 g, 34.4 mmol) in five portions. Upon completion of addition, the reaction was slowly allowed to warm to room temperature and stir for 16 hr. The reaction was then cooled to 0 °C, diluted with CHCl₃, and quenched with the addition of 2.0 M HCl. The layers were separated, and the organic layer was washed with 2.0 M HCl x 2, brine, dried over MgSO₄, filtered,

concentrated, and purified via flash chromatography (Teledyne ISCO flash purification system; silica gel column; hexanes:EtOAc; 0-5% EtOAc gradient) to afford the desired product as a colorless oil (4.02 g, 69% yield). Spectral data were in accordance with reported literature values.^{42,52}



Synthesis of (S)-2-methylpent-4-en-1-yl 4-methylbenzenesulfonate (4.30b)

4.30b was synthesized as described above in 80% yield, using **4.35b** as the starting material. Spectral data were in accordance with reported literature values.^{42,52}



Synthesis of (6R,9S)-9-methyldodec-11-en-6-yl ((S)-3-(4-(benzyloxy)phenyl)-2-((tert-butoxycarbonyl)(methyl)amino)propanoate (4.39a)

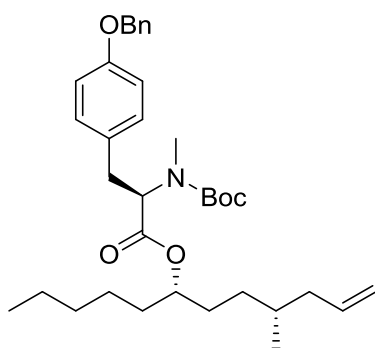
To a solution of **4.30a** (1.0 g, 3.93 mmol) in DMA (13.0 mL) was added lithium iodide (789 mg, 5.90 mmol) in one portion. The resulting suspension was then heated to 80 °C for 2 hr, whereupon TLC analysis indicated complete consumption of starting material. Upon cooling to room temperature, the reaction was diluted with Et₂O and water. The layers were separated, and the aqueous layer was washed with Et₂O x 2. The combined organic material was washed with water x 2, sat. Na₂S₂O₃, brine, dried over

MgSO₄, filtered, and carefully concentrated to afford a crude, colorless oil which was carried forward to the next step immediately, assuming quantitative yield.

In a separate RBF, Et₂O (6.5 mL) was added and cooled to -78 °C before the sequential addition of *t*-BuLi (1.98 mL, 2.38 mmol, 1.2 M solution in pentane) and a solution of the crude oil described above (250 mg, 1.19 mmol) in Et₂O (1.0 mL). The resulting reaction was stirred at -78 °C for 1 hr before the dropwise addition of lithium 2-thienylcyanocuprate (4.76 mL, 1.19 mmol, 0.25 M solution in THF). The reaction was warmed to 0 °C and stirred for an additional 30 min before the addition of a solution of **4.29a** (113 mg, 0.990 mmol) in THF (1.0 mL). The reaction was warmed to room temperature and stirred for 4 hr before being quenched with the addition of sat. NH₄Cl. The layers were separated, and the aqueous layer was washed with Et₂O x 3. The combined organic material was dried over MgSO₄, filtered, concentrated, and passed through a short silica plug to afford crude alcohol (120 mg, 0.605 mmol) which was carried forward immediately without further purification.

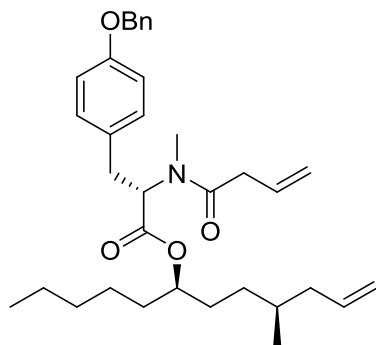
In a separate vial, **4.26a** (268 mg, 0.698 mmol) was dissolved in toluene (2.5 mL), and triethylamine (0.118 mL, 0.847 mmol) and 2,4,6-trichlorobenzoyl chloride (0.108 mL, 0.696 mmol) were sequentially added at room temperature. This reaction mixture was stirred for 30 min before the addition of a solution of crude alcohol described above (120 mg, 0.605 mmol) and DMAP (114 mg, 0.932 mmol) in toluene (3.0 mL). The reaction was stirred for 16 hr at room temperature before the addition of EtOAc and sat. NH₄Cl. The layers were separated, and the aqueous layer was washed with EtOAc x 3. The combined organic material was washed with sat. NaHCO₃, brine, dried over MgSO₄, filtered, concentrated, and purified via flash chromatography (Teledyne ISCO flash

purification system; silica gel column; hexanes:EtOAc; 0-15% EtOAc gradient) to afford the desired product as a colorless oil (262 mg, 47% yield over three steps, mixture of rotamers). $[\alpha]_D^{25} = -20.8$ ($c = 1.60$, CHCl_3). $^1\text{H NMR}$ (400 MHz, CDCl_3) δ 7.43-7.30 (m, 5H), 7.17-7.09 (m, 2H), 6.89 (d, $J = 8.0$ Hz, 2H), 5.76 (m, 1H), 5.03-4.97 (m, 4H), 4.92-4.72 (m, 2H), 3.33-3.19 (m, 1H), 2.99-2.87 (m, 1H), 2.77 and 2.72 (s, 3H, NCH_3 rotamers), 2.08-2.02 (m, 1H), 1.91-1.85 (m, 1H), 1.61-1.13 (m, 22H), 0.88-0.86 (m, 6H); $^{13}\text{C NMR}$ (100 MHz, CDCl_3) $\delta = 171.4, 171.1, 157.7, 157.6, 155.9, 155.4, 137.5, 137.4, 137.2, 130.8, 130.1, 130.0, 129.6, 129.1, 128.7, 128.0, 127.6, 116.0, 115.9, 115.0, 114.9, 80.2, 79.9, 75.9, 75.6, 70.2, 61.0, 59.6, 41.4, 38.1, 34.5, 34.3, 34.0, 32.8, 31.9, 31.8, 31.6, 31.2, 29.8, 29.3, 28.4, 28.2, 25.0, 22.6, 19.5, 14.1$. HRMS (TOF, ES+) calc'd for $\text{C}_{35}\text{H}_{52}\text{NO}_5$ $[\text{M}+\text{H}]^+$, 566.3840; found, 566.3841.



Synthesis of (6*S*,9*R*)-9-methyldodec-11-en-6-yl (*R*)-3-(4-(benzyloxy)phenyl)-2-((tert-butoxycarbonyl)(methyl)amino)propanoate (4.39b)

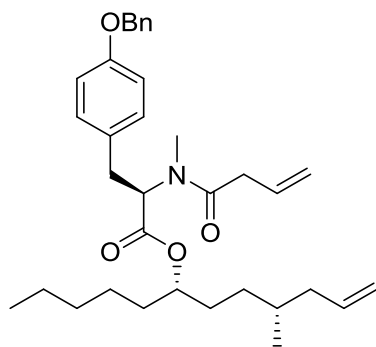
4.39b was synthesized as described above in 31% yield over three steps, using **4.30b**, **4.29b**, and **4.26b** as the starting material and necessary reagents. Spectral data matched that of **4.39a** except for $[\alpha]_D^{25} = +21.1$ ($c = 0.83$, CHCl_3).



Synthesis of (6*R*,9*S*)-9-methyldodec-11-en-6-yl (S)-3-(4-(benzyloxy)phenyl)-2-(*N*-methylbut-3-enamido)propanoate (4.40a)

To a solution of **4.39a** (200 mg, 0.353 mmol) in DCM (2.5 mL) cooled to 0 °C was added trifluoroacetic acid (0.541 mL, 7.07 mmol) dropwise. Upon completion of addition, the reaction was warmed to room temperature and stirred for 1 h, whereupon LCMS analysis showed complete consumption of starting material. The reaction was concentrated *in vacuo* to afford a crude red oil which was subsequently dissolved in DCM (2.5 mL). This solution was cooled to 0 °C before the sequential addition of vinylacetic acid **4.27** (0.0451 mL, 0.530 mmol), PyBroP (247 mg, 0.530 mmol), and *N,N*-diisopropylethyl amine (0.246 mL, 1.41 mmol). The reaction was allowed to slowly warm to room temperature and stir for 3 hr, whereupon LCMS analysis indicated complete consumption of starting material. The reaction was diluted with DCM and quenched with the addition of sat. NH₄Cl. The layers were separated, and the aqueous layer was washed with DCM x 3. The combined organic material was washed with sat. NaHCO₃, brine, dried over MgSO₄, filtered, concentrated, and purified via flash chromatography (Teledyne ISCO flash purification system; silica gel column; hexanes:EtOAc; 0-20% EtOAc gradient) to afford the desired product as a colorless oil (168 mg, 89% yield). $[\alpha]_D^{25} = -26.7$ (c = 0.79, CHCl₃). ¹H NMR (400 MHz, CDCl₃) δ 7.43-7.30 (m, 5H), 7.13-

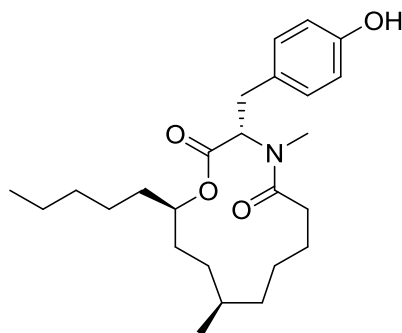
7.06 (m, 2H), 6.89 (m, 2H), 5.84-5.71 (m, 2H), 5.39 (m, 1H), 5.09-4.84 (m, 6H), 3.32-3.23 (m, 1H), 3.05-2.90 (m, 4H), 2.85 (s, 2H), 2.08-2.00 (m, 1H), 1.92-1.85 (m, 1H), 1.59 (s, 2H), 1.56-1.43 (m, 4H), 1.31-1.08 (m, 8H), 0.89-0.84 (m, 6H); ^{13}C NMR (100 MHz, CDCl_3) δ = 171.5, 170.9, 158.1, 157.7, 137.5, 137.3, 137.2, 131.5, 131.1, 130.2, 130.0, 129.5, 128.8, 128.7, 128.2, 128.1, 127.6, 117.9, 116.1, 115.9, 115.4, 115.0, 76.0, 70.2, 62.4, 58.0, 41.4, 39.1, 38.6, 34.8, 34.2, 34.0, 32.8, 32.7, 31.9, 31.8, 31.5, 30.0, 29.7, 25.0, 22.7, 19.5, 14.2. HRMS (TOF, ES⁺) calc'd for $\text{C}_{34}\text{H}_{48}\text{NO}_4$ $[\text{M}+\text{H}]^+$, 534.3578; found, 534.3580.



Synthesis of (6*S*,9*R*)-9-methyldodec-11-en-6-yl (*R*)-3-(4-(benzyloxy)phenyl)-2-(*N*-methylbut-3-enamido)propanoate (4.40b)

4.40b was synthesized as described above, using **4.39b** as the starting material.

Spectral data were identical to **4.40a** except for $[\alpha]_D^{25} = +27.2$ ($c = 1.16$, CHCl_3).

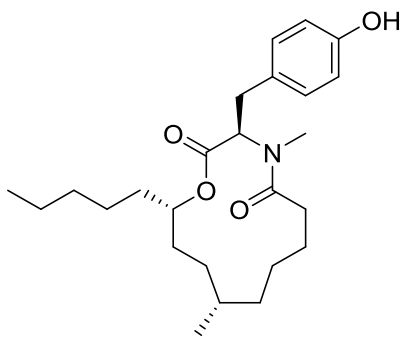


Synthesis of (3*S*,10*R*,13*R*)-3-(4-hydroxybenzyl)-4,10-dimethyl-13-pentyl-1-oxa-4-azacyclotridecane-2,5-dione (4.41a)

To a solution of **4.40a** (113 mg, 0.212 mmol) in toluene (42.3 mL) was sequentially added titanium (IV) isopropoxide (0.0626 mL, 0.212 mmol) and Grubbs Catalyst™ 2nd Generation (18.0 mg, 0.021 mmol) at room temperature. The resulting solution was degassed by vigorously bubbling argon through the reaction mixture for 15 min. The reaction was then heated to 90 °C for 7 hr, whereupon LCMS showed consumption of starting material. Upon cooling to room temperature, the reaction was diluted with EtOAc, quenched with the addition of brine, and filtered over a pad of celite. The layers were separated, and the aqueous layer was washed with EtOAc x 3. The combined organic material was dried over MgSO₄, filtered, concentrated, and passed through a short silica plug to afford a crude, colorless oil (80 mg, 0.158 mmol) which was taken forward to the next step without further purification.

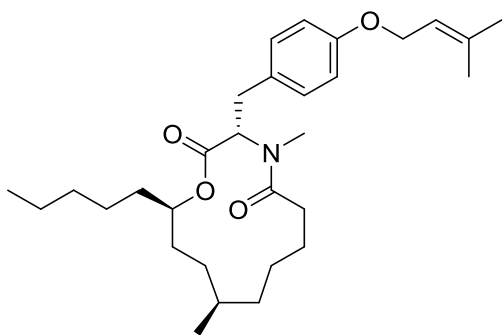
To a solution of this crude oil (80 mg, 0.158 mmol) in EtOAc (1.05 mL) was added Pd/C (33.7 mg, 0.0158 mmol, 5% Pd by mass). The flask was evacuated and back-flushed with hydrogen three times, and the reaction was stirred under a static atmosphere of hydrogen (hydrogen balloon) for 16 hr. Excess hydrogen gas was evacuated, and the reaction suspension was diluted with EtOAc and filtered through a pad of celite. The combined organic material was concentrated and purified via flash chromatography (Teledyne ISCO flash purification system; silica gel column; hexanes:EtOAc; 0-30% EtOAc gradient) to afford the desired product as a white solid (53.4 mg, 60% yield over two steps). $[\alpha]_D^{25} = -83.2$ (c = 0.74, CHCl₃). ¹H NMR (400 MHz, CDCl₃) δ 7.09-7.00 (m, 2H), 6.74 (m, 2H), 5.89 (m, 1H), 4.92-4.84 (m, 1H), 3.17-3.12 (m, 1H), 3.05-2.91 (m, 3H), 2.72-2.59 (m, 1H), 2.17-2.14 (m, 1H), 1.62-1.11 (m, 20H), 0.91-0.83 (m, 7H); ¹³C

NMR (100 MHz, CDCl₃) δ = 175.2, 174.8, 171.2, 170.4, 155.9, 155.7, 129.9, 129.6, 127.5, 127.1, 116.0, 115.5, 76.0, 74.8, 62.1, 55.5, 35.1, 34.9, 34.0, 33.7, 33.0, 32.7, 31.8, 30.8, 29.9, 29.7, 29.3, 28.6, 28.5, 28.2, 26.6, 25.4, 25.3, 25.0, 23.9, 23.6, 23.1, 22.7, 20.7, 20.2, 14.2. HRMS (TOF, ES⁺) calc'd for C₂₅H₄₀NO₄ [M+H]⁺, 418.2952; found, 418.2953.



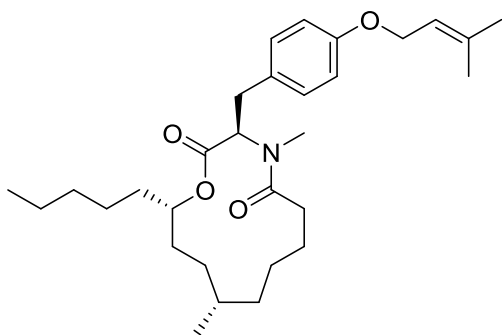
Synthesis of (3*R*,10*S*,13*S*)-3-(4-hydroxybenzyl)-4,10-dimethyl-13-pentyl-1-oxa-4-azacyclotridecane-2,5-dione (4.41b)

4.41b was synthesized as described above in 65% yield over two steps, using **4.40b** as the starting material. Spectral data were identical to **4.41a** except for $[\alpha]_D^{25} = +85.6$ ($c = 0.56$, CHCl₃).



Synthesis of (-)-Melearoride A (4.8a)

To a solution of **4.41a** (7.0 mg, 0.0168 mmol), 3-methyl-2-buten-1-ol (**4.28**) (0.00255 mL, 0.0251 mmol), and triphenylphosphine (7.03 mg, 0.0268 mmol) in THF (0.120 mL) cooled to 0 °C was added a solution of DIAD (0.00528 mL, 0.0268 mmol) in THF (0.120 mL) dropwise. Upon completion of addition, the reaction was allowed to warm to room temperature and stir for 2 hr, whereupon LCMS analysis showed complete consumption of starting material. The reaction mixture was concentrated and purified via flash chromatography (Teledyne ISCO flash system; silica gel column; hexanes:EtOAc; 0-30% EtOAc gradient) to afford the desired product as a colorless oil (5.6 mg, 69% yield) in ~93:7 d.r. by ¹H NMR. $[\alpha]_D^{25} = -95.5$ (c = 0.48, MeOH). ¹H NMR (600 MHz, CDCl₃) δ see **Table 4.2**; ¹³C NMR (150 MHz, CDCl₃) δ = see **Table 4.2**. HRMS (TOF, ES+) calc'd for C₃₀H₄₈NO₄ [M+H]⁺, 486.3578; found, 486.3582.



Synthesis of (+)-Melearoride A (**4.8b**)

4.8b was synthesized as described above in 72% yield, using **4.41b** as the starting material. Spectral data were identical to **4.8a** except for $[\alpha]_D^{25} = +96.7$ (c = 0.52, MeOH).

Isolated Melearoride A			Synthetic Melearoride A (4.8a)		
Position	δ_C^a	δ_H (J in Hz) ^b	Position	δ_C^c	δ_H (J in Hz) ^d
1	173.3		1	173.3	
	173.8			173.8	
2	32.9	2.44, t (J = 13.1 Hz)	2	32.9	2.44, t (J = 13.0 Hz)
	34.1	2.18, m		34.0	2.18, m
3	23.9	1.33, m	3	23.8	1.32, m
	24	1.33, m		24.0	1.32, m
4	33.7	2.69, m	4	33.6	2.69, m
	33.7	2.69, m		33.7	2.69, m
	34.1	2.19, m; 2.69, m		34.0	2.19, m; 2.69, m
5	26.5	1.87-1.94, m	5	26.5	1.86-1.94, m
6	28.2	1.37-1.53, m	6	28.2	1.39-1.53, m
	29.4	1.19-1.40, m		29.4	1.20-1.39, m
7	25.3	1.06, m	7	25.2	1.05, m
8	28.3	1.37-1.53, m	8	28.3	1.39-1.53, m
	28.7	1.37-1.53, m		28.7	1.39-1.53, m
	29	1.37-1.53, m		28.9	1.39-1.53, m
	29.7	1.37-1.53, m		29.7	1.39-1.53, m
9	74.5	4.85, m	9	74.6	4.85, m
	75.2	4.85, m		75.2	4.85, m
	75.8	4.85, m		75.8	4.85, m
10	23.4	1.53, m	10	23.4	1.54, m
	23.7	1.27, m		23.7	1.26, m
11	24.7	1.24, m	11	24.7	1.23, m
	25	1.27, m		25.0	1.26, m
12	31.6	1.27, m	12	31.5	1.26, m
	31.7	1.19, m		31.6	1.18, m
	31.8	1.19, m		31.8	1.18, m
13	22.5	1.19-1.40, m	13	22.5	1.20-1.39, m
	22.9	1.37, m		22.9	1.38, m
14	14	0.88, t (J = 6.9 Hz)	14	14.0	0.88, m
15	20	0.84, d (J = 6.9 Hz)	15	20.0	0.84, m
	20.5	0.84, d (J = 6.9 Hz)		20.5	0.84, m
1'	170.2		1'	170.2	
	171.1			171.1	
2'	55.4	5.81, t (J = 8.3 Hz)	2'	55.4	5.81, t (J = 8.2 Hz)
	61.6	4.58, dd (J = 10.3 Hz, 5.5 Hz)		61.6	4.57, dd (J = 10.2 Hz, 5.2 Hz)
	67.3	3.52, dd (J = 11.2 Hz, 4.1 Hz)		67.4	3.53, dd (J = 11.1 Hz, 4.0 Hz)
3'	33	2.83, dd (J = 14.3 Hz, 7.7 Hz)	3'	33.0	2.83, dd (J = 14.2 Hz, 7.8 Hz)
	33.5	3.20, dd (J = 14.3 Hz, 8.9 Hz)		33.5	3.21, m
		3.43, dd (J = 14.5 Hz, 11.5 Hz)			3.42, dd (J = 14.0 Hz, 11.6 Hz)
	35	3.01, m		34.9	3.01, m
	35.1	3.01, m		35.1	3.01, m
4'	128.1		4'	128.1	
	128.4			128.4	
5' 9'	129.5	7.09, d (J = 8.6 Hz)	5' 9'	129.5	7.09, d (J = 8.4 Hz)
	130	7.18, d (J = 8.6 Hz)		130.0	7.18, d (J = 8.5 Hz)
6' 8'	114.5	6.83, d (J = 8.6 Hz)	6' 8'	114.5	6.83, d (J = 8.5 Hz)
	114.9	6.85, d (J = 8.6 Hz)		114.9	6.85, d (J = 8.5 Hz)
7'	157.5		7'	157.5	
	157.9			157.9	
10'	64.6	4.45, d (J = 7.2 Hz)	10'	64.6	4.45, m
	64.7	4.78, d (J = 7.2 Hz)		64.7	4.78, d (J = 7.4 Hz)
11'	119.5	5.51, t (J = 7.2 Hz)	11'	119.5	5.51, t (J = 7.5 Hz)
	119.7	5.50, t (J = 7.2 Hz)		119.7	5.50, t (J = 7.4 Hz)
12'	138		12'	137.9	
	138.3			138.2	
13'	25.8	1.81, s	13'	25.8	1.81, d (J = 5.9 Hz)
14'	18.2	1.74, s	14'	18.1	1.75, d (J = 8.9 Hz)
N-CH3	29.3	3.03, s	N-CH3	29.2	3.03, s
	30.7	2.95, s		30.6	2.94, s
	40.3	2.71, s		40.3	2.70, s

Comparison of NMR Spectroscopic Data (in ppm) for Isolated and Synthetic Melearoride A.

^a ¹³C NMR (125 MHz) at room temperature in CDCl₃ (solvent calibrated to 77.0 ppm)

^b ¹H NMR (500 MHz) at -20 °C in CDCl₃ (solvent calibrated to 7.28 ppm)

^c ¹³C NMR (150 MHz) at room temperature in CDCl₃ (solvent calibrated to 77.0 ppm)

^d ¹H NMR (600 MHz) at -20 °C in CDCl₃ (solvent calibrated to 7.28 ppm)

Table 4.2: Comparison of ¹H and ¹³C NMR data of isolated **4.8a** and synthetic **4.8a**

References for Chapter IV

1. Cragg, G. M.; Newman, D. J. Biodiversity: a continuing source of novel drug leads. *Pure Appl. Chem.* **2005**, *77*, 7-24.
2. Eberhardt, L.; Kumar, K.; Waldmann, H. Exploring and exploiting biologically relevant chemical space. *Curr. Drug Targets* **2011**, *12*, 1531-1546.
3. Wright, G. D. Unlocking the potential of natural products in drug discovery. *Microbial Biotechnology* **2019**, *12*, 55-57.
4. Dias, D. A.; Urban, S.; Roessner, U. A historical overview of natural products in drug discovery. *Metabolites* **2012**, *2*, 303-336.
5. Bharate, S. S.; Mignani, S.; Vishwakarma, R. A. Why are the majority of active compounds in the CNS domain natural products? A critical analysis. *J. Med. Chem.* **2018**, *61*, 10345-10374.
6. Raskin, I. Role of salicylic acid in plants. *Annu. Rev. Physiol. Plant Mol. Biol.* **1992**, *43*, 439-463.
7. Ji, H-F.; Li, X-J.; Zhang, H-Y. Natural products and drug discovery: can thousands of years of ancient medical knowledge lead us to new and powerful drug combinations in the fight against cancer and dementia? *EMBO Reports* **2009**, *10*, 194-200.
8. Hunter, P. Harnessing nature's wisdom: turning to nature for inspiration and avoiding her follies. *EMBO Reports* **2008**, *9*, 838-840.
9. Wani, M. C.; Taylor, H. L.; Wall, M. E.; Coggon, P.; McPhail, A. T. Plant antitumor agents. VI. Isolation and structure of taxol, a novel antileukemic and antitumor agent from *Taxus brevifolia*. *J. Am. Chem. Soc.* **1971**, *93*, 2325-2327.
10. Garrod, L. P. Relative antibacterial activity of three penicillins. *Br. Med. J.* **1960**, 527-529.
11. Endo, A. A historical perspective on the discovery of statins. *Proc. Jpn. Acad., Ser. B.* **2010**, *86*, 484-493.
12. Sneader, W. The discovery of heroin. *The Lancet* **1998**, *352*, 1697-1699.
13. Shekelle, P. G.; Newberry, S. J.; Fitzgerald, J. D.; Motala, A.; O'Hanlon, C. E.; Tariq, A.; Okunogbe, A.; Han, D.; Shanman, R. Management of gout: a systematic review in support of an American college of physicians clinical practice guideline. *Ann. Intern. Med.* **2017**, *166*, 37-51.
14. Krishna, S.; Bustamante, L.; Haynes, R. K.; Staines, H. M. Artemisinin: their growing importance in medicine. *Trends Pharmacol. Sci.* **2008**, *29*, 520-527.
15. Harvey, A. L.; Edrada-Ebel, R.; Quinn, R. J. The re-emergence of natural products for drug discovery in the genomics era. *Nat. Rev. Drug Disc.* **2015**, *14*, 111-129.
16. Nicolaou, K. C. The chemistry-biology-medicine continuum and the drug discovery and development process in academia. *Chemistry and Biology* **2014**, *21*, 1039-1045.
17. Vasilevich, N. I.; Kombarov, R. V.; Genis, D. V.; Kirpichenok, M. A. Lessons from natural products chemistry can offer novel approaches for synthetic chemistry in drug discovery. *J. Med. Chem.* **2012**, *55*, 7003-7009.
18. Koehn, F. E.; Carter, G. T. The evolving role of natural products in drug discovery. *Nat. Rev. Drug Disc.* **2005**, *4*, 206-220.

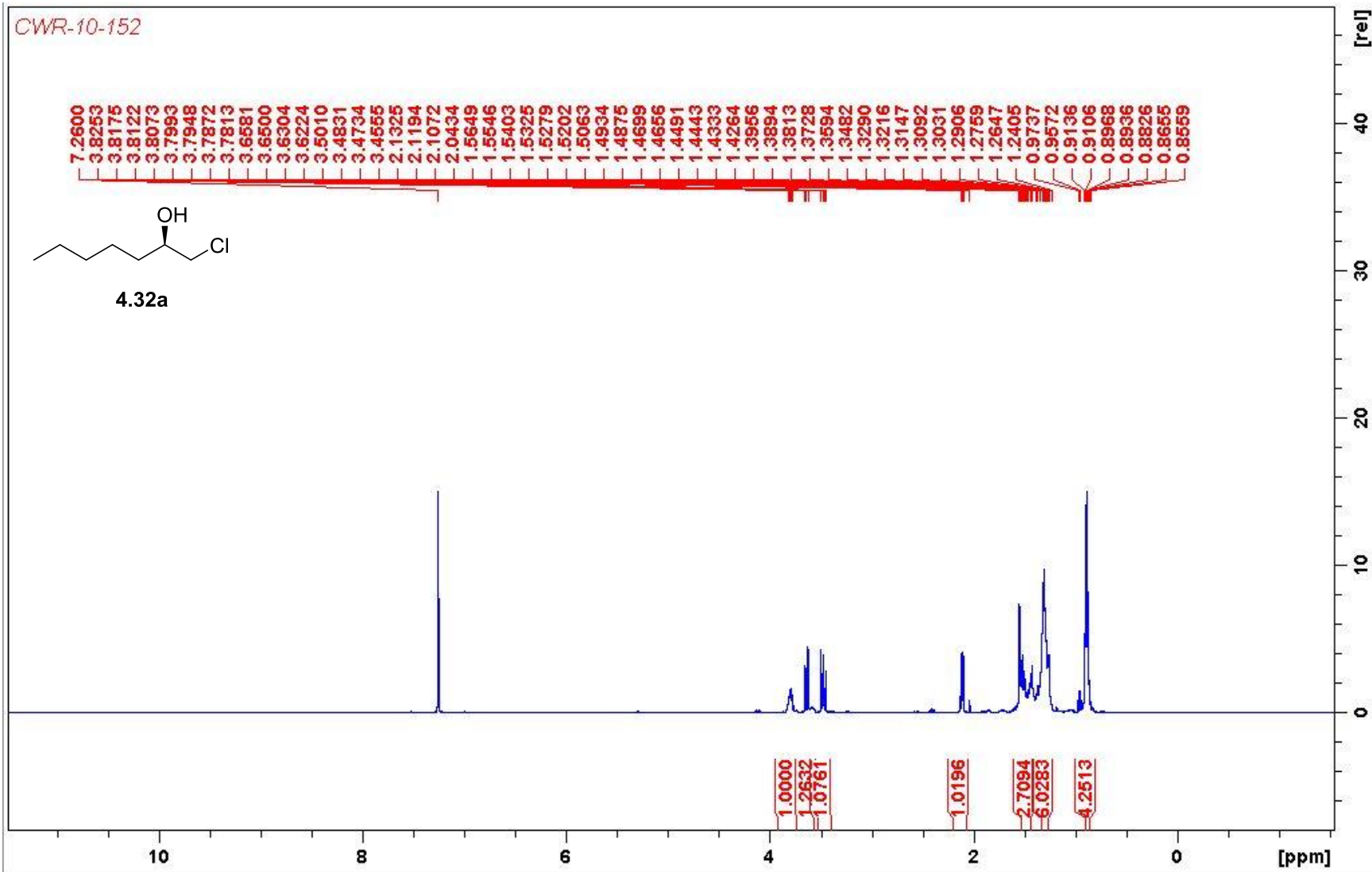
19. Wang, S.; Dong, G.; Sheng, C. Structural simplification of natural products. *Chem. Rev.* **2019**, *119*, 4180-4220.
20. Rodrigues, T.; Reker, D.; Schneider, P.; Schneider, G. Counting on natural products for drug design. *Nature Chemistry* **2016**, *8*, 531-541.
21. Swinney, D. C.; Anthony, J. How were new medicines discovered? *Nat. Rev. Drug Disc.* **2011**, *10*, 507-519.
22. Bebbington, M. W. P. Natural product analogues: towards a blueprint for analogue-focused synthesis. *Chem. Soc. Rev.* **2017**, *46*, 5059-5109.
23. Okabe, M.; Sugita, T.; Kinoshita, K.; Koyama, K. Macrolides from a marine-derived fungus, *Penicillium meleagrinum* var. *viridiflavum*, showing synergistic effects with fluconazole against azole-resistant *Candida albicans*. *J. Nat. Prod.* **2016**, *79*, 1208-1212.
24. Nose, H.; Seki, A.; Yaguchi, T.; Hosoya, A.; Sasaki, T.; Hoshiko, S.; Shomura, T. PF1163A and B, New Antifungal Antibiotics Produced by *Penicillium* sp. I. Taxonomy of producing strain, fermentation, isolation, and biological activities. *J. Antibiot.* **2000**, *53*, 33-37.
25. Sasaki, T.; Nose, H.; Hosoya, A.; Yoshida, S.; Kawaguchi, M.; Watanabe, T.; Usui, T.; Ohtsuka, Y.; Shomura, T. PF1163A and B, New Antifungal Antibiotics Produced by *Penicillium* sp. II. Physico-chemical properties and structure elucidation. *J. Antibiot.* **2000**, *53*, 38-44.
26. Nose, H.; Fushimi, H.; Seki, A.; Sasaki, T.; Watabe, H.; Hoshiko, S. PF1163A, a novel antifungal agent, inhibit ergosterol biosynthesis at C-4 sterol methyl oxidase. *J. Antibiot.* **2002**, *55*, 969-974.
27. Ghannoum, M. A.; Rice, L. B. Antifungal agents: mode of action, mechanisms of resistance, and correlation of these mechanisms with bacterial resistance. *Clin. Microbiol. Rev.* **1999**, *12*, 501-517.
28. Di Santo, R. Natural products as antifungal agents against clinically relevant pathogens. *Nat. Prod. Rep.* **2010**, *27*, 1084-1098.
29. Tatsuta, K.; Takano, S.; Ikeda, Y.; Nakano, S.; Miyazaki, S. The total synthesis and absolute structure of antifungal antibiotics (-)-PF1163A and B. *J. Antibiot.* **1999**, *52*, 1146-1151.
30. Kumar, H.; Reddy, A. S.; Subba Reddy, B. V. The stereoselective total synthesis of PF1163A. *Tetrahedron Lett.* **2014**, *55*, 1519-1522.
31. Krishna, P. R.; Srinivas, P. Total synthesis of the antifungal antibiotic PF1163A. *Tetrahedron Asymmetry* **2012**, *23*, 769-774.
32. Yadav, J. S.; Venkalesh, M.; Thrimurtulu, N.; Prasad, A. R. Stereoselective synthesis of (-)-PF1163A via Prins cyclization. *Synlett* **2010**, *8*, 1255-1259.
33. Bouazza, F.; Renoux, B.; Bachmann, C.; Gesson, J-P. Total synthesis and conformational analysis of the antifungal agent (-)-PF1163B. *Org. Lett.* **2003**, *5*, 4049-4052.
34. Takahashi, H.; Kawakita, T.; Ohno, M.; Yoshioka, M.; Kobayashi, S. A catalytic enantioselective reaction using a C₂-symmetric disulfonamide as a chiral ligand: alkylation of aldehydes catalyzed by disulfonamide-Ti(O*i*Pr₄)-dialkyl zinc system. *Tetrahedron*, **1992**, *48*, 5691-5700.
35. Knochel, P. Stereoselective reactions mediated by functionalized diorganozincs. *Synlett*, **1995**, *5*, 393-403.

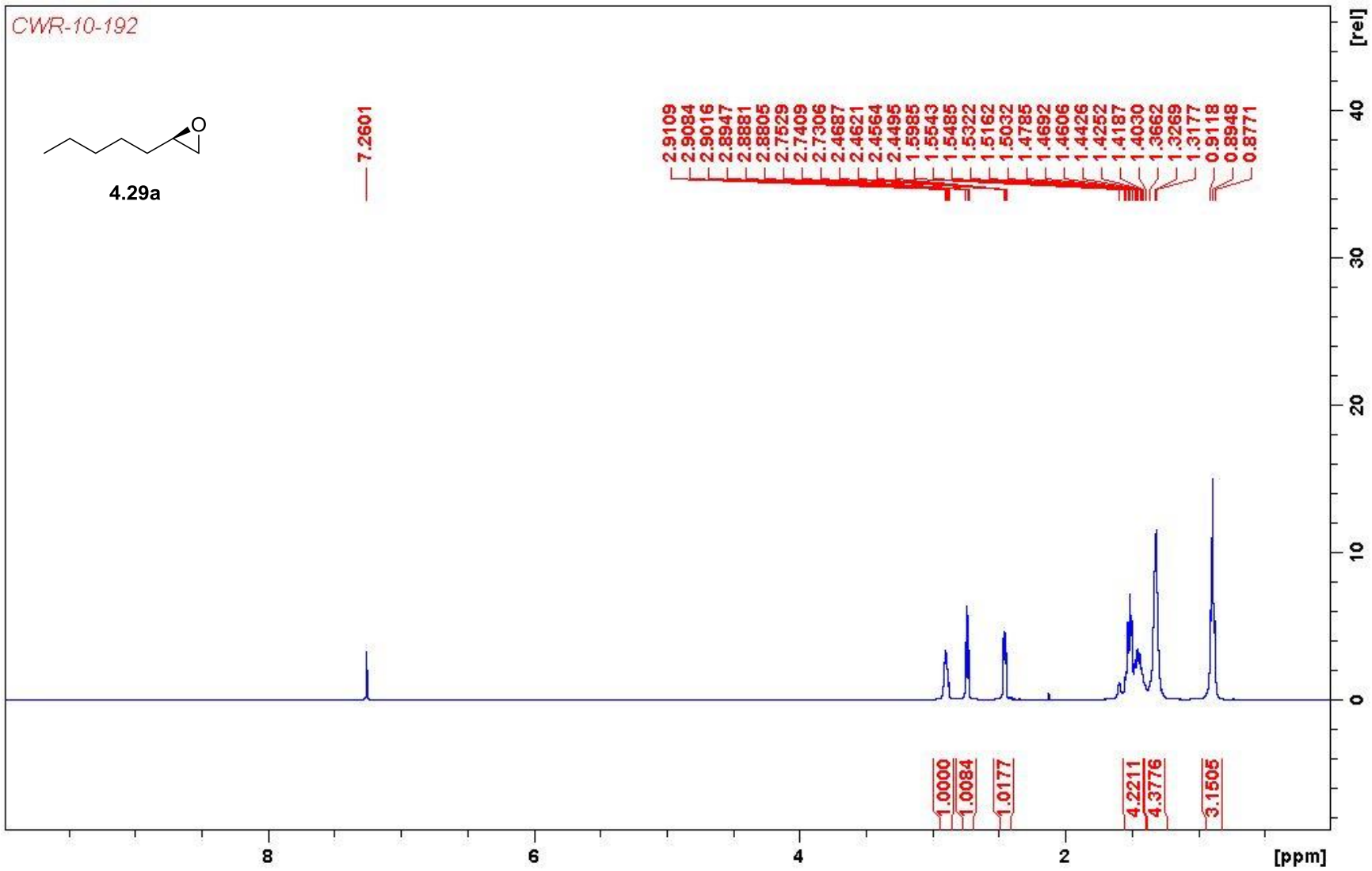
36. Reed, C. W.; Fulton, M. G.; Nance, K. D.; Lindlsey, C. W. Total synthesis of natural (-)- and unnatural (+)-Melearoride A. *Tetrahedron Lett.* **2019**, *60*, 743-745.
37. Batiste, S. M.; Blackwell, D. J.; Kim, K.; Kryshal, D. O.; Gomez-Hurtado, N.; Rebbeck, R. T.; Cornea, R. L.; Johnston, J. N.; Knollmann, B. C. Unnatural verticilide enantiomer inhibits type 2 ryanodine receptor-mediated calcium leak and is antiarrhythmic. *Proc. Natl. Acad. Sci.* **2019**, *116*, 4810-4815.
38. Hahn, K. N.; Fadeyi, O. O.; Cho, H. P.; Lindsley, C. W. Synthesis and biological evaluation of cremastrine and an unnatural analogue. *Tetrahedron Lett.* **2012**, *53*, 3577-3580.
39. Moriarty, R. M.; Rani, N.; Enache, L. A.; Rao, M. S.; Batra, H.; Guo, I.; Penmasta, R. A.; Staszewski, J. P.; Tuladhar, S. M.; Prakash, O.; Crich, D.; Hirtopeanu, A.; Gilardi, R. The intramolecular asymmetric Pauson-Khand cyclization as a novel and general stereoselective route to benzindene prostacyclins: synthesis of UT-15 (Trepstinil). *J. Org. Chem.* **2004**, *69*, 1890-1902.
40. Jana, S.; Sarpe, V. A.; Kulkarni, S. S. Total synthesis of Emmyguyacins A and B, potential fusion inhibitors of influenza virus. *Org. Lett.* **2018**, *20*, 6938-6942.
41. Hansen, D. B.; Starr, M. L.; Tolstoy, N.; Joullie, M. M. A stereoselective synthesis of (2*S*,4*R*)- δ -hydroxyleucine methyl ester: a component of cyclomarin A. *Tetrahedron Asymmetry* **2005**, *16*, 3623-3627.
42. Pack, S. K.; Molander, G. A. Determining the scope of the organolanthanide-catalyzed, sequential intramolecular amination/cyclization reaction: formation of substituted quinolizidines, indolizidines, and pyrrolizidines. *J. Org. Chem.* **2003**, *68*, 9214-9220.
43. Teerlinck, C. E.; Bowyer, W. J. Reactivity of magnesium surfaces during the formation of Grignard reagents. *J. Org. Chem.* **1996**, *61*, 1059-1064.
44. Tilstam, U.; Weinmann, H. Activation of Mg metal for safe formation of Grignard reagents on plant scale. *Org. Process Res. Dev.* **2002**, *6*, 906-910.
45. Lipshutz, B. H.; Koerner, M.; Parker, D. A. 2-thienyl(cyano)copper lithium. A lower order, stable "cuprate in a bottle" precursor to higher order reagents. *Tetrahedron Lett.* **1987**, *28*, 945-948.
46. Inanaga, J.; Hirata, K.; Saeki, H.; Katsuki, T.; Yamaguchi, M. A rapid esterification by means of mixed anhydride and its application to large-ring lactonization. *Bull. Chem. Soc. Jpn.* **1979**, *52*, 1989-1993.
47. Furstner, A.; Langemann, K. Total synthesis of (+)-ricinelaidic acid lactone and of (-)-gloeosporone based on transition-metal-catalyzed C-C bond formations. *J. Am. Chem. Soc.* **1997**, *119*, 9130-9136.
48. Yang, Q.; Xiao, W.-J.; Yu, Z. Lewis acid assisted ring-closing metathesis of chiral diallylamines: an efficient approach to enantiopure pyrrolidine derivatives. *Org. Lett.* **2005**, *7*, 871-874.
49. Gage, J. R.; Evans, D. A. Diastereoselective aldol condensation using a chiral oxazolidinone auxiliary: (2*S*,3*S*)-3-hydroxy-3-phenyl-2-methylpropanoic acid. *Org. Synth.* **1990**, *68*, 83-91.
50. Matousek, V.; Togni, A.; Bizet, V.; Cahard, D. Synthesis of α -CF₃-substituted carbonyl compounds with relative and absolute stereocontrol using electrophilic CF₃-transfer reagents. *Org. Lett.* **2011**, *13*, 5762-5765.

51. Clark, J. S.; Labre, F.; Thomas, L. H. Concise synthesis of the C-1-C-12 fragment of amphidinolides T1-T5. *Org. Biomol. Chem.* **2011**, *9*, 4823-4830.
52. Fujimoto, S.; Yoshikawa, K.; Itoh, M.; Kitahara, T. Synthesis of (*R*)- and (*S*)-Muscone. *Bioscience, Biotechnology, and Biochemistry* **2002**, *66*, 1389-1392.

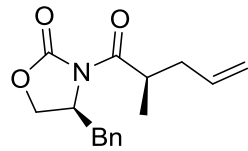
Appendix D

Relevant Spectra for Chapter IV

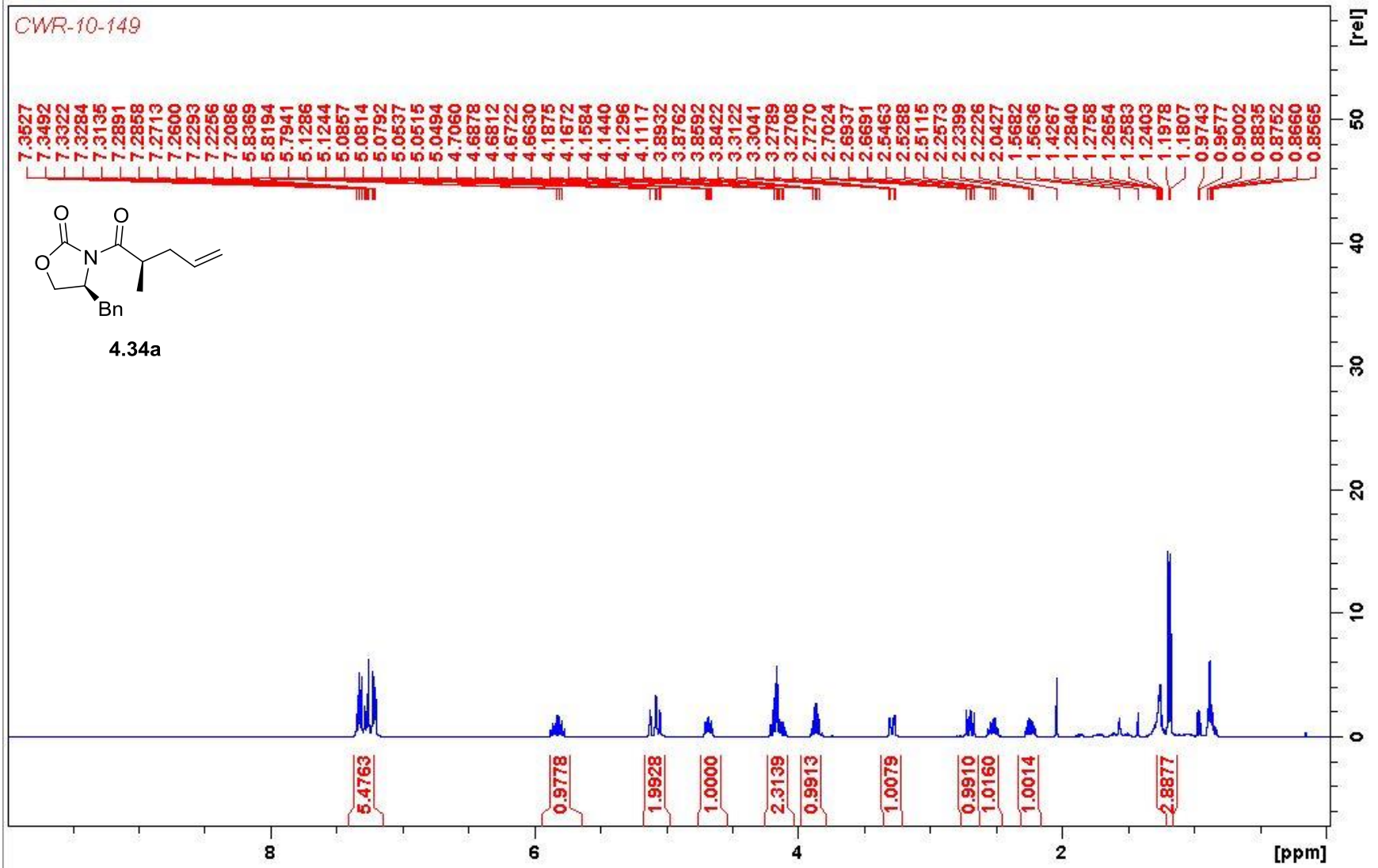




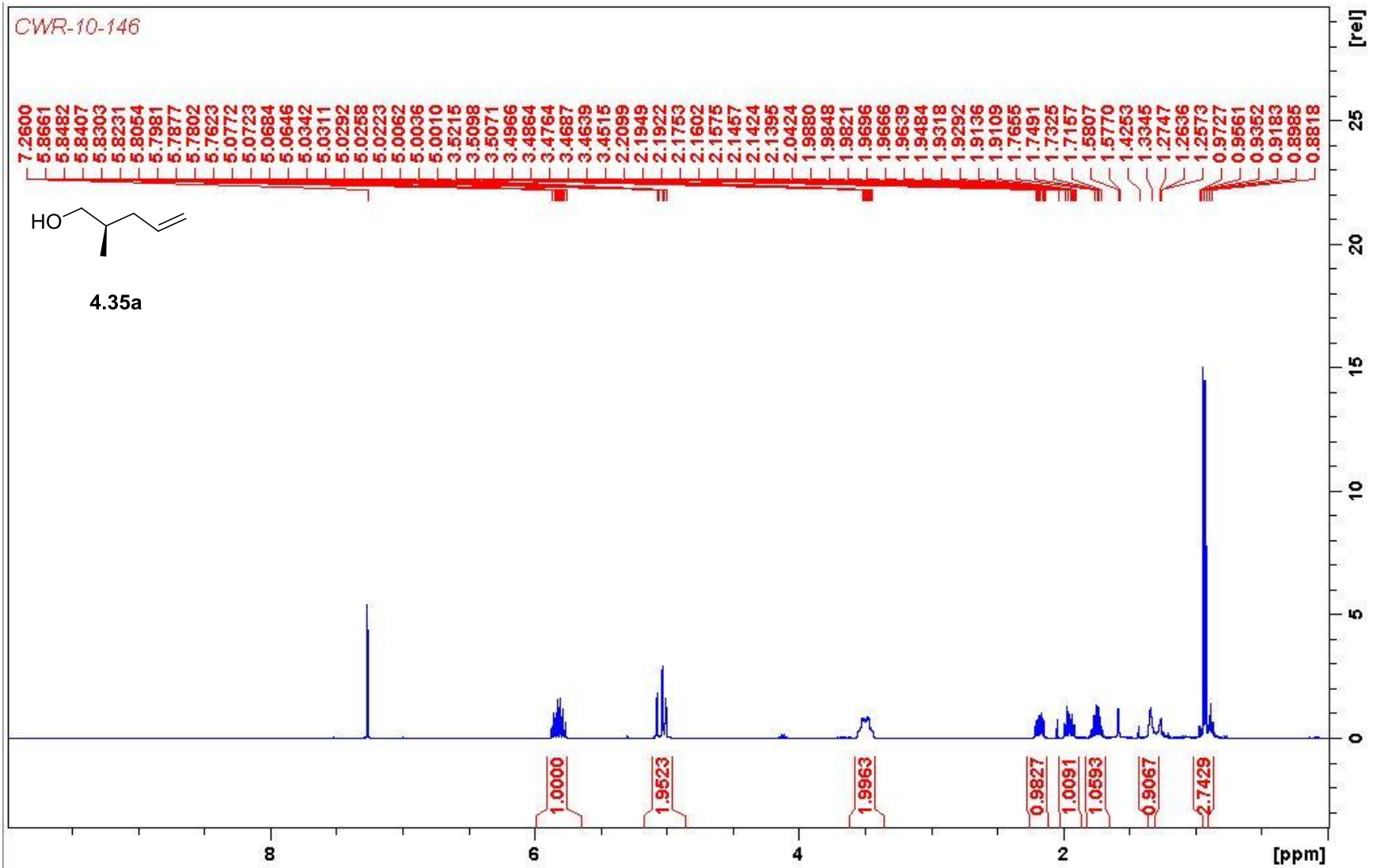
CWR-10-149



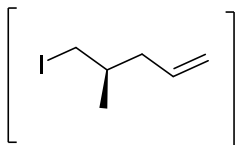
4.34a



CWR-10-146

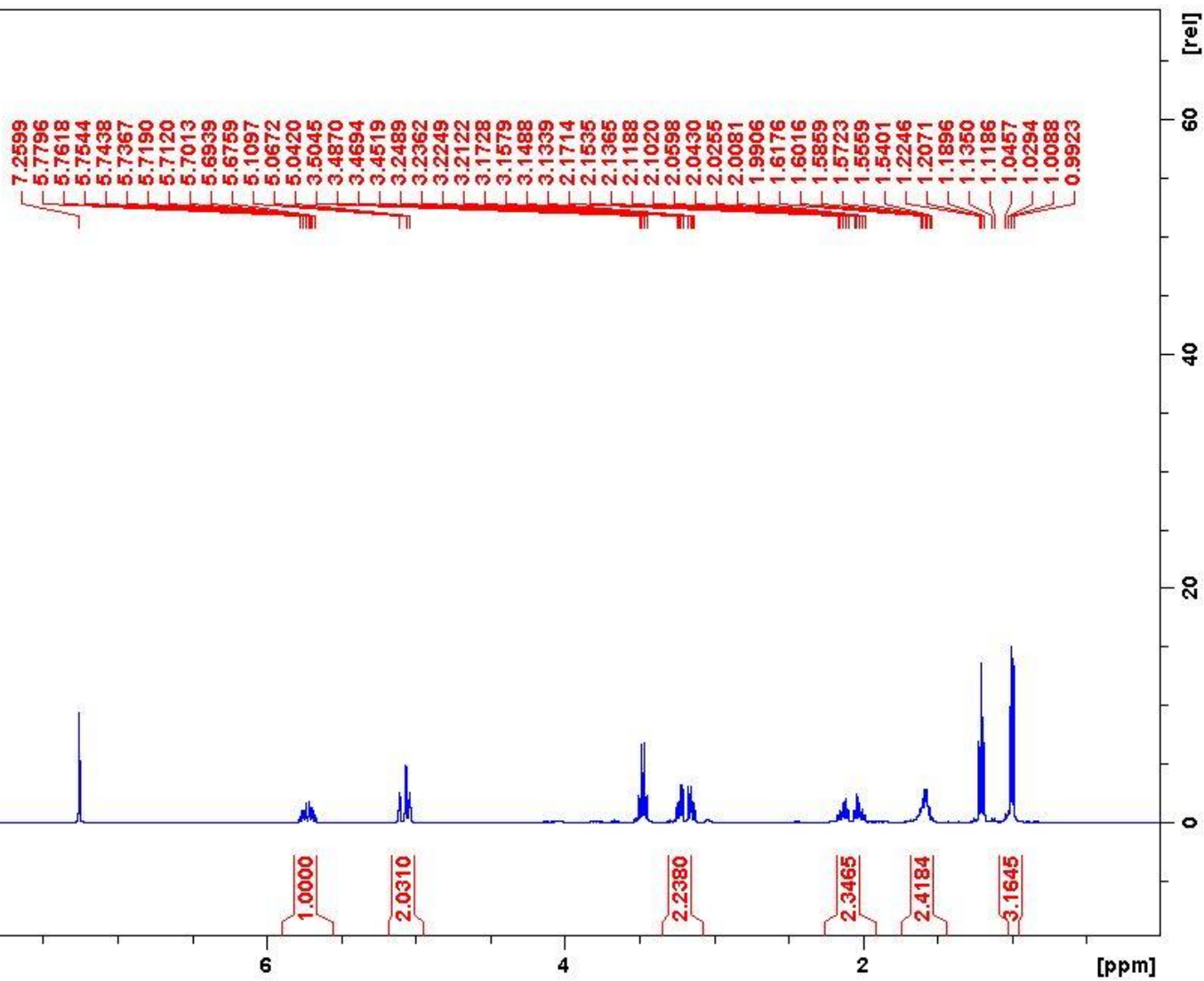


CWR-10-188

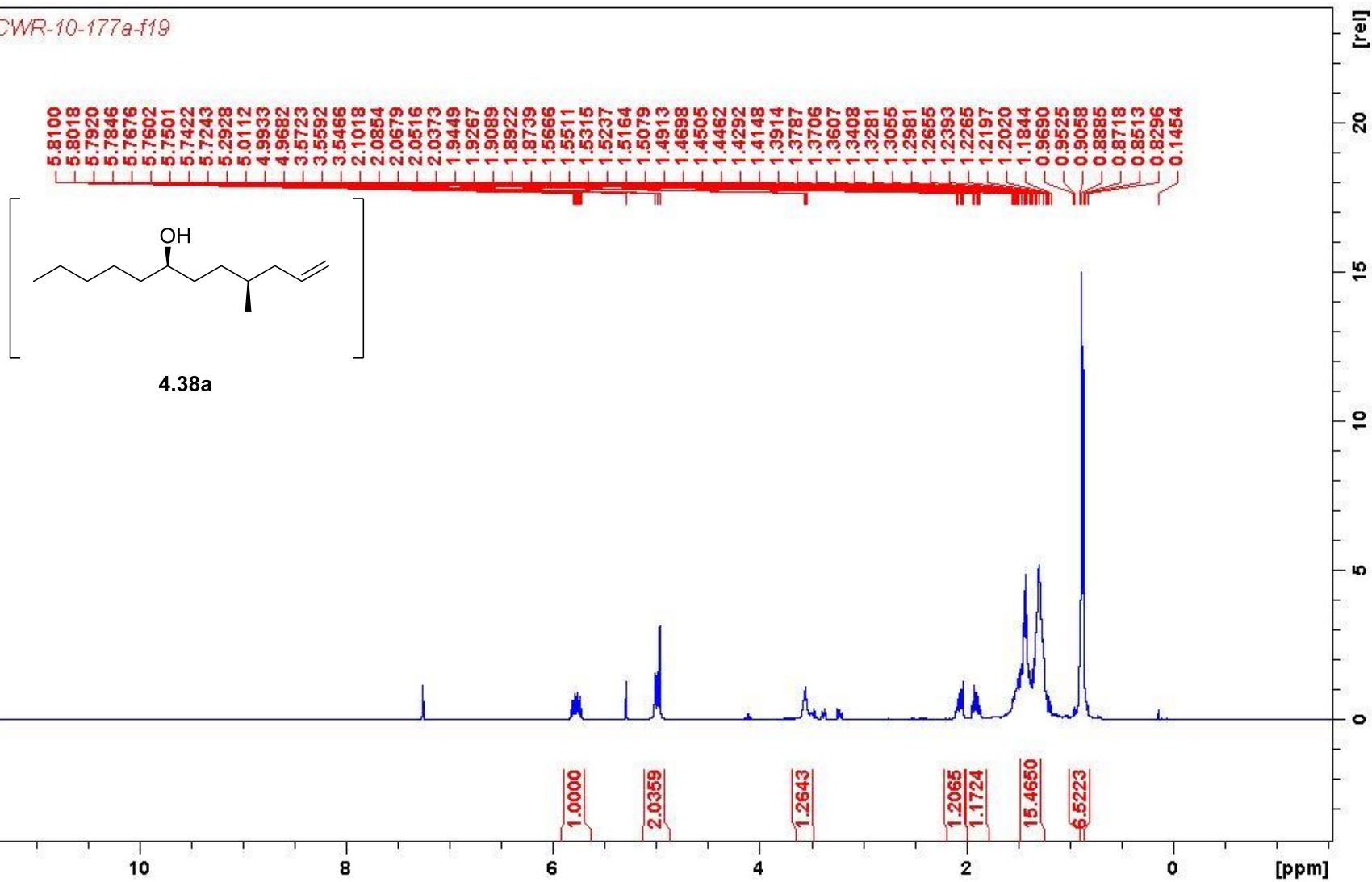


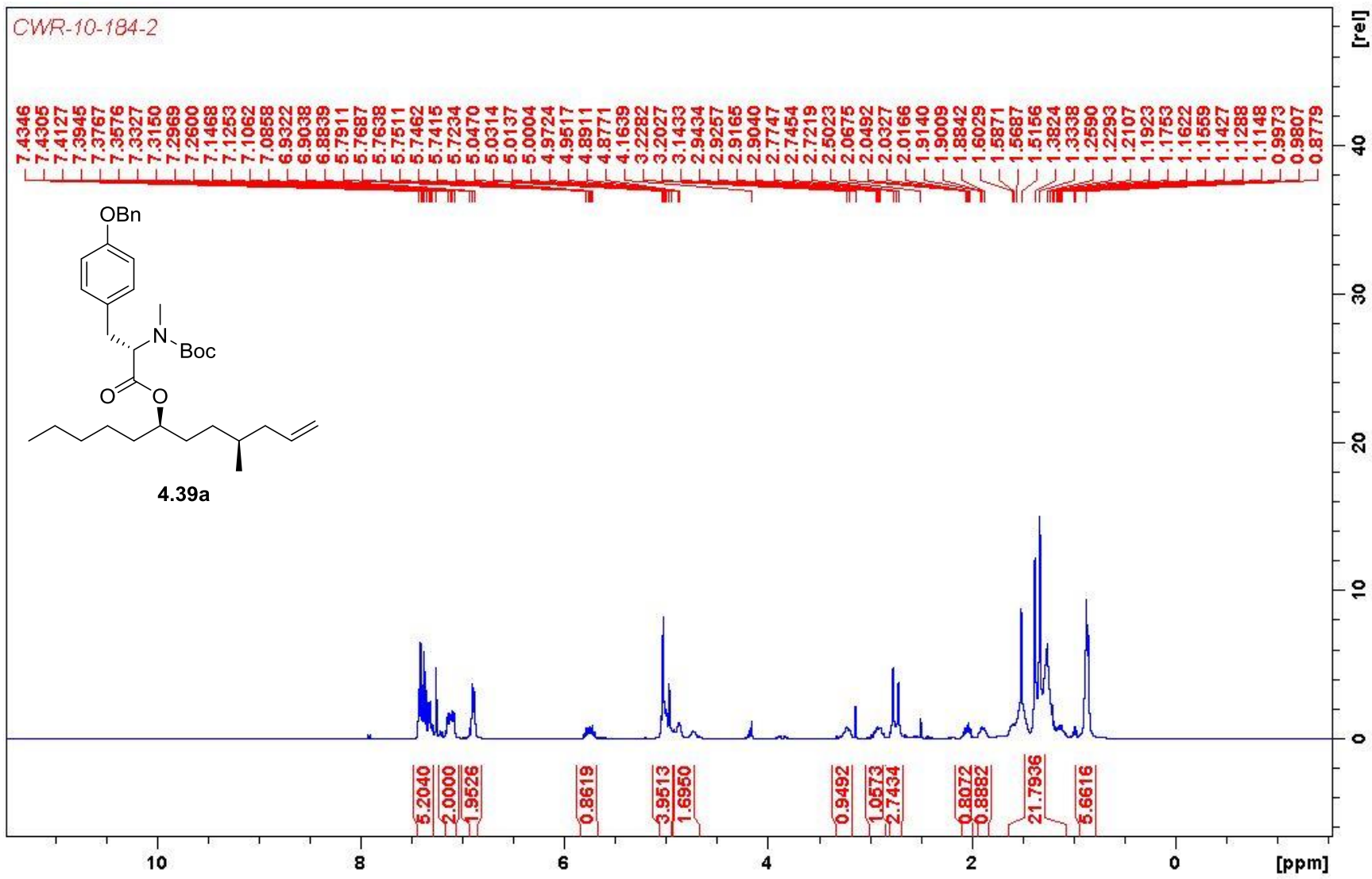
4.37a

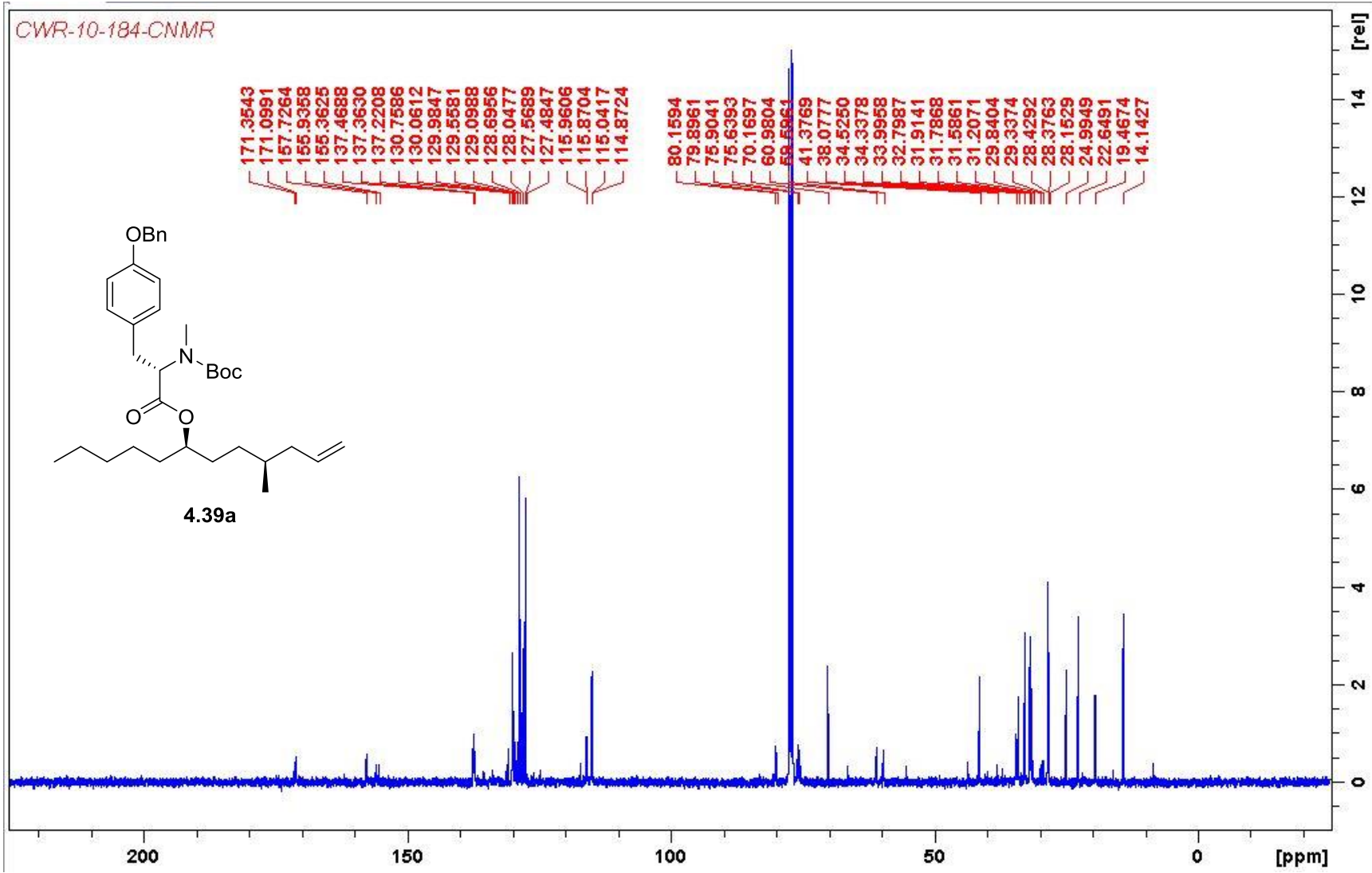
as a solution in Et₂O

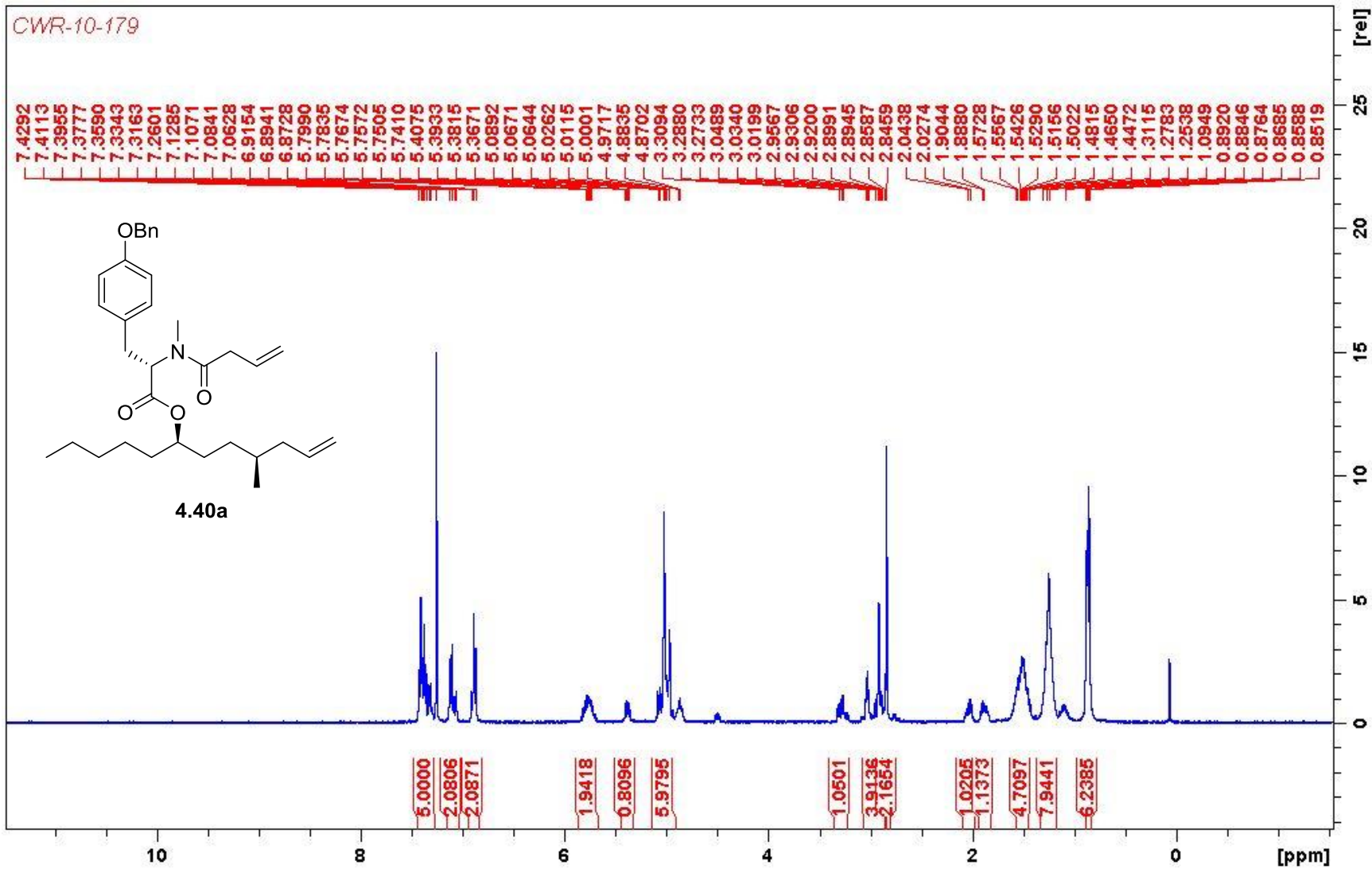


CWR-10-177a-f19

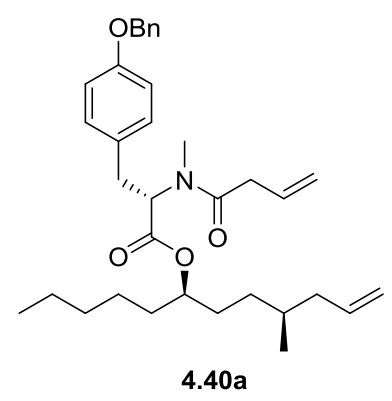






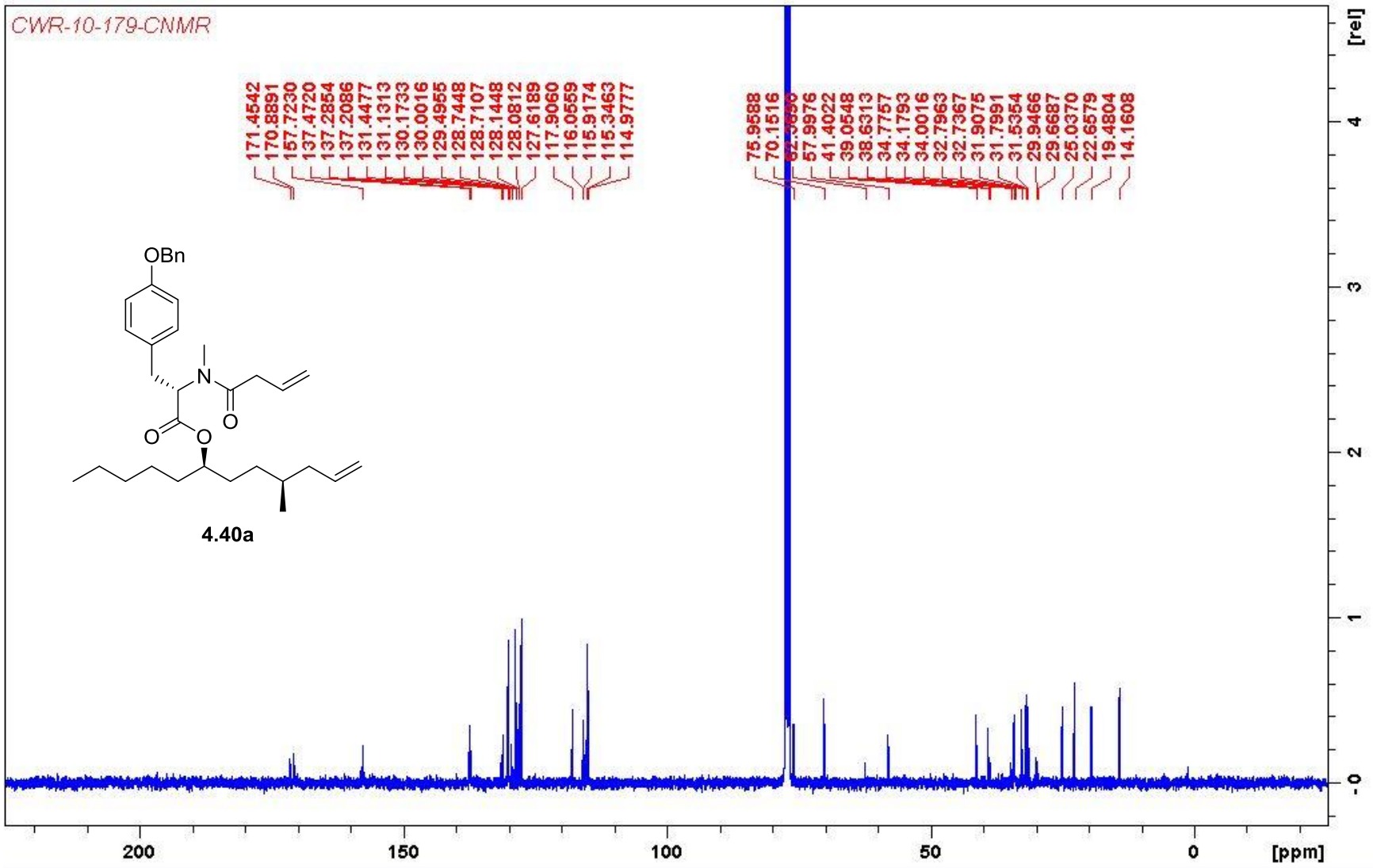


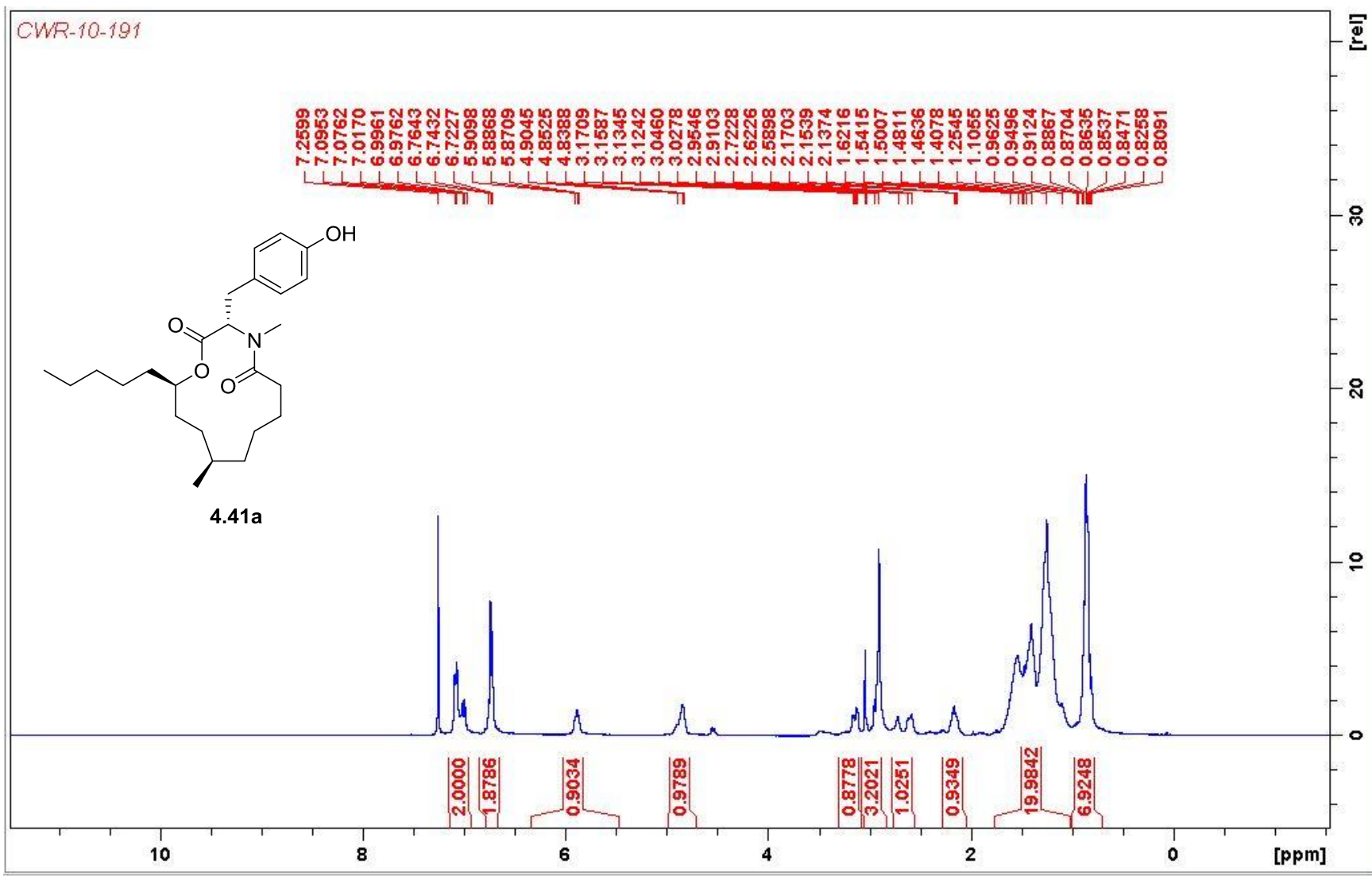
CWR-10-179-CNMR

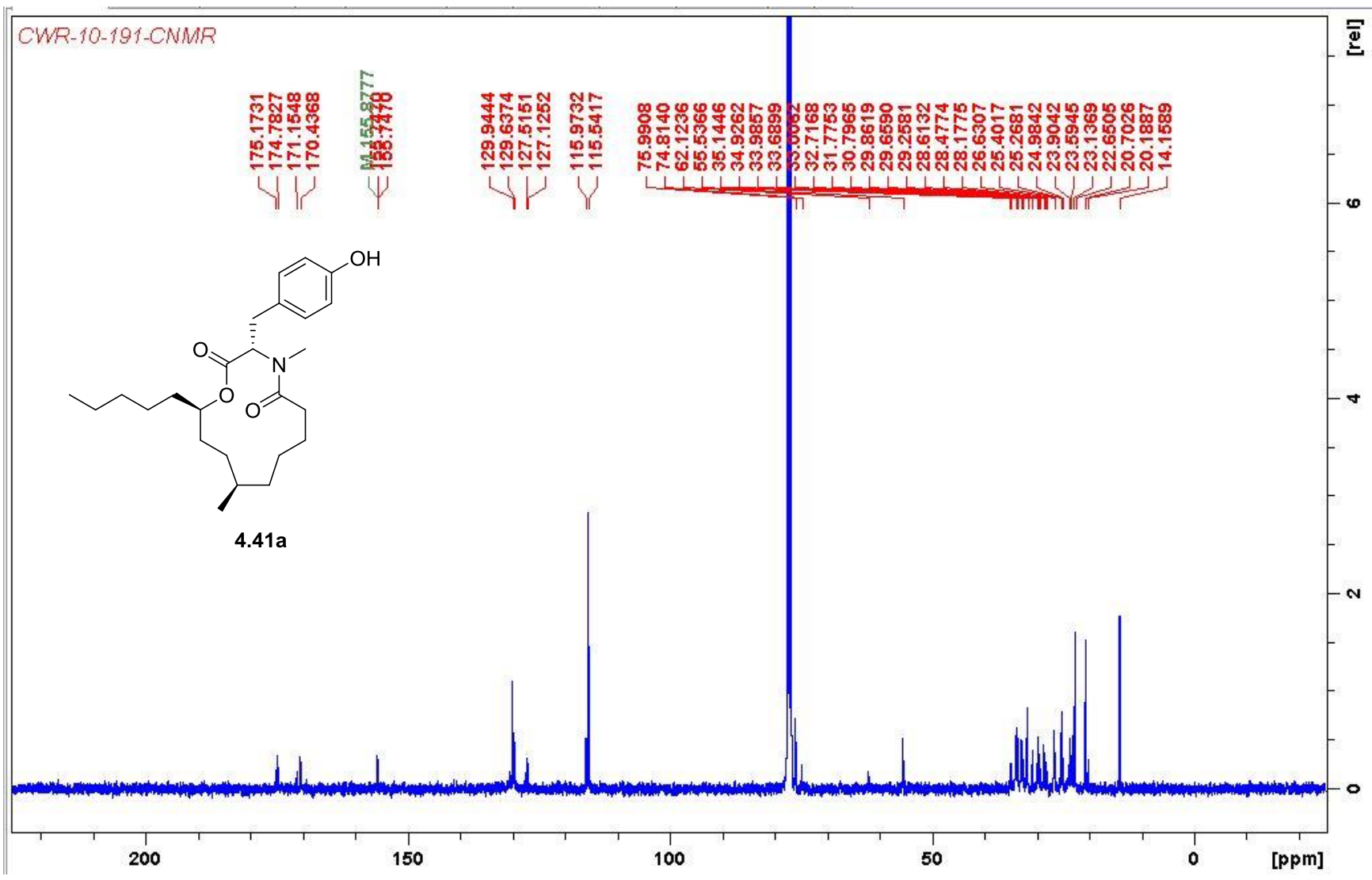


171.4542
170.8891
157.7230
137.4720
137.2854
137.2086
131.4477
131.1313
130.1733
130.0016
129.4955
128.7448
128.7107
128.1448
128.0812
127.6189
117.9060
116.0559
115.9174
115.3463
114.9777

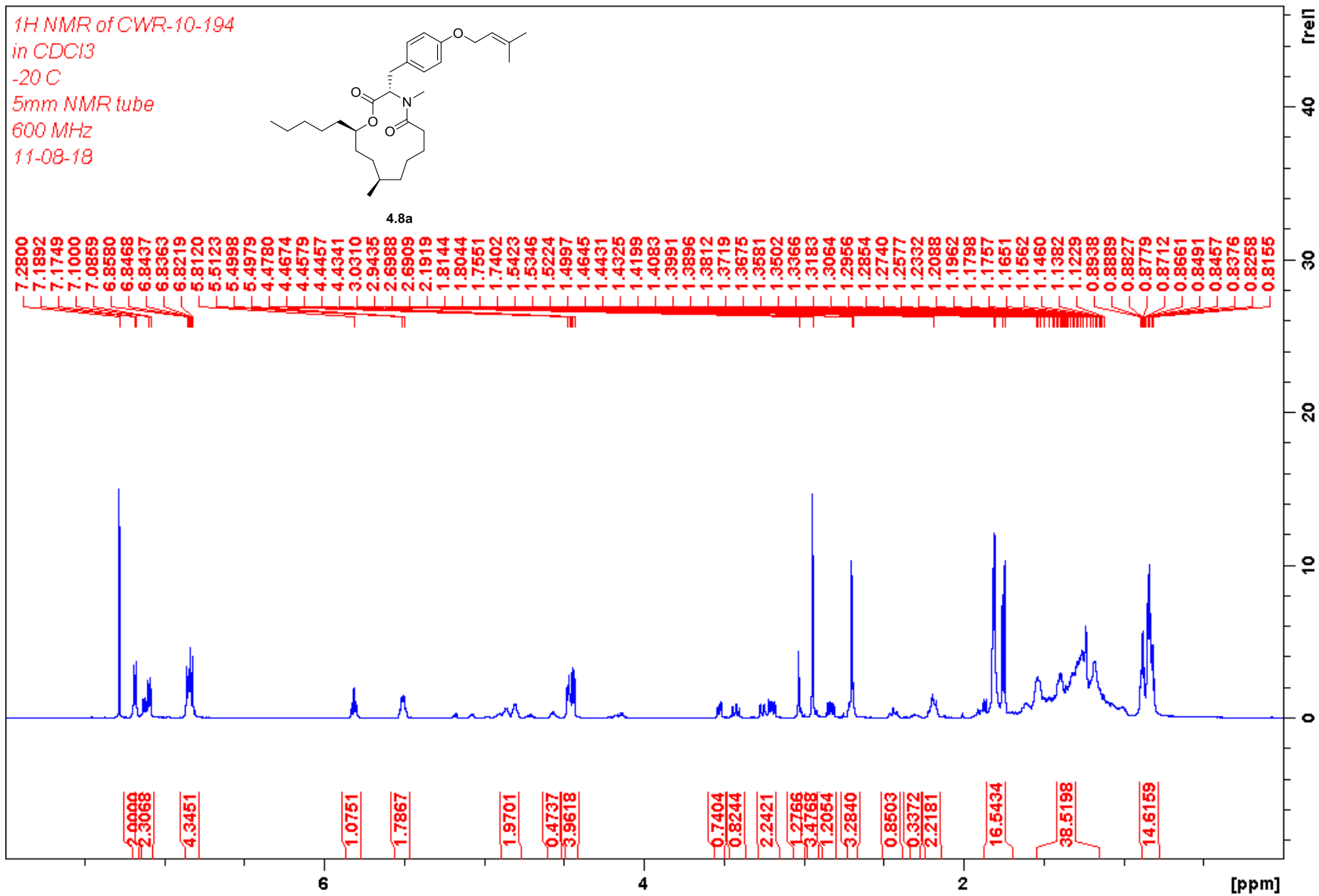
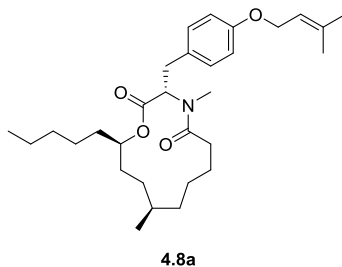
75.9588
70.1516
62.3650
57.9976
41.4022
39.0548
38.6313
34.7757
34.1793
34.0016
32.7963
32.7367
31.9075
31.7991
31.5354
29.9466
29.6687
25.0370
22.6579
19.4804
14.1608

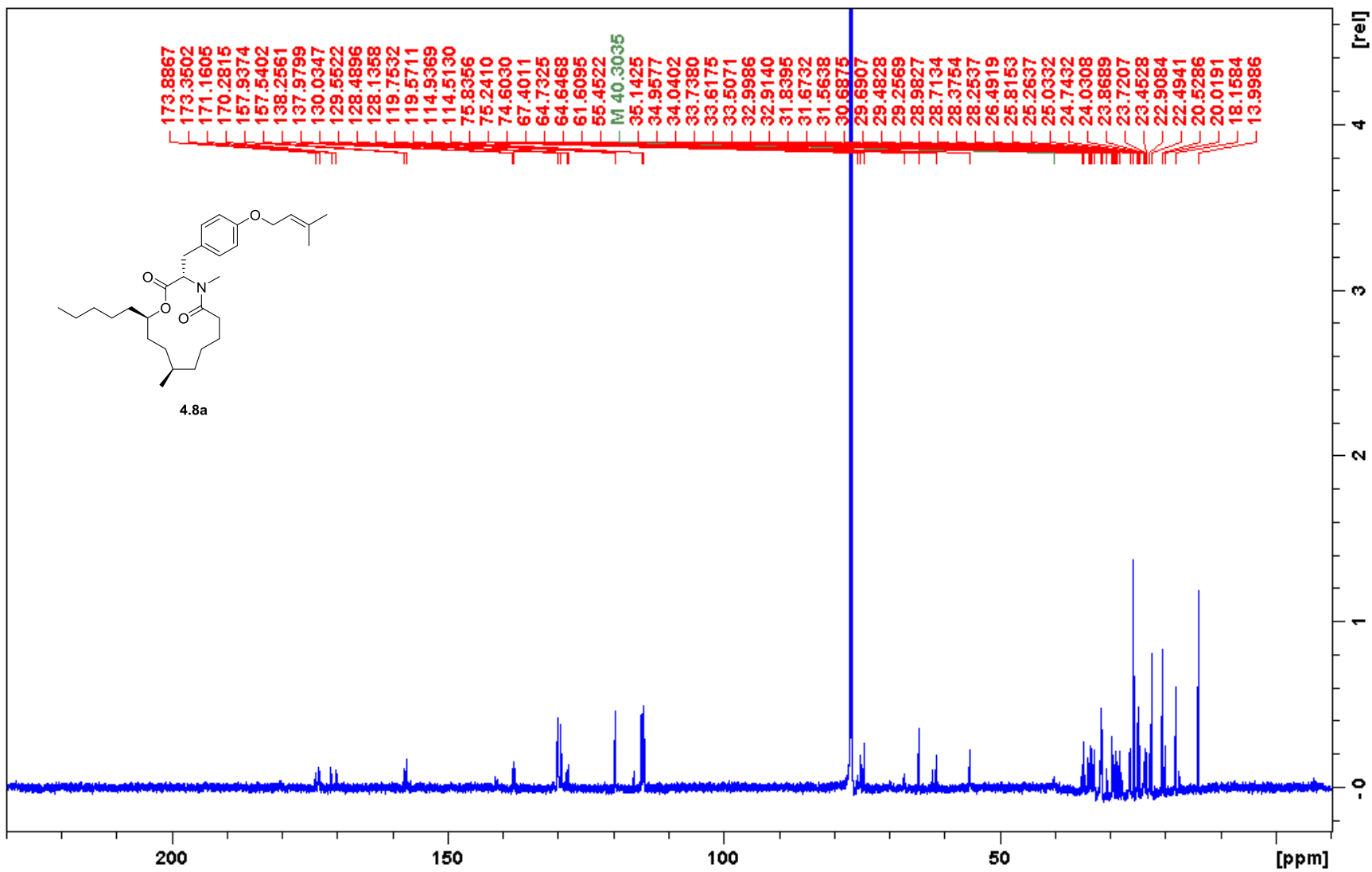


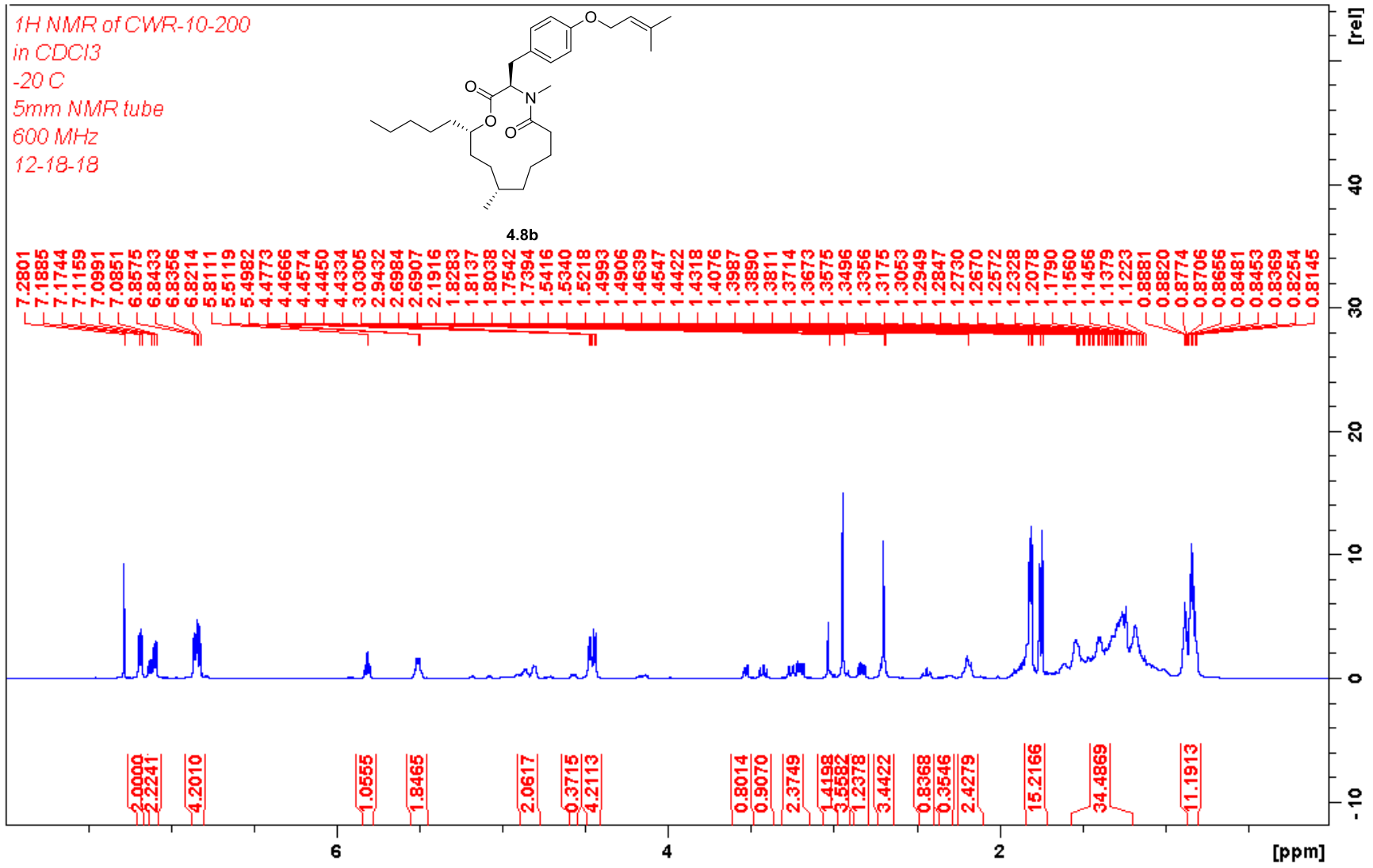


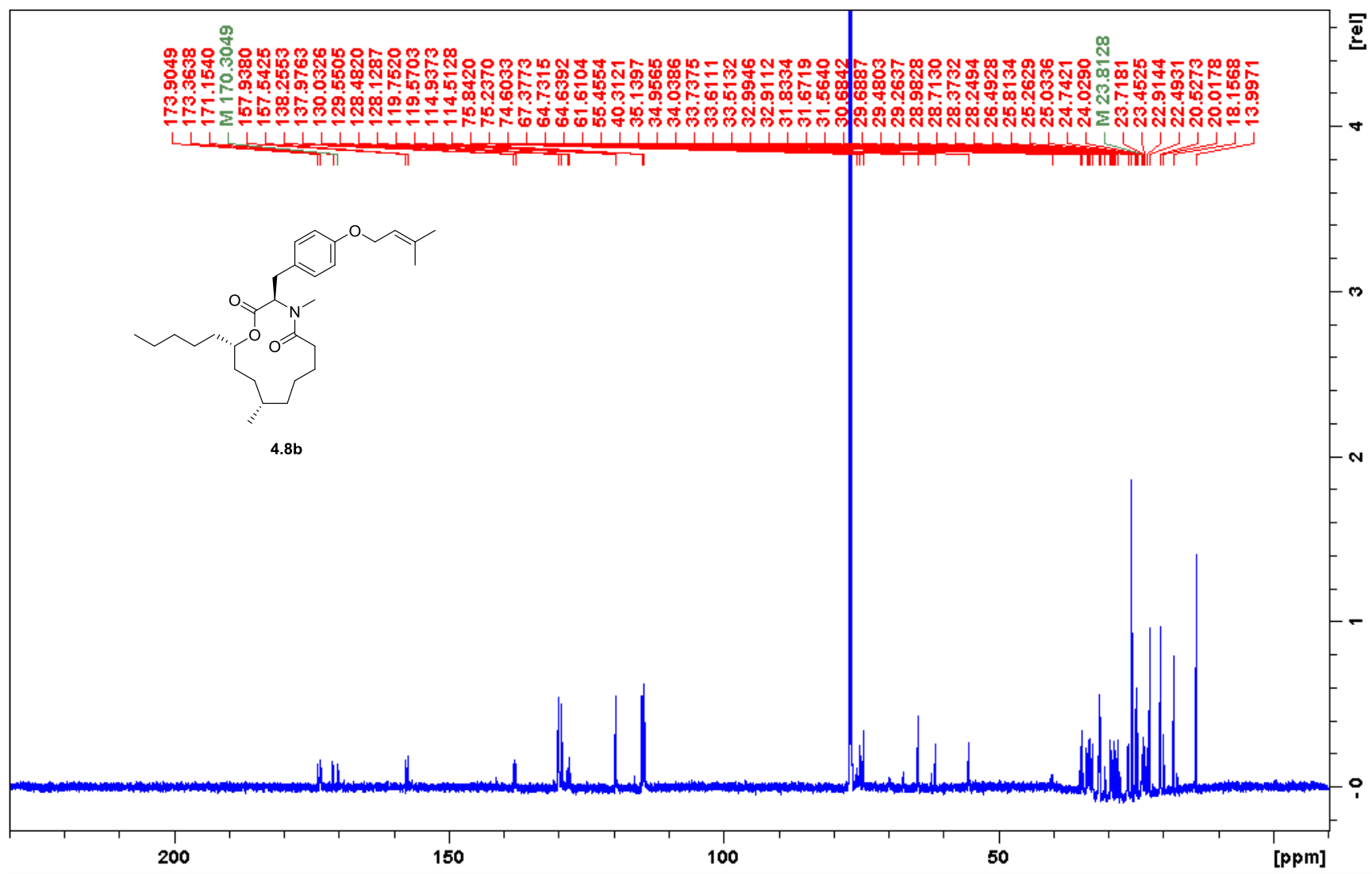


*1H NMR of CWR-10-194
in CDCl3
-20 C
5mm NMR tube
600 MHz
11-08-18*









Sections of this dissertation have been reprinted with permission from the following:

VU6010608, a Novel mGlu₇ NAM from a Series of *N*-(2-(1*H*-1,2,4-Triazol-1-yl)-5-(trifluoromethoxy)phenyl)benzamides. Carson W. Reed, Kevin M. McGowan, Paul K. Spearing, Branden J. Stansley, Hanna F. Roenfanz, Darren W. Engers, Alice L. Rodriguez, Eileen M. Engelberg, Vincent B. Luscombe, Matthew T. Loch, Daniel H. Remke, Jerri M. Rook, Anna L. Blobaum, P. Jeffrey Conn, Colleen M. Niswender, and Craig W. Lindsley. *ACS Med. Chem. Lett.* **2017**, *8*, 1326-1330. DOI: 10.1021/acsmchemlett.7b00429. Copyright © 2017 American Chemical Society.

Discovery of an Orally Bioavailable and Central Nervous System (CNS) Penetrant mGlu₇ Negative Allosteric Modulator (NAM) *in vivo* Tool Compound: *N*-(2-(1*H*-1,2,4-triazol-1-yl)-5-(trifluoromethoxy)phenyl)-4-(cyclopropylmethoxy)-3-methoxybenzamide (VU6012962). Carson W. Reed, Samantha E. Yohn, Jordan P. Washecheck, Hanna F. Roenfanz, Marc Q. Quitalig, Vincent B. Luscombe, Matthew T. Jenkins, Alice L. Rodriguez, Darren W. Engers, Anna L. Blobaum, P. Jeffrey Conn, Colleen M. Niswender, and Craig W. Lindsley. *J. Med. Chem.* **2019**, *62*, 1690-1695. DOI: 10.1021/acs.jmedchem.8b01810. Copyright © 2019 American Chemical Society.